AN ABSTRACT OF THE DISSERTATION OF

Juan D. Chavez for the degree of Doctor of Philosophy in Chemistry on

December 10, 2009

Title: Mass Spectrometry-based Identification and Characterization of Protein and Peptide Adducts of Lipoxidation-Derived Aldehydes

Abstract approved:_____

Claudia S. Maier

Oxidative stress is recognized as an important underlying factor in the pathogenesis of many degenerative diseases as well as normal senescence. The free radicals, reactive oxygen species (ROS) and electrophiles produced during oxidative stress are capable of modifying nucleic acids, lipids and proteins. There are a variety of oxidative modifications that occur to proteins including: cleavage of the protein backbone, direct oxidation of amino acid side chains by ROS, and adduction by electrophilic species such as lipid peroxidation products. Many of these oxidative modifications result in the introduction of carbonyl groups into the proteins. Protein carbonylation levels are commonly used as a biomarker to assess the degree of oxidative damage to a system. However the most commonly employed methods for measuring oxidative modifications to proteins, typically fail to provide any information about the identity of the modified protein, site of modification, or the chemical nature of the modification.

In the present study we develop an analytical technique based on affinity labeling with N'-aminooxymethylcarbonylhydrazino-D-biotin (aldehyde reactive probe, ARP), along with mass spectrometric analysis which allows for the full characterization of protein carbonylation modifications. The ability of the ARP method was first demonstrated for the case of oxylipid peptide and protein conjugates formed by Michael addition-type conjugation reactions with α,β-unsaturated aldehydic lipid peroxidation products with nucleophilic amino acid residue side chains. ARP was used to label a 4-hydroxy-2-nonenal (HNE) modified cysteine containing model peptide, and HNE modified *E. coli* thioredoxin, which were characterized using ESI-MS/MS and MALDI-MS/MS. ARP was also used to label the oxidative modifications alpha-aminoadipic semialdehyde (AAS) and gamma-glutamic semialdehyde (GGS), formed during the metal catalyzed oxidation of GAPDH.

After demonstrating the utility of the technique on model systems, it was then applied to complex biological systems. In one case, subsarcolemmal mitochondria (SSM) isolated from rat cardiac tissue. Mitochondria are well known to be a major source of ROS within the cell. They are therefore important mediators of oxidative stress, as well as regulators of cell death. We were able to identify 39 unique sites on 27 mitochondrial proteins which were modified by six different α,β-unsaturated aldehydes, including acrolein, β-hydroxyacrolein,

crotonaldehyde, 4-hydroxy-2-hexenal, 4-hydroxy-2-nonenal and 4-oxo-2-nonenal. Additionally we identified nine Lys residues on four mitochondrial proteins that were oxidized to AAS and subsequently labeled with ARP. The proteins identified with oxidative modifications include members of the mitochondrial electron transport chain, TCA cycle, membrane transport, lipid metabolism, and other important mitochondrial enzymes.

The ARP technique was also applied to identify protein targets of 4-hyroxy-2-nonenal in human monocytic THP-1 cells that were exogenously exposed to HNE. It was shown previously that exposure of THP-1 cells to HNE resulted in apoptosis, necrosis and protein carbonylation. We applied a multi-pronged proteomic approach involving electrophoretic, immunoblotting and mass spectrometric analysis to unequivocally identify eighteen sites of HNE modification on sixteen proteins. It was also demonstrated in this study that pretreatment of THP-1 cells with ascorbic acid resulted in decreased levels of HNE-protein conjugate formation.

Mass Spectrometry-based Identification and Characterization of Protein and Peptide Adducts of Lipoxidation-Derived Aldehydes

by

Juan D. Chavez

A DISSERTATION

submitted to

Oregon State University

in partial fulfillment of
the requirements for the
degree of

Doctor of Philosophy

Presented December 10, 2009
Commencement June 2010

Doctor of Philosophy dissertation Juan D. Chavez presented on December 10, 2009

APPROVED:

Major Professor, representing Chemistry

Chair of the Department of Chemistry

Dean of the Graduate School

I understand that my dissertation will become part of the permanent collection of Oregon State University libraries. My signature below authorizes release of my dissertation to any reader upon request.

Juan D. Chavez, Author

AKNOWLEDGEMENTS

I would like to thank Professor Claudia Maier for providing guidance, support, and encouragement throughout my time at Oregon State University. Thanks to all of the members who have served on my committee: Dr. Doug Barofsky, Dr. Tory Hagen, Dr. Phil Watson, Dr. Manish Gupta, Dr. Larry Daley, and Dr. Fred Stevens.

I would also like to thank the current and past members of the Maier laboratory for their collaboration. In particular Walter Wu, Jing Wang, New City Tzeng, Sasidhar Nirudodhi, Val Miranda, and Woon-Gye Chung for their friendship, support, and keeping the lab interesting.

Thanks to Brian Arbogast, Jeff Morre, Mike Hare, Lilo Barofsky and the rest of members of the mass spectrometry facility at OSU for all of their support and assistance in operating and maintaining the mass spectrometric instrumentation.

I would also like to thank my family and all of the many friends I've made here at OSU for your support and friendship over the last few years. I would like to offer special thanks to my wife, Cynthia for her love, patience and understanding.

CONTRIBUTION OF AUTHORS

Jianyong (Walter) Wu contributed to the writing of the first chapter. He also assisted with the data collection and writing of the work presented in chapters two, three and four. Dr. Bingnan Han and Dr. Woon-Gye Chung also assisted with the data collection and writing of the work presented in chapter three. Although not an author, Duane Mooney assisted with the early development of the work presented in chapter 3.

Dr. William Bisson assisted with the analysis of the protein crystal structures, contributing to the work in presented in chapters four and six.

Dr. Cristobal Miranda and Dr. Woon-Gye Chung contributed to the SDS-PAGE and Western blot analysis presented in chapter five. Dr. Mudita Singhal contributed to the analysis of the functions of the proteins presented in chapter 5. Dr. Jan F. Stevens contributed to the writing, editing, and provided financial support for the work presented in chapter 5.

TABLE OF CONTENTS

TABLE OF CONTENTS (Continued)

TABLE OF CONTENTS (Continued)

LIST OF FIGURES

LIST OF FIGURES (Continued)

LIST OF TABLES

LIST OF APPENDIX FIGURES

LIST OF APPENDIX FIGURES (Continued)

LIST OF APPENDIX FIGURES (Continued)

LIST OF APPENDIX FIGURES (Continued)

LIST OF APPENDIX FIGURES (Continued)

LIST OF APPENDIX FIGURES (Continued)

LIST OF APPENDIX FIGURES (Continued)

LIST OF APPENDIX TABLES

Mass Spectrometry-based Identification and Characterization of Protein and Peptide Adducts of Lipoxidation-Derived Aldehydes

Chapter 1

Introduction

Molecular oxygen (O_2) is essential for the cellular respiration of all aerobic organisms. While it's chemical reactivity provides a source of energy to drive the process of life, it also makes O_2 a potentially dangerous toxin. Reactive oxygen species (ROS) are highly reactive byproducts formed as a result of the use of oxygen. A host of ROS including superoxide, hydrogen peroxide, hydroxyl radical, peroxy radical and peroxynitrite are produced endogenously through numerous metabolic pathways, including oxidative phosphorylation, oxidation of xanthine by xanthine oxidase, cytochrome P-450 detoxification reaction and oxidation of NADPH by NADPH oxidase (1-3). Besides endogenous sources, ROS can also be formed by exogenous agents like ozone, pesticides, photochemical smog and ionizing radiation (3). Although at high levels ROS are potentially damaging to key cellular components, at lower levels they also play an important role in cell signaling (4, 5). Additionally they are very important in immune response, where they are generated by neutrophils in lethal quantities to kill pathogens (6). Conditions of oxidative stress can nonetheless result when cellular homeostasis is disrupted due to excessive production of ROS and/or

failure of the biological system's ability to detoxify the reactive intermediates or repair the resulting damage.

Mitochondria and Oxidative Stress

Serving as the primary energy plant for the cell, and consuming approximately 90% of the molecular oxygen taken in during aerobic respiration (7), mitochondria are central to studies of oxidative stress. The mitochondrial electron transport chain (ETC) complexes serve to reduce molecular oxygen into water, and in turn generate a proton gradient across the inner mitochondrial membrane, which drives the process of ATP production. Although electron transport through the complexes is a highly efficient process, many studies have shown that a small but significant percentage of the molecular oxygen consumed by the mitochondria, is nonetheless converted into reactive oxygen species including the radical anion superoxide ($O_2^{\cdot -}$) and H_2O_2, due to electron “leakage” from the ETC complexes (8, 9). Mitochondria are therefore a major source of superoxide within the cell (10). On its own, superoxide is relatively stable and innocuous, however it serves as a precursor for other, more reactive and damaging ROS including hydrogen peroxide, peroxynitrite, and the hydroxyl radical (11). Although there is some debate about the actual mechanism of electron leakage, generally Complex I, and Complex III are regarded as the primary production sites of ROS from the ETC. In addition to the ETC, mitochondria contain a multiplicity of other ROS-producing sources including

cytochrome b5 reductase, monoamine oxidases, dihydrooroate dehydrogenase, dehydrogenase of α-glycerophosphate, succinate dehydrogenase, aconitase, and α-ketoglutarate dehydogenase. However the contribution to the total mitochondrial ROS production by these seven sources remains unknown (Andreyev et al Biochem 2005).

Antioxidant defense system

Under normal physiological conditions a balance of the ROS produced during respiration is maintained by a complex multi-leveled antioxidant defense system (12, 13). This network of enzymes and non-enzymatic antioxidants serve to protect proteins, DNA and other important biomolecules critical to the function of the cell. The mitochondrial superoxide dismutase (Mn-SOD) serves to eliminate superoxide by dismutation to form hydrogen peroxide, which can then be catalytically decomposed into water and O_2 through the action of peroxidases. When the concentration of $O_2^{\cdot -}$ or H_2O_2 gets too high, H_2O_2 can react with superoxide to form the extremely reactive hydoxyl radical ($HO^{\cdot}$). Additionally H_2O_2 can undergo the Fenton reaction with divalent metal cations such as Fe^{2+} and Cu^{2+} producing $HO^{\cdot}$.

The mitochondrial membrane, being rich in polyunsaturated fatty acids (PUFAs), is particularly susceptible to ROS damage resulting in the lipid peroxidation process. Typically antioxidants such as ubiquinione, ascorbic acid (vitamin C) and the lipid soluble α-tocopherol (vitamin E), serve as radical scavengers,

thereby protecting the vulnerable PUFAs. Additionally other small molecule antioxidants including pyruvate, flavonoids, and carotenoids help to scavenge ROS (12). One of the most important and thoroughly studied mechanisms of antioxidant defense is the glutathione-based detoxification system. Consisting chiefly of thiol containing tripeptide, glutathione (GSH, L-γ-glutamyl-L-cysteinylgylcine), mitochondria utilize this system as both a renewable radical scavenger and as a sacrificial consumable antioxidant (14). Glutathione exists in reduced (GSH) and oxidized states (GSSG). In the reduced state, GSH can scavenge unstable ROS including superoxide and hydroxyl radicals by functioning as an electron donor to eliminate the reactive radicals. As a result GSH is converted into its oxidized disulfide form GSSG. The reduced form of GSH can be enzymatically regenerated in the mitochondrial matrix by GSSG and glutaredoxin. Additionally, in conjunction with the enzyme glutathione peroxidase, GSH can serve as an electron donor in the conversion of hydrogen peroxide to water. Acting in a sacrificial manner, the free thiol in GSH can react with electrophilic 2-alkenals derived from the lipid peroxidation process, either non-enzymatically or in a catalyzed reaction with the aid of glutathione-S-transferase. The glutathione-oxylipid conjugate can then be secreted from the mitochondria and the cell (15). Mitochondrial GSH is consumed in this process and therefore, needs to be replenished from the cytosolic GSH pool. Typically, mitochondria maintain a relatively high concentration of GSH. If a high enough

concentration of GSH cannot be maintained then oxidative stress-induced damage will occur.

Under conditions of oxidative stress the antioxidant system becomes overwhelmed and a host of lipid peroxidation products are formed. Among these, include the α,β-unsaturated aldehydes, such as HNE, ONE, HHE, acrolein etc. (16). These lipid-derived electrophiles are known to be potent cellular toxins, longer lived, and potentially more damaging to the cell than the ROS that generated them (17). They are capable of covalently modifying proteins at nucleophilic sites including Cys, His and Lys through Michael-type addition or Schiff base mechanisms, which can lead to enzymatic inhibition, increased ROS production, and contribute to a cataclysmic cycle of oxidative stress-induced cellular damage. Figure 1.1 illustrates examples of Michael adducts and Schiff base adducts between peptides and lipid peroxidation products.

Mitochondria are known to play a key role in the regulation of the cellular death mechanisms of apoptosis and necrosis (18). Damage induced by ROS and lipid peroxidation products can lead to compromised mitochondrial integrity and the release of proteins from the intermembrane space leading to cell death (19). The involvement of the mitochondrial permeability transition (MPT) in cell death is a complex detailed subject which is outside the scope of this paper but has been covered in many reviews (18, 20-23). Basically, oxidative stress can trigger the

mitochondrial permeability transition (MPT), in which nonspecific pores are opened in the mitochondrial membrane leading to a drop in the mitochondrial membrane potential ($\Delta\psi$), and release of molecules such as cytochrome c and Ca^{2+}, that then activate programmed cell death pathways (24). MPT is known to play a role in several pathological conditions including ischemia, stroke and myocardial infarction. The voltage-dependent anion selective channel (VDAC) and adenine nucleotide transporter (ANT) are both proteins known to be important in the formation of MPT pores, and oxidative damage to these proteins could play a role in the MPT process (25).

Protein Oxidation

The oxidative modification of proteins is a complex phenomenon, taking on many forms and depending on a multitude of various factors. The accumulation of oxidized proteins has been associated with a number of diseases as well as the general aging process. However, the role of these modified proteins in the etiology of disease is not well understood. Oxidative modification to proteins can take many forms including radical-induced cleavage of the peptide backbone, direct oxidation of amino acid residue side chains, nitration and nitrosylation by peroxynitrite, and conjugation with bioactive aldehydes, such as lipid peroxidation products.

The formation of protein carbonyl derivatives is widely used as a marker to assess ROS-induced damage during oxidative stress related to aging or age-related diseases. Protein carbonylation can occur as a result of direct oxidation of the side chains of lysine, arginine, proline, and threonine by ROS such as $HO^{\cdot}$, resulting in the formation of α-amino adipic semialdehyde for the case of lysine, γ-glutamic semialdehyde for the case of proline and arginine, and aminoketobutyrate for the case of threonine. Furthermore, carbonylated proteins are formed by the reaction between the side chains of cysteine, histidine, and lysine with α,β-unsaturated aldehydes, such as HNE and acrolein. The C3 atom of α,β-unsaturated aldehydes is electrophilic and readily reacts with the nucleophilic sulfhydryl group of cysteine, the imidazole group of histidine and the ε-amino group of lysine, to form a Michael-type addition product. Regardless of how the carbonyl group is introduced, they exist as relatively reactive sites on the protein molecule and can contribute to protein crosslinking by forming Schiff base products with free amino groups in the same protein or on neighboring proteins. Oxidatively crosslinked proteins are often enzymatiallly inactive and resistant to proteolytic degradation (26-28). It comes as no surprise that diseases associated with an increase in protein carbonylation often also see an increase in protein aggregate formation due to crosslinking.

Analytical methods for measuring protein carbonylation

Protein carbonylation is frequently used as a measure of oxidative stress-induced damage. Therefore, a myriad of techniques have been developed for the analysis of protein carbonyls. Some of the earliest developed, and most widely employed methods rely on spectrophotometric analysis following derivatization with thiobarbituric acid (TBARS) or 2,4-dinitrophenylhydrazine (DNPH) (29, 30). These methods are able to provide a measure of the global level of protein carbonylation within a biological sample and are therefore useful in assessing the degree of oxidative damage. However they are not able to conclusively identify the protein, specific amino acid site, or chemical nature of the oxidative modification. Several methods have been developed to identify the carbonylated proteins using the traditional proteomics analysis tools of gel electrophoresis and Western blotting. Perhaps the most widely employed of these methods again relies on the use DNPH as a labeling agent followed by immunochemical detection with an anti-DNP antibody (31). Similar approaches have used biotin hydrazide instead of DNPH, as a labeling agent, which can then be detected with the use of avidin analogs and fluorescence or chemiluminescence detection (32, 33). However, due to the lack of specificity of these hydrazine-based reagents towards the various types of carbonylation (e.g. 2-alkenal-protein adduct vs. directly oxidized amino acid side chain), the chemical nature of the modification remains unknown. To this end several studies have employed immunological detection using antibodies specific for the different types of alkenal-protein

adducts (i.e. anti-HNE or anti-acrolein antibodies) (34-37). While these methods can be highly specific for the differing forms of oxidative modification the identity of the amino acid residue site of modification remains tentative at best. Complete characterization of the chemical nature and amino acid site of modification is important to truly understand the biological impact of protein carbonylation. Technological advances in mass spectrometry have provided researchers with powerful tools to characterize post-translational modifications (PTM) to proteins. Mass spectrometry provides several advantages over other approaches for the characterization of PTMs including the ability for unequivocal identification of the amino acid site, chemical nature of PTM, discovery of novel PTMs, and the ability to quantify relative changes in PTMs (38). A variety of studies have employed mass spectrometry to study protein carbonylation in model systems in which purified proteins are incubated with LPO products or subjected to MCO reactions (39-45). These studies are useful for developing new analytical methods or for detailed structural and functional analysis of proteins of interest, however the ultimate goal remains the analysis of protein carbonyls in complex biological matrices. Several gel-free, mass spectrometric methods have been developed in which researchers are able to identify the protein target, amino acid site, and type of carbonylation in biological samples. Due to the low abundance of endogenously carbonylated proteins and the extreme complexity of biological samples affinity enrichment is necessary prior to detection. Even still, many studies add exogenous agents to carbonylate proteins *in vitro* before

identifying the protein targets. Using the biotin-tagged electrophile probes N-iodoacetyl- N biotinylhexylene-diamine (IAB) and 1-biotinamido-4-(4'-[maleimidoethylcyclohexane]-carboxamido)butane (BMCC) researchers from the Liebler group were able to identify 897 different cysteine residues from 539 proteins from nuclear and cytosolic fractions, and 1693 different cysteine residues from 809 proteins from the mitochondria (46, 47). Several studies have employed the use of biotin-hydrazide derivatives as labeling reagents for the enrichment and subsequent mass spectrometric analysis of protein carbonyls (48-50). Recently, our group has developed an analogous technique employing N' aminooxymethylcarbonylhydrazino-D-biotin (Aldehyde Reactive Probe, ARP) to label, enrich and characterize oxidative modifications to proteins (51). This method represents an attractive alternative to hydrazine-based derivatization methods for oxidized peptides and proteins because the reduction step necessary for the transformation of the hydrazone bond to the chemically more stable hydrazine bond can be omitted. Incubating mitochondrial proteins with HNE followed by biotin hydrazide labeling, affinity enrichment and mass spectrometric detection, Condreanu et al. were able to identify 18 specific sites of HNE adduction. The flexibility of modern mass spectrometers allows for different data-dependent acquisition methods combined with different dissociation techniques including CID and ECD, to be applied for the identification of carbonylated positions in peptides and proteins (39, 52-54). Stevens el al. identified 24 sites of Michael-type histidine-HNE adducts on 15 unique proteins

using neutral loss-driven MS^3 on a LTQ-FT mass spectrometer (54). Employing a solid phase hydrazide enrichment strategy and neutral loss driven MS^3 Roe et al. mapped 125 sites of HNE adduction to 67 proteins from a yeast cell lysate to which HNE had been added (53). These in vitro studies demonstrate the powerful potential of mass spectrometry in proteomics, and have proven useful for identifying putative sites and protein targets of oxidative modification, however it is still important to characterize the carbonyl modifications to proteins occurring endogenously in complex biological systems. Applying our ARP based analytical strategy to proteins isolated from rat cardic mitochondria, we were able to identify 39 unique sites on 27 proteins as being modified by a variety of 2-alkenal products including acrolein, β-hydroxyacrolein, crotonaldehyde, 4-hydroxy-2-hexenal, 4-hydroxy-2-nonenal and 4-oxo-2-nonenal (unpublished results).

Quantitative analysis of carbonylated proteins based on Mass spectrometry

Mass spectrometry based protein quantification has been developed greatly recently. One major approach is based on isotope-labeled amino acids or peptides, which can be recognized by a mass spectrometer according to their mass difference (55-58). Another major approach is label-free quantification including two different strategies: (i) measuring and comparing signal intensity of peptides from proteins; (ii) counting and comparing the number of identified-peptide spectra from a particular protein (59-64) (for an excellent review, see

Ref(65)). All these approaches can be applied to quantification for carbonylated proteins as long as the targeted peptides are replaced by carbonylated ones. However, low abundance of carbonylated proteins in biological samples requires enrichment methods not only for identification but also for quantification. Light and heavy isotope labeled Girard's P reagents, which can enrich carbonylated peptides by ion exchange columns, were applied to establish the linear dynamic range for quantification of a model carbonylated peptide by LC-MS (66). Griffin's group applied multiplexed iTRAQ reagents to label digested peptides of oxidized proteins from rat muscle mitochondria to establish the quantitative reproducibility of the avidin enrichment strateg by LC-MS/MS (67). Recently, our group designed and synthesized an aldehyde-reactive, hydrazide-functionalized, isotope-coded affinity tag (HICAT) and applied it to mitochondrial proteins modified in vitro with HNE for quantitative analysis by nanoLC-MALDI-MS (68). One acrolein-modified peptide from ADP/ATP translocase from rat mitochondria was also successfully quantified between young and old rats in vivo. A new quantitative method without isotope-labeling is also being developed in our group. The reagent N'-aminooxymethylcarbonylhydrazino-D-biotin (ARP) and iodoacetyl-PEO_2-Biotin (IPB) were used to enrich acrolein-modified Cys-containing peptides and the corresponding unmodified ones from mitochondrial samples. The ratios between them are determined by nanoLC-SRM analysis using a hybrid linear ion trap mass spectrometer. While there have been significant advances in the mass spectrometric identification and quantification of

carbonylated proteins, there is still much room for improvement on the current methods. More efficient and specific enrichment methods are critical since most of quantitative MS analysis of endogenously carbonylated proteins only works well for the most abundant of the low abundance target proteins, and there is frequently significant interference from the very abundant non-modified proteins.

References

1. Geiszt M, Kopp JB, Varnai P and Leto TL: Identification of renox, an NAD(P)H oxidase in kidney. Proc. Natl. Acad. Sci. U. S. A. 97: 8010-4, 2000.
2. Sayre LM, Smith MA and Perry G: Chemistry and biochemistry of oxidative stress in neurodegenerative disease. Curr. Med. Chem. 8: 721-38, 2001.
3. Pacifici RE and Davies KJ: Protein, lipid and DNA repair systems in oxidative stress: the free-radical theory of aging revisited. Gerontology 37: 166-80, 1991.
4. D'Autreaux B and Toledano MB: ROS as signalling molecules: mechanisms that generate specificity in ROS homeostasis. Nat. Rev. Mol. Cell. Biol. 8: 813-24, 2007.
5. Nemoto S, Takeda K, Yu ZX, Ferrans VJ and Finkel T: Role for mitochondrial oxidants as regulators of cellular metabolism. Mol. Cell. Biol. 20: 7311-8, 2000.
6. Fialkow L, Wang Y and Downey GP: Reactive oxygen and nitrogen species as signaling molecules regulating neutrophil function. Free Radic. Biol. Med. 42: 153-64, 2007.
7. Nohl H: Is Redox-Cycling Ubiquinone Involved In Mitochondrial Oxygen Activation? Free Radic. Res. 8: 307 - 315, 1990.
8. Boveris A and Chance B: The mitochondrial generation of hydrogen peroxide. General properties and effect of hyperbaric oxygen. Biochem. J. 134: 707-16, 1973.
9. St-Pierre J, Buckingham JA, Roebuck SJ and Brand MD: Topology of superoxide production from different sites in the mitochondrial electron transport chain. J. Biol. Chem. 277: 44784-90, 2002.
10. Lambert AJ and Brand MD: Reactive oxygen species production by mitochondria. Methods Mol. Biol. 554: 165-81, 2009.
11. Beckman JS and Koppenol WH: Nitric oxide, superoxide, and peroxynitrite: the good, the bad, and ugly. Am. J. Physiol. 271: C1424-37, 1996.
12. Finkel T and Holbrook NJ: Oxidants, oxidative stress and the biology of ageing. Nature 408: 239-47, 2000.
13. Andreyev AY, Kushnareva YE and Starkov AA: Mitochondrial metabolism of reactive oxygen species. Biochemistry (Mosc) 70: 200-14, 2005.
14. Pompella A, Visvikis A, Paolicchi A, De Tata V and Casini AF: The changing faces of glutathione, a cellular protagonist. Biochem. Pharmacol. 66: 1499-503, 2003.
15. Hayes JD and McLellan LI: Glutathione and glutathione-dependent enzymes represent a co-ordinately regulated defence against oxidative stress. Free Radic. Res. 31: 273-300, 1999.

16. Esterbauer H, Schaur RJ and Zollner H: Chemistry and biochemistry of 4-hydroxynonenal, malonaldehyde and related aldehydes. Free Radic. Biol. Med. 11: 81-128, 1991.
17. Esterbauer H: Cytotoxicity and genotoxicity of lipid-oxidation products. Am. J. Clin. Nutr. 57: 779S-785S; discussion 785S-786S, 1993.
18. Kroemer G and Reed JC: Mitochondrial control of cell death. Nat. Med. 6: 513-9, 2000.
19. Orrenius S, Gogvadze V and Zhivotovsky B: Mitochondrial oxidative stress: implications for cell death. Annu. Rev. Pharmacol. Toxicol. 47: 143-83, 2007.
20. Rasola A and Bernardi P: The mitochondrial permeability transition pore and its involvement in cell death and in disease pathogenesis. Apoptosis 12: 815-33, 2007.
21. Tsujimoto Y and Shimizu S: Role of the mitochondrial membrane permeability transition in cell death. Apoptosis 12: 835-40, 2007.
22. Grimm S and Brdiczka D: The permeability transition pore in cell death. Apoptosis 12: 841-55, 2007.
23. Crompton M: The mitochondrial permeability transition pore and its role in cell death. Biochem. J. 341 (Pt 2): 233-49, 1999.
24. Yang JC and Cortopassi GA: Induction of the mitochondrial permeability transition causes release of the apoptogenic factor cytochrome c. Free Radic. Biol. Med. 24: 624-31, 1998.
25. Choksi KB, Boylston WH, Rabek JP, Widger WR and Papaconstantinou J: Oxidatively damaged proteins of heart mitochondrial electron transport complexes. Biochim. Biophys. Acta 1688: 95-101, 2004.
26. Friguet B: Oxidized protein degradation and repair in ageing and oxidative stress. FEBS Lett. 580: 2910-6, 2006.
27. Friguet B and Szweda LI: Inhibition of the multicatalytic proteinase (proteasome) by 4-hydroxy-2-nonenal cross-linked protein. FEBS Lett. 405: 21-5, 1997.
28. Grune T and Davies KJ: The proteasomal system and HNE-modified proteins. Mol. Aspects Med. 24: 195-204, 2003.
29. Ohkawa H, Ohishi N and Yagi K: Assay for lipid peroxides in animal tissues by thiobarbituric acid reaction. Anal. Biochem. 95: 351-8, 1979.
30. Fields R and Dixon HB: Micro method for determination of reactive carbonyl groups in proteins and peptides, using 2,4-dinitrophenylhydrazine. Biochem. J. 121: 587-9, 1971.
31. Nakamura A and Goto S: Analysis of protein carbonyls with 2,4-dinitrophenyl hydrazine and its antibodies by immunoblot in two-dimensional gel electrophoresis. J. Biochem. 119: 768-74, 1996.
32. Oh-Ishi M, Ueno T and Maeda T: Proteomic method detects oxidatively induced protein carbonyls in muscles of a diabetes model Otsuka Long-Evans Tokushima Fatty (OLETF) rat. Free Radic. Biol. Med. 34: 11-22, 2003.

33. Yoo BS and Regnier FE: Proteomic analysis of carbonylated proteins in two-dimensional gel electrophoresis using avidin-fluorescein affinity staining. Electrophoresis 25: 1334-41, 2004.
34. Toroser D, Orr WC and Sohal RS: Carbonylation of mitochondrial proteins in Drosophila melanogaster during aging. Biochem. Biophys. Res. Commun. 363: 418-24, 2007.
35. Chung WG, Miranda CL and Maier CS: Epigallocatechin gallate (EGCG) potentiates the cytotoxicity of rotenone in neuroblastoma SH-SY5Y cells. Brain Res. 1176: 133-42, 2007.
36. Chung WG, Miranda CL, Stevens JF and Maier CS: Hop proanthocyanidins induce apoptosis, protein carbonylation, and cytoskeleton disorganization in human colorectal adenocarcinoma cells via reactive oxygen species. Food Chem. Toxicol. 47: 827-36, 2009.
37. Tanaka N, Tajima S, Ishibashi A, Uchida K and Shigematsu T: Immunohistochemical detection of lipid peroxidation products, protein-bound acrolein and 4-hydroxynonenal protein adducts, in actinic elastosis of photodamaged skin. Arch. Dermatol. Res. 293: 363-7, 2001.
38. Larsen MR, Trelle MB, Thingholm TE and Jensen ON: Analysis of posttranslational modifications of proteins by tandem mass spectrometry. Biotechniques 40: 790-8, 2006.
39. Rauniyar N, Stevens SM, Jr. and Prokai L: Fourier transform ion cyclotron resonance mass spectrometry of covalent adducts of proteins and 4-hydroxy-2-nonenal, a reactive end-product of lipid peroxidation. Anal. Bioanal. Chem. 389: 1421-8, 2007.
40. Zhu X, Tang X, Anderson VE and Sayre LM: Mass Spectrometric Characterization of Protein Modification by the Products of Nonenzymatic Oxidation of Linoleic Acid. Chem. Res. Toxicol.: 2009.
41. Bolgar MS and Gaskell SJ: Determination of the Sites of 4-Hydroxy-2-nonenal Adduction to Protein by Electrospray Tandem Mass Spectrometry. Anal. Chem. 68: 2325-2330, 1996.
42. Carini M, Aldini G and Facino RM: Mass spectrometry for detection of 4-hydroxy-trans-2-nonenal (HNE) adducts with peptides and proteins. Mass Spectrom. Rev. 23: 281-305, 2004.
43. Doorn JA and Petersen DR: Covalent modification of amino acid nucleophiles by the lipid peroxidation products 4-hydroxy-2-nonenal and 4-oxo-2-nonenal. Chem. Res. Toxicol. 15: 1445-50, 2002.
44. Isom AL, Barnes S, Wilson L, Kirk M, Coward L and Darley-Usmar V: Modification of Cytochrome c by 4-hydroxy- 2-nonenal: evidence for histidine, lysine, and arginine-aldehyde adducts. J. Am. Soc. Mass Spectrom. 15: 1136-47, 2004.
45. Temple A, Yen TY and Gronert S: Identification of specific protein carbonylation sites in model oxidations of human serum albumin. J. Am. Soc. Mass Spectrom. 17: 1172-80, 2006.

46. Dennehy MK, Richards KA, Wernke GR, Shyr Y and Liebler DC: Cytosolic and nuclear protein targets of thiol-reactive electrophiles. Chem. Res. Toxicol. 19: 20-9, 2006.
47. Wong HL and Liebler DC: Mitochondrial protein targets of thiol-reactive electrophiles. Chem. Res. Toxicol. 21: 796-804, 2008.
48. Mirzaei H and Regnier F: Affinity chromatographic selection of carbonylated proteins followed by identification of oxidation sites using tandem mass spectrometry. Anal. Chem. 77: 2386-92, 2005.
49. Soreghan BA, Yang F, Thomas SN, Hsu J and Yang AJ: High-throughput proteomic-based identification of oxidatively induced protein carbonylation in mouse brain. Pharm. Res. 20: 1713-20, 2003.
50. Grimsrud PA, Picklo MJ, Sr., Griffin TJ and Bernlohr DA: Carbonylation of adipose proteins in obesity and insulin resistance: identification of adipocyte fatty acid-binding protein as a cellular target of 4-hydroxynonenal. Mol. Cell. Proteomics 6: 624-37, 2007.
51. Chavez J, Wu J, Han B, Chung WG and Maier CS: New role for an old probe: affinity labeling of oxylipid protein conjugates by N'-aminooxymethylcarbonylhydrazino d-biotin. Anal. Chem. 78: 6847-54, 2006.
52. Rauniyar N, Stevens SM, Prokai-Tatrai K and Prokai L: Characterization of 4-hydroxy-2-nonenal-modified peptides by liquid chromatography-tandem mass spectrometry using data-dependent acquisition: neutral loss-driven MS3 versus neutral loss-driven electron capture dissociation. Anal. Chem. 81: 782-9, 2009.
53. Roe MR, Xie H, Bandhakavi S and Griffin TJ: Proteomic mapping of 4-hydroxynonenal protein modification sites by solid-phase hydrazide chemistry and mass spectrometry. Anal. Chem. 79: 3747-56, 2007.
54. Stevens SM, Jr., Rauniyar N and Prokai L: Rapid characterization of covalent modifications to rat brain mitochondrial proteins after ex vivo exposure to 4-hydroxy-2-nonenal by liquid chromatography-tandem mass spectrometry using data-dependent and neutral loss-driven MS3 acquisition. J. Mass. Spectrom. 42: 1599-605, 2007.
55. Gygi SP, Rist B, Gerber SA, Turecek F, Gelb MH and Aebersold R: Quantitative analysis of complex protein mixtures using isotope-coded affinity tags. Nat. Biotechnol. 17: 994-9, 1999.
56. Heck AJ and Krijgsveld J: Mass spectrometry-based quantitative proteomics. Expert. Rev. Proteomics 1: 317-26, 2004.
57. Oda Y, Huang K, Cross FR, Cowburn D and Chait BT: Accurate quantitation of protein expression and site-specific phosphorylation. Proc. Natl. Acad. Sci. U. S. A. 96: 6591-6, 1999.
58. Ong SE and Mann M: Mass spectrometry-based proteomics turns quantitative. Nat. Chem. Biol. 1: 252-62, 2005.
59. Bondarenko PV, Chelius D and Shaler TA: Identification and relative quantitation of protein mixtures by enzymatic digestion followed by capillary

reversed-phase liquid chromatography-tandem mass spectrometry. Anal. Chem. 74: 4741-9, 2002.
60. Bylund D, Danielsson R, Malmquist G and Markides KE: Chromatographic alignment by warping and dynamic programming as a pre-processing tool for PARAFAC modelling of liquid chromatography-mass spectrometry data. J. Chromatogr. A 961: 237-44, 2002.
61. Gilchrist A, Au CE, Hiding J, Bell AW, Fernandez-Rodriguez J, Lesimple S, Nagaya H, Roy L, Gosline SJ, Hallett M, Paiement J, Kearney RE, Nilsson T and Bergeron JJ: Quantitative proteomics analysis of the secretory pathway. Cell 127: 1265-81, 2006.
62. Liu H, Sadygov RG and Yates JR, 3rd: A model for random sampling and estimation of relative protein abundance in shotgun proteomics. Anal. Chem. 76: 4193-201, 2004.
63. Wang P, Tang H, Fitzgibbon MP, McIntosh M, Coram M, Zhang H, Yi E and Aebersold R: A statistical method for chromatographic alignment of LC-MS data. Biostatistics 8: 357-67, 2007.
64. Washburn MP, Wolters D and Yates JR, 3rd: Large-scale analysis of the yeast proteome by multidimensional protein identification technology. Nat. Biotechnol. 19: 242-7, 2001.
65. Bantscheff M, Schirle M, Sweetman G, Rick J and Kuster B: Quantitative mass spectrometry in proteomics: a critical review. Anal. Bioanal. Chem. 389: 1017-31, 2007.
66. Mirzaei H and Regnier F: Identification and quantification of protein carbonylation using light and heavy isotope labeled Girard's P reagent. J. Chromatogr. A 1134: 122-33, 2006.
67. Meany DL, Xie H, Thompson LV, Arriaga EA and Griffin TJ: Identification of carbonylated proteins from enriched rat skeletal muscle mitochondria using affinity chromatography-stable isotope labeling and tandem mass spectrometry. Proteomics 7: 1150-63, 2007.
68. Han B, Stevens JF and Maier CS: Design, synthesis, and application of a hydrazide-functionalized isotope-coded affinity tag for the quantification of oxylipid-protein conjugates. Anal. Chem. 79: 3342-54, 2007.

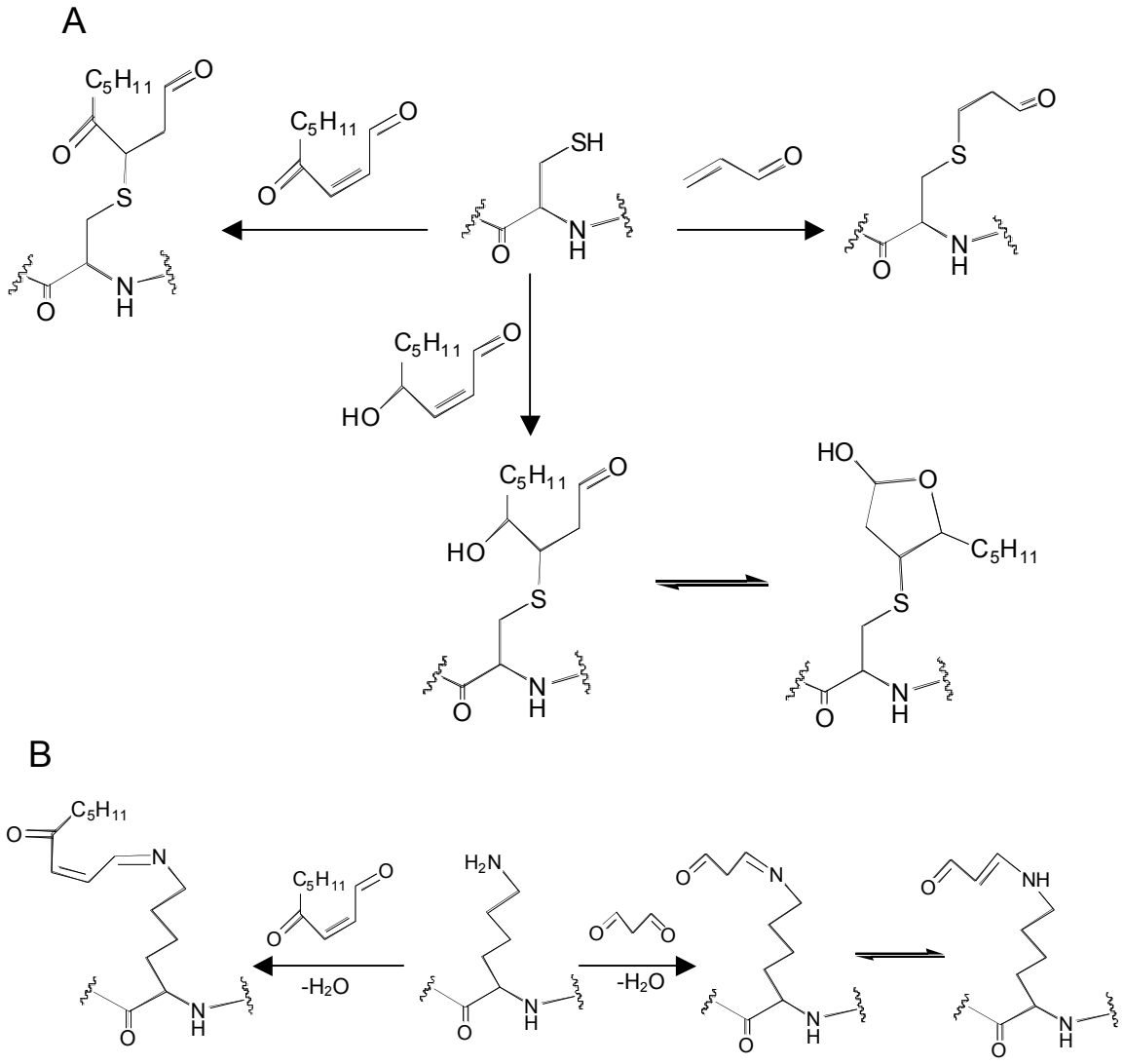

Figure 1.1 - Michael adducts formed from Cys-containing peptides with ACR, ONE and HNE (A), C-2 can also be the active site for ONE; Schiff bases formed from Lys-containing peptides with MDA and ONE (B).

Chapter 2

Methods

Mass Spectrometry for the Analysis of Biomolecules

Mass spectrometry (MS) is an analytical technique for the structural elucidation of molecules by measuring their mass-to-charge ratio (m/z). Mass spectrometric measurements are carried out on ions in the gas phase. All mass spectrometers consist of three basic components: an ionization source to convert the analyte into gas phase ions, a mass analyzer to separate the ions according to their m/z, and a detector to record the number of ions at each m/z. Over the last three decades technological advances in mass spectrometric instrumentation, specifically the advent of the 'soft' ionization techniques of electrospray ionization (ESI) (1) and matrix-assisted laser desorption ionization (MALDI) (2), have allowed for an explosive growth of the field of biomolecular mass spectrometry. Additionally, improvements in mass analyzer technology and the widespread commercial availability of a variety of MS instrumentation has allowed biomolecular MS analysis to become commonplace in many labs. The most common mass analyzers used for biomolecular analysis include the quadrupole (Q), ion trap (IT), time-of-flight (TOF), Fourier transform ion cyclotron resonance (FT-ICR), and the more recently developed Orbitrap (OT). Each of the different type of analyzers have there own particular strengths and weaknesses. Many modern mass spectrometers are hybrid instruments that contain two or more

types of mass analyzers and are able to combine the strengths of the various types of analyzers.

Ionization Methods

Prior to the 1980's mass spectrometry was limited to the analysis of small and relatively volatile molecules. The advent of ESI and MALDI allowed for the analysis of biological macromolecules including proteins, DNA and carbohydrates, and are now the most common ionization sources for biomolecular mass spectrometry (1, 2).

Electrospray ionization

ESI produces gas phase ions directly from a liquid solution (Figure 2.1). A solution containing the analyte is passed through a needle electrode, which is typically maintained at a voltage of 1-5kV. A fine aerosol of charged droplets is generated as the solvent sprays from the tip of the needle. The droplets undergo evaporation, which is often aided by flowing a desolvation gas (N_2) coaxially with the spray. As the droplets decrease in size, the charge density increases resulting in Coulombic explosion and the generation of smaller droplets. Finally, gas phase ions are produced through either an ion evaporation mechanism or the charged residue mechanism and are passed on to the mass analyzer (3, 4). For peptides and proteins the ESI process results in multiply charged ions, typically doubly and triply charged for tryptic peptide ions. ESI has

the particular advantage that it can be coupled directly to the eluate flow from an HPLC, thereby allowing for the hybrid analytical technique of LC-MS, which combines the separation capabilities of HPLC with the mass analysis capabilities of MS resulting in a technique with high specificity and sensitivity.

Matrix-Assisted Laser Desorption Ionization (MALDI)

MALDI employs the use of a laser to transfer ionizing energy to a sample of the analyte that is co-crystalized with an organic acid matrix (Figure 2.2). The most common matrix materials are derivatives of cinnamic acid, which are mixed at a high molar ratio with the analyte and co-crystallized on a metal target plate. The matrix molecules serve to absorb a majority of the laser energy, thereby protecting the analyte and making MALDI a 'soft' ionization technique. Although the exact desorption/ionization mechanism is not completely understood, irradiation of the sample generates a gaseous plume of matrix and analyte ions. The gas phase ions are then electrostatically driven from the ionization source into the mass analyzer. MALDI generates primarily singly charged ions for peptides and proteins. LC-MS analysis is also possible with MALDI instruments, but only in an offline fashion, where the LC separation is performed first and the eluate is spotted onto a MALDI target plate, followed by the MS analysis.

Tandem mass spectrometry for the analysis of peptides and proteins

Tandem mass spectrometry, MS/MS or MS^n, employs two or more stages of mass spectrometric analysis. This type of analysis is carried out using hybrid mass spectrometers that contain multiple mass analyzers such as; the quadrupole-time-of-flight (Q-TOF), time-of-flight/time-of-flight (TOF/TOF), or triple quadrupole (QQQ) instruments, or, alternatively, by using instruments with ion trapping mass analyzers such as; quadrupole ion traps (IT), ion cyclotron resonance (ICR), or the Orbitrap (OT). Regardless of the type of instrument used, the fundamental principles of MS/MS experiments remain the same. First a precursor ion of a selected m/z is isolated and fragmented, followed by the analysis of the m/z values of the resulting fragment ions. Several different fragmentation mechanisms exist, however the most common ones used for the analysis of peptides and proteins are collision-induced dissociation (CID), electron transfer dissociation (ETD), and electron capture dissociation (ECD). CID is by far the most common method of fragmentation used in MS/MS experiments. In CID experiments, selected precursor ions are accelerated into a collision cell where they undergo collisions with an inert gas, often nitrogen, helium, or argon. These collisions result in the formation of characteristic fragment ions, which when analyzed, provide structural information about the precursor ion. The CID fragmentation of protonated peptide ions primarily results in the fragmentation of the peptide bond and the formation of, so called, y and b type ions according to the Roepstorff nomenclature (5), modified by

Biemann (6) (figure 2.3). The CID process can be performed in either a low energy regime, (which occurs on the millisecond timescale, consisting of multiple collisions between the ions and the collision gas with a collision energy typically in the range of 30-100 eV) or the high energy regime (occurring on the microsecond timescale, consisting of one or two collisions between the ions and collision gas with a collision energy > 1 keV). Ideally one would like to aquire a MS/MS spectrum with a complete series of y and/or b ions, thereby allowing the amino acid sequence of the peptide to be deduced. Realistically this is not always the case and some peptides, for example those with non-tryptic sequences, or post-translational modifications can be notoriously difficult to sequence using CID experiments.

The alternative fragmentation techniques of ECD and ETD both operate on the principle of transferring an electron (eitherby direct capture in the case of ECD, or by way of an electron transfer reaction with an anionic radical, typically fluoranthene) to a peptide or protein cation, thereby inducing its dissociation into fragment ions. Both ECD and ETD result primarily in the formation of c and z type ions, which originate through the dissociation of the N-C_α bond (7, 8). This cleavage occurs randomly across the peptide backbone and has made these techniques particularly useful in fragmenting large peptides (>10 residues) and complete proteins as needed in the top-down proteomics approach. Additionally ECD and ETD have proven, in general, to be more effective than CID in

preserving PTMs during the dissociation process, making it possible to identify the chemical nature and amino acid site of the modification. Recently, it has been shown that ETD is truly a complimentary technique to CID and by employing both in concert, more useful information can be obtained from a single experiment than using either technique alone (9, 10). As MS technology continues to advance and more instruments become available that can operate using multiple dissociation techniques, it is likely that the use of a single type of fragmentation in bioanalytical MS experiments will become a thing of the past.

Mass Spectrometry-Based Proteomics

Proteomics refers to the study of the proteome, with the goal of understanding the structural and functional properties of proteins. Mass spectrometry-based proteomics experiments typically fall into one of two categories; top down proteomics, and bottom-up proteomics. The most widely used approach is bottom-up proteomics, in which proteins are digested with an enzyme such as trypsin, and the resulting peptides are analyzed by mass spectrometry. The mass spectrometric analysis takes place in two stages, first a MS analysis that determines the m/z of the precursor peptide ion followed by a MS^2 analysis in which a precursor ion of interest is fragmented to obtain the peptide sequence information (see tandem mass spectrometry section above). Sequenced peptides are then compared with genome derived, protein sequence databases to identify their proteins of origin. In the top down approach, intact proteins are

ionized and introduced into the mass spectrometer, where again the analysis takes place in multiple stages. First, MS analysis measures the m/z of the intact protein, followed by fragmentation of the protein and MS^2 measurement of the m/z of the resulting fragment ions. Typically top-down analysis is performed using FT-ICR instruments, which allow for further MS^n analysis to be performed, consisting of isolating the primary fragment ions generated by MS^2 and subjecting them to another round of fragmentation and measurement of the secondary fragment ions mass-to-charge ratios (m/z). The information generated from the analysis of the fragment ions, is used to construct a fragment ion ladder that can be used to deduce the complete protein sequence.

Instrumentation

As stated above all mass spectrometers consist of three main components; an ionization source, a mass analyzer, and a detector, however there are many different variations of each of these three components and, thus, a wide variety in available types of instrumentation. Each type of mass spectrometer has specific advantages and disadvantages, depending on the application. The three different types of mass spectrometers used for the research in this dissertation are described below.

Quadrupole-Time-Of-Flight Mass Spectrometer (Q-TOF)

The Micromass/Waters Q-TOF Ultima Global is a quadrupole-time-of-flight hybrid mass spectrometer used primarily with an ESI source (Figure 2.4). Ions generated at the ESI source are focused through a series of ion optics that pass the ion beam through to the quadrupole, which serves as the first mass analyzer. Ions of interest can then be selectively passed through the quadrupole into a hexapole collision cell where ions can undergo low energy collision-induced dissociation (CID) generating fragment ions. The fragment ions along with any remaining precursor ions are then passed on to the TOF analyzer with an upper m/z range of 20,000 where they are separated according to their m/z and detected on a multi-channel plate (MCP) detector.

Linear Ion Trap Ion Cyclotron Resonance Mass Spectrometer (LTQ-FT)

The Thermo Scientific LTQ-FT Ultra hybrid mass spectrometer is a linear ion trap-Fourier transform ion cyclotron resonance instrument operated primarily with an ESI source (Figure 2.5). Ions generated at the source will pass through transfer optics into the 2D-linear quadrupole ion trap where they can be analyzed according to their m/z or undergo low energy CID and passed on to the cylindrical ICR cell. In the ICR cell accurate masses of the ions can be obtained with a resolving power of up to 100,000 at m/z 400. This instrument has a scan range of 50-4000 m/z. The combination of the linear ion trap and ICR mass

analyzers offer the capability to perform MS^n experiments as well as electron capture dissociation in the ICR cell.

Time-Of-Flight/Time-Of-Flight Mass Spectrometer (MALDI-TOF/TOF)

The Applied Biosystems 4700 Proteomics Analyzer generates ions with a MALDI source, which are then analyzed with tandem time-of-flight mass analyzers. (Figure 2.6) The MALDI source consists of Nd:YAG laser operating at 355nm. In MS mode ions are accelerated down the flight tube where they can be analyzed in linear mode for ions > 5000 m/z or in reflectron mode for smaller ions. In MS/MS mode ions can be selected by the first TOF analyzer, which functions as a timed ion selector to allow ions of interest to pass into the collision cell where they can undergo high energy CID (1 keV). Fragment ions are then accelerated down the second TOF tube where they are analyzed in reflectron mode.

Isolation of Mitochondria

The Institutional Animal Care and Use Committee (IACUC) at Oregon State University approved the experimental protocol for the use of animals in this study. Male Fisher 344 rats, obtained from the National Institute of Aging (Bethesda, MD), were housed in individual plastic cages covered with Hepa filters and allowed free access to food and water. Rats were anesthetized with diethyl ether and a midlateral incision was made in the chest to remove the heart.

The hearts were perfused with phosphate buffered saline (PBS), rinsed with saline, blotted dry and weighted. Subsarcolemmal mitochondria (SSM) and interfibrillar mitochondria (IFM) were isolated from the rat hearts by differential centrifugation according to the procedures of Palmer (11) with minor modifications by Suh et. al. (12) and stored at -80^{o}C until needed. Briefly, after trimming excess fat and removing the atria, the ventricles were minced and homogenized 1:5 (w/v) with buffer A1 (220 mM mannitol, 70mM sucrose, 5 mM MOPS, 0.2 % BSA, pH 7.4). The minced heart tissues were homogenized with a glass homogenizer and pestle attached to a drill. The homogenates were then centrifuged at 500 × *g* for 10 min at 4°C (all remaining centrifugation steps were also performed at 4°C). The supernatant was saved and the pellet was resuspended in 10 volumes (mL/g) of Buffer A1 and centrifuged at 500 × *g* for 10 min. The two supernatants were subsequently pooled and centrifuged at 3000 × *g* for 10 min to obtain SSM, while the pellet obtained in the second low-speed centrifugation step was saved for IFM isolation. This pellet was resuspended in 3 volumes of Buffer B1 (100 mM KCl, 50 mM MOPS, 2 mM EGTA, 0.2 % BSA, pH 7.4). Subtilisin A (3 mg/g wet weight tissue) was added to the tissue pellet, incubated on ice for 0.5 min, and homogenized. The homogenate was then diluted 7-fold with Buffer B1 and centrifuged at 5000 × *g* for 5 min. The supernatant was discarded and the pellet resuspended in the original volume of buffer. The resuspended pellet was centrifuged at 500 × *g* for 10 min to yield the nuclear pellet. The supernatant was saved and the pellet was resuspended and

centrifuged at 500 × *g* for 10 min. This step was repeated once more with the supernatant being saved after each spin. The supernatants from the three low-speed spins were combined and centrifuged at 3000 × *g* for 10 min to obtain the IFM pellet. The final SSM and IFM pellets were resuspended in one volume of respiration buffer (300 mM mannitol, 10 mM KCl, 2 mM HEPES, 5 mM KH_2PO_4, pH 7.2) and frozen at -80^{o}C. A flow chart illustrating a simplified version of the mitochondrial isolation is shown in figure 2.7.

Preparation of Mitochondrial Protein Samples

In preparation of protein samples from mitochondria, the mitochondrial membranes needed to be disrupted. To evaluate three different methods of preparing the mitochondrial protein samples a proteomics LC-MS/MS analysis was performed. In the first method, the mitochondria were ruptured by four rounds of freeze/thaw cycles which involved rapid freezing with liquid N_2 followed by thawing in a cold water bath with mild sonication. The second method involved dissolving the mitochondrial membranes with a buffer solution containing triton X-100, a mild non-ionic detergent. The third method involved using RapiGest^{TM} SF, an acid labile surfactant available through Waters. The proteins were reduced, alkylated and digested with trypsin and the resulting peptide samples were analyzed on the Q-TOF. Mascot was used to for protein identification and Scaffold was used for comparison of the samples. Samples were evaluated by the total number of proteins identified, using the criteria in

Scaffold of 95% peptide and protein probability with a minimum of 2 peptides per protein. The results were as follows; freeze/thaw method identified a total of 91 proteins, triton X-100 method identified a total of 92 proteins, and the RapiGest method identified a total of 93 proteins with a total of 67 proteins being common to the three methods. These values indicated that there was not a significant difference between the three methods and are summarized in a Venn diagram in figure 2.8. Mitochondrial protein samples used for the research described in this dissertation were prepared using either the freeze/thaw or triton X-100 methods.

SDS-PAGE and Western Blotting

Sodium dodecyl sulfate polyacrylamide gel electrophoresis (SDS-PAGE) is a widely used technique for separating proteins according to their electrophoretic mobility (13). The electrophoretic mobility of a molecule is a function of it's size, shape and net charge. In SDS-PAGE, the anionic detergent SDS denatures and binds to the protein at a constant ratio of 1.4 grams SDS per gram protein. This imparts each protein with an overall negative charge, which is proportional to the length of the peptide backbone, or it's molecular mass. Therefore the observed electrophoretic mobility of SDS-protein complexes becomes a function of the molecular mass, being inversely proportional to the logarithm of the length of the peptide backbone (14). An electric field is applied across the gel causing the negatively charged SDS-protein complexes to migrate through the gel toward the anode. Pores in the gel cause proteins of different sizes to move at different

rates through the gel with smaller proteins moving more quickly and larger proteins moving slower. Separated protein bands can then be visualized by staining the gel with Coomassie Blue R-250. A Coomassie stained SDS-PAGE is shown in figure 2.9A. In this dissertation SDS-PAGE was used as a tool to separate protein samples, which were then typically analyzed by mass spectrometry or Western blotting.

Western blotting is an immunochemical technique used to detect specific proteins of interest, after they have been separated by gel electrophoresis. The proteins are electrophoretically transferred from the gel to a membrane, usually composed of nitrocellulose or PVDF. The membrane is then probed with an antibody that is specific for the protein of interest. Reactive protein bands are visualized using a chemiluminescent reaction in which horseradish peroxidase (HRP), which is conjugated to the antibody, oxidizes luminol, which emits light at 428 nm. The emitted light can be detected spectrophotometrically or by using photographic film. In this dissertation, NeutrAvidin-HRP was used as a probe in Western blotting to detect ARP labeled proteins. A typical Western blot image can be seen in figure 2.9B

Blue-Native Gel Electrophoresis

Blue native polyacrylamide gel electrophoresis (BN-PAGE) is a technique developed in the early 1990's for the separation of membrane proteins and large protein complexes in the molecular mass range of 10 kDa to 10,000 kDa (15). In

opposition to SDS-PAGE, separation in BN-PAGE takes place under mild non-denaturing conditions so the proteins maintain their native structure, and their enzymatic activity throughout the process. The underlying principle of BN-PAGE relies on the fact that anionic Coomassie blue dyes bind to membrane protein complexes providing an overall negative charge to the protein complexes necessary for electrophoretic mobility. This technique has been widely applied to study the mitochondrial electron transport chain (ETC) complexes (16-19). A technique using BN-PAGE was developed in hopes of being able to analyze oxidative stress induced damage to the mitochondrial ETC complexes in greater detail. The ETC complexes were successfully separated with BN-PAGE and identified by mass spectrometry. Attempts were made to combine BN-PAGE with Western blotting however no specificity could be obtained in the detection of ARP labeled ETC proteins in the Western blot. Figure 2.10 displays a typical BN-PAGE and corresponding Western blot, illustrating the lack of specificity when probed by NeutrAvidin-HRP. In a collaboration with members of the Hagen group, BN-PAGE was used in conjunction with MALDI-TOF/TOF analysis to show that supercomplexes of the mitochondrial ETC decline with age in the rat heart (20).

Avidin-Biotin Affinity Chromatography

Affinity chromatography takes advantage of the high specificity of biochemical interactions, and is frequently employed to enrich low abundance target molecules from complex biological matrices. The avidin-biotin system is one of

the most widely employed for affinity enrichment methods. Avidin is a tetrameric glycoprotein, consisting of four identical subunits with a combined mass of 67-68 KDa, which naturally occurs in the egg whites of birds, reptiles and amphibians. Each monomer of avidin binds biotin (vitamin H) with a high degree of affinity and specificity. In fact the binding is the strongest non-covalent interaction known in nature with a $K_D \approx 10^{-15}$ M (21, 22). The binding interaction occurs very rapidly and once formed is stable under a wide range of conditions, including extremes of pH, temperature, solvents and denaturing agents. These features of the avidin-biotin interaction make immobilized avidin particularly useful for purifying biotinylated molecules of interest. However the exceptionally high strength of the binding often makes it hard to elute the bound molecules, typically requiring harsh denaturing conditions, such as boiling in 8M guandine-HCl, pH 1.5 or sodium-dodecyl-sulfate (SDS) buffer. Such harsh conditions are often not desirable as they may damage the biomolecular analyte, and are incompatible with downstream analysis such as LC-MS. Therefore many applications employ the use of an immobilized monomeric form of avidin which binds biotin reversibly, with a $K_D \approx 10^{-7}$ M (23). This allows elution of the biotinylated molecules of interest from the avidin support using milder conditions. The research described in this dissertation used Pierce UltraLink® monomeric avidin available through Thermo Scientific, for the enrichment of biotinylated carbonyl-modified peptides.

References

1. Fenn JB, Mann M, Meng CK, Wong SF and Whitehouse CM: Electrospray ionization for mass spectrometry of large biomolecules. Science 246: 64-71, 1989.
2. Tanaka K, Waki H, Ido Y, Akita S, Yoshida Y, Yoshida T and Matsuo T: Protein and polymer analyses up to m/z 100 000 by laser ionization time-of-flight mass spectrometry. Rapid Communications in Mass Spectrometry 2: 151-153, 1988.
3. Nguyen S and Fenn JB: Gas-phase ions of solute species from charged droplets of solutions. Proc. Natl. Acad. Sci. U. S. A. 104: 1111-7, 2007.
4. Kebarle P and Verkerk UH: Electrospray: From ions in solution to ions in the gas phase, what we know now. Mass Spectrom. Rev.: 2009.
5. Roepstorff P and Fohlman J: Proposal for a common nomenclature for sequence ions in mass spectra of peptides. Biomed. Mass Spectrom. 11: 601, 1984.
6. Biemann K: Sequencing of peptides by tandem mass spectrometry and high-energy collision-induced dissociation. Methods Enzymol. 193: 455-79, 1990.
7. McLafferty FW, Horn DM, Breuker K, Ge Y, Lewis MA, Cerda B, Zubarev RA and Carpenter BK: Electron capture dissociation of gaseous multiply charged ions by Fourier-transform ion cyclotron resonance. J. Am. Soc. Mass Spectrom. 12: 245-9, 2001.
8. Syka JE, Coon JJ, Schroeder MJ, Shabanowitz J and Hunt DF: Peptide and protein sequence analysis by electron transfer dissociation mass spectrometry. Proc. Natl. Acad. Sci. U. S. A. 101: 9528-33, 2004.
9. Zubarev RA, Zubarev AR and Savitski MM: Electron capture/transfer versus collisionally activated/induced dissociations: solo or duet? J. Am. Soc. Mass Spectrom. 19: 753-61, 2008.
10. Coon JJ: Collisions or electrons? Protein sequence analysis in the 21st century. Anal. Chem. 81: 3208-15, 2009.
11. Palmer JW, Tandler B and Hoppel CL: Biochemical properties of subsarcolemmal and interfibrillar mitochondria isolated from rat cardiac muscle. J. Biol. Chem. 252: 8731-9, 1977.
12. Suh JH, Heath SH and Hagen TM: Two subpopulations of mitochondria in the aging rat heart display heterogenous levels of oxidative stress. Free Radic. Biol. Med. 35: 1064-72, 2003.
13. Shapiro AL, Vinuela E and Maizel JV, Jr.: Molecular weight estimation of polypeptide chains by electrophoresis in SDS-polyacrylamide gels. Biochem. Biophys. Res. Commun. 28: 815-20, 1967.
14. Creighton TE: Proteins: Structures and Molecular Properties. W. H. Freeman and Company, New York, NY, 1993.

15. Schagger H and von Jagow G: Blue native electrophoresis for isolation of membrane protein complexes in enzymatically active form. Anal. Biochem. 199: 223-31, 1991.
16. Schagger H: Native electrophoresis for isolation of mitochondrial oxidative phosphorylation protein complexes. Methods. Enzymol. 260: 190-202, 1995.
17. Jung C, Higgins CM and Xu Z: Measuring the quantity and activity of mitochondrial electron transport chain complexes in tissues of central nervous system using blue native polyacrylamide gel electrophoresis. Anal. Biochem. 286: 214-23, 2000.
18. Nijtmans LG, Henderson NS and Holt IJ: Blue Native electrophoresis to study mitochondrial and other protein complexes. Methods 26: 327-34, 2002.
19. Van Coster R, Smet J, George E, De Meirleir L, Seneca S, Van Hove J, Sebire G, Verhelst H, De Bleecker J, Van Vlem B, Verloo P and Leroy J: Blue native polyacrylamide gel electrophoresis: a powerful tool in diagnosis of oxidative phosphorylation defects. Pediatr. Res. 50: 658-65, 2001.
20. Gomez LA, Monette JS, Chavez JD, Maier CS and Hagen TM: Supercomplexes of the mitochondrial electron transport chain decline in the aging rat heart. Arch. Biochem. Biophys. 490: 30-5, 2009.
21. Green NM: Avidin. 1. the Use of (14-C)Biotin for Kinetic Studies and for Assay. Biochem. J. 89: 585-91, 1963.
22. Melamed MD and Green NM: Avidin. 2. Purification and Composition. Biochem. J. 89: 591-9, 1963.
23. Kohanski RA and Lane MD: Monovalent avidin affinity columns. Methods Enzymol. 184: 194-200, 1990.

Figures

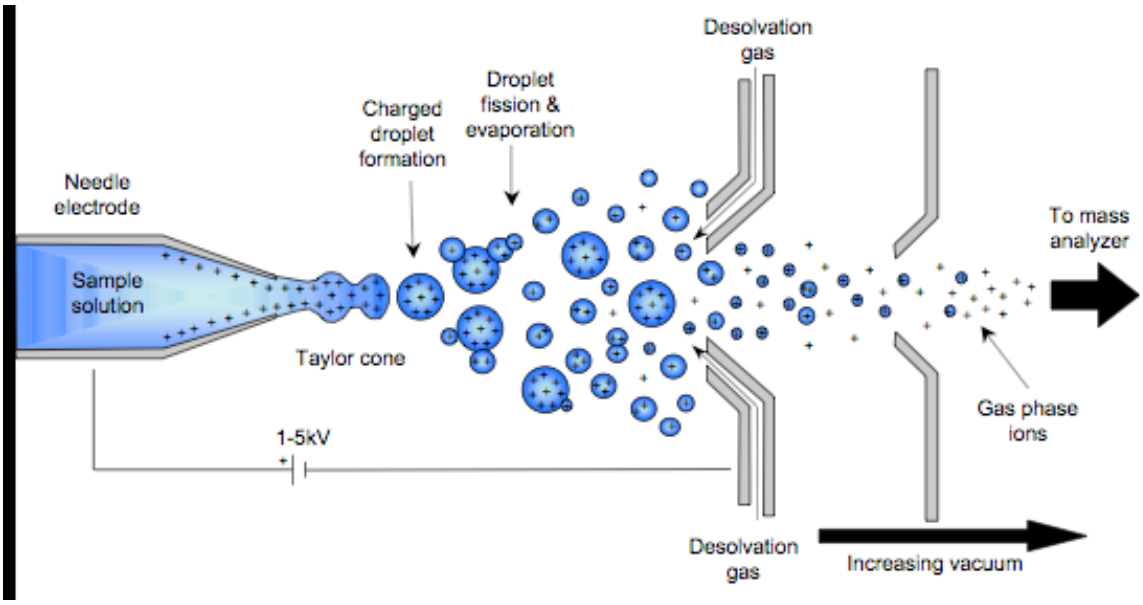

Figure 2.1 – Electrospray Ionization

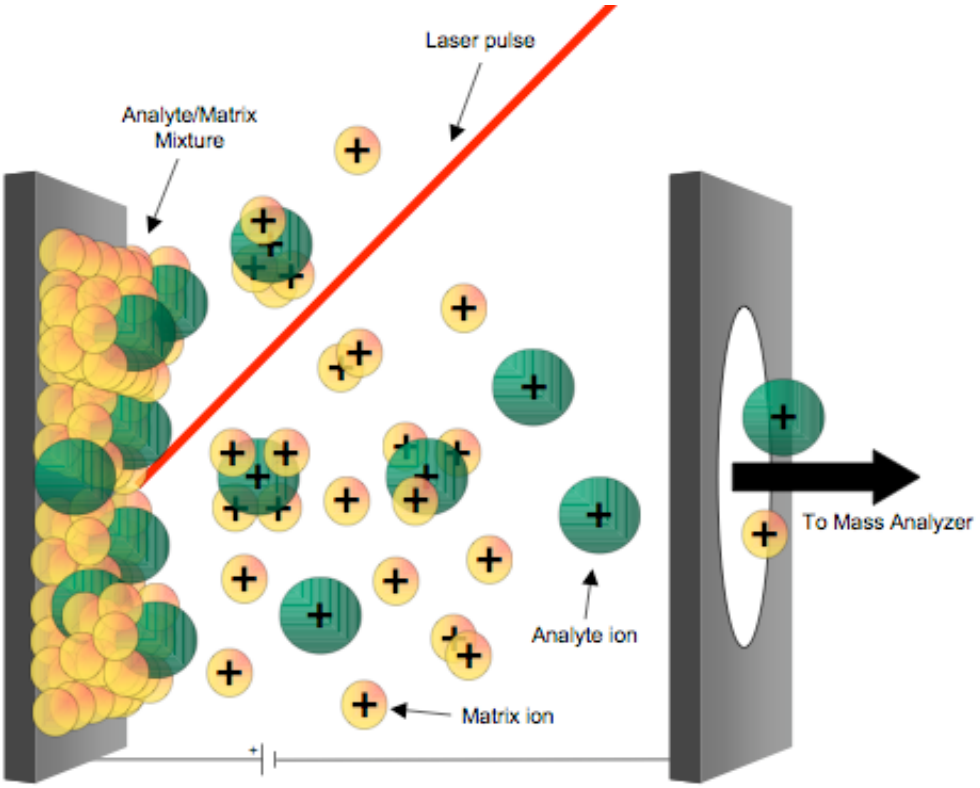

Figure 2.2 – Matrix-Assisted Laser Desorption Ionization

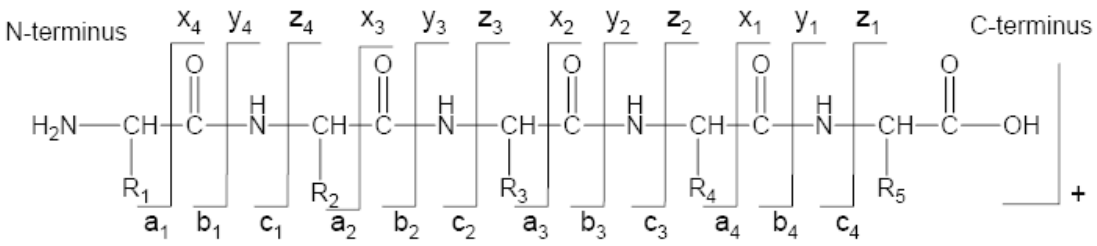

Figure 2.3 – The nomenclature of peptide fragmentation

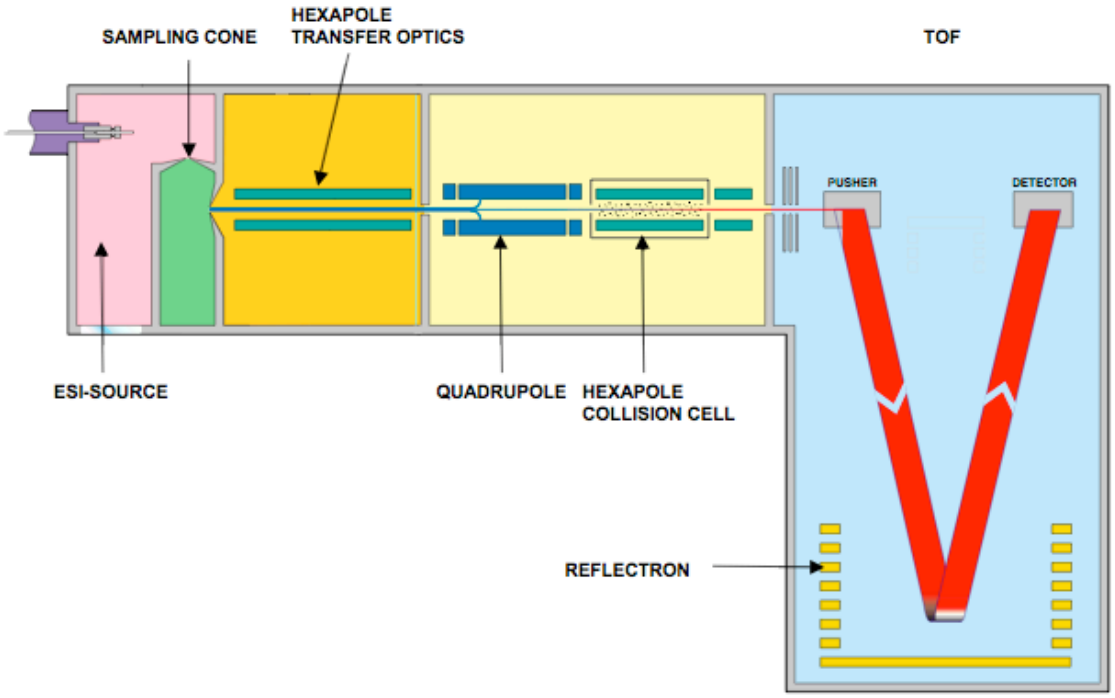

Figure 2.4 – Micromass/Waters Q-TOF Ultima Global. Image modified from Waters Corp. (Milford, MA).

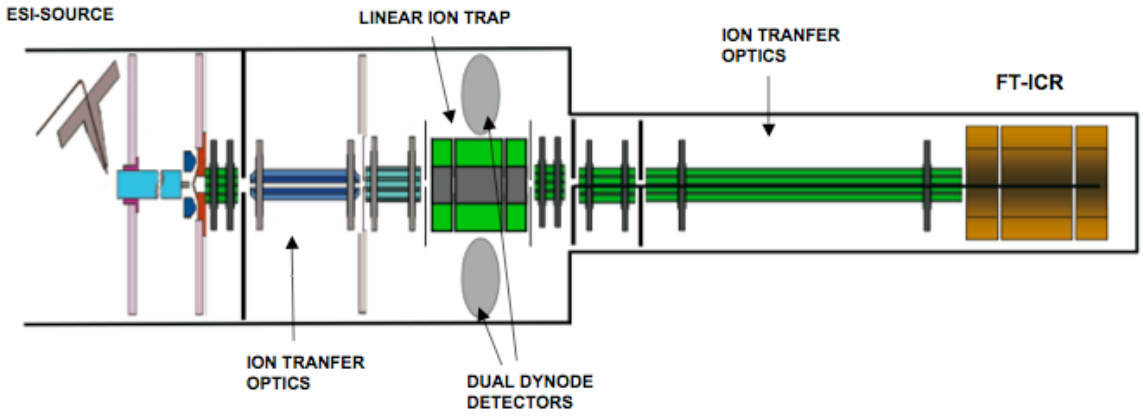

Figure 2.5 – Thermo Scientific LTQ-FT Ultra. Image modified from Thermo Fisher Scientific (Waltham, MA).

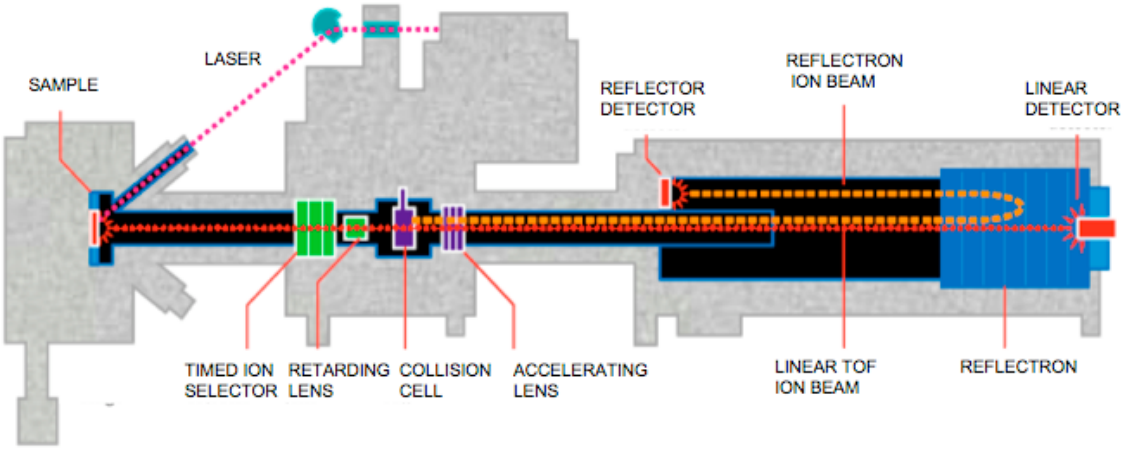

Figure 2.6 – Applied Biosystems 4700 Proteomics Analyzer MALDI-TOF/TOF. Image modified from Applied Biosystems Inc. (Foster City, CA).

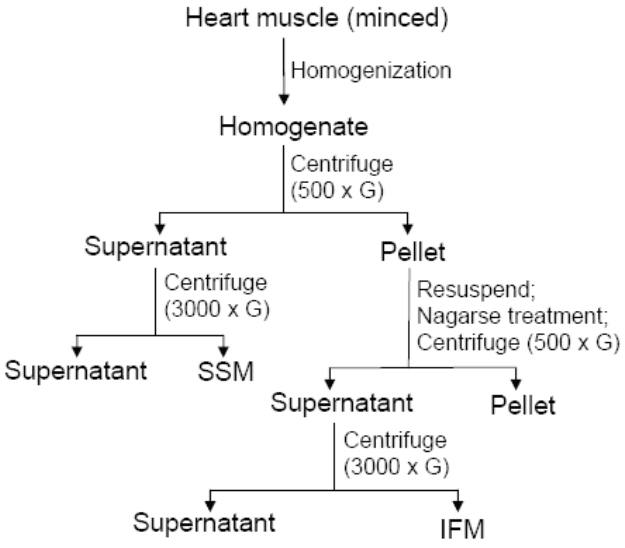

Figure 2.7 – Flow chart for isolation of cardiac mitochondria

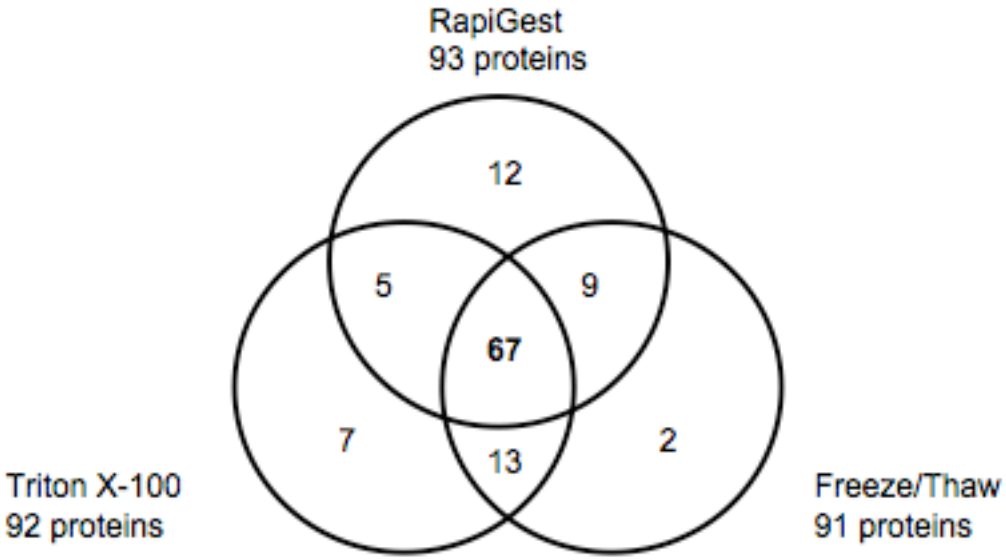

Figure 2.8 – Venn diagram comparing three different methods of preparing mitochondrial protein samples. The total number of proteins identified by each of the three methods were very similar and over 58% of the proteins identified were common to the three methods.

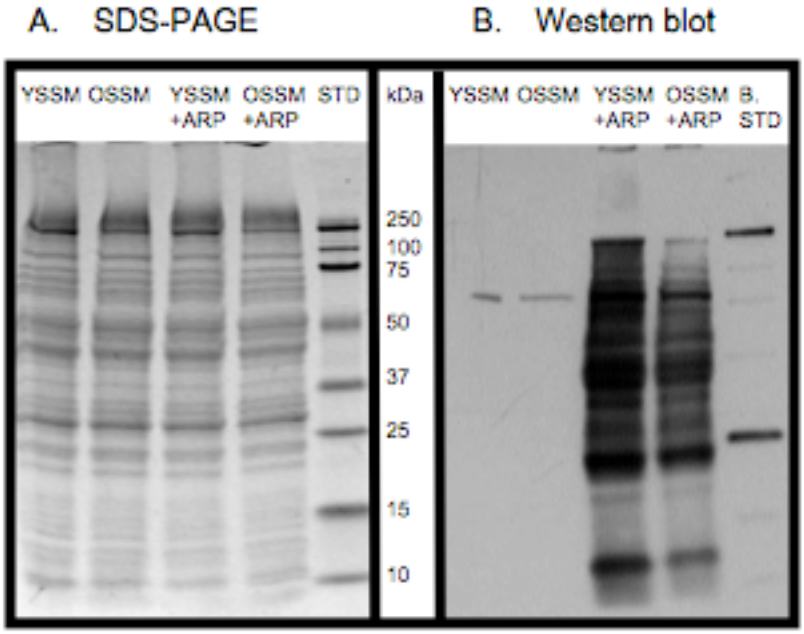

Figure 2.9 – A. Coomassie stained SDS-PAGE of SSM of the following mitochondrial samples: YSSM (young SSM); OSSM (old SSM); YSSM+ARP (ARP labeled young SSM); OSSM+ARP (ARP labeled old SSM). B. Corresponding Western blot probed with NeutrAvidin-HRP. The absence of signal observed in Western for the YSSM and OSSM samples indicates selective detection of ARP labeled proteins by NeutrAvidin-HRP.

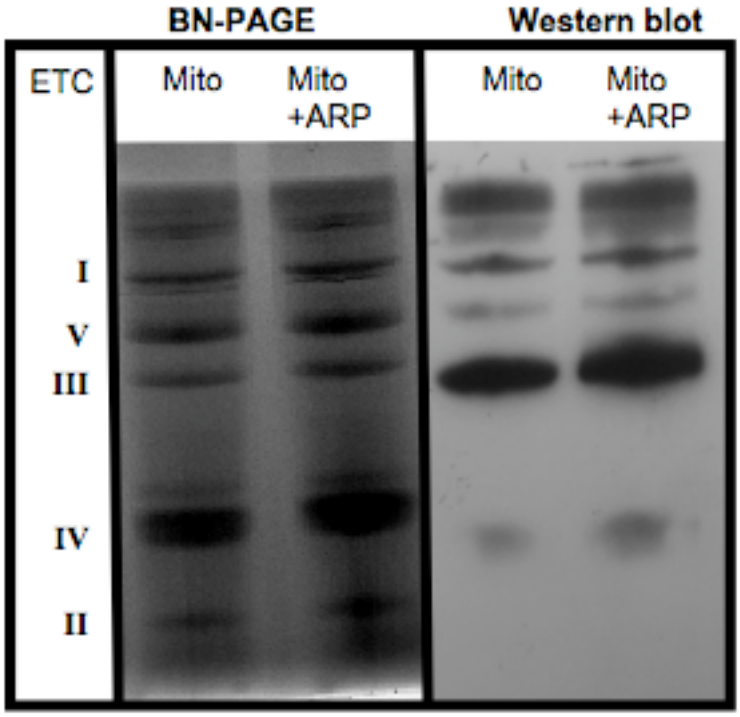

Figure 2.10 – BN-PAGE and corresponding Western blot probed with NeutrAvidin-HRP. The bands corresponding to the five ETC complexes are labeled with Roman numerals on the left. The equivalent signals between the ARP labeled and negative ARP control mitochondria samples observed in the Western blot indicate that the NeutrAvidin-HRP is not specific for ARP labeled ETC complexes.

Chapter 3

New Role for an Old Probe: Affinity Labeling of Oxylipid Protein Conjugates by N'-Aminooxymethylcarbonylhydrazino D-biotin

Juan Chavez, Jianyong Wu, Bingnan Han, Woon-Gye Chung and Claudia S. Maier*

Department of Chemistry, Oregon State University, Corvallis, OR 97331

*To whom correspondence should be addressed. Tel: 541-737-9533. Fax: 541-737-2062. Email: claudia.maier@oregonstate.edu

Analytical Chemistry

American Chemical Society

1155 Sixteenth Street N.W., Washington DC, 20036

Vol. 78, No. 19, October 1, 2006, 6847-6854

Abstract

Free radicals, electrophiles and endogenous reactive intermediates are generated during normal physiological processes, and are capable of modifying DNA, lipids and proteins. However, elevated levels of oxidative modifications of proteins by reactive species are implicated in the etiology and pathology of oxidative stress-mediated diseases, neurodegeneration and aging. A mass spectrometry-based approach is reported that aids to the identification and characterization of carbonyl modified proteins. The method uses N'-aminooxymethylcarbonylhydrazino-D-biotin, a biotinylated hydroxylamine derivative, that forms an oxime derivative with the aldehyde/keto group found in oxidatively modified proteins. In this paper, the method is demonstrated for one class of carbonyl-modified proteins, namely oxylipid peptide and protein conjugates formed by Michael addition-type conjugation reactions of α,β-unsaturated aldehydic lipid peroxidation products with nucleophilic peptide side chains. This new application of an “old” probe, which has been used for the detection of abasic sites in DNA strands, introduces a biotin moiety into the oxylipid peptide conjugate. The biotin-modified oxylipid peptide conjugates is then amenable to enrichment using avidin affinity capture. The described method represents an attractive alternative to hydrazine-based derivatization methods for oxidized peptides and proteins because the reduction step necessary for the transformation of the hydrazone bond to the chemically more stable hydrazine bond can be omitted. Tandem mass spectrometry of the labeled oxylipid peptide

conjugates indicates that the biotin moiety is at least partially retained on the fragment ion during the collisionally induced dissociation experiments, a prerequisite for the use of automated database searching of uninterpreted tandem mass spectra. The reported approach is outlined for the detection, identification and characterization of oxylipid peptide conjugates but the labeling chemistry may also be applicable to other carbonyl-modified proteins.

Introduction

Free-radical injury is central to the etiology and pathology of inflammatory diseases and age-related disorders. The burden of reactive oxygen species (ROS) is counteracted by an intricate antioxidant system, which includes antioxidant enzymes, e.g. SOD, catalase and glutathione peroxidase, and non-enzymatic, low molecular weight antioxidants, perhaps most importantly glutathione and ascorbic acid. However, the extent of the imbalance of ROS production and antioxidant defenses determines the degree of oxidative stress (1). Oxidative-stress mediated modifications occur on DNA, proteins, and lipids (1-5). Oxidative modification of proteins proceeds according to variety of mechanisms, (2, 5-7) some of which lead to backbone peptide bond cleavage or to side chain modifications. The latter includes the introduction of carbonyl functionalities, i.e. aldehyde or keto groups, by direct oxidation of most residues or via conjugation reactions of reactive secondary oxidation products that arise, for example, from lipid peroxidation processes (7).

Polyunsaturated fatty acids of membrane lipids are highly susceptible to peroxidation by oxygen radicals. Exposure of linoleic acid, the major ω-6 polyunsaturated fatty acid in mammalian tissues, to reactive oxygen species leads to the formation of lipid peroxidation (LPO) products. In Esterbauer's studies on the production of cytotoxic compounds in LPO processes, 4-hydroxy-2-nonenal (HNE) was described as a major LPO product (8, 9). To date, HNE is

the best studied LPO product with cytotoxic potential. LPO products that contain α,β-unsaturated aldehyde/keto functionalities are highly reactive electrophiles that react readily with nucleophilic sites in proteins, such as cysteine sulfhydryls, histidine imidazole moieties and with ε-amino groups of lysine residues, forming Michael addition-type conjugates and Schiff's base-derived products (4, 10). Oxylipid-protein conjugates have been implicated in the pathogenesis of inflammatory,(11) neurodegenerative and age-related diseases.(12, 13) Consequently, there is a high interest in analytical methodology that are capable of identifying and characterizing oxidative protein modifications.

Traditionally, the total amount of protein-bound carbonyls was determined colorimetrically (14). Many protocols for detecting oxidative protein modifcations are based on 2,4-dinitrophenylhydrazine (DNPH) derivatization followed by UV spectroscopy (15) or immunochemical detection using an anti-dinitrophenyl primary antibody (16, 17). Although these methods are capable of detecting oxidatively modified proteins with high sensitivity, they fail to provide information such as the identity of the modified proteins, the chemical nature and site of the modification. Mass spectrometry-based approaches are, at least in part, capable of overcoming some of these latter limitations. For instance, matrix-assisted laser desorption/ionization time-of-flight (MALDI-ToF) mass spectrometry was used for identifying HNE-modified lysine residues in tryptic digests of in vitro modified glucose-6-phosphate dehydrogenase (18). Also, the characterization of HNE-

modified peptides directly from unfractionated digests of model proteins after using DNPH as MALDI matrix has been reported (19). In 1996, Bolgar and Gaskell reported the detection of HNE-modified His-residues of oxidized low density lipoprotein by electrospray ionization (ESI) tandem mass spectrometry (MS/MS) (20). Since then, numerous in vitro studies have been reported using ESI-MS/MS for identifying the site of modifications by LPO products in proteins. For example, ESI-MS/MS was employed for detecting HNE modifications in hemoglobin, (21) subunit VIII of bovine heart cytochrome c oxidase, (22) glyceraldehyde-3-phosphate dehydrogenase, (23) the heat shock proteins hsp72 and hsp90, (24, 25) and protein disulfide isomerase (26). Labeling of carbonyl groups formed by metal-catalyzed oxidation of amino acid side chains by biotin hydrazine for both gel-based and mass spectrometric detection have been reported recently (27-29).

As a new alternative to hydrazine-based reagents for MS-based characterization strategies of oxidative stress-induced protein modifications, this study reports the use of N'-aminooxymethylcarbonylhydrazino D-biotin, a biotinylated hydroxylamine derivative which reacts with aldehyde/keto groups found in oxidatively modified proteins under formation of an oxime derivative which is amenable to tandem mass spectral analysis.(30) This aldehyde-reactive probe (ARP) is commonly used for the detection of DNA modifications that resulted in the formation of an aldehyde group from the oxidative damage on the abasic

(AP) sites of DNA strands (31, 32). The hydroxylamine moiety of ARP forms a stable C=N bond with the aldehyde functionality of the Michael-type oxylipid conjugate (Figure 3.1). Thus, the reduction step which is necessary for the stabilization of the hydrazone bond formed during the derivatization of the protein carbonyl with hydrazide-based reagents becomes obsolete. The derivatization of oxidized proteins by ARP enables the use of avidin affinity selection protocols for enrichment of ARP-labeled peptides with oxidative modification. To demonstrate the applicability of the ARP approach for the characterization of oxidatively modified proteins we focus in this paper on one group of carbonylated proteins, namely Michael addition-type oxylipid conjugates.

Specifically, we describe the derivatization of HNE-modified peptide conjugates by ARP, and the selective affinity enrichment and MS-based detection of ARP-labeled peptides from tryptic digests of HNE-conjugated thioredoxin (TRX). ARP-labeled oxylipid peptide conjugates were studied by tandem mass spectrometry. Successful database searching of uninterpreted mass spectra of ARP-labeled HNE-conjugated peptides was also performed demonstrating the potential of ARP as a new adjunct to the analysis of protein carbonyls.

Experimental Section

Materials

Thioredoxin and sequencing grade-modified trypsin were from Promega Corporation (Madison, WI). HNE (10 mg/mL in ethanol) was obtained from

Cayman Chemical (Ann Arbor, MI). Aldehyde Reactive Probe (ARP, N-aminooxymethylcarbonylhydrazino D-biotin) was purchased from Dojindo Laboratories (Kumamoto, Japan). UltraLink immobilized monomeric avidin was obtained from Pierce (Rockford, IL).

Methods.

Synthesis, modification with HNE and labeling with ARP of the peptide Ac-SVVDLTCR-amide.

The peptide Ac-Ser-Val-Val-Asp-Leu-Thr-Cys-Arg-amide (Ac-SVVDLTCR-amide) was synthesized using a PS3 automated solid phase peptide synthesizer (Protein Technologies, Inc., Tucson, AZ). 9-Fluoroenylmethoxy-carbonyl (Fmoc) derivatives of the amino acids were from SynPep Co. (Dublin, CA). The first residue, i.e. the C-terminal residue of the final peptide product bound to the Fmoc-Arg(pbf)-Rink Amide-MBHA resin was purchased from AnaSpec Inc. (San Jose, CA).

One mg of the synthetic peptide in 1mL 10 mM phosphate buffer, pH 7.4 was reacted with 13 μL HNE (10 mg/mL) at room temperature for two hours. The HNE-adducted peptide was purified by HPLC on a C_{18} column (Vydac, 4.6 x 250 mm, 5 μm), lyophilized, and its mass confirmed by MALDI-MS. HNE-adducted peptide (100 μg) was reacted with 200 μL 10 mM ARP in 10 mM sodium phosphate buffer, pH 7.4, for one hour at room temperature. The ARP-labeled

HNE-peptide conjugate was isolated by HPLC as described above and lyophilized.

HNE modification and ARP-Labeling of *E. coli* Thioredoxin.

Adduction of thioredoxin (TRX) with HNE was accomplished by dissolving 1 mg (82 nMole) TRX in 1 mL 10 mM sodium phosphate, pH 7.4, to which a 10-fold molar excess (13 μL) of HNE (10 mg/ml) was added. The reaction mixture was then incubated at 37 ^{o}C for 2 hr. The TRX-HNE adduct was purified from unreacted HNE by reverse-phase HPLC using a C_4 column (Vydac, 10 x 250 mm, 5 μm). The isolated product was lyophilized and analyzed by MALDI-MS. Affinity labeling of TRX-HNE was carried out by the addition 250 μL of 10 mM ARP to the TRX-HNE reconstituted in 750 μL 10 mM sodium phosphate, pH 7.4. The reaction mixture was incubated at 37 ^{o}C for 3.5 hr. Unreacted ARP was removed using the same HPLC method as described above. After lyophilization, ARP-labeled HNE-modified TRX adduct was digested using trypsin at a ratio of 1:50 at 37 ^{o}C for 18 hr.

Affinity chromatography.

Ultralink monomeric avidin (100 μl) was packed into the tip of a glass pasteur pipette plugged with glass wool. The column was equilibrated to room temperature and washed with five column volumes of PBS buffer. The irreversible binding sites were blocked by washing the column with three column

volumes of 2 mM D-biotin. Excess biotin was removed from the reversible binding sites by washing the column with five column volumes of 0.1 M glycine, pH 2.8. The column was re-equilibrated by rinsing with five columns of PBS buffer. One hundred microliters of TRX-HNE-ARP tryptic digest was loaded onto the column and incubated for one hour. Non-labeled peptides were eluted from the column by rinsing with 10 column volumes of PBS buffer and collected in five 200 μL fractions. The HNE-ARP labeled peptides were eluted using 10 column volumes of 0.3 % formic acid and were also collected in five 200 μL fractions. The fractions were analyzed by MALDI-MS/MS and ESI-MS/MS.

Oxidation of a Trp-containing peptide and ARP treatment

The model peptide QAKWRLQTL (from AnaSpec Inc., San Jose, CA) was treated with H_2O_2 overnight and reaction was stopped by adding catalase. ARP (20 molar excess, 10 mM sodium phosphate buffer, pH 7.4) was added to the oxidized peptide. The reaction mixture was incubated at 37 ^{o}C for 1 hr.

Identification of carbonylated proteins in mitochondria.

Rat cardiac mitochondria were isolated by differential centrifugation and stored at -80^{o}C. (33). The mitochondria were ruptured by several freeze thaw cycles. Protein concentration was determined by the Pierce-Coomassie protein assay. Membrane and soluble proteins were reacted with 5mM ARP for 2 hr at 37^{o}C. Excess ARP was removed by buffer exchange using Amicon Microcon

centrifugal filters (10kDa MWCO). Proteins were digested with a 1:50 ratio of trypsin at 37 ^{o}C overnight. The resulting tryptic peptides were filtered through Amicon Microcon centrifugal filters (10 kDa MWCO) to remove trypsin and membrane fragments. The peptide solutions were passed through a monomeric avidin cartridge (Applied Biosystems) following the manufacturer's instructions to enrich ARP-labeled peptides. The fraction containing the ARP-labeled peptides was analyzed by nano-LC MALDI-TOF/TOF mass spectrometry. The MS/MS spectra were interpreted both manually and in an automated fashion with Mascot software.

Mass Spectrometry.

MALDI-MS/MS analysis was performed on an ABI 4700 Proteomics Analyzer with TOF/TOF optics equipped with a 200-Hz frequency-tripled Nd:YAG laser operating at a wavelength of 355 nm (Applied Biosystems, Inc., Framingham, MA). Protein mass spectra were acquired in the linear mode, whereas all peptide mass spectra were obtained in the reflector mode. For both operational modes the accelerating voltage was set to 20 kV. For MS/MS experiments, the collision energy, which is defined by the potential difference between the source acceleration voltage (8 kV) and the floating collision cell (7 kV), was set at 1 kV. The precursor ion was selected by operating the timed gate window with 3-10 Da. Gas pressure (air) in the collision cell was set to 6 x 10^{-7} Torr. Fragment ions were accelerated by 15 kV into the reflector. Data were acquired in a mass range

of m/z 700-4000 with external calibration using AB's 4700 calibration mixture consisting of the following peptides (in brackets the monoisotopic mass of the singly protonated ion is given in Da): des-Arg^1-bradykinin (904.4681), angiotensin I (1296.6853), Glu^1-fibrinopeptide B (1570.6774) and ACTH 18-39 (2465.1989).

ESI-MS/MS was performed using a quadrupole orthogonal time-of-flight mass spectrometer (Q-ToF Ultima Global, Micromass/Waters, Manchester, UK) coupled to a nanoAcquity Ultra Performance LC (Waters, Milford, MA). Peptide mixtures were trapped and washed on a nanoAcquity column (Symmetry C_{18}, 5 μm, 180 μm x 20 mm) for 3 min using 2 % acetonitrile containing 0.1 % formic acid at 4 μL/min. Peptide fractionation was accomplished using an in-house packed 12 cm x 75 μm Jupiter C_5 or C_{18} (5 μm; Phenomenex Inc., Torrance, CA) picofrit column (New Objectives, Woburn, MA). Peptides were eluted using a binary gradient system consisting of solvent A, 0.1 % formic acid and solvent B, acetonitrile containing 0.1 % formic acid.

The electrospray ion source was operated in the positive ion mode with a spray voltage of 3.5 kV. The data-dependent MS/MS mode was used with a 0.6 s survey scan and 2.4 s MS/MS scans on the three most abundant ion signals in the MS survey scan, with previously selected m/z values being excluded for 60 s. The collision energy for MS/MS (25 to 65 eV) was dynamically selected based on the charge state of the ion selected by the quadrupole analyzer (q1). Mass spectra were calibrated using fragment ions of Glu^1-fibrinopeptide B (MH^+

1570.6774 Da, monoisotopic mass). In addition, to compensate for temperature drifts, lock mass correction was used every 30 s for 1 scan using the doubly charged ion of Glu^1-fibrinopepide B ($[M+2H]^{2+}$ 785,8426 Da, monoisotopic mass).

Mascot software (Matrix Science, London, UK) was used to aid in the interpretation of tandem mass spectra. Searches were performed using the SwissProt database with Met oxidation (147.04 Da, monoisotopic mass), ARP-HNE labeled Cys, His, and Lys (monoisotopic masses 572.2 Da, 606.2 Da, and 597.2 Da, respectively) as variable peptide modifications. Trypsin/P was selected as the digesting enzyme allowing for the possibility of one missed cleavage site. Mass tolerances were set to ± 100 ppm for the precursor ion and ± 0.1 Da for the fragment ions. The principal fragment ions were labeled according to the nomenclature of Biemann.(34)

Results and Discussion

Labeling of a HNE-modified Cys-containing peptide with N'-Aminooxymethyl-carbonylhydrazino-D-biotin and tandem mass spectrometric characterization

To evaluate the potential of N'-aminooxymethylcarbonylhydrazino D-biotin as a biotin-labeled aldehyde reactive reagent, we used as a model system the synthetic peptide Ac-SVVDLTCR-amide. Cysteine sulfhydryl side chains are considered as likely targets for the electrophile HNE due to their nucleophilic

properties (10). After reaction with HNE in phosphate buffer (pH 7.4) for 2 hours, the HNE-conjugated peptide was purified by reverse-phase HPLC and lyophilized. Mass analysis of the HNE-peptide-conjugate indicated a mass shift by 156 Da compared to the unmodified peptide confirming that the Michael-type conjugate was obtained. The oxylipid peptide conjugate was subsequently reacted with ARP at room temperature for 1 hr. The reaction product was isolated chromatographically. Successful derivatization of the aldehyde functionality by ARP was confirmed by tandem mass spectrometry.

Tandem mass spectrometric analysis of the ARP-labeled HNE-Cys containing model peptide, Ac-SVVDLTCR-amide (Pep-HNE-ARP) was achieved by using high energy collision dissociation on a MALDI tandem time-of-flight mass spectrometer with TOF/TOF optics (Figure 3.2). The tandem mass spectrum exhibited an almost complete b_n-ion series (b_2 to b_6). The first C-terminal ion, the y_1 ion, was seen at m/z 174.1. More importantly, we observed the C-terminal fragment ions, y_2* to y_5* which retained the ARP-HNE moiety. This ion series was accompanied by series of ions that indicate neutral loss of the ARP-HNE moiety from the respective y_n* ions (i.e. Δm/z = 469.3 Th) and these ions are annotated y_4, y_3 and y_2 in Figure 3.2. The presence of an Asp-residue in this peptide causes the relative predominance of the y_4* fragment ion. The enhanced cleavage probability of the peptide amide bond C-terminal to the Asp-residue in this peptide is particularly pronounced due to the presence of the C-terminal Arg-

residue sequestering the proton (35-37). Collectively, the observed peptide fragment ions confirm that the cysteine residue is modified by a HNE-ARP moiety. Neutral loss of the HNE-ARP moiety from the precursor ion MH^+ 1402.8 is also evident resulting in the ion at m/z 933.4. The fragment ions F1 and F2 indicate side-chain fragmentation of the ARP-HNE moiety to some degree. Noteworthy, the observation of fragment ions that retained the HNE-ARP moiety are a prerequisite for peptide identification based on the use of uninterpreted tandem mass spectra acquired under high energy collision experimental conditions in conjugation with automated database searching.

Specificity of ARP towards carbonylated protein modifications. The oxidation of tryptophan leads to the formation of N-formylkynurenine by dioxygenation and ring breakage. We tested if the –NH-CHO moiety in the N-formylkynurenine residue shows reactivity towards ARP. The model peptide QAKWRLQTL (MH^+ 1143.7; Figure SA1 A in Appendix A) was treated with H_2O_2 overnight and reaction was stopped by adding catalase. The mass spectrum of the reaction products showed the expected peptide ions that indicated oxidation of the Trp residue at m/z 1159.7 (+16 Th), m/z 1175.7 (+32 Th) and m/z 1147.7 (+4 Th) (for structures corresponding to those mass shifts see Figure SA1 A in Appendix A). ARP (20 molar excess) was added to the oxidized peptide mixture. Mass spectral analysis of the reaction mixture after treatment with ARP indicated that the –NH-CHO moiety in N-formylkynurenine is unreactive towards ARP

(Figure SA1 C in appendix A) due to its tautomeric stabilization (–NH-CHO and –N=CH(OH)). Similarly, no ARP reaction product was observed for the decarboxylation product of N-formylkynurenine (structure 3 in Figure SA1 A in appendix A). These results demonstrate that ARP has specificity in its reactivity towards different forms of protein carbonyl groups.

ARP labeling and mass spectrometry of a Michael-type oxylipid protein conjugate.

In proteins, products of lipid peroxidation, such as the α,β-unsaturated aldehyde HNE, are able to modify nucleophilic amino acid residues. In particular, Cys and His residues form readily Michael-type conjugates (10). In addition, Schiff's base formation with the ε-amino group of Lys is also observed and this route leads potentially to formation of 2-pentylpyrrole (38). For studying the applicability of ARP for the efficient labeling of Michael-type oxylipid moieties in proteins we used *E.coli* thioredoxin (TRX) as a simple model protein. TRX is composed of 108 amino acid residues, of which 10 are Lys residues. TRX possesses only one His residue located at position 6. In the oxidized protein, the two cysteine residues, Cys-32 and Cys-35, are disulfide-linked and, thus, not available for HNE modification. Using oxidized TRX in our ARP labeling studies enabled us to focus on the derivatization and characterization of oxylipid-His conjugates and, accordingly, to complement our Cys-containing peptide model studies.

Adducts of oxidized thioredoxin (TRX) to HNE were obtained by dissolving 1 mg (82 nMole) thioredoxin in 1 mL 10 mM sodium phosphate buffer (pH 7.4) to which a 10-fold molar excess of HNE was added. The reaction mixture was incubated for 2 hr at 37 ^{o}C. The stoichiometry of HNE conjugation was checked by MALDI-MS (Figure 3.3A). The mass spectral peak at m/z 11,674.9 represents the unmodified TRX and the ion peak at m/z 11,832.8 corresponds to the addition of one HNE molecule (Δm/z 157.9 Th). The mass spectral analysis also indicated that, although a 10-fold molar excess of HNE to TRX was used in the modification reaction, a large amount of the TRX remained unmodified. After confirming the presence of the HNE adduct by MALDI-MS analysis the HNE-conjugated thioredoxin (TRX-HNE) was reacted with ARP. In the mass spectrum displayed in Figure 3.3B it can be seen that the TRX-HNE peak at m/z 11,832.8 is replaced by a peak at m/z 12,145.3 resulting from the ARP-labeled oxylipid protein conjugate, TRX-HNE-ARP.

A potential problem of approaches that are designed to label the aldehyde functionality of HNE-peptide or -protein conjugates is the fact that the HNE conjugate can undergo an intramolecular cyclization reaction in which the hydroxyl group at position C-4 reacts with C-1 of the aldehyde group to form a hemiacetal product (9). Because the hemiacetal no longer contains an aldehyde-functional group, it is unreactive toward aldehyde-specific reagents and, therefore, would not be detected using ARP. However, the cyclization equilibrium

is controlled by the pH value. The result from the MALDI-MS analysis shows that nearly all of the TRX-HNE adduct has been converted to TRX-HNE-ARP which suggests that the condensation reaction of the aldehyde functionality with ARP is very efficient under the conditions used, namely 10 mM sodium phosphate, pH 7.4.

Tandem mass spectrometric characterization of the ARP-labeled HNE-modified tryptic peptide T2.

After confirming that the oxylipid-protein conjugate was successfully labeled by ARP, the unreacted ARP was removed by HPLC. This was followed by digestion of the sample with trypsin and avidin affinity chromatography to enrich the ARP-labeled peptides of TRX. The enrichment was performed on the tryptic peptide mixture rather than the protein so that only the ARP-labeled peptides would be enriched. The ARP-labeled peptides were isolated from the crude tryptic digest using an immobilized monomeric avidin column. Avidin is naturally a tetrameric protein with a very high binding affinity for biotin necessitating very harsh elution conditions for retrieving biotin-labeled sample. Therefore, monomeric avidin was used which binds to biotinylated compounds reversibly and allows for milder elution conditions. The non-labeled peptides were eluted by washing with PBS buffer. Subsequently, the ARP-labeled peptides were eluted using 0.3 % formic acid instead of 2 mM biotin in PBS (as described in the manufacturer's instruction) in order to facilitate good compatibility with mass spectrometric analyses. Figure 3.4 shows the MALDI-MS spectra of the tryptic digest of TRX-

HNE-ARP (Figure 3.4A) as well as the affinity-enriched peptide fraction (Figure 3.4B). Selective enrichment of the peptide with MH^+ 2201.2 is evident implying that this is an ARP-labeled peptide (Figure 3.4B). MALDI-MS/MS was performed on the peptide ion at m/z 2201.2 to confirm ARP labeling and identify the site of modification (Figure 3.5).

High energy collision induced dissociation tandem mass spectrometry on the MALDI ToF/ToF instrument yielded a fragment ion spectrum which identified the ARP-labeled peptide as the tryptic peptide T2, encompassing the residue 4 to 18 (Figure 3.5). This peptide contains only one nucleophilic site, namely His-6. Indeed, the m/z difference of 606.3 Th between the y_{12} and y_{13} fragment ions confirmed the presence of a His-HNE-ARP residue in position 6 (Figure 3.5). The b_n-ions (b_3 to b_7, b_{10}, b_{12} and b_{13}) were consistently shifted by 469.3 Th to higher m/z values compared to the m/z-values that would be expected for an unmodified peptide with corresponding sequence. The fragment ion at m/z 1731.8 indicates the neutral loss of the ARP-HNE moiety from the precursor ion MH^+ 2201.2. Worth noting is the ARP-HNE-modified His immonium ion prominently visible at m/z 579.4. The intensive immonium ion formation from HNE-modified His residue has been also described previously by Bolgar and Gaskell (20) and Fenaille et al (39).

We also studied the low energy collision induced dissociation behavior of the ARP-labeled HNE-modified T2 peptide using a quadrupole time-of flight instrument equipped with an electrospray ionization source. The triply-charged molecular ion of the ARP-labeled HNE-modified peptide T2, i.e. the $[M+3H]^{3+}$ ion at m/z 734.4, was selected as precursor ion (Figure 3.6). Almost complete y_n and b_n fragment ion series were observed. The m/z difference between the b_2 ion (at m/z 227) and the b_3 ion (at m/z 833) locates the HNE-ARP moiety to the His residue. Accordingly, the b_4 to b_{12} ions were consistently shifted by 469 Th to higher m/z values. The modification of the His residue by an ARP-HNE moiety is also confirmed by the observation of the doubly charged y_{13} ion at m/z 988 and an intense His immonium ion at m/z 579.4. Ions that indicate extensive loss and/or side chain fragmentation of the ARP-HNE moiety were not observed in the tandem mass spectra acquired under the low energy CID conditions which are common to qTOF-type instruments.

In order to test the usefulness of the ARP labeling procedure for proteomic-type applications, we searched the uninterpreted tandem mass spectra from both the TOF/TOF and the q-TOF instrument against the SwissProt database using the Mascot software. The HNE-ARP moiety was implemented as variable modifications on Cys, His and Lys residues. The tandem mass spectrum of the ARP-labeled T2 peptide acquired on the MALDI-MS/MS instrument obtained an ion score of 68. Data-dependant analysis on the qToF instrument yielded tandem

mass spectra for the doubly as well as the triply charged ion of the ARP-labeled T2 peptide; these spectra obtained excellent scores of 78 (data not shown) and 110 (Figure 3.6), respectively.

Identification of carbonylated proteins in mitochondria

The ARP labeling approach is currently used in our laboratory for the detection and identification of oxidatively modified proteins in mitochondria isolated from rat hearts. We repeatedly found several proteins modified by lipid peroxidation products. For example, the long chain-specific acyl-CoA dehydrogenase, (ACADL_RAT) was identified as an *in vivo* target of oxidative modification by lipid peroxidation products. The tandem mass spectrum of the ARP-labeled HNE-conjugated peptide (MH^+ 2415,09) is depicted in Figure 3.7. The observed y_n fragment ions (y_1, y_3-y_6, y_9, y_{11}, and y_{12}) identify the peptide as the partial sequence 166-185 of ACADL_RAT. The fragment ion at m/z 2099.3, annotated as F_2, is generated by side chain cleavage at the oxime bond (-O-N=CH-) whereby the oxylipid moiety is retained at the peptide. In agreement with our previous observations (see Figures 3.2 and 3.5) the fragment ion at m/z 1946.2 arises from neutral loss of the ARP-HNE moiety (Δm = 468.9 Th). Because the identified peptide encompasses only a single nucleophilic residue, i.e.Cys-166, the tandem mass spectral data support the notion that Cys-166 is an *in vivo* target site for HNE conjugation. Noteworthy, the same peptide was also found to

be modified by 4-oxo-2-nonenal (data not shown). We will communicate these findings in combination with other biochemical studies in greater detail shortly.

Conclusion

In the above described study, N'-aminooxymethylcarbonylhydrazino D-biotin (also known as ARP) is introduced as a new reagent for the efficient labeling of carbonyl groups in proteins and peptides. ARP is a hydroxyl amine-functionalized biotin-containing probe which efficiently reacts with aldehyde/keto groups, thereby forming an oxime-type (C=N) bond which is sufficiently stable in tandem mass spectrometric fragmentation studies to allow potentially the localization of the site of modification. The labeling procedure is a one-step reaction and proceeds readily under near physiological conditions in phosphate buffer at pH 7.4 at ambient temperature. A potentially important new application for this "old" probe, which was hitherto used for the detection of abasic sites in DNA, is the exciting field of proteins as targets of oxidative modifications, for example, by lipid peroxidation products. The described methodology allows the affinity-enrichment of biotinylated oxylipid peptide conjugates and enables their identification and characterization by mass spectrometry. However, it should be noted that oxidative modifications to proteins occur via many different pathways (2, 4). The chemical diversity of oxidative protein modifications makes it at best very difficult to use automated searching of uninterpreted tandem mass spectra as the sole mean of mass spectral data interpretation.

The proof-of-concept study described in this paper introduces ARP as a potentially useful and alternative probe to hydrazine-based reagents for the detection and characterization of carbonylated proteins. Studies are currently ongoing that use the described ARP labeling approach for the detection and identification of oxidatively modified proteins in cardiac mitochondria.

Acknowledgements

Many thanks are due to Duane T. Mooney for his assistance during the early periods of this project. This work was supported by grants from the NIH/NIA (AG025372) and Oregon's Agricultural Research Foundation. The mass spectrometry core facility of the Environmental Health Sciences Center at Oregon State University is supported in part by a grant from NIEHS (ES00210).

Supporting Information Available

Mass spectra of the Trp-containing model peptide after oxidation and ARP-treatment. This material is available in appendix A or free of charge via the internet at http://pubs.acs.org.

References

1. Finkel T and Holbrook NJ: Oxidants, oxidative stress and the biology of ageing. Nature 408: 239-47, 2000.
2. Stadtman ER: Protein oxidation in aging and age-related diseases. Ann. N. Y. Acad. Sci. 928: 22-38, 2001.
3. West JD and Marnett LJ: Endogenous reactive intermediates as modulators of cell signaling and cell death. Chem. Res. Toxicol. 19: 173-94, 2006.
4. Marnett LJ, Riggins JN and West JD: Endogenous generation of reactive oxidants and electrophiles and their reactions with DNA and protein. J. Clin. Invest. 111: 583-93, 2003.
5. Levine RL and Stadtman ER: Oxidative modification of proteins during aging. Exp. Gerontol. 36: 1495-502, 2001.
6. Dean RT, Fu S, Stocker R and Davies MJ: Biochemistry and pathology of radical-mediated protein oxidation. Biochem. J. 324 (Pt 1): 1-18, 1997.
7. Levine RL: Carbonyl modified proteins in cellular regulation, aging, and disease. Free Radic. Biol. Med. 32: 790-6, 2002.
8. Benedetti A, Comporti M and Esterbauer H: Identification of 4-hydroxynonenal as a cytotoxic product originating from the peroxidation of liver microsomal lipids. Biochim. Biophys. Acta 620: 281-96, 1980.
9. Esterbauer H, Schaur RJ and Zollner H: Chemistry and biochemistry of 4-hydroxynonenal, malonaldehyde and related aldehydes. Free Radic. Biol. Med. 11: 81-128, 1991.
10. Doorn JA and Petersen DR: Covalent modification of amino acid nucleophiles by the lipid peroxidation products 4-hydroxy-2-nonenal and 4-oxo-2-nonenal. Chem. Res. Toxicol. 15: 1445-50, 2002.
11. Anderson MM, Hazen SL, Hsu FF and Heinecke JW: Human neutrophils employ the myeloperoxidase-hydrogen peroxide-chloride system to convert hydroxy-amino acids into glycolaldehyde, 2-hydroxypropanal, and acrolein. A mechanism for the generation of highly reactive alpha-hydroxy and alpha,beta-unsaturated aldehydes by phagocytes at sites of inflammation. J. Clin. Invest. 99: 424-32, 1997.
12. Sayre LM, Smith MA and Perry G: Chemistry and biochemistry of oxidative stress in neurodegenerative disease. Curr. Med. Chem. 8: 721-38, 2001.
13. Andersen JK: Oxidative stress in neurodegeneration: cause or consequence? Nat. Med. 10 Suppl: S18-25, 2004.
14. Ohkawa H, Ohishi N and Yagi K: Assay for lipid peroxides in animal tissues by thiobarbituric acid reaction. Anal. Biochem. 95: 351-8, 1979.
15. Levine RL, Garland D, Oliver CN, Amici A, Climent I, Lenz AG, Ahn BW, Shaltiel S and Stadtman ER: Determination of carbonyl content in oxidatively modified proteins. Methods Enzymol. 186: 464-78, 1990.

16. Reinheckel T, Korn S, Mohring S, Augustin W, Halangk W and Schild L: Adaptation of protein carbonyl detection to the requirements of proteome analysis demonstrated for hypoxia/reoxygenation in isolated rat liver mitochondria. Arch. Biochem. Biophys. 376: 59-65, 2000.
17. Korolainen MA, Goldsteins G, Alafuzoff I, Koistinaho J and Pirttila T: Proteomic analysis of protein oxidation in Alzheimer's disease brain. Electrophoresis 23: 3428-33, 2002.
18. Grace JM, MacDonald TL, Roberts RJ and Kinter M: Determination of site-specific modifications of glucose-6-phosphate dehydrogenase by 4-hydroxy-2-nonenal using matrix assisted laser desorption time-of-flight mass spectrometry. Free Radic. Res. 25: 23-9, 1996.
19. Fenaille F, Tabet JC and Guy PA: Identification of 4-hydroxy-2-nonenal-modified peptides within unfractionated digests using matrix-assisted laser desorption/ionization time-of-flight mass spectrometry. Anal. Chem. 76: 867-73, 2004.
20. Bolgar MS, Yang CY and Gaskell SJ: First direct evidence for lipid/protein conjugation in oxidized human low density lipoprotein. J. Biol. Chem. 271: 27999-8001, 1996.
21. Bruenner BA, Jones AD and German JB: Direct characterization of protein adducts of the lipid peroxidation product 4-hydroxy-2-nonenal using electrospray mass spectrometry. Chem. Res. Toxicol. 8: 552-9, 1995.
22. Musatov A, Carroll CA, Liu YC, Henderson GI, Weintraub ST and Robinson NC: Identification of bovine heart cytochrome c oxidase subunits modified by the lipid peroxidation product 4-hydroxy-2-nonenal. Biochemistry 41: 8212-20, 2002.
23. Ishii T, Tatsuda E, Kumazawa S, Nakayama T and Uchida K: Molecular basis of enzyme inactivation by an endogenous electrophile 4-hydroxy-2-nonenal: identification of modification sites in glyceraldehyde-3-phosphate dehydrogenase. Biochemistry 42: 3474-80, 2003.
24. Carbone DL, Doorn JA, Kiebler Z, Ickes BR and Petersen DR: Modification of heat shock protein 90 by 4-hydroxynonenal in a rat model of chronic alcoholic liver disease. J. Pharmacol. Exp. Ther. 315: 8-15, 2005.
25. Carbone DL, Doorn JA, Kiebler Z, Sampey BP and Petersen DR: Inhibition of Hsp72-mediated protein refolding by 4-hydroxy-2-nonenal. Chem. Res. Toxicol. 17: 1459-67, 2004.
26. Carbone DL, Doorn JA, Kiebler Z and Petersen DR: Cysteine modification by lipid peroxidation products inhibits protein disulfide isomerase. Chem. Res. Toxicol. 18: 1324-31, 2005.
27. Yoo BS and Regnier FE: Proteomic analysis of carbonylated proteins in two-dimensional gel electrophoresis using avidin-fluorescein affinity staining. Electrophoresis 25: 1334-41, 2004.
28. Mirzaei H and Regnier F: Affinity chromatographic selection of carbonylated proteins followed by identification of oxidation sites using tandem mass spectrometry. Anal. Chem. 77: 2386-92, 2005.

29. Soreghan BA, Yang F, Thomas SN, Hsu J and Yang AJ: High-throughput proteomic-based identification of oxidatively induced protein carbonylation in mouse brain. Pharm. Res. 20: 1713-20, 2003.
30. Ide H, Akamatsu K, Kimura Y, Michiue K, Makino K, Asaeda A, Takamori Y and Kubo K: Synthesis and damage specificity of a novel probe for the detection of abasic sites in DNA. Biochemistry 32: 8276-83, 1993.
31. Kubo K, Ide H, Wallace SS and Kow YW: A novel, sensitive, and specific assay for abasic sites, the most commonly produced DNA lesion. Biochemistry 31: 3703-8, 1992.
32. Atamna H, Cheung I and Ames BN: A method for detecting abasic sites in living cells: age-dependent changes in base excision repair. Proc. Natl. Acad. Sci. U. S. A. 97: 686-91, 2000.
33. Palmer JW, Tandler B and Hoppel CL: Biochemical properties of subsarcolemmal and interfibrillar mitochondria isolated from rat cardiac muscle. J. Biol. Chem. 252: 8731-9, 1977.
34. Biemann K: Contributions of Mass Spectrometry to Peptide and Protein Structure. Biomed. Environ. Mass Spectrom. 16: 99-111, 1988.
35. Herrmann KA, Wysocki VH and Vorpagel ER: Computational investigation and hydrogen/deuterium exchange of the fixed charge derivative tris(2,4,6-trimethoxyphenyl) phosphonium: implications for the aspartic acid cleavage mechanism. J. Am. Soc. Mass Spectrom. 16: 1067-80, 2005.
36. Wysocki VH, Tsaprailis G, Smith LL and Breci LA: Mobile and localized protons: a framework for understanding peptide dissociation. J. Mass Spectrom. 35: 1399-406, 2000.
37. Gu C, Tsaprailis G, Breci L and Wysocki VH: Selective gas-phase cleavage at the peptide bond C-terminal to aspartic acid in fixed-charge derivatives of Asp-containing peptides. Anal. Chem. 72: 5804-13, 2000.
38. Salomon RG, Kaur K, Podrez E, Hoff HF, Krushinsky AV and Sayre LM: HNE-derived 2-pentylpyrroles are generated during oxidation of LDL, are more prevalent in blood plasma from patients with renal disease or atherosclerosis, and are present in atherosclerotic plaques. Chem. Res. Toxicol. 13: 557-64, 2000.
39. Fenaille F, Guy PA and Tabet JC: Study of protein modification by 4-hydroxy-2-nonenal and other short chain aldehydes analyzed by electrospray ionization tandem mass spectrometry. J. Am. Soc. Mass Spectrom. 14: 215-26, 2003.

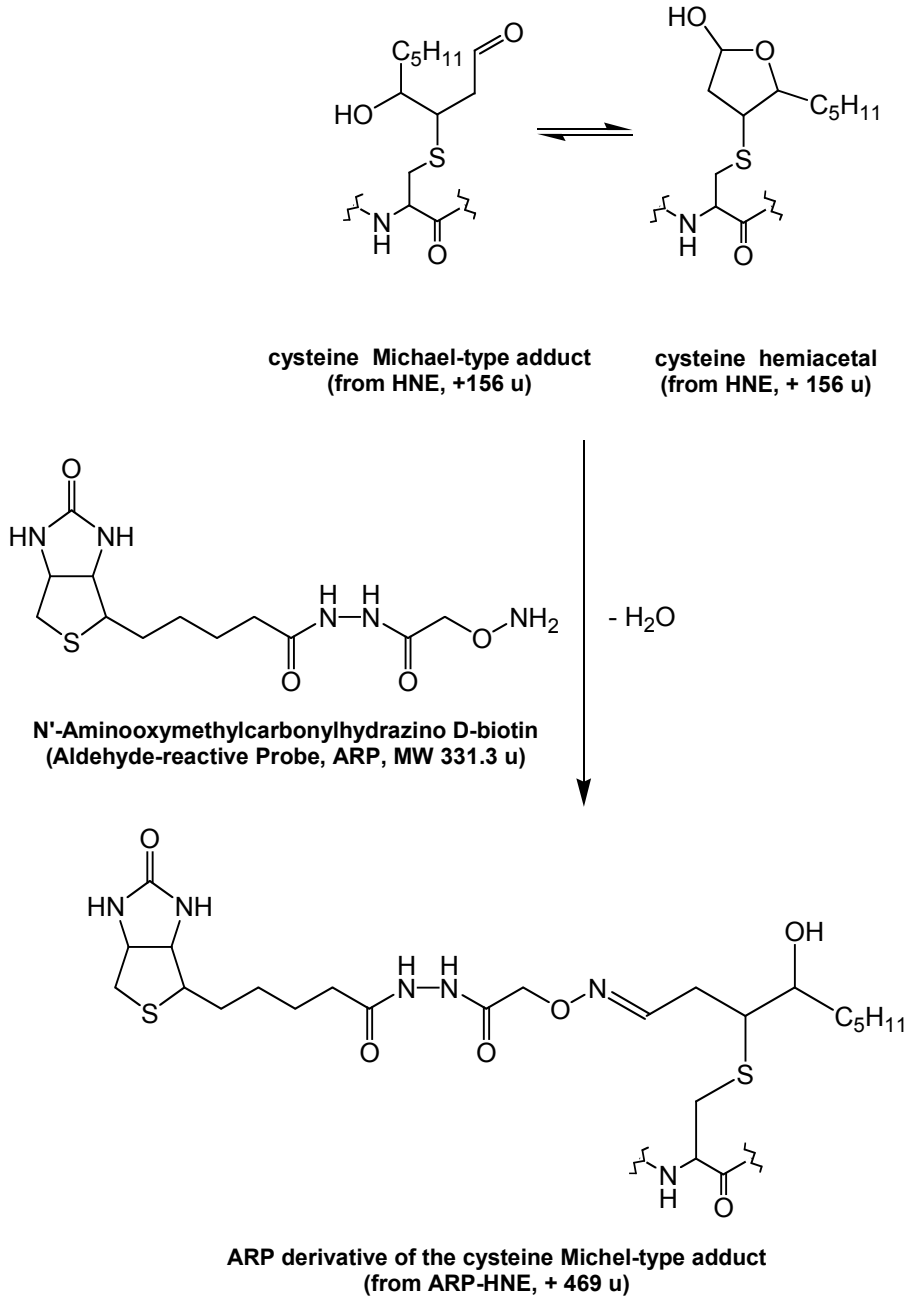

Figure 3.1 - Structure and reaction of N'-Aminooxymethylcarbonylhydrazineo D-biotin (Aldehyde-reactive probe, ARP) for labeling oxylipid–peptide conjugates, e.g. a HNE-modified cysteine-containing peptide.

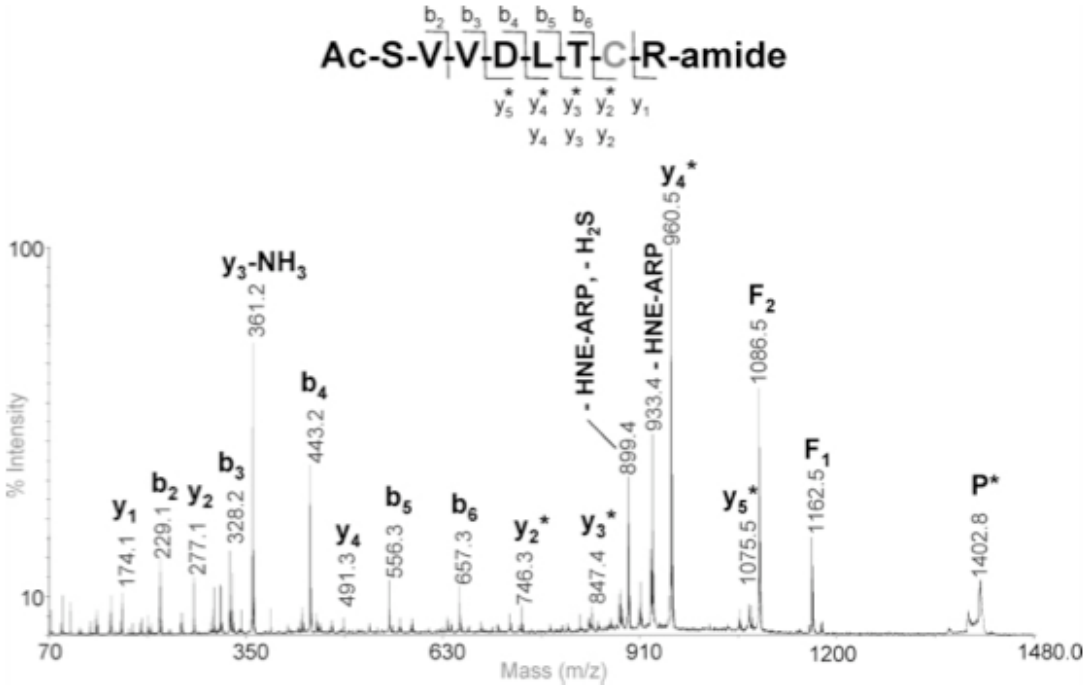

Figure 3.2 - Tandem mass spectrum of the ARP-labeled HNE-peptide conjugate Ac-SVVDLTCR-amide. Michael-type conjugation of the model peptide was observed on the Cys-residue. Note, unequivocal localization of the ARP-HNE moiety to the Cys-residue is obtained by the y_n-fragment ions annotated with an asterisk *.

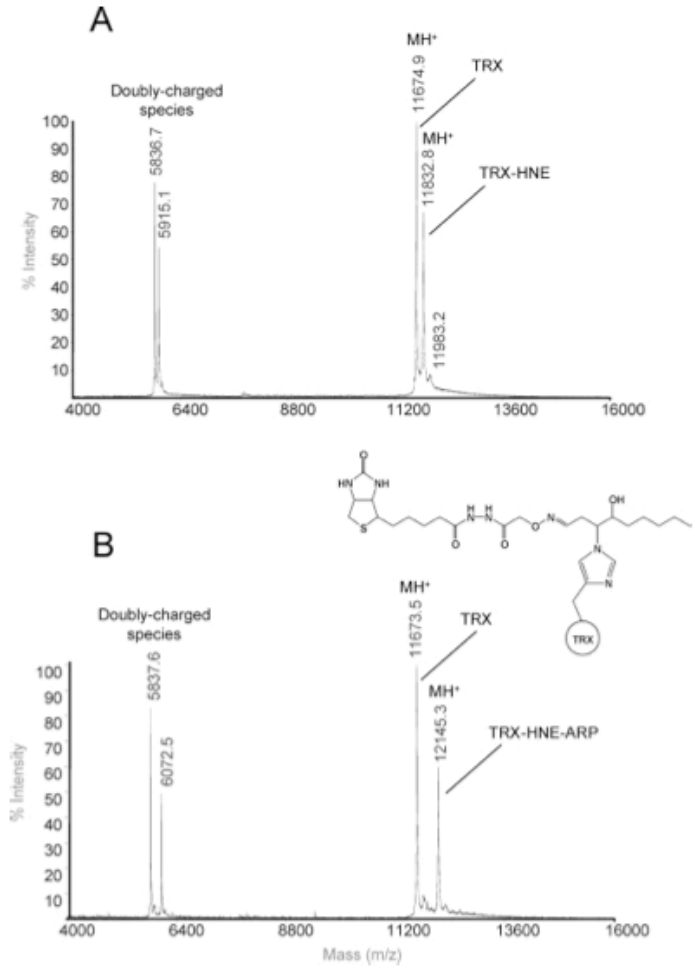

Figure 3.3 - MALDI-MS spectra *E.coli* thioredoxin (TRX) after HNE-modification (A) and ARP-labeling (B). (A), the difference of ~158 Th between the mass peak at m/z 11,675 and m/z 11,833 indicates monoadduction by HNE *via* Michael-type addition. The low abundant ion at m/z 11,983 may indicate modification of TRX by a second HNE moiety but *via* Schiff's base formation (Δm/z 150 Th). (B), the difference of ~472 Th between the mass peak at m/z 11,674 and m/z 12,145 provides evidence that ARP labeling of the HNE moiety under formation of an oxime derivative was successful and highly efficient.

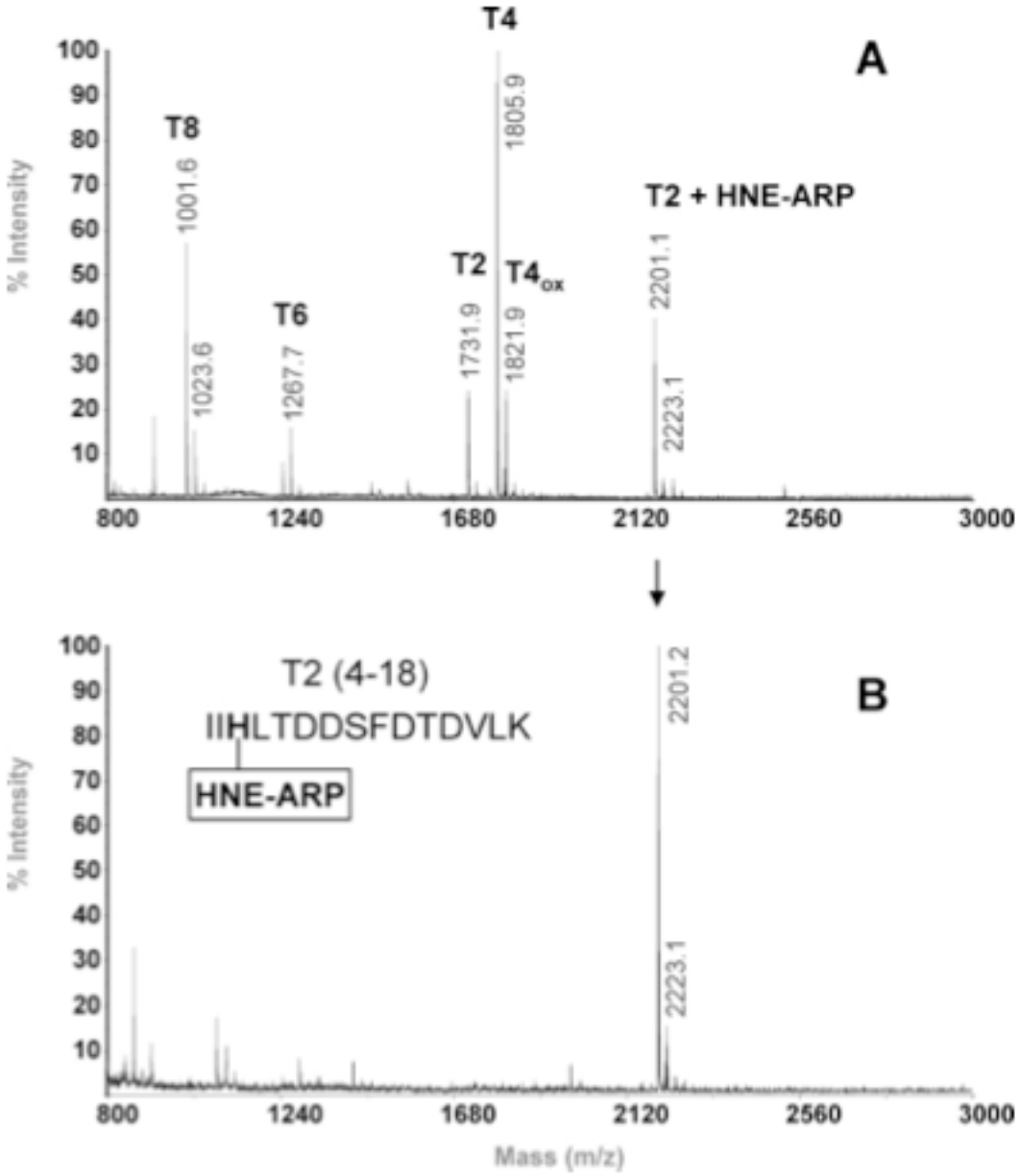

Figure 3.4 - Affinity chromatographic enrichment of the ARP-labeled HNE-peptide conjugate. (A), MALDI mass spectrum of the unfractionated tryptic digest of HNE-modified thioredoxin and (B), the avidin affinity-enriched fraction containing the ARP-labeled HNE-conjugate of peptide T2. The following non-labeled tryptic peptides were observed: T2, IIHLTDDSFDTDVLK (1731.9 Da), T4, MIAPILDEIADEYQGK (1806.1 Da), T6, LNIDQNPGTAPK (1267.4 Da) and T8 GIPTLLLFK (1001.3 Da).

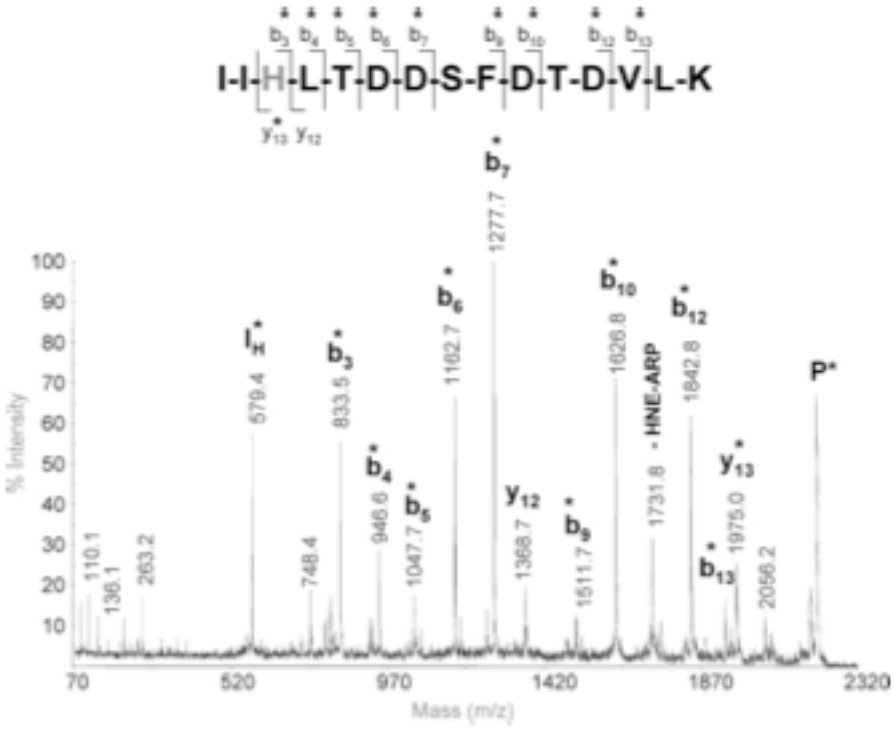

Figure 3.5 - MALDI tandem mass spectrometric identification of the ARP-labeled tryptic peptide T2. Fragment ions marked with an asterisk * retained the ARP-HNE moiety during high energy collision induced fragmentation. The ion at m/z 579.4 corresponds to the immonium ion of the ARP-labeled HNE-conjugated histidine residue. The prominent ion at 1731.8 indicates neutral loss of the ARP-HNE moiety. This spectrum obtained a Mascot score of 68.

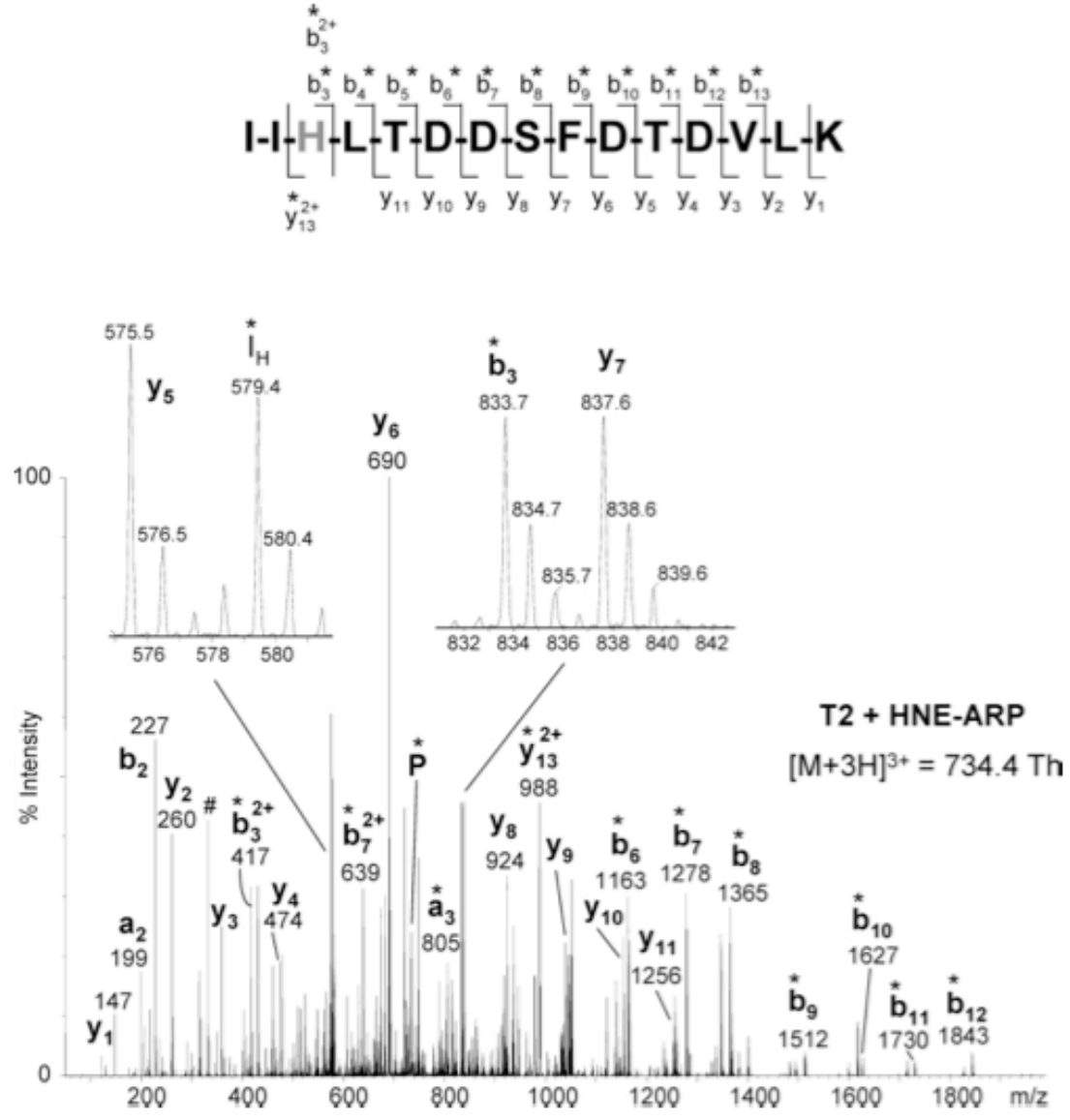

Figure 3.6 - ESI tandem mass spectrum of the ARP-labeled tryptic peptide T2. The triply charged ion at m/z 734.4 was selected for low energy collision induced fragmentation. Product ions marked with an asterisk * retained the ARP-HNE moiety. The ion at m/z 579.4 corresponds to the immonium ion of the ARP-labeled HNE-conjugated histidine residue. The ion marked with # may represent an internal fragment ion, i.e. [TDD]. This spectrum obtained a Mascot score of 110.

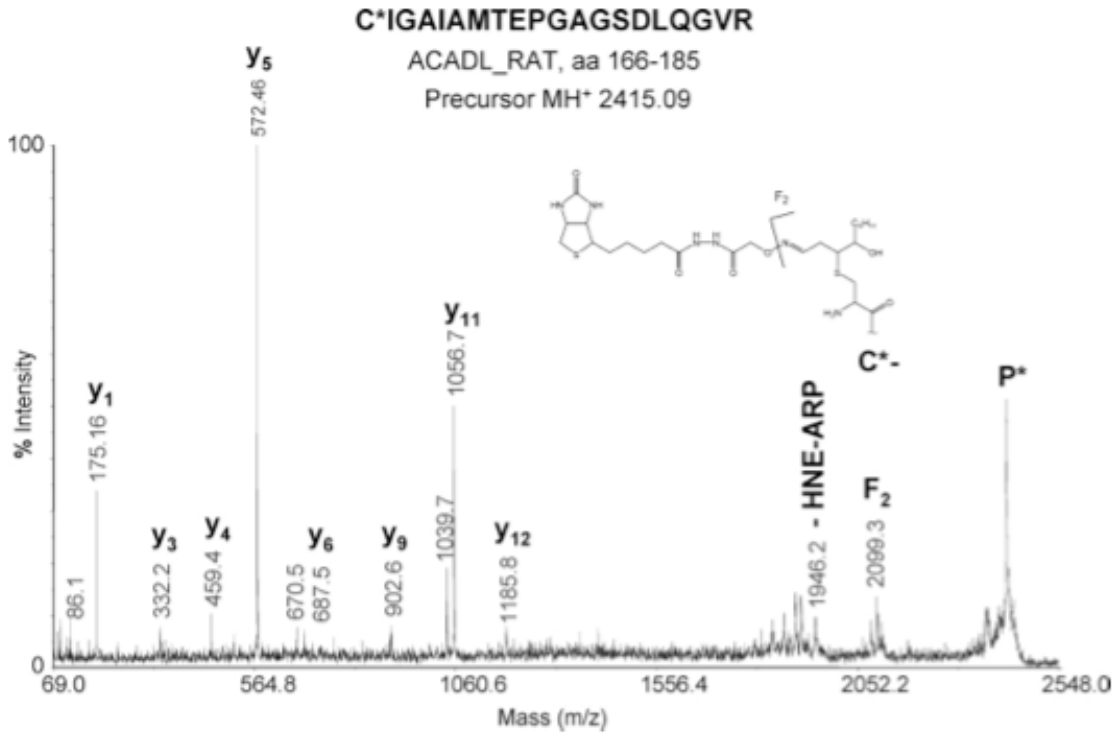

Figure 3.7 - MALDI tandem mass spectrum of the ARP-labeled *in vivo* HNE-modified peptide from the long chain-specific acyl-CoA dehydrogenase (ACADL_RAT, aa 166-185) found in rat heart mitochondria. The fragment ion F_2 at m/z 2099.3 indicates side chain fragmentation at the oxime bond whereby the oxylipid moiety remains bound to the peptide. The ion at m/z 1946.2 indicates neutral loss of the ARP-HNE moiety. This spectrum obtained a Mascot score of 31.

Chapter 4

Diversity of 2-Alkenal Adducts to Mitochondrial Proteins

Juan Chavez, Jianyong Wu, William Bisson, Claudia Maier

Abstract

The modification of proteins by lipid peroxidation products is thought to be an underlying molecular factor in the pathogenesis of many degenerative diseases and age related disorders. Here we report on the identification of protein targets of electophilic 2-alkenals which are formed as a byproduct of naturally occurring oxidative stress. We employ the use of N'-aminooxymethylcarbonylhydrazino-D-biotin as an aldehyde reactive probe (ARP) to label and enrich carbonyl-modified peptides and proteins. The enriched ARP-labeled peptides are then detected and sequenced using LC-MS/MS analysis. Employing this method for the analysis of proteins isolated from rat cardiac mitochondria, 39 unique sites on 27 proteins were identified as being modified by a variety of 2-alkenal products including acrolein, β-hydroxyacrolein, crotonaldehyde, 4-hydroxy-2-hexenal, 4-hydroxy-2-nonenal and 4-oxo-2-nonenal. These sites represent susceptible targets for oxidative modification and many of the sites are known to be important in the catalytic function of key mitochondrial enzymes.

Introduction

Since the 1950's when Harman's "free radical theory of aging" was introduced there have been a considerable number of studies focused on understanding the molecular mechanisms of oxidative stress and it's impact on living systems (1, 2). It is widely accepted that oxidative stress plays a role in an increasing number of human health disorders and the aging process(3-9). Within the rapidly advancing field of proteomics, several efforts have been devoted to identifying changes to the proteome in relation to oxidative stress.

Mitochondria are central to studies of oxidative stress, as they are known to be generators of reactive oxygen species (ROS) within the cell and play a pivotal role in cell death (7, 8, 10, 11). There are a number of ROS producing sites within the mitochondria including Complex I and Complex III of the mitochondrial electron transport chain (12, 13). Being that the ROS are generated in close proximity to the mitochondrial membrane, which is rich in polyunsaturated fatty acids, a whole host of reactive lipid peroxidation products are formed. These lipid peroxidation products are relatively long lived compared to the free radical ROS which led to their formation, allowing them to diffuse further from their site of production to potentially react with proteins and other biomolecules within the mitochondria. Among the most abundant and studied of these are the highly

electrophilic α,β-unsaturated aldehydes such as 4-hydroxy-2-nonenal (HNE), 4-oxo-2-nonenal (ONE), 4-hydroxy-2-hexenal (HHE), and acrolein (14).

A number of techniques exist for measuring the oxidative modification to proteins and other biomolecules. Among the most widely used of these techniques are assays based on the use of either 2,4 –dinitrophenylhydrazine (DNPH) or thiobarbituric acid (TBARS) derivatization. While these methods are able to provide researchers with a general overview of levels of oxidative stress induced modifications, they fail to provide specific information such as the identity of the modified proteins, and the site and chemical nature of the modification. In addition to the traditional colorimetric and immunochemical based methods of analysis, mass spectrometry has emerged as a powerful technique for studying the oxidative modification to biomolecules in ageing and disease related research (15). Towards the goal of identifying the sites of oxidative modification in proteins, a variety of methods involving chemical derivatization followed by mass spectrometric detection have been developed. A variety of interesting chemistries have been employed to label and detect oxidatively modified sites in proteins including; hydrazide-functionalized probes, Girard's P reagent, and Click chemistry to name a few (16-18). One limitation of the many hydrazine-based reagents for labeling protein carbonyls is the pH-dependant reversibility of the hydrazone bond and the need for a reduction step to form a stable hydrazine adduct. We recently demonstrated an alternative approach to the hydrazine-based chemistry, using N'-aminooxymethycarbonylhydrazino-D-biotin, a

hydroxylamine-functionalized biotin derivative, which forms stable oxime bonds with protein aldehydes, thus negating the need for a reduction step.

Several recent studies have been devoted to identifying the protein targets and sites of these lipid-derived electrophiles, in particular targets of HNE (19-21). Numerous in vitro studies have demonstrated that α,β-unsaturated aldehydes, being electrophilic in nature, covalently modify proteins at nucleophilic sites, in particular cysteine, histidine and lysine. Cysteine, with its thiol functional group being the most nucleophilic side chain, and being important to the structure and function of many enzymes has garnered many studies set out to identify target cysteine residues in proteins (22-24). While there has been much success in identifying protein targets from in vitro studies, there is a void of results when it comes to the identification of oxidative modifications that occur in vivo. This information is truly of great importance and interest towards increasing our understanding of the effects of lipid-derived aldehydes on the proteome, and is the focus of the current study.

Here we expand upon our previously described technique of using N'-aminooxymethylcarbonylhydrazino-D-biotin as an aldehyde reactive probe (ARP) which allows for a labeling, affinity enrichment and mass spectrometry-based approach to identify the sites and chemical nature of carbonyl modifications to proteins within the mitochondria. In our current study, we have found this method to be successful in identifying a number of protein targets with

susceptible nucleophilic sites, which turn out to be modified by a surprising variety of electrophilic 2-alkenal products. We are able to conclusively identify both the site and nature of the modification, thus advancing the study of protein-oxylipid conjugates to a new level of detail.

Materials and Methods

Chemical Reagents

N'-aminooxymethylcarbonyl hydrazino-D-biotin (Aldehyde Reactive Probe, ARP) was purchased from Dojindo Molecular Technologies Inc. (Rockville, MD). Ultralink Monomeric Avidin, Zeba Spin Desalting columns, SuperSignal West Pico Chemiluminescent substrate were purchased from Thermo Scientific (Rockford, IL). Neutravidin-HRP was purchased from Pierce. Sequencing grade modified trypsin was purchased from Promega (Madison, WI). 12% Tris-HCl Ready Gels were purchased from Bio-Rad. Immobilon-P PVDF membranes were purchased from Millipore.

Preparation of rat cardiac mitochondria*:*

The Institutional Animal Care and Use Committee (IACUC) at Oregon State University approved the experimental protocol for the use of animals in this study. Male Fischer 344 rats, obtained from the National Institute of Aging (Bethesda, MD), were housed in individual plastic cages covered with Hepa filters and allowed free access to food and water. Rats were anethetized with

diethyl ether and a midlateral incision was made in the chest to remove the heart. Subsarcolemmal mitochondria were isolated from the rat hearts by differential centrifugation according to the procedures of Palmer with minor modifications by Suh et al and stored at -80^{o}C until needed (25, 26). Mitochondrial samples containing approximately 1mg total protein were washed twice with 0^{o}C 10mM NaH_2PO_4 pH 7.4. The mitochondria were then resuspended in 200μl of 10mM NaH_2PO_4 pH 7.4. The mitochondria were ruptured by four rounds of freeze/thaw cycles which involved rapid freezing with liquid N_2 followed by thawing in a cold water bath with 10 minutes of sonication. Soluble and membrane proteins were separated by centrifugation at 14,000g for 15min. Pierce Coomassie Plus protein assay was used to determine the protein concentration.

ARP labeling of Mitochondrial Proteins.

ARP labeling of mitochondrial proteins was accomplished by simultaneously adjusting the protein concentration to ~1μg/μl and the ARP concentration to 5mM in 10mM NaH_2PO_4 buffer pH 7.4. The mixture was then allowed to react for up to one hour at room temperature. Excess ARP was removed using Zeba desalting spin columns (Pierce) with a molecular weight cut-off of around 7kDa. Protein samples were digested with a 1:50 w/w ratio of modified trypsin in 100mM NH_4HCO_3 pH 8.3 for 6-18 hours at 37^{o}C.

SDS-PAGE and Western Blot

One dimension SDS-PAGE was accomplished by loading 20μg of mitochondrial protein per well of Bio-Rad 12% tris-HCl readymade gels and running them at a constant 130 V for 60 minutes. For visualization of the protein bands the gels were incubated with Biosafe Coomassie dye for 1 hr. Western blotting was accomplished by transferring the proteins from the gel to a PVDF membrane by applying a constant current of 150 mA for 2 hours. The blot was then blocked with 5% milk in TBS buffer with 0.1% tween-20 and then washed extensively before being incubated with 40 ng/mL of HRP-NeutrAvidin for one hour. After several additional wash steps the gel was exposed to the PicoWest chemiluminescent substrate for 10 minutes and developed using Kodak BioMax X-Ray film.

Affinity Enrichment of ARP-labeled peptides

100-300μl of Ultralink monomeric avidin was packed into Handee Mini Spin Columns, which accommodate solvent addition with a Luer Lok syringe. The column was washed with 1.5ml of 10mM NaH_2PO_4, pH 7.4. Irreversible binding sites, consisting of tetrameric avidin, were blocked by washing with three column volumes of 2mM D-biotin. To remove excess D-biotin the column was washed with five column volumes of 2M Glycine-HCl pH 2.8. The column was then re-equilibrated by washing with 2mL of 2x phosphate buffered saline (PBS, 20mM NaH_2PO_4 300mM NaCl). The mitochondrial peptide sample was then slowly

added to the affinity column and the flow thru collected. To remove non-labeled and non-specifically bound peptides the column was washed with 1mL 2 x PBS followed by 1mL of 10mM NaH_2PO_4 and finally 1.5mL of 50mM NH_4HCO_3 20% CH_3OH. The column was then rinsed with 1mL of MilliQ H_2O before eluting the ARP-labeled peptides with 0.4% formic acid 30% acetonitrile. Collected fractions were then concentrated using vacuum centrifugation and stored at -20^{o}C before mass spectrometric analysis.

LC-MS/MS Analysis

The resulting ARP-enriched peptides were analyzed by LC-MS/MS using a quadrupole orthogonal time-of-flight mass spectrometer (Q-TOF Ultima Global, Micromass/ Waters, Manchester, UK) mass spectrometer equipped with a NanoAcquity UPLC system. Peptides were fractionated by reversed-phase chromatography on a 100 μm i.d x 200mm long BEH column (Waters, Milford, MA) using a linear gradient of a binary solvent system consisting of solvent A (2% acetonitrile with 0.1% formic acid in water) and solvent B (acetonitrile containing 0.1% formic acid). The electrospray source was operated in the positive mode with a spray of 3.5kV. The mass spectrometer was operated in data-dependant MS/MS mode, performing 0.6 second MS scans followed by 2.4 second MS/MS scans, on the three most abundant precursor ions in the MS scan with a 60 second dynamic exclusion of previously selected ions. The MS/MS collision energy (25-65 eV) was dynamically selected based on the charge state

of the precursor ion selected by the quadrupole analyzer. Mass spectra were calibrated using fragment ions of Glu^1-fibrinopeptide B (MH^+ 1570.6774 Da, monoisotopic mass). Additionally, lock spray mass correction was performed on the doubly charged ion of Glu^1-fibrinopeptide ($[M+2H]^{2+}$ 785.8426 Th) every 30 seconds during the MS/MS run.

Peptide samples were also analyzed by LC-MALDI-MS/MS by performing off-line reversed-phase fractionation on a Dionex/LC Packings Ultimate nanoLC system coupled to a Probot target spotter. Peptides were fractionated over a 75 μm i.d x 150mm C_{18} PepMap 100 column (LC-Packings) using a binary gradient consisting of solvent A (5% acetonitrile with 0.1% trifluoroacetic acid (TFA) in water) and solvent B (80% acetonitrile with 0.1% TFA in water). A Probot was used to mix the eluting peptides with α-cyano-4-hydroxycinnamic acid (2mg/mL in 50% acetonitrile containing 0.1% TFA) and spot the mixture to a 144 spot stainless steel MALDI target plate. MALDI-MS/MS analysis was performed on an ABI 4700 proteomics analyzer with TOF/TOF optics equipped with a 200-Hz frequency-tripled Nd:YAG laser operating at a wavelength of 355 nm (Applied Biosystems, Inc., Framingham, MA). Operating in a data-dependent reflectron mode, full MS scans was obtained for the range m/z 700-4000 followed by MS/MS scans on the 10 most abundant ion signals in the MS scan. Collision-induced dissociation was performed using a collision energy of 1 keV in a collision cell with a gas pressure of 6×10^{-7} Torr. Mass spectra were calibrated

externally using the ABI 4700 calibration mixture consisting of the following peptides des-Arg^1-bradykinin ([M+H]$^+$ 904.4675 Da), angiotensin I ([M+H]$^+$ 1296.6847 Da), Glu^1-fibrinopeptide B ([M+H]$^+$ 1570.6768 Da), and ACTH 18-39 ([M+H]$^+$ 2465.1983 Da).

MS/MS data analysis and identification of ARP-labeled peptides

Tandem mass spectrometric data generated on the Q-TOF were processed into peak list files using ProteinLynx Global Server v2.3 (PLGS Waters, Manchester, UK). Both the MS survey and MS/MS scans were calibrated using the lock mass of m/z 785.8426 with a lock spray tolerance of 0.1Da. MS/MS spectra were smoothed using the Savitzky-Golay algorithm performing 2 iterations over a smoothing window of 3 channels. The survey scan was deisotoped and centroided using a fast algorithm performing 30 iterations. MS and MS/MS spectra were centroided with a minimum peak width of 4 channels centroiding the top 80% with a TOF resolution set at 10,000 and a NP multiplier of 0.7. MALDI-MS/MS data were processed into peak list files using the Peaks to Mascot tool in 4000 Series Explorer V3.0 (Applied BIosystems). Default settings were used except for the peak density for MS/MS spectra was set to a max of 10 peaks per 200 Da, the minimum S/N was set to 10 with a minimum peak area of 500 and a max peak/precursor set to 40.

Peak list files of the tandem mass spectrometric data were analyzed with the aid of Mascot v2.1 (Matrix Science, London, UK) and Peaks Studio v4.5 (Bioinformatic Solutions Inc., Waterloo, ON Canada) protein database search engines. The Swiss Prot database v50 (270778 sequences, 99412397 residues) and the following parameters: taxonomy rodentia (20991 sequences), ± 0.2 Da mass tolerances for the precursor and fragment ions, possibility of 3 missed proteolytic cleavage sites, with trypsin/P or semitrypsin selected as the digesting enzyme, and ARP-HHE (CHK), ARP-HNE (CHK), ARP-Acrolein (CHK), ARP-ONE (CHK), ARP-MDA (KR), ARP-β-hydroxyacrolein, ARP-crotonaldehyde and methionine oxidation (M) selected as variable modifications at the residues specified in parenthesis. A false discovery rate (FDR) for peptide identification was obtained by searching a decoy database containing randomized protein sequences with the same average amino acid content as the target database (Swiss Prot, rodentia), using Mascot's decoy search function. The average false discovery rate for all datasets (6 MALDI-MS/MS and 6 ESI-MS/MS) was then calculated by taking the sum of the total number of peptide matches above the homology or identity threshold ($p<0.05$) from the decoy database divided by the sum of the total number of peptide matches above the homology or identity threshold ($p<0.05$) from the Swiss Prot rodentia database. This ratio is then expressed as a percentage.

Calculation of B-factor and Solvent Accessible Area (SAA).

The 3D coordinates of porcine heart mitochondrial type II malate dehydrogenase (MDH) was retrieved from the crystal structures available in the Protein Data Bank (Pdb) 1MLD (27). The B-factor and SAA values for all cysteine residues of MDH protein in the tetramer conformation were calculated using the program Molsoft ICM v3.5-1p. The mean B-factor values were derived from the atomic crystallographic data for each cysteine residue in each of the four monomers of the tetramer complex of MDH. The reported B-Factor values for each cysteine residue are the average of the four monomers. The solvent accessible areas were calculated using a faster modification of the Shrake and Rupley alogorithm accounting for the presence of hydrogen atoms in the protein structure and using a water probe radius of 1.4 Å (28). SAA values were calculated as the average of a span of three residues, including ±1 residue from the cysteine for each of the monomers of the tetrameric complex of MDH. The reported SAA values for each cysteine are the average of the four monomers.

Functional Pathway Network Analysis

The carbonyl-modified proteins identified by LC-MS/MS analysis were evaluated for their functional biological pathways using the Kyoto Encyclopeda of Genes and Genomes (KEGG) database. Cytoscape (v. 2.6.2) was used to construct a

visual representation of the network connections between the modified proteins and their functional pathways.

Results

Global Analysis of ARP Labeling of Carbonyl-Modified Mitochondrial Proteins

Mitochondria are well known sources of ROS and oxidative modification of mitochondrial proteins is associated with many human health disorders as well as the aging process (29, 30). To identify mitochondrial protein targets of electrophilic, 2-alkenal, lipid peroxidation products, we employed a chemical labeling and affinity enrichment technique using ARP. The relatively low abundance of carbonylated proteins under physiological conditions requires the use of an affinity enrichment approach. The hydroxylamine functionality of ARP reacts, through a condensation mechanism, with the carbonyl group on the oxidized protein to form a stable oxime product, adding a mass of 313.1 Da to the carbonylated protein. This is a particular advantage of the ARP based approach over similar affinity labeling methods such as those employing hydrazide functionalized probes such as DNPH and biotin hydrazide, which require reduction of the hydrazone bond to form a stable adduct. The biotin moiety present in the ARP tag allows for the use of avidin affinity enrichment of low-level modified peptides, which can then be characterized using LC-MS/MS analysis. Rat cardiac mitochondria were used for this study based on related

studies indicating that oxidative modification to proteins may play a role in mitochondrial decay observed in aging and age related diseases (31).

In order to demonstrate the utility of ARP labeling for the detection of oxidatively modified proteins in rat cardiac mitochondria, we applied a previously demonstrated method to produce an “ARP-blot” (32). Mitochondrial protein samples were reacted with 5mM ARP and then were separated by 1D-SDS-PAGE followed by Western blotting on a PVDF membrane. HRP conjugated NeutrAvidin was used with PicoWest chemiluminescent reagents (Pierce) to visualize the ARP reactive bands (figure 4.1). Several ARP reactive protein bands are visible in the Western blot from the mitochondrial sample that was reacted with ARP. The control sample, to which no ARP was added, shows relatively no signal. Although not conclusively identified, the single HRP-NeutrAvidin-reactive protein band visible in the control is likely due to a naturally biotinylated protein such as one of the mitochondrial carboxylase enzymes.

Identification of ARP-labeled, carbonylated proteins by affinity enrichment and tandem mass spectrometry

Oxidatively modified mitochondrial proteins were labeled with ARP according to the previously described procedure. ARP-labeled mitochondrial proteins were tryptically digested, enriched with monomeric avidin and analyzed by LC-MS/MS using ESI-Q-TOF and MALDI-TOF/TOF. The resulting MS/MS data were searched against the Swiss Prot database with the aid of Mascot and Peaks

software. Database search parameters allowed for the possibility of the specified ARP-labeled post-translational modifications listed in the methods section. Mascot's decoy search function was used to search a decoy database containing randomized sequences with the same average amino acid content as the target database (Swiss Prot, rodentia) to obtain false positive (FP) matches. The false discovery rate (FDR) for peptides above the homology or identity threshold is calculated as the number of FP peptide matches to the decoy database divided by the number of peptide matches from the Swiss Prot, rodentia database. The average FDR for our datasets (6 MALDI-MS/MS; 6 ESI-MS/MS) was 3.7% for peptide matches above the homology or identity threshold ($p<0.05$). However it should be noted that not all of the identified ARP-labeled peptide sequences identified were above the significance threshold of $p<0.05$ and are therefore not included in the calculation of the false discovery rate. It should also be noted that in targeted proteomics experiments, such as the ones described in this study, the datasets are often too small to provide an accurate determination of the false discovery rate.

The identification of post-translationally modified peptides with tandem mass spectrometry remains a challenging task. Modified peptides often display atypical and complicated fragmentation patterns that are difficult for automated search algorithms such as Mascot and Peaks to identify. In our previous studies we identified several unique features of ARP-labeled peptides, which aid in their

identification by manual inspection (33, 34). Identification of ARP-labeled 2-alkenal modified peptides was accomplished by first putatively identifying MS/MS spectra of ARP-labeled 2-alkenal-modified peptides in the Mascot and Peaks search results. These spectra were then subjected to rigorous manual inspection before being considered as positive identifications. Manual analysis included assigning a continuity of b- and y- type ion series, comparison to homologous peptides with high scores, as well as inspection for the presence of fragment ions characteristic to ARP-labeled peptides. All tandem mass spectra from the ARP-labeled 2-alkenal modified peptides with fragment ion annotation are included in the supplemental materials in appendix B.

Using this approach we identified a variety of oxidative modifications to peptides originating from several mitochondrial proteins, the results of which are summarized in table 1. The annotated tandem mass spectra from each of the assigned ARP-labeled peptides are available as supplemental figures SB1-SB77. In total we identified 39 unique sites of modification in 27 mitochondrial proteins. The types of modifications identified consisted of six different 2-alkenal products including; acrolein, β-hydroxyacrolein, crotonaldehyde, 4-hydroxy-2-hexenal, 4-hydroxy-2-nonenal, and 4-oxo-2-nonenal. Three of the modified peptides including; NALANPLYCPDYR from ubiquinol-cytochrome-c reductase core protein 2, ETECTYFSTPLLLGK from malate dehydrogenase, and

CIGAIAMTEPGAGDLQGVR from long-chain specific acyl-CoA dehydrogenase, were identified with more than one type of modification to the same residue. Several of the proteins identified in table 1 are components of the mitochondrial electron transport chain (ETC). Many of these protein subunits have been previously identified as being carbonylated or modified by HNE in gel-based studies, which employed Western blot detection using anti-DNP or anti-HNE antibodies. For example succinate dehydrogenase [ubiquinone] flavoprotein subunit, ATP synthase α-chain, ATP synthase β-chain, ATP synthase γ-chain, cytochrome c oxidase subunit VIb isoform 1, and NADH dehydrogenase [ubiquinone] flavoprotein 1 were identified with carbonylation and/or HNE modifications, however the sites and types of modifications were not conclusively identified (35, 36).

By comparing the results in table 1 with other reports in the literature of studies aimed at identifying sites of oxidative modification to proteins by the exogenous addition of electrophiles, there is some overlap of the sites and proteins identified. This is particularly interesting in that it suggests that the modified residues identified in table 1 represent susceptible targets for adduction by lipid peroxidation products. For example in comparison with previous results from our group in which we utilized a novel synthetic probe (HICAT) to label and quantify mitochondrial protein targets of HNE, we identified eight of the same proteins and sites of modification, including; H 227 of ATP synthase β-subunit, Cys-100 of

ATP synthase D chain, Cys-141 of ATP synthase O subunit, Cys-256 of ADP/ATP translocase 1, Cys-166 of long-chain specific acyl-CoA dehydrogenase, Cys-93 and Cys-285 of malate dehydrogenase, and Cys-191 of ubiquinol-cytochorme-c reductase complex core protein 2 (18). In a recent study by Wong and Liebler in which they added two thiol-reactive electrophilic probes (IAB & BMCC) to mitochondrial samples from HEK293 cells, they were able to identify 1693 sites of adduction belonging two 809 proteins. By comparing their results with the modified protein sites identified in our study, we can see that there are seven cases of overlap between the modified residues identified. These sites include Cys-385 of acontiase, Cys-256 of ADP/ATP translocase, Cys-100 of ATP synthase D chain, Cys-317 of methylmalonate-semialdehyde dehydrogenase, Cys-936 of NAD(P) transhydrogenase, Cys-191 of ubiquinol-cytochrom-c-reductase complex core protein 2, and Cys-231 of voltage-dependant anion selective channel protein 1. The fact that only seven common sites exist out of the 1693 residues identified by Wong & Liebler and the 39 residues identified in this study raises some interesting questions as to what actually represent biologically significant targets of oxidiative stress, and what is the best approach to identify them. Clearly in vitro studies in which relatively high concentrations of electrophilic probes are added are capable of identifying a large number of potential target sites, however such artificial situations may not accurately reflect the most biologically relevant sites. There is also the question of the site specificity of various electrophiles based on their differing chemical

structures and physicochemical properties. Our results include a few examples that indicate that despite the variation in size and chemical structure of these 2-alkenals, their common electrophilic properties allow them to modify the same nucleophilic sites on proteins. Perhaps the most striking of these examples is the case of the long chain specific acyl-CoA dehydrogenase, which was identified with modifications from an unprecedented, five different types of 2-alkenal lipid peroxidation products to Cys-166. These modifications included acrolein, β-hydroxyacrolein, 4-hydroxy-2-hexenal, 4-hydroxy-2-nonenal, and 4-oxo-2-nonenal. Figure 4.2 displays the MALDI-TOF/TOF generated tandem mass spectra of the tryptic peptide CIGAIAMTEPGAGSDLQGVR spanning residues 166 to 185 illustrating the diversity of modifications identified on the N-terminal cysteine.

Several of the sites identified in this study are known to be very important to the function of the specific proteins. For example the tryptic peptide including residue Cys-166 from the long chain specific acyl-CoA dehydrogenase contains several residues which make up part of a FAD binding site, and adduction of this site by LPO's would very likely interfere with the protein's ability to bind FAD and therefore inhibit it's ability to catalyze the first step in the β-oxidation of fatty acids.

Another example is cysteine 385 of aconitase, which was identified with an ARP-acrolein modification. Aconitase has been shown to be inhibited by acrolein in a concentration dependent manner (37). Aconitase is found in the mitochondrial matrix and is involved in the second step of the citric acid cycle, catalyzing the reversible isomerization of citrate and isocitrate with cis-aconitate as a reaction intermediate. We identified the tryptic peptide VGLIGSCTNSSYEDMGR to be modified on Cys-385 by ARP-acrolein. This same peptide was also identified in a separate study performed in our group in which (4-iodobutyl)triphenylphosphonium (IBTP) was used as a thiol reactive probe (24). Taken together this evidence supports the notion that the susceptibility of cysteine 385 to modification by electrophilic species could account for the sensitivity and corresponding loss of activity of aconitase frequently observed under conditions of oxidative stress (38). Cysteine 385 is known to be part of a 4Fe-4S iron sulfur cluster which is required for the catalytic activity. A specific Fe(II) atom, called Fe_{α}, is thought to coordinate the OH group of the substrate so as to facilitate it's elimination. Unlike many iron sulfur clusters this iron-sulfur cluster is not associated with a redox process. Instead it has been postulated that the electronic properties of the 4Fe-4S cluster permit Fe_{α} to expand its coordination shell from the four ligands observed in the x-ray structure of the free enzyme (three S^{2-} and one OH^{-}) to the six octahedrally arranged ligands observed in the enzyme substrate complex. The modification of Cys-385 by a lipid peroxidation product would undoubtedly inhibit the function of this enzyme,

as irreversible oxidative disruption of the 4Fe-4S cluster is known to cause a loss of enzymatic activity (39, 40).

The peptide spanning residues 317 to 330 from methylmalonate-semialdehyde dehydrogenase was identified by both ESI-Q-TOF and MALDI-TOF/TOF analysis as containing a ARP-acrolein modification to Cys-317. This is particularly significant in that Cys-317 is the nucleophilic acitive site of this enzyme, which catalyzes the irreversible oxidative decarboxylation of malonsemialdehyde and methylmalonate semialdehyde to acetyl-CoA and propionyl-CoA respectively. Obviously such a modification would inhibit the function of this enzyme. The ESI-Q-TOF generated MS/MS is shown in figure 4.3. Note the presence of fragment ions at 227.09 m/z and 332.14 m/z, which are generated by the fragmentation of the ARP tag and are useful as diagnostic peaks to assist in the identification of ARP-labeled peptides.

The fact that proteins contain sites susceptible to modification by lipid peroxidation products raises the question of what this means in terms of the folded structure of the protein molecules. Why are certain residues targeted over others? Clearly one would think that in order to be modified, a residue would need to be located on or near the surface of the protein, and be reasonably exposed to the surrounding environment. A residues susceptibility to modification would also undoubtedly depend on the side chains pKa value and

the chemical microenvironment in which it is located. We attempted to address this question for the case of mitochondrial malate dehydrogenase (MDH), which was found modified by lipid peroxidation products on five cysteine residues (Cys 89, 93, 212, 275, 285). Structural analysis was performed on the crystal structure of porcine heart (MDH) using the protein modeling software Molsoft ICM V3.5-1p. Normalized B-Factor values, which serve as a measure of local flexibility of the protein structure over a given region, were obtained for all eight cysteine residues in a monomer of MDH in the tetramer conformation. The solvent accessible areas (SAA) for each of the eight cysteines, which provide a measure of how exposed each residue is to the surrounding solvent, were also calculated using a water probe radius of 1.4 Å. Four out of the five cysteine residues we identified as modified correspond with the cysteine residues with the largest B-Factor values. Cys-285, which has the largest B-Factor and second largest SAA of all of cysteines in MDH, was identified being modified by ARP-acrolein and ARP-HHE. The MALDI-TOF/TOF generated tandem mass spectra of the ARP-acrolein and ARP-HHE modified peptides spanning residues 282-296 are shown below in figure 4.4 along with the ribbon structure of MDH illustrating the position of Cys-285 and a table with the corresponding average B-Factor and SAA values for all cysteine residues in a MDH tetramer. Thus for the case of malate dehydrogenase it seems that B-factor and SAA values correspond with the susceptibility of residues towards oxidative modification.

Functional Network Analysis of 2-alkenal Modified Proteins

In order to get an understanding of the potential impact of 2-alkenal modification to mitochondrial proteins on a systems level we performed a network analysis of the functional pathways of our identified proteins. The KEGG database was queried to obtain the functional pathway information and Cytoscape was used to visualize the connections between the proteins and their pathways. The network of modified proteins is depicted in figure 4.5. The network analysis shows that many of the proteins identified in this study are involved in the functional pathways of degenerative diseases including Alzheimer's disease, Huntington's disease, and Parkinson's disease, all in which oxidative stress induced modification to proteins has been implicated to play an important role. Many of the identified proteins are also involved in calcium signaling, which is involved in mitochondrial regulation of cell death.

Discussion

To the best of our knowledge this work represents the most exhaustive analysis of endogenously occuring oxidative modifications to mitochondrial proteins by 2-alkenal lipid derived compounds, through the use of affinity enrichment and mass spectrometry. In total we identified 27 proteins containing 39 unique nucleophilic sites that were modified by six varieties of 2-alkenals. The majority of modified proteins identified (40%) were members of the respiratory chain. This is to be expected as the electron transport enzymes are both a major source of ROS

within the mitochondria and in close proximity to a high concentration of polyunsaturated fatty acids present in the inner mitochondrial membrane. TCA cycle proteins comprised the second most abundant category of identified modified proteins at 19%. A pie chart displaying the percentages of all identified proteins and modified sites is shown in figure 4.6A. Eighty five percent of the 2-alkenal Michael type additions characterized were present on cysteine residues, while 12% of the modification sites were to histidine with 3% occurring on lysine (figure 4.6B). This is also not surprising as cysteine is well known to be the most nucleophilic of the three residues. The proteins and modified sites identified in this study represent targets within the mitochondrial proteome that are susceptible to oxidative damage by electrophilic lipid peroxidation products. A few of the sites identified in this study match with those identified by other studies employing invitro addition of HNE or other electrophilic probes, followed by affinity enrichment and mass spectrometry. However there are a number of sites, which are exclusive to either this study, or the in vitro studies. In order to get a better understanding of the role that oxidative modifications play in biological processes, we feel it is important to characterize the naturally occurring modifications.

Acrolein modification of Mitochondrial Proteins

The Michael type addition of acrolein to nuleophilic sites in proteins is by far the most common modification we identified in this experiment, occurring on 26 out

of the 27 carbonylated proteins and comprising a total of 84% of the 2-alkenal modifications identified (figure 4.6C). Acrolein is known to be the most reactive of the α,β–unsaturated aldehydes and is common environmental toxin which can be formed from combustion of organic matter or formed biologically through the metabolism of allyl compounds, lipid peroxidation of polyunsaturated fatty acids, and the amine-oxidase mediated degradation of polyamines (14, 41, 42). The toxicity of acrolein has been shown to be approximately one to three orders of magnitude greater than formaldehyde, acetaldehyde, and HNE (43). Exposure to acrolein induces conditions of oxidative stress by depleting protective nucleophiles such as glutathione (GSH) and ascorbic acid (42, 44). Recent studies have shown concentrations of acrolein as low as 1 μM can induce oxidative stress damage resulting in functional impairment of mitochondria (37). Acrolein's higher reactivity towards protein nucleophiles could in part explain why we have it detected more frequently than other α,β–unsaturated aldehydes. Uchida et al. reported the formation of N^{ε}-(3-formyl-3,4-dehydropiperidino) lysine (FDP-lysine) as a major reaction product between acrolein and Lys residues. However although the structure of FDP-lysine contains a free aldehyde group, which would be reactive with ARP, we were not able to identify any of these types of adducts in our experiments (41). Being that FDP lysine requires two molar equivalents of acrolein per nucleophilic residue to form it is likely that FDP-lysine modifications only form under in vitro conditions containing relatively high concentrations of acrolein and are unlikely to occur under normal physiological

conditions. It is important to note that most anti-acrolein antibodies used for the immunochemical detection of acrolein-protein adducts are specific for FDP-lysine derivatives, so their sensitivity towards acrolein Micheal type adducts of cysteine residues, such as those primarily identified in this study, remains unknown. It is possible that the ARP approach and the immunological approach are sensitive to two different populations of acrolein adducts. Recent studies have shown acrolein to be a mitochondrial toxin inhibiting electron transport and increasing overall oxidative stress damage in brain and liver mitochondria (37, 43). Several important mitochondrial enzymes including aconitase, ADP/ATP translocase, Complex I, Complex II, pyruvate dehydrogenase and alpha ketogluterate dehydrogenase have been shown to be inhibited by acrolein (37, 43). Out of those six enzymes we were able to identify the sites of acrolein modifications to aconitase, ADP/ATP translocase, Complex I, and Complex II in our experiments.

Other Lipid peroxidation products

In addition to acrolein we also identified a few cases of other lipid peroxidation products adducted to mitochondrial proteins. These other products include 4-hyroxy-2-hexenal, 4-hydroxy-2-nonenal, 4-oxo-2-nonenal, crotonaldehyde, beta-hyroxyacrolein. 4-hydroxy-2-nonenal and 4-oxo-2-nonenal arise primarily from the lipid peroxidation of the ω–6 fatty acids, linoleic and arachadonic acids, while 4-Hydroxy-2-hexenal on the other hand, is an end product of the peroxidation of ω-3 fatty acids, including α-linolenic, eicosapentaenoic, and docosahexanoic

acids. Combined, these other 2-alkenal products comprised only 16% of the modifications identified (figure 4.6C). It is quite surprising that this wide variety of LPO's were all identified as adducting to the same residue sites.

To assess the structural implications of why certain residues are susceptible to modification we performed structural analysis of malate dehydrogenase by integrating our mass spectrometry data identifying sites of modification with the known x-ray crystal structure for MDH. This proved useful in that the sites of acrolein and HHE adduction correspond to the cysteine residues with high B-factors and solvent accessible areas. Further studies will be necessary to see if this correlation extends to other protein systems and if B-factor and SAA values may be useful in predicting susceptible sites of modification by lipid derived electrophiles

Evaluation and method validation of the ARP approach (Possible pitfalls & limitations with ARP approach)

With the rapidly increasing number of new analytical proteomics techniques it is of critical importance to perform validation of the analytical method to ensure the results are scientifically sound. Do to the extreme sample complexity, biological variability and absence of reference standards this becomes a daunting task. We assessed the robustness of the ARP labeling and enrichment method on several levels in an attempt to validate our analytical approach. We tested the reproducibility of our method by repeating our analysis several times using new

sample preparations from different animals and analyzing the samples on multiple instruments. We found that 20 of the ARP-labeled oxylipid modified peptides belonging to 15 proteins were reproducibly identifiable in repeated sample preparations. The overwhelming presence of acrolein modified peptides towards other oxylipids raised the question as to whether or not our method was in some way biased towards acrolein modifications vs. HNE, ONE and other LPO adducts. However the results of our previous study with human THP-1 cells which were exposed exogenously to HNE, resulted in the identification of sixteen protein targets of HNE (34). These results demonstrate that our method is not discriminating against HNE modified peptides, as when HNE is added, we enrich and detect HNE adducted peptides. Instead we suggest the abundance of acrolein modifications is likely due to a relatively high concentration of acrolein compared to other LPO's in the mitochondria as well as acrolein's higher reactivity towards protein nucleophilic sites.

Additionally, many of the modified proteins identified are known to be of relatively high abundance in the mitochondria. With such a large dynamic range of protein concentrations present in the mitochondria, it is extremely difficult to sample the proteins of lower abundance. This problem becomes exaggerated by the fact that LPO-modified proteins are already of very low abundance compared to their non-modified variants. It's possible that this problem could be overcome by employing a variety of additional fractionation techniques, however this would

also require a larger amount of starting material to be sure to have enough of the lowest abundance modified proteins.

It's important to consider the possibility that oxidative modifications can occur during the processing of the sample. However, even if such modifications do occur as artifacts of sample preparation the proteins and amino acid residue sites that were modified still represent susceptible targets to oxidative damage and are therefore still relevant. It's also worth noting that the majority of modified proteins identified in this study are located on the matrix side of the mitochondrial inner membrane, where the major sites of ROS production are thought to be, supporting the notion that these modifications occurred while the mitochondria were intact.

The results shown here are important to increasing our understanding of these types of modifications to proteins and the biological implications such modifications may have. The present study is a discovery effort with the goal of identifying the sites and types of endogenously occurring, 2-alkenal modifications to mitochondrial proteins. Now that we have characterized a number of these adducts, future experiments are needed to determine what impact these modifications have on the proteins structure and function as well as the function of the mitochondria and cell as a whole. Ongoing experiments in our laboratory include performing quantitative analysis of acrolein, modified peptides in the

mitochondria to better understand how the levels of these modifications change with ageing. Additionally, in preliminary unpublished results from our laboratory we have identified several of the same cysteine containing peptide sequences as being modified by glutathione.

Acknowledgements

This work was supported by grants from the NIH/NIA (AG025372). The mass spectrometry core facility of the Environmental Health Sciences Center at Oregon State University is supported in part by a grant from NIEHS (ES00210).

Supporting Information Available

Annotated tandem mass spectra for all ARP labeled peptides are provided in figures SB1 through SB77 available in appendix B.

References

1. Harman D: Aging: a theory based on free radical and radiation chemistry. Journal of Gerontology 11: 298-300, 1956.
2. Harman D: The aging process. Proc. Natl. Acad. Sci. U. S. A. 78: 7124-8, 1981.
3. Berlett BS and Stadtman ER: Protein oxidation in aging, disease, and oxidative stress. J. Biol. Chem. 272: 20313-6, 1997.
4. Stadtman ER: Protein oxidation in aging and age-related diseases. Ann. N. Y. Acad. Sci. 928: 22-38, 2001.
5. Gibson BW: The human mitochondrial proteome: oxidative stress, protein modifications and oxidative phosphorylation. Int. J. Biochem. Cell. Biol. 37: 927-34, 2005.
6. Liebler DC: The poisons within: application of toxicity mechanisms to fundamental disease processes. Chem. Res. Toxicol. 19: 610-3, 2006.
7. Sastre J, Pallardo FV and Vina J: Mitochondrial oxidative stress plays a key role in aging and apoptosis. IUBMB Life 49: 427-35, 2000.
8. Linford NJ, Schriner SE and Rabinovitch PS: Oxidative damage and aging: spotlight on mitochondria. Cancer Res. 66: 2497-9, 2006.
9. Cadenas E and Davies KJ: Mitochondrial free radical generation, oxidative stress, and aging. Free Radic. Biol. Med. 29: 222-30, 2000.
10. Orrenius S, Gogvadze V and Zhivotovsky B: Mitochondrial oxidative stress: implications for cell death. Annu. Rev. Pharmacol. Toxicol. 47: 143-83, 2007.
11. Ott M, Gogvadze V, Orrenius S and Zhivotovsky B: Mitochondria, oxidative stress and cell death. Apoptosis 12: 913-22, 2007.
12. Andreyev AY, Kushnareva YE and Starkov AA: Mitochondrial metabolism of reactive oxygen species. Biochemistry (Mosc) 70: 200-14, 2005.
13. O'Malley Y, Fink BD, Ross NC, Prisinzano TE and Sivitz WI: Reactive oxygen and targeted antioxidant administration in endothelial cell mitochondria. J. Biol. Chem. 281: 39766-75, 2006.
14. Esterbauer H, Schaur RJ and Zollner H: Chemistry and biochemistry of 4-hydroxynonenal, malonaldehyde and related aldehydes. Free Radic. Biol. Med. 11: 81-128, 1991.
15. Schoneich C: Mass spectrometry in aging research. Mass Spectrom. Rev. 24: 701-18, 2005.
16. Vila A, Tallman KA, Jacobs AT, Liebler DC, Porter NA and Marnett LJ: Identification of protein targets of 4-hydroxynonenal using click chemistry for ex vivo biotinylation of azido and alkynyl derivatives. Chem. Res. Toxicol. 21: 432-44, 2008.
17. Mirzaei H and Regnier F: Identification and quantification of protein carbonylation using light and heavy isotope labeled Girard's P reagent. J. Chromatogr. A 1134: 122-33, 2006.

18. Han B, Stevens JF and Maier CS: Design, synthesis, and application of a hydrazide-functionalized isotope-coded affinity tag for the quantification of oxylipid-protein conjugates. Anal. Chem. 79: 3342-54, 2007.
19. Codreanu SG, Zhang B, Sobecki SM, Billheimer DD and Liebler DC: Global analysis of protein damage by the lipid electrophile 4-hydroxy-2-nonenal. Mol. Cell. Proteomics 8: 670-80, 2009.
20. Grimsrud PA, Picklo MJ, Sr., Griffin TJ and Bernlohr DA: Carbonylation of adipose proteins in obesity and insulin resistance: identification of adipocyte fatty acid-binding protein as a cellular target of 4-hydroxynonenal. Mol. Cell. Proteomics 6: 624-37, 2007.
21. Meany DL, Xie H, Thompson LV, Arriaga EA and Griffin TJ: Identification of carbonylated proteins from enriched rat skeletal muscle mitochondria using affinity chromatography-stable isotope labeling and tandem mass spectrometry. Proteomics 7: 1150-63, 2007.
22. Wong HL and Liebler DC: Mitochondrial protein targets of thiol-reactive electrophiles. Chem. Res. Toxicol. 21: 796-804, 2008.
23. Landar A, Oh JY, Giles NM, Isom A, Kirk M, Barnes S and Darley-Usmar VM: A sensitive method for the quantitative measurement of protein thiol modification in response to oxidative stress. Free Radic. Biol. Med. 40: 459-68, 2006.
24. Marley K, Mooney DT, Clark-Scannell G, Tong TT, Watson J, Hagen TM, Stevens JF and Maier CS: Mass tagging approach for mitochondrial thiol proteins. J. Proteome Res. 4: 1403-12, 2005.
25. Palmer JW, Tandler B and Hoppel CL: Biochemical properties of subsarcolemmal and interfibrillar mitochondria isolated from rat cardiac muscle. J. Biol. Chem. 252: 8731-9, 1977.
26. Suh JH, Heath SH and Hagen TM: Two subpopulations of mitochondria in the aging rat heart display heterogenous levels of oxidative stress. Free Radic. Biol. Med. 35: 1064-72, 2003.
27. Gleason WB, Fu Z, Birktoft J and Banaszak L: Refined crystal structure of mitochondrial malate dehydrogenase from porcine heart and the consensus structure for dicarboxylic acid oxidoreductases. Biochemistry 33: 2078-88, 1994.
28. Shrake A and Rupley JA: Environment and exposure to solvent of protein atoms. Lysozyme and insulin. J. Mol. Biol. 79: 351-71, 1973.
29. Stadtman ER: Protein oxidation and aging. Free Radic. Res. 40: 1250-8, 2006.
30. Wallace DC: Mitochondrial diseases in man and mouse. Science 283: 1482-8, 1999.
31. Hagen TM, Moreau R, Suh JH and Visioli F: Mitochondrial decay in the aging rat heart: evidence for improvement by dietary supplementation with acetyl-L-carnitine and/or lipoic acid. Ann. N. Y. Acad. Sci. 959: 491-507, 2002.
32. Chung WG, Miranda CL and Maier CS: Detection of carbonyl-modified proteins in interfibrillar rat mitochondria using N'-aminooxymethylcarbonylhydrazino-D-biotin as an aldehyde/keto-reactive probe

in combination with Western blot analysis and tandem mass spectrometry. Electrophoresis 29: 1317-24, 2008.
33. Chavez J, Wu J, Han B, Chung WG and Maier CS: New role for an old probe: affinity labeling of oxylipid protein conjugates by N'-aminooxymethylcarbonylhydrazino d-biotin. Analytical Chemistry 78: 6847-54, 2006.
34. Chavez J, Chung WG, Miranda CL, Singhal M, Stevens JF and Maier CS: Site-specific protein adducts of 4-hydroxy-2(E)-nonenal in human THP 1 monocytic cells: Protein carbonylation is diminished by ascorbic acid. Chem. Res. Toxicol.: 2009.
35. Choksi KB, Boylston WH, Rabek JP, Widger WR and Papaconstantinou J: Oxidatively damaged proteins of heart mitochondrial electron transport complexes. Biochim. Biophys. Acta 1688: 95-101, 2004.
36. Wen JJ and Garg N: Oxidative modification of mitochondrial respiratory complexes in response to the stress of Trypanosoma cruzi infection. Free Radic. Biol. Med. 37: 2072-81, 2004.
37. Luo J and Shi R: Acrolein induces oxidative stress in brain mitochondria. Neurochem. Int. 46: 243-52, 2005.
38. Bulteau AL, Ikeda-Saito M and Szweda LI: Redox-dependent modulation of aconitase activity in intact mitochondria. Biochemistry 42: 14846-55, 2003.
39. Bulteau AL, Lundberg KC, Ikeda-Saito M, Isaya G and Szweda LI: Reversible redox-dependent modulation of mitochondrial aconitase and proteolytic activity during in vivo cardiac ischemia/reperfusion. Proc. Natl. Acad. Sci. U. S. A. 102: 5987-91, 2005.
40. Matasova LV and Popova TN: Aconitate hydratase of mammals under oxidative stress. Biochemistry (Mosc) 73: 957-64, 2008.
41. Uchida K, Kanematsu M, Morimitsu Y, Osawa T, Noguchi N and Niki E: Acrolein is a product of lipid peroxidation reaction. Formation of free acrolein and its conjugate with lysine residues in oxidized low density lipoproteins. J. Biol. Chem. 273: 16058-66, 1998.
42. Stevens JF and Maier CS: Acrolein: sources, metabolism, and biomolecular interactions relevant to human health and disease. Mol. Nutr. Food Res. 52: 7-25, 2008.
43. Sun L, Luo C, Long J, Wei D and Liu J: Acrolein is a mitochondrial toxin: effects on respiratory function and enzyme activities in isolated rat liver mitochondria. Mitochondrion 6: 136-42, 2006.
44. Horton ND, Mamiya BM and Kehrer JP: Relationships between cell density, glutathione and proliferation of A549 human lung adenocarcinoma cells treated with acrolein. Toxicology 122: 111-22, 1997.

Table 4.1 - Summary of the mitochondrial proteins modified by lipid peroxidation derived 2-alkenals and subsequently labeled with ARP and identified by tandem mass spectrometry. The MS/MS identified peptide sequences containing the ARP label and 2-alkenal modification from each of the corresponding carbonylated proteins is shown. The amino acid residue and chemical nature of the modification are indicated for each case. Biological and functional assignments were made on the basis of information from the NCBI (www.ncbi.nlm.nih.gov/Pubmed) and the UniProt Knowledgebase (http: http://www.uniprot.org) websites.

Table 1. ARP-labeled 2-alkenal Modified Peptides Identified from Rat Cardiac Mitochondrial Proteins‡

Biological Function	SwissProt ID	UniProt Accession	Protein Name	Peptide Sequence	Modified Residue	Modifications
Respiratory Chain	AT5F1_RAT	P19511	ATP synthase B chain	C*IGDLK[a,b]	C239	ARP-acrolein
	ATP5H_RAT	P31399	ATP synthase D chain	NC*AQFVTGSQAR[a,b,c]	C100	ARP-acrolein
	ATPA_RAT	P15999	ATP synthase subunit alpha	GC*SMGEYFR[a,b,c,d]	C294	ARP-acrolein
				SGC*SMGEYFR[a,b,c,d]	C294	ARP-acrolein
				YSGC*SMGEYFR[a,b,d]	C294	ARP-acrolein
				LAPYSGC*SMGEYFR[a,c]	C294	ARP-acrolein
	ATPB_RAT	P10719	ATP synthase subunit beta	H*GGYSVFAGVGER[a,b,c,d]	H227	ARP-crotonaldehyde
	ATPG_RAT	P35435	ATP synthase gamma chain	GLC*GAIHSSVAK[a,b,c]	C78	ARP-acrolein
				H*SDQFLVSFK[a,b]	H120	ARP-acrolein
	ATPO_RAT	Q06647	ATP synthase O subunit	GEVPC*TVTTAFPLDEAVLSELK[a,b,c]	C141	ARP-acrolein
	CX6B1_MOUSE‡ (EDM07730)	P56391	Cytochrome c oxidase subunit VIb isoform 1	GGDVSVC*EWYR[a,c]	C54	ARP-acrolein
	NDUV1_MOUSE‡ (AAH83709)	Q91YT0	NADH dehydrogenase [ubiquinone] flavoprotein 1	QIEGHTIC*ALGDGAAWPVQGLIR[a]	C425	ARP-acrolein
	QCR1_RAT	Q68FY0	Ubiquinol-cytochrome-c reductase complex core protein 1	NALISHLDGTTPVC*EDIGR[a,b,c]	C410	ARP-acrolein
				YFYDQC*PAVAGYGPIEQLSDYNR[b]	C453	ARP-acrolein
	QCR2_RAT	P32551	Ubiquinol-cytochrome-c reductase complex core protein 2	NALANPLYC*PDYR[a,b,c]	C191	ARP-acrolein, ARP-HNE
				NPLYC*PDYR[a,d]	C191	ARP-acrolein
	DHSA_RAT	Q920L2	Succinate	GH*SLLHTLYGR[a,b]	H190	ARP-acrolein

Table 4.1 (Continued)

			dehydrogenase [ubiquinone] flavoprotein subunit			
Transport	Q6IRH6_RAT	Q6IRH6	Slc25a3 protein	AVEEQYSC*EYGSGR[b,d]	C52	ARP-acrolein
	ADT1_RAT	Q05962	ADP/ATP translocase 1	GADIMYTGTVDC*WR[a,b,c]	C256	M(ox), ARP-acrolein
				TGTVDC*WR[a,c,d]	C256	ARP-acrolein
				EFNGLGDC*LTK[a,c]	C159	ARP-acrolein
				YFAGNLASGGAAGATSLC*[a,d]	C128	ARP-acrolein
				C*FVYPLDFAR[a,b,c]	C128	ARP-acrolein
				DIMYTGTVDC*WR[b]	C256	ARP-acrolein
				KGADIMYTGTVDC*WR[b]	C256	ARP-acrolein
	ADT2_RAT	Q09073	ADP/ATP translocase 2	VSFAK*DFLAGGVAAAISK[a,c]	K10	ARP-HNE
				TGTLDC*WR[a,d]	C257	ARP-acrolein
	VDAC1_RAT	Q9Z2L0	Voltage-dependent anion-selective channel protein 1	YQVDPDAC*FSAK[a,b,c]	C232	ARP-acrolein
	VDAC3_RAT	Q9R1Z0	Voltage-dependent anion-selective channel protein 3	VC*NYGLIFTQK[a]	C65	ARP-acrolein
TCA cycle	ACON_RAT	Q9ER34	Aconitate hydratase	VGLIGSC*TNSSYEDMGR[a,b]	C385	ARP-acrolein
				VAVPSTIHC*DHLIEAQLGGEK[a]	C126	ARP-acrolein
	IDHP_RAT	P56574	Isocitrate dehydrogenase [NADP]	C*ATITPDEAR[b]	C184	ARP-acrolein
				DLAGC*IHGLSNVK[a]	C418	ARP-acrolein
	MDHM_RAT	P04636	Malate dehydrogenase	ETEC*TYFSTPLLLGK[a,b,c]	C285	ARP-acrolein, ARP-HHE
				TEC*TYFSTPLLLGK[a,b,d]	C285	ARP-acrolein
				EGVIEC*SFVQSK[a]	C275	ARP-acrolein
				GYLGPEQLPDC*LK[a]	C89	ARP-acrolein
				TIIPLISQC*TPK[a]	C212	ARP-acrolein
				GC*DVVVIPAFVPR[a]	C93	ARP-acrolein
	ODPA_RAT	P26284	Pyruvate dehydrogenase E1	VDGMDILC*VR[b]	C261	ARP-acrolein
			component alpha subunit	H*GFTFTR[a]	H121	ARP-crotonaldehyde
	ODPB_RAT	P49432	Pyruvate dehydrogenase E1 component subunit beta	EGIEC*EVINLR[a]	C263	ARP-acrolein
Oxidoreductase	ETFD_RAT	Q6UPE1	Electron transfer flavoprotein-ubiquinone oxidoreductase	AAQIGHTLSGAC*LDPAAFK[a,b]	C117	ARP-acrolein
	MMSA_RAT	Q02253	Methylmalonate-semialdehyde dehydrogenase	C*MALSTAVLVGEAK[a,b]	C317	ARP-acrolein
	NNTM_MOUSE‡ (AAH91271)	Q61941	NAD(P) transhydrogenase	EANSIVITPGYGLC*AAK[a,b,c]	C936	ARP-acrolein
Chaperone	CH60_RAT	P63039	60 kDa heat shock protein	C*EFQDAYVLLSEK[b]	C237	ARP-acrolein
Lipid Metabolism	ACADL_RAT	P15650	Long-chain specific acyl-CoA dehydrogenase	C*IGAIAMTEPGAGSDLQGVR[a,b,c]	C166	ARP-Acrolein, ARP-βHA, ARP-HHE, ARP-HNE, ARP-ONE
Kinase	KCRB_RAT	P07335	Creatine Kinase B Type	LGYILTC*PSNLGTGLR[a,c]	C283	ARP-acrolein
				ILTC*PSNLGTGLR[a,d]	C283	ARP-acrolein

An * marks the ARP-labeled 2-alkenal modified residue. ‡ Rat version not present in Swiss Prot database, gene bank accession numbers for rat proteins containing the equivalent peptide sequences provided. All MS/MS spectra were visually inspected and fragment ions annotated manually and are available in the supplemental material. [a]= peptide identified by ESI-Q-TOF [b]= peptide identified by MALDI-TOF/TOF [c]= peptide identified in repeated biological sample preparations [d]= identified peptide sequence is semi-tryptic

Figures

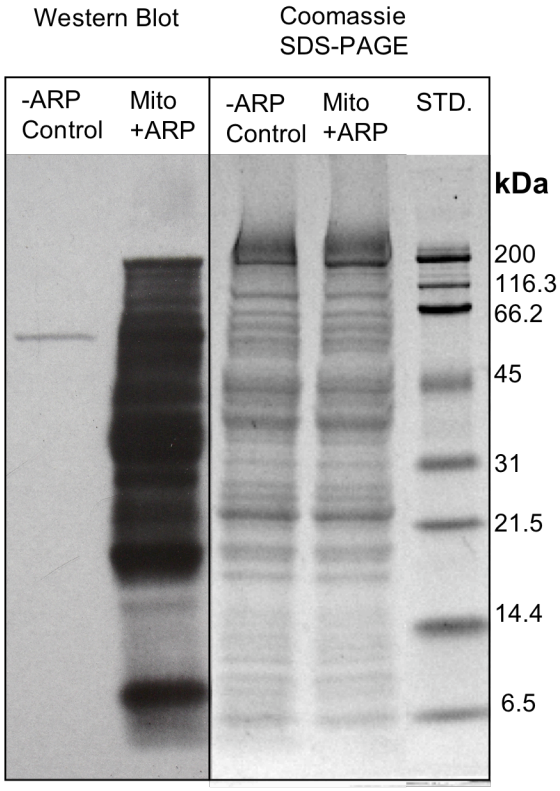

Figure 4.1 - SDS-PAGE and Western blot of mitochondrial proteins from rat hearts. The difference in signal between –ARP control and the +ARP mitochondrial samples demonstrates the presence of a large number or ARP reactive proteins, as well as the selectivity of NeutrAvidin-HRP for the ARP-labeled proteins.

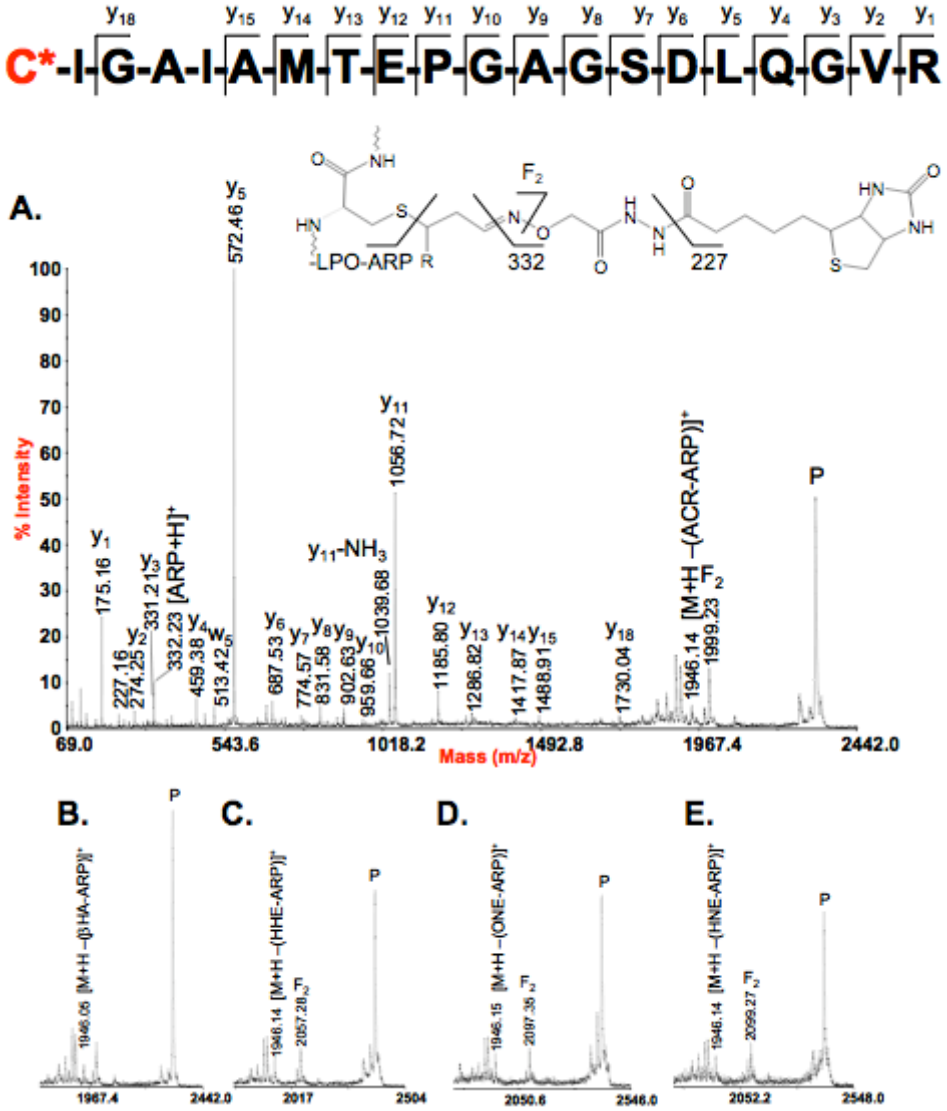

Figure 4.2 - Tandem mass spectra from the peptide spanning residues 166 to 185 from the long chain specific acyl-CoA dehydrogenase which was found to be modified on Cys-166 by a surprising variey of lipid peroxidation products and subsequently labeled with ARP. **A.** Full tandem mass spectrum of the ARP-acrolein modified version of the peptide. **B.,C.,D., and E.** display the high m/z region of the tandem mass spectra for the ARP-β-hydroxyacrolein modified, ARP-HHE modified, ARP-ONE modified, and ARP-HNE modified versions of the peptide respectively.

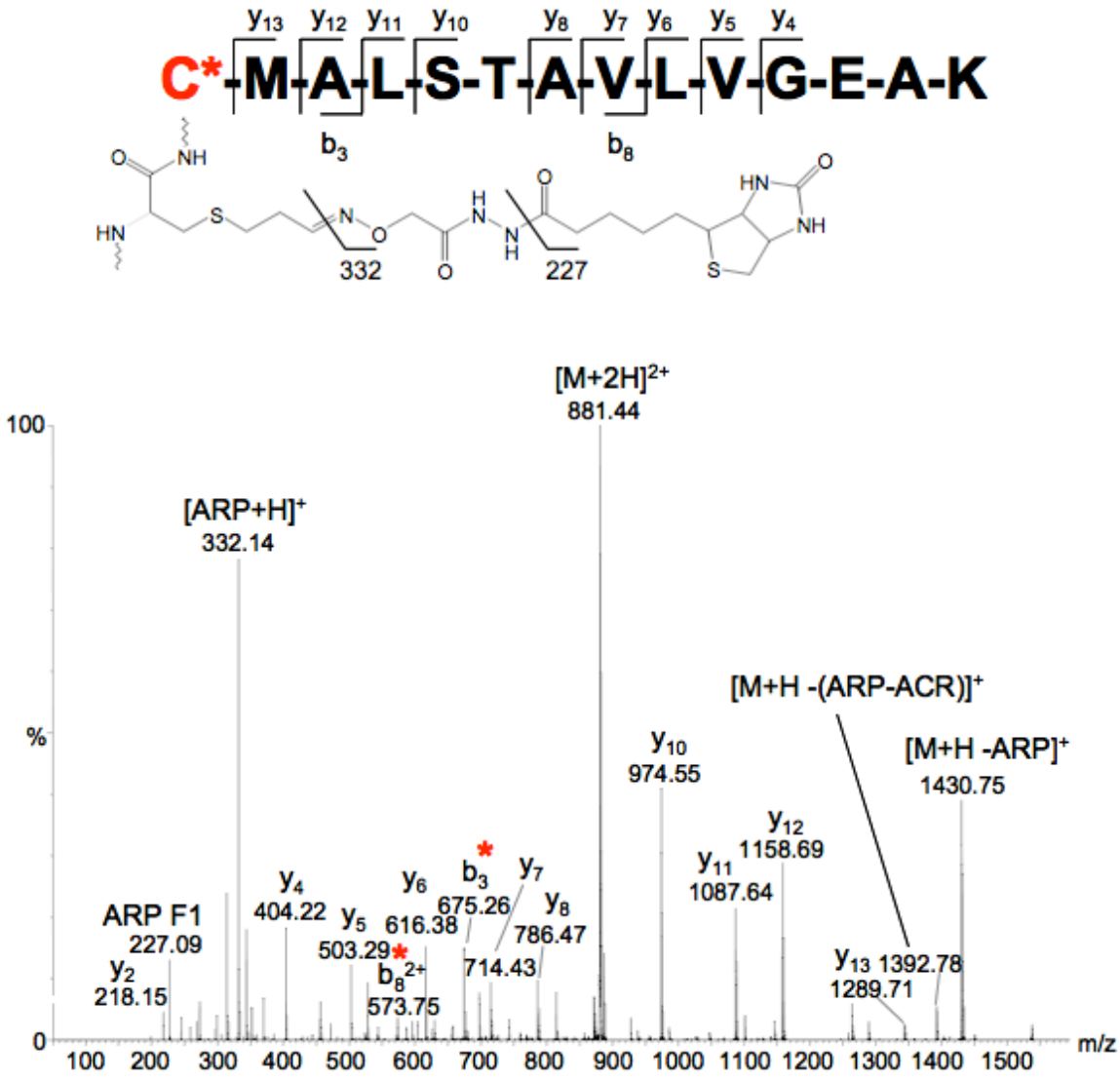

Figure 4.3 - ESI-Q-TOF generated MS/MS of the peptide CMALSTAVLVGEAK, spanning residues 317-330 of methylmalonate-semialdehyde dehydrogenase containing an ARP-acrolein modification at Cys-317. Cys-317 also happens to be the nucleophilic active site for this enzyme. This spectrum also contains the fragment ions at 332.22 m/z and 227.15 m/z, which are generated from the ARP tag and are diagnostic of ARP labeling.

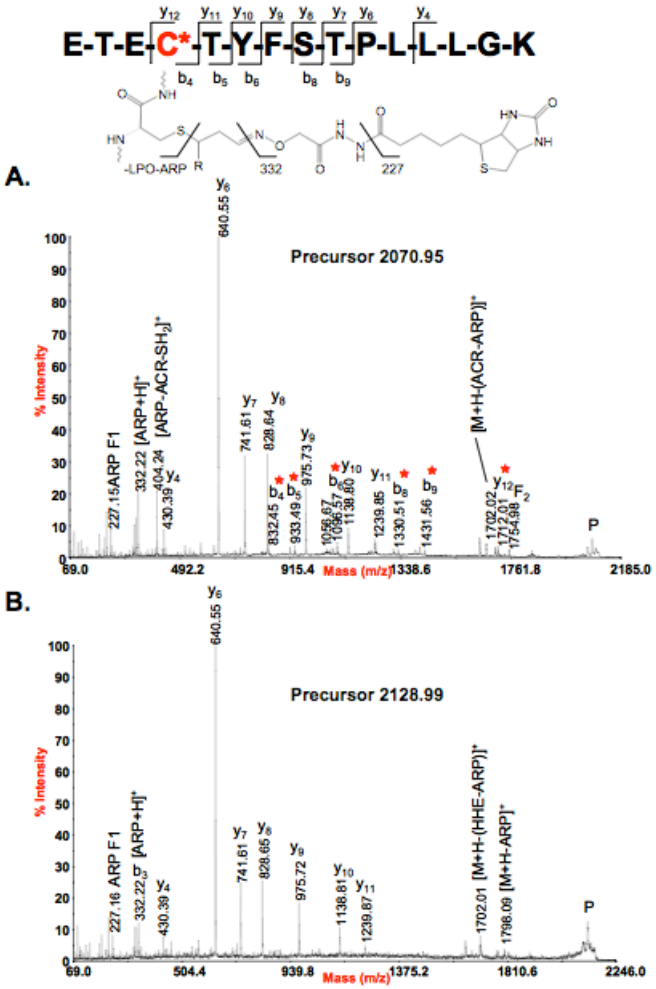

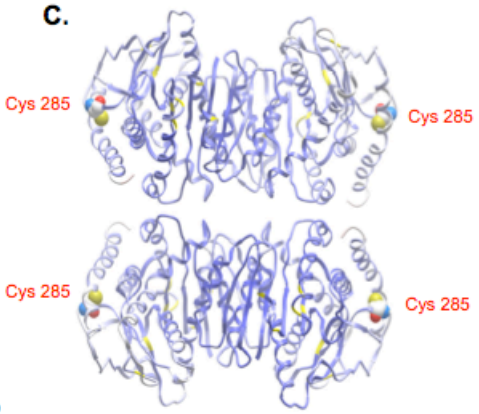

D.

Cys #	B-Factor	SAA (Å²)
89	26.22	24.49
93	26.17	20.55
128	22.32	2.14
132	24.51	22.71
138	19.61	0.22
212	33.71	45.95
275	20.72	2.25
285	35.78	43.84

Figure 4.4 - A.MALDI-TOF/TOF generated tandem mass spectrum of the peptide spanning residues 282-296 from malate dehydrogenase which was found with the ARP-acrolein and ARP-HHE modifications on Cys-285. Cys-285 is the most solvent accessible Cys residue according to solvent accessibility analysis. **B.** Tandem mass spectrum of the ARP-HHE modified version of the same peptide. **C.** Porcine heart MDH tetramer (PDB:1MLD) with the protein backbone displayed as ribbon (cysteine amino acids colored in yellow) and colored by B-Factor (ICM v3.6-1d, Molsoft). The residue Cys-285 is displayed as cpk and colored by atom type with the carbon atoms in white. **D.** Table listing the average B-Factor and solvent accessible area values data of all Cys residues of MDH protein in tetramer conformation

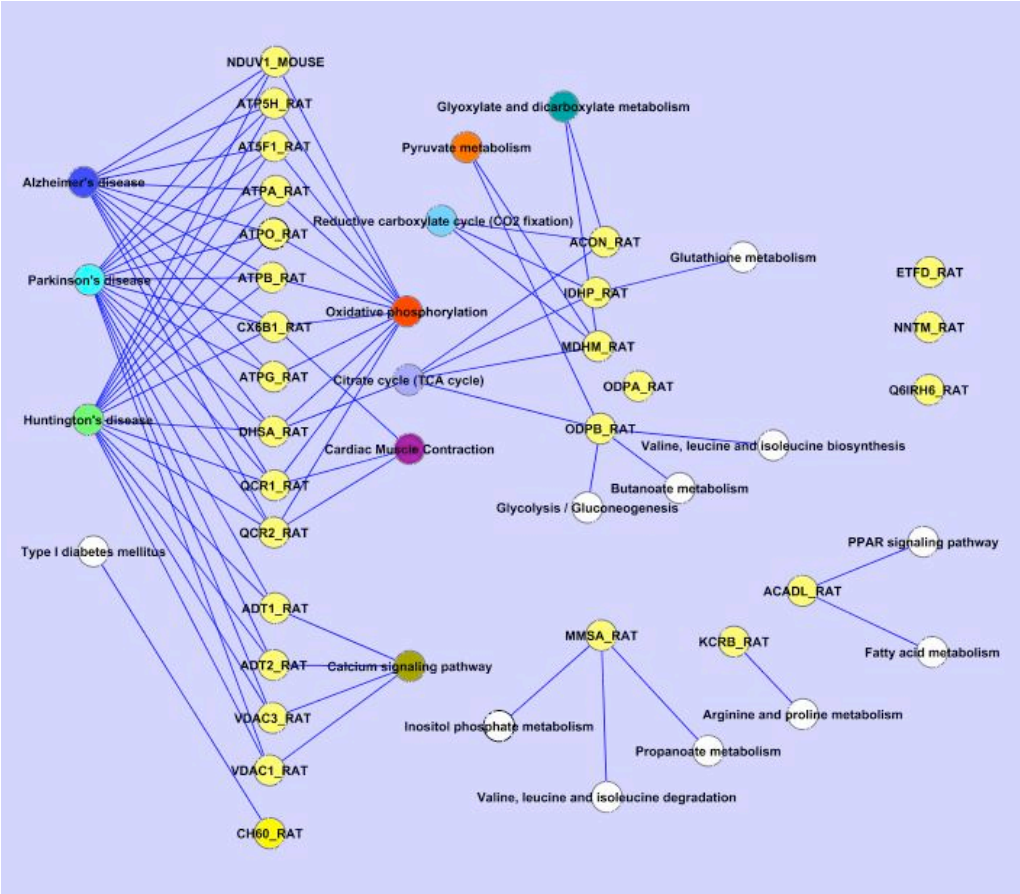

Figure 4.5 - Biological pathway analysis from the network of carbonylated proteins generated with funcation data from the KEGG database. Carbonylated proteins are colored as yellow nodes and the functional pathways are displayed as colored nodes. White colored nodes represent pathways for which only one protein was identified.

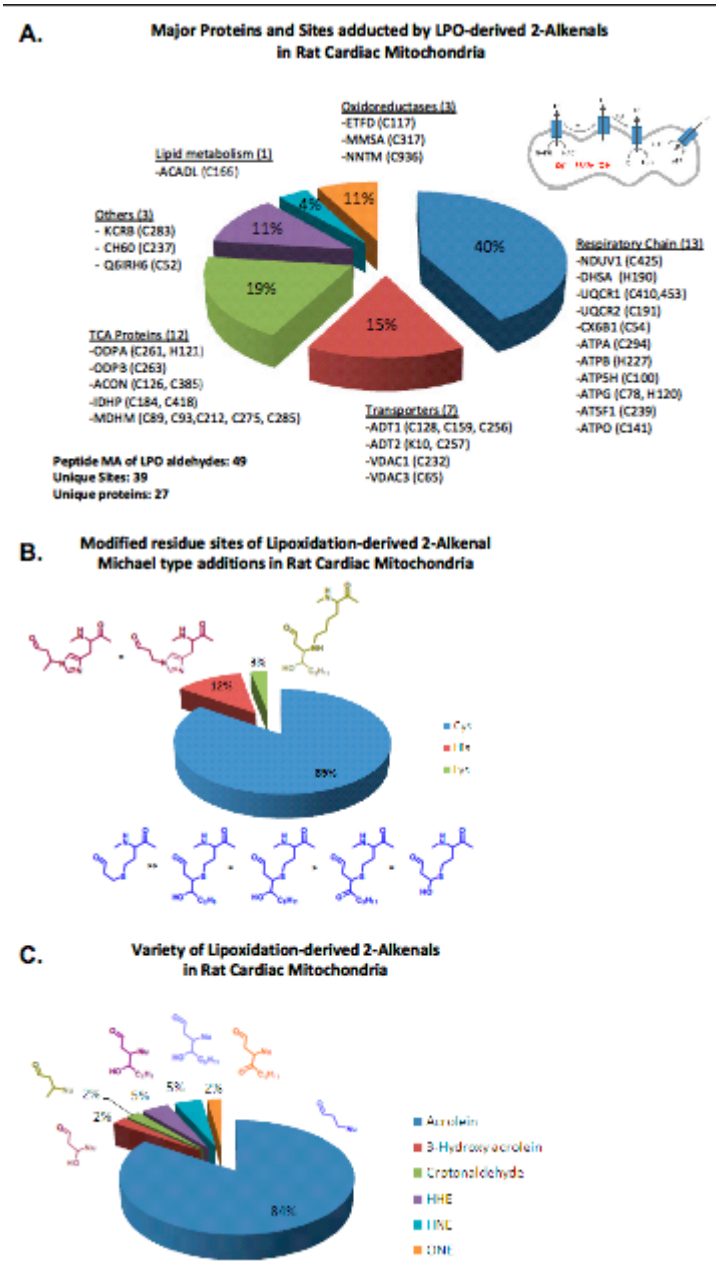

Figure 4.6 - A. Pie chart displaying the mitochondrial proteins and amino acid residue sites identified with modifications by lipid peroxidation derived 2-alkenals. **B.** Pie chart illustrating the percentage breakdown of the types of residues identified with Micheal-type additions of lipid peroxidation derived 2-alkenals. **C.** Pie chart indicating the percentages of the different types of lipid peroxidation derived 2-alkenals identified in this study.

Chapter 5

Site-specific protein adducts of 4-hydroxy-2(E)-nonenal in human THP-1 monocytic cells: Protein carbonylation is diminished by ascorbic acid

Juan Chavez[†], Woon-Gye Chung[†], Cristobal L. Miranda[†,‡,§], Mudita Singhal[¥], Jan F. Stevens[‡,§], and Claudia S. Maier[†,*]

[†]Department of Chemistry, [‡]Linus Pauling Institute, and [§]Department of Pharmaceutical Sciences, Oregon State University, Corvallis, Oregon 97331; [¥]Applied Computer Science Group, Pacific Northwest National Laboratory, Richland, WA 99352, USA

*To whom correspondence should be addressed. Tel: 541-737-9533. Fax: 541-737-2062. Email: claudia.maier@oregonstate.edu

Chemical Research in Toxicology

American Chemical Society

1155 Sixteenth Street N.W., Washington DC, 20036

In Press

Abstract

The protein targets and sites of modification by 4-hydroxy-2(E)-nonenal (HNE) in human monocytic THP-1 cells after exogenous exposure to HNE were examined using a multi-pronged proteomic approach involving electrophoretic, immunoblotting and mass spectrometric methods. Immunoblot analysis using monoclonal anti-HNE antibodies showed several proteins as targets of HNE adduction. Pretreatment of THP-1 cells with ascorbic acid resulted in reduced levels of HNE-protein adducts. Biotinylation of Michael-type HNE adducts using an aldehyde-reactive hydroxylamine-functionalized probe (aldehyde-reactive probe, ARP) and subsequent enrichment facilitated the identification and site-specific assignment of the modifications by LC-MS/MS analysis. Sixteen proteins were unequivocally identified as targets of HNE adduction and eighteen sites of HNE modification at Cys and His residues were assigned. HNE exposure of THP-1 cells resulted in the modification of proteins involved in cytoskeleton organization and regulation, proteins associated with stress responses and enzymes of the glycolytic and other metabolic pathways. This study yielded the first evidence of site-specific adduction of HNE to Cys-295 in tubulin α-1B chain, Cys-351 and Cys-499 in α-actinin-4, Cys-328 in vimentin, Cys-369 in D-3-phosphoglycerate dehydrogenase and His-246 in aldolase A.

Introduction

Reactive oxygen species initiate lipid peroxidation resulting in the formation of lipid peroxides which further decompose to reactive intermediates, such as aldehydic end products. 4-Hydroxy-2-nonenal (HNE) is a major lipid peroxidation product generated by oxidation of lipids containing polyunsaturated ω-6 fatty acids, such as linoleic and arachidonic acid (1, 2). HNE has been linked to the cytotoxic effects of oxidative stress by mechanisms involving adduct formation with DNA (3) and proteins, including protein constituents of the cytoskeleton (4, 5), signaling pathway (6, 7), protein folding (8) and degradation machinery (9), and the mitochondrial electron transport chain complexes (10). As an α,β-unsaturated hydroxyalkenal, HNE reacts predominately with nucleophilic sites in proteins yielding Michael-type adducts. In some cases, a Schiff base and pyrrole formation with Lys residues has been reported (11). Intramolecular or intermolecular protein cross-links occur when HNE forms a Michael adduct involving the electrophilic carbon at position 3 and a Schiff base with the ε-amino group of a Lys residue (11). Elevated levels of HNE, as observed under conditions of oxidative stress, have been associated with the impairment of protein function, initiation of cell death pathways, disruption of cellular, organelle and organ functions (12, 13). However, more recently, it has also been recognized that HNE and related α,β-unsaturated aldehydes seem to promote cell proliferation, induction of antioxidant genes and cellular stress responses that

reflect the importance of electrophiles in modulating diverse cell signaling pathways (7, 14).

Because the modification of proteins by HNE (and other α,β-unsaturated aldehydic lipid peroxidation products) has been linked to the etiology and progression of various diseases (12, 13) as well as degenerative processes associated with aging (15), an extensive repertoire of analytical methods has been described to detect HNE-modified proteins in complex biological matrices. Routinely, protein carbonyls are measured by derivatization of the carbonyl groups with 2,4-dinitrophenylhydrazine (DNPH) and the DNP-modified protein carbonyls are subsequently detected by immunochemical methods, such as ELISAs or Western blots. These methods provide the total protein carbonyl content, but lack specificity for distinct modifications by lipid peroxidation products or other oxidative processes that lead to the introduction of aldehyde/keto groups into proteins (10, 16). A hallmark for HNE-related research was the introduction of anti-HNE antibodies. These antibodies show only minor reactivity with other protein-bound aldehydes, but are not necessarily specific for the site of adduction (8, 10, 17, 18). Consequently, anti-HNE immunostaining protocols based on gel-electrophoretic methods and tandem mass spectrometry provide putative identifications of protein targets of modification by HNE, but site-specific assignment of the HNE adduction is rarely possible with gel-based approaches.

More recently, mass spectrometry-based proteomics approaches have become available that allow the unequivocal identification of protein targets of modifications and the residue-specific determination of the site of adduction by reactive lipid peroxidation products (19-24). Because of the low abundance of oxidatively modified proteins in complex biological samples, enrichment protocols have been developed that make these distinct sub-groups of proteins amenable to detailed mass spectrometric analyses. Some analytical strategies employ hydrazine-functionalized beads for the selective capture and release of HNE-modified peptides (23, 24) and others are based on chemical tagging of the carbonyl group by aldehyde-specific probes that enable biotin-avidin affinity enrichment or selective chromatographic separations (19-22). An alternative approach uses HNE analogs which retain the electrophilic and hydrophobic properties of HNE and have a reactivity group allowing for the subsequent derivatization with a biotinylation reagent via click chemistry (25). Our group has explored the use of hydrazine-functionalized isotope-coded affinity probes (HICATs) (21) and a biotinylated hydroxylamine derivative, N'-aminooxymethylcarbonylhydrazino D-biotin (aldehyde-reactive probe, ARP) for chemical tagging, enrichment and tandem mass spectrometric (MS/MS) characterization of carbonyl-modified proteins (19).

In the present study, we applied the ARP labeling strategy to identify protein targets of HNE in the human monocytic cell line THP-1, a cell line which has

properties similar to human monocyte-derived macrophages and is widely used for studying mechanisms of foam cell formation associated with atherosclerosis (26). Our previous studies have demonstrated that exposure of THP-1 cells to HNE resulted in apoptosis, necrosis, and protein carbonylation. THP-1 cells have the ability to accumulate ascorbic acid (Asc) in millimolar concentrations and Asc pretreatment of these cells enhanced the efflux of GSH-HNE phase I metabolites and lessened the formation of protein carbonyls detected by ELISA using an anti-DNPH antibody (27). In order to gain a deeper understanding of the mechanisms that link the protein modifications caused by HNE to the observed cytotoxic effects of HNE exposure and prevention by Asc pretreatment in human THP-1 cells, we combined gel-based approaches, anti-HNE immunostaining and a targeted mass spectrometry-based proteomics strategy to unequivocally identify the protein targets and sites of adduction of HNE in THP-1 cells.

Experimental Section

Materials. Fetal bovine serum, phenol red-free RPMI 1640, penicillin, streptomycin and trypsin-EDTA were purchased from Invitrogen (Carlsbad, CA, USA). HNE (10 mg/mL in ethanol) was obtained from Cayman Chemical (Ann Arbor, MI). Monoclonal anti-HNE IgG and monoclonal anti-β actin IgG were purchased from Oxis International, Inc. (Foster City, CA) and Santa Cruz Biotechnology Inc. (Santa Cruz, CA), respectively. Goat anti-mouse IgG-HRP conjugate and SuperSignal West Pico Chemiluminescent Substrate were obtained from Pierce Biotechnology, Inc. (Rockford, IL). Aldehyde-reactive probe (ARP, N-aminooxymethylcarbonylhydrazino-D-biotin) was purchased from Dojindo Laboratories (Kumamoto, Japan). UltraLink-immobilized monomeric avidin was obtained from Pierce (Rockford, IL).

Cell culture and treatment. THP-1 cells (American Type Culture Collection (Manassas, VA) were routinely cultured in 75 cm^2 flasks in RPMI 1640 medium supplemented with 10% fetal bovine serum (FBS), 2 mM glutamine, 100 units/mL penicillin, 100 μg/mL streptomycin and 0.05 mM 2-mercaptoethanol. The cells were incubated in humidified atmosphere of 5% carbon dioxide at 37 ºC.

THP-1 cells were incubated in 6-well plates (2 mL/well) with or without 1 mM Asc for 18 h in phenol red-free RPMI 1640 medium with 10% FBS and 50 μM 2-

mercaptoethanol. After an 18-h incubation at 37 ºC in 5% CO_2, the cells were centrifuged at 500 x g. The cells were washed with PBS and then resuspended in HBSS, 2 mL/well (3 x 10^6 cells/mL). HNE (or ethanol for control wells) was added to the wells to a final concentration of 100 μM. After 3 h of incubation with HNE, the cells were pelleted by centrifugation. The cell pellet was resuspended in 250 μl of PBS, lysed by sonication and frozen at -80 ºC prior to analysis by Western blotting and mass spectrometry.

SDS-PAGE, Western blotting and putative assignment of HNE-modified proteins by mass spectrometry. The protein samples (20 μg), mixed with Laemmli sample buffer (Bio-Rad cat. no. 161-0737) and heated at 95 ºC for 5 min, were loaded onto a 10-well 12% Tris-HCl gel (Bio-Rad Cat. no. 161-1102). After 1-dimensional SDS-PAGE (1-DE), proteins were transferred to a nitrocellulose membrane at 0.3 A for 2 h. Membranes were blocked with 5% non-fat milk in TBS containing 0.1% (v/v) Tween 20 (TBS-T) at room temperature for 2 h. For detection of protein-HNE adducts, the membranes were incubated with anti-HNE antibody for 1 h. After washing the blots 6 times in TBS-T for 5 min each, the membranes were incubated with 1:3000 diluted goat anti-mouse HRP-conjugated IgG in 40 mL TBS-T for 1 h. Subsequently, the blots were washed 6 times in TBS-T for 5 min each and then incubated in SuperSignal West Pico Chemiluminescent substrate (Pierce). Protein bands were visualized by exposing the membranes to X-ray film.

For identification, an identical duplicate was stained with Bio-Safe Coomassie-staining solution (Bio-Rad, 161-0787) for 2 h at room temperature. The protein bands that were found to correspond to those in the Western blot to be immunoreactive with anti-HNE antibody were selected, excised, digested with trypsin (28) and the resulting peptides were separated using a nano-LC system (Dionex Corporation, Sunnyvale, CA) using a PepMap C_{18} column (75 μm i.d. x 150 mm, 3 μm 100 Å, Dionex), spotted onto a MALDI target plate and subjected to MALDI tandem mass spectrometry as described in detail below.

Two-dimensional electrophoresis (2-DE) and Western blotting. 2-D electrophoresis followed by Western blotting was performed as described by Chung et. al. (5) to aid in the identification of HNE-modified proteins in THP-1 cells. Proteins (100 μg), dissolved in rehydration buffer [7 M urea, 2 M thiourea, 2% CHAPS, 0.2% (v/v) biolytes, 100 mM dithiothreitol (DTT), and 0.001% bromophenol blue], were applied to a Ready Strip IPG (pH 3–10). After covering with mineral oil, the strips were loaded in a Protean IEF isoelectric focusing cell (BioRad, Hercules, CA) and rehydrated overnight at 50 V. Isoelectric focusing (IEF) was performed at 20 °C by conditioning the strips at 250 V for 15 min and then ramped to 8000 V over 2.5 h and held at 35,000 V·h. The strips were removed and stored at -80 °C. Prior to SDS-PAGE, the strips were equilibrated for 10 min in 375 mM Tris–HCl (pH 8.8) containing 6 M urea, 2% (w/v) sodium dodecyl sulfate, 20% (v/v) glycerol, and 2% DTT. The strips were then

equilibrated for 10 min in the same buffer containing 2.5% iodoacetamide instead of DTT. Subsequently, the strips were mounted on Gradient criterion Tris–HCl gels (8-16%, Bio-Rad) to perform the second dimension electrophoresis at 130 V for 115 min. The separated proteins were then transferred to a nitrocellulose membrane before probing with anti-HNE IgG. The membrane was incubated with goat anti-mouse IgG-HRP conjugate and then incubated with SuperSignal West Pico Chemiluminescent Substrate for detection of HNE-positive spots on X-ray film.

To identify the HNE-positive spots in the Western blot, a second dimension electrophoresis gel was performed in parallel. After electrophoresis, the gel was placed in a gel fixative (10% methanol, 7% acetic acid) for 1 h at room temperature. The gel was then rinsed with MilliQ water and stained with Bio-Safe Coomassie-staining solution for 2 h at room temperature. Protein spots corresponding to the HNE-positive bands on the Western blot were excised, digested with trypsin and the extracted peptides analyzed by nanoLC-MALDI-MS/MS (29).

Identification of HNE-modified proteins in THP-1 cells following ARP labeling and tandem mass spectrometry. THP-1 cell proteins were labeled with ARP and enriched as described by Chavez et al. (19). Briefly, THP1 cells (1 mg protein) were lysed by incubation with 1% Triton X-100 in 50 mM sodium

phosphate buffer, pH 7.4, for 10 minutes. The lysate was then incubated with 5 mM ARP in 50 mM sodium phosphate buffer (pH 7.4) for 1 h at room temperature and excess ARP was removed by buffer exchange using Millipore BioMax centrifugal filters (10 kDa MWCO). The protein mixture was digested overnight with a 1:50 ratio of trypsin at 37 ^{o}C in 100 mM ammonium bicarbonate (pH 8.0). Peptides were then filtered (Amicon Microcon centrifugal filters, 10 kDa MWCO) to remove trypsin and membrane fragments. Peptides containing the ARP label were enriched using a 100 μL monomeric avidin affinity column (Ultralink monomeric avidin, Thermo). After removing non-labeled peptides with extensive washing, ARP-labeled peptides were eluted from the affinity column with 0.4% formic acid in 30% aqueous acetonitrile. The enriched ARP-labeled peptide fraction was concentrated using vacuum centrifugation before being submitted to LC-MS/MS analysis.

The ARP-labeled peptide samples were fractionated by reversed-phase (RP) liquid chromatography and spotted to a MALDI stainless steel target plate using a Dionex/LC Packings Ultimate nanoLC system coupled to a Probot™ target spotter. Peptides were trapped on a 300 μm i.d. x 1 mm PepMap™ C18 trap and washed at 30 μL/min for 3 minutes with solvent A (0.1% trifluoroacetic acid (TFA) in 5% aqueous acetonitrile). A PepMap C_{18} column (75 μm i.d. x 150 mm, 3 μm particles, 100 Å pore size; LC-Packings, Sunnyvale, CA) was used for the chromatographic separations. Separation was achieved by performing a 60-

minute linear gradient from 10% B to 60% B (0.1% TFA in 80% aqueous acetonitrile). Flow rate was 260 nL/min. The eluate from the column was transferred to the Probot^{TM} target spotter, where it was mixed with the MALDI matrix (2 mg/mL α-cyano-4-hydroxycinnamic acid in 50% aqueous acetonitrile acidified with 0.1% TFA) and spotted to a 144-spot MALDI target plate. Fraction collection began after a delay period of 20 minutes. The fraction collection/spotting time was set to 25 seconds.

Mass spectrometric analysis was performed using an Applied Biosystems 4700 MALDI-TOF/TOF instrument equipped with a Nd:YAG laser operating at a wavelength of 355 nm. All data were acquired in the positive reflector mode. External mass calibration was performed prior to analysis using the ABI 4700 calibration mixture consisting of the following peptides: des-Arg^1-bradykinin ($[M+H]^+$ at m/z_{calc} 904.4675), angiotensin 1 ($[M+H]^+$ at m/z_{calc} 1296.6847, Glu^1-fibrinopeptide B ($[M+H]^+$ at m/z_{calc} 1570.6768), and ACTH 18-39 ($[M+H]^+$ at m/z_{calc} 2465.1983). For peptide analyses, the instrument was operated in the data-dependent acquisition mode in which for each spot a survey mass spectrum (m/z 700-4000) was obtained followed by MS/MS analysis on the 10 most abundant ion signals detected. Tandem mass spectral data was acquired by accelerating the precursor ions to 8 keV and selecting them with the timed gate set to a nominal precursor mass window of 50 ppm. Collision-induced dissociation was performed with a collision energy of 1 keV and a collision gas

pressure of 6 x 10^{-7} Torr. Fragment ions were accelerated to 14 keV before entering the reflector.

MALDI-MS/MS data were processed into peak list files using 4000 Series Explorer v3.0. Default settings were used except for the peak density for MS/MS spectra which was set to a maximum of 10 peaks per 200 Da. The minimum signal-to-noise (S/N) ratio was set to 10, with a minimum peak area of 500. A setting of 40 was used for the maximum number of fragment ion peaks per precursor.

Mascot was used to search the MS/MS data against the Swiss Prot Database v56.8 (410518 sequences; 148080998 residues) limited to human taxonomy (20401 sequences). The Mascot search settings were as follows: the digesting enzyme was set to Trypsin/P and 2 missed cleavage sites were allowed. Both precursor and fragment ion tolerances were set to 0.2 Da with the instrument type set to MALDI-TOF/TOF. Dynamic modifications included ARP-HNE (+469.2359 Da) for Cys, His, and Lys residues, and oxidation (+15.9949 Da) for Met residues. Tandem mass spectra of potential ARP-HNE modified peptides were then manually inspected for verification of the sequence and modification.

ESI-MS/MS was performed using a ThermoFinnigan LTQ-FT Ultra (Thermo Scientific, San Jose, CA) equipped with a Michrom ADVANCE electrospray

ionization source (Bio Resource, Inc., Cotati, CA) and coupled to a capillary HPLC (CapLC, Waters). The ADVANCE source was operated at 1.8 kV. Peptide mixtures were separated on a C_{18} column (Agilent Zorbax 300SB-C_{18}, 250 x 0.3 mm, 5 μm) using a flow rate of 4 μL/min with a binary solvent system consisting of solvent A, 0.1% formic acid in water, and solvent B, 0.1% formic acid in acetonitrile. Peptides were trapped on a Michrom 'captrap' and washed for 3 min using 0.1% aqueous formic acid containing 1% acetonitrile at a flow rate of 6 μL/min. After trapping, peptides were separated on the analytical column using a linear gradient starting at 10% solvent B and rising to 30 % B over 50 minutes.

The LTQ-FT mass spectrometer was operated in the data-dependent MS/MS acquisition mode. Preview FTMS option was enabled. ESI-MS acquisitions were performed in the ICR cell over the range of 400-1800 m/z. The resolving power was set to 100,000 at m/z 400. MS scans were acquired using 1 microscan with a maximum ion accumulation time of 1000 ms. Centroided MS/MS spectra were acquired in the linear ion trap on the five most abundant doubly or triply charged precursor ions. Precursor ions were selected with an isolation width of 2 *Th* and subjected to collision-induced dissociation (CID) in the linear ion trap using a normalized collision energy of 35% with an activation Q of 0.250 and activation time of 30 ms. MS/MS scans were performed using 3 microscans with a maximum ion accumulation time of 50 ms. MS/MS data was recorded using a

dynamic exclusion period of 60s for previously analyzed precursor ions. Prior to analysis, the mass spectrometer was tuned with Glu^1-fibrinopeptide B (EGVNDNEEGFFSAR) using the following tune parameters: source voltage of 1.80 kV, a capillary temperature of 180 ^oC, a capillary voltage of 49.00 V, and a tube lens voltage of 155 V. For FT-MS scans the automatic gain control (AGC) target value was set to 1×10^6, while an AGC setting of 30,000 was used for MS/MS scans in the ion trap. Mass calibration was performed using the Supelco MSCAL5 ProteoMass^{TM} LTQ/FT hybrid ESI Pos. Mode Calibration Mixture (Sigma-Aldrich).

Sequence Database Searching

MALDI-MS/MS: Mascot version 2.2.04 was used to search the MALDI-MS/MS data against the Swiss Prot Database v56.8 (410518 sequences; 148080998 residues) limited to human taxonomy (20401 sequences). The Mascot search settings were as follows: the digesting enzyme was set to Trypsin/P and 2 missed cleavage sites were allowed. Both precursor and fragment ion tolerances were set to 0.2 Da with the instrument type set to MALDI-TOF/TOF. Dynamic modifications included ARP-HNE (+469.235890 Da) for Cys, His, and Lys residues, and oxidation (+15.994915 Da) for Met residues. MALDI tandem mass spectra of potential ARP-HNE modified peptides were then manually inspected for verification of the sequence and modification.

LTQ-FT MS/MS data: Thermo RAW data files were processed with Proteome Discoverer v1.0 using default parameters except for a S/N threshold setting of 10. For grouping spectra with the same measured *m/z*, a precursor tolerance of 10 ppm and a maximum retention time difference of 1.5 min was applied. A Mascot search of the Swiss Prot Database v56.9 (412525 sequences; 148809765 residues) was launched from Proteome Discoverer with the following search parameters: the taxonomy was limited to Homo sapiens (20401 sequences), the digesting enzyme was set to trypsin/P and two missed cleavage sites were allowed; peptide cut-off score was 10 and the protein cut-off score was 20. The instrument type was set to ESI-TRAP. The precursor ion mass tolerance was set to 10 ppm, while a fragment ion tolerance of 0.5 Da was used. Dynamic modifications included ARP-HNE (+469.235890 Da) for Cys, His, and Lys residues, and oxidation (+15.994915 Da) for Met residues. The tandem mass spectra of ARP-HNE modified peptides were visually inspected to verify (1) peptide fragment ions and (2) ions originating from the fragmentation of the ARP tag and (3) ions resulting from the loss of the ARP tag and the ARP-HNE moiety from the precursor ions. The proposed mechanisms for ARP and ARP-HNE loss fragmentations as well as proposed structures for the ARP-specific fragment ions are provided in the supporting information in Figure SC26.

Mascot uses a decoy database, containing randomized sequences with the same average amino acid content as the target database (Swiss Prot, human), to

obtain false positive (FP) matches. The false discovery rate (FDR) is calculated by dividing the number of FP matches by the number of peptide identifications above the identity or extensive homology threshold ($p<0.05$). This ratio is expressed as a percentage. The average false discovery rate of our datasets (1 MALDI-MS/MS; 2 ESI-MS/MS datasets) was 6.4% for peptide matches above the homology or identity threshold ($p<0.05$). However, it should be noted that not all of the identified ARP-HNE modified peptide sequences were above the significance threshold of $p<0.05$, and are therefore not included in the calculation of the false discovery rate. A point of caution, in targeted proteomics experiments, such as the ones described in this study, the datasets are often too small to provide an accurate determination of a false discovery rate.

Results

Western blotting and tandem mass spectrometric analysis of putative protein-HNE adducts in Asc-deficient and Asc-adequate THP-1 cells.

Assignments of immunoreactive bands were made by aligning the protein bands in the Western blot with the protein bands in the parallel gel stained with Coomassie (Figure 5.1). Protein bands of interest were then excised, and subjected to in-gel trypsin digestion followed by nanoLC-MALDI-MS/MS analysis to identify the proteins by mass spectrometric peptide sequencing

(Supplementary material Table SC1). The protein assignments of the immunoreactive bands are at best tentative since in some cases, multiple proteins were detected in the excised gel piece. For example, immunoreactive bands 7 and 13 were composed of 3 proteins (protein disulfide isomerase A3, adenylyl cyclase-associated protein 1, and vimentin) and 2 proteins (carbonic anhydrase 2 and 14-3-3 protein β/α), respectively. Using the alignment procedure, other proteins in THP-1 cells recognized by anti-HNE antibody were tentatively assigned as follows: heat shock protein HSP 90-β, heat shock cognate 71 kDa protein, α-enolase, cytoplasmic 1 actin (β-actin), carbonic anhydrase 2, 14-3-3 protein β/α, A, peroxiredoxin-6, and histone H2B type 1-M.

The intensity of immunoreactive bands varied according to treatment of cells. HNE-treated cells showed the darkest bands, and the intensity of these bands was reduced by Asc pretreatment of THP-1 cells. Control THP-1 cells or cells treated with Asc alone showed no or only weak staining for HNE-modified proteins (Figure 5.1B).

2-D Gel electrophoresis, Western blotting and MALDI tandem mass spectrometry of HNE-protein adducts. Since the SDS-PAGE did not show a clear separation of some proteins, a 2-DE separation was performed followed by Western blotting to determine the identity of the HNE-adducted proteins with higher confidence (Figure 5.2). Anti-HNE immunoreactive spots in the Western

were aligned with corresponding Coomassie-stained spots from the 2-D gel and the respective protein spots were excised, subjected to tryptic digestion and protein identities established by nanoLC-MALDI-MS/MS analysis. The following proteins were identified: ribonuclease inhibitor; protein disulfide-isomerase A1; tubulin beta-2C; β-actin*; 14-3-3 protein β/α; keratin, type II cytoskeletal 1; coronin-1A; stress-induced-phosphoprotein 1; α-enolase*; purine nucleoside phosphorylase; and carbonic anhydrase 2*. β-actin and α-enolase were found in 4 spots and 2 spots, respectively, implying post-translational modification or different protein isoforms. Four of the 11 immunoreactive proteins were also detected in the 1-DE blot and these are marked by an asterisk (see also Table 1). However, even with the 2-DE approach, the identification of the HNE-modified proteins remains putative at best due to the known difficulties associated with gel-based approaches that are based on matching gel spots detected by a visual staining method with spots detected on an immunoblot. Visual staining methods are commonly biased toward the most abundant proteins while immunochemical detections on membranes are exquisitely sensitive and specific. The limitation of the 2D gel-based approach becomes apparent by comparing the shapes of some of the protein spots detected on the immunoblot with the supposedly corresponding spots on the 2D gel (Figure 5.2). Discrepancies in the shape of some of the protein spots detected by Western blotting and Coomassie-stained 2D-gel may indicate that, with the 2D-PAGE protocol used in this study, separation of the cellular protein mixture into a single protein per gel spot was not

consistently achieved. Consequently, LC-MS/MS-based analyses of tryptic peptides extracted from gel spots containing multiple proteins are skewed towards identifying preferentially the most abundant protein(s). For that reason, unambiguous identification of HNE-modified proteins relies on the detection of the HNE-peptide adduct and the site-specific localization of the residue modified by the lipid aldehyde.

Detection and characterization of ARP-labeled peptides by LC-MS/MS analysis. Employing the ARP-labeling strategy, enrichment and LC-MS/MS analysis, 18 peptides belonging to 16 proteins were identified with ARP-HNE modifications to distinct cysteine or histidine residues (Cys, His with asterisk, Table 1). Ten peptides were detected and characterized using the LTQ-FT mass spectrometer, one peptide was identified exclusively by MALDI-TOF/TOF tandem mass spectral analysis and seven peptides were detected and sequenced by both instruments. Fourteen of the identified peptides contain a Michael-type adduct of HNE to cysteine residues while the remaining four have Michael-type adducts to histidine residues. The four peptides containing modified histidine residues were only detected by the LTQ-FT mass spectrometer. Annotated tandem mass spectra for the peptides identified with the ARP-HNE modification are available in the supporting information (Figures SC1-SC25).

Identification of post-translationally modified peptides in targeted proteomics approach remains a challenging undertaking. Peptides containing PTMs often have complex or atypical fragmentation patterns, and although traditional proteomics search engines, such as Mascot, include the ability to search for PTMs, they often struggle to assign peaks resulting from neutral loss of the PTMs, or fail to annotate non-peptide ions related to the modification. The tandem mass spectra of ARP-labeled peptides display several unique characteristics that, although generate problems for the database search software used in this study, aid in the manual inspection to unequivocally identify ARP-labeled peptides. Diagnostic ions frequently observed in our laboratory include the ions observed at m/z 227.1 (F1) and m/z 332.2 ($[ARP+H]^+$) which originate from the ARP tag. Additionally, ions resulting from the loss of the ARP and HNE-ARP moiety from the precursor ion were observed. Several fragmentation pathways seem to be possible. We noticed that the charge state of the precursor ion, the ionization technique and CID conditions used may at least partly determine which of the fragmentation mechanisms prevails (Supplementary Material, Figure SC26). In the MALDI-MS/MS analyses, the precursor ions are singly charged with the charge residing primarily on the C-terminal Lys or Arg residue, therefore we observe ions resulting from the neutral loss of ARP (-331.2 Da) and ARP-HNE (-469 Da) from the precursor ion. In the ESI-MS/MS analyses reported the precursor ions were multiply charged, allowing for a higher probability that a protonation site resides on the ARP tag. Therefore,

in the ESI-MS/MS spectra of ARP-labeled peptides we observed frequently ions resulting from a) the loss of protonated ARP (-332.2 Da) and b) the loss of protonated ARP followed by the neutral loss of the dehydrated HNE moiety (additional loss of -138.10 Da) from the multiply charged precursor ion. This proposed mechanism would account for the reduction of the charge state observed for these diagnostic ions compared to the precursor ion used for the CID experiment (Supporting Information, Figure SC26). Occasionally, ESI-MS/MS spectra did also display ion peaks which indicate neutral loss of the ARP-HNE moiety from the precursor ion, e.g. the $[M+3H-(ARP-HNE)]^{3+}$ ion at m/z 668.3 in the ESI-MS/MS spectrum of the $[M+3H]^{3+}$ ion of the dynein light chain peptide (Figure SC13).

Figure 5.3 depicts tandem mass spectra of the tubulin α-1B peptide encompassing the partial sequence 340-352 in which Cys-347 was identified as being modified by the ARP-HNE moiety. The low energy CID fragment ion mass spectrum of the doubly protonated molecular ion of the HNE-modified peptide SIQFVDWC*PTGFK obtained with the linear ion trap of the LTQ-FT instrument is depicted in Figure 5.3A. In this peptide, Cys-347 was identified as being modified by the ARP-HNE moiety. Modification of the cysteine residue results in a m/z-difference of 572.2 Th between the y_5 (m/z 549.3) and y_6 ion (m/z 1121.4). Unequivocal assignment of the site of modification was further supported by additional y-type fragment ions, y_6 and higher, and b-type fragment ions, b_8 (m/z

1448.5) and b_{12} (m/z 1850.6), which show a mass shift of 469.2 Da due to the ARP-HNE modification. In addition, the singly charged ions at m/z 1665.6 and 1527.5 were characteristic for the loss of a protonated ARP tag (-332 Da) and the loss of the protonated ARP tag followed by neutral loss of the dehydrated HNE moiety (-470 Da) from the doubly charged precursor ion, respectively. The facile loss of the protonated ARP tag and subsequent loss of the dehydrated HNE moiety were frequently observed in tandem mass spectra acquired with the LTQ for peptides containing a HNE-modified cysteine residue. The use of the LTQ-FT mass spectrometer enabled exact mass measurements of modified peptides with high resolution which significantly increased the confidence of the peptide assignments. For example, high resolution mass analysis of the $[M+2H]^{2+}$ ion of the HNE-modified peptide SIQFVDWC*PTGFK enabled the observation of the monoisotopic ion at m/z 998.9862 (expected m/z 998.9866) with an accuracy of 0.4 ppm (Supplemental information, Figure SC1).

Figure 5.3B depicts the MALDI-TOF/TOF tandem mass spectrum of the same HNE-modified peptide, SIQFVDWC*PTGFK, obtained by high energy (1 keV) collision-induced fragmentation of the singly protonated molecular ion ($[M+H]^{+}$, m/z 1997.1). HNE adduction of the Cys residue in this peptide is confirmed by the y_6, y_7 and y_8 ions observed at m/z 1121.7, 1307.7 and 1422.8, respectively. Neutral loss of the ARP-HNE moiety (-469.2 Da) from the singly protonated precursor ion results in the ion at m/z 1527.9. Additional fragment ions related to

the ARP label were observed at m/z 227.1 (ARP-F1) and 332.2 ($[ARP+H]^+$). Fragmentation of the oxime bond (-O-N=CH-) resulted in the formation of the fragment ion F_2 at m/z 1681.0.

As an example of a tandem mass spectrum that permitted the identification of a His residue as the site of ARP-HNE modification, the low energy CID-MS/MS spectrum of the peptide, FSH*EEIAMATVTALR, is shown in Figure 5.4A. This peptide represents the partial sequence 244-258 of fructose-bisphosphate aldolase A containing His-246 modified by HNE and ARP. CID was performed on the triply protonated molecular ion $[M+3H]^{3+}$ (m/z 715.7). The resulting tandem mass spectrum was dominated by doubly charged b-type ions, b_5-b_7, b_9-b_{11}, b_{13} and b_{14}, which indicated that the ARP-HNE modification is located in the N-terminal region of the peptide. Because there is only one nucleophilic residue in this region we concluded that the His residue must be the site of modification by the ARP-HNE moiety. This assignment was in line with the observed y-type ions, y_3-y_6, y_8, and y_9, which were observed at the predicted m/z values without a mass shift related to the modification. In addition, the exact mass determination of the triply charged molecular ion $[M+3H]^{3+}$ with m/z 715.7001 (m/z_{calc} 715.6992; accuracy Δ(m/z) 1.2 ppm) using the FT-MS capabilities of the LTQ-FT instrument supported the identification of this HNE-peptide adduct with high confidence.

Discussion

Protein carbonylation may contribute to the cytotoxicity of HNE observed in THP-1 cells. We have chosen for the present study an exposure concentration of 100 μM, because our previous work indicated that at this concentration HNE triggers apoptotic and necrotic processes associated with elevated levels of protein carbonyls as determined by anti-DNP ELISA (27). Indeed, exposure of THP-1 cells at 100 μM HNE resulted in the formation of covalent protein-HNE adducts that were readily detected by anti-HNE immunostaining (Figure 5.1B). The attenuating effect of Asc on protein-HNE adduct levels was demonstrated by the lower intensity of the HNE-positive bands (Figure 5.1B). Thus, it would be conceivable that Asc attenuates HNE toxicity by preventing or inhibiting protein-HNE adduct formation. Our previous work has indicated a possible route for the observed diminishing effect of Asc on protein carbonylation. Asc promotes detoxification by enhancing HNE metabolite formation and their cellular export. Rapid inactivation of the electrophilic properties of HNE by glutathionylation and subsequent elimination of the respective HNE metabolites will result in lower cellular HNE levels and reduced protein-HNE adduct formation (27).

So far, only a few studies have attempted to identify protein targets of modification of HNE in complex biological systems. In our present study we combined gel-based and gel-free mass spectrometry-based approaches to detect, identify and characterize protein targets of HNE in THP-1 cells

(summarized in Table 1). Immunostaining using an anti-HNE antibody in combination with mass spectrometry enabled the tentative assignment of 18 immunoreactive proteins (12 in 1-DE and seven additional ones in 2-DE). The four immunoreactive proteins that were assigned in both methods were β-actin, α-enolase, the 14-3-3 protein β/α and carbonic anhydrase (Table 1). In the 1-DE, protein disulfide isomerase A3 co-migrated with adenylyl cyclase-associated protein 1 and vimentin, and carbonic anhydrase co-migrated with 14-3-3 protein β/α. The subsequent 2-DE analysis resolved some of the ambiguities and confirmed the 14-3-3 protein β/α and carbonic anhydrase as proteins modified by HNE.

In the current study, mass spectrometric analysis of the immunoreactive proteins resolved on 1-DE or 2-DE gels did not yield the actual amino acid residues modified by HNE. Therefore, a gel-free strategy was employed, in which the aldehyde/keto-reactive reagent, ARP, was used for the biotinylation of Michael-type protein-HNE adducts, followed by trypsin digestion and subsequent enrichment using monomeric avidin. Using this targeted approach, 18 HNE-modified peptides belonging to 16 proteins were successfully identified by LC-MS/MS analysis, enabling the assignment of the ARP-HNE modification to specific Cys or His residues (Table 1). Of the 16 ARP-HNE modified proteins identified, four matched with proteins tentatively detected in the 1D and 2D immunoblotting analyses, namely β-actin, vimentin, adenylyl cyclase associated

protein 1 and tubulin α-1B. These proteins are all highly abundant structural proteins and it is therefore not too surprising that these proteins were identified by different approaches.

In this study THP-1 cells were exposed to 100 μM HNE. In our previous study, this HNE concentration has been shown to induce apoptosis and necrosis in this cell line (27). At 100 μM, HNE may induce necrosis and apoptosis by adducting to proteins that are involved in the regulation of cell death or are important for cell survival. We found proteins associated with the cytoskeleton comprised the major group of HNE-modified proteins which are important for cellular survival (30), namely β-actin, vimentin, α-actinin-1, α-actinin-4, cofilin-1, F-actin-capping protein, one of the dynein light chains and tubulin α-1B chain. All of these proteins were detected using the ARP labeling strategy in combination with tandem mass spectrometry and as site of adduction distinct Cys and His residues were identified (Table 1). Additional cytoskeletal proteins were found by Western blotting analysis using a monoclonal anti-HNE antibody and these were tentatively assigned as: coronin-1A, type II cytoskeletal 1 keratin and tubulin beta-2C. However, the site of HNE modification in these immunoreactive proteins was not detected by mass spectrometry.

Cytoskeletal proteins are important in maintaining cell shape and intracellular transport. These proteins contribute to cellular organization and differentiation.

Agents that specifically disrupt the cytoskeleton have been shown to stimulate apoptosis (31). β-Actin is a component of the actin cytoskeleton and serves as a mediator of internal cell motility (32). β-Actin is a target of carbonylation in Alzheimer's disease brain (4). Alpha-actinin binds to actin filaments and associates with cytoskeletal and signaling molecules, cytoplasmic domains of transmembrane receptors and ion channels (33). Cofilins promote cytoskeletal dynamics by depolymerizing actin filaments (34). Coronins are conserved actin binding proteins that help regulate cellular processes associated with cytoskeletal remodeling, endocytosis and cell motility (35). F-actin-capping proteins bind to the fast growing ends of actin filaments (barbed end) thereby blocking the growth of the actin filament at the barbed ends (36). Depolymerization of F-actin and degradation of intermediate filaments has been shown to be an important in the early stages of apoptosis (37). Vimentin is an intermediate filament protein and found in THP-1 derived macrophages (38). Tubulin α and tubulin β are components of the microtubule cytoskeleton.

Changes in cytoskeletal proteins could be one of the molecular bases for morphological changes occurring in the cell induced by oxidative stress and toxic chemicals (5). The adduction of Cys residues in α- and β-tubulins may have important implications on the structure of the microtubule cytoskeleton. Microtubules are in a dynamic state, alternately assembling and disassembling on the basis of the changing needs of the cell. Apoptotic phenomena, such as

cell rounding, contraction and compaction of cellular organelles, require microtubule reorganization (31). Microtubule assembly can be impaired by HNE and destruction of microtubule structure has been observed in certain cells exposed to HNE (39). Modification of tubulin at Cys residues by lipid aldehydes could lead to the inhibition of polymerization because Cys residues are critical for tubulin polymerization (40). α-Tubulin has been identified as a major target of oxidative modification by HNE in rat primary neuronal cells, PC12 cells, and rat fibroblasts (39).

Two proteins of the glycolytic pathway, α-enolase and fructose-bisphosphate aldolase A (aldolase A), were identified by anti-HNE 2D Western blot and LC ESI-MS/MS analysis, respectively. In certain cancer cells glycolytic enzymes are upregulated due to the Warburg effect (41) which may at least partially explain why these proteins were identified as two of the major protein targets of HNE adduction in THP-1 cells. α-Enolase can bind cytoskeletal and chromatin structures and may serve as a cell surface plasminogen receptor and as a heat-shock protein (42). Increased carbonylation of α-enolase has been found in the brain of patients with mild cognitive impairment (43) and Alzheimer's disease (44). Several studies have identified fructose-bisphosphate aldolase (aldolase A) as a target of oxidative stress-related modifications (45, 46). However, the site of modification in aldolase A has not been previously identified. Our results suggest that His-246 is a susceptible target site for Michael-type addition by HNE. The

location of His-246, at the start of the 9th α-helix, can be seen in the protein ribbon structure of aldolase A (pdb:2ald) shown in Figure 5.4B. Aldolase A has been described of having a dual functionality as glycolytic enzyme that also interacts with monomeric or multimeric forms of actin including actin filaments (47) and the α subunit of tubulin (48).

Other proteins that were tentatively identified as targets of modification by HNE were proteins related to stress response, including heat shock proteins, protein disulfide isomerase (the A1 and A3 isoforms) and peroxiredoxin-6. Heat-shock proteins function as molecular chaperones in response to cellular stress. Protein disulfide isomerase is an endoplasmic reticulum chaperone that promotes correct disulfide formation in newly synthesized proteins and has been shown to be modified by HNE at a Cys residue at the active site of the enzyme (18). Peroxiredoxin-6, an important antioxidant protein, is at Cys-91 susceptible to modification by HNE resulting in a cross-link, involving the residues Cys-91 and Lys-209, and inactivation of the protein (49). Carbonic anhydrase, an enzyme involved in the reversible hydration of carbon dioxide and aldehydes (50), has been shown to be a major intracellular target of HNE in erythrocytes (51), ventilatory muscles (46), skeletal muscles (52) and AD brain (53).

Our ARP labeling and enrichment strategy for the mass spectrometry-based identification and characterization of HNE-adducted peptides in THP-1 cells is

analogous to the Codreanu et al. method which uses biotin hydrazide and capture with streptavidin to identify HNE-adducted proteins in human colon carcinoma RKO cells treated with 50 or 100 μM HNE (20). Codreanu et al. describe distinct adduction sites for 18 proteins. A comparison of the modification site assignments made in the RKO and the current THP-1 cell exposure studies revealed that only two HNE modification sites, namely Cys-347 in the tubulin α-1B chain and Cys-47 of the voltage-dependent anion-selective protein, were found at equivalent sequence positions in both systems. The minimal overlap between the two exposure studies suggests that the protein targets of HNE may be cell-specific and/or that there might be differences in the efficacy of the ARP/monomeric avidin method and biotin-hydrazide/streptavidin method for the analysis of protein-HNE adducts.

Prokai and coworkers introduced a solely mass spectrometry-based approach employing data-dependent and neutral loss-driven MS^3 acquisition for the selective detection and identification of HNE-modified proteins in rat brain mitochondria exposed to HNE ex vivo (54). In this study, the majority of HNE adducts were found to be on His residues. Codreanu et al. (20) and we used prior enrichment of biotin-tagged HNE adducts and subsequent mass spectrometric analysis. The majority of the HNE targets in the RKO cells were modified on cysteine residue; only one His residue was observed to be adducted to HNE (20). In the present study, the sites of Michael-type addition involved

predominately Cys residue and to a lesser degree His residues. It is not known at this time if the analytical LC-MS/MS-based strategy employed introduces a bias for which Michael-type adducts are observed. In general, it should be noted that proteomics-type analyses of protein targets of HNE adduction are commonly skewed toward highly abundant proteins. Also, HNE exposure studies of cellular systems may not necessarily reveal the protein targets of HNE formed endogenously due to the presence of ROS-generating centers and the compartmentalization of cellular systems (55).

Conclusions

The present study describes protein targets of HNE in the human monocytic cell line THP-1, a cell line which exhibits properties similar to monocyte-derived macrophages and is used for studying foam cell formation associated with atherosclerotic processes. A multifaceted strategy, involving electrophoretic, immunochemical and mass spectrometric methods, was employed to detect and identify HNE-protein adducts in THP-1 cells after exogenous exposure to HNE. Gel-based approaches in combination with immunoblotting using monoclonal anti-HNE antibodies were used to demonstrate a diminishing effect of ascorbic acid on protein modification by HNE. In addition, a chemical proteomic analysis based on the biotinylation of Michael-type HNE adducts using an aldehyde-reactive hydroxylamine-functionalized probe (aldehyde-reactive probe, ARP), enrichment and LC-MS/MS analysis enabled site-specific assignments of

Michael-type HNE adductions. A total of 16 proteins were unequivocally identified as protein-HNE adducts. HNE adduction was predominately found at Cys residues (14-times out of 18); the remaining target sites were His residues. The majority of the HNE-modified proteins were involved in cytoskeleton organization/regulation and actin binding, stress response and glycolysis. This study provides the first site-specific assignments of adduction of HNE to Cys-295 in tubulin α-1B chain, Cys-351 and Cys-499 in α-actinin-4, Cys-328 in vimentin, Cys-369 in D-3-phosphoglycerate dehydrogenase and His-246 in aldolase A.

Acknowledgement. We thank Brian Arbogast for technical assistance on the LTQ-FT instrument. This study was supported by NIH Grants R01HL081721 and R01AG025372. We acknowledge the use of the Mass Spectrometry Facility and the Cell Culture Facility of Oregon State University's Environmental Health Sciences Center (NIH Grant P30ES00210). PNNL is a multiprogram national laboratory operated by Battelle for the U.S. Department of Energy under Contract DE-AC06-76RL01830.

Supporting Information Available: Table SC1 summarizes the mass spectrometry data of proteins tentatively identified in the gel regions (Fig. 1a) that matched to the immunoreactive bands in Figure 5.1B. Table SC2 lists the mass spectrometry data of the HNE-positive protein spots assigned in the 2D blot depicted in Figure 5.2. Figures SC1 to SC25 display the annotated MS/MS

spectra of ARP-HNE-modified peptides. Figure SC26 depicts the proposed mechanisms for the CID fragmentations observed for ARP-labeled HNE-peptide adducts and proposed chemical structures of the non-peptide fragment ions characteristic for the collision-induced fragmentation of the ARP-tag. This material is available free of charge via the Internet at http://pubs.acs.org.

References

1. Esterbauer H, Schaur RJ and Zollner H: Chemistry and biochemistry of 4-hydroxynonenal, malonaldehyde and related aldehydes. Free Radic. Biol. Med. 11: 81-128, 1991.
2. Uchida K: 4-Hydroxy-2-nonenal: a product and mediator of oxidative stress. Prog. Lipid Res. 42: 318-43, 2003.
3. Chung FL, Pan J, Choudhury S, Roy R, Hu W and Tang MS: Formation of trans-4-hydroxy-2-nonenal- and other enal-derived cyclic DNA adducts from omega-3 and omega-6 polyunsaturated fatty acids and their roles in DNA repair and human p53 gene mutation. Mutat. Res. 531: 25-36, 2003.
4. Butterfield DA: Amyloid beta-peptide (1-42)-induced oxidative stress and neurotoxicity: implications for neurodegeneration in Alzheimer's disease brain. A review. Free Radic. Res. 36: 1307-13, 2002.
5. Chung WG, Miranda CL, Stevens JF and Maier CS: Hop proanthocyanidins induce apoptosis, protein carbonylation, and cytoskeleton disorganization in human colorectal adenocarcinoma cells via reactive oxygen species. Food Chem. Toxicol. 47: 827-36, 2009.
6. Forman HJ, Fukuto JM, Miller T, Zhang H, Rinna A and Levy S: The chemistry of cell signaling by reactive oxygen and nitrogen species and 4-hydroxynonenal. Arch. Biochem. Biophys. 477: 183-95, 2008.
7. West JD and Marnett LJ: Endogenous reactive intermediates as modulators of cell signaling and cell death. Chem. Res. Toxicol. 19: 173-94, 2006.
8. Carbone DL, Doorn JA, Kiebler Z, Sampey BP and Petersen DR: Inhibition of Hsp72-mediated protein refolding by 4-hydroxy-2-nonenal. Chem. Res. Toxicol. 17: 1459-67, 2004.
9. Ferrington DA and Kapphahn RJ: Catalytic site-specific inhibition of the 20S proteasome by 4-hydroxynonenal. FEBS Lett. 578: 217-23, 2004.
10. Choksi KB, Boylston WH, Rabek JP, Widger WR and Papaconstantinou J: Oxidatively damaged proteins of heart mitochondrial electron transport complexes. Biochim. Biophys. Acta 1688: 95-101, 2004.
11. Sayre LM, Lin D, Yuan Q, Zhu X and Tang X: Protein adducts generated from products of lipid oxidation: focus on HNE and one. Drug Metab. Rev. 38: 651-75, 2006.
12. Poli G, Schaur RJ, Siems WG and Leonarduzzi G: 4-hydroxynonenal: a membrane lipid oxidation product of medicinal interest. Med. Res. Rev. 28: 569-631, 2008.
13. Romero FJ, Bosch-Morell F, Romero MJ, Jareno EJ, Romero B, Marin N and Roma J: Lipid peroxidation products and antioxidants in human disease. Environ. Health Perspect. 106 Suppl 5: 1229-34, 1998.

14. Lee HP, Zhu X, Zhu X, Skidmore SC, Perry G, Sayre LM, Smith MA and Lee HG: The essential role of ERK in 4-oxo-2-nonenal-mediated cytotoxicity in SH-SY5Y human neuroblastoma cells. J. Neurochem. 108: 1434-41, 2009.
15. Poon HF, Calabrese V, Scapagnini G and Butterfield DA: Free radicals and brain aging. Clin. Geriatr. Med. 20: 329-59, 2004.
16. Toroser D, Orr WC and Sohal RS: Carbonylation of mitochondrial proteins in Drosophila melanogaster during aging. Biochem. Biophys. Res. Commun. 363: 418-24, 2007.
17. Carbone DL, Doorn JA, Kiebler Z, Ickes BR and Petersen DR: Modification of heat shock protein 90 by 4-hydroxynonenal in a rat model of chronic alcoholic liver disease. J. Pharmacol. Exp. Ther. 315: 8-15, 2005.
18. Carbone DL, Doorn JA, Kiebler Z and Petersen DR: Cysteine modification by lipid peroxidation products inhibits protein disulfide isomerase. Chem. Res. Toxicol. 18: 1324-31, 2005.
19. Chavez J, Wu J, Han B, Chung WG and Maier CS: New role for an old probe: affinity labeling of oxylipid protein conjugates by N'-aminooxymethylcarbonylhydrazino d-biotin. Analytical Chemistry 78: 6847-54, 2006.
20. Codreanu SG, Zhang B, Sobecki SM, Billheimer DD and Liebler DC: Global analysis of protein damage by the lipid electrophile 4-hydroxy-2-nonenal. Mol. Cell. Proteomics 8: 670-80, 2009.
21. Han B, Stevens JF and Maier CS: Design, synthesis, and application of a hydrazide-functionalized isotope-coded affinity tag for the quantification of oxylipid-protein conjugates. Anal. Chem. 79: 3342-54, 2007.
22. Mirzaei H and Regnier F: Affinity chromatographic selection of carbonylated proteins followed by identification of oxidation sites using tandem mass spectrometry. Anal. Chem. 77: 2386-92, 2005.
23. Rauniyar N, Stevens SM, Prokai-Tatrai K and Prokai L: Characterization of 4-hydroxy-2-nonenal-modified peptides by liquid chromatography-tandem mass spectrometry using data-dependent acquisition: neutral loss-driven MS3 versus neutral loss-driven electron capture dissociation. Anal. Chem. 81: 782-9, 2009.
24. Roe MR, Xie H, Bandhakavi S and Griffin TJ: Proteomic mapping of 4-hydroxynonenal protein modification sites by solid-phase hydrazide chemistry and mass spectrometry. Anal. Chem. 79: 3747-56, 2007.
25. Vila A, Tallman KA, Jacobs AT, Liebler DC, Porter NA and Marnett LJ: Identification of protein targets of 4-hydroxynonenal using click chemistry for ex vivo biotinylation of azido and alkynyl derivatives. Chemical research in toxicology 21: 432-44, 2008.
26. Banka CL, Black AS, Dyer CA and Curtiss LK: THP-1 cells form foam cells in response to coculture with lipoproteins but not platelets. J. Lipid Res. 32: 35-43, 1991.

27. Miranda CL, Reed RL, Kuiper HC, Alber S and Stevens JF: Ascorbic acid promotes detoxification and elimination of 4-hydroxy-2(E)-nonenal in human monocytic THP-1 cells. Chemical research in toxicology 22: 863-74, 2009.
28. Chung WG, Miranda CL and Maier CS: Detection of carbonyl-modified proteins in interfibrillar rat mitochondria using N'-aminooxymethylcarbonylhydrazino-D-biotin as an aldehyde/keto-reactive probe in combination with Western blot analysis and tandem mass spectrometry. Electrophoresis 29: 1317-24, 2008.
29. Chung WG and Maier CS: Mass Spectrometry-based Identification and Characterization of Oxylipid-Protein Conjugates. In: Current Protocols in Toxicology. 2008, p Unit 17.9.
30. Papakonstanti EA and Stournaras C: Cell responses regulated by early reorganization of actin cytoskeleton. FEBS Lett. 582: 2120-7, 2008.
31. Raffray M and Cohen GM: Apoptosis and necrosis in toxicology: a continuum or distinct modes of cell death? Pharmacol. Ther. 75: 153-77, 1997.
32. Hunter T and Garrels JI: Characterization of the mRNAs for alpha-, beta- and gamma-actin. Cell 12: 767-81, 1977.
33. Sjoblom B, Salmazo A and Djinovic-Carugo K: Alpha-actinin structure and regulation. Cell. Mol. Life Sci. 65: 2688-701, 2008.
34. Fialkow L, Wang Y and Downey GP: Reactive oxygen and nitrogen species as signaling molecules regulating neutrophil function. Free Radic. Biol. Med. 42: 153-64, 2007.
35. Gandhi M and Goode BL: Coronin: the double-edged sword of actin dynamics. Subcell. Biochem. 48: 72-87, 2008.
36. Barron-Casella EA, Torres MA, Scherer SW, Heng HH, Tsui LC and Casella JF: Sequence analysis and chromosomal localization of human Cap Z. Conserved residues within the actin-binding domain may link Cap Z to gelsolin/severin and profilin protein families. J. Biol. Chem. 270: 21472-9, 1995.
37. Bursch W, Hochegger K, Torok L, Marian B, Ellinger A and Hermann RS: Autophagic and apoptotic types of programmed cell death exhibit different fates of cytoskeletal filaments. J. Cell Sci. 113 (Pt 7): 1189-98, 2000.
38. Kang JH, Ryu HS, Kim HT, Lee SJ, Choi UK, Park YB, Huh TL, Choi MS, Kang TC, Choi SY and Kwon OS: Proteomic analysis of human macrophages exposed to hypochlorite-oxidized low-density lipoprotein. Biochim. Biophys. Acta 1794: 446-58, 2009.
39. Kokubo J, Nagatani N, Hiroki K, Kuroiwa K, Watanabe N and Arai T: Mechanism of destruction of microtubule structures by 4-hydroxy-2-nonenal. Cell Struct. Funct. 33: 51-9, 2008.
40. Stewart BJ, Doorn JA and Petersen DR: Residue-specific adduction of tubulin by 4-hydroxynonenal and 4-oxononenal causes cross-linking and inhibits polymerization. Chemical research in toxicology 20: 1111-9, 2007.
41. Unwin RD, Craven RA, Harnden P, Hanrahan S, Totty N, Knowles M, Eardley I, Selby PJ and Banks RE: Proteomic changes in renal cancer and co-

ordinate demonstration of both the glycolytic and mitochondrial aspects of the Warburg effect. Proteomics 3: 1620-32, 2003.
42. Pancholi V: Multifunctional alpha-enolase: its role in diseases. Cell. Mol. Life Sci. 58: 902-20, 2001.
43. Reed T, Perluigi M, Sultana R, Pierce WM, Klein JB, Turner DM, Coccia R, Markesbery WR and Butterfield DA: Redox proteomic identification of 4-hydroxy-2-nonenal-modified brain proteins in amnestic mild cognitive impairment: insight into the role of lipid peroxidation in the progression and pathogenesis of Alzheimer's disease. Neurobiol. Dis. 30: 107-20, 2008.
44. Butterfield DA, Poon HF, St Clair D, Keller JN, Pierce WM, Klein JB and Markesbery WR: Redox proteomics identification of oxidatively modified hippocampal proteins in mild cognitive impairment: insights into the development of Alzheimer's disease. Neurobiol. Dis. 22: 223-32, 2006.
45. Martinez A, Dalfo E, Muntane G and Ferrer I: Glycolitic enzymes are targets of oxidation in aged human frontal cortex and oxidative damage of these proteins is increased in progressive supranuclear palsy. J. Neural. Transm. 115: 59-66, 2008.
46. Hussain SN, Matar G, Barreiro E, Florian M, Divangahi M and Vassilakopoulos T: Modifications of proteins by 4-hydroxy-2-nonenal in the ventilatory muscles of rats. Am. J. Physiol. Lung Cell. Mol. Physiol. 290: L996-1003, 2006.
47. Wang J, Morris AJ, Tolan DR and Pagliaro L: The molecular nature of the F-actin binding activity of aldolase revealed with site-directed mutants. J. Biol. Chem. 271: 6861-5, 1996.
48. Volker KW and Knull H: A glycolytic enzyme binding domain on tubulin. Arch. Biochem. Biophys. 338: 237-43, 1997.
49. Roede JR, Carbone DL, Doorn JA, Kirichenko OV, Reigan P and Petersen DR: In vitro and in silico characterization of peroxiredoxin 6 modified by 4-hydroxynonenal and 4-oxononenal. Chemical research in toxicology 21: 2289-2299, 2008.
50. Pocker Y and Dickerson DG: The catalytic versatility of erythrocyte carbonic anhydrase. V. Kinetic studies of enzyme-catalyzed hydrations of aliphatic aldehydes. Biochemistry 7: 1995-2004, 1968.
51. Uchida K, Hasui Y and Osawa T: Covalent attachment of 4-hydroxy-2-nonenal to erythrocyte proteins. J. Biochem. 122: 1246-51, 1997.
52. Chen CN, Ferrington DA and Thompson LV: Carbonic anhydrase III and four-and-a-half LIM protein 1 are preferentially oxidized with muscle unloading. J. Appl. Physiol. 105: 1554-61, 2008.
53. Sultana R, Boyd-Kimball D, Poon HF, Cai J, Pierce WM, Klein JB, Merchant M, Markesbery WR and Butterfield DA: Redox proteomics identification of oxidized proteins in Alzheimer's disease hippocampus and cerebellum: an approach to understand pathological and biochemical alterations in AD. Neurobiol. Aging 27: 1564-76, 2006.

54. Stevens SM, Jr., Rauniyar N and Prokai L: Rapid characterization of covalent modifications to rat brain mitochondrial proteins after ex vivo exposure to 4-hydroxy-2-nonenal by liquid chromatography-tandem mass spectrometry using data-dependent and neutral loss-driven MS3 acquisition. J. Mass Spectrom. 42: 1599-605, 2007.
55. Taylor SW, Fahy E, Murray J, Capaldi RA and Ghosh SS: Oxidative post-translational modification of tryptophan residues in cardiac mitochondrial proteins. J. Biol. Chem. 278: 19587-90, 2003.

Table 5.1 - Summary of THP-1 proteins modified by Michael-type adduction of HNE based on tandem mass spectral data (MS/MS), proteins that are putative (based on anti-HNE 2D blots) and tentative (based on anti-HNE 1D blots) targets of HNE modifications. Proteins marked by $ and #, respectively, co-migrated in the 1D GE analysis. LTQ-FT: tandem mass spectral data acquired with the linear ion trap of the ESI LTQ-FT system; TOF/TOF: tandem mass spectral data obtained with the MALDI TOF/TOF instrument. Biological and functional assignments were made on the basis of information from the NCBI (www.ncbi.nlm.nih.gov/Pubmed) and the UniProt Knowledgebase (http: http://www.uniprot.org) websites.

Protein (Swiss Prot ID, residue modified if available)	**ARP-HNE Modified Peptides (modified residue)**	**MS/MS**	**2D**	**1D**
Proteins linked to cytoskeleton structure, organization and regulation				
α-actinin-1(ACTN1_Human)	IC*DQWDNLGALTQK (Cys-480)	LTQ-FT		
α-actinin-4 (ACTN4_Human)	IC*DQWDALGSLTHSR (Cys-499)	LTQ-FT TOF/TOF		
	C*QLEINFNTLQTK (Cys-351)	LTQ-FT		
Adenylyl cyclase associated protein 1 (CAP1_Human)$^{\$}$	ALLVTASQC*QQPAENK (Cys-93)	LTQ-FT		x
β-actin (ACTB_Human)	H*QGVM^{ox}VGM^{ox}GQK (His-40)	LTQ-FT	x	x
Cofilin 1 (COF1_Human)	HELQANC*YEVKDR (Cys-139)	LTQ-FT TOF/TOF		
Coronin-1A (COR1A_Human)			x	
Dynein light chain Tctex-type 3 (DYLT3_Human)	H*CDEVGFNAEEAHNIVK (His-7)	LTQ-FT		

Table 5.1 (Continued)

F-actin capping protein (CAPZB_Human)	GC*WDSIHVVEVQEK (Cys-93)	LTQ-FT TOF/TOF		
Keratin, type II cytoskeletal 1 (K2C1_Human)			x	
Vimentin (VIME_Human)[$]	QVQSLTC*EVDALK (Cys-328)	LTQ-FT		x
Tubulin α-1B chain (TBA1B_Human)	SIQFVDWC*PTGFK (Cys-347)	LTQ-FT TOF/TOF		x
	AYHEQLSVAEITNAC*FEPANQMVK (Cys295)	LTQ-FT		
Tubulin β-2C (TBB2C_Human)			x	
Proteins associated with stress and immune responses				
Heat shock protein HSP90β (HSB90B_Human)				x
Heat shock protein 71kDa (HSP7C_Human)				x
Peroxiredoxin-6 (PRDX6_Human)				x
Protein disulfide isomerase A1 (PDIA1_Human)			x	
Protein disulfide isomerase A3 (PDIA3_Human)[$]				x
Purine nucleoside phosphorylase (PNPH_Human)			x	

Table 5.1 (Continued)

SAM domain and HD domain binding protein (MOP-5) (SAMH1_Human)	NPIDHVSFYC*K (Cys-522)	TOF/TOF		
Stress-induced-phosphoprotein 1 (STIP1_Human)			x	
Proteins involved in glycolysis				
Fructose-bisphosphate aldolase A (ALDOA_Human)	FSH*EEIAMATVTALR (His-246)	LTQ-FT		
α-Enolase (ENOA_HUMAN)			x	x
Proteins involved in other metabolic processes				
Carbonic anhydrase (CAH2_Human)[#]			x	x
D-3-phosphoglycerate dehydrogenase (SERA_Human)	NAGNC*LSPAVIVGLLK (Cys-369)	LTQ-FT		
Proteins involved in (negative) regulation of translation and RNA binding				
Plasminogen activator inhibitor 1 RNA-binding protein (PAIR_Human)	PGHLQEGFGC*VVTNR (Cys-11)	LTQ-FT TOF/TOF		

Table 5.1 (Continued)

Ribonuclease inhibitor (RINI_Human)			x	
Signal recognition particle 9 kDa protein (SRP09_Human)	VTDDLVC*LVYK (Cys-48)	LTQ-FT TOF/TOF		
Others				
14-3-3 protein β/α (1433B_Human)[#]			x	x
Histone H2B type 1-M (H2B1M_Human)				x
Leucine-rich repeat-containing protein 59 (LRC59_Human)	RH*EILQWVLQTDSQQ (His-294)	LTQ-FT		
Voltage-dependent anion-selective channel protein 2 (VDAC2_Human)	SC*SGVEFSSGSSNTDTGK (Cys-47)	LTQ-FT TOF/TOF		

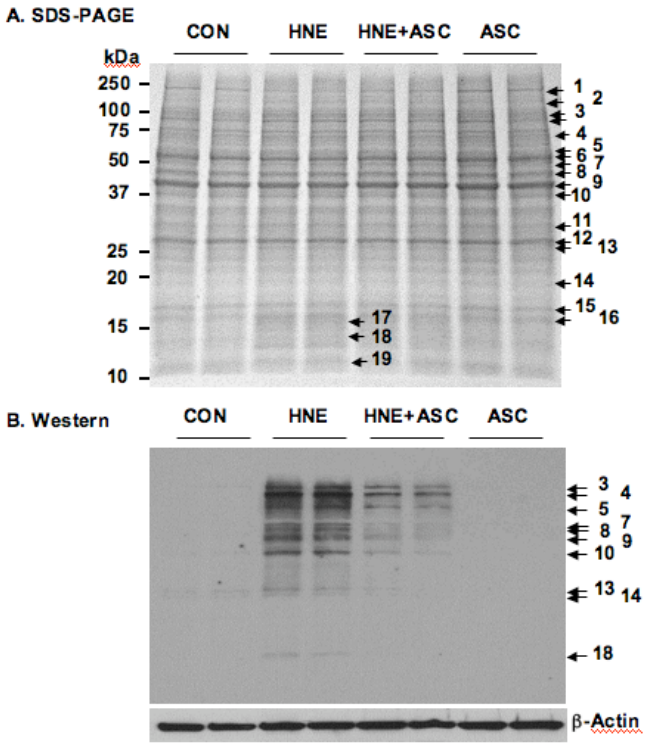

Figure 5.1 - SDS-PAGE (A) and corresponding Western blot probed with monoclonal anti-HNE antibody (B) of cell lysates from THP-1 cells pretreated with 0 or 1 mM ascorbic acid for 18 h before exposure to 0 or 0.1 mM HNE for 3 h. The proteins were tentatively identified as follows: 1: Myosin-9 (MYH9-Human, MW 226,392); 2: ATP-citrate synthase (ACLY_Human, MW 120,762); 3: Heat shock protein HSP 90-β (HS90B_Human, MW 83,212); 4: Heat shock cognate 71 kDa protein (HSP7C_Human, MW 70,854); 5-1: Protein disulfide-isomerase precursor (PDIA1_Human, MW 57,081); 5-2:Pyruvate kinase isomerase M1/M2 (KPYM_Huamn, MW 57,900); 5-3: 60 kDa heat shock protein (CH60_Human, MW 61,016); 6-1: Protein disulfide isomerase A3 (PDIA3_Human, MW 56,747); 6-2: Adenylyl cyclase-associated protein 1 (CAP1_Huamn, MW 51,823); 6-3: Vimentin (VIME_Human, MW 53,619); 7: Tubulin α-1B (TBA1B_Human, MW 50,120); 8: α-Enolase (ENOA_Human, MW 47,139); 9: β-Actin (ACTB_Human, MW 41,710); 10: Fructose-bisphosphate aldolase A (ALDOA_Human, 39,395); 11: Voltage-dependent anion selective channel protein (VDAC1_Human, MW 30,754); 12-1: Carbonic anhydrase 2(CAH2_Human, MW 22,298); 12-2: 14-3-3 protein β/α (1433B_Human, MW 28,065); 13: Peroxiredoxin-6 (PRDX6_Human, MW 25,019); 14: 60S ribosomal protein L18a (RL18A_Human, MW 20,749); 15: Histone H3.1t (H31T_Human, MW 15,499); 16,17: Histone H2B type 1-M (H2B1M_Human, MW 13,981); 18: Histone H2A type 2-C (H2A2C_Human, MW 13,980); 19: Histone 4 (H4_Human, MW 11,360).

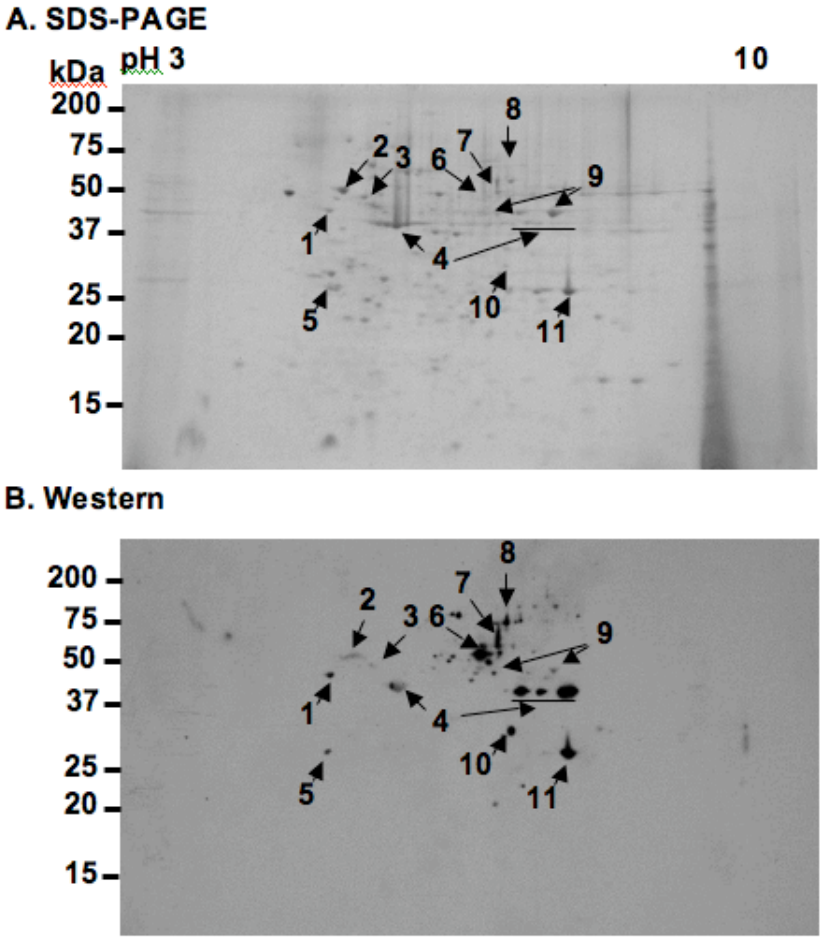

Figure 5.2 - Coomassie Blue G250-stained gel (A) after 2-dimensional electrophoresis of HNE-treated THP-1 cells and the parallel Western blot (B) probed with anti-HNE IgG. The identities of the spots are as follows: 1, Ribonuclease inhibitor (RINI_Human); 2, Protein disulfide-isomerase* (PDIA1_Human); 3, Tubulin beta-2C (TBB2C_Human); 4, β-Actin* (ACTB_Human); 5, 14-3-3 protein β/α* (1433B_Human); 6, Keratin, type II cytoskeletal 1 (K2C1_Human); 7, Coronin-1A (COR1A_Human); 8, Stress-induced-phosphoprotein 1 (STIP1_Human); 9, α-enolase (ENOA_Human)*; 10, Purine nucleoside phosphorylase (PNPH_Human); and 11, Carbonic anhydrase 2 (CAH2_Human)*. Proteins marked with asterisks (*) were also detected by anti-HNE immunostaining on the 1-D blot (Figure 1B).

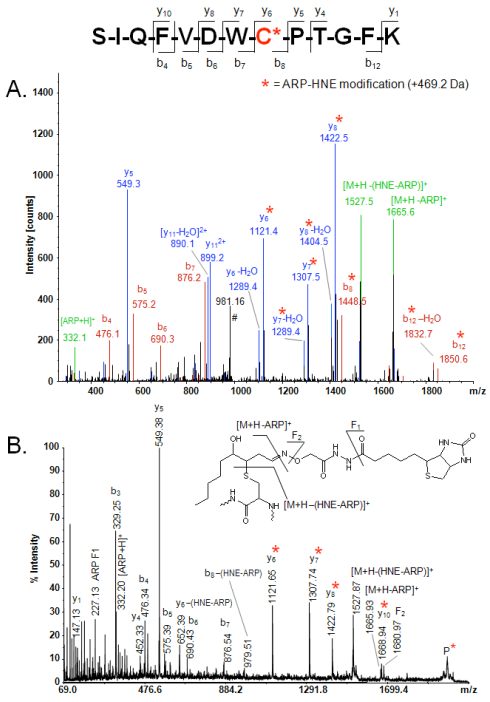

Figure 5.3 - Tandem mass spectral analysis of the ARP-labeled HNE-modified peptide SIQFVDWC*PTGFK from tubulin α-1B chain. **A.** ESI-MS/MS spectrum of its doubly protonated precursor ion, $[M+2H]^{2+}$ (m/z 999.0) obtained with the linear ion trap of the LTQ-FT mass spectrometer. The peak at m/z 981.2 (marked with "#") indicates neutral loss of two H_2O molecules from the doubly protonated precursor ion. The prominent ions with m/z 1665.6 and 1527.5 reflect loss of the protonated ARP tag and loss of the protonated ARP tag followed by a neutral loss of the dehydrated HNE moiety, respectively, from the doubly protonated precursor ion. Fragment ions marked with an asterisk (*) retained the ARP-HNE moiety during collision-induced fragmentation and allowed the unequivocal localization of the ARP-HNE moiety to the Cys residue at position 8 in this peptide. FTICR full-scan mass analysis of the doubly protonated molecular ion ($[M+2H]^{2+}$) yielded *m/z* 998.9862 (m/z_{calc} 998.9866 (monoisotopic ion); accuracy Δ(m/z) -0.4 ppm) and supported the identification of this peptide as the partial sequence encompassing the residues 340 to 352 of tubulin α-1B chain. **B.** MALDI-MS/MS spectrum of the same ARP-labeled HNE-peptide adduct, SIQFVDWC*PTGFK. High-energy collision-induced fragmentation of the singly protonated precursor ion, $[M+H]^+$ at m/z 1997.1 (marked with P), resulted in b- and y-type fragment ions. The short y-fragment ion series, y_6-y8 and y10, highlighted by an asterisk (*), confirmed the localization of the ARP-HNE modification to the Cys residue at position 8. P, precursor ion; F1 and F2, non-peptide fragment ions related to the ARP-tag (insert and Figure SC26)

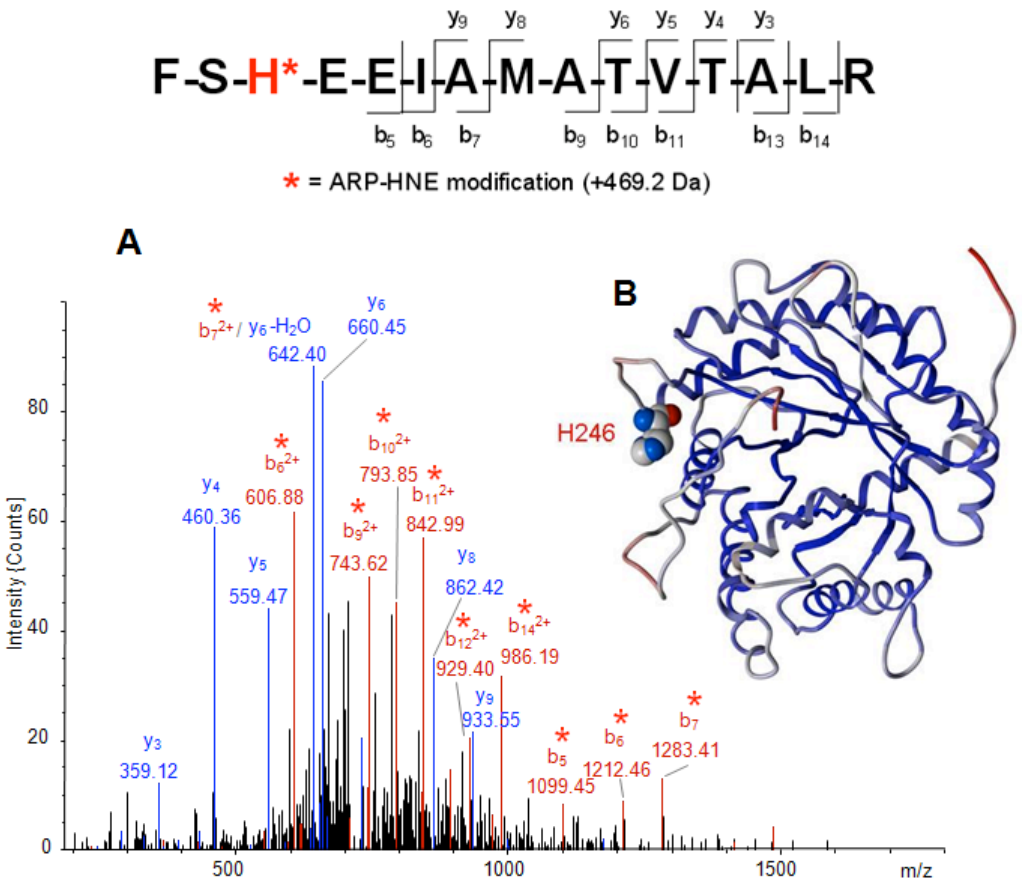

Figure 5.4 - A. Tandem mass spectral analysis of the ARP-labeled HNE-modified peptide, FSH*EEIAMATVTALR, from fructose-bisphosphate aldolase A. The triply protonated molecular ion $[M+3H]^{3+}$ (m/z 715.7) was used for collision-induced fragmentation in the linear ion trap of the LTQ-FT MS instrument. The ion peak marked with (#) at m/z 703.8 corresponds to the 'neutral loss'-derived ion $[M+3H - 2H_2O]^{3+}$. The b-type fragment ions marked with an asterisk (*) enabled the localization of the ARP-HNE moiety to the His residue at position 3 of this peptide, which corresponds to the partial sequence 244-258 of aldolase A (ALDOA_Human). Full-scan FTICR analysis yielded for the monoisotopic $[M+3H]^{3+}$ ion m/z 715.7001 (m/z_{calc} 715.6992; accuracy $\Delta(m/z)$ 1.2 ppm). **B.** Crystal structure of fructose-bisphosphate aldolase A (pdb:2ald) with the protein backbone displayed as ribbon and colored according to the B-factors reported for the structure pdb:2ald. The residue His-246, which was identified as site of the ARP-HNE modification, is displayed in CPK style and colored by atom type with the carbon atoms in white, nitrogen in blue and oxygen in red.

Chapter 6

Characterization of α-aminoadipic and γ-glutamic semialdehydes with affinity labeling and mass spectrometry

Juan D. Chavez[a], William Bisson[b], and Claudia S. Maier[a]*

[a]Department of Chemistry, and [b]Cancer Biology Laboratory, Environmental Health Sciences Center, Oregon State University, Corvallis, Oregon 97331

Abstract

The formation of carbonyl groups in proteins is frequently used as a measure of oxidative stress. Reactive oxygen species (ROS) produced during conditions of oxidative stress, such as the hydroxyl radical, can introduce carbonyl groups into proteins by oxidizing the side chains of certain amino acids. The products alpha-aminoadipic semialdehyde (AAS) and gamma-glutamic semialdehyde (GGS) are considered major carbonylation products in oxidized proteins, resulting from the oxidation of Lys, or Arg and Pro respectively. Several analytical methods exist to measure protein carbonylation, however, most of these methods only measure changes to the global level of carbonylation and ignore details such as what proteins are being carbonylated, at what site on the protein is the carbonylation occurring, and what is the chemical nature of the carbonylation. In this report, we describe a method to label carbonylation sites in proteins with a biotinylation reagent, followed by affinity enrichment and mass spectrometric analysis. This method is able to provide complete characterization of the protein identity, site and chemical nature of the carbonylation. We identify AAS and GGS as the major carbonyl products formed during the metal-catalyzed oxidation of glyceraldehyde-3-phosphate dehydrogenase (GAPDH), locating these modifications to six specific sites on the protein. Additionally we are able to identify nine AAS modification sites to lysine residues on four different mitochondrial proteins, namely ATP synthase alpha subunit, ubiquinol

cytochrome-c-reductase core protein 2, ADP/ATP translocase 1, and ADP/ATP translocase 2. These results indicate this technique is able to provide important details about the nature of oxidative modifications to proteins, which the current commonly employed methods do not.

Introduction

The oxidative modification of proteins is widely thought to be an important factor in the etiology and progression of several diseases (1-3). Protein oxidation can take many forms including the direct oxidation of amino acid side chains by reactive oxygen species (ROS), cleavage of the peptide backbone, protein crosslinking or adduction by reactive intermediates such as α,β-unsaturated aldehydes. The formation of protein carbonyls is commonly used as a marker for assessing levels of oxidative damage to proteins. Many studies have identified α-aminoadipic semialdehyde (AAS) and γ-glutamic semialdehyde (GGS) to be major products of oxidized amino acid sidechains present in carbonylated proteins (4). Both AAS and GGS are readily formed through metal-catalyzed oxidation (MCO) reactions in vitro and in vivo. AAS is formed from the oxidative deamination of lysine residues while GGS originates from the oxidation of arginine and proline residues (scheme 1).

Some of the earliest developed, and most widely employed methods for measuring protein carbonyls rely on spectrophotometric analysis following

derivatization with thiobarbituric acid (TBARS) or 2,4-dinitrophenylhydrazine (DNPH) (5, 6). While these methods have proven useful for measuring the total levels of protein carbonyls, they lack specificity and are unable to provide information on the chemical nature of the modification or identify the amino acid residue sites where the modification occurs. Recently several new methods have been developed which overcome some of these problems. Akagawa et al. developed a technique using *p*-aminobenzoic acid (ABA) derivatization and HPLC with fluorometric detection for the quantitative analysis of AAS and GGS (7, 8). Recently Estévez et al. applied the ABA labeling in conjunction with LC-ESI-MS analysis for the analysis of AAS and GGS in food proteins (9). One limitation of the current ABA-based methods is that they rely on complete acid hydrolysis of the proteins, and therefore lose information about the site of modification.

We recently introduced a method using and aldehyde reactive probe (ARP) for the affinity labeling, enrichment, and mass spectrometric characterization of protein carbonyls (10). This method is able to identify both the amino acid site and chemical nature of carbonyl modifications to proteins. Here we describe the use of the ARP-based method for the analysis of the protein carbonyl products AAS and GGS.

Materials and Methods

Chemicals

N'-aminooxymethylcarbonyl hydrazine-D-biotin (ARP) was purchased from Dojindo Molecular Technologies Inc. (Rockville, MD). Rabbit muscle glycderaldehyde-3-phosphate dehydrogenase (GAPDH) was obtained from Sigma-Aldrich (St. Luis, MO). Pierce UltraLink® monomeric avidin was obtained from Thermo Scientific (Rockford, IL).

Metal Catalyzed Oxidation of GAPDH

GAPDH was dissolved at a concentation of 5mg/mL in a 50mM sodium phosphate buffer at pH 7.4. The Fenton reaction was carried out with a Fe^{2+} concentation of 100 μM and H_2O_2 concentration of 1mM. Alternatively the oxidation reaction was carried out with 100 μM Cu^{2+} and 1mM ascorbate. The oxidation reaction was carried out at 37°C for two hours. The sample was then transferred to a Biomax 10 KDa molecular weight cut off ultrafiltration device and washed four times with 500 μL of fresh 50mM sodium phosphate buffer. The oxidized GAPDH was then labeled with ARP at a final concentation of 5mM for one hour at room temperature. The protein sample was then was washed again with the Biomax 10 KDa ultrafiltration device as done previously. The sample was then digested for 16 hours at 37°C using a 1:50 ratio of trypsin.

ARP labeling of carbonylated proteins in rat cardiac mitochondria

Subsarcolemmal mitochondria (SSM) samples were isolated from the heart tissue of male Fisher 344 rats according to the procedures of Palmer (11) with minor modifications by Suh et al. (12). The total protein concentration was determined using the Pierce Coomassie Plus protein assay. Mitochondrial samples containing 1 mg total protein were washed twice with 50 mM sodium phosphate buffer pH 7.4. The mitochondrial membranes were disrupted by resuspending the mitocondira in 50mM sodium phosphate buffer pH 7.4 containing 1% triton x-100. The ARP labeling reaction was carried out using a concentration of 5 mM ARP for 1 hour at room temperature. Excess ARP was then removed by pelleting the remaining membrane fragments at 14,000 g for 15 minutes and transferring the supernatant to a Biomax 10 KDa ultrafiltration device and washing with fresh 50 mM sodium phosphate buffer as done previously with GAPDH. The ARP-labeled mitochondrial protein samples were then digested for 16 hours at 37^{o}C using a 1:50 ratio of trypsin in 100mM ammonium bicarbonate buffer at pH 8.3.

Affinity enrichment of ARP labeled peptides

ARP labeled peptide samples were enriched using UltraLink® monomeric avidin as previously described (13). Briefly, protein samples were added to 100 μL avidin columns and washed extensively first with 10 mM sodium phosphate, 150

mM sodium chloride pH 7.4 (PBS buffer) followed by washes with 50 mM ammonium bicarbonate pH 8.3 containing 20% methanol, to remove the non labeled peptides. The column was then washed with MilliQ H_2O to reduce the salt concentration before the ARP-labeled peptides were eluted using 0.4% formic acid, 30% acetonitrile. ARP-labeled peptide fractions were concentrated using vacuum centrifugation at stored at -80^{0}C until mass spectrometric analysis.

Mass Spectrometry

The resulting ARP enriched peptides were analyzed by LC-MS/MS using a quadrupole orthogonal time-of-flight mass spectrometer (Q-TOF Ultima Global, Micromass/ Waters, Manchester, UK) mass spectrometer equipped with a NanoAcquity UPLC system and additionally using an Applied Biosystems 4700 Proteomics Analyzer MALDI-TOF/TOF instrument coupled in an offline fashion with a Dionex/LC Packings Ultimate nano-LC system equipped with a Probot target spotter as previously published (10).

Identification of ARP-labeled oxidized peptides

Tandem mass spectrometric data generated on the Q-TOF were processed into peak list files using ProteinLynx Global Server v2.3 (Waters, Manchester, UK). MALDI-MS/MS data were processed into peak list files using the Peaks to Mascot tool in 4000 Series Explorer V3.0 (Applied Biosystems). Peak list files of the tandem mass spectrometric data were analyzed with the aid of Mascot v2.1

(Matrix Science, London, UK). The Swiss Prot database v50 (270778 sequences, 99412397 residues) and the following parameters: taxonomy rodentia (20991 sequences), ± 0.2 Da mass tolerances for the precursor and fragment ions, possibility of 3 missed proteolytic cleavage sites, with trypsin/P or semitrypsin selected as the digesting enzyme, and ARP-α-aminoadipic semialdehyde, ARP – γ-glutamic semialdehyde, and methionine oxidation (M) selected as variable modifications at the residues specified in parenthesis.

Protein Modeling.

The 3D coordinates of rabbit muscle glyceraldeyde-3-phosphate dehydrogenase (GADPH) was retrieved from the crystal structures available in the Protein Data Bank (Pdb) 1J0X (14). The structure was energetically refined in the internal coordinate space with Molsoft ICM v3.5-1p.

Calculation of B-factor and Residue Accessible Area (RAA).

The B-factor and RAA values for all residues Arginine, Lysine of the GADPH protein monomer in the tetramer conformation in the presence and in the absence of NAD+ were calculated using the program ICM v3.5-1p. The normalized B-factor values were derived from the atomic crystallographic data and the average for each fragment made of a specific string of residues was calculated (14).The atomic accessible surfaces are calculated using a faster modification of the Shrake and Rupley alogorithm (15) with a water probe radius

of 1.4 Å. The relative RAA is expressed by an integer number in a scale from 0 to 9 (0-fully buried, 9-fully exposed). The average RAA of each fragment was then normalized to the highest value obtained.

Results

Analysis of AAS and GGS in GAPDH

First we subjected GAPDH to a MCO reaction, inducing the formation of AAS and GGS. After an hour MCO reaction the carbonylated residues were labeled with the affinity reagent ARP. We then digested the labeled protein with trypsin, enriched the ARP labeled peptides using an immobilized monomeric avidin column and sequenced the peptides by LC-MS/MS analysis. Using this approach we identified six amino acid residue sites that had been oxidized to AAS or GGS and subsequently labeled with ARP, summarized in figure 6.1. These sites included Lys-3, and Lys-192 being oxidized to AAS, and Arg-11, Arg-78, Pro-122, and Pro-127 being oxidized to GGS. The modification of Lys and Arg always resulted in a tryptic missed cleavage site occurring at the modified residue, as would be expected. Both Pro oxidations occurred on the same tryptic peptide sequence spanning residues 117 to 137, however this peptide was only detected by LC-MS/MS with a single modification occurring either on Pro-122 or Pro-127 and never with both modifications occurring simultaneously on the same peptide. All of the tandem mass spectra from the identified ARP labeled,

semialdehyde modified peptides are included in the supplemental figures (SD1-SD21) in appendix D. Examination of the tandem mass spectra of the ARP labeled semialdehyde modified peptides reveled some common features, which can aid in the identification under manual inspection, however, complicate the identification by automated search algorithms such as MASCOT. The first of these features is the neutral loss of the ARP moiety from the y ion in which the ARP labeled residue is the N-terminal residue. This results in the respective y ion appearing at -331 m/z from its expected value. In some cases the neutral loss is not complete and the respective y ion also appears at the expected m/z including the mass of the ARP tag. The other two features commonly observed in the tandem mass spectra of ARP labeled peptides are the fragment ions present at m/z 227 and m/z 332. These ions originate from fragmentation of the ARP moiety, with the ion at m/z 227 resulting from fragmentation of the amide bond in ARP, while m/z 332 represents the protonated ARP ion. The structures of these ions are shown in supplemental figure SD22.

The x-ray diffraction derived crystal structure of rabbit muscle GAPDH (PDB 1j0x) was downloaded from the PDB and analyzed using Molsoft ICM v 3.5-1p. B-factor values (BF) were calculated for all Lys and Arg residues present in the tetramer form of GAPDH. Lys and Arg residues having a B-factor value of less than 45 were filtered off and the solvent accessibility values (SA) were calculated for the Lys and Arg residues with B-factors greater than 45. SA values span the

range of 0-9 with 0 corresponding to residues that are completely buried, while SA values of 9 represent residues that are totally exposed to the surrounding solvent. The results of this analysis suggest that Arg-78 (BF 69.3, SA 6) and Lys-192 (BF 48.2, SA 9) are the most susceptible residues to undergo metal catalyzed oxidation due to their relatively high flexibility (BF) and solvent accessibility (SA). Five of the six modified residues (Lys-3, Arg-11, Arg-78, Pro-122, and Pro-127) are present on the NAD domain of the protein, while Lys-192 is present on the catalytic domain figure 6.2a. The ICMpkFinder was used to locate the NAD ligand binding pocket in the tetramer form of GAPDH. Interestingly, Arg-78 and Lys-192 are both located near the entrance of the NAD binding pocket, with Lys-192 being present on a very flexible loop region which may act as a gate, opening and closing to allow or deny access to the ligand binding pocket figure 6.2b.

Analysis of ARP-labeled carbonylation sites in mitochondrial proteins

Next we employed the ARP labeling procedure to rat cardiac mitochondrial samples. ARP reacts with the naturally occurring carbonylation sites on the proteins. We then digested the protein mixture with trypsin, used immobilized monomeric avidin to enrich the ARP labeled peptides and analyzed the resulting peptide mixture by LC-MS/MS. We then used our in house Mascot server to analyze the MS/MS data searching specifically for the ARP labeled AAS and ARP labeled GGS modifications. This resulted in the identification of nine

different amino acid residue sites with the AAS modification occurring on four mitochondrial proteins. ADP/ATP translocase 1 contained six Lys residues that were oxidized to AAS and labeled with ARP. ADP/ATP translocase 2 contained a single Lys residue that was oxidized to AAS and labeled with ARP. ATP synthase α chain was identified with a single Lys residue that was oxidized to AAS and labeled with ARP. Ubiquinol cytochrome C reductase complex core protein 2 contained one Lys residue that was oxidized to AAS and labeled with ARP. These results are summarized in table 6.1. In each case the modified Lys residue resulted in a missed tryptic cleavage site.

Discussion

In this report, we have described the application of our ARP affinity labeling, enrichment and LC-MS/MS analytical method for the characterization of AAS and GGS modifications present in carbonylated proteins. By applying this method to GAPDH, which had been subjected to MCO, we identified six sites of modification. GAPDH is a key enzyme in glycolysis, playing a central role in cellular energy production. Several studies have shown that GAPDH is susceptible to oxidative stress induced damage resulting in loss of activity or degradation of the enzyme. The lipid derived aldehyde products 4-hydoxy-2-nonenal (HNE) and 4-hydroxy-2-hexenal (HHE) have been shown to modify GAPDH and trigger it's degradation (16). Oxidative stress present in mouse models of amyotrophic lateral sclerosis (ALS) has been shown to induce

conformational changes accompanied by reduction in biological activity of GAPDH (17). Additionally S-nitrosylated GAPDH has been shown to induce apoptosis in cultured cells (18). We believe that the six sites of carbonylation identified in this study, which include arginine, lysine, and proline residues, represent sites in the GAPDH molecule that are susceptible to oxidative modification during conditions of oxidative stress.

To examine the formation of AAS and GGS in vivo, we applied the ARP labeling technique to cardiac mitochondria isolated from rats. Mitochondria serve as the cellular power plants but are also known to be a major source of ROS within the cell, and are important regulators of oxidative stress (19-21). Oxidative damage to mitochondrial proteins has been implicated in a host of human ailments, including cancer, heart disease and neurological disorders (22). Employing LC-MS/MS analysis we were able to characterize nine sites of AAS modification occurring on four key mitochondrial proteins, namely ADP/ATP translocase 1 (ANT1), ADP/ATP translocase 2 (ANT2), ATP synthase α subunit (ATPA) and ubiquinol cytochrome-c-reductase core complex protein 2 (UQCR2). Interestingly, each of these proteins are involved in critical roles in mitochondrial energy production.

ADP/ATP translocase functions to transport ADP and ATP across the inner mitochondrial membrane (IMM). The abundance of ANT has been estimated to

constitute up to 10% of the inner mitochondrial membrane proteins making it the single most abundant protein in the IMM (23, 24). These residues appear to be susceptible sites to damage by ROS which could, through sterically induced conformational changes, lead to decreased activity of this membrane transport protein. In their recent study Jian Luo et al. showed that acrolein inhibits ADP/ATP translocase activity which could lead to an overall increase in the production of ROS in the mitochondria resulting in a detrimental cycle of increased oxidative stress damage (25). It has been hypothesized by Wallace that a decreased ANT activity would reduce the concentration of ADP in the mitochondrial matrix limiting ADP-dependant proton transport through complex V, which would hyperpolarize the IMM and inhibit the electron transport chain (26). An accumulation of electrons would then result in an increased production ROS and increased oxidative stress.

Two proteins from the mitochondrial electron transport chain (ETC) complexes were identified with AAS modifications. From ETC complex V, ATP synthase alpha subunit forms part of the catalytic core of the F1 complex of ATP synthase, consisting of three copies of the alpha subunit and three copies of the beta subunit. ATP synthase alpha subunit was identified with an AAS modification to Lys-175. The alpha subunit of ATP synthase has been shown to be a distinct target of oxidative stress induced damage, leading to a decrease in ATP synthase activity in the early stages of Alzheimer's disease (27). The

second protein identified, with an AAS modification to Lys-161, is ubiquinol cytochrome-c-reductase core complex protein 2 from the ETC complex III. Complex III is widely considered to be a major source of ROS within the mitochondria. Complex III contains two ROS generating centers: the Q_o center, oriented toward the intermembrane space, and the Q_i center that faces the mitochondrial matrix (28). While the core protein 2 has no catalytic activity it is required for assembly of the complex. Being in close proximity to the major sites of ROS production likely makes Lys -161 a susceptible target to oxidative damage.

Conclusions

Protein carbonylation is widely accepted as a marker of oxidative stress. Most of the commonly used methods to measure protein carbonylation only measure changes to the global levels of carbonylation with no regard to the identity of the protein, amino acid residue site, or chemical type of carbonylation occurring. AAS and GGS have been identified as major forms of carbonylation resulting from the direct oxidation of the amino acid side chains of Lys, Arg, and Pro residues by ROS. Here we've described an analytical technique using affinity labeling, enrichment and LC-MS/MS analysis, which is able to identify the carbonylated protein, as well distinguish between the different forms of carbonylation including AAS and GGS. We believe this technique is a valuable

new tool to provide critical information to researchers studying oxidative stress induced damage to proteins.

Acknowledgements

This study was supported by NIH grant R01AG025372. We acknowledge the use of the Mass Spectrometric Facility of the Environmental Health Sciences Center at Oregon State University supported in part by NIH grant P30ES00210.

Supporting Information Available

The annotated tandem mass spectra for each of the modified peptides identified in this study are available in figures SD1 to SD21 in appendix D. A diagram illustrating the neutral loss of ARP from y ions with an ARP-labeled AAS or ARP-labeled GGS residue located at the N-terminal location is displayed in figure SD22.

References

1. Berlett BS and Stadtman ER: Protein oxidation in aging, disease, and oxidative stress. J. Biol. Chem. 272: 20313-6, 1997.
2. Stadtman ER: Protein oxidation in aging and age-related diseases. Ann. N. Y. Acad. Sci. 928: 22-38, 2001.
3. Korolainen MA, Goldsteins G, Alafuzoff I, Koistinaho J and Pirttila T: Proteomic analysis of protein oxidation in Alzheimer's disease brain. Electrophoresis 23: 3428-33, 2002.
4. Requena JR, Chao CC, Levine RL and Stadtman ER: Glutamic and aminoadipic semialdehydes are the main carbonyl products of metal-catalyzed oxidation of proteins. Proc Natl Acad Sci U S A 98: 69-74, 2001.
5. Ohkawa H, Ohishi N and Yagi K: Assay for lipid peroxides in animal tissues by thiobarbituric acid reaction. Anal. Biochem. 95: 351-8, 1979.
6. Fields R and Dixon HB: Micro method for determination of reactive carbonyl groups in proteins and peptides, using 2,4-dinitrophenylhydrazine. Biochem. J. 121: 587-9, 1971.
7. Akagawa M, Sasaki D, Ishii Y, Kurota Y, Yotsu-Yamashita M, Uchida K and Suyama K: New method for the quantitative determination of major protein carbonyls, alpha-aminoadipic and gamma-glutamic semialdehydes: investigation of the formation mechanism and chemical nature in vitro and in vivo. Chem. Res. Toxicol. 19: 1059-65, 2006.
8. Akagawa M, Suyama K and Uchida K: Fluorescent detection of alpha-aminoadipic and gamma-glutamic semialdehydes in oxidized proteins. Free Radic. Biol. Med. 46: 701-6, 2009.
9. Estevez M, Ollilainen V and Heinonen M: Analysis of protein oxidation markers alpha-aminoadipic and gamma-glutamic semialdehydes in food proteins using liquid chromatography (LC)-electrospray ionization (ESI)-multistage tandem mass spectrometry (MS). J. Agric. Food Chem. 57: 3901-10, 2009.
10. Chavez J, Wu J, Han B, Chung WG and Maier CS: New role for an old probe: affinity labeling of oxylipid protein conjugates by N'-aminooxymethylcarbonylhydrazino d-biotin. Analytical Chemistry 78: 6847-54, 2006.
11. Palmer JW, Tandler B and Hoppel CL: Biochemical properties of subsarcolemmal and interfibrillar mitochondria isolated from rat cardiac muscle. J. Biol. Chem. 252: 8731-9, 1977.
12. Suh JH, Heath SH and Hagen TM: Two subpopulations of mitochondria in the aging rat heart display heterogenous levels of oxidative stress. Free Radic. Biol. Med. 35: 1064-72, 2003.
13. Chavez J, Chung WG, Miranda CL, Singhal M, Stevens JF and Maier CS: Site-specific protein adducts of 4-hydroxy-2(E)-nonenal in human THP 1 monocytic cells: Protein carbonylation is diminished by ascorbic acid. Chem. Res. Toxicol.: 2009.

14. Cowan-Jacob SW, Kaufmann M, Anselmo AN, Stark W and Grutter MG: Structure of rabbit-muscle glyceraldehyde-3-phosphate dehydrogenase. Acta Crystallogr. D. Biol. Crystallogr. 59: 2218-27, 2003.
15. Shrake A and Rupley JA: Environment and exposure to solvent of protein atoms. Lysozyme and insulin. J. Mol. Biol. 79: 351-71, 1973.
16. Tsuchiya Y, Yamaguchi M, Chikuma T and Hojo H: Degradation of glyceraldehyde-3-phosphate dehydrogenase triggered by 4-hydroxy-2-nonenal and 4-hydroxy-2-hexenal. Arch. Biochem. Biophys. 438: 217-22, 2005.
17. Pierce A, Mirzaei H, Muller F, De Waal E, Taylor AB, Leonard S, Van Remmen H, Regnier F, Richardson A and Chaudhuri A: GAPDH is conformationally and functionally altered in association with oxidative stress in mouse models of amyotrophic lateral sclerosis. J. Mol. Biol. 382: 1195-210, 2008.
18. Hara MR, Agrawal N, Kim SF, Cascio MB, Fujimuro M, Ozeki Y, Takahashi M, Cheah JH, Tankou SK, Hester LD, Ferris CD, Hayward SD, Snyder SH and Sawa A: S-nitrosylated GAPDH initiates apoptotic cell death by nuclear translocation following Siah1 binding. Nat. Cell. Biol. 7: 665-74, 2005.
19. Cadenas E and Davies KJ: Mitochondrial free radical generation, oxidative stress, and aging. Free Radic. Biol. Med. 29: 222-30, 2000.
20. Orrenius S, Gogvadze V and Zhivotovsky B: Mitochondrial oxidative stress: implications for cell death. Annu. Rev. Pharmacol. Toxicol. 47: 143-83, 2007.
21. Ott M, Gogvadze V, Orrenius S and Zhivotovsky B: Mitochondria, oxidative stress and cell death. Apoptosis 12: 913-22, 2007.
22. Gibson BW: The human mitochondrial proteome: oxidative stress, protein modifications and oxidative phosphorylation. Int. J. Biochem. Cell. Biol. 37: 927-34, 2005.
23. Fiore C, Trezeguet V, Le Saux A, Roux P, Schwimmer C, Dianoux AC, Noel F, Lauquin GJ, Brandolin G and Vignais PV: The mitochondrial ADP/ATP carrier: structural, physiological and pathological aspects. Biochimie 80: 137-50, 1998.
24. Klingenberg M and Nelson DR: Structure-function relationships of the ADP/ATP carrier. Biochim. Biophys. Acta 1187: 241-4, 1994.
25. Luo J and Shi R: Acrolein induces oxidative stress in brain mitochondria. Neurochem. Int. 46: 243-52, 2005.
26. Wallace DC: Mitochondrial diseases in man and mouse. Science 283: 1482-8, 1999.
27. Terni B, Boada J, Portero-Otin M, Pamplona R and Ferrer I: Mitochondrial ATP-Synthase in the Entorhinal Cortex Is a Target of Oxidative Stress at Stages I/II of Alzheimer's Disease Pathology. Brain Pathol.: 2009.
28. Chen Q, Vazquez EJ, Moghaddas S, Hoppel CL and Lesnefsky EJ: Production of reactive oxygen species by mitochondria: central role of complex III. J. Biol. Chem. 278: 36027-31, 2003.

Table 6.1 – Table listing the mitochondrial proteins identified with AAS modifications to Lys residues. The trypic peptide sequences indicating the location of the modification are listed with the modified residue marked with an asterisk. Superscripts "a" and "b" indicate whether the peptide was detected by ESI-Q-TOF or MALDI-TOF/TOF respectively.

Biological function	Swiss Prot ID	Uniprot Accession	Protein Name	Peptide Sequence	Modification
Respiratory Chain	ATPA_RAT	P15999	ATP synthase subunit alpha	VGLK*APGIIPR[a]	AAS (K175)
	QCR2_RAT	P32551	Ubiquinol-cytochrome-c reductase complex core protein 2	IDK*AVAFQNPQTR[b]	AAS (K161)
Membrane Transport	ADT1_RAT	Q05962	ADP/ATP translocase 1	YFPTQALNFAFK*DK[b]	AAS (K91)
				HK*QFWR[a]	AAS (K107)
				VLVLYDEIK*K[a]	AAS (K295)
				YK*QIFLGGVDR[a]	AAS (K52)
				VK*LLLQVQHASK[b]	AAS (K33)
				IPK*EQGFLSFWR[a,b]	AAS (K63)
	ADT2_RAT	Q09073	ADP/ATP translocase 2	LLLQVQHASK*QITADK[a]	AAS (K43)

Figures

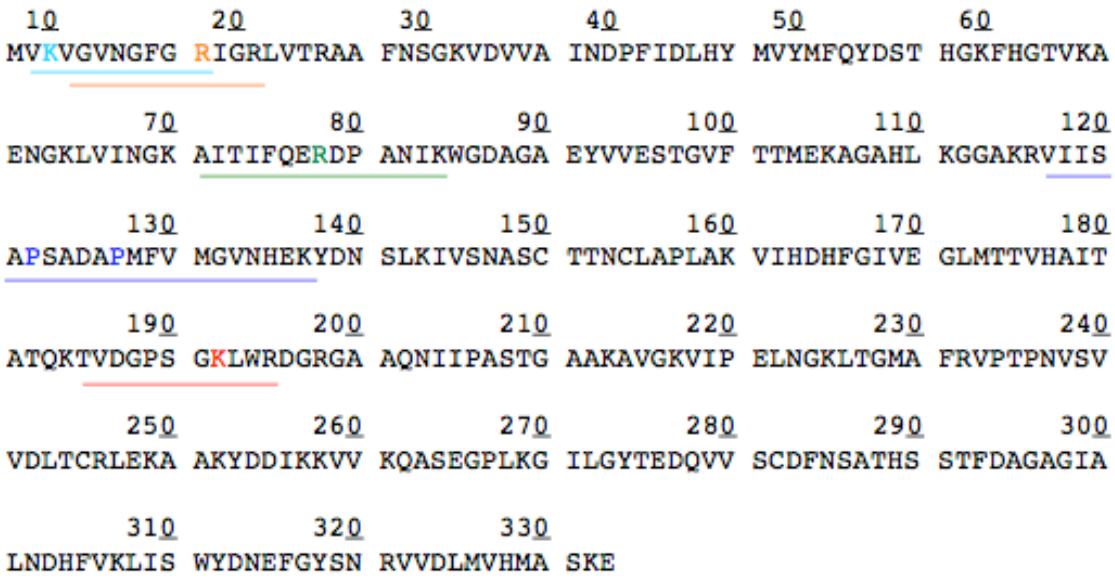

Peptide	Modification	ESI-Q-TOF	MALDI-TOF/TOF
VK*VGVNGFGR	AAS (K3)	✓	✓
VGVNGFGR*IGR	GGS (R11)	✓	✓
AITIFQER*DPANIK	GGS (R78)	✓	✓
VIISAP*SADAPMFVMGVNHEK	GGS (P122)	✓	✓
VIISAPSADAP*MFVMGVNHEK	GGS (P127)		✓
TVDGPSGK*LWR	AAS (K192)	✓	✓

Figure 6.1 – Primary sequence of GAPDH from rabbit muscle, with the residues identified with AAS, or GGS modifications indicated by color. Colored bars, matching the color of the modified residues, indicate the tryptic peptide sequence in which the modified residue was detected with mass spectrometry. Additionally the peptide sequences are listed in a table indicating the type and site of modification, as well as the instrument that the peptide was detected with.

A.

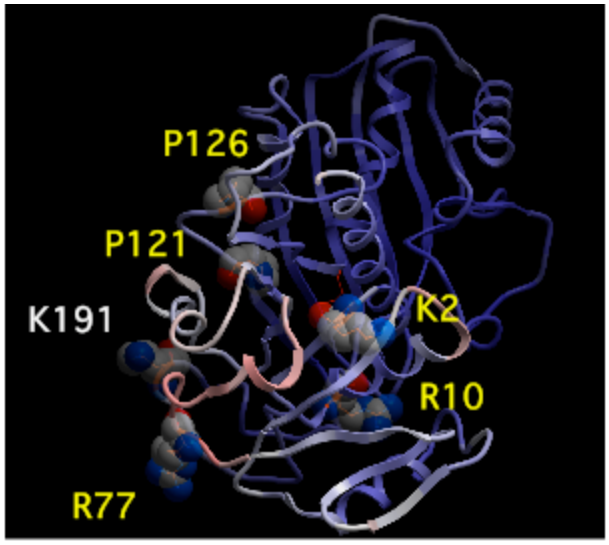

B.

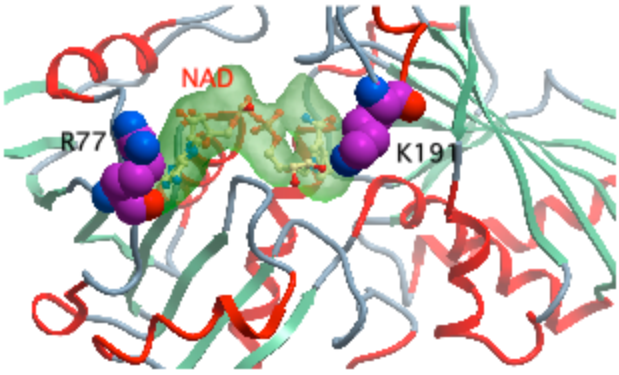

Figure 6.2 – A) Crystal structure of rabbit muscle GAPDH (PDB = 1j0x) with the residues identified with semialdehyde modifications and labeled with ARP shown as CPK and labeled. **B)** Image illustrating the proximity of Arg-77 and Lys-191 to the NAD binding pocket of GAPDH.

Chapter 7

Conclusions

This dissertation describes the development and application of an analytical technique, involving affinity labeling with ARP, avidin affinity enrichment, and mass spectrometric analysis, for the characterization of peptide and protein based carbonyls. The utility of the technique to detect peptide and protein Michael adducts of α,β-unsaturated aldehydes such as 4-hydoxy-2-nonenal (HNE), was demonstrated using model systems, including a HNE-modified Cys containing peptide, and HNE-modified *E. coli* thioredoxin. Additionally the technique was shown to be effective for the characterization of the carbonyl products α-aminoadipic semialdehyde (AAS) and γ-glutamic semialdehyde (GGS), which result from the direct oxidation of Lys, Arg, and Pro sidechains by ROS, using metal catalyzed oxidation on glyceraldehyde-3-phosphate dehydrogenase (GAPDH).

Applying this technique to protein samples from rat cardiac mitochondria, 39 unique sites on 27 proteins were identified as being modified by a variety of 2-alkenal lipid peroxidation products including: acrolein, β-hydroxyacrolein, crotonaldehyde, 4-hydroxy-2-hexenal, 4-hydroxy-2-nonenal and 4-oxo-2-nonenal. The majority (40%) of the identified modified proteins were members of

the mitochondrial electron transport chain. Nineteen percent were proteins from the TCA cycle, while the remaining proteins were involved in membrane transport, lipid metabolism or other metabolic processes. Nine additional sites on four proteins were identified with AAS modifications to Lys residues. These four proteins, namely: ADP/ATP tranlocase 1, ADP/ATP translocase 2, ubiquinol-cytochrome-c reductase core protein 2, and ATP synthase α chain, are all located within the mitochondrial inner membrane, close to the sites of ROS production within the mitochondria.

A multifaceted strategy, involving gel electrophoresis, immunochemical analysis, ARP labeling, enrichment, and mass spectrometry, was used to characterize the protein targets of HNE in human monocytic THP-1 cells. THP-1 cells are commonly used for studying foam cell formation in atherosclerosis. Exogenous exposure of THP-1 cells to HNE has been shown to induce apoptosis, necrosis, and an increase in protein carbonylation. Pretreatment of the cells with ascorbic acid resulted in a protective effect, diminishing the levels of protein carbonylation. A total of 18 HNE modified sites on 16 proteins were characterized. The HNE modification occurred primarily on Cys residues (14 out of 18), with the remaining modifications occurring on His residues. The majority of HNE-modified proteins were involved in cytoskeletal organization/regulation and actin binding, stress response and glycolysis.

Traditional methods to measure protein carbonylation typically fail to provide information on protein identities, sites of modification and the chemical nature of the modification. With the recent advancement of proteomic technologies, particularly in mass spectrometry, there has been much interest in developing new techniques that overcome the shortfalls of the traditional methods. The targeted proteomics approach described in this dissertation provides researchers with an alternative technique, which is able to unequivocally characterize carbonylation modifications to proteins and peptides.

Bibliography

1. Akagawa M, Sasaki D, Ishii Y, Kurota Y, Yotsu-Yamashita M, Uchida K and Suyama K: New method for the quantitative determination of major protein carbonyls, alpha-aminoadipic and gamma-glutamic semialdehydes: investigation of the formation mechanism and chemical nature in vitro and in vivo. Chem. Res. Toxicol. 19: 1059-65, 2006.

2. Akagawa M, Suyama K and Uchida K: Fluorescent detection of alpha-aminoadipic and gamma-glutamic semialdehydes in oxidized proteins. Free Radic. Biol. Med. 46: 701-6, 2009.

3. Andersen JK: Oxidative stress in neurodegeneration: cause or consequence? Nat Med 10 Suppl: S18-25, 2004.

4. Anderson MM, Hazen SL, Hsu FF and Heinecke JW: Human neutrophils employ the myeloperoxidase-hydrogen peroxide-chloride system to convert hydroxy-amino acids into glycolaldehyde, 2-hydroxypropanal, and acrolein. A mechanism for the generation of highly reactive alpha-hydroxy and alpha,beta-unsaturated aldehydes by phagocytes at sites of inflammation. J Clin Invest 99: 424-32, 1997.

5. Andreyev AY, Kushnareva YE and Starkov AA: Mitochondrial metabolism of reactive oxygen species. Biochemistry (Mosc) 70: 200-14, 2005.

6. Atamna H, Cheung I and Ames BN: A method for detecting abasic sites in living cells: age-dependent changes in base excision repair. Proc Natl Acad Sci U S A 97: 686-91, 2000.

7. Banka CL, Black AS, Dyer CA and Curtiss LK: THP-1 cells form foam cells in response to coculture with lipoproteins but not platelets. J. Lipid Res. 32: 35-43, 1991.

8. Bantscheff M, Schirle M, Sweetman G, Rick J and Kuster B: Quantitative mass spectrometry in proteomics: a critical review. Anal. Bioanal. Chem. 389: 1017-31, 2007.

9. Barron-Casella EA, Torres MA, Scherer SW, Heng HH, Tsui LC and Casella JF: Sequence analysis and chromosomal localization of human Cap Z. Conserved residues within the actin-binding domain may link Cap Z to gelsolin/severin and profilin protein families. J. Biol. Chem. 270: 21472-9, 1995.

10. Beckman JS and Koppenol WH: Nitric oxide, superoxide, and peroxynitrite: the good, the bad, and ugly. Am. J. Physiol. 271: C1424-37, 1996.

11. Benedetti A, Comporti M and Esterbauer H: Identification of 4-hydroxynonenal as a cytotoxic product originating from the peroxidation of liver microsomal lipids. Biochim Biophys Acta 620: 281-96, 1980.

12. Berlett BS and Stadtman ER: Protein oxidation in aging, disease, and oxidative stress. J. Biol. Chem. 272: 20313-6, 1997.

13. Biemann K: Contributions of Mass Spectrometry to Peptide and Protein Structure. Biomed. Environ. Mass Spectrom. 16: 99-111, 1988.

14. Biemann K: Sequencing of peptides by tandem mass spectrometry and high-energy collision-induced dissociation. Methods Enzymol. 193: 455-79, 1990.

15. Bolgar MS and Gaskell SJ: Determination of the Sites of 4-Hydroxy-2-nonenal Adduction to Protein by Electrospray Tandem Mass Spectrometry. Anal. Chem. 68: 2325-2330, 1996.

16. Bolgar MS, Yang CY and Gaskell SJ: First direct evidence for lipid/protein conjugation in oxidized human low density lipoprotein. J Biol Chem 271: 27999-8001, 1996.

17. Bondarenko PV, Chelius D and Shaler TA: Identification and relative quantitation of protein mixtures by enzymatic digestion followed by capillary reversed-phase liquid chromatography-tandem mass spectrometry. Anal. Chem. 74: 4741-9, 2002.

18. Boveris A and Chance B: The mitochondrial generation of hydrogen peroxide. General properties and effect of hyperbaric oxygen. Biochem. J. 134: 707-16, 1973.

19. Bruenner BA, Jones AD and German JB: Direct characterization of protein adducts of the lipid peroxidation product 4-hydroxy-2-nonenal using electrospray mass spectrometry. Chem Res Toxicol 8: 552-9, 1995.

20. Bulteau AL, Ikeda-Saito M and Szweda LI: Redox-dependent modulation of aconitase activity in intact mitochondria. Biochemistry 42: 14846-55, 2003.

21. Bulteau AL, Lundberg KC, Ikeda-Saito M, Isaya G and Szweda LI: Reversible redox-dependent modulation of mitochondrial aconitase and proteolytic activity during in vivo cardiac ischemia/reperfusion. Proc. Natl. Acad. Sci. U. S. A. 102: 5987-91, 2005.

22. Bursch W, Hochegger K, Torok L, Marian B, Ellinger A and Hermann RS: Autophagic and apoptotic types of programmed cell death exhibit different fates of cytoskeletal filaments. J. Cell Sci. 113 (Pt 7): 1189-98, 2000.

23. Butterfield DA: Amyloid beta-peptide (1-42)-induced oxidative stress and neurotoxicity: implications for neurodegeneration in Alzheimer's disease brain. A review. Free Radic. Res. 36: 1307-13, 2002.

24. Butterfield DA, Poon HF, St Clair D, Keller JN, Pierce WM, Klein JB and Markesbery WR: Redox proteomics identification of oxidatively modified hippocampal proteins in mild cognitive impairment: insights into the development of Alzheimer's disease. Neurobiol. Dis. 22: 223-32, 2006.

25. Bylund D, Danielsson R, Malmquist G and Markides KE: Chromatographic alignment by warping and dynamic programming as a pre-processing tool for PARAFAC modelling of liquid chromatography-mass spectrometry data. J. Chromatogr. A 961: 237-44, 2002.

26. Cadenas E and Davies KJ: Mitochondrial free radical generation, oxidative stress, and aging. Free Radic. Biol. Med. 29: 222-30, 2000.

27. Carbone DL, Doorn JA, Kiebler Z, Ickes BR and Petersen DR: Modification of heat shock protein 90 by 4-hydroxynonenal in a rat model of chronic alcoholic liver disease. J Pharmacol Exp Ther 315: 8-15, 2005.

28. Carbone DL, Doorn JA, Kiebler Z and Petersen DR: Cysteine modification by lipid peroxidation products inhibits protein disulfide isomerase. Chem Res Toxicol 18: 1324-31, 2005.

29. Carbone DL, Doorn JA, Kiebler Z, Sampey BP and Petersen DR: Inhibition of Hsp72-mediated protein refolding by 4-hydroxy-2-nonenal. Chem Res Toxicol 17: 1459-67, 2004.

30. Carini M, Aldini G and Facino RM: Mass spectrometry for detection of 4-hydroxy-trans-2-nonenal (HNE) adducts with peptides and proteins. Mass Spectrom. Rev. 23: 281-305, 2004.

31. Chavez J, Chung WG, Miranda CL, Singhal M, Stevens JF and Maier CS: Site-specific protein adducts of 4-hydroxy-2(E)-nonenal in human THP 1 monocytic cells: Protein carbonylation is diminished by ascorbic acid. Chem. Res. Toxicol.: 2009.

32. Chavez J, Wu J, Han B, Chung WG and Maier CS: New role for an old probe: affinity labeling of oxylipid protein conjugates by N'-aminooxymethylcarbonylhydrazino d-biotin. Anal. Chem. 78: 6847-54, 2006.

33. Chen CN, Ferrington DA and Thompson LV: Carbonic anhydrase III and four-and-a-half LIM protein 1 are preferentially oxidized with muscle unloading. J. Appl. Physiol. 105: 1554-61, 2008.

34. Chen Q, Vazquez EJ, Moghaddas S, Hoppel CL and Lesnefsky EJ: Production of reactive oxygen species by mitochondria: central role of complex III. J. Biol. Chem. 278: 36027-31, 2003.

35. Choksi KB, Boylston WH, Rabek JP, Widger WR and Papaconstantinou J: Oxidatively damaged proteins of heart mitochondrial electron transport complexes. Biochim. Biophys. Acta 1688: 95-101, 2004.

36. Chung FL, Pan J, Choudhury S, Roy R, Hu W and Tang MS: Formation of trans-4-hydroxy-2-nonenal- and other enal-derived cyclic DNA adducts from omega-3 and omega-6 polyunsaturated fatty acids and their roles in DNA repair and human p53 gene mutation. Mutat. Res. 531: 25-36, 2003.

37. Chung WG and Maier CS: Mass Spectrometry-based Identification and Characterization of Oxylipid-Protein Conjugates. In: Current Protocols in Toxicology. 2008, p Unit 17.9.

38. Chung WG, Miranda CL and Maier CS: Epigallocatechin gallate (EGCG) potentiates the cytotoxicity of rotenone in neuroblastoma SH-SY5Y cells. Brain Res. 1176: 133-42, 2007.

39. Chung WG, Miranda CL and Maier CS: Detection of carbonyl-modified proteins in interfibrillar rat mitochondria using N'-aminooxymethylcarbonylhydrazino-D-biotin as an aldehyde/keto-reactive probe in combination with Western blot analysis and tandem mass spectrometry. Electrophoresis 29: 1317-24, 2008.

40. Chung WG, Miranda CL, Stevens JF and Maier CS: Hop proanthocyanidins induce apoptosis, protein carbonylation, and cytoskeleton disorganization in human colorectal adenocarcinoma cells via reactive oxygen species. Food Chem. Toxicol. 47: 827-36, 2009.

41. Codreanu SG, Zhang B, Sobecki SM, Billheimer DD and Liebler DC: Global analysis of protein damage by the lipid electrophile 4-hydroxy-2-nonenal. Mol. Cell. Proteomics 8: 670-80, 2009.

42. Coon JJ: Collisions or electrons? Protein sequence analysis in the 21st century. Anal. Chem. 81: 3208-15, 2009.

43. Cowan-Jacob SW, Kaufmann M, Anselmo AN, Stark W and Grutter MG: Structure of rabbit-muscle glyceraldehyde-3-phosphate dehydrogenase. Acta Crystallogr. D. Biol. Crystallogr. 59: 2218-27, 2003.

44. Creighton TE: Proteins: Structures and Molecular Properties. W. H. Freeman and Company, New York, NY, 1993.

45. Crompton M: The mitochondrial permeability transition pore and its role in cell death. Biochem. J. 341 (Pt 2): 233-49, 1999.

46. D'Autreaux B and Toledano MB: ROS as signalling molecules: mechanisms that generate specificity in ROS homeostasis. Nat. Rev. Mol. Cell. Biol. 8: 813-24, 2007.

47. Dean RT, Fu S, Stocker R and Davies MJ: Biochemistry and pathology of radical-mediated protein oxidation. Biochem J 324 (Pt 1): 1-18, 1997.

48. Dennehy MK, Richards KA, Wernke GR, Shyr Y and Liebler DC: Cytosolic and nuclear protein targets of thiol-reactive electrophiles. Chem. Res. Toxicol. 19: 20-9, 2006.

49. Doorn JA and Petersen DR: Covalent modification of amino acid nucleophiles by the lipid peroxidation products 4-hydroxy-2-nonenal and 4-oxo-2-nonenal. Chem. Res. Toxicol. 15: 1445-50, 2002.

50. Esterbauer H: Cytotoxicity and genotoxicity of lipid-oxidation products. Am. J. Clin. Nutr. 57: 779S-785S; discussion 785S-786S, 1993.

51. Esterbauer H, Schaur RJ and Zollner H: Chemistry and biochemistry of 4-hydroxynonenal, malonaldehyde and related aldehydes. Free Radic. Biol. Med. 11: 81-128, 1991.

52. Estevez M, Ollilainen V and Heinonen M: Analysis of protein oxidation markers alpha-aminoadipic and gamma-glutamic semialdehydes in food proteins using liquid chromatography (LC)-electrospray ionization (ESI)-multistage tandem mass spectrometry (MS). J. Agric. Food Chem. 57: 3901-10, 2009.

53. Fenaille F, Guy PA and Tabet JC: Study of protein modification by 4-hydroxy-2-nonenal and other short chain aldehydes analyzed by electrospray ionization tandem mass spectrometry. J Am Soc Mass Spectrom 14: 215-26, 2003.

54. Fenaille F, Tabet JC and Guy PA: Identification of 4-hydroxy-2-nonenal-modified peptides within unfractionated digests using matrix-assisted laser desorption/ionization time-of-flight mass spectrometry. Anal Chem 76: 867-73, 2004.

55. Fenn JB, Mann M, Meng CK, Wong SF and Whitehouse CM: Electrospray ionization for mass spectrometry of large biomolecules. Science 246: 64-71, 1989.

56. Ferrington DA and Kapphahn RJ: Catalytic site-specific inhibition of the 20S proteasome by 4-hydroxynonenal. FEBS Lett. 578: 217-23, 2004.

57. Fialkow L, Wang Y and Downey GP: Reactive oxygen and nitrogen species as signaling molecules regulating neutrophil function. Free Radic. Biol. Med. 42: 153-64, 2007.

58. Fields R and Dixon HB: Micro method for determination of reactive carbonyl groups in proteins and peptides, using 2,4-dinitrophenylhydrazine. Biochem. J. 121: 587-9, 1971.

59. Finkel T and Holbrook NJ: Oxidants, oxidative stress and the biology of ageing. Nature 408: 239-47, 2000.

60. Fiore C, Trezeguet V, Le Saux A, Roux P, Schwimmer C, Dianoux AC, Noel F, Lauquin GJ, Brandolin G and Vignais PV: The mitochondrial ADP/ATP carrier: structural, physiological and pathological aspects. Biochimie 80: 137-50, 1998.

61. Forman HJ, Fukuto JM, Miller T, Zhang H, Rinna A and Levy S: The chemistry of cell signaling by reactive oxygen and nitrogen species and 4-hydroxynonenal. Arch. Biochem. Biophys. 477: 183-95, 2008.

62. Friguet B: Oxidized protein degradation and repair in ageing and oxidative stress. FEBS Lett. 580: 2910-6, 2006.

63. Friguet B and Szweda LI: Inhibition of the multicatalytic proteinase (proteasome) by 4-hydroxy-2-nonenal cross-linked protein. FEBS Lett. 405: 21-5, 1997.

64. Gandhi M and Goode BL: Coronin: the double-edged sword of actin dynamics. Subcell. Biochem. 48: 72-87, 2008.

65. Geiszt M, Kopp JB, Varnai P and Leto TL: Identification of renox, an NAD(P)H oxidase in kidney. Proc. Natl. Acad. Sci. U. S. A. 97: 8010-4, 2000.

66. Gibson BW: The human mitochondrial proteome: oxidative stress, protein modifications and oxidative phosphorylation. Int. J. Biochem. Cell. Biol. 37: 927-34, 2005.

67. Gilchrist A, Au CE, Hiding J, Bell AW, Fernandez-Rodriguez J, Lesimple S, Nagaya H, Roy L, Gosline SJ, Hallett M, Paiement J, Kearney RE, Nilsson T and Bergeron JJ: Quantitative proteomics analysis of the secretory pathway. Cell 127: 1265-81, 2006.

68. Gleason WB, Fu Z, Birktoft J and Banaszak L: Refined crystal structure of mitochondrial malate dehydrogenase from porcine heart and the consensus structure for dicarboxylic acid oxidoreductases. Biochemistry 33: 2078-88, 1994.

69. Gomez LA, Monette JS, Chavez JD, Maier CS and Hagen TM: Supercomplexes of the mitochondrial electron transport chain decline in the aging rat heart. Arch. Biochem. Biophys. 490: 30-5, 2009.

70. Grace JM, MacDonald TL, Roberts RJ and Kinter M: Determination of site-specific modifications of glucose-6-phosphate dehydrogenase by 4-hydroxy-2-nonenal using matrix assisted laser desorption time-of-flight mass spectrometry. Free Radic Res 25: 23-9, 1996.

71. Green NM: Avidin. 1. the Use of (14-C)Biotin for Kinetic Studies and for Assay. Biochem. J. 89: 585-91, 1963.

72. Grimm S and Brdiczka D: The permeability transition pore in cell death. Apoptosis 12: 841-55, 2007.

73. Grimsrud PA, Picklo MJ, Sr., Griffin TJ and Bernlohr DA: Carbonylation of adipose proteins in obesity and insulin resistance: identification of adipocyte fatty acid-binding protein as a cellular target of 4-hydroxynonenal. Mol. Cell. Proteomics 6: 624-37, 2007.

74. Grune T and Davies KJ: The proteasomal system and HNE-modified proteins. Mol. Aspects Med. 24: 195-204, 2003.

75. Gu C, Tsaprailis G, Breci L and Wysocki VH: Selective gas-phase cleavage at the peptide bond C-terminal to aspartic acid in fixed-charge derivatives of Asp-containing peptides. Anal Chem 72: 5804-13, 2000.

76. Gygi SP, Rist B, Gerber SA, Turecek F, Gelb MH and Aebersold R: Quantitative analysis of complex protein mixtures using isotope-coded affinity tags. Nat. Biotechnol. 17: 994-9, 1999.

77. Hagen TM, Moreau R, Suh JH and Visioli F: Mitochondrial decay in the aging rat heart: evidence for improvement by dietary supplementation with acetyl-L-carnitine and/or lipoic acid. Ann. N. Y. Acad. Sci. 959: 491-507, 2002.

78. Han B, Stevens JF and Maier CS: Design, synthesis, and application of a hydrazide-functionalized isotope-coded affinity tag for the quantification of oxylipid-protein conjugates. Anal. Chem. 79: 3342-54, 2007.

79. Hara MR, Agrawal N, Kim SF, Cascio MB, Fujimuro M, Ozeki Y, Takahashi M, Cheah JH, Tankou SK, Hester LD, Ferris CD, Hayward SD, Snyder SH and Sawa A: S-nitrosylated GAPDH initiates apoptotic cell death by nuclear translocation following Siah1 binding. Nat. Cell. Biol. 7: 665-74, 2005.

80. Harman D: Aging: a theory based on free radical and radiation chemistry. Journal of Gerontology 11: 298-300, 1956.

81. Harman D: The aging process. Proc. Natl. Acad. Sci. U. S. A. 78: 7124-8, 1981.

82. Hayes JD and McLellan LI: Glutathione and glutathione-dependent enzymes represent a co-ordinately regulated defence against oxidative stress. Free Radic. Res. 31: 273-300, 1999.

83. Heck AJ and Krijgsveld J: Mass spectrometry-based quantitative proteomics. Expert. Rev. Proteomics 1: 317-26, 2004.

84. Herrmann KA, Wysocki VH and Vorpagel ER: Computational investigation and hydrogen/deuterium exchange of the fixed charge derivative tris(2,4,6-trimethoxyphenyl) phosphonium: implications for the aspartic acid cleavage mechanism. J Am Soc Mass Spectrom 16: 1067-80, 2005.

85. Horton ND, Mamiya BM and Kehrer JP: Relationships between cell density, glutathione and proliferation of A549 human lung adenocarcinoma cells treated with acrolein. Toxicology 122: 111-22, 1997.

86. Hunter T and Garrels JI: Characterization of the mRNAs for alpha-, beta- and gamma-actin. Cell 12: 767-81, 1977.

87. Hussain SN, Matar G, Barreiro E, Florian M, Divangahi M and Vassilakopoulos T: Modifications of proteins by 4-hydroxy-2-nonenal in the

ventilatory muscles of rats. Am. J. Physiol. Lung Cell. Mol. Physiol. 290: L996-1003, 2006.

88. Ide H, Akamatsu K, Kimura Y, Michiue K, Makino K, Asaeda A, Takamori Y and Kubo K: Synthesis and damage specificity of a novel probe for the detection of abasic sites in DNA. Biochemistry 32: 8276-83, 1993.

89. Ishii T, Tatsuda E, Kumazawa S, Nakayama T and Uchida K: Molecular basis of enzyme inactivation by an endogenous electrophile 4-hydroxy-2-nonenal: identification of modification sites in glyceraldehyde-3-phosphate dehydrogenase. Biochemistry 42: 3474-80, 2003.

90. Isom AL, Barnes S, Wilson L, Kirk M, Coward L and Darley-Usmar V: Modification of Cytochrome c by 4-hydroxy- 2-nonenal: evidence for histidine, lysine, and arginine-aldehyde adducts. J. Am. Soc. Mass Spectrom. 15: 1136-47, 2004.

91. Jung C, Higgins CM and Xu Z: Measuring the quantity and activity of mitochondrial electron transport chain complexes in tissues of central nervous system using blue native polyacrylamide gel electrophoresis. Anal. Biochem. 286: 214-23, 2000.

92. Kang JH, Ryu HS, Kim HT, Lee SJ, Choi UK, Park YB, Huh TL, Choi MS, Kang TC, Choi SY and Kwon OS: Proteomic analysis of human macrophages exposed to hypochlorite-oxidized low-density lipoprotein. Biochim. Biophys. Acta 1794: 446-58, 2009.

93. Kebarle P and Verkerk UH: Electrospray: From ions in solution to ions in the gas phase, what we know now. Mass Spectrom. Rev.: 2009.

94. Klingenberg M and Nelson DR: Structure-function relationships of the ADP/ATP carrier. Biochim. Biophys. Acta 1187: 241-4, 1994.

95. Kohanski RA and Lane MD: Monovalent avidin affinity columns. Methods Enzymol. 184: 194-200, 1990.

96. Kokubo J, Nagatani N, Hiroki K, Kuroiwa K, Watanabe N and Arai T: Mechanism of destruction of microtubule structures by 4-hydroxy-2-nonenal. Cell Struct. Funct. 33: 51-9, 2008.

97. Korolainen MA, Goldsteins G, Alafuzoff I, Koistinaho J and Pirttila T: Proteomic analysis of protein oxidation in Alzheimer's disease brain. Electrophoresis 23: 3428-33, 2002.

98. Kroemer G and Reed JC: Mitochondrial control of cell death. Nat. Med. 6: 513-9, 2000.

99. Kubo K, Ide H, Wallace SS and Kow YW: A novel, sensitive, and specific assay for abasic sites, the most commonly produced DNA lesion. Biochemistry 31: 3703-8, 1992.

100. Lambert AJ and Brand MD: Reactive oxygen species production by mitochondria. Methods Mol. Biol. 554: 165-81, 2009.

101. Landar A, Oh JY, Giles NM, Isom A, Kirk M, Barnes S and Darley-Usmar VM: A sensitive method for the quantitative measurement of protein thiol modification in response to oxidative stress. Free Radic. Biol. Med. 40: 459-68, 2006.

102. Larsen MR, Trelle MB, Thingholm TE and Jensen ON: Analysis of posttranslational modifications of proteins by tandem mass spectrometry. Biotechniques 40: 790-8, 2006.

103. Lee HP, Zhu X, Zhu X, Skidmore SC, Perry G, Sayre LM, Smith MA and Lee HG: The essential role of ERK in 4-oxo-2-nonenal-mediated cytotoxicity in SH-SY5Y human neuroblastoma cells. J. Neurochem. 108: 1434-41, 2009.

104. Levine RL: Carbonyl modified proteins in cellular regulation, aging, and disease. Free Radic Biol Med 32: 790-6, 2002.

105. Levine RL, Garland D, Oliver CN, Amici A, Climent I, Lenz AG, Ahn BW, Shaltiel S and Stadtman ER: Determination of carbonyl content in oxidatively modified proteins. Methods Enzymol 186: 464-78, 1990.

106. Levine RL and Stadtman ER: Oxidative modification of proteins during aging. Exp Gerontol 36: 1495-502, 2001.

107. Liebler DC: The poisons within: application of toxicity mechanisms to fundamental disease processes. Chem. Res. Toxicol. 19: 610-3, 2006.

108. Linford NJ, Schriner SE and Rabinovitch PS: Oxidative damage and aging: spotlight on mitochondria. Cancer Res. 66: 2497-9, 2006.

109. Liu H, Sadygov RG and Yates JR, 3rd: A model for random sampling and estimation of relative protein abundance in shotgun proteomics. Anal. Chem. 76: 4193-201, 2004.

110. Luo J and Shi R: Acrolein induces oxidative stress in brain mitochondria. Neurochem. Int. 46: 243-52, 2005.

111. Marley K, Mooney DT, Clark-Scannell G, Tong TT, Watson J, Hagen TM, Stevens JF and Maier CS: Mass tagging approach for mitochondrial thiol proteins. J. Proteome Res. 4: 1403-12, 2005.

112. Marnett LJ, Riggins JN and West JD: Endogenous generation of reactive oxidants and electrophiles and their reactions with DNA and protein. J Clin Invest 111: 583-93, 2003.

113. Martinez A, Dalfo E, Muntane G and Ferrer I: Glycolitic enzymes are targets of oxidation in aged human frontal cortex and oxidative damage of these proteins is increased in progressive supranuclear palsy. J. Neural. Transm. 115: 59-66, 2008.

114. Matasova LV and Popova TN: Aconitate hydratase of mammals under oxidative stress. Biochemistry (Mosc) 73: 957-64, 2008.

115. McLafferty FW, Horn DM, Breuker K, Ge Y, Lewis MA, Cerda B, Zubarev RA and Carpenter BK: Electron capture dissociation of gaseous multiply charged ions by Fourier-transform ion cyclotron resonance. J. Am. Soc. Mass Spectrom. 12: 245-9, 2001.

116. Meany DL, Xie H, Thompson LV, Arriaga EA and Griffin TJ: Identification of carbonylated proteins from enriched rat skeletal muscle mitochondria using affinity chromatography-stable isotope labeling and tandem mass spectrometry. Proteomics 7: 1150-63, 2007.

117. Melamed MD and Green NM: Avidin. 2. Purification and Composition. Biochem. J. 89: 591-9, 1963.

118. Miranda CL, Reed RL, Kuiper HC, Alber S and Stevens JF: Ascorbic acid promotes detoxification and elimination of 4-hydroxy-2(E)-nonenal in human monocytic THP-1 cells. Chem. Res. Toxicol. 22: 863-74, 2009.

119. Mirzaei H and Regnier F: Affinity chromatographic selection of carbonylated proteins followed by identification of oxidation sites using tandem mass spectrometry. Anal. Chem. 77: 2386-92, 2005.

120. Mirzaei H and Regnier F: Identification and quantification of protein carbonylation using light and heavy isotope labeled Girard's P reagent. J. Chromatogr. A 1134: 122-33, 2006.

121. Musatov A, Carroll CA, Liu YC, Henderson GI, Weintraub ST and Robinson NC: Identification of bovine heart cytochrome c oxidase subunits modified by the lipid peroxidation product 4-hydroxy-2-nonenal. Biochemistry 41: 8212-20, 2002.

122. Nakamura A and Goto S: Analysis of protein carbonyls with 2,4-dinitrophenyl hydrazine and its antibodies by immunoblot in two-dimensional gel electrophoresis. J. Biochem. 119: 768-74, 1996.

123. Nemoto S, Takeda K, Yu ZX, Ferrans VJ and Finkel T: Role for mitochondrial oxidants as regulators of cellular metabolism. Mol. Cell. Biol. 20: 7311-8, 2000.

124. Nguyen S and Fenn JB: Gas-phase ions of solute species from charged droplets of solutions. Proc. Natl. Acad. Sci. U. S. A. 104: 1111-7, 2007.

125. Nijtmans LG, Henderson NS and Holt IJ: Blue Native electrophoresis to study mitochondrial and other protein complexes. Methods 26: 327-34, 2002.

126. Nohl H: Is Redox-Cycling Ubiquinone Involved In Mitochondrial Oxygen Activation? . Free Radic. Res. 8: 307 - 315, 1990.

127. O'Malley Y, Fink BD, Ross NC, Prisinzano TE and Sivitz WI: Reactive oxygen and targeted antioxidant administration in endothelial cell mitochondria. J. Biol. Chem. 281: 39766-75, 2006.

128. Oda Y, Huang K, Cross FR, Cowburn D and Chait BT: Accurate quantitation of protein expression and site-specific phosphorylation. Proc. Natl. Acad. Sci. U. S. A. 96: 6591-6, 1999.

129. Oh-Ishi M, Ueno T and Maeda T: Proteomic method detects oxidatively induced protein carbonyls in muscles of a diabetes model Otsuka Long-Evans Tokushima Fatty (OLETF) rat. Free Radic. Biol. Med. 34: 11-22, 2003.

130. Ohkawa H, Ohishi N and Yagi K: Assay for lipid peroxides in animal tissues by thiobarbituric acid reaction. Anal. Biochem. 95: 351-8, 1979.

131. Ong SE and Mann M: Mass spectrometry-based proteomics turns quantitative. Nat. Chem. Biol. 1: 252-62, 2005.

132. Orrenius S, Gogvadze V and Zhivotovsky B: Mitochondrial oxidative stress: implications for cell death. Annu. Rev. Pharmacol. Toxicol. 47: 143-83, 2007.

133. Ott M, Gogvadze V, Orrenius S and Zhivotovsky B: Mitochondria, oxidative stress and cell death. Apoptosis 12: 913-22, 2007.

134. Pacifici RE and Davies KJ: Protein, lipid and DNA repair systems in oxidative stress: the free-radical theory of aging revisited. Gerontology 37: 166-80, 1991.

135. Palmer JW, Tandler B and Hoppel CL: Biochemical properties of subsarcolemmal and interfibrillar mitochondria isolated from rat cardiac muscle. J. Biol. Chem. 252: 8731-9, 1977.

136. Pancholi V: Multifunctional alpha-enolase: its role in diseases. Cell. Mol. Life Sci. 58: 902-20, 2001.

137. Papakonstanti EA and Stournaras C: Cell responses regulated by early reorganization of actin cytoskeleton. FEBS Lett. 582: 2120-7, 2008.

138. Pierce A, Mirzaei H, Muller F, De Waal E, Taylor AB, Leonard S, Van Remmen H, Regnier F, Richardson A and Chaudhuri A: GAPDH is conformationally and functionally altered in association with oxidative stress in mouse models of amyotrophic lateral sclerosis. J. Mol. Biol. 382: 1195-210, 2008.

139. Pocker Y and Dickerson DG: The catalytic versatility of erythrocyte carbonic anhydrase. V. Kinetic studies of enzyme-catalyzed hydrations of aliphatic aldehydes. Biochemistry 7: 1995-2004, 1968.

140. Poli G, Schaur RJ, Siems WG and Leonarduzzi G: 4-hydroxynonenal: a membrane lipid oxidation product of medicinal interest. Med. Res. Rev. 28: 569-631, 2008.

141. Pompella A, Visvikis A, Paolicchi A, De Tata V and Casini AF: The changing faces of glutathione, a cellular protagonist. Biochem. Pharmacol. 66: 1499-503, 2003.

142. Poon HF, Calabrese V, Scapagnini G and Butterfield DA: Free radicals and brain aging. Clin. Geriatr. Med. 20: 329-59, 2004.

143. Raffray M and Cohen GM: Apoptosis and necrosis in toxicology: a continuum or distinct modes of cell death? Pharmacol. Ther. 75: 153-77, 1997.

144. Rasola A and Bernardi P: The mitochondrial permeability transition pore and its involvement in cell death and in disease pathogenesis. Apoptosis 12: 815-33, 2007.

145. Rauniyar N, Stevens SM, Jr. and Prokai L: Fourier transform ion cyclotron resonance mass spectrometry of covalent adducts of proteins and 4-hydroxy-2-nonenal, a reactive end-product of lipid peroxidation. Anal. Bioanal. Chem. 389: 1421-8, 2007.

146. Rauniyar N, Stevens SM, Prokai-Tatrai K and Prokai L: Characterization of 4-hydroxy-2-nonenal-modified peptides by liquid chromatography-tandem mass spectrometry using data-dependent acquisition: neutral loss-driven MS3 versus neutral loss-driven electron capture dissociation. Anal. Chem. 81: 782-9, 2009.

147. Reed T, Perluigi M, Sultana R, Pierce WM, Klein JB, Turner DM, Coccia R, Markesbery WR and Butterfield DA: Redox proteomic identification of 4-hydroxy-2-nonenal-modified brain proteins in amnestic mild cognitive impairment: insight into the role of lipid peroxidation in the progression and pathogenesis of Alzheimer's disease. Neurobiol. Dis. 30: 107-20, 2008.

148. Reinheckel T, Korn S, Mohring S, Augustin W, Halangk W and Schild L: Adaptation of protein carbonyl detection to the requirements of proteome analysis demonstrated for hypoxia/reoxygenation in isolated rat liver mitochondria. Arch Biochem Biophys 376: 59-65, 2000.

149. Requena JR, Chao CC, Levine RL and Stadtman ER: Glutamic and aminoadipic semialdehydes are the main carbonyl products of metal-catalyzed oxidation of proteins. Proc Natl Acad Sci U S A 98: 69-74, 2001.

150. Roe MR, Xie H, Bandhakavi S and Griffin TJ: Proteomic mapping of 4-hydroxynonenal protein modification sites by solid-phase hydrazide chemistry and mass spectrometry. Anal. Chem. 79: 3747-56, 2007.

151. Roede JR, Carbone DL, Doorn JA, Kirichenko OV, Reigan P and Petersen DR: In vitro and in silico characterization of peroxiredoxin 6 modified by 4-hydroxynonenal and 4-oxononenal. Chem. Res. Toxicol. 21: 2289-2299, 2008.

152. Roepstorff P and Fohlman J: Proposal for a common nomenclature for sequence ions in mass spectra of peptides. Biomed. Mass Spectrom. 11: 601, 1984.

153. Romero FJ, Bosch-Morell F, Romero MJ, Jareno EJ, Romero B, Marin N and Roma J: Lipid peroxidation products and antioxidants in human disease. Environ. Health Perspect. 106 Suppl 5: 1229-34, 1998.

154. Salomon RG, Kaur K, Podrez E, Hoff HF, Krushinsky AV and Sayre LM: HNE-derived 2-pentylpyrroles are generated during oxidation of LDL, are more prevalent in blood plasma from patients with renal disease or atherosclerosis, and are present in atherosclerotic plaques. Chem Res Toxicol 13: 557-64, 2000.

155. Sastre J, Pallardo FV and Vina J: Mitochondrial oxidative stress plays a key role in aging and apoptosis. IUBMB Life 49: 427-35, 2000.

156. Sayre LM, Lin D, Yuan Q, Zhu X and Tang X: Protein adducts generated from products of lipid oxidation: focus on HNE and one. Drug Metab. Rev. 38: 651-75, 2006.

157. Sayre LM, Smith MA and Perry G: Chemistry and biochemistry of oxidative stress in neurodegenerative disease. Curr. Med. Chem. 8: 721-38, 2001.

158. Schagger H: Native electrophoresis for isolation of mitochondrial oxidative phosphorylation protein complexes. Methods. Enzymol. 260: 190-202, 1995.

159. Schagger H and von Jagow G: Blue native electrophoresis for isolation of membrane protein complexes in enzymatically active form. Anal. Biochem. 199: 223-31, 1991.

160. Schoneich C: Mass spectrometry in aging research. Mass Spectrom. Rev. 24: 701-18, 2005.

161. Shapiro AL, Vinuela E and Maizel JV, Jr.: Molecular weight estimation of polypeptide chains by electrophoresis in SDS-polyacrylamide gels. Biochem. Biophys. Res. Commun. 28: 815-20, 1967.

162. Shrake A and Rupley JA: Environment and exposure to solvent of protein atoms. Lysozyme and insulin. J. Mol. Biol. 79: 351-71, 1973.

163. Sjoblom B, Salmazo A and Djinovic-Carugo K: Alpha-actinin structure and regulation. Cell. Mol. Life Sci. 65: 2688-701, 2008.

164. Soreghan BA, Yang F, Thomas SN, Hsu J and Yang AJ: High-throughput proteomic-based identification of oxidatively induced protein carbonylation in mouse brain. Pharm. Res. 20: 1713-20, 2003.

165. St-Pierre J, Buckingham JA, Roebuck SJ and Brand MD: Topology of superoxide production from different sites in the mitochondrial electron transport chain. J. Biol. Chem. 277: 44784-90, 2002.

166. Stadtman ER: Protein oxidation in aging and age-related diseases. Ann N Y Acad Sci 928: 22-38, 2001.

167. Stadtman ER: Protein oxidation and aging. Free Radic. Res. 40: 1250-8, 2006.

168. Stevens JF and Maier CS: Acrolein: sources, metabolism, and biomolecular interactions relevant to human health and disease. Mol. Nutr. Food Res. 52: 7-25, 2008.

169. Stevens SM, Jr., Rauniyar N and Prokai L: Rapid characterization of covalent modifications to rat brain mitochondrial proteins after ex vivo exposure to 4-hydroxy-2-nonenal by liquid chromatography-tandem mass spectrometry using data-dependent and neutral loss-driven MS3 acquisition. J. Mass Spectrom. 42: 1599-605, 2007.

170. Stewart BJ, Doorn JA and Petersen DR: Residue-specific adduction of tubulin by 4-hydroxynonenal and 4-oxononenal causes cross-linking and inhibits polymerization. Chem. Res. Toxicol. 20: 1111-9, 2007.

171. Suh JH, Heath SH and Hagen TM: Two subpopulations of mitochondria in the aging rat heart display heterogenous levels of oxidative stress. Free Radic. Biol. Med. 35: 1064-72, 2003.

172. Sultana R, Boyd-Kimball D, Poon HF, Cai J, Pierce WM, Klein JB, Merchant M, Markesbery WR and Butterfield DA: Redox proteomics identification of oxidized proteins in Alzheimer's disease hippocampus and cerebellum: an approach to understand pathological and biochemical alterations in AD. Neurobiol. Aging 27: 1564-76, 2006.

173. Sun L, Luo C, Long J, Wei D and Liu J: Acrolein is a mitochondrial toxin: effects on respiratory function and enzyme activities in isolated rat liver mitochondria. Mitochondrion 6: 136-42, 2006.

174. Syka JE, Coon JJ, Schroeder MJ, Shabanowitz J and Hunt DF: Peptide and protein sequence analysis by electron transfer dissociation mass spectrometry. Proc. Natl. Acad. Sci. U. S. A. 101: 9528-33, 2004.

175. Tanaka K, Waki H, Ido Y, Akita S, Yoshida Y, Yoshida T and Matsuo T: Protein and polymer analyses up to m/z 100 000 by laser ionization time-of-flight mass spectrometry. Rapid Communications in Mass Spectrometry 2: 151-153, 1988.

176. Tanaka N, Tajima S, Ishibashi A, Uchida K and Shigematsu T: Immunohistochemical detection of lipid peroxidation products, protein-bound acrolein and 4-hydroxynonenal protein adducts, in actinic elastosis of photodamaged skin. Arch. Dermatol. Res. 293: 363-7, 2001.

177. Taylor SW, Fahy E, Murray J, Capaldi RA and Ghosh SS: Oxidative post-translational modification of tryptophan residues in cardiac mitochondrial proteins. J. Biol. Chem. 278: 19587-90, 2003.

178. Temple A, Yen TY and Gronert S: Identification of specific protein carbonylation sites in model oxidations of human serum albumin. J. Am. Soc. Mass Spectrom. 17: 1172-80, 2006.

179. Terni B, Boada J, Portero-Otin M, Pamplona R and Ferrer I: Mitochondrial ATP-Synthase in the Entorhinal Cortex Is a Target of Oxidative Stress at Stages I/II of Alzheimer's Disease Pathology. Brain Pathol.: 2009.

180. Toroser D, Orr WC and Sohal RS: Carbonylation of mitochondrial proteins in Drosophila melanogaster during aging. Biochem. Biophys. Res. Commun. 363: 418-24, 2007.

181. Tsuchiya Y, Yamaguchi M, Chikuma T and Hojo H: Degradation of glyceraldehyde-3-phosphate dehydrogenase triggered by 4-hydroxy-2-nonenal and 4-hydroxy-2-hexenal. Arch. Biochem. Biophys. 438: 217-22, 2005.

182. Tsujimoto Y and Shimizu S: Role of the mitochondrial membrane permeability transition in cell death. Apoptosis 12: 835-40, 2007.

183. Uchida K: 4-Hydroxy-2-nonenal: a product and mediator of oxidative stress. Prog. Lipid Res. 42: 318-43, 2003.

184. Uchida K, Hasui Y and Osawa T: Covalent attachment of 4-hydroxy-2-nonenal to erythrocyte proteins. J. Biochem. 122: 1246-51, 1997.

185. Uchida K, Kanematsu M, Morimitsu Y, Osawa T, Noguchi N and Niki E: Acrolein is a product of lipid peroxidation reaction. Formation of free acrolein and its conjugate with lysine residues in oxidized low density lipoproteins. J. Biol. Chem. 273: 16058-66, 1998.

186. Unwin RD, Craven RA, Harnden P, Hanrahan S, Totty N, Knowles M, Eardley I, Selby PJ and Banks RE: Proteomic changes in renal cancer and co-ordinate demonstration of both the glycolytic and mitochondrial aspects of the Warburg effect. Proteomics 3: 1620-32, 2003.

187. Van Coster R, Smet J, George E, De Meirleir L, Seneca S, Van Hove J, Sebire G, Verhelst H, De Bleecker J, Van Vlem B, Verloo P and Leroy J: Blue native polyacrylamide gel electrophoresis: a powerful tool in diagnosis of oxidative phosphorylation defects. Pediatr. Res. 50: 658-65, 2001.

188. Vila A, Tallman KA, Jacobs AT, Liebler DC, Porter NA and Marnett LJ: Identification of protein targets of 4-hydroxynonenal using click chemistry for ex vivo biotinylation of azido and alkynyl derivatives. Chem. Res. Toxicol. 21: 432-44, 2008.

189. Volker KW and Knull H: A glycolytic enzyme binding domain on tubulin. Arch. Biochem. Biophys. 338: 237-43, 1997.

190. Wallace DC: Mitochondrial diseases in man and mouse. Science 283: 1482-8, 1999.

191. Wang J, Morris AJ, Tolan DR and Pagliaro L: The molecular nature of the F-actin binding activity of aldolase revealed with site-directed mutants. J. Biol. Chem. 271: 6861-5, 1996.

192. Wang P, Tang H, Fitzgibbon MP, McIntosh M, Coram M, Zhang H, Yi E and Aebersold R: A statistical method for chromatographic alignment of LC-MS data. Biostatistics 8: 357-67, 2007.

193. Washburn MP, Wolters D and Yates JR, 3rd: Large-scale analysis of the yeast proteome by multidimensional protein identification technology. Nat. Biotechnol. 19: 242-7, 2001.

194. Wen JJ and Garg N: Oxidative modification of mitochondrial respiratory complexes in response to the stress of Trypanosoma cruzi infection. Free Radic. Biol. Med. 37: 2072-81, 2004.

195. West JD and Marnett LJ: Endogenous reactive intermediates as modulators of cell signaling and cell death. Chem Res Toxicol 19: 173-94, 2006.

196. Wong HL and Liebler DC: Mitochondrial protein targets of thiol-reactive electrophiles. Chem. Res. Toxicol. 21: 796-804, 2008.

197. Wysocki VH, Tsaprailis G, Smith LL and Breci LA: Mobile and localized protons: a framework for understanding peptide dissociation. J Mass Spectrom 35: 1399-406, 2000.

198. Yang JC and Cortopassi GA: Induction of the mitochondrial permeability transition causes release of the apoptogenic factor cytochrome c. Free Radic. Biol. Med. 24: 624-31, 1998.

199. Yoo BS and Regnier FE: Proteomic analysis of carbonylated proteins in two-dimensional gel electrophoresis using avidin-fluorescein affinity staining. Electrophoresis 25: 1334-41, 2004.

200. Zhu X, Tang X, Anderson VE and Sayre LM: Mass Spectrometric Characterization of Protein Modification by the Products of Nonenzymatic Oxidation of Linoleic Acid. Chem. Res. Toxicol.: 2009.

201. Zubarev RA, Zubarev AR and Savitski MM: Electron capture/transfer versus collisionally activated/induced dissociations: solo or duet? J. Am. Soc. Mass Spectrom. 19: 753-61, 2008.

APPENDICES

Appendix A

Supplemental Material for Chapter 1

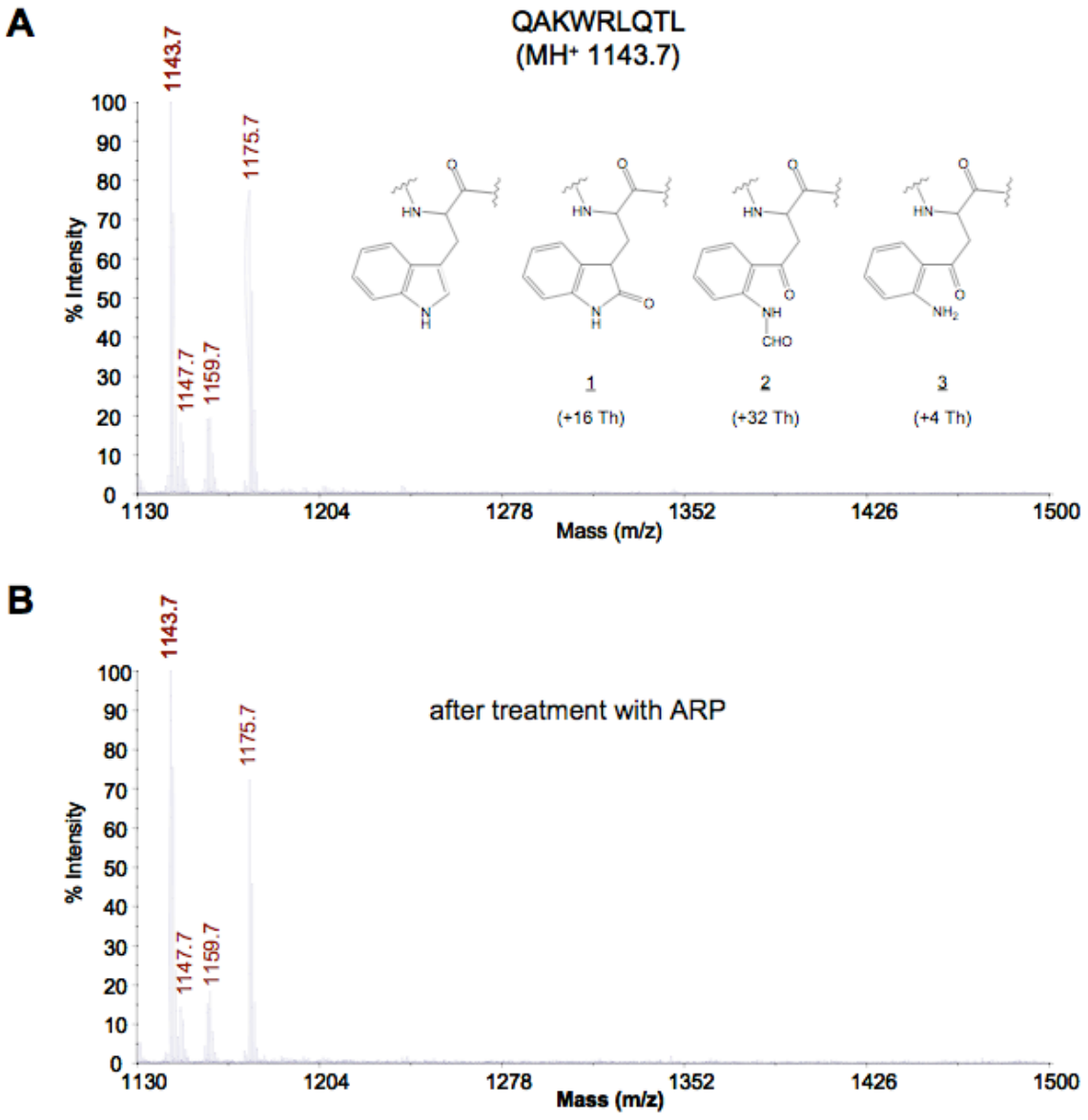

Figure SA1 - (A) MALDI mass spectrum of the model peptide QAKWRLQTL after oxidation by H2O2; Ions at m/z 1159.7 (+16 Th), m/z 1175.7 (+32 Th) and m/z 1147.7 (+4 Th) indicate oxidation of the Trp residue. Structures of the oxidized Trp derivatives and the respective mass shifts are depicted. (B) Mass spectrum of the oxidized peptide mixture after treatment with ARP. MS shows no mass changes that would reflect modification by ARP.

Appendix B

Supplemental Material for Chapter 4

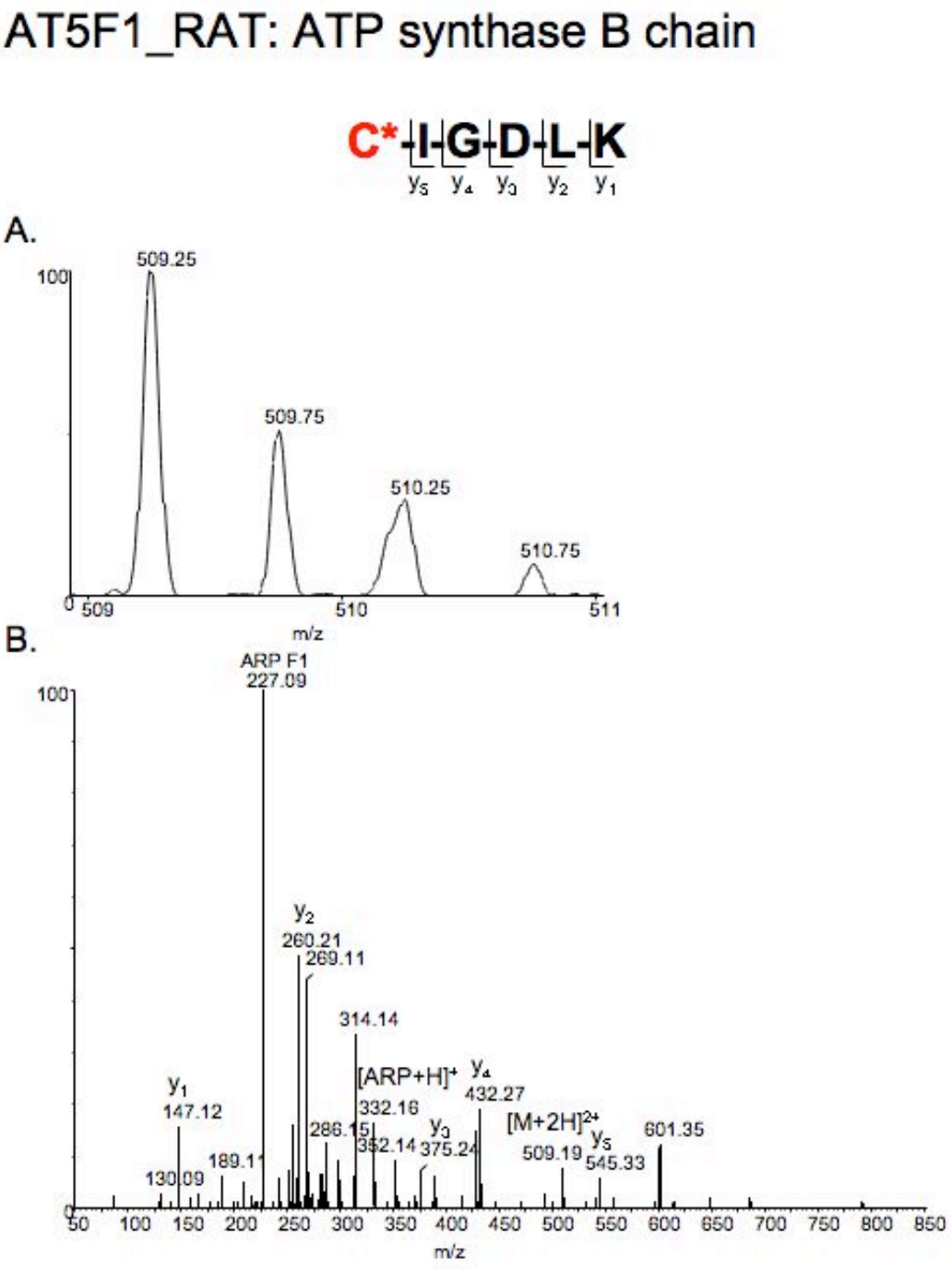

Figure SB1. (A) Full mass spectrum and (B) MS/MS spectrum acquired by ESI-Q-TOF of the $[M+2H]^{2+}$ ion of the ARP labeled, acrolein modified peptide C*IGDLK; monoisotopic m/z_{calc} 509.25; accuracy **Δ**(m/z) = 0.00 m/z

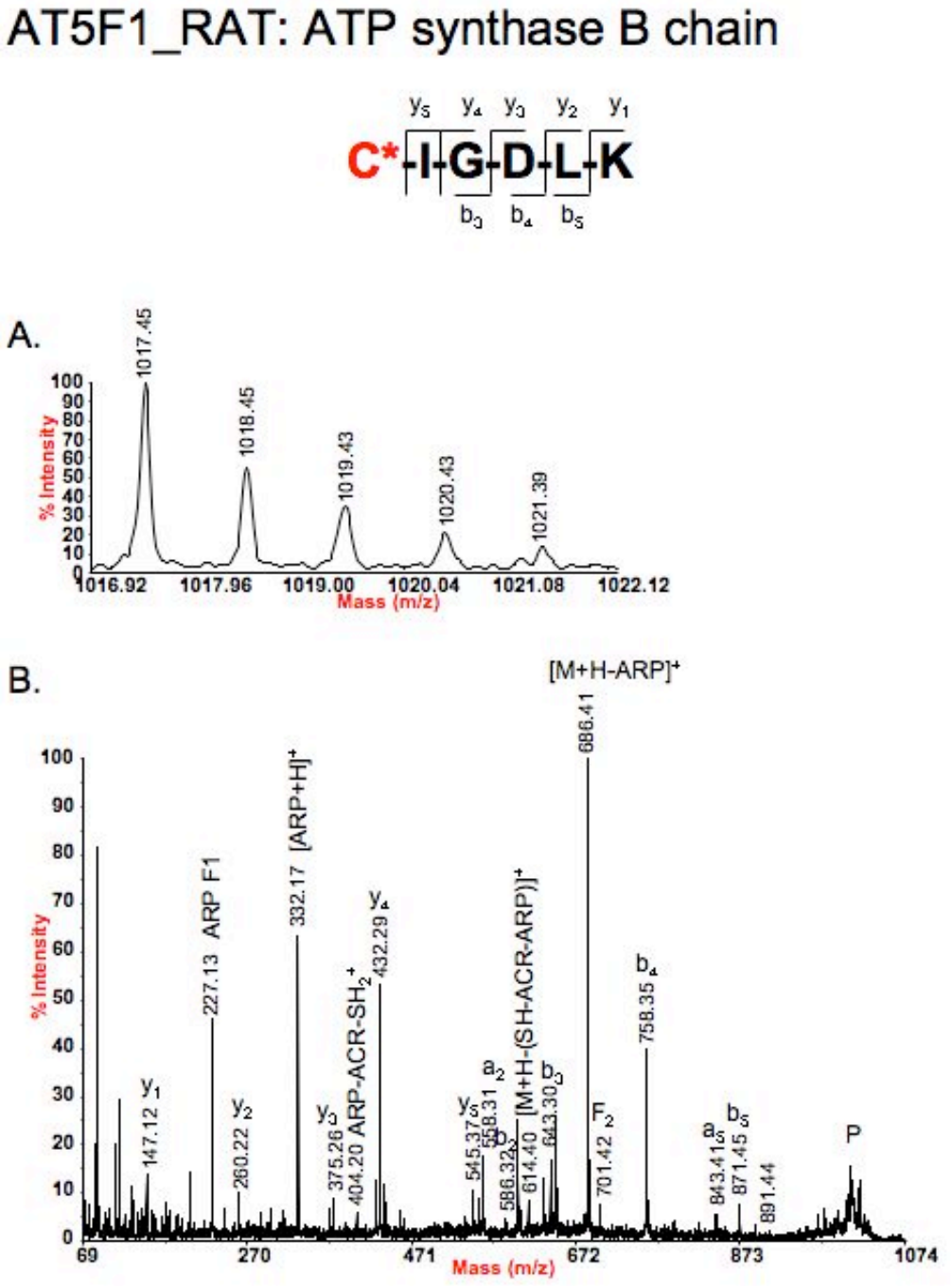

Figure SB2. (A) Full mass spectrum and (B) MS/MS spectrum acquired by MALDI-TOF/TOF of the $[M+H]^+$ ion of the ARP labeled, acrolein modified peptide C*IGDLK; monoisotopic m/z_{calc} 1017.49; accuracy **Δ**(m/z) = -0.04 m/z

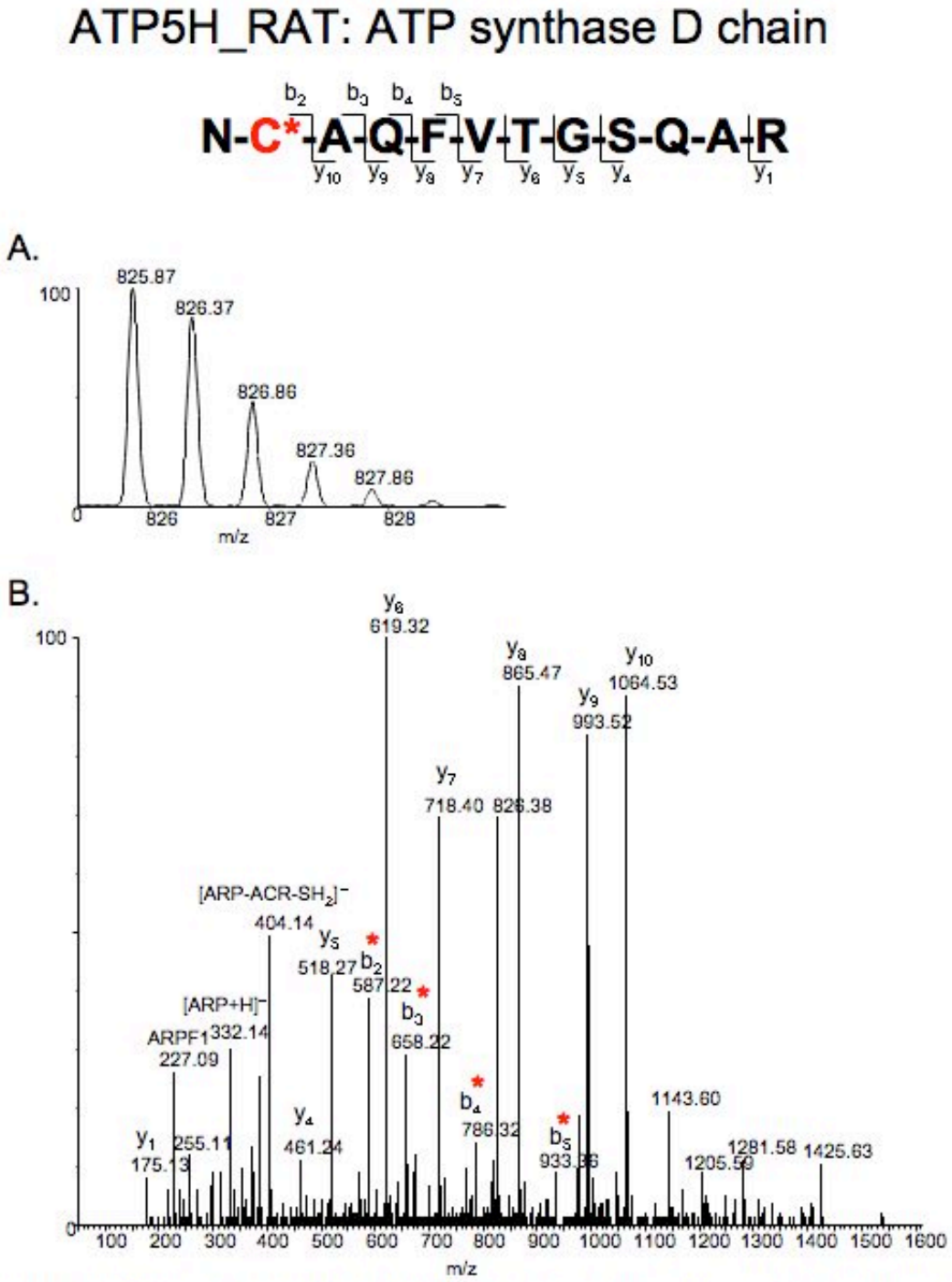

Figure SB3. (A) Full mass spectrum and (B) MS/MS spectrum acquired by ESI-Q-TOF of the $[M+2H]^{2+}$ ion of the ARP labeled, acrolein modified peptide NC*AQFVTGSQAR; monoisotopic m/z_{calc} 825.88; accuracy $\Delta(m/z)$ = -0.01 m/z

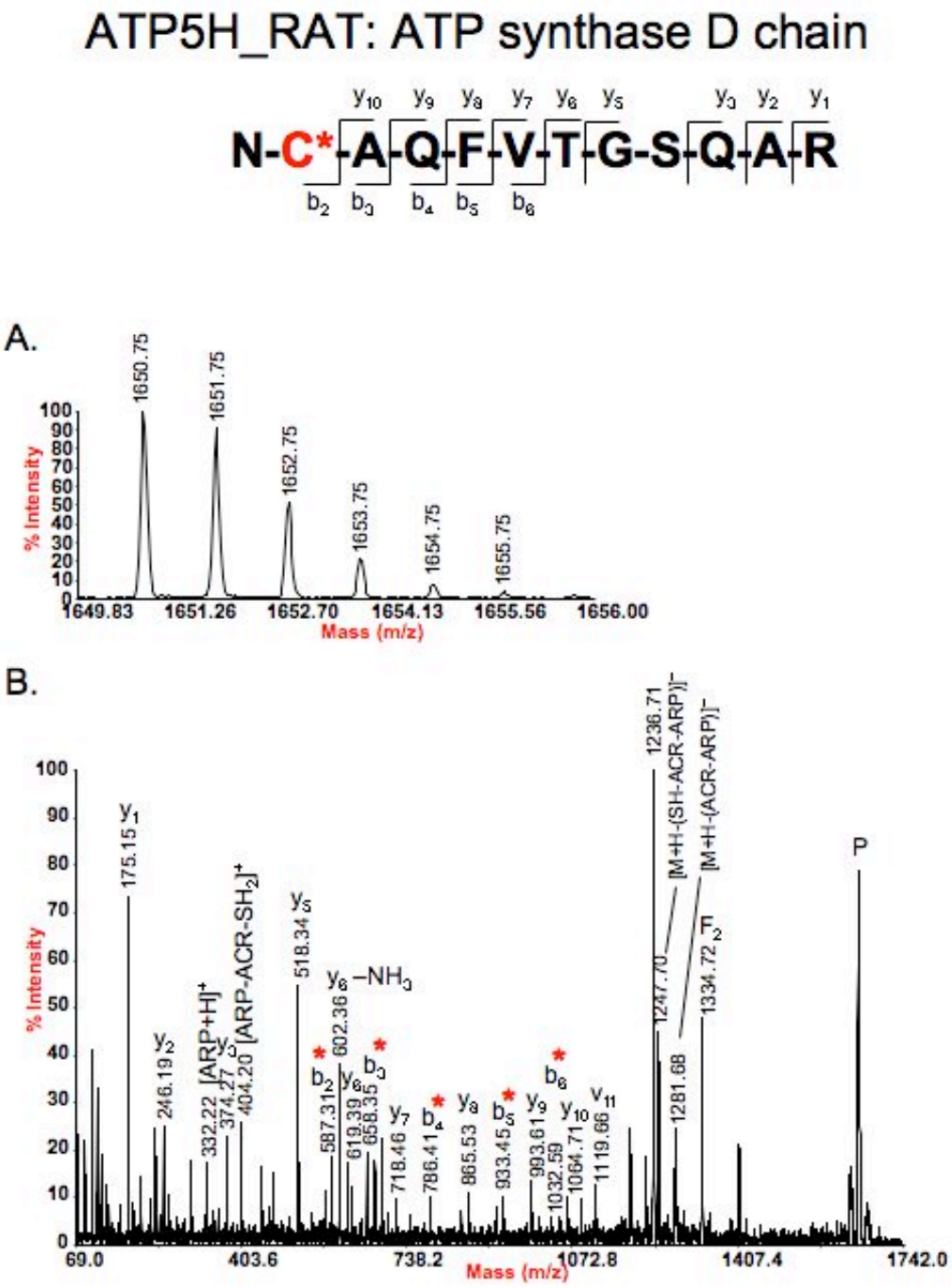

Figure SB4. (A) Full mass spectrum and (B) MS/MS spectrum acquired by MALDI-TOF/TOF of the $[M+H]^+$ ion of the ARP labeled, acrolein modified peptide NC*AQFVTGSQAR; monoisotopic m/z_{calc} 1650.75; accuracy **Δ**(m/z) = 0.00 m/z

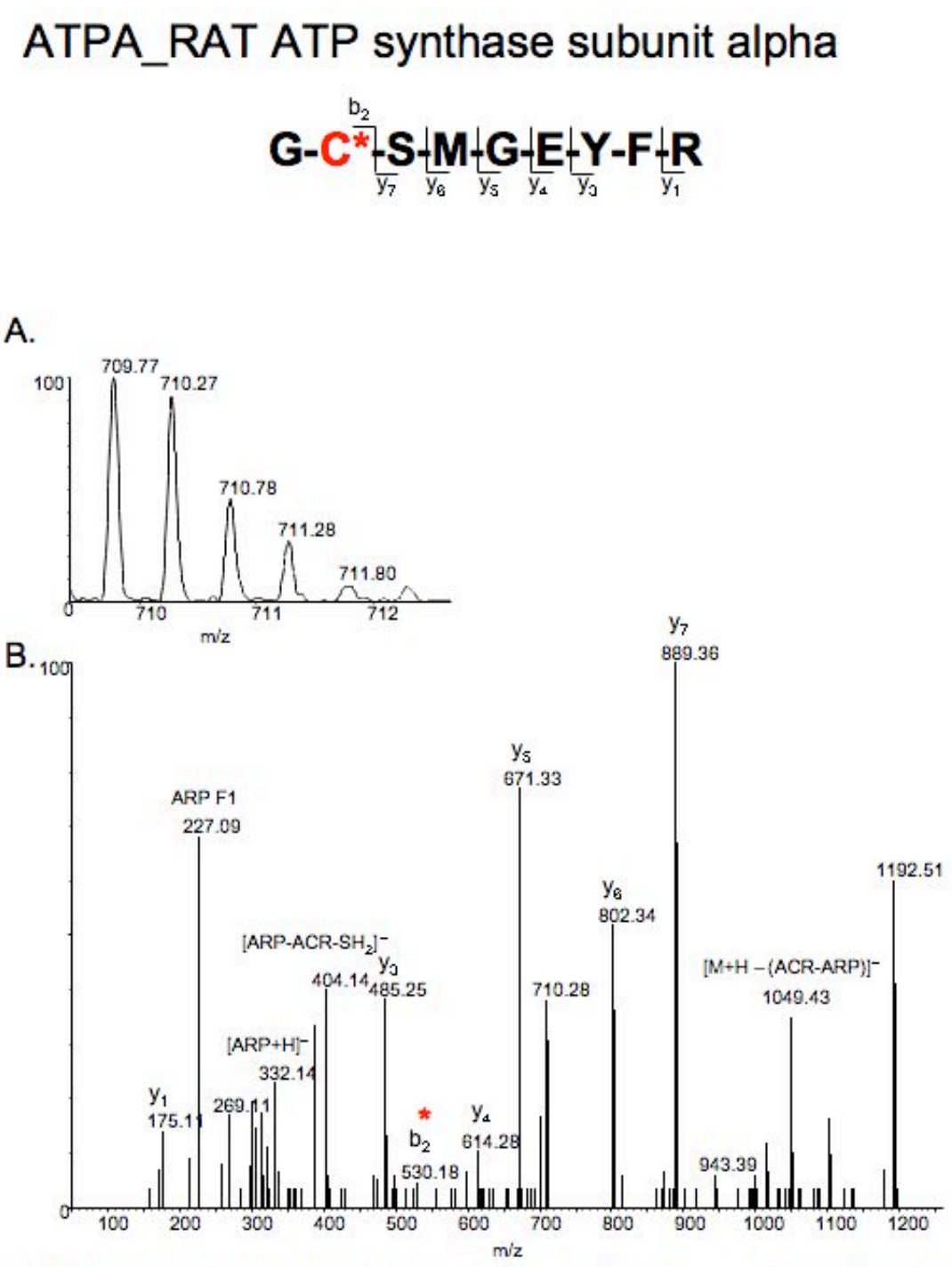

Figure SB5. (A) Full mass spectrum and (B) MS/MS spectrum acquired by ESI-Q-TOF of the $[M+2H]^{2+}$ ion of the ARP labeled, acrolein modified peptide GC*SMGEYFR; monoisotopic m/z_{calc} 709.79; accuracy **Δ**(m/z) = -0.02 m/z

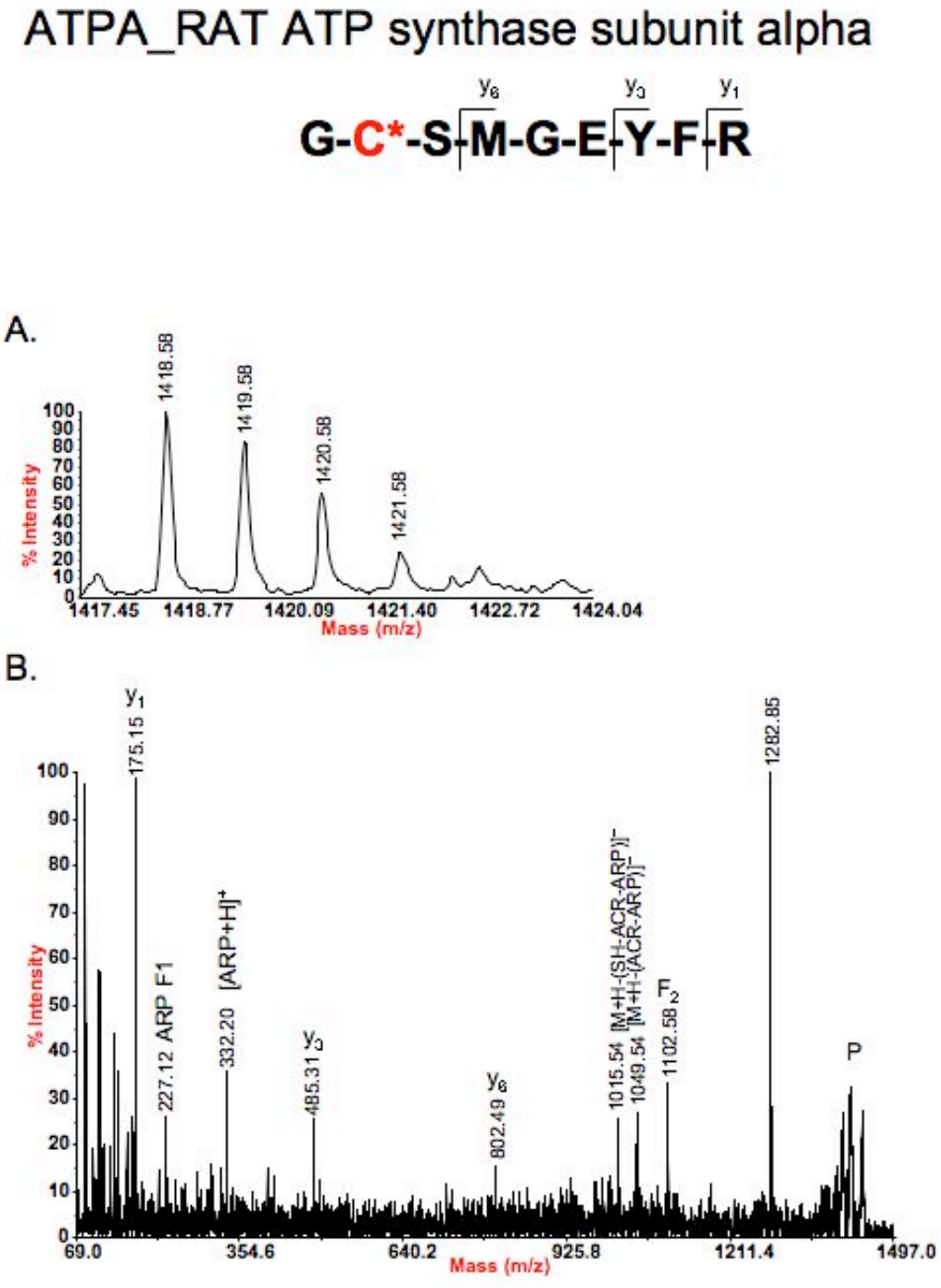

Figure SB6. (A) Full mass spectrum and (B) MS/MS spectrum acquired byMALDI-TOF/TOF of the $[M+H]^+$ ion of the ARP labeled, acrolein modified peptide GC*SMGEYFR; monoisotopic m/z_{calc} 1418.57; accuracy **Δ**(m/z) = 0.01 m/z

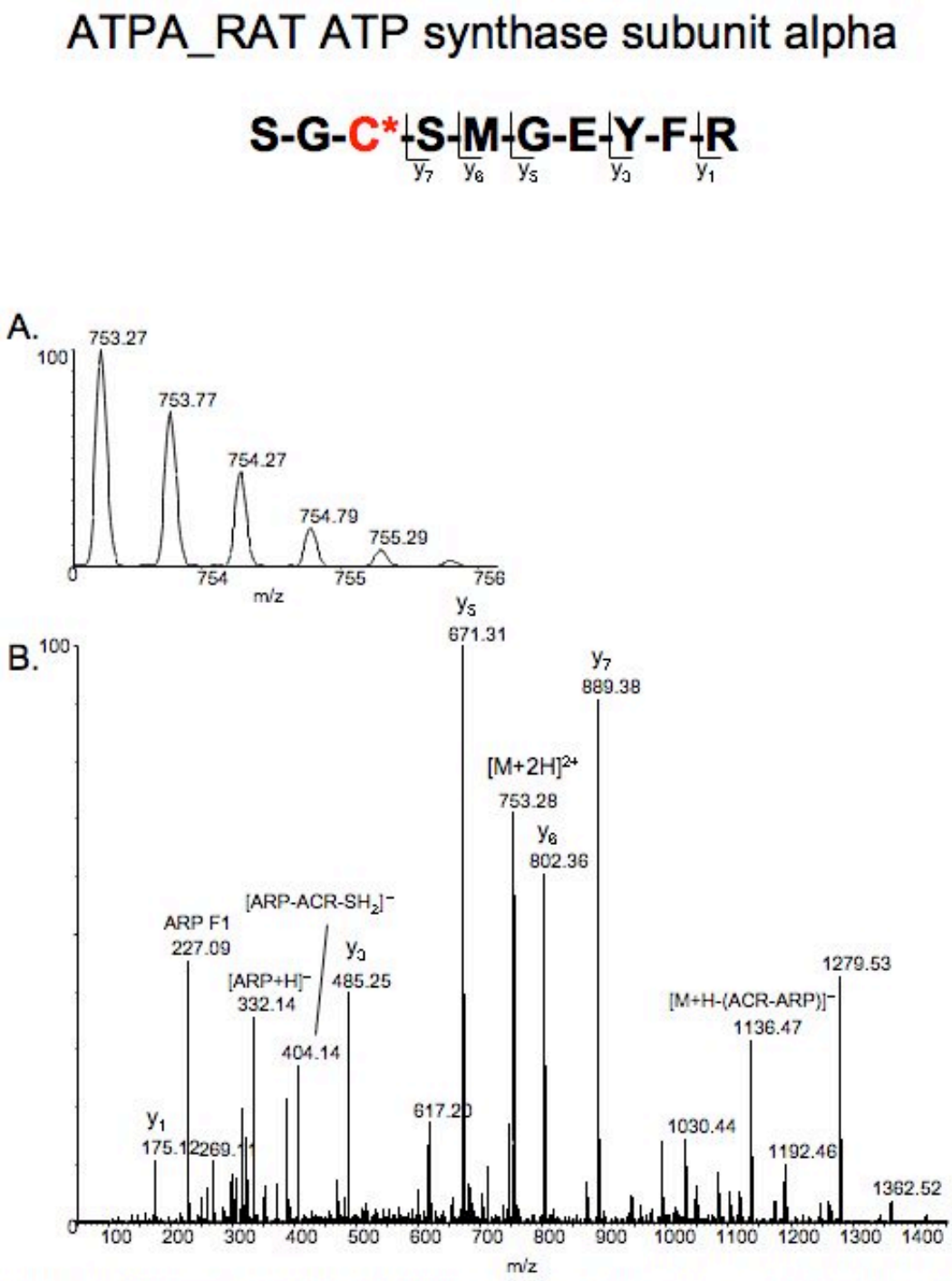

Figure SB7. (A) Full mass spectrum and (B) MS/MS spectrum acquired by ESI-Q-TOF of the $[M+2H]^{2+}$ ion of the ARP labeled, acrolein modified peptide SGC*SMGEYFR; monoisotopic m/z_{calc} 753.30; accuracy **Δ**(m/z) = -0.03 m/z

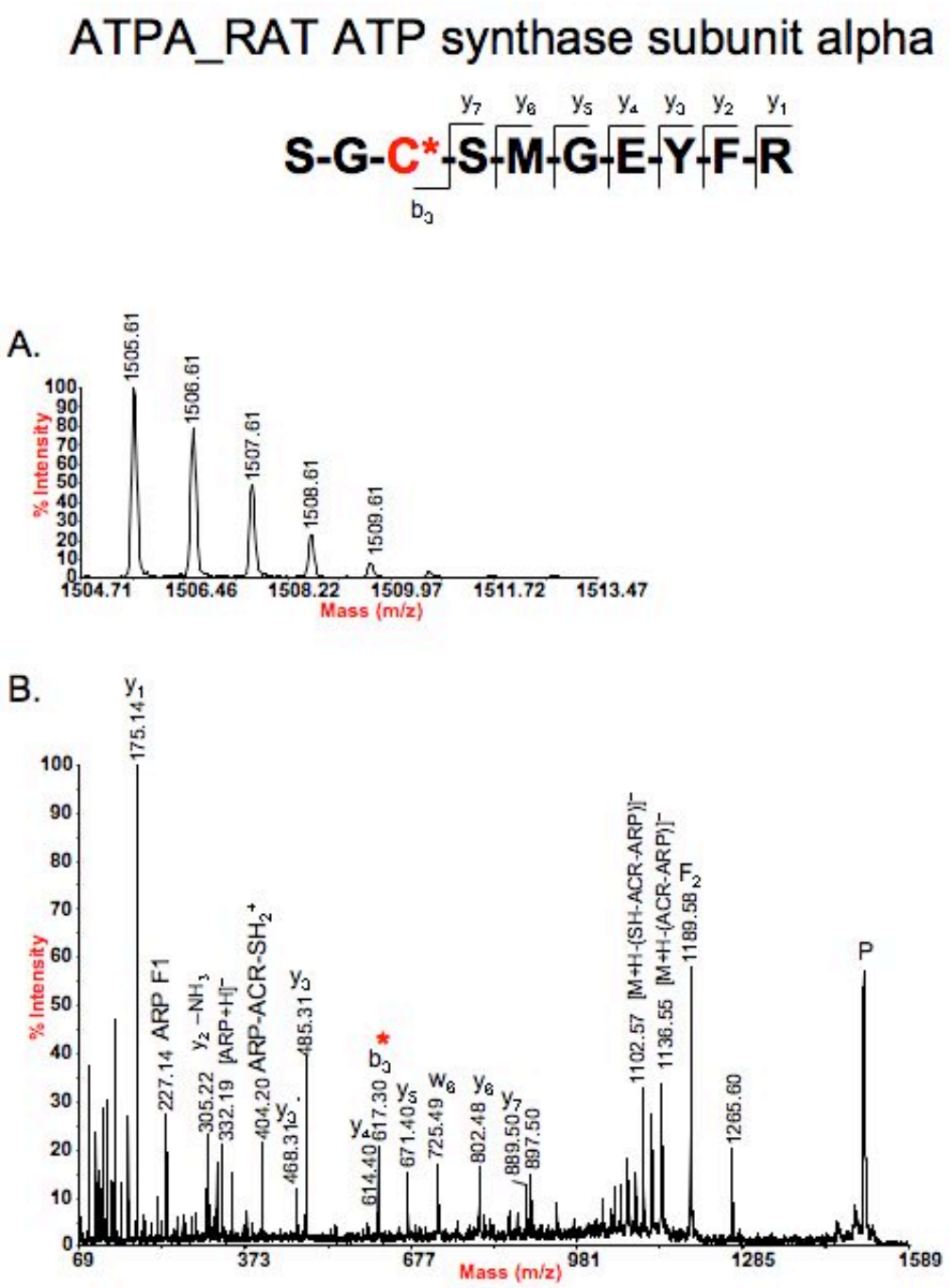

Figure SB8. (A) Full mass spectrum and (B) MS/MS spectrum acquired by MALDI-TOF/TOF of the $[M+H]^+$ ion of the ARP labeled, acrolein modified peptide SGC*SMGEYFR; monoisotopic m/z_{calc} 1505.60; accuracy **Δ**(m/z) = 0.01 m/z

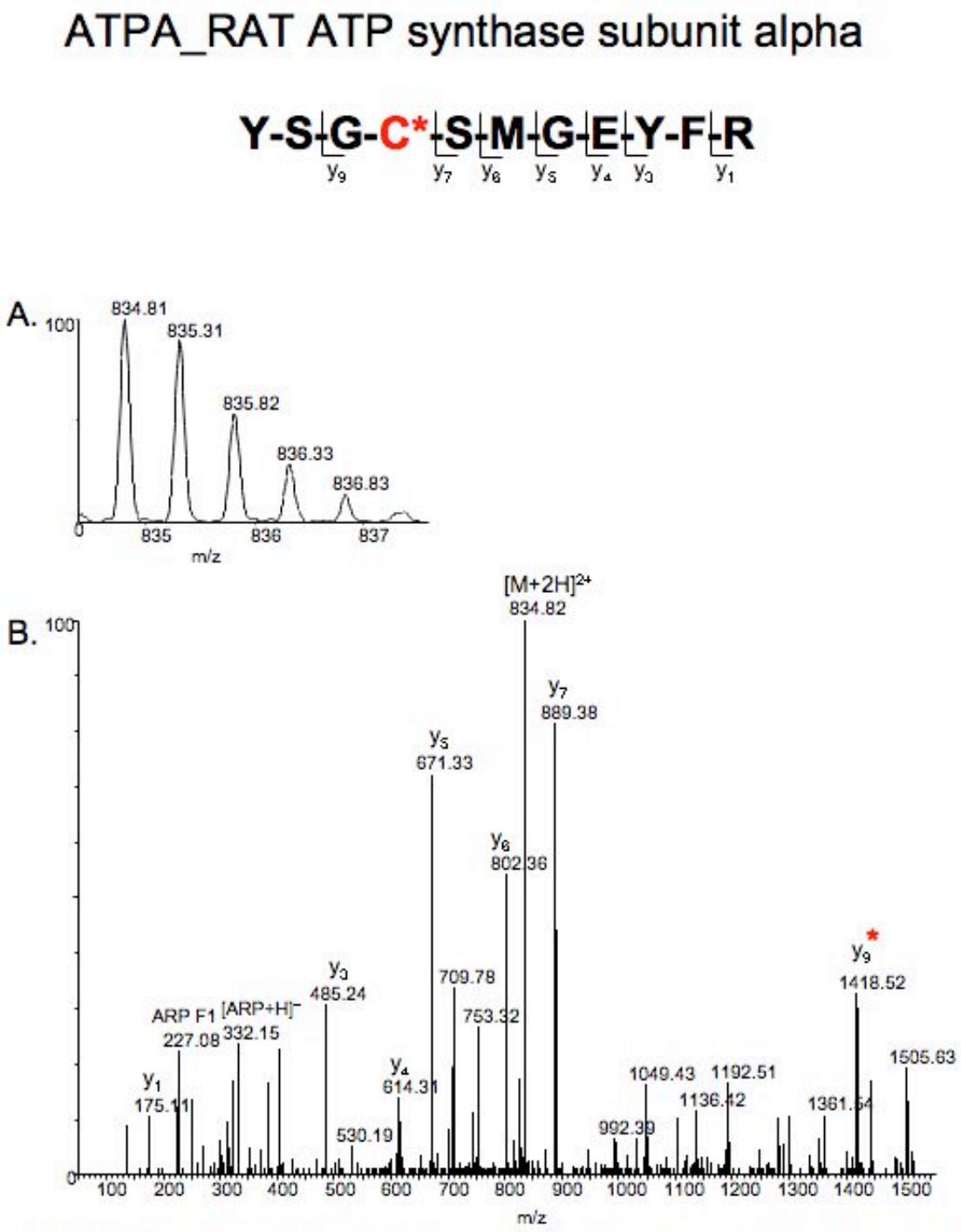

Figure SB9. (A) Full mass spectrum and (B) MS/MS spectrum acquired by ESI-Q-TOF of the $[M+2H]^{2+}$ ion of the ARP labeled, acrolein modified peptide YSGC*SMGEYFR; monoisotopic m/z_{calc} 834.83; accuracy **Δ**(m/z) = -0.02 m/z

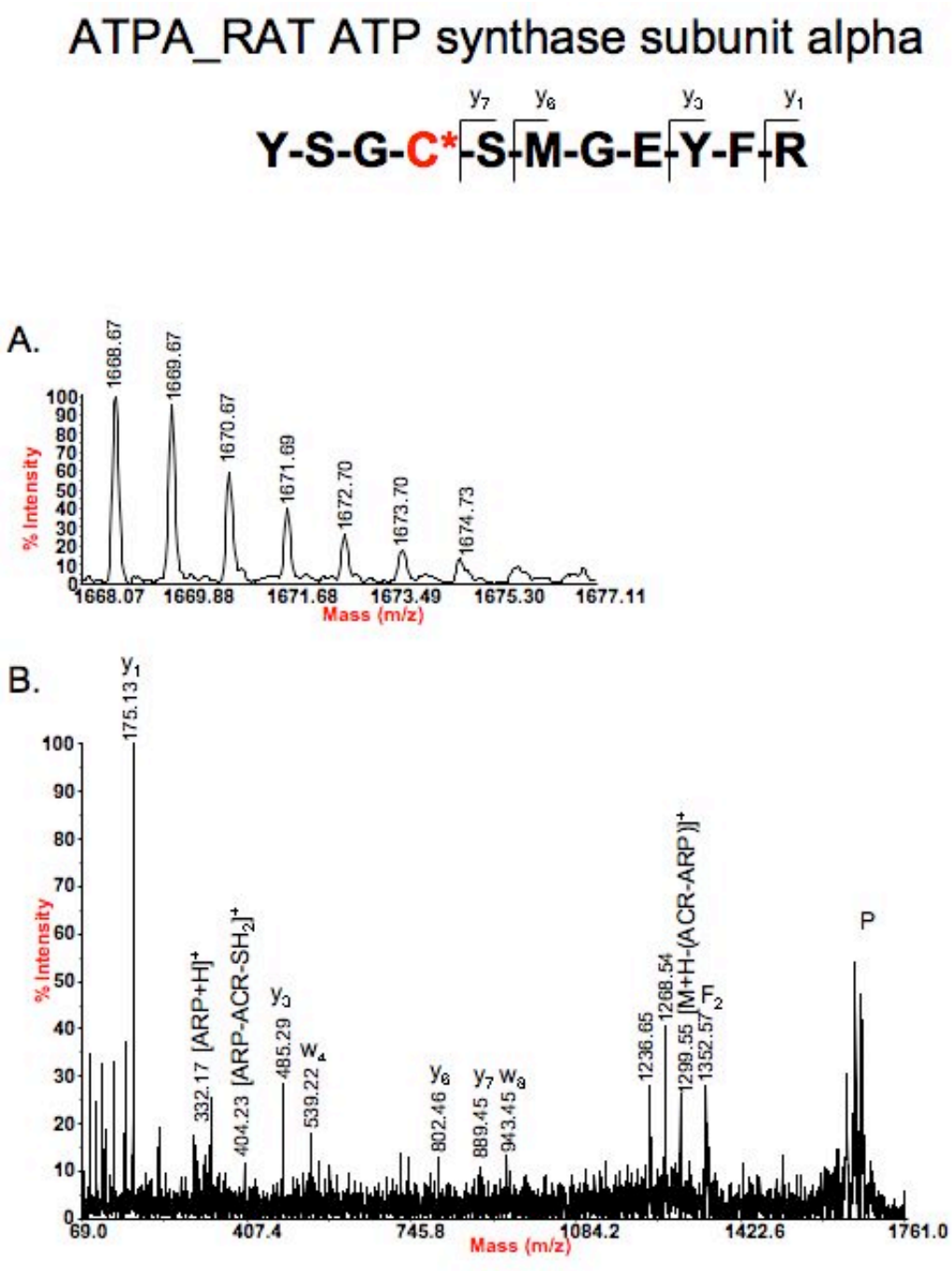

Figure SB10. (A) Full mass spectrum and (B) MS/MS spectrum acquired by MALDI-TOF/TOF of the $[M+H]^+$ ion of the ARP labeled, acrolein modified peptide YSGC*SMGEYFR; monoisotopic m/z_{calc} 1668.66; accuracy **Δ**(m/z) = -0.01 m/z

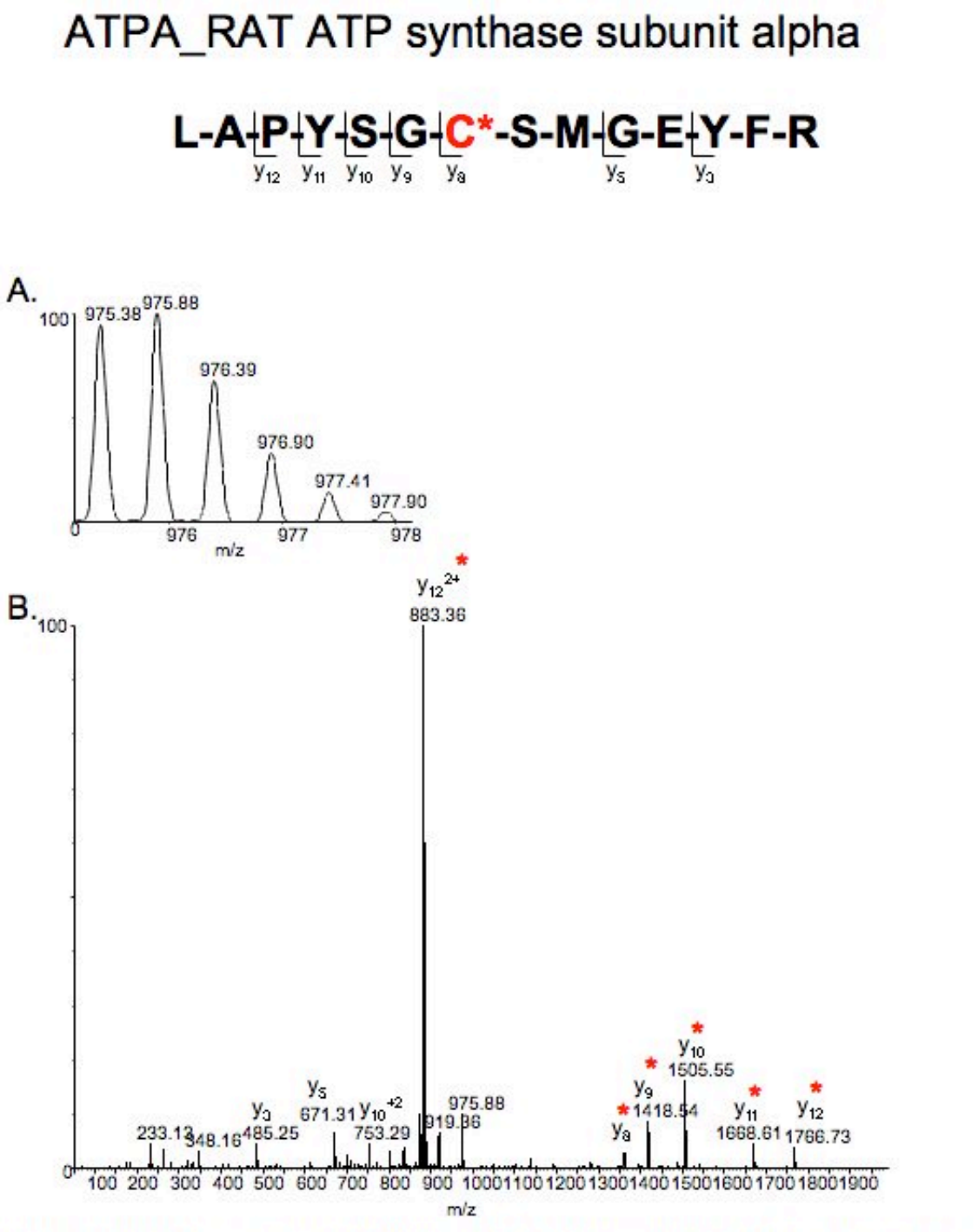

Figure SB11. (A) Full mass spectrum and (B) MS/MS spectrum acquired by ESI-Q-TOF of the $[M+2H]^{2+}$ ion of the ARP labeled, acrolein modified peptide LAPYSGC*SMGEYFR; monoisotopic m/z_{calc} 975.42; accuracy $\Delta(m/z)$ = -0.04 m/z

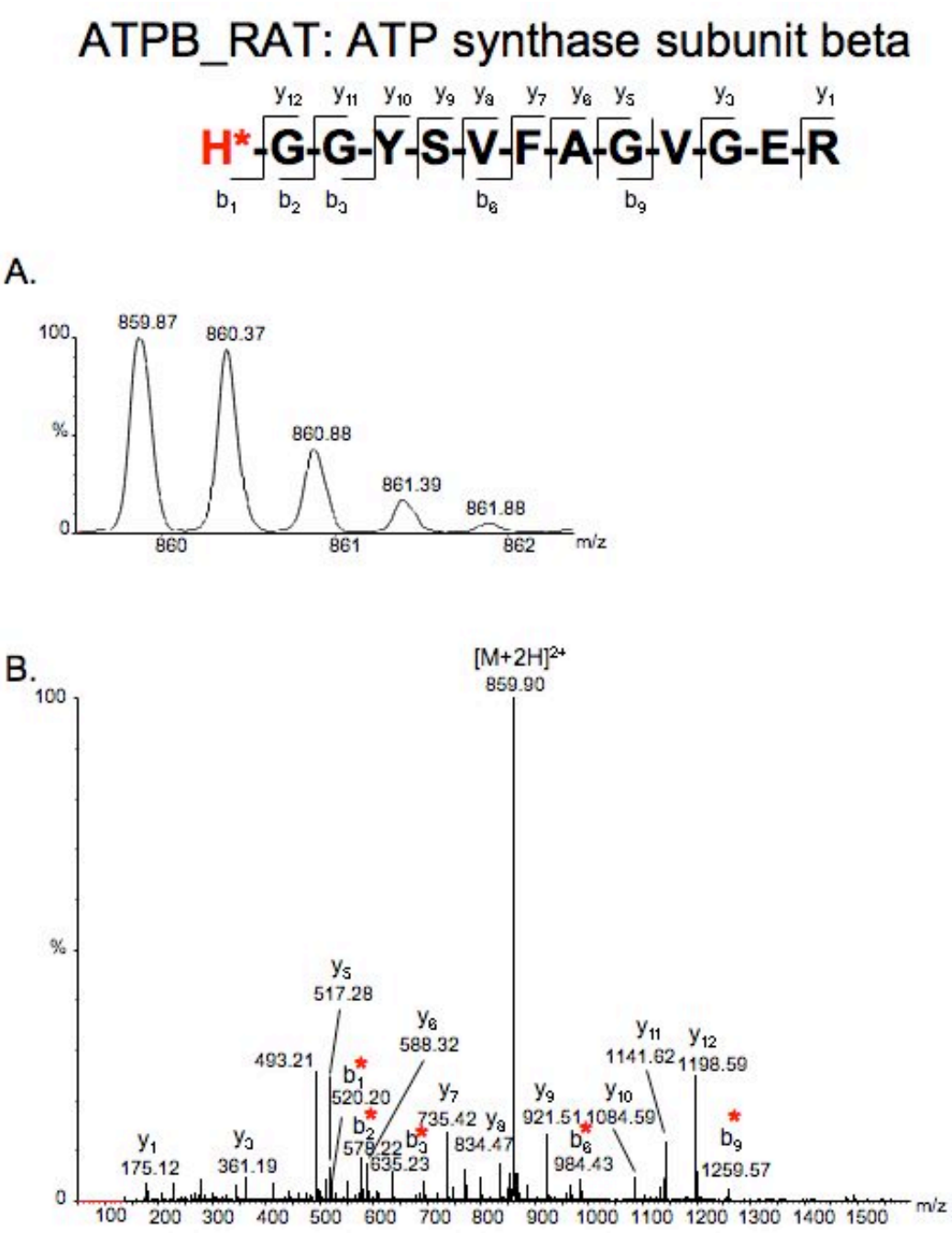

Figure SB12. (A) Full mass spectrum and (B) MS/MS spectrum acquired by ESI-Q-TOF of the $[M+2H]^{2+}$ ion of the ARP labeled, crotonaldehyde modified peptide H*GGYSVFAGVGER; monoisotopic m/z_{calc} 859.91; accuracy **Δ**(m/z) = -0.04 m/z

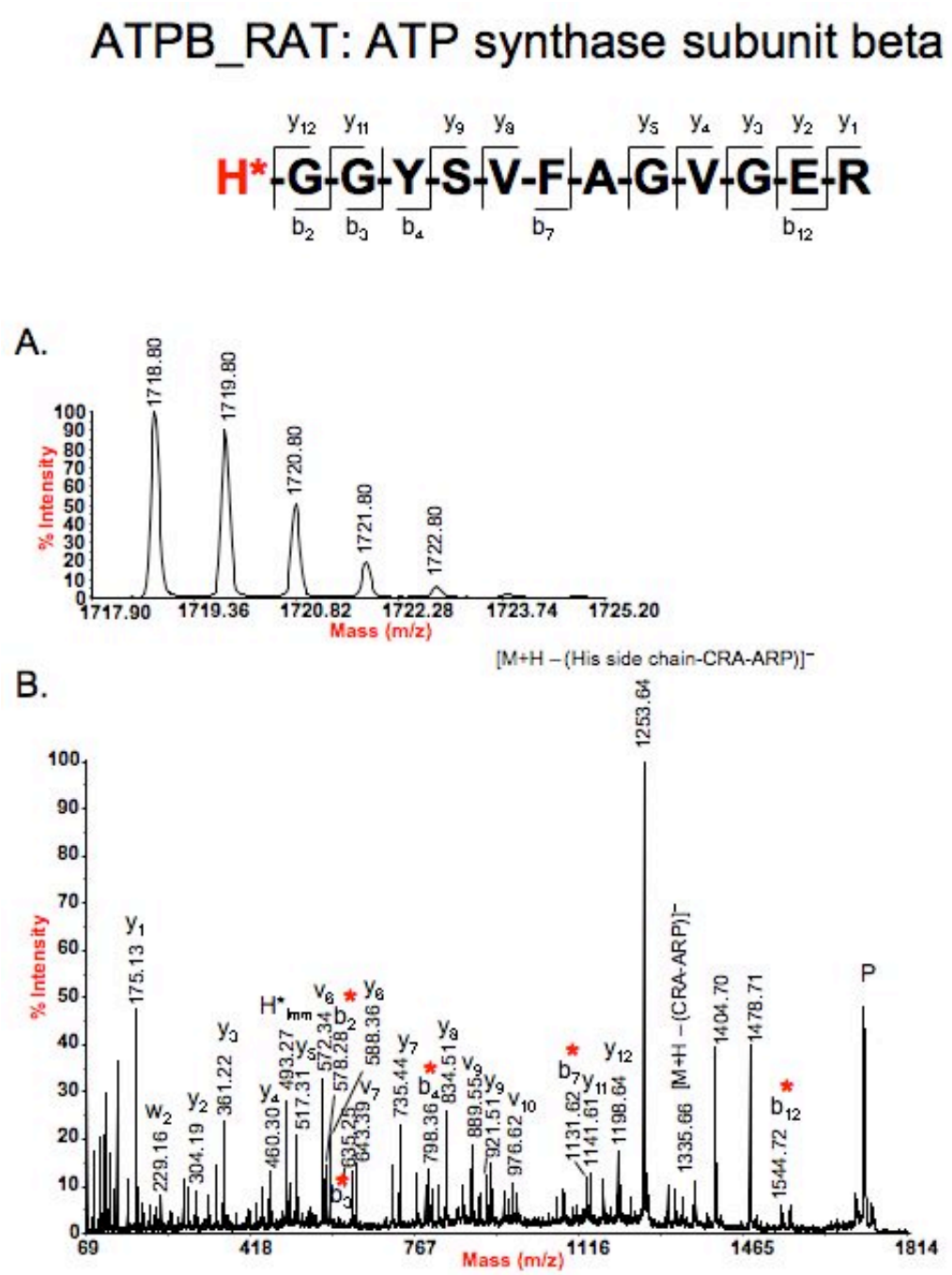

Figure SB13. (A) Full mass spectrum and (B) MS/MS spectrum acquired by MALDI-TOF/TOF of the $[M+H]^+$ ion of the ARP labeled, crotonaldehyde modified peptide H*GGYSVFAGVGER; monoisotopic m/z_{calc} 1718.81; accuracy **Δ**(m/z) = -0.01 m/z

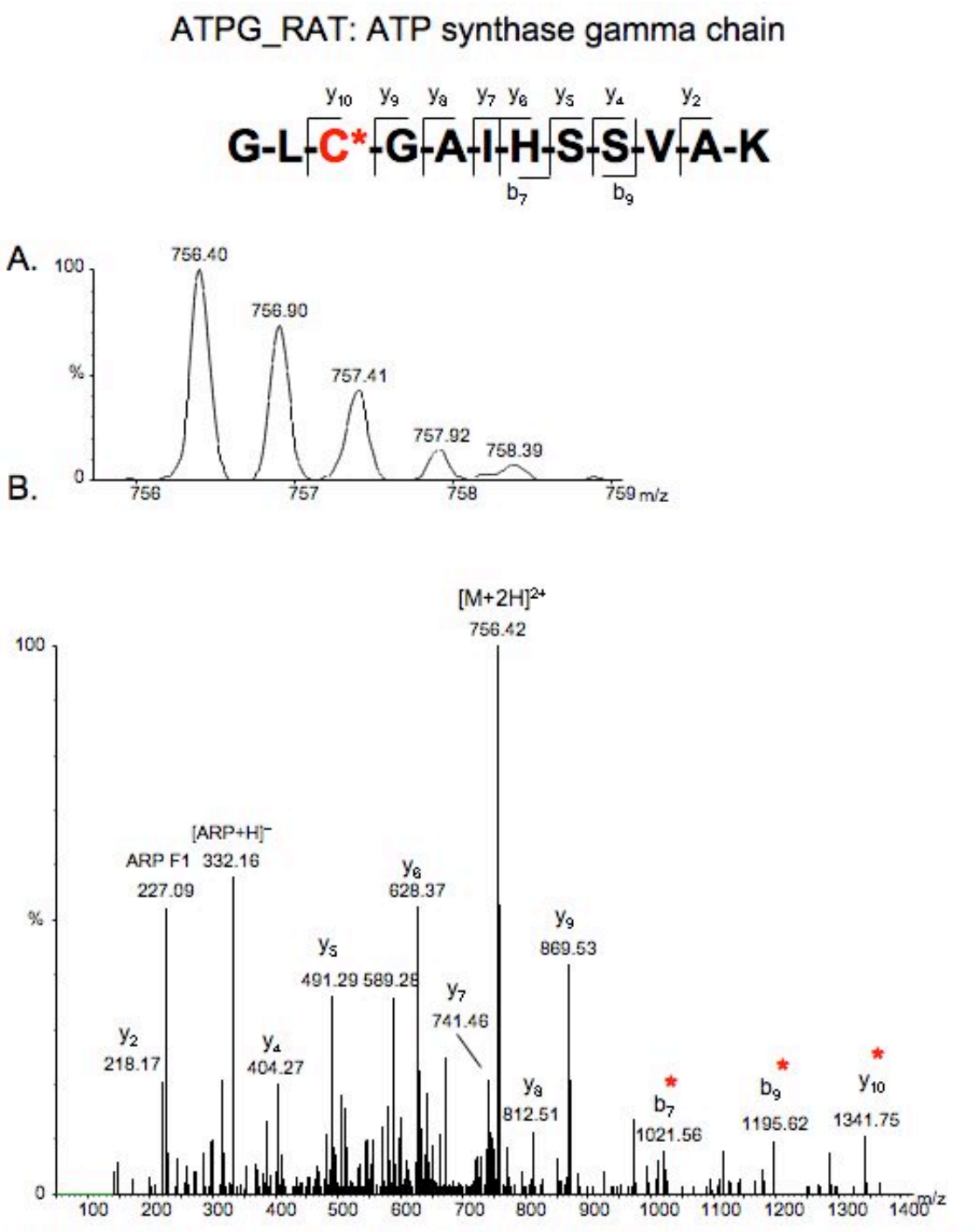

Figure SB14. (A) Full mass spectrum and (B) MS/MS spectrum acquired by ESI-Q-TOF of the $[M+2H]^{2+}$ ion of the ARP labeled, acrolein modified peptide GLC*GAIHSSVAK; monoisotopic m/z_{calc} 756.38; accuracy **Δ**(m/z) = 0.02 m/z

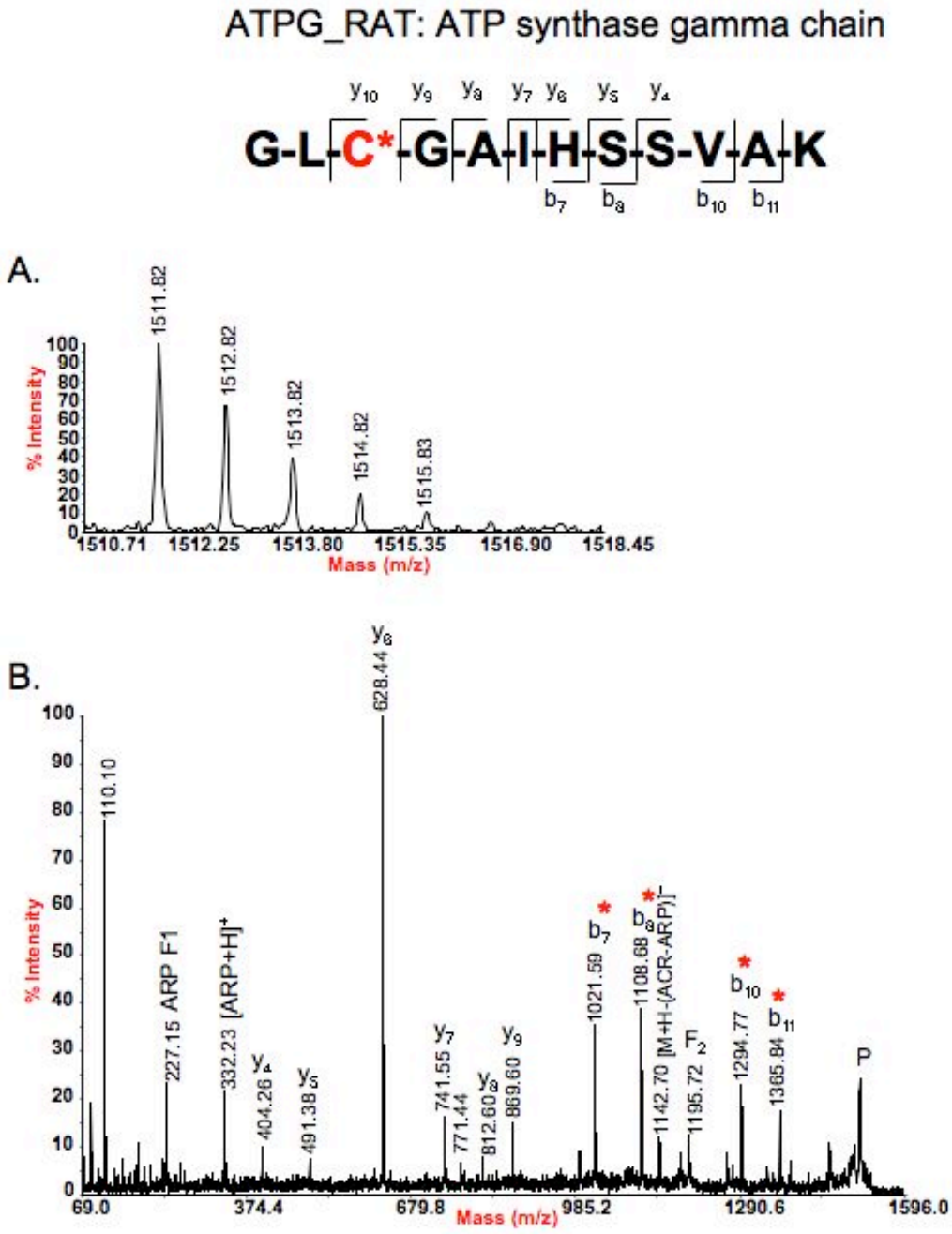

Figure SB15. (A) Full mass spectrum and (B) MS/MS spectrum acquired by MALDI-TOF/TOF of the $[M+H]^+$ ion of the ARP labeled, acrolein modified peptide GLC*GAIHSSVAK; monoisotopic m/z_{calc} 1511.75; accuracy $\Delta(m/z)$ = 0.07 m/z

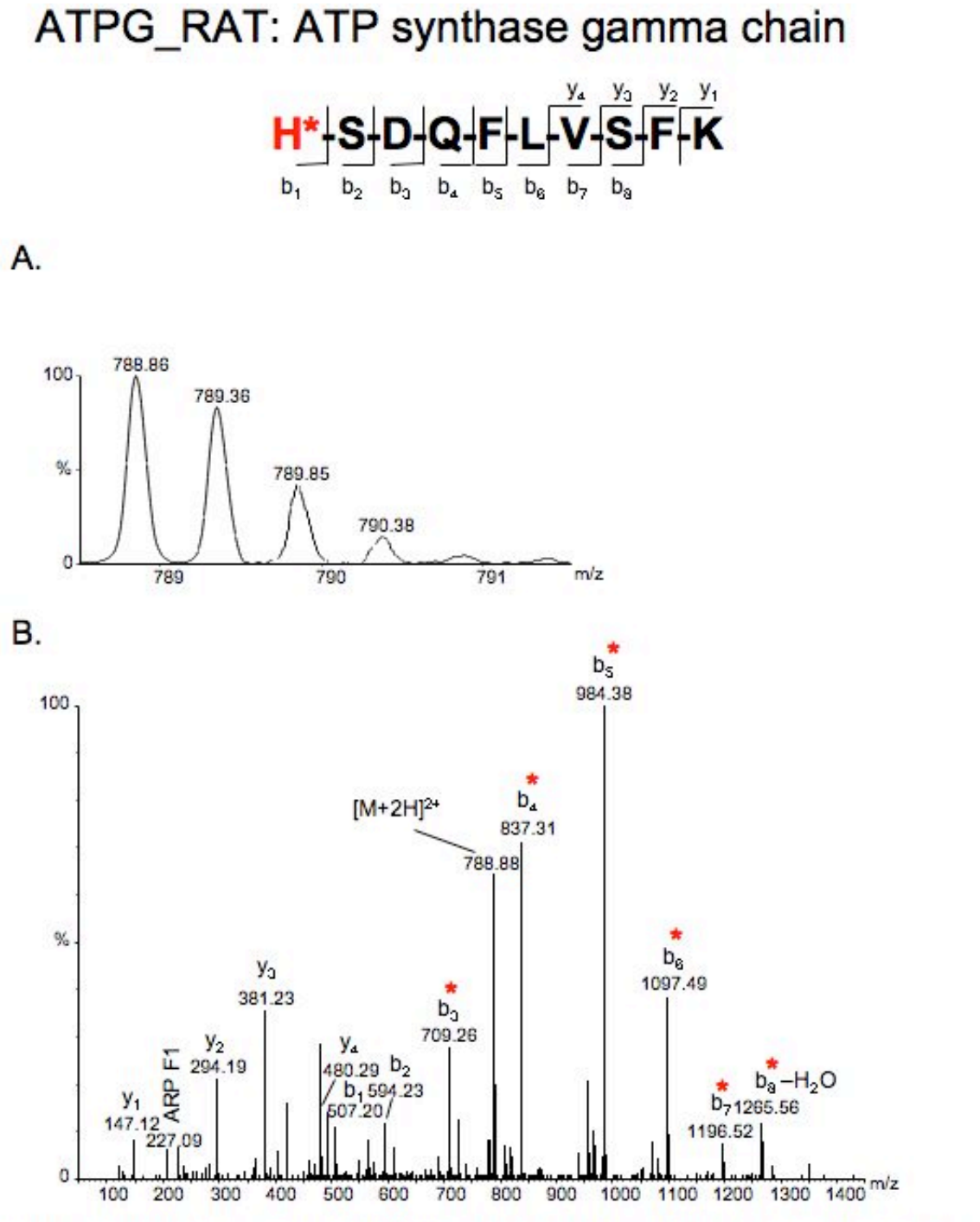

Figure SB16. (A) Full mass spectrum and (B) MS/MS spectrum acquired by ESI-Q-TOF of the $[M+2H]^{2+}$ ion of the ARP labeled, acrolein modified peptide H*SDQFLVSFK; monoisotopic m/z_{calc} 788.88; accuracy **Δ**(m/z) = -0.02 m/z

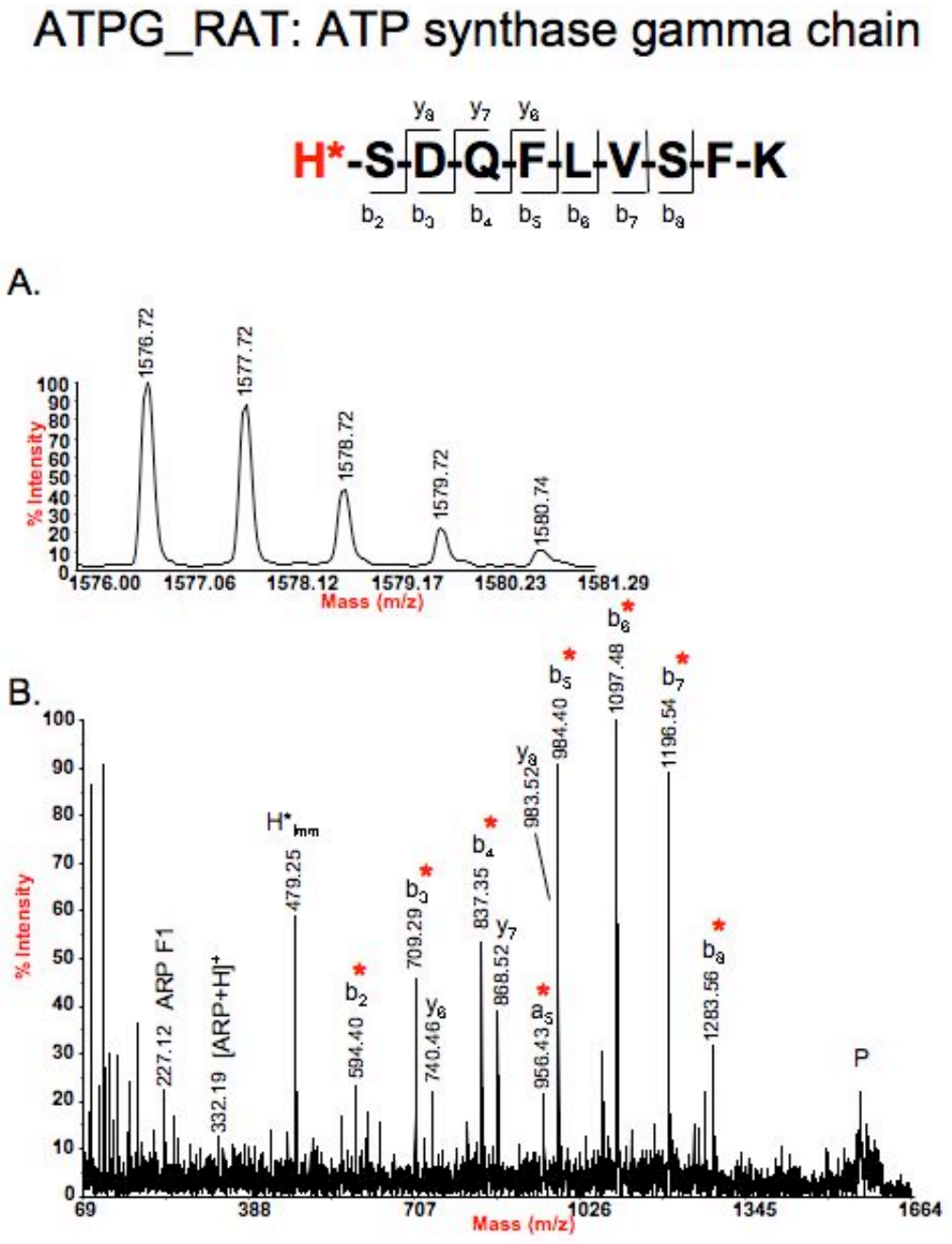

Figure SB17. (A) Full mass spectrum and (B) MS/MS spectrum acquired by MALDI-TOF/TOF of the $[M+H]^+$ ion of the ARP labeled, acrolein modified peptide H*SDQFLVSFK; monoisotopic m/z_{calc} 1576.76; accuracy **Δ**(m/z) = -0.04 m/z

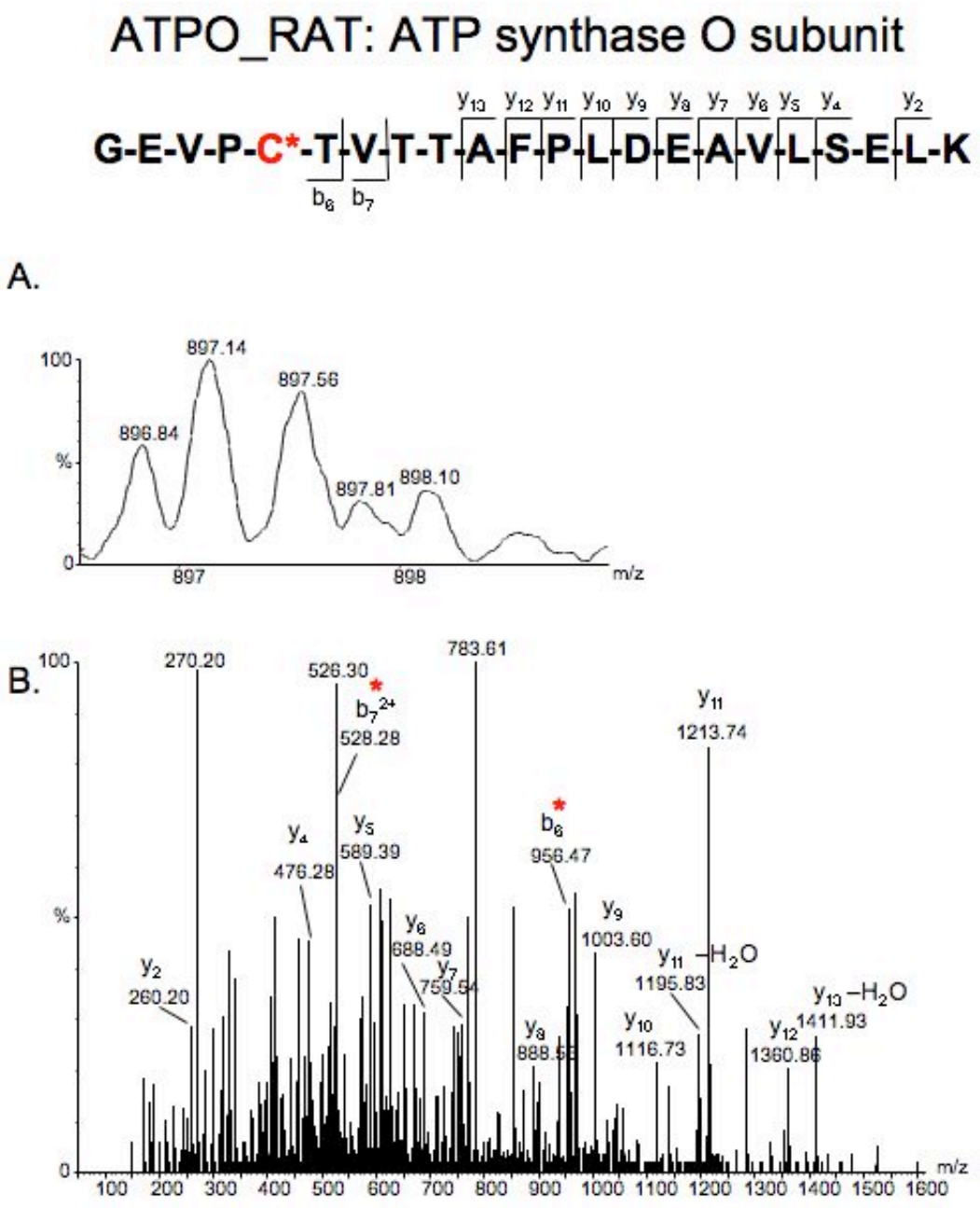

Figure SB18. (A) Full mass spectrum and (B) MS/MS spectrum acquired by ESI-Q-TOF of the $[M+3H]^{3+}$ ion of the ARP labeled, acrolein modified peptide GEVPC*TVTTAFPLDEAVLSELK; monoisotopic m/z_{calc} 896.78; accuracy **Δ**(m/z) = 0.06 m/z

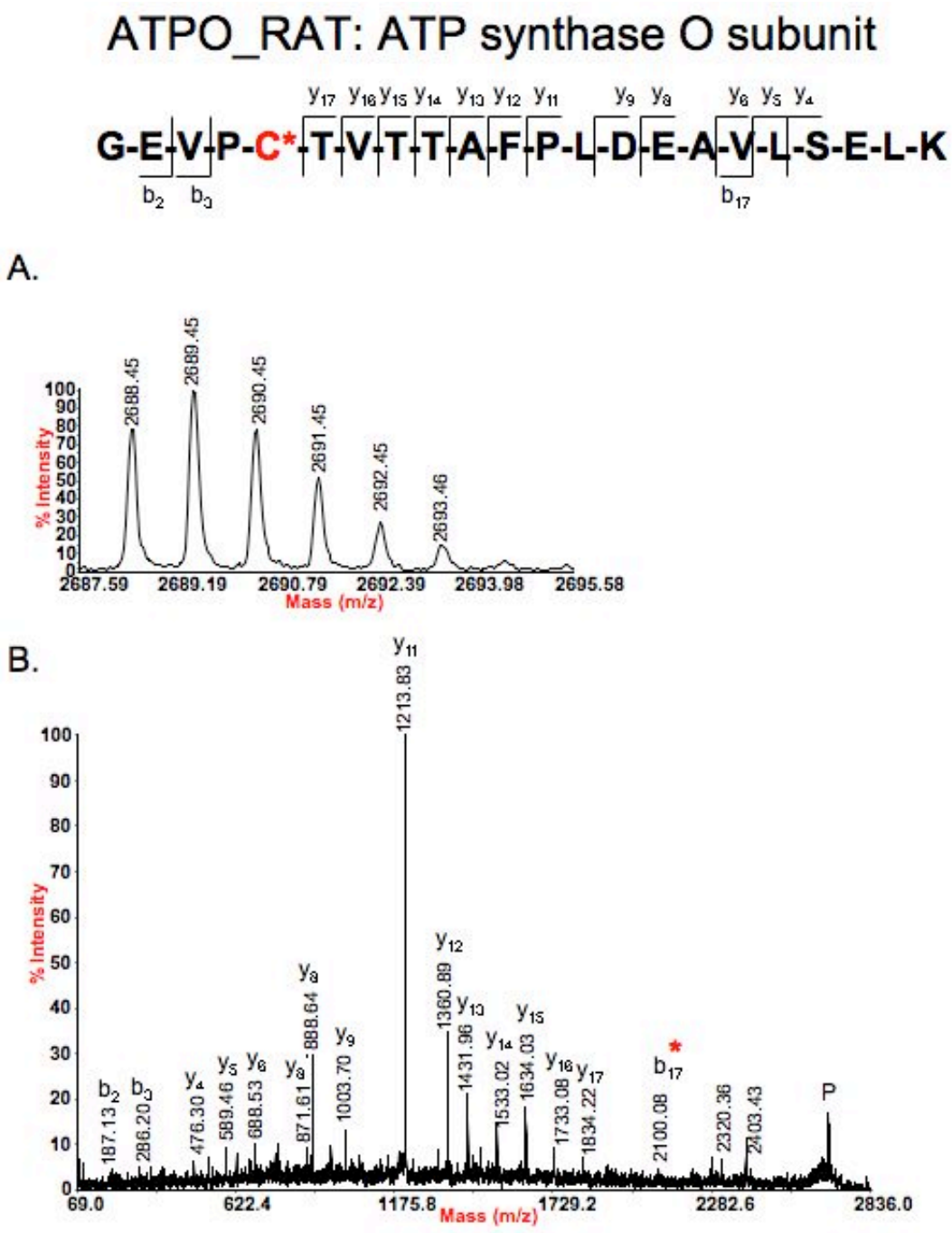

Figure SB19. (A) Full mass spectrum and (B) MS/MS spectrum acquired by MALDI-TOF/TOF of the $[M+H]^+$ ion of the ARP labeled, acrolein modified peptide GEVPC*TVTTAFPLDEAVLSELK; monoisotopic m/z_{calc} 2688.33; accuracy **Δ**(m/z) = 0.12 m/z

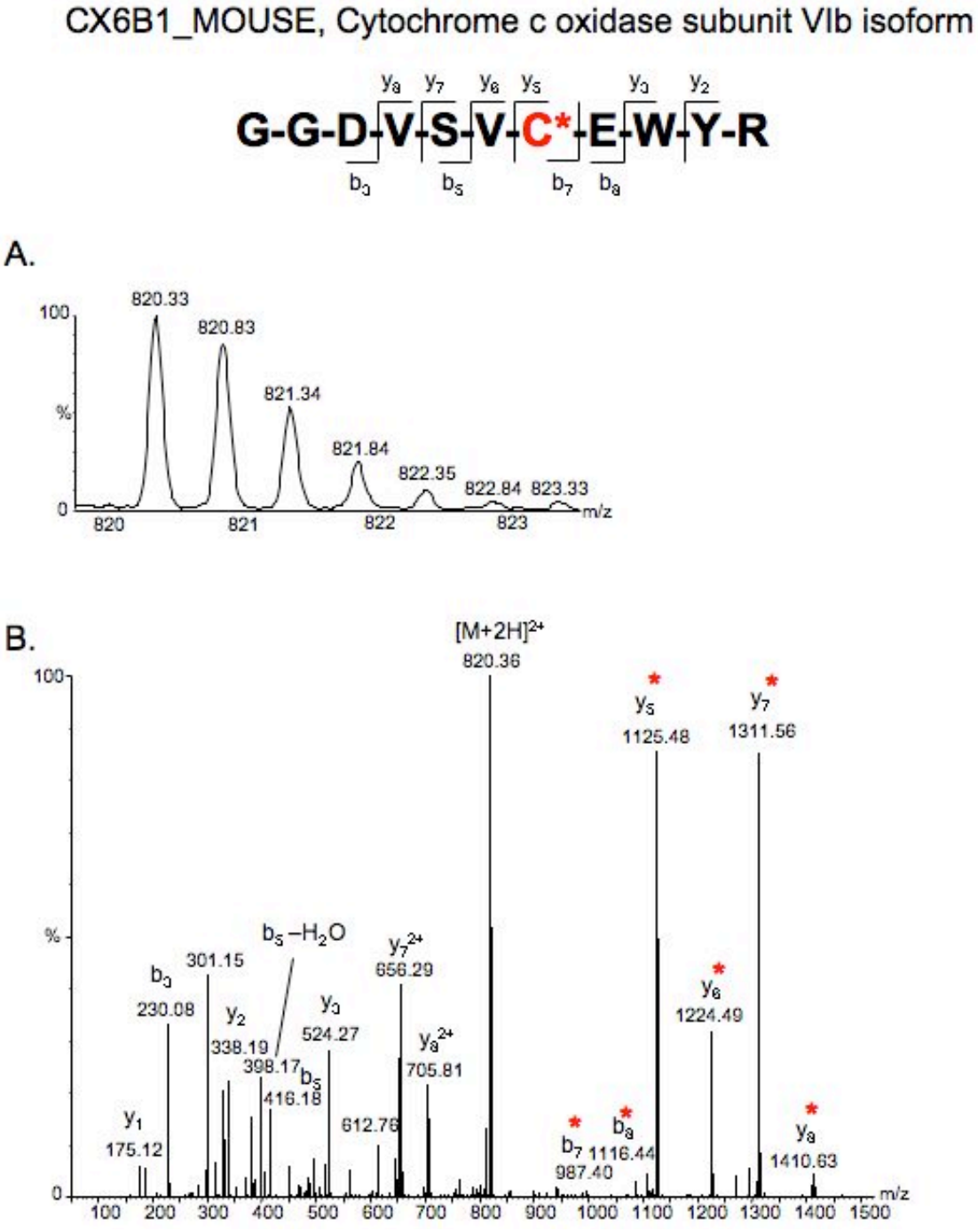

Figure SB20. (A) Full mass spectrum and (B) MS/MS spectrum acquired by ESI-Q-TOF of the $[M+2H]^{2+}$ ion of the ARP labeled, acrolein modified peptide GGDVSVC*EWYR; monoisotopic m/z_{calc} 820.35; accuracy **Δ**(m/z) = -0.02 m/z

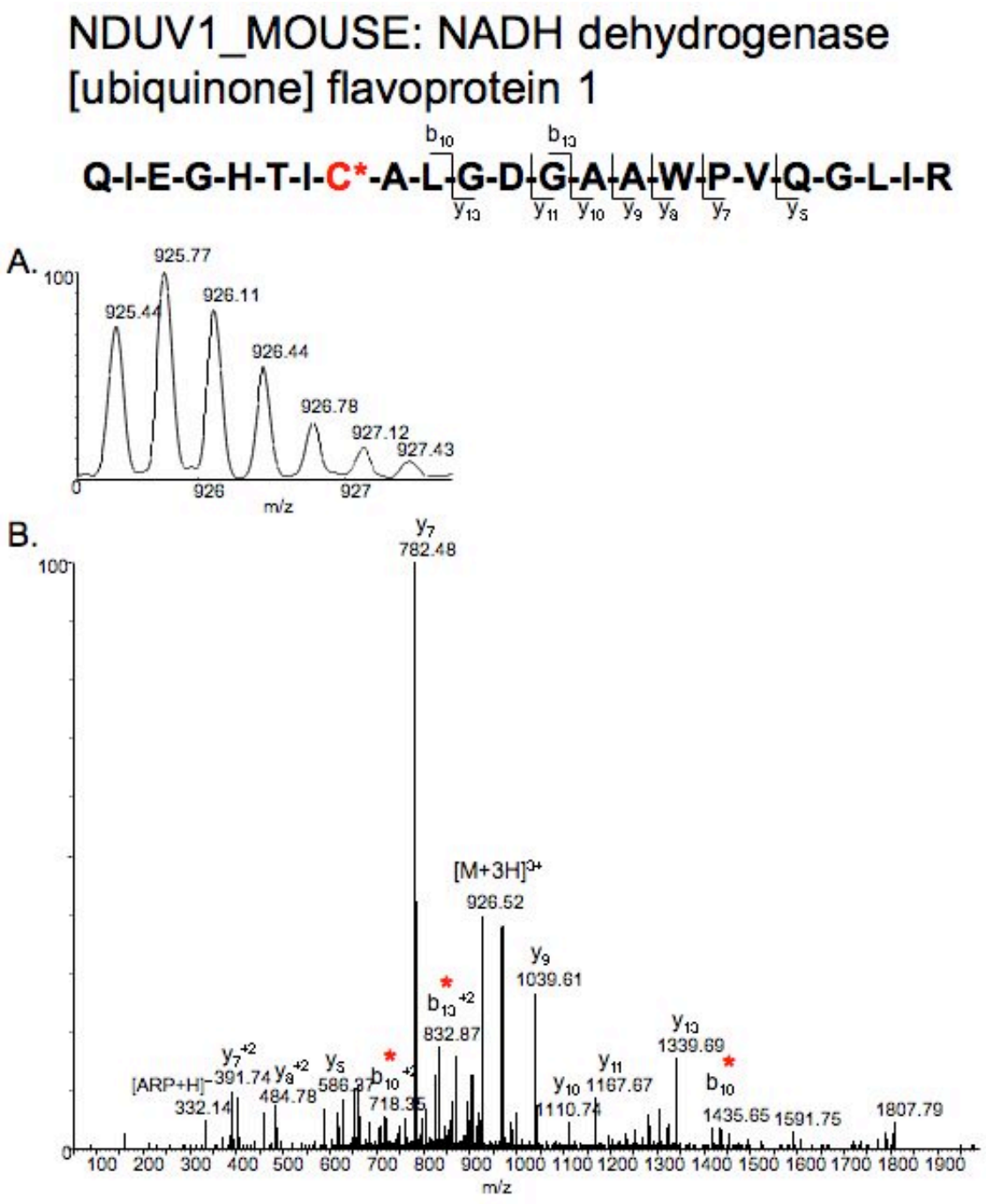

Figure SB21. (A) Full mass spectrum and (B) MS/MS spectrum acquired by ESI-Q-TOF of the $[M+3H]^{3+}$ ion of the ARP labeled, acrolein modified peptide QIEGHTIC*ALGDGAAWPVQGLIR; monoisotopic m/z_{calc} 925.47; accuracy **Δ**(m/z) = -0.03 m/z

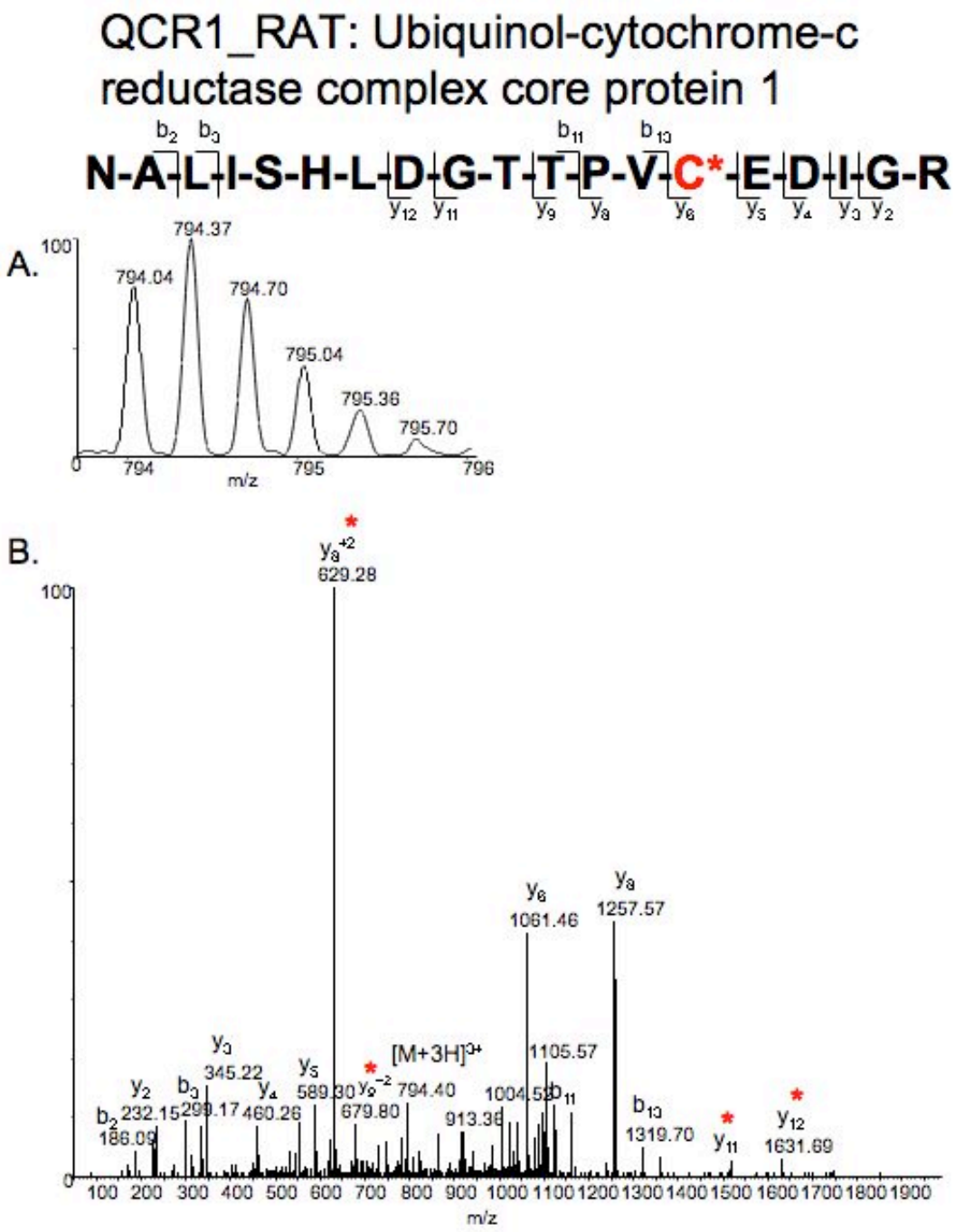

Figure SB22. (A) Full mass spectrum and (B) MS/MS spectrum acquired by ESI-Q-TOF of the $[M+3H]^{3+}$ ion of the ARP labeled, acrolein modified peptide NALISHLDGTTPVC*EDIGR; monoisotopic m/z_{calc} 794.05; accuracy **Δ**(m/z) = -0.01 m/z

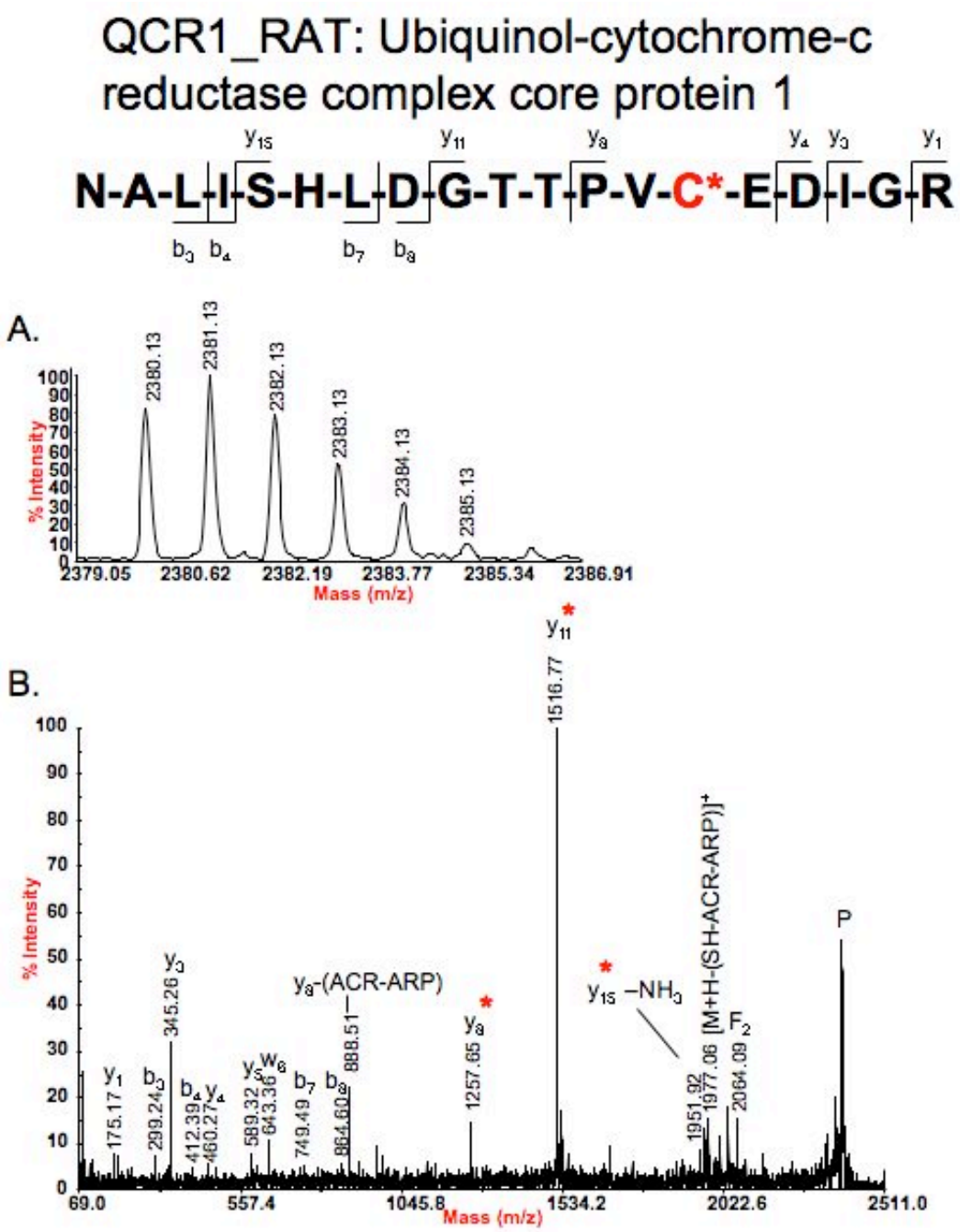

Figure SB23. (A) Full mass spectrum and (B) MS/MS spectrum acquired by MALDI-TOF/TOF of the $[M+H]^+$ ion of the ARP labeled, acrolein modified peptide NALISHLDGTTPVC*EDIGR; monoisotopic m/z_{calc} 2380.14; accuracy **Δ**(m/z) = -0.01 m/z

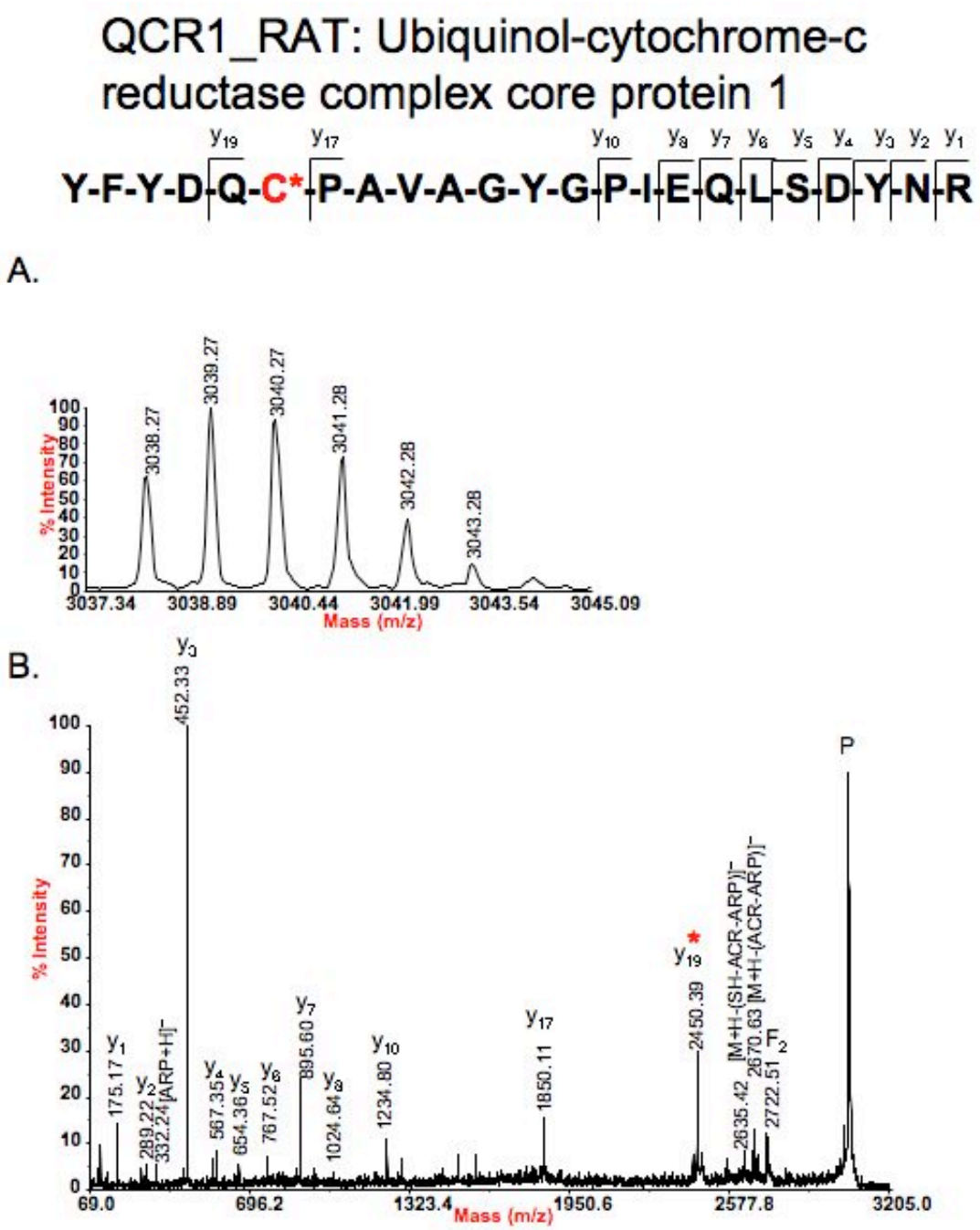

Figure SB24. (A) Full mass spectrum and (B) MS/MS spectrum acquired by MALDI-TOF/TOF of the $[M+H]^+$ ion of the ARP labeled, acrolein modified peptide YFYDQC*PAVAGYGPIEQLSDYNR; monoisotopic m/z_{calc} 3038.34; accuracy **Δ**(m/z) = -0.07 m/z

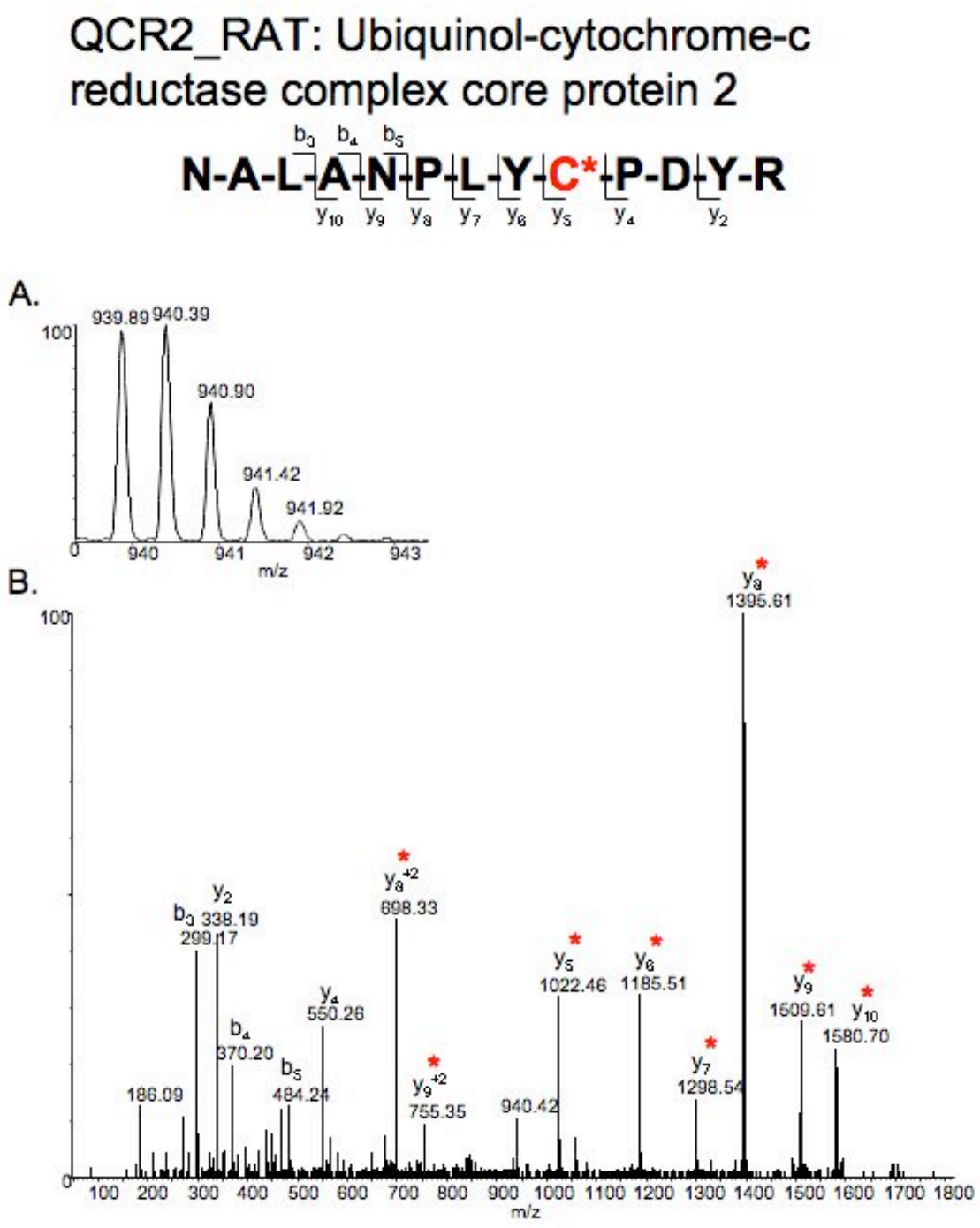

Figure SB25. (A) Full mass spectrum and (B) MS/MS spectrum acquired by ESI-Q-TOF of the $[M+2H]^{2+}$ ion of the ARP labeled, acrolein modified peptide NALANPLYC*PDYR; monoisotopic m/z_{calc} 939.93; accuracy **Δ**(m/z) = -0.04 m/z

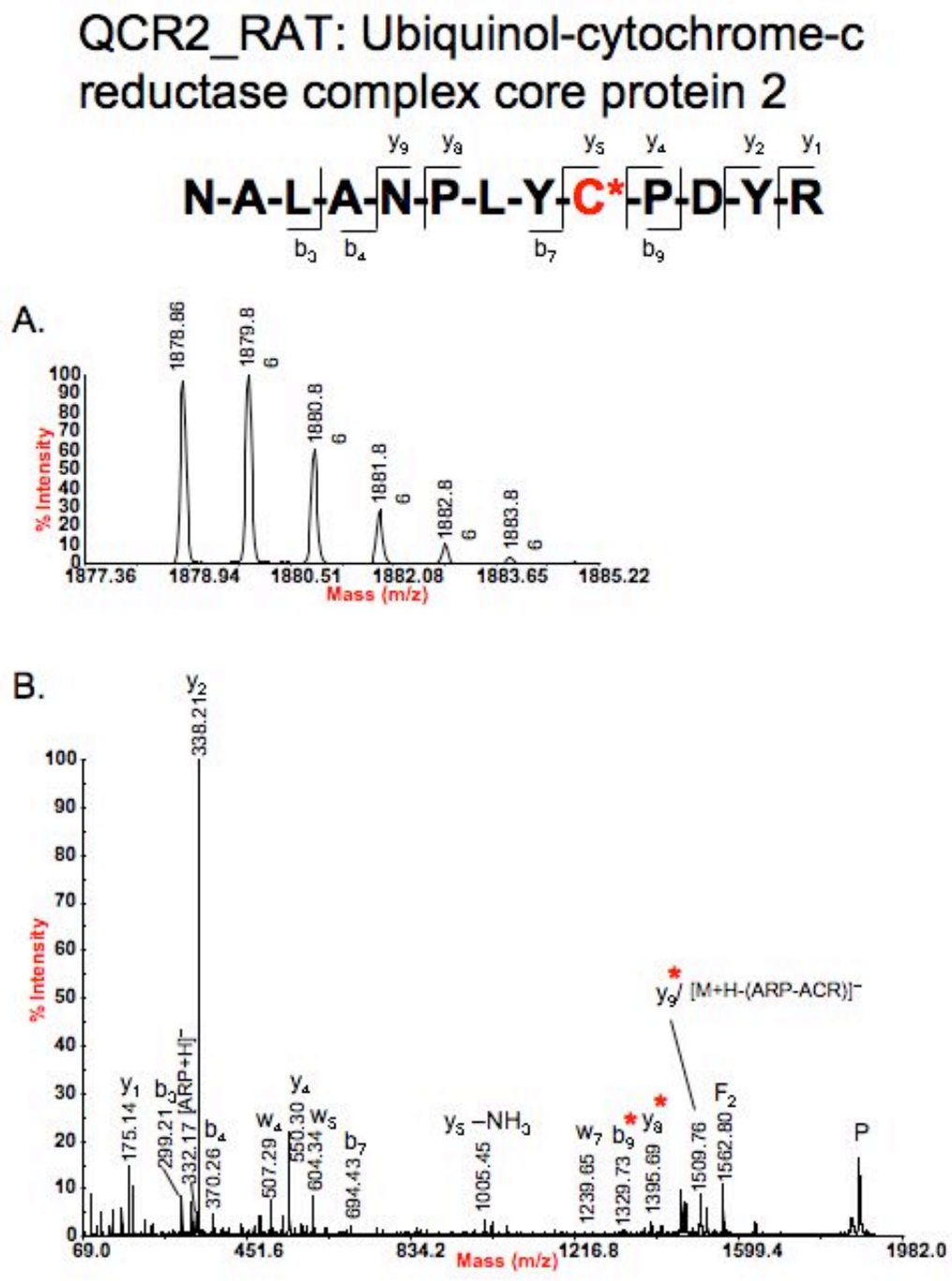

Figure SB26. (A) Full mass spectrum and (B) MS/MS spectrum acquired by MALDI-TOF/TOF of the $[M+H]^+$ ion of the ARP labeled, acrolein modified peptide NALANPLYC*PDYR; monoisotopic m/z_{calc} 1878.86; accuracy Δ(m/z) = 0.00 m/z

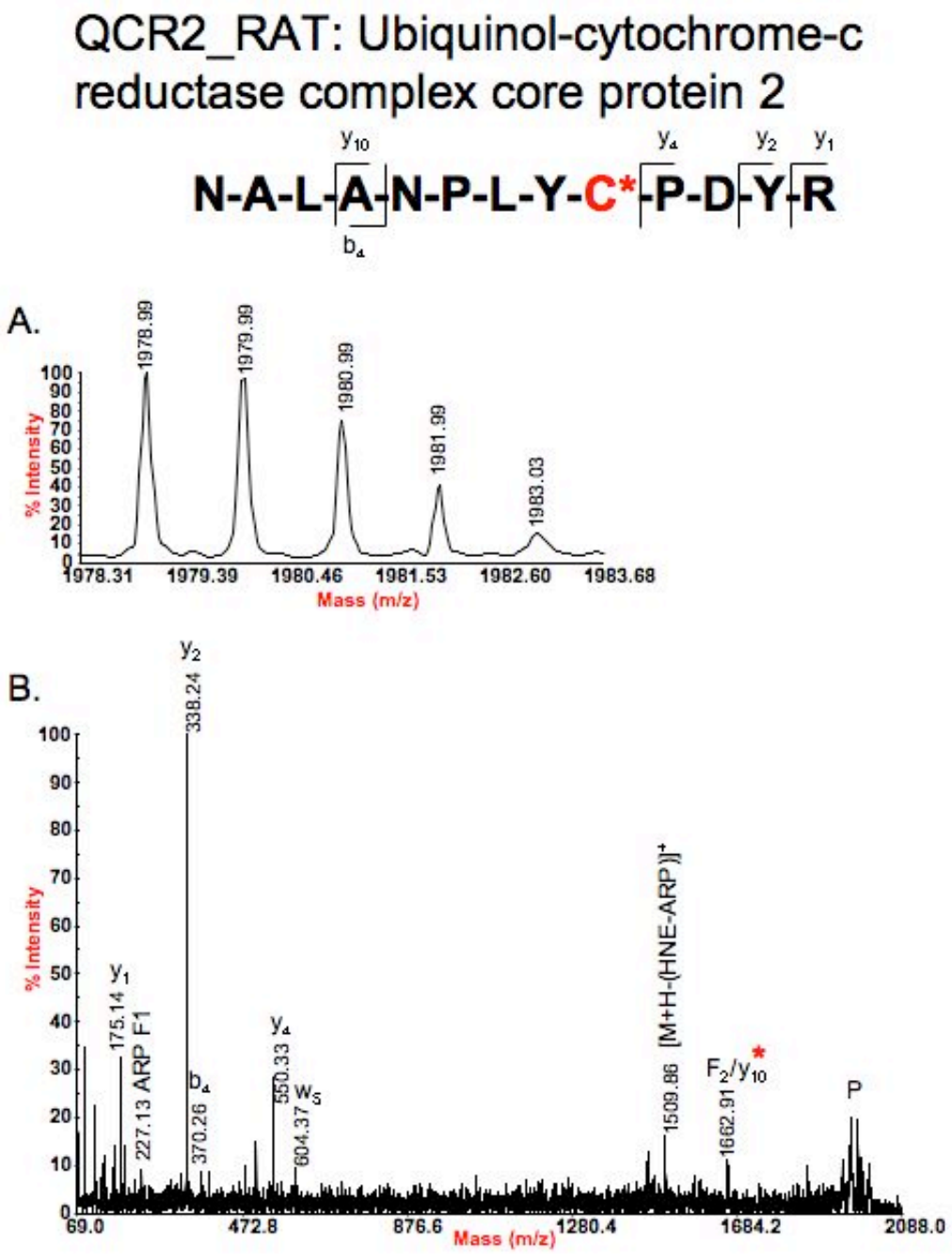

Figure SB27. (A) Full mass spectrum and (B) MS/MS spectrum acquired by MALDI-TOF/TOF of the $[M+H]^+$ ion of the ARP labeled, HNE modified peptide NALANPLYC*PDYR; monoisotopic m/z_{calc} 1978.95; accuracy **Δ**(m/z) = 0.04 m/z

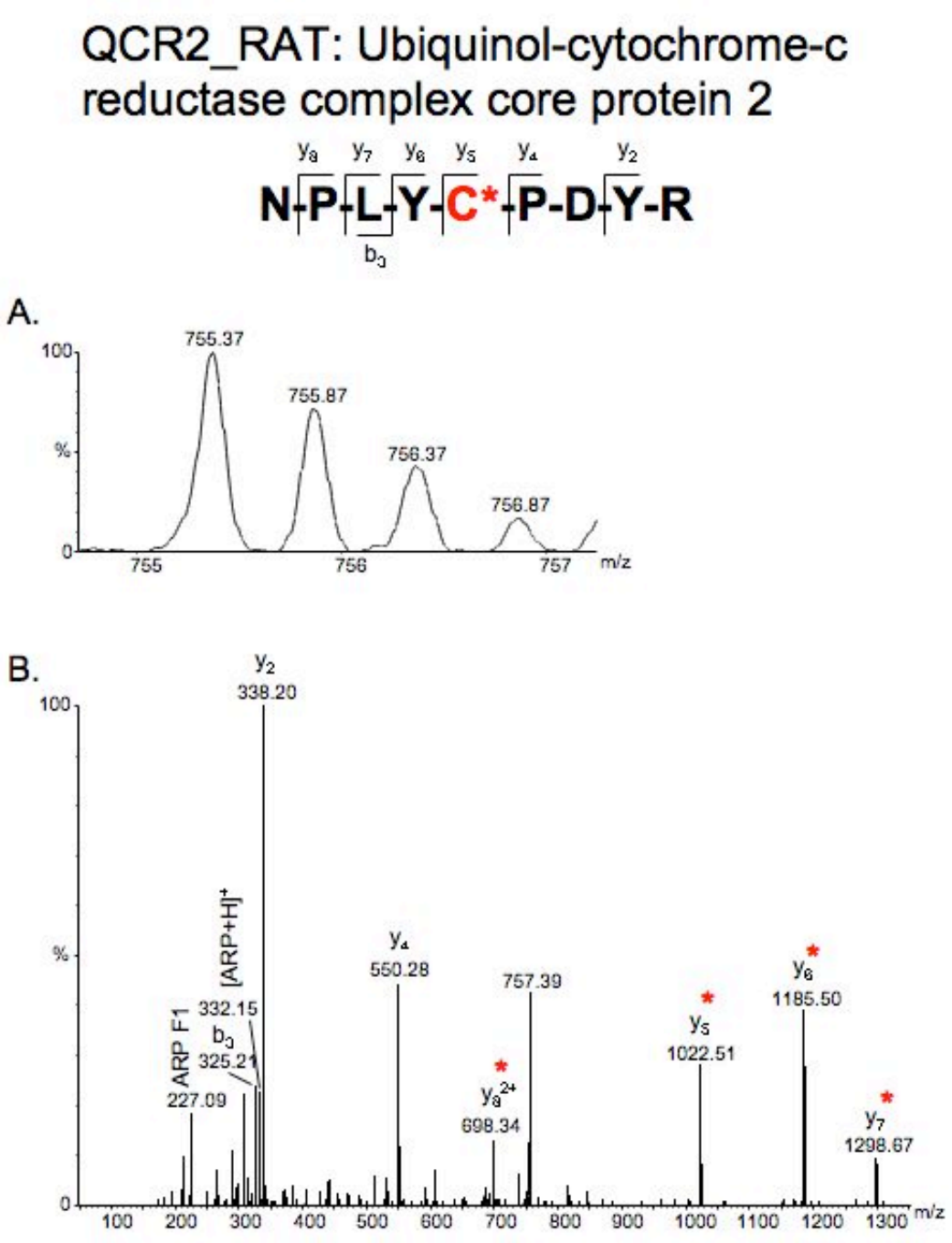

Figure SB28. (A) Full mass spectrum and (B) MS/MS spectrum acquired by ESI-Q-TOF of the $[M+2H]^{2+}$ ion of the ARP labeled, acrolein modified peptide NPLYC*PDYR; monoisotopic m/z_{calc} 755.33; accuracy **Δ**(m/z) = 0.04 m/z

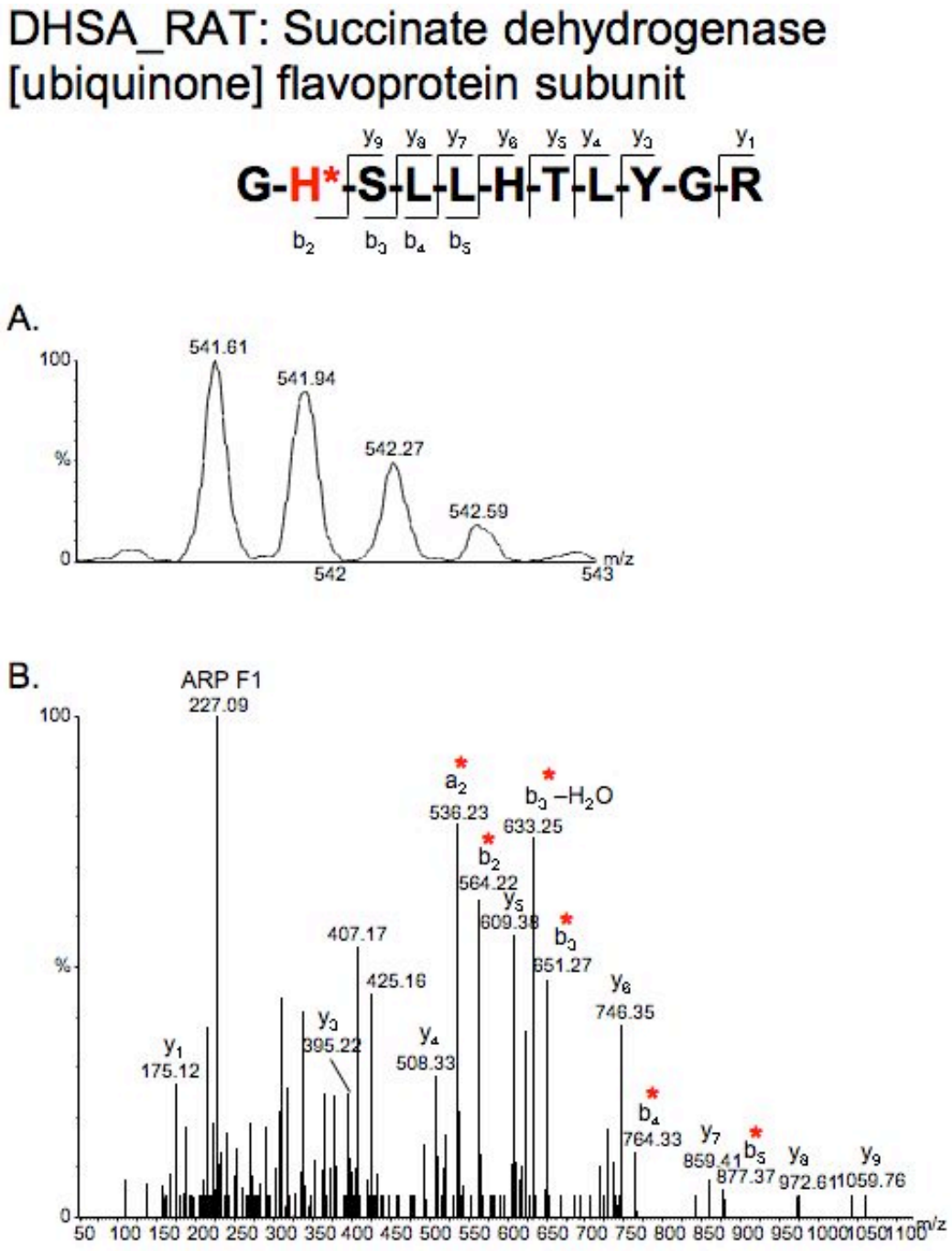

Figure SB29. (A) Full mass spectrum and (B) MS/MS spectrum acquired by ESI-Q-TOF of the $[M+3H]^{3+}$ ion of the ARP labeled, acrolein modified peptide GH*SLLHTLYGR; monoisotopic m/z_{calc} 541.61; accuracy **Δ**(m/z) = 0.00 m/z

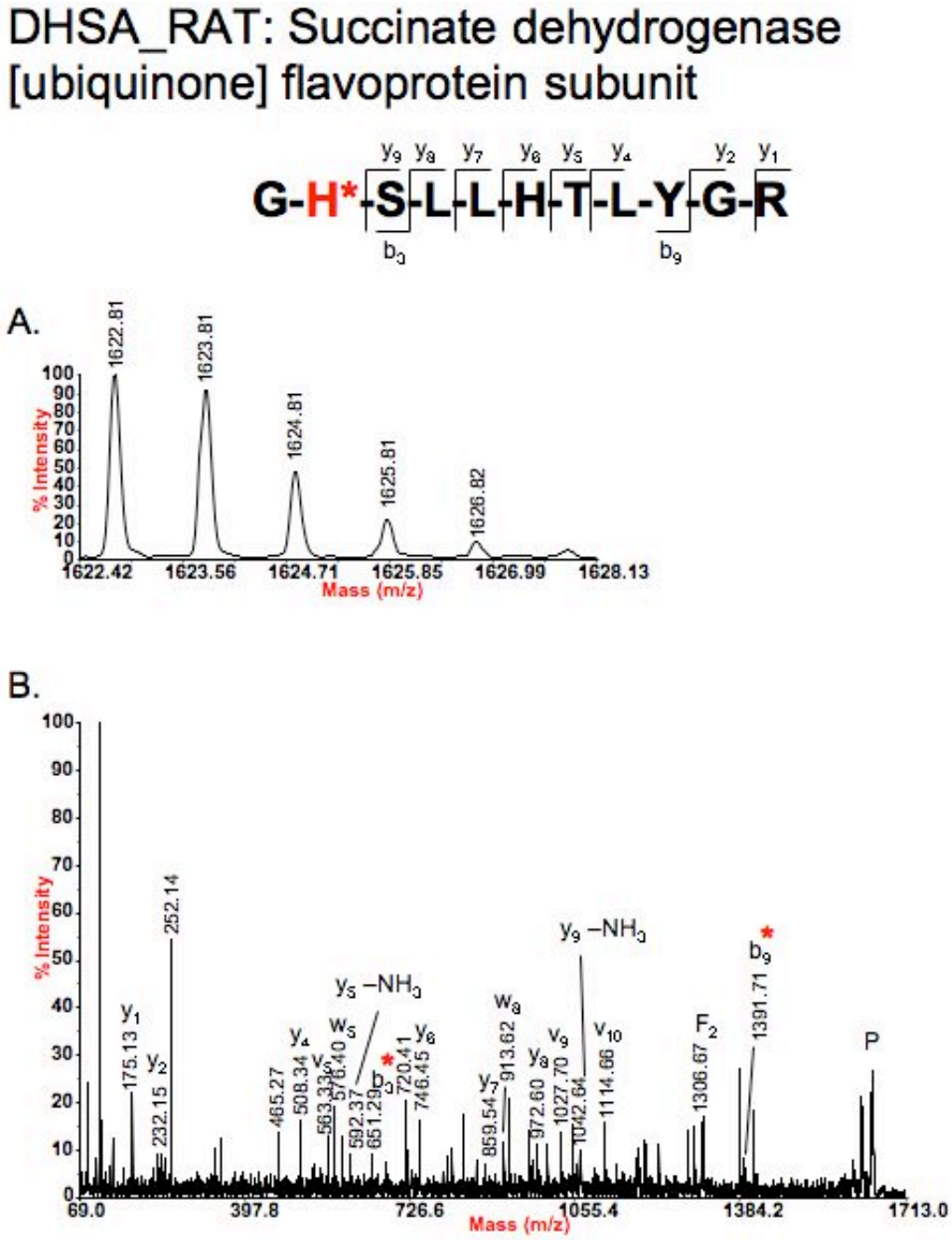

Figure SB30. (A) Full mass spectrum and (B) MS/MS spectrum acquired by MALDI-TOF/TOF of the $[M+H]^+$ ion of the ARP labeled, acrolein modified peptide GH*SLLHTLYGR; monoisotopic m/z_{calc} 1622.82; accuracy **Δ**(m/z) = -0.01 m/z

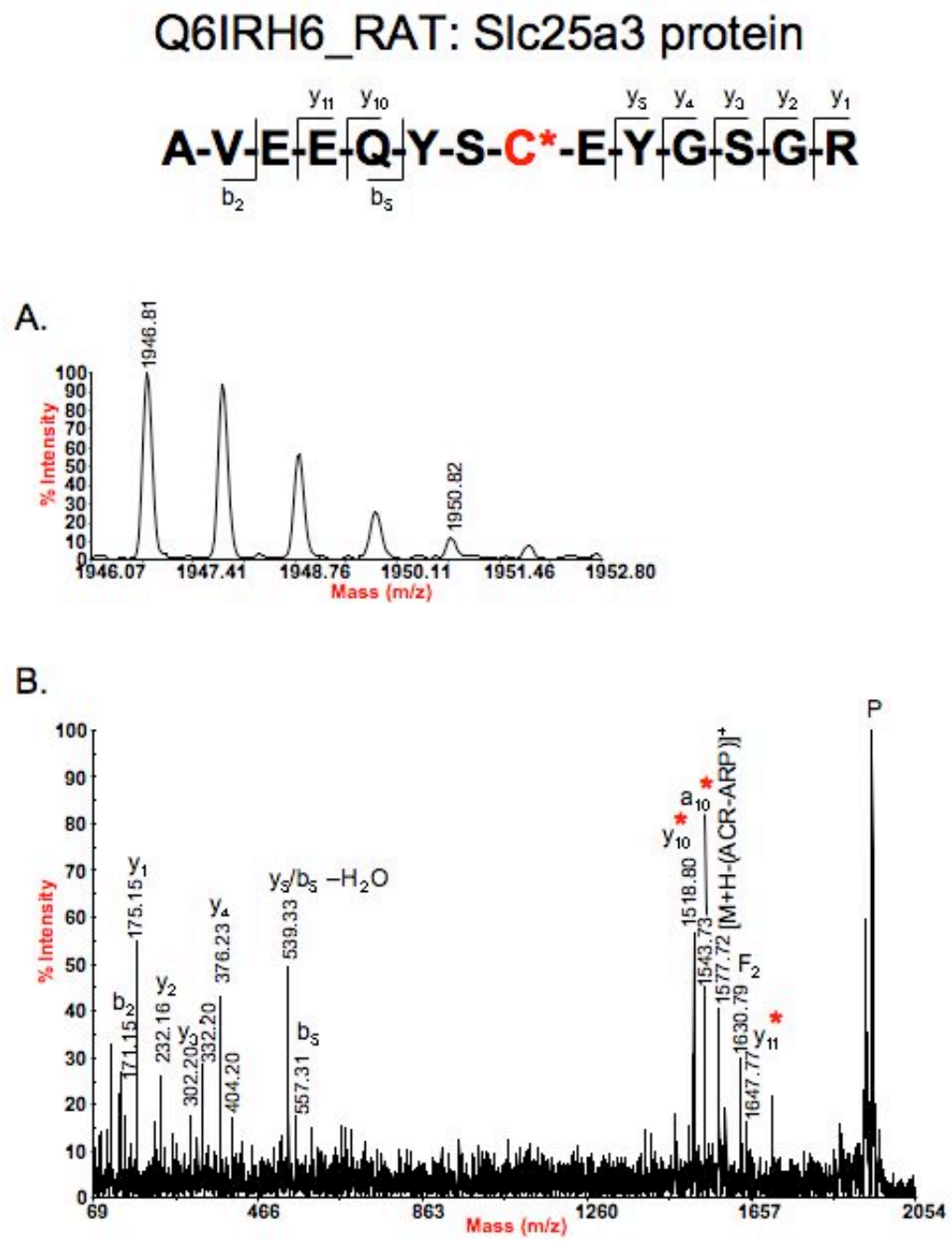

Figure SB31. (A) Full mass spectrum and (B) MS/MS spectrum acquired by MALDI-TOF/TOF of the $[M+H]^+$ ion of the ARP labeled, acrolein modified peptide AVEEQYSC*EYGSGR; monoisotopic m/z_{calc} 1946.80; accuracy **Δ**(m/z) = 0.01 m/z

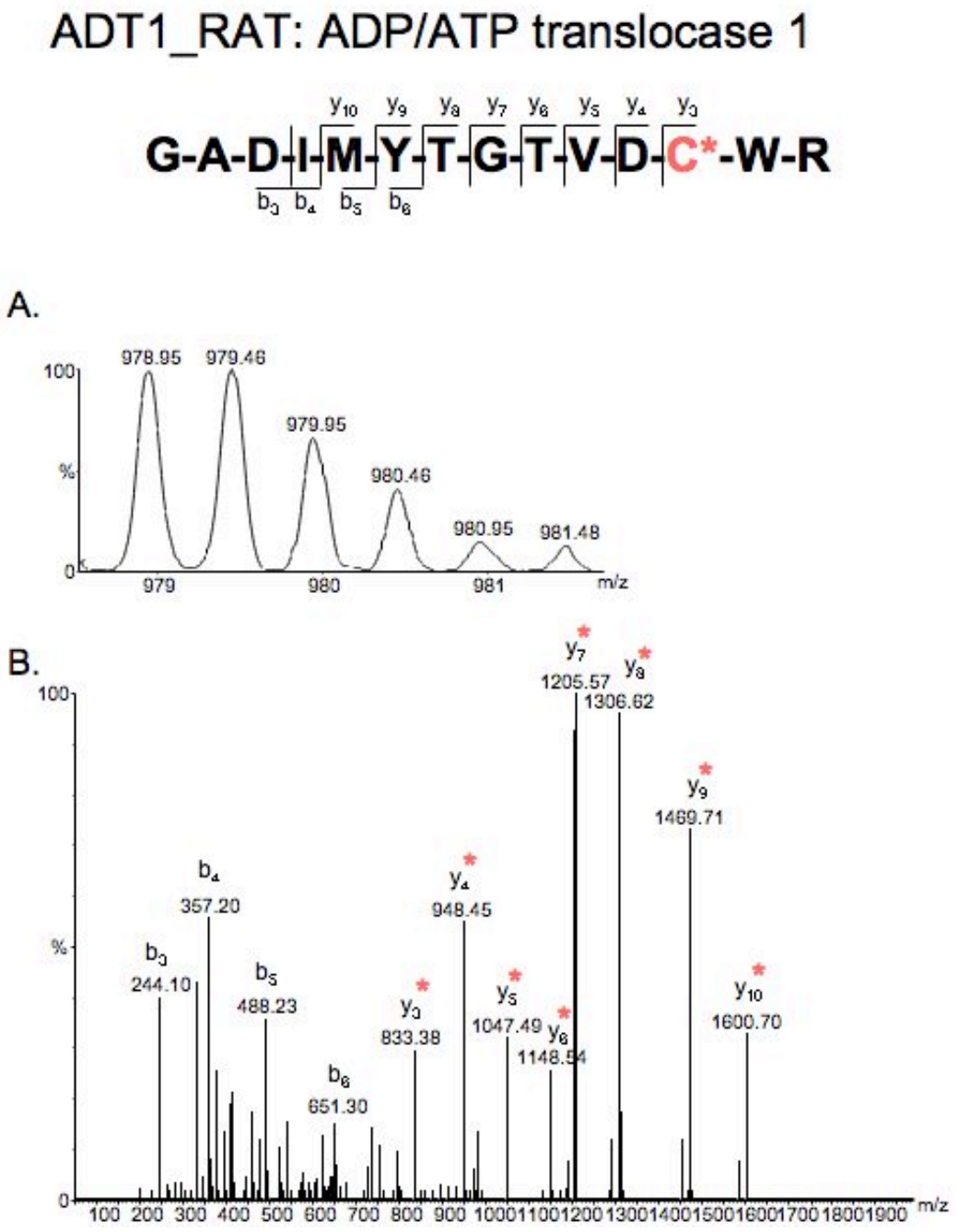

Figure SB32. (A) Full mass spectrum and (B) MS/MS spectrum acquired by ESI-Q-TOF of the $[M+2H]^{2+}$ ion of the ARP labeled, acrolein modified peptide GADIMYTGTVDC*WR; monoisotopic m/z_{calc} 978.92; accuracy **Δ**(m/z) = 0.03 m/z

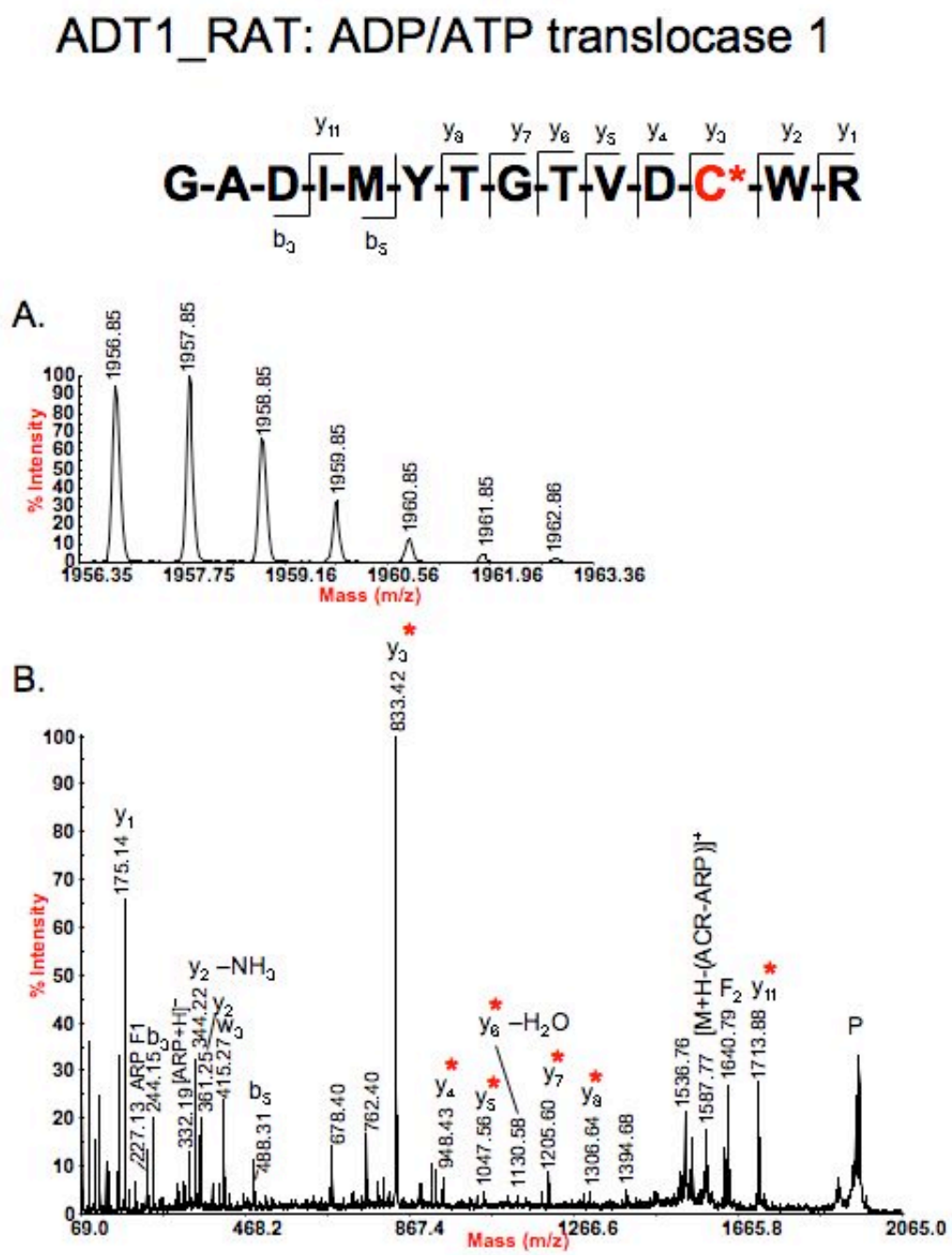

Figure SB33. (A) Full mass spectrum and (B) MS/MS spectrum acquired by MALDI-TOF/TOF of the $[M+H]^+$ ion of the ARP labeled, acrolein modified peptide GADIMYTGTVDC*WR; monoisotopic m/z_{calc} 1956.84; accuracy **Δ**(m/z) = 0.01 m/z

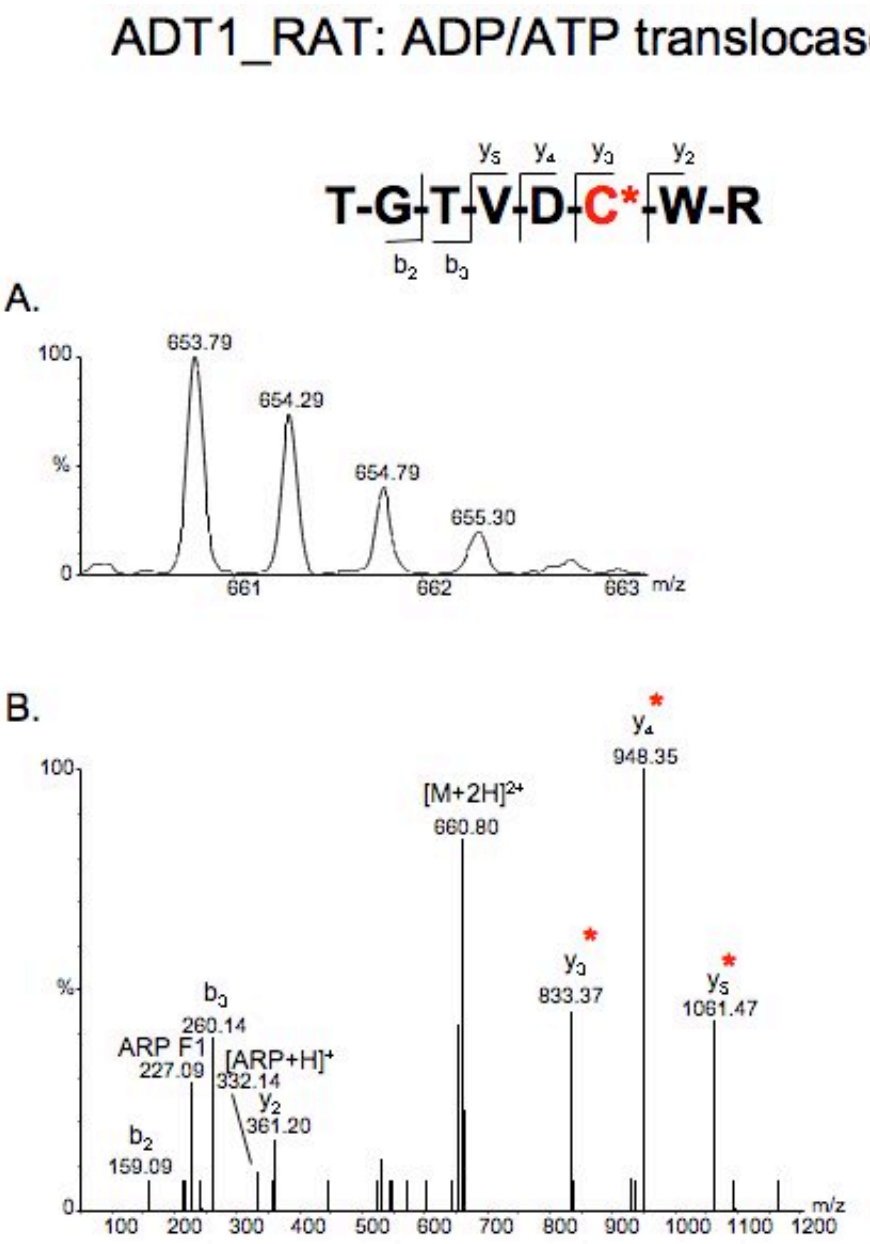

Figure SB34. (A) Full mass spectrum and (B) MS/MS spectrum acquired by ESI-Q-TOF of the $[M+2H]^{2+}$ ion of the ARP labeled, acrolein modified peptide TGTVDC*WR; monoisotopic m/z_{calc} 653.79; accuracy **Δ**(m/z) = 0.00 m/z

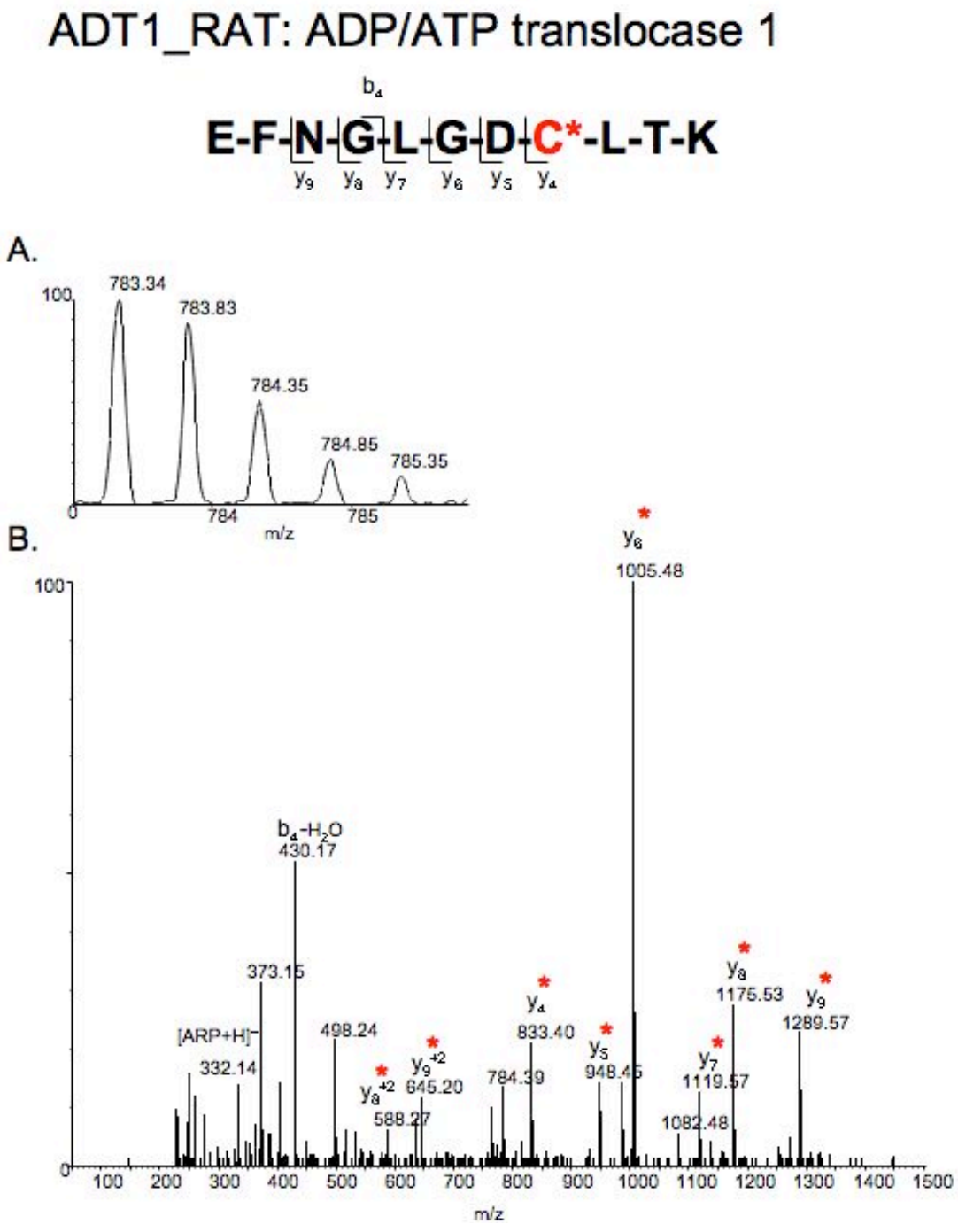

Figure SB35. (A) Full mass spectrum and (B) MS/MS spectrum acquired by ESI-Q-TOF of the $[M+2H]^{2+}$ ion of the ARP labeled, acrolein modified peptide EFNGLGDC*LTK; monoisotopic m/z_{calc} 783.36; accuracy **Δ**(m/z) = -0.02 m/z

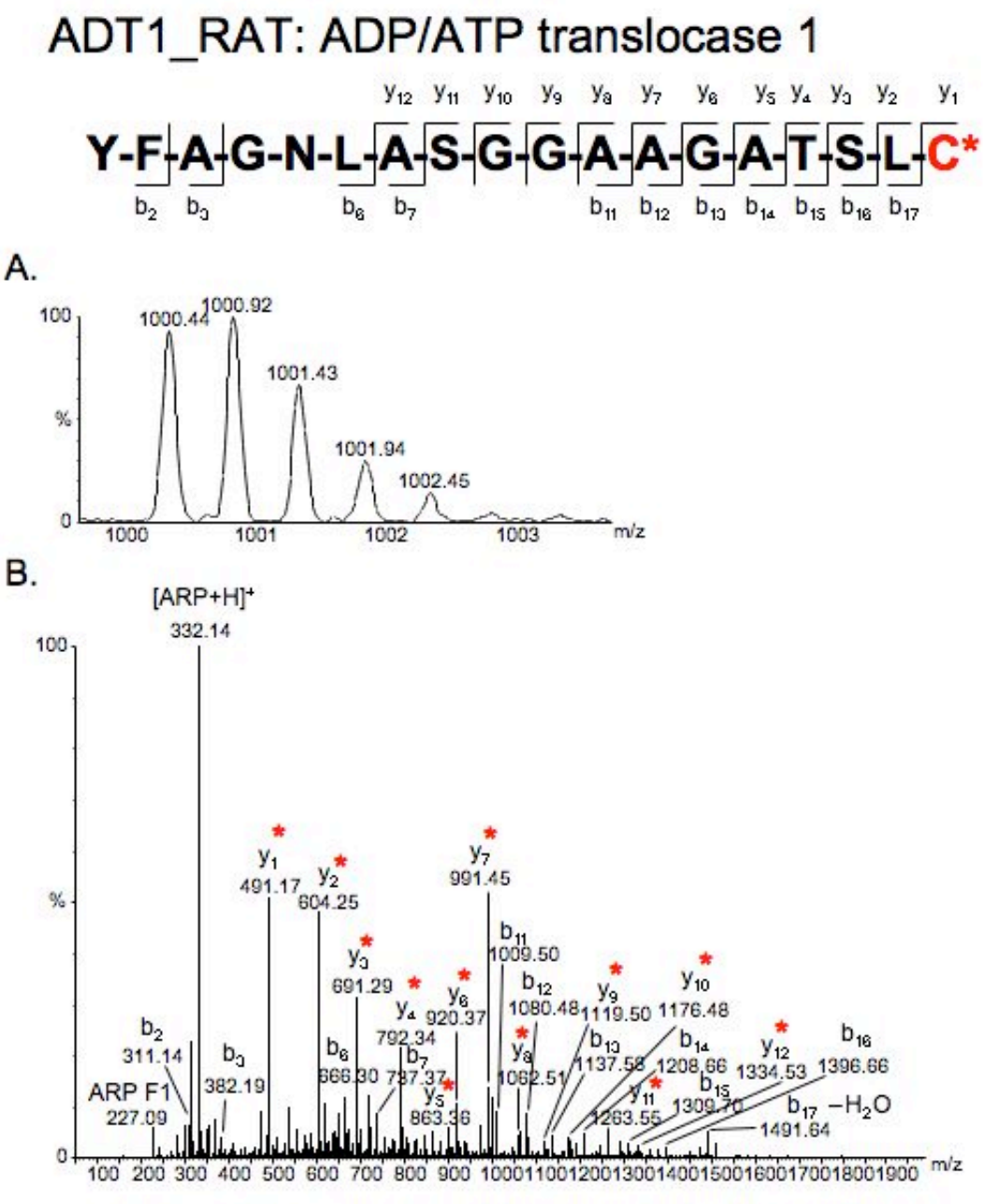

Figure SB36. (A) Full mass spectrum and (B) MS/MS spectrum acquired by ESI-Q-TOF of the $[M+2H]^{2+}$ ion of the ARP labeled, acrolein modified peptide YFAGNLASGGAAGATSLC*; monoisotopic m/z_{calc} 1000.45; accuracy **Δ**(m/z) = -0.01 m/z

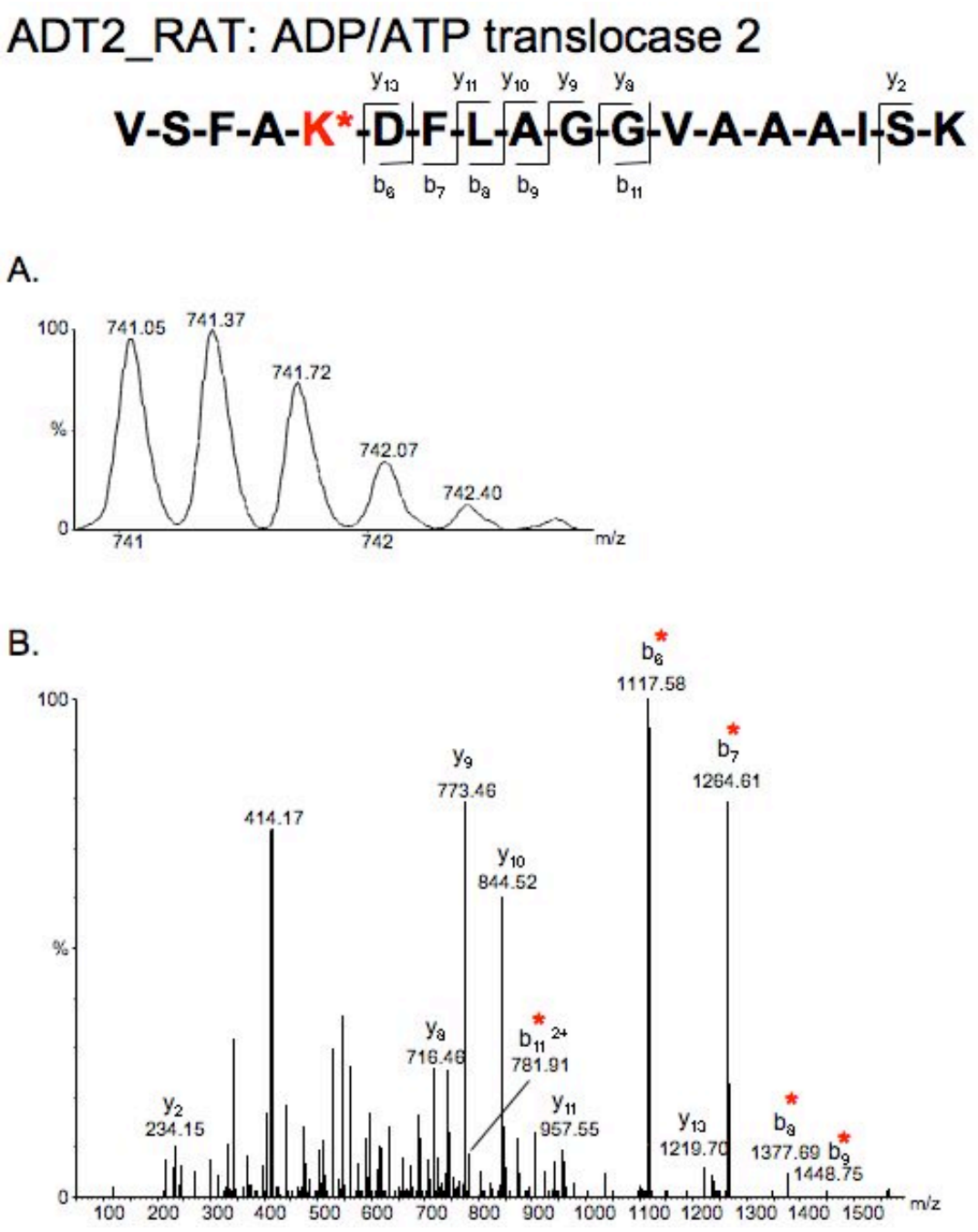

Figure SB37. (A) Full mass spectrum and (B) MS/MS spectrum acquired by ESI-Q-TOF of the $[M+3H]^{3+}$ ion of the ARP labeled, HNE modified peptide VSFAK*DFLAGGVAAAISK; monoisotopic m/z_{calc} 741.07; accuracy **Δ**(m/z) = -0.02 m/z

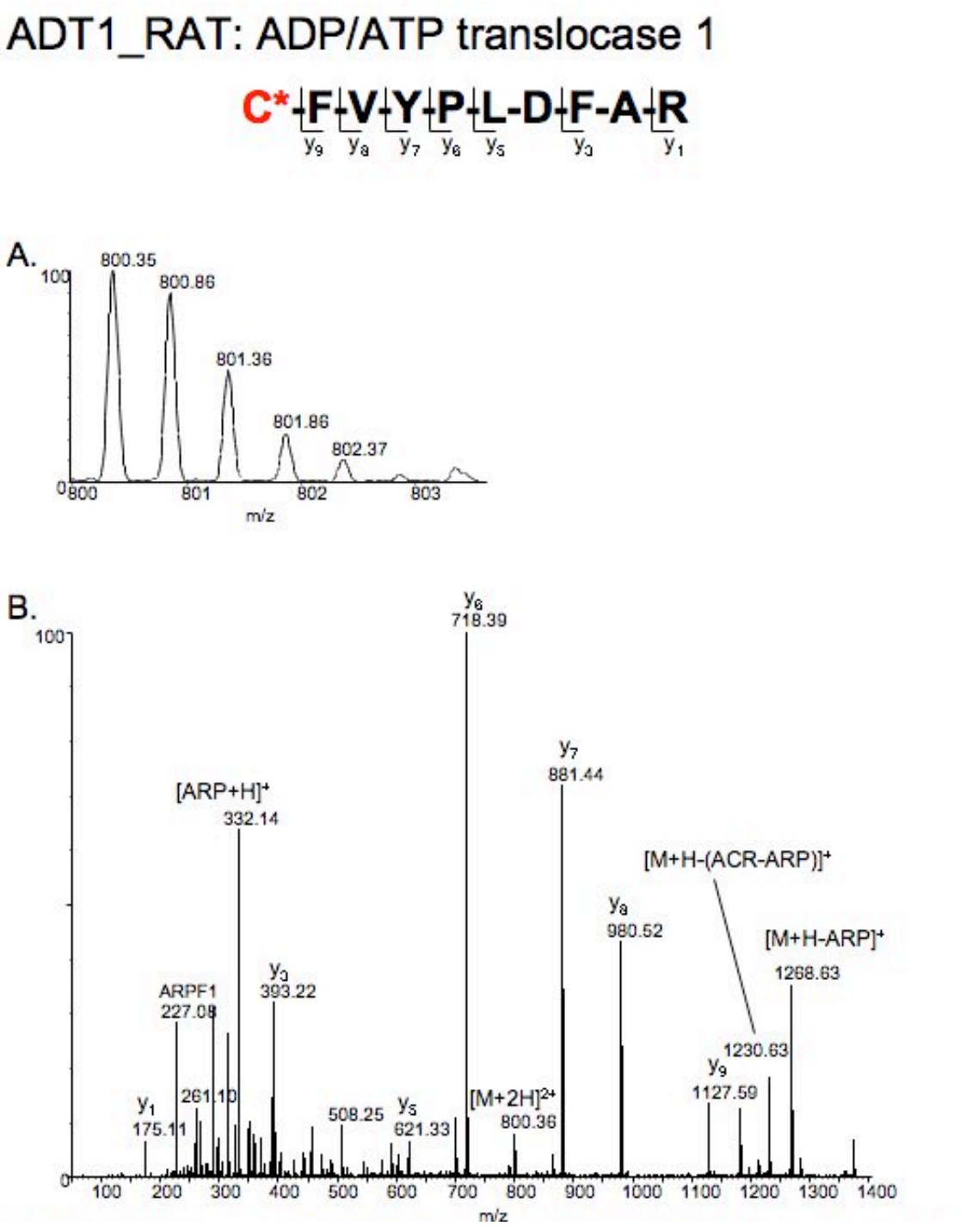

Figure SB38. (A) Full mass spectrum and (B) MS/MS spectrum acquired by ESI-Q-TOF of the $[M+2H]^{2+}$ ion of the ARP labeled, acrolein modified peptide C*FVYPLDFAR; monoisotopic m/z_{calc} 800.38; accuracy **Δ**(m/z) = -0.03 m/z

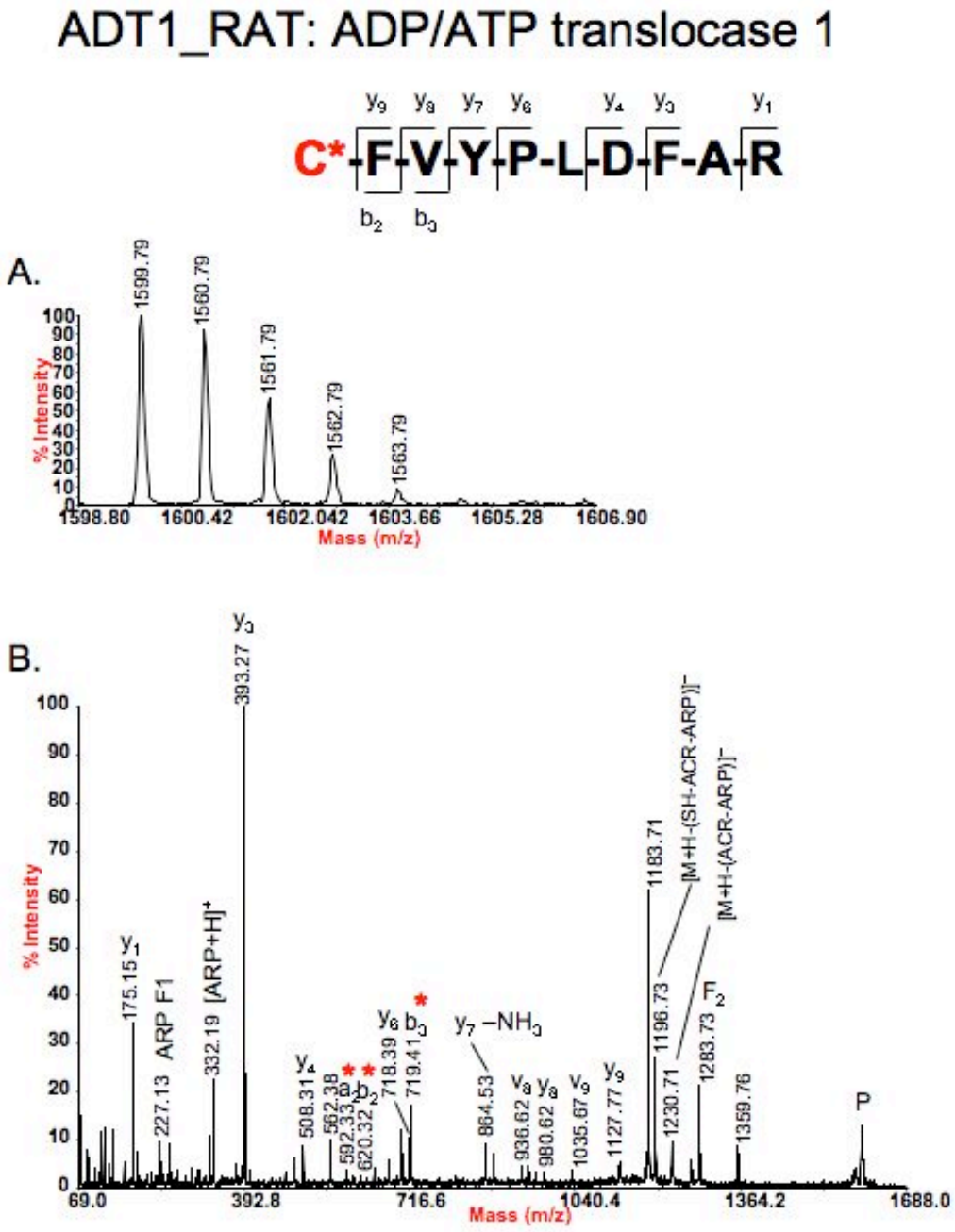

Figure SB39. (A) Full mass spectrum and (B) MS/MS spectrum acquired by MALDI-TOF/TOF of the $[M+H]^+$ ion of the ARP labeled, acrolein modified peptide C*FVYPLDFAR; monoisotopic m/z_{calc} 1599.74; accuracy **Δ**(m/z) = 0.05 m/z

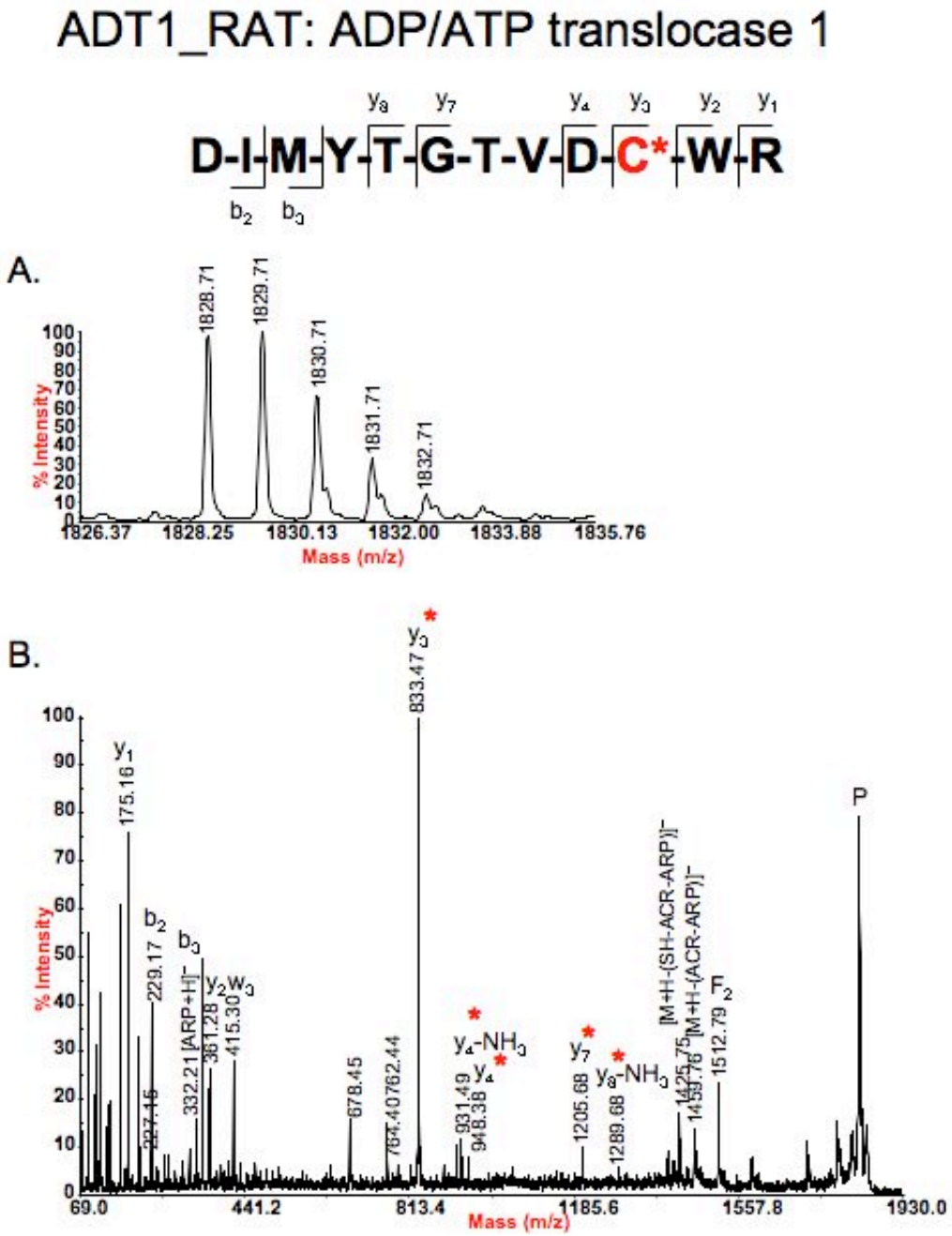

Figure SB40. (A) Full mass spectrum and (B) MS/MS spectrum acquired by MALDI-TOF/TOF of the $[M+H]^+$ ion of the ARP labeled, acrolein modified peptide DIMYTGTVDC*WR; monoisotopic m/z_{calc} 1828.78; accuracy **Δ**(m/z) = -0.07 m/z

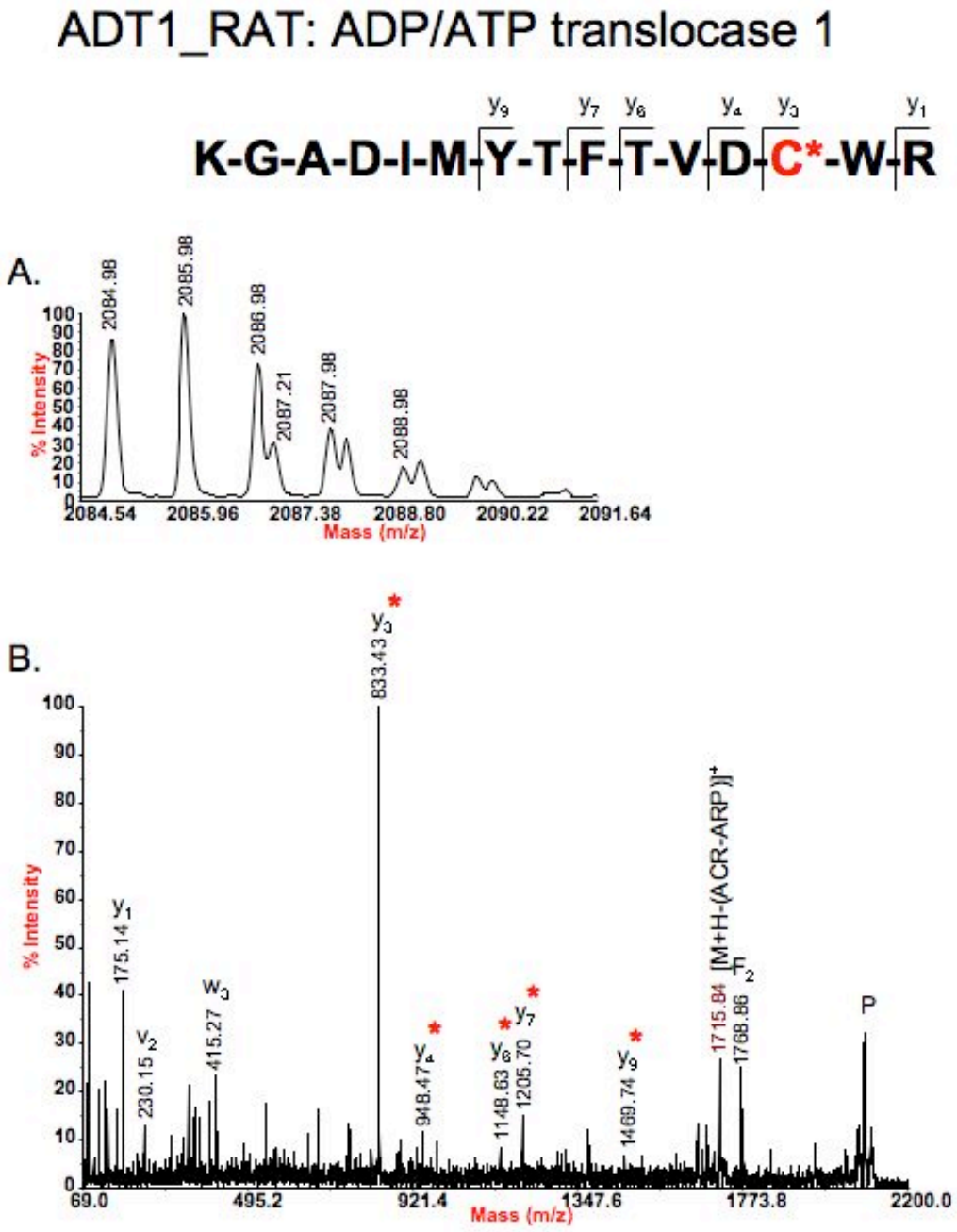

Figure SB41. (A) Full mass spectrum and (B) MS/MS spectrum acquired by MALDI-TOF/TOF of the $[M+H]^+$ ion of the ARP labeled, acrolein modified peptide KGADIMYTGTVDC*WR; monoisotopic m/z_{calc} 2084.94; accuracy **Δ**(m/z) = 0.04 m/z

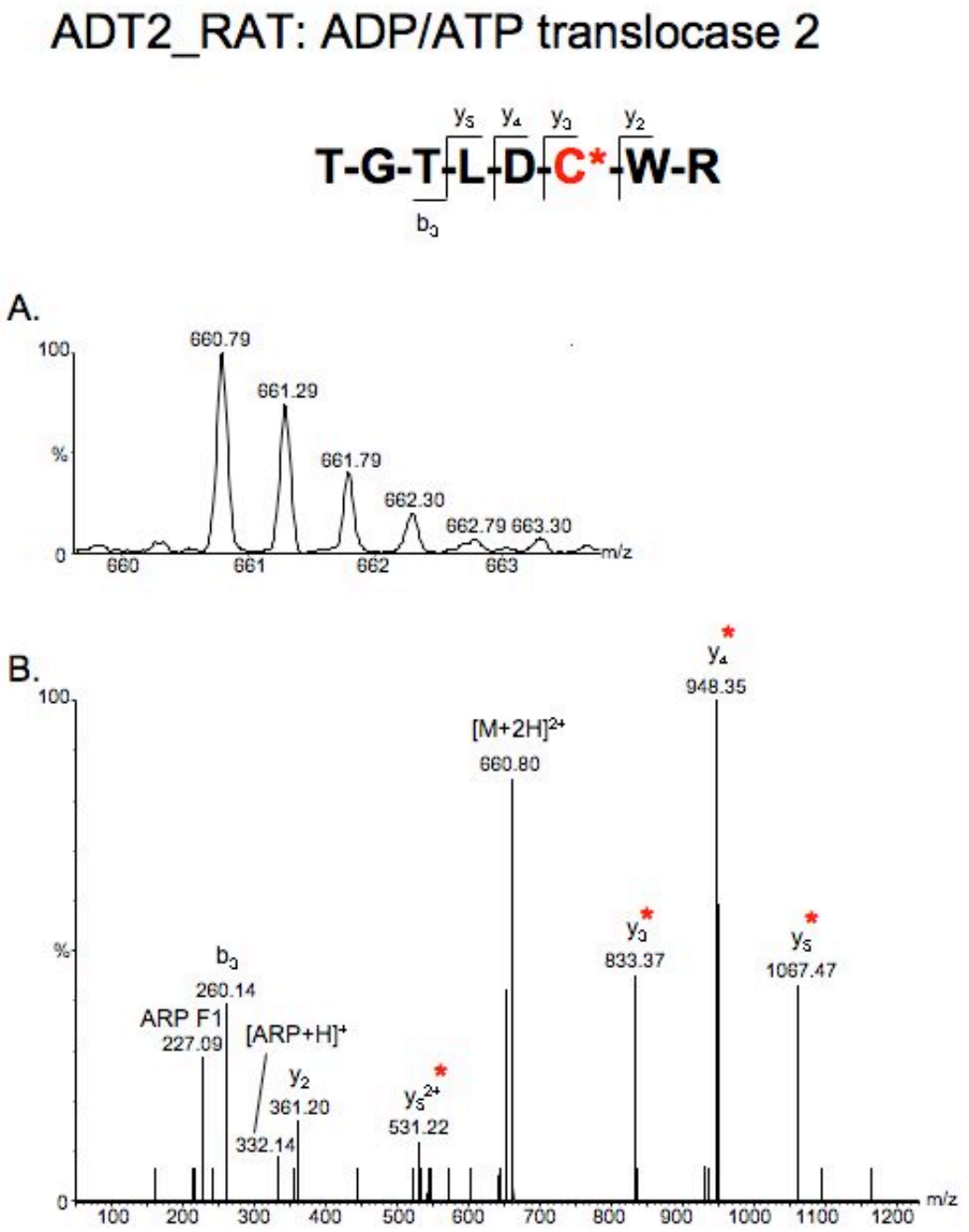

Figure SB42. (A) Full mass spectrum and (B) MS/MS spectrum acquired by ESI-Q-TOF of the $[M+2H]^{2+}$ ion of the ARP labeled, acrolein modified peptide TGTLDC*WR; monoisotopic m/z_{calc} 660.79; accuracy **Δ**(m/z) = 0.00 m/z

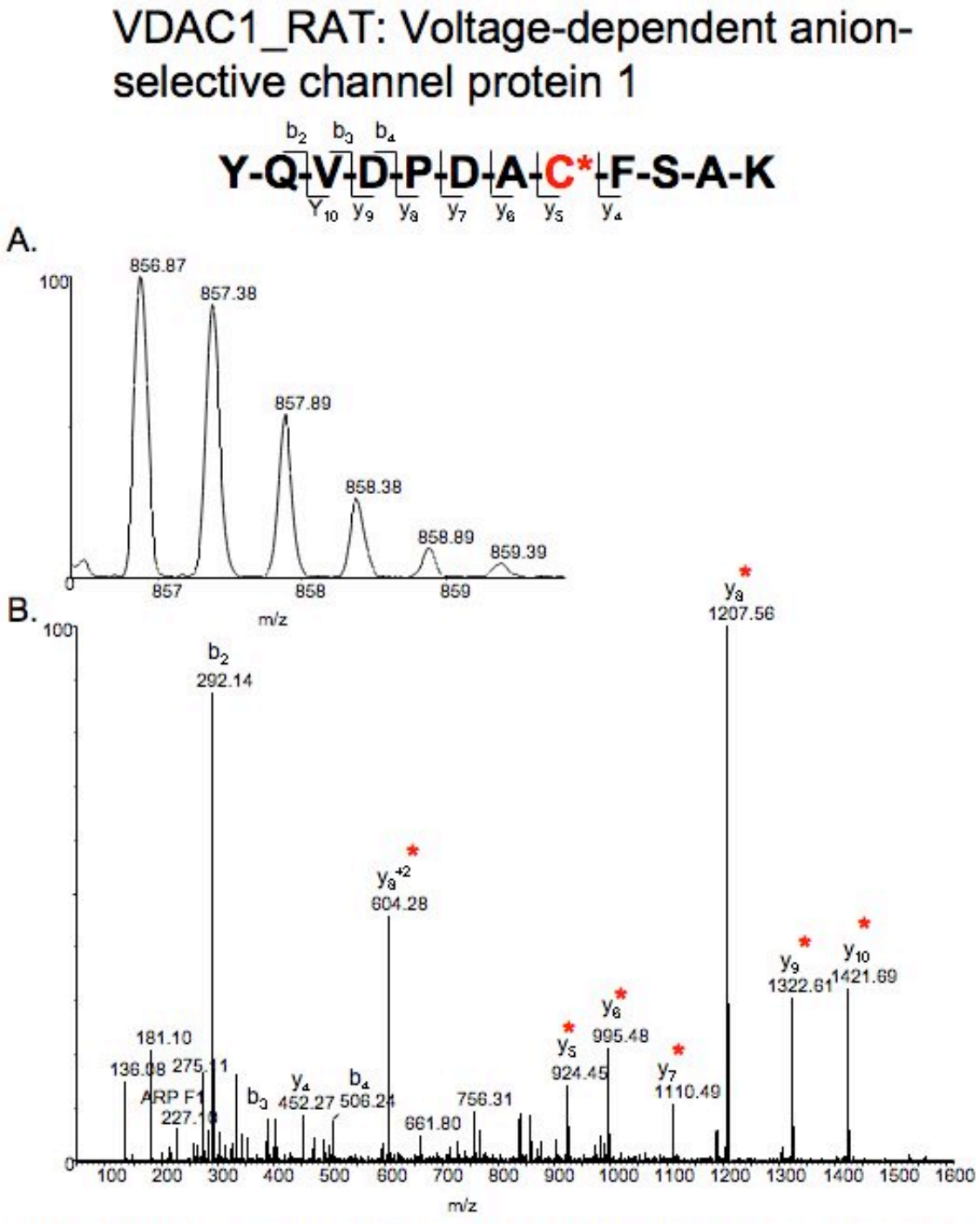

Figure SB43. (A) Full mass spectrum and (B) MS/MS spectrum acquired by ESI-Q-TOF of the $[M+2H]^{2+}$ ion of the ARP labeled, acrolein modified peptide YQVDPDAC*FSAK; monoisotopic m/z_{calc} 856.87; accuracy **Δ**(m/z) = 0.00 m/z

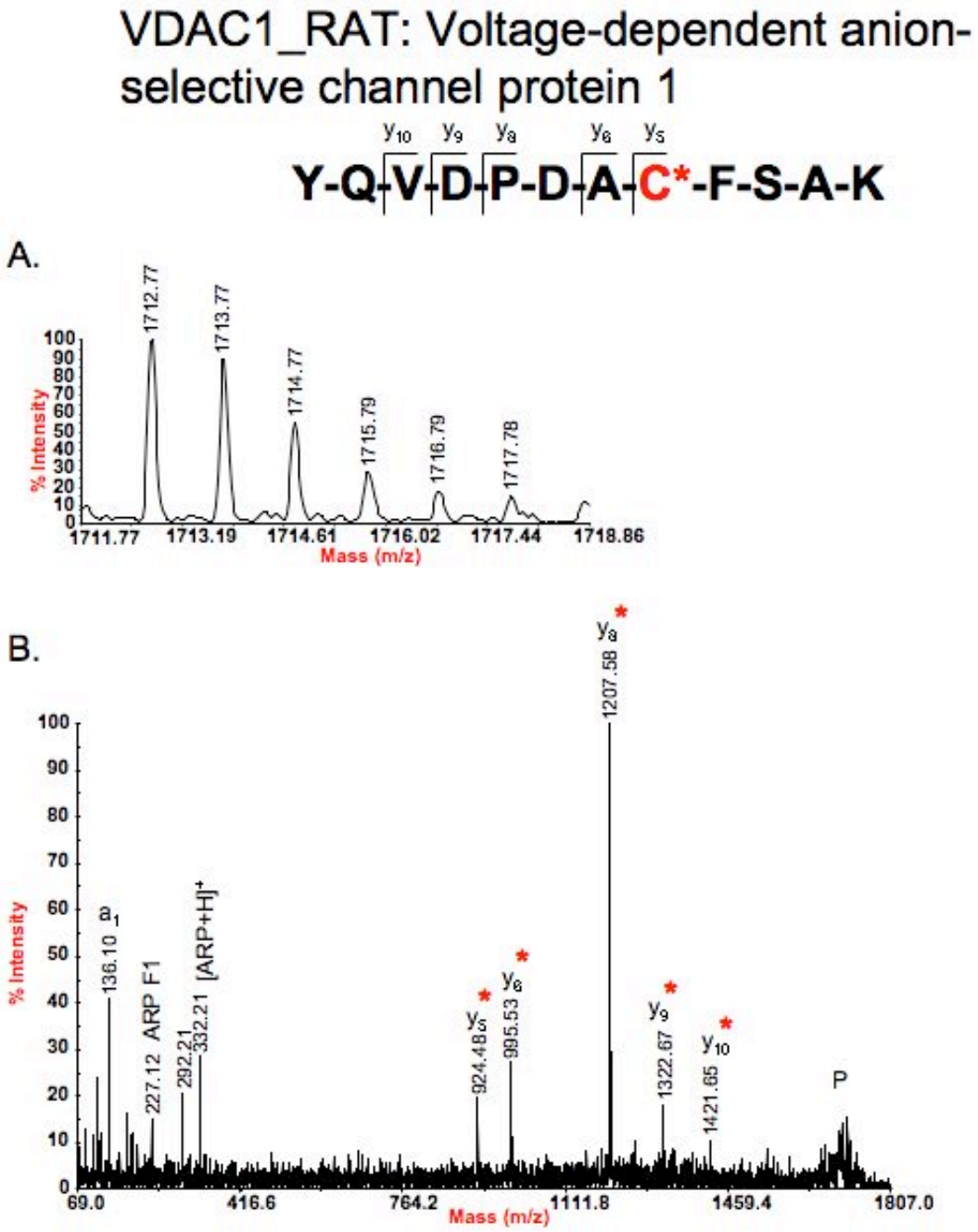

Figure SB44. (A) Full mass spectrum and (B) MS/MS spectrum acquired by MALDI-TOF/TOF of the $[M+H]^+$ ion of the ARP labeled, acrolein modified peptide YQVDPDAC*FSAK; monoisotopic m/z_{calc} 1712.74; accuracy **Δ**(m/z) = 0.03 m/z

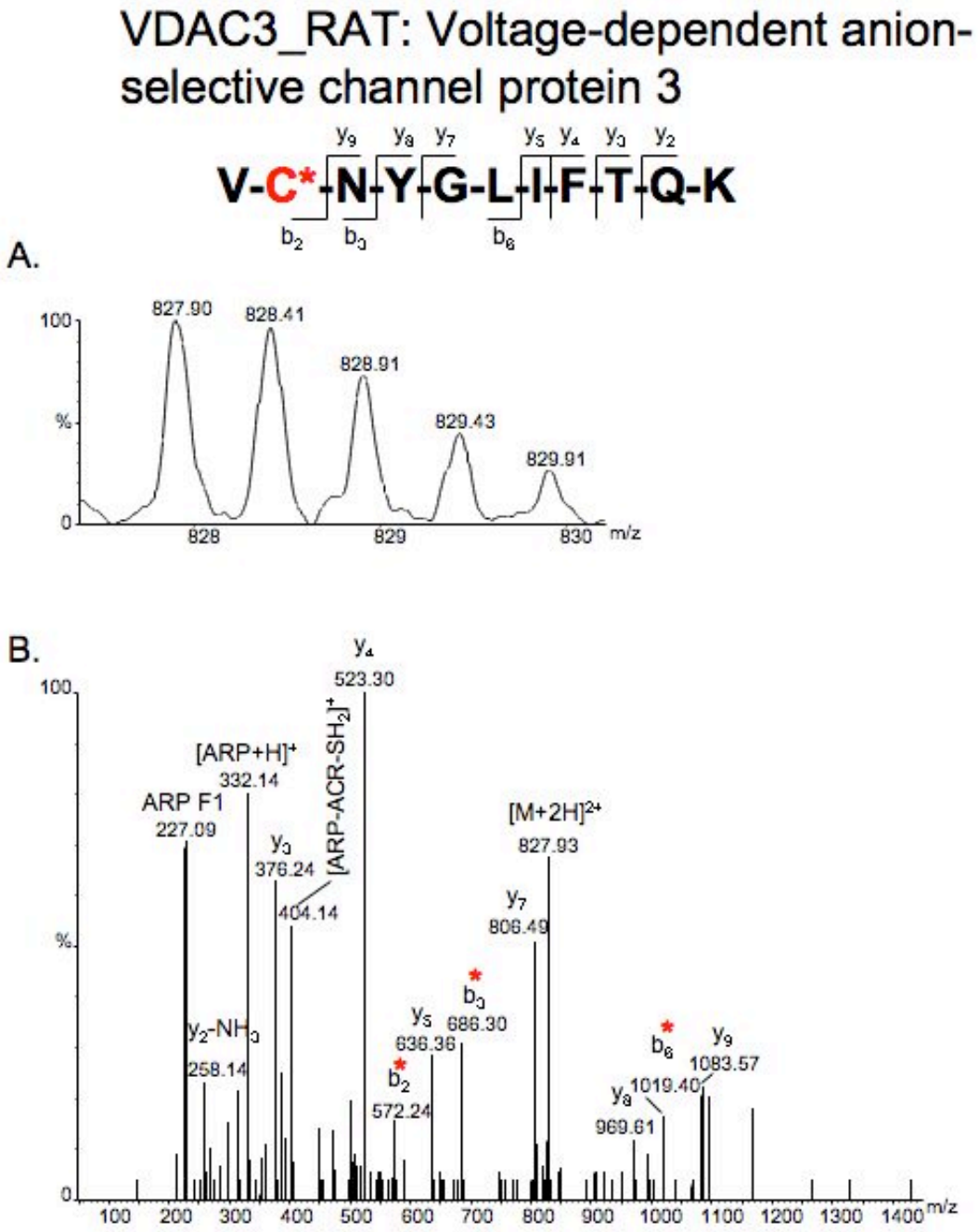

Figure SB45. (A) Full mass spectrum and (B) MS/MS spectrum acquired by ESI-Q-TOF of the $[M+2H]^{2+}$ ion of the ARP labeled, acrolein modified peptide VC*NYGLIFTQK; monoisotopic m/z_{calc} 827.91; accuracy **Δ**(m/z) = -0.01 m/z

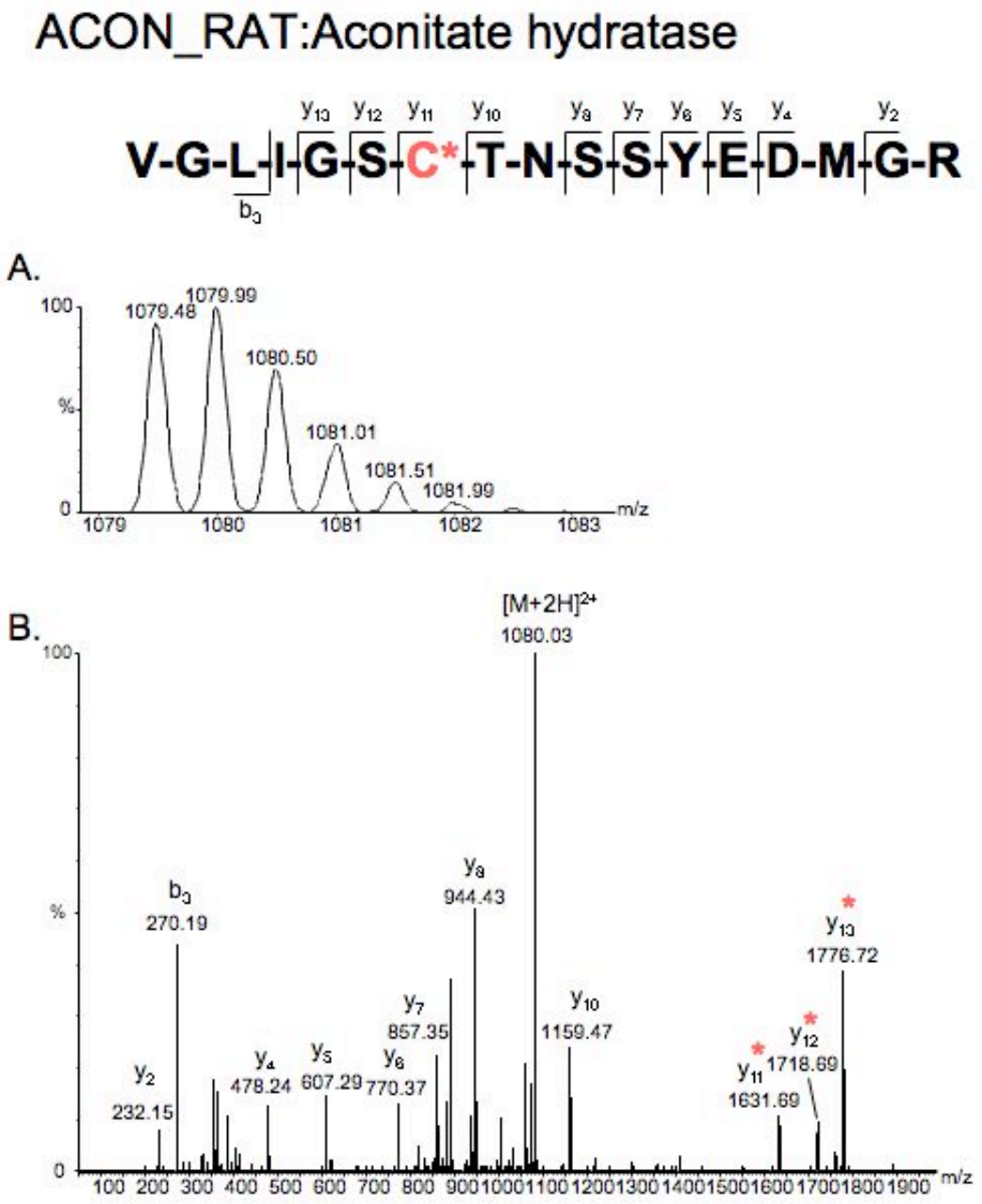

Figure SB46. (A) Full mass spectrum and (B) MS/MS spectrum acquired by ESI-Q-TOF of the $[M+2H]^{2+}$ ion of the ARP labeled, acrolein modified peptide VGLIGSC*TNSSYEDMGR; monoisotopic m/z_{calc} 1079.47; accuracy **Δ**(m/z) = 0.01 m/z

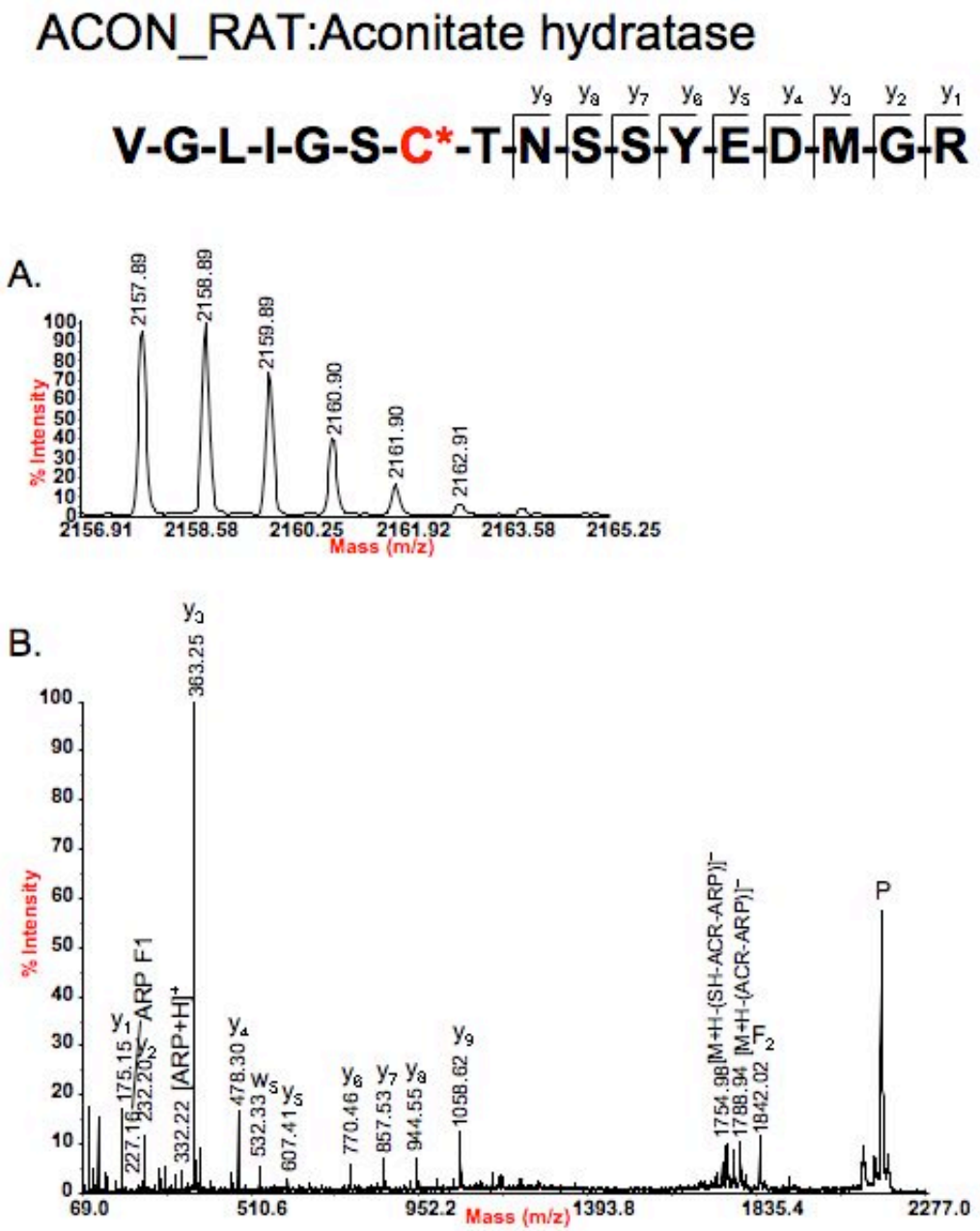

Figure SB47. (A) Full mass spectrum and (B) MS/MS spectrum acquired by MALDI-TOF/TOF of the $[M+H]^+$ ion of the ARP labeled, acrolein modified peptide VGLIGSC*TNSSYEDMGR; monoisotopic m/z_{calc} 2157.94; accuracy **Δ**(m/z) = -0.05 m/z

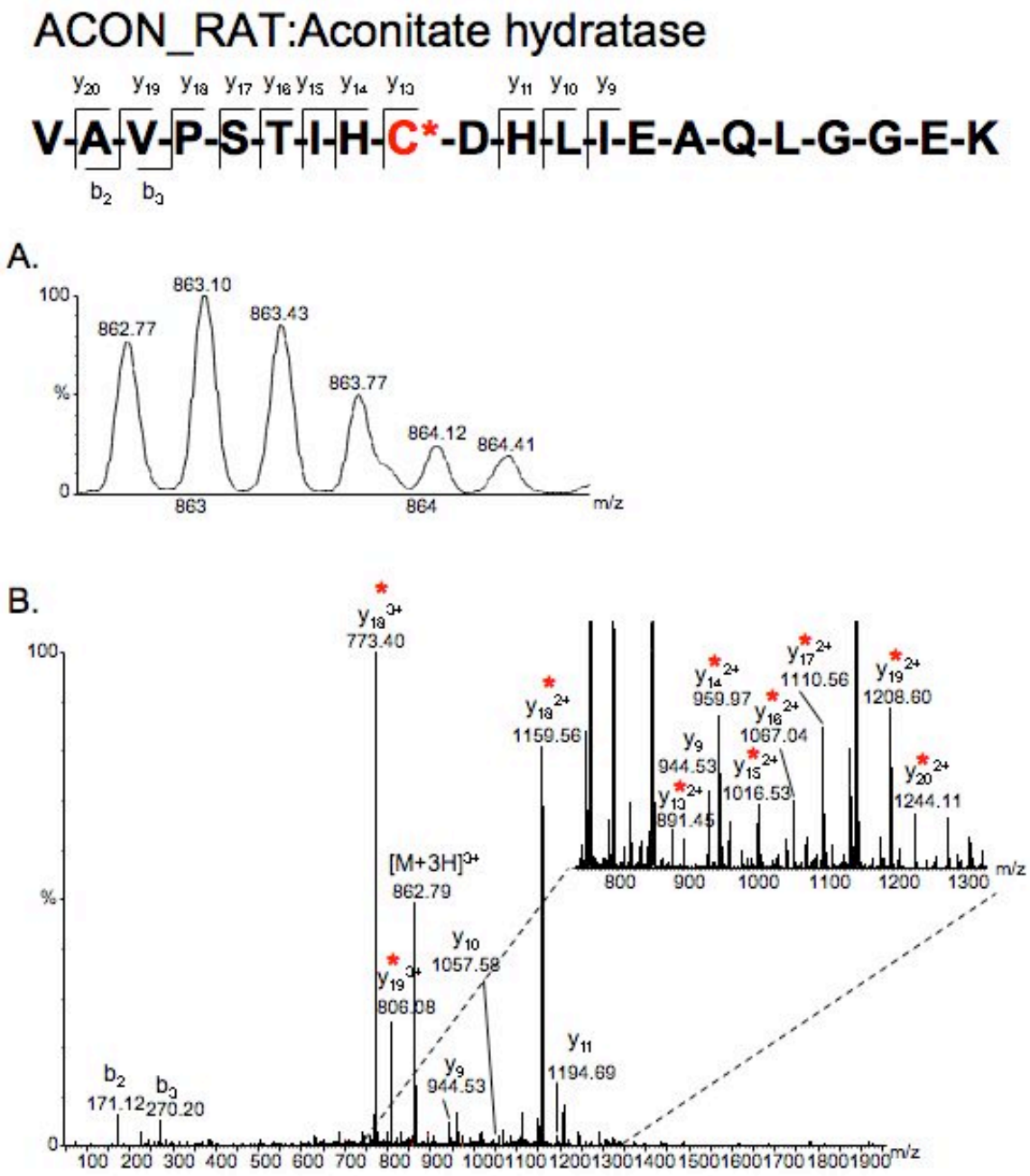

Figure SB48. (A) Full mass spectrum and (B) MS/MS spectrum acquired by ESI-Q-TOF of the $[M+3H]^{3+}$ ion of the ARP labeled, acrolein modified peptide VAVPSTIHC*DHLIEAQLGGEK; monoisotopic m/z_{calc} 862.77; accuracy **Δ**(m/z) = 0.00 m/z

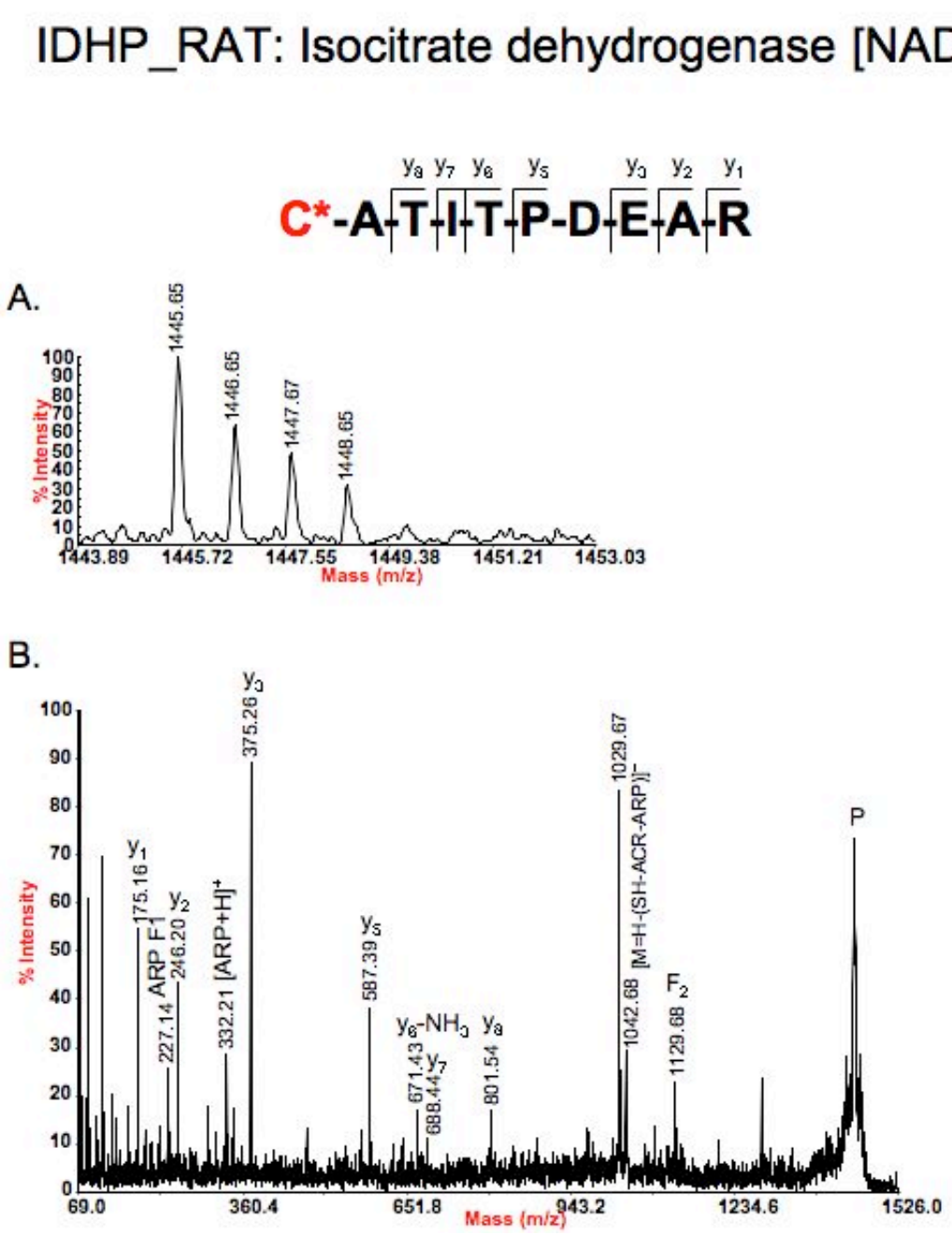

Figure SB49. (A) Full mass spectrum and (B) MS/MS spectrum acquired by MALDI-TOF/TOF of the $[M+H]^+$ ion of the ARP labeled, acrolein modified peptide C*ATITPDEAR; monoisotopic m/z_{calc} 1445.65; accuracy **Δ**(m/z) = 0.00 m/z

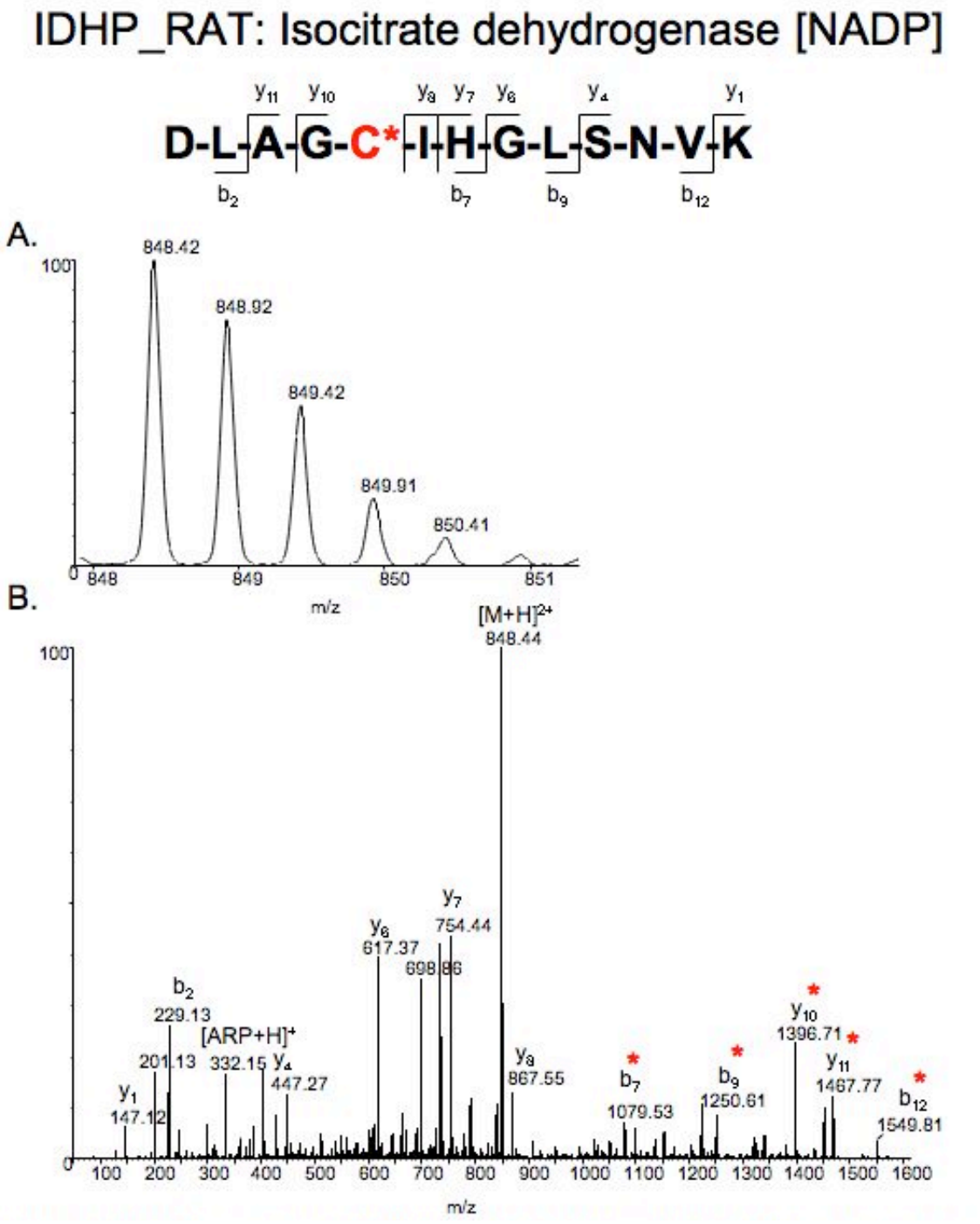

Figure SB50. (A) Full mass spectrum and (B) MS/MS spectrum acquired by ESI-Q-TOF of the $[M+2H]^{2+}$ ion of the ARP labeled, acrolein modified peptide DLAGC*IHGLSNVK; monoisotopic m/z_{calc} 848.42; accuracy **Δ**(m/z) = 0.00 m/z

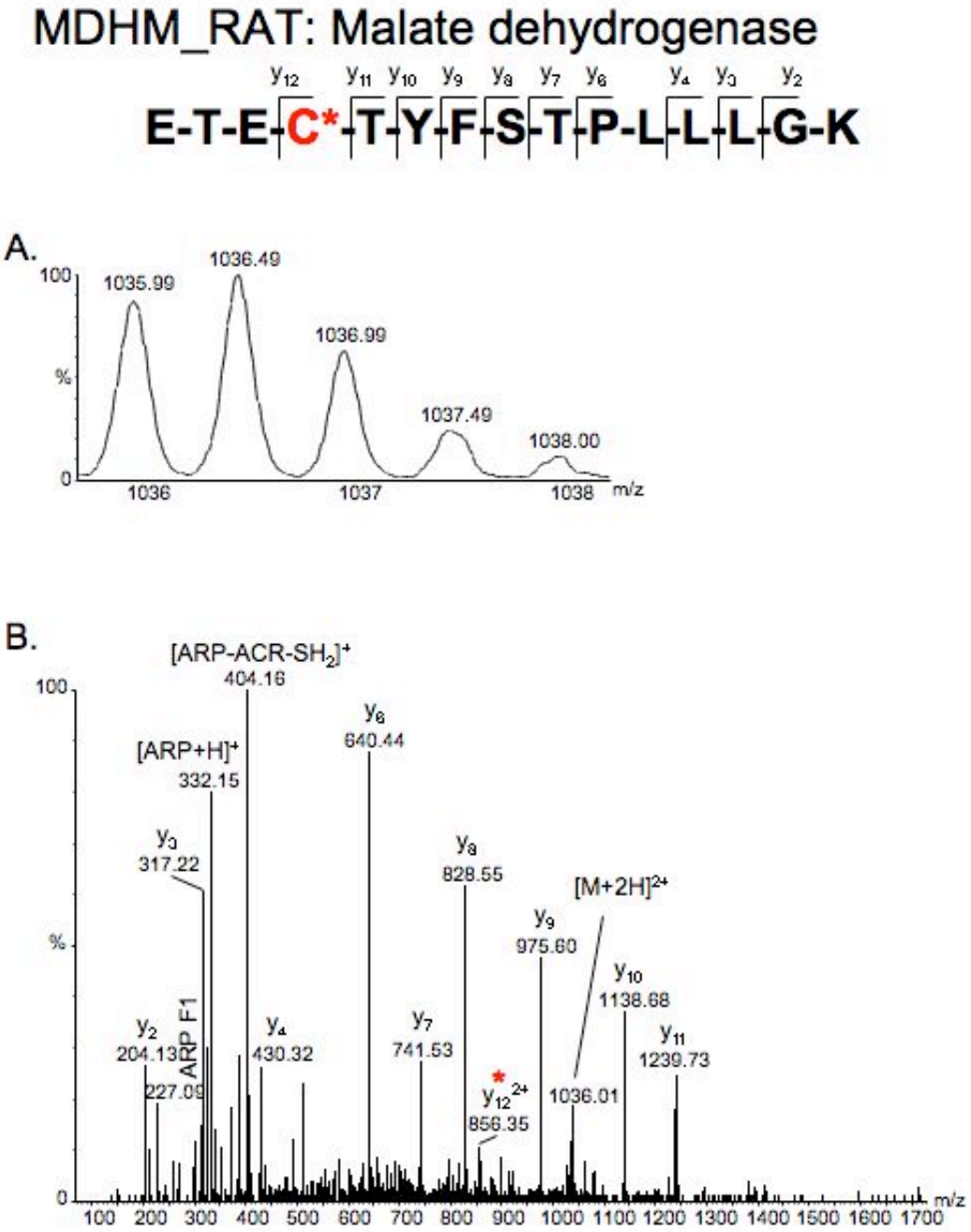

Figure SB51. (A) Full mass spectrum and (B) MS/MS spectrum acquired by ESI-Q-TOF of the $[M+2H]^{2+}$ ion of the ARP labeled, acrolein modified peptide ETEC*TYFSTPLLLGK; monoisotopic m/z_{calc} 1036.00; accuracy **Δ**(m/z) = -0.01 m/z

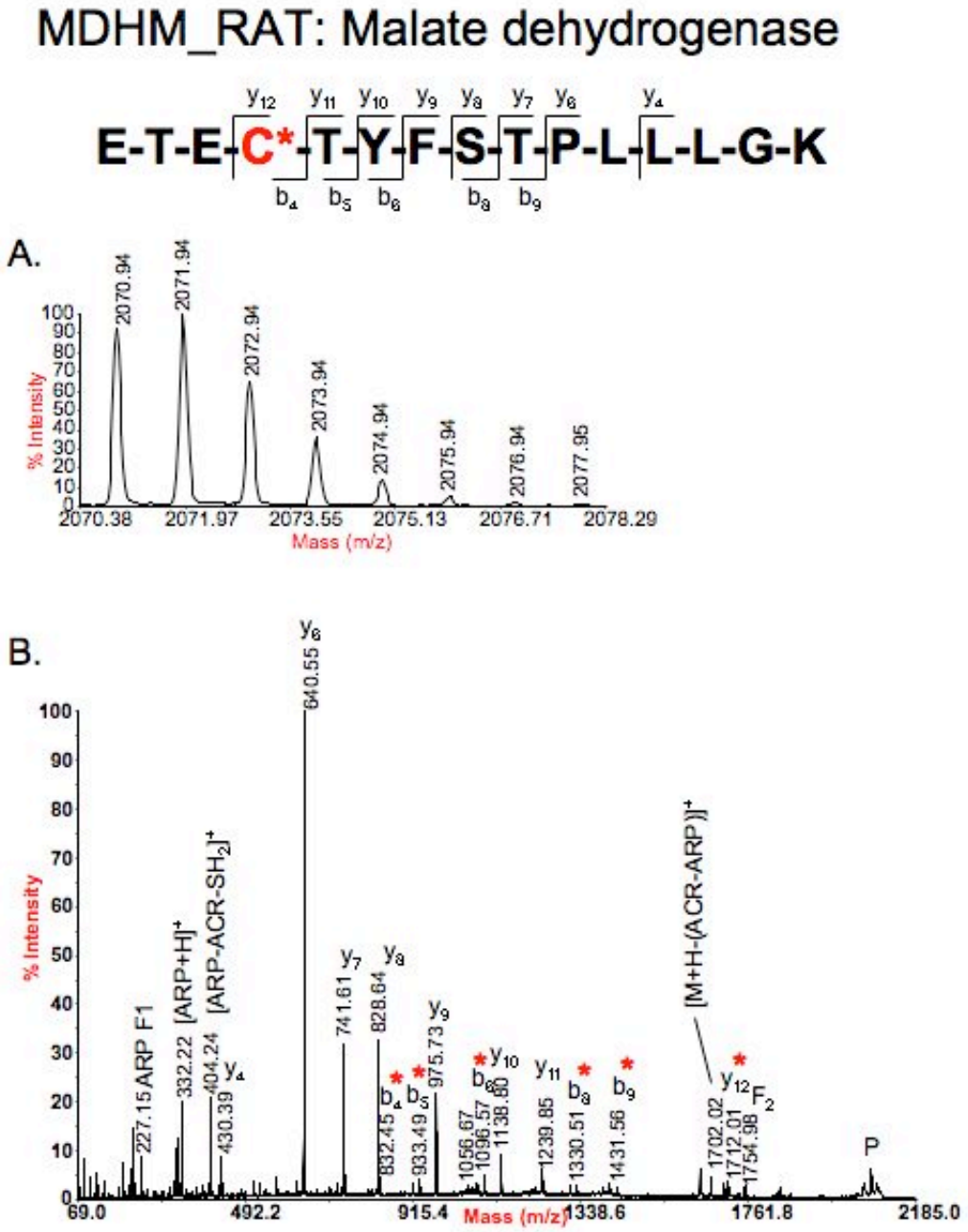

Figure SB52. (A) Full mass spectrum and (B) MS/MS spectrum acquired by MALDI-TOF/TOF of the $[M+H]^+$ ion of the ARP labeled, acrolein modified peptide ETEC*TYFSTPLLLGK; monoisotopic m/z_{calc} 2070.99; accuracy **Δ**(m/z) = -0.05 m/z

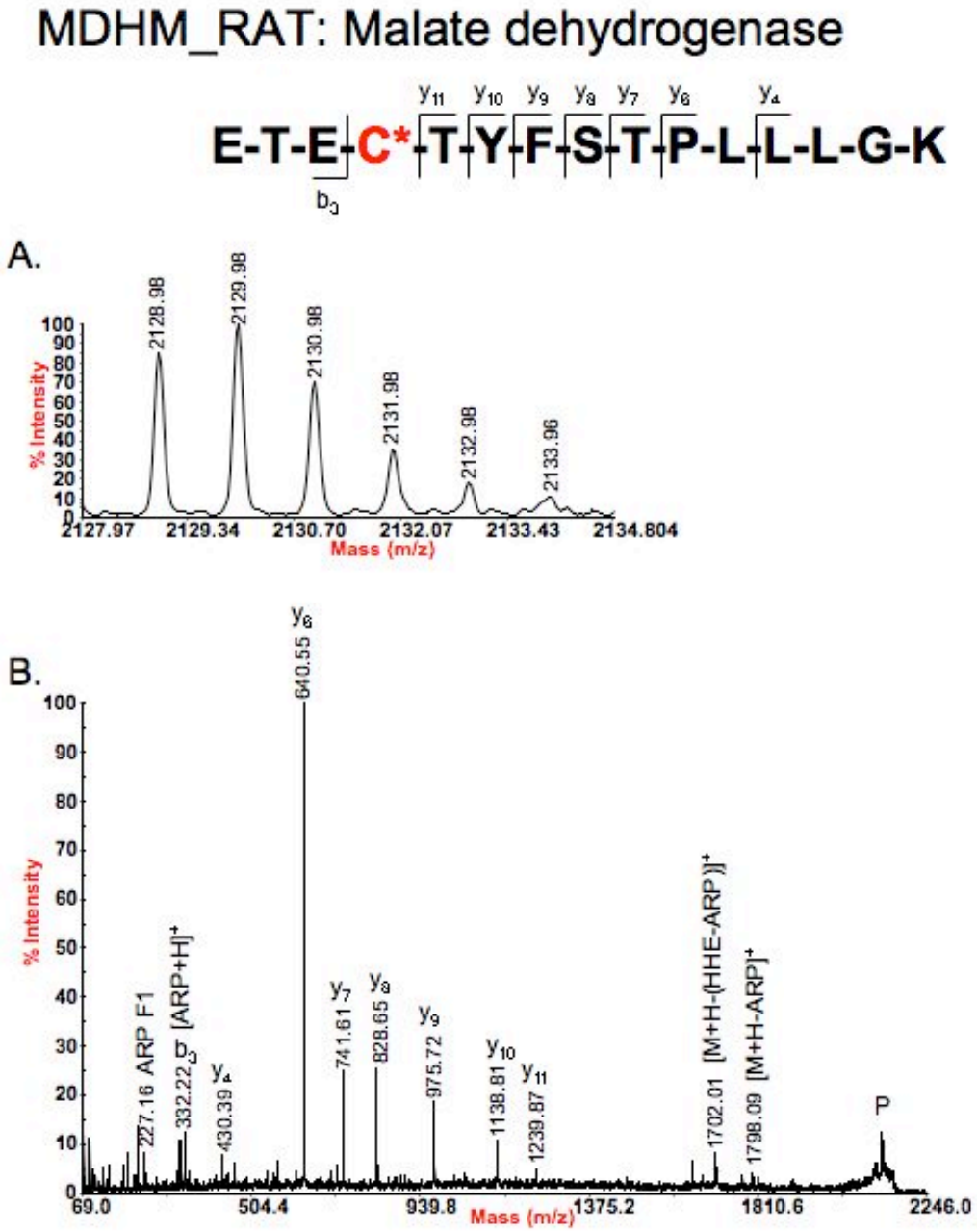

Figure SB53. (A) Full mass spectrum and (B) MS/MS spectrum acquired by MALDI-TOF/TOF of the $[M+H]^+$ ion of the ARP labeled, HHE modified peptide ETEC*TYFSTPLLLGK; monoisotopic m/z_{calc} 2129.03; accuracy **Δ**(m/z) = -0.05 m/z

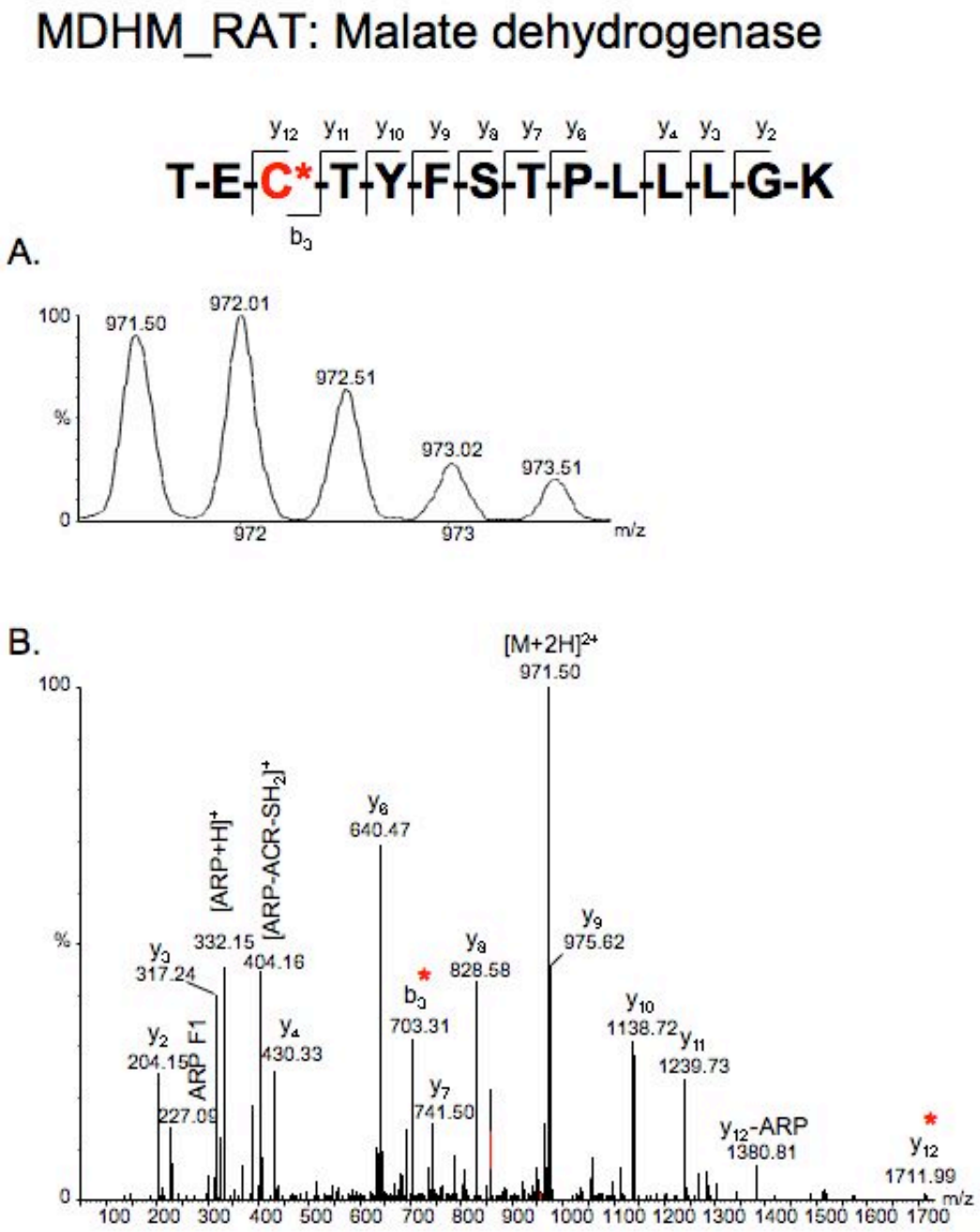

Figure SB54. (A) Full mass spectrum and (B) MS/MS spectrum acquired by ESI-Q-TOF of the $[M+2H]^{2+}$ ion of the ARP labeled, acrolein modified peptide TEC*TYFSTPLLLGK; monoisotopic m/z_{calc} 971.48; accuracy **Δ**(m/z) = 0.02 m/z

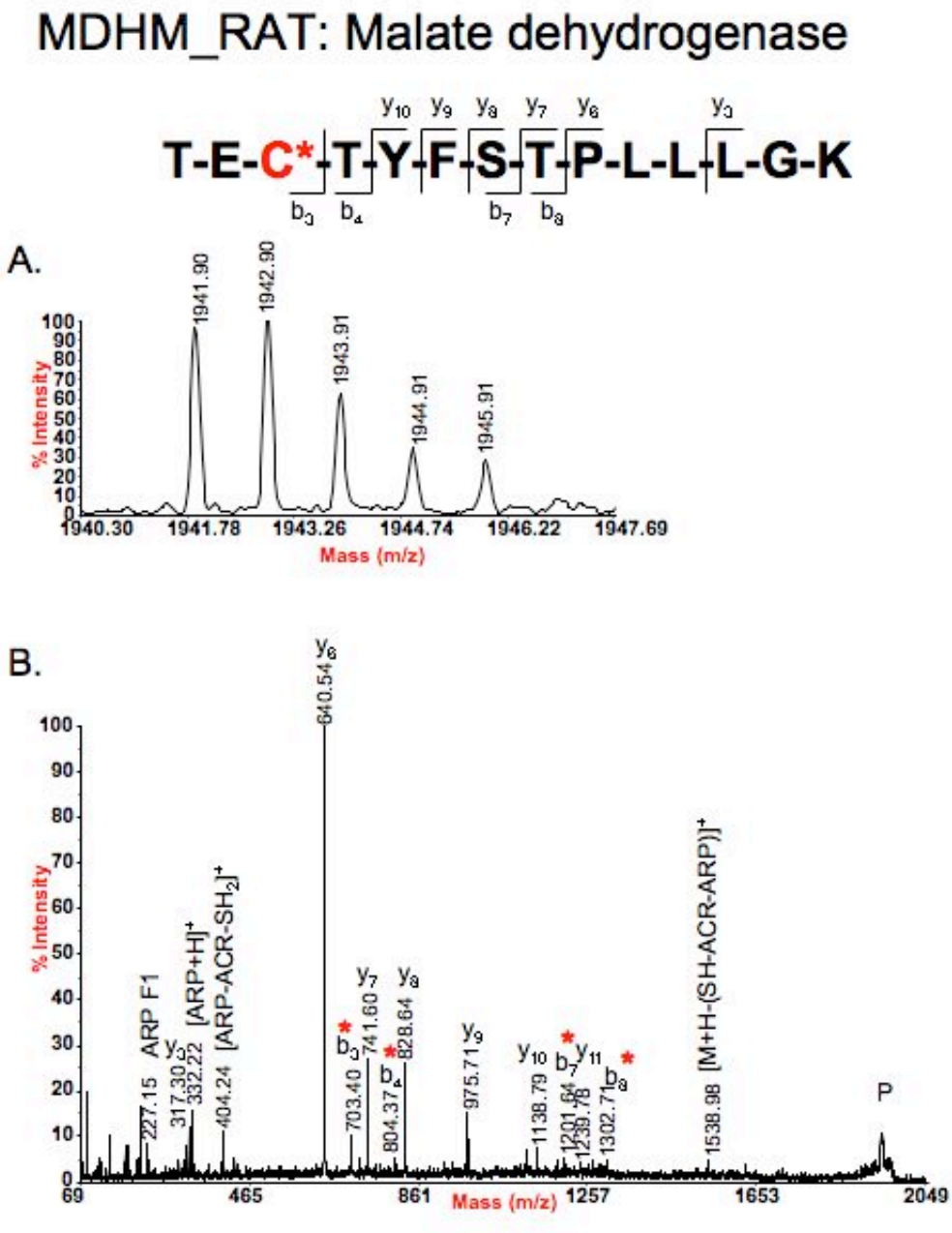

Figure SB55. (A) Full mass spectrum and (B) MS/MS spectrum acquired by MALDI-TOF/TOF of the $[M+H]^+$ ion of the ARP labeled, acrolein modified peptide TEC*TYFSTPLLLGK; monoisotopic m/z_{calc} 1941.94; accuracy **Δ**(m/z) = -0.04 m/z

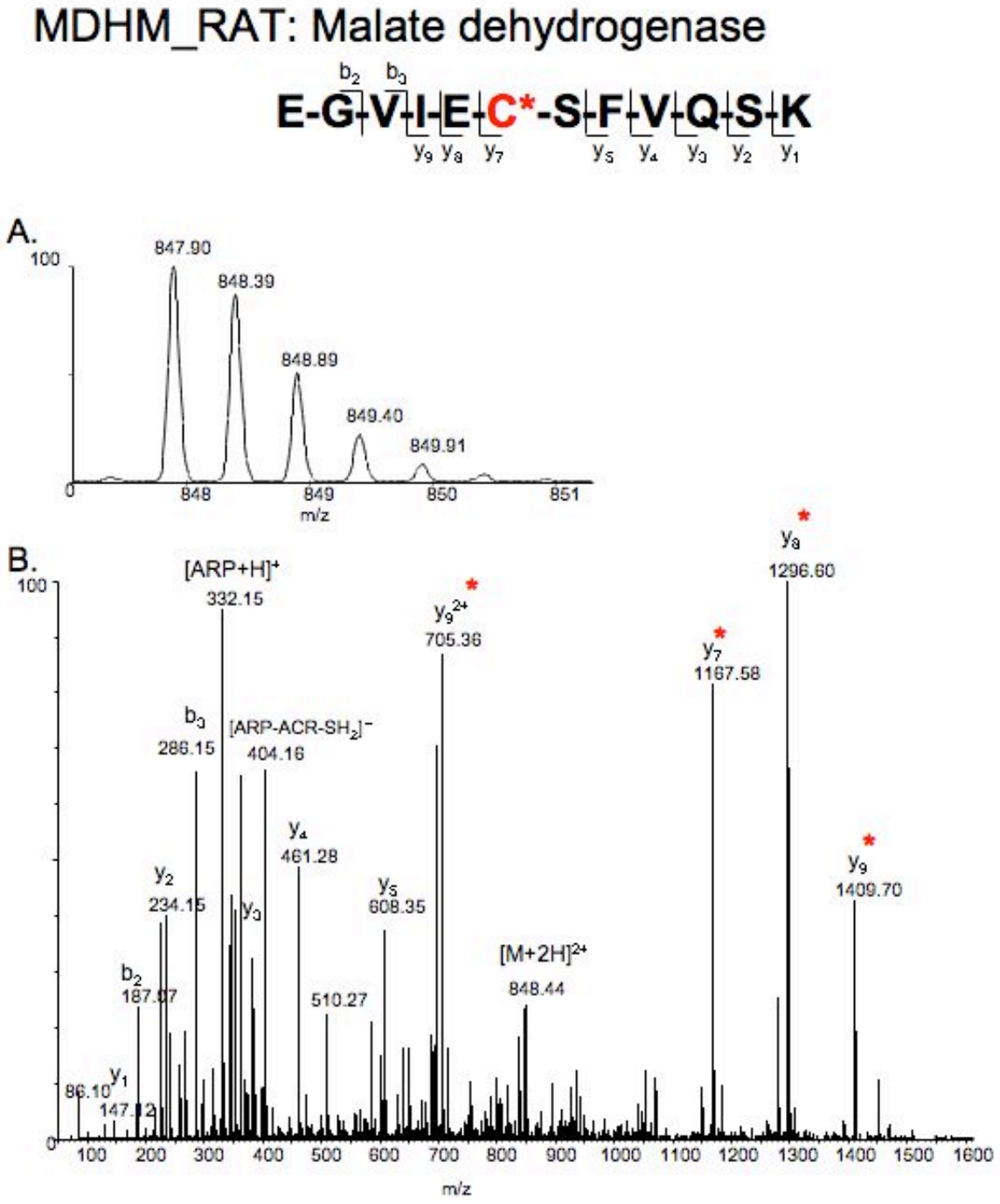

Figure SB56. (A) Full mass spectrum and (B) MS/MS spectrum acquired by ESI-Q-TOF of the $[M+2H]^{2+}$ ion of the ARP labeled, acrolein modified peptide EGVIEC*SFVQSK; monoisotopic m/z_{calc} 847.90; accuracy **Δ**(m/z) = 0.00 m/z

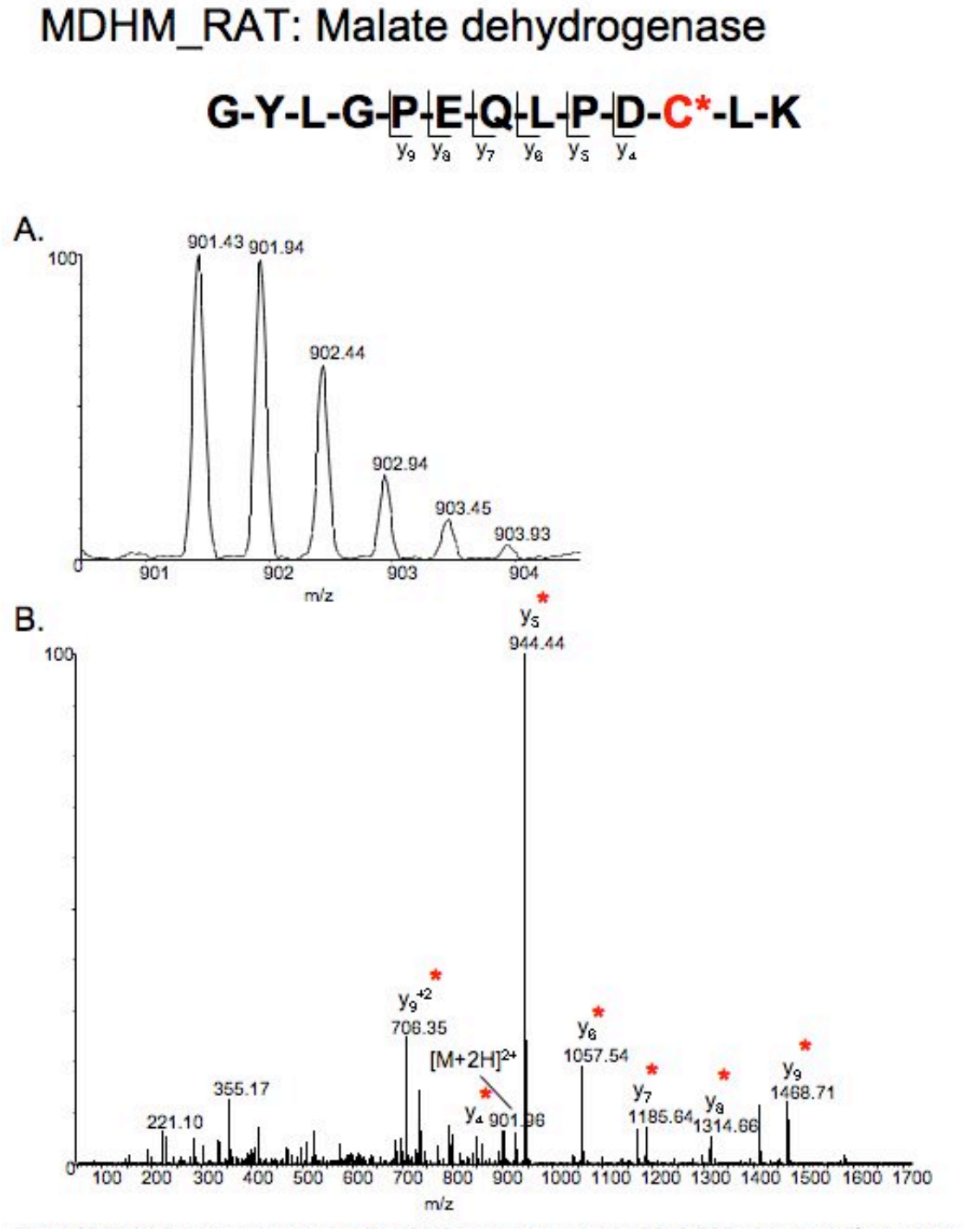

Figure SB57. (A) Full mass spectrum and (B) MS/MS spectrum acquired by ESI-Q-TOF of the $[M+2H]^{2+}$ ion of the ARP labeled, acrolein modified peptide GYLGPEQLPDC*LK; monoisotopic m/z_{calc} 901.43; accuracy **Δ**(m/z) = 0.00 m/z

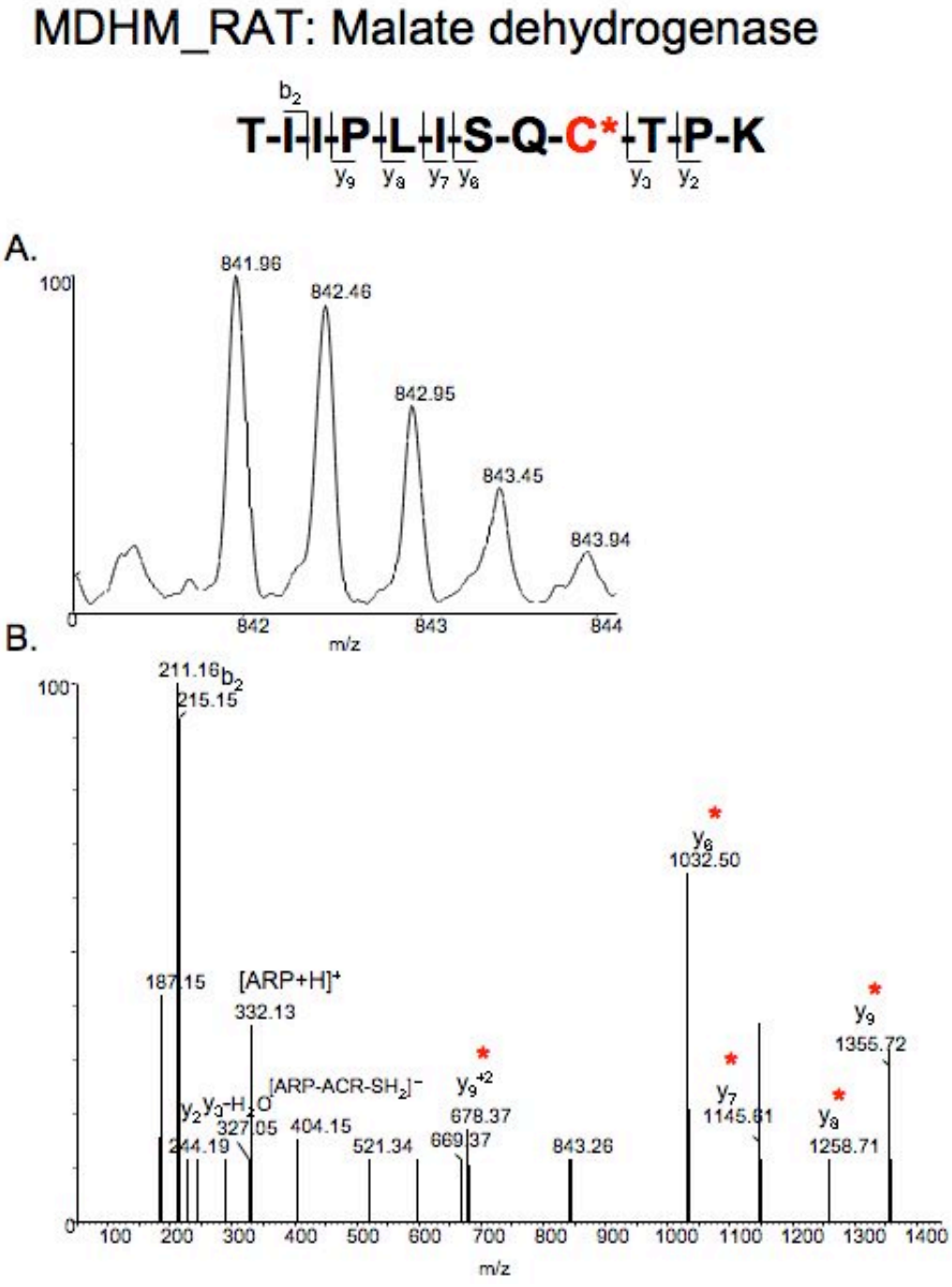

Figure SB58. (A) Full mass spectrum and (B) MS/MS spectrum acquired by ESI-Q-TOF of the $[M+2H]^{2+}$ ion of the ARP labeled, acrolein modified peptide TIIPLISQC*TPK; monoisotopic m/z_{calc} 841.95; accuracy **Δ**(m/z) = 0.01 m/z

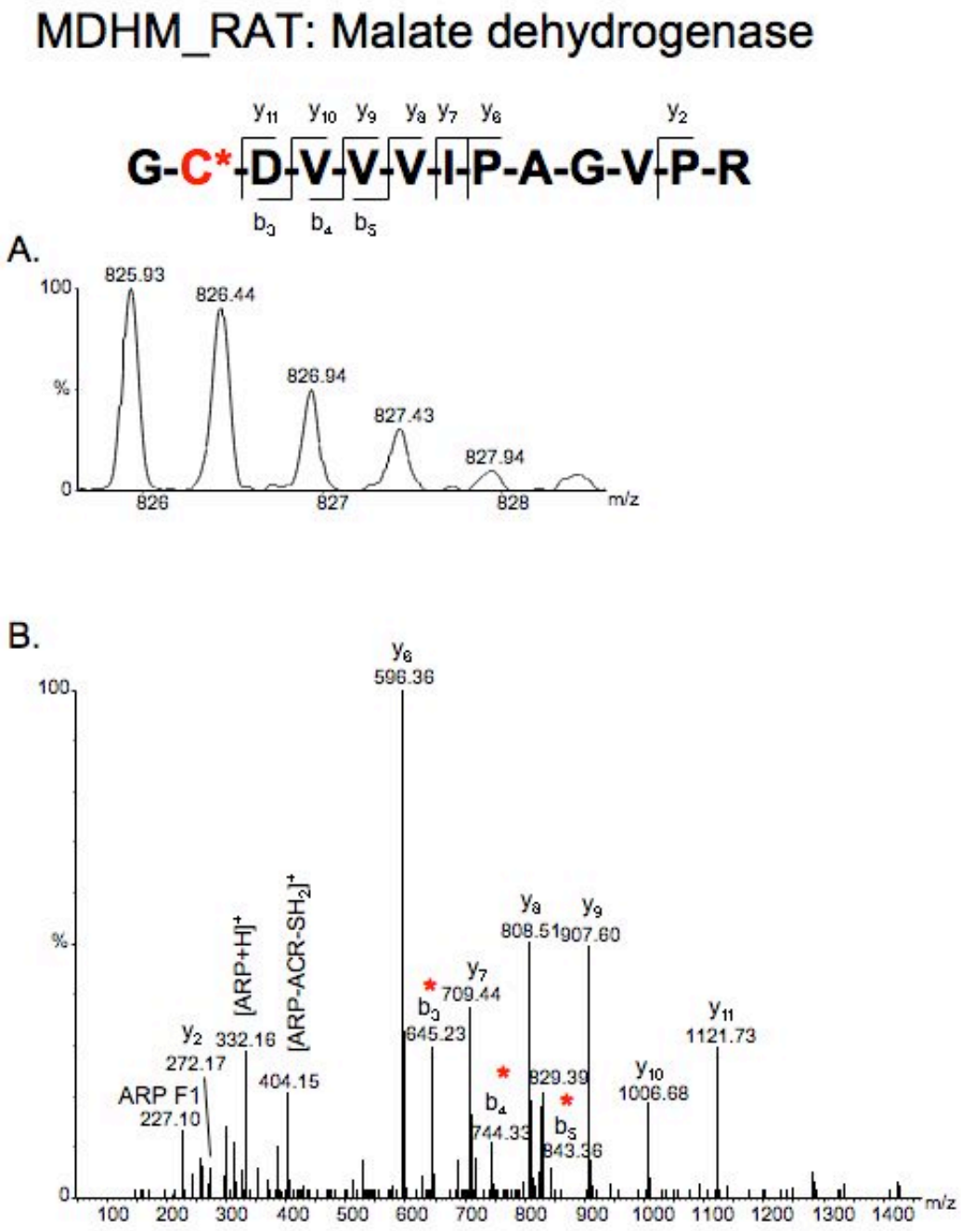

Figure SB59. (A) Full mass spectrum and (B) MS/MS spectrum acquired by ESI-Q-TOF of the $[M+2H]^{2+}$ ion of the ARP labeled, acrolein modified peptide GC*DVVVIPAGVPR; monoisotopic m/z_{calc} 825.93; accuracy **Δ**(m/z) = 0.00 m/z

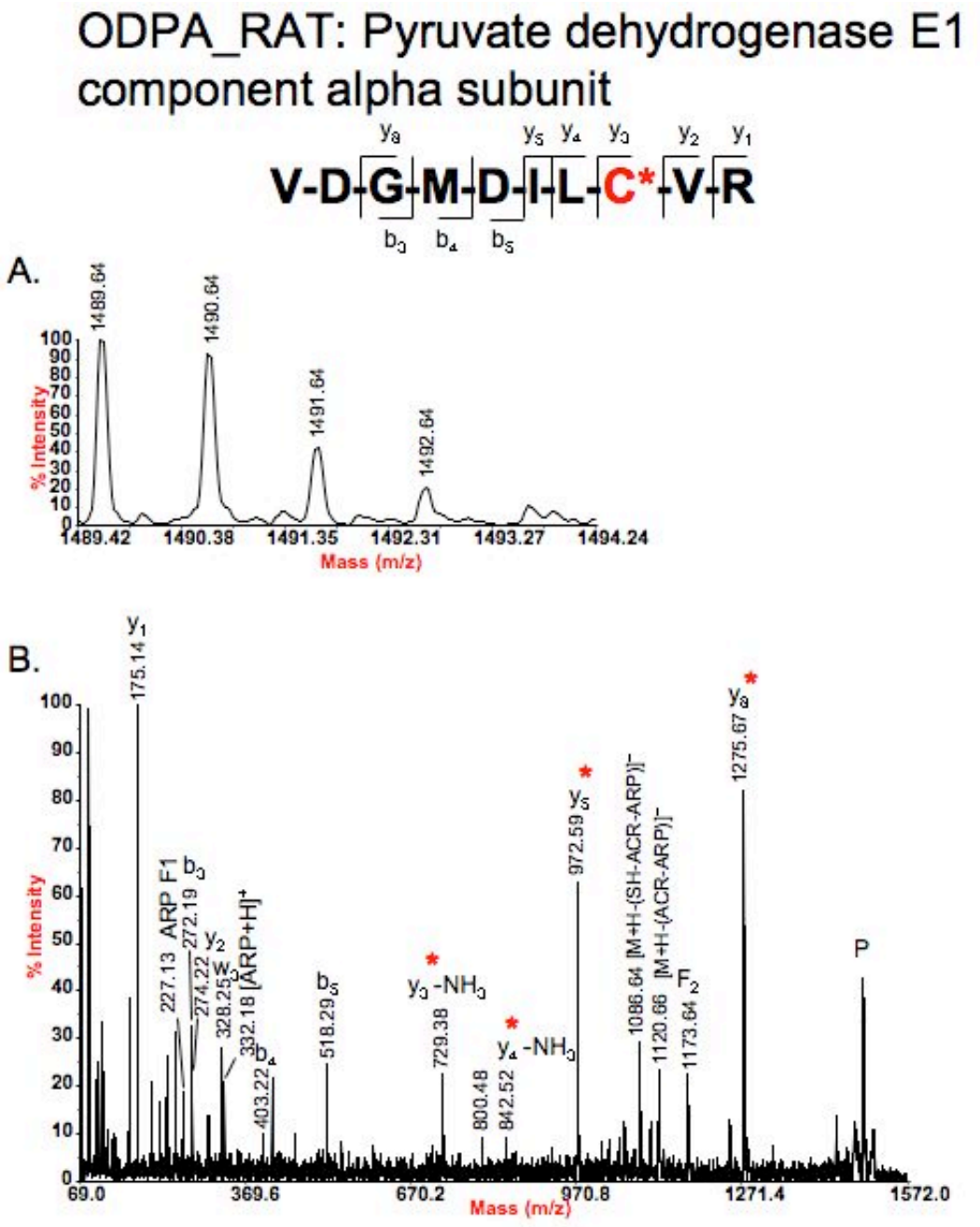

Figure SB60. (A) Full mass spectrum and (B) MS/MS spectrum acquired by MALDI-TOF/TOF of the $[M+H]^+$ ion of the ARP labeled, acrolein modified peptide VDGMDILC*VR; monoisotopic m/z_{calc} 1489.70; accuracy **Δ**(m/z) = -0.06 m/z

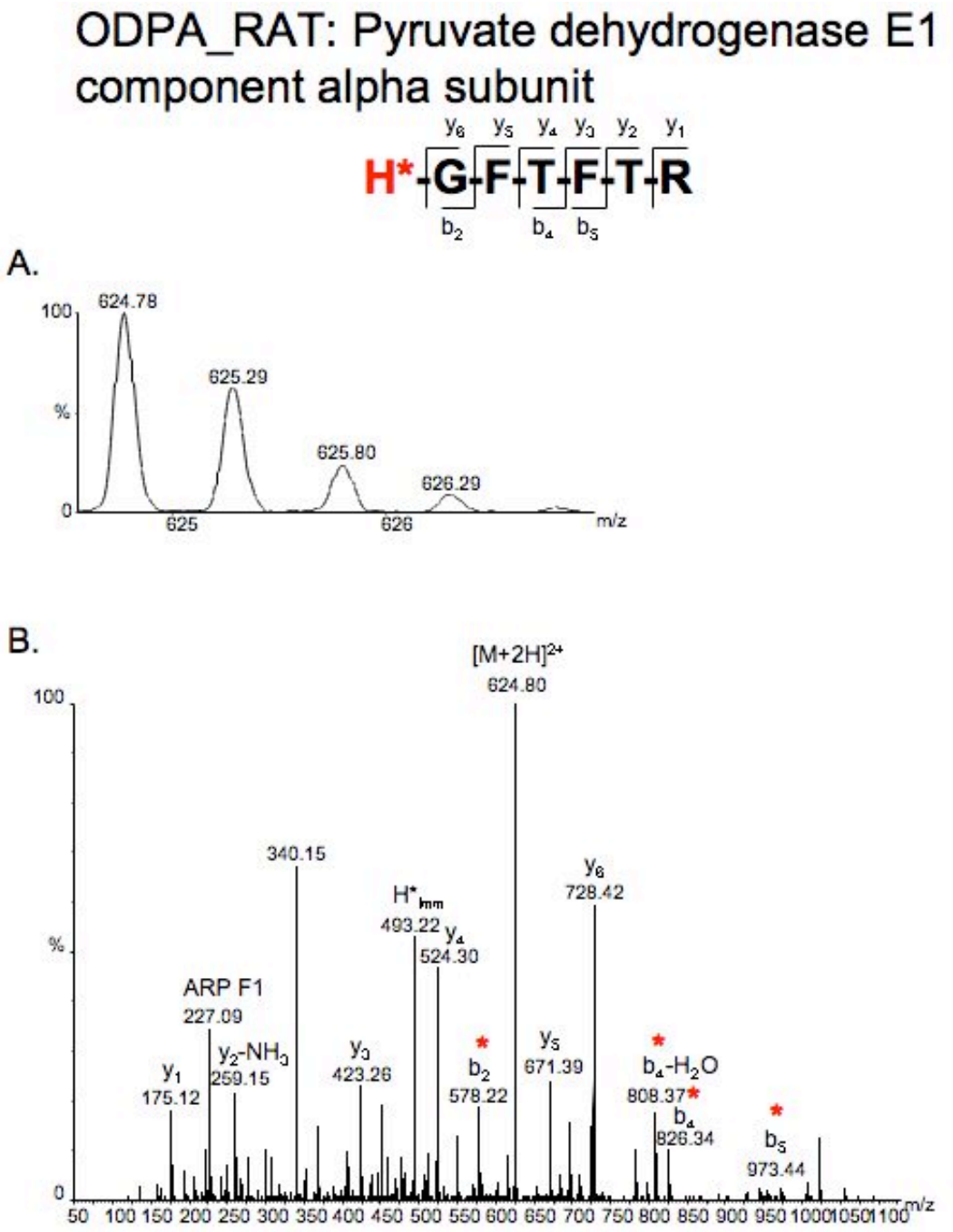

Figure SB61. (A) Full mass spectrum and (B) MS/MS spectrum acquired by ESI-Q-TOF of the $[M+2H]^{2+}$ ion of the ARP labeled, crotonaldehyde modified peptide H*GFTFTR; monoisotopic m/z_{calc} 624.80; accuracy **Δ**(m/z) = -0.02 m/z

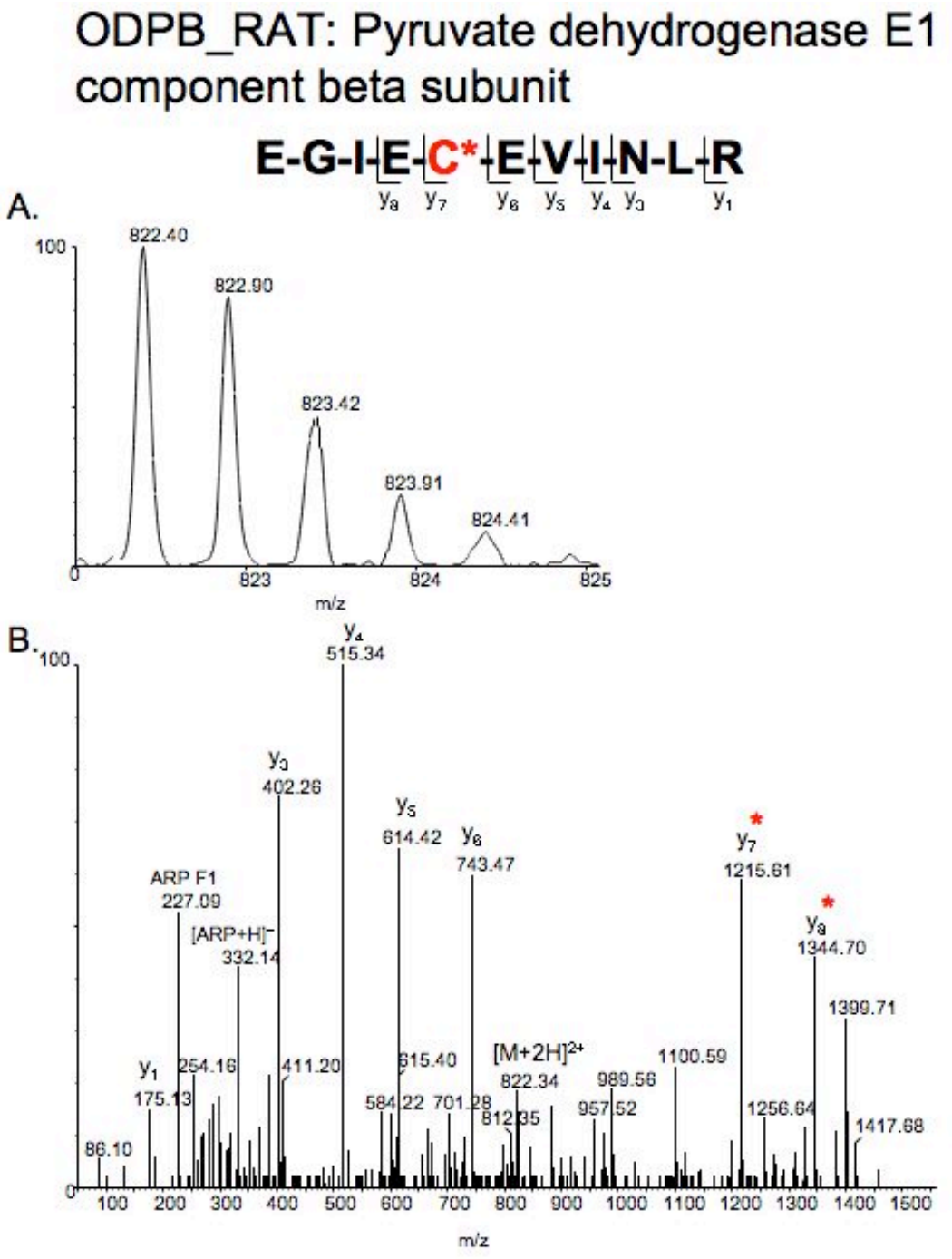

Figure SB62. (A) Full mass spectrum and (B) MS/MS spectrum acquired by ESI-Q-TOF of the $[M+2H]^{2+}$ ion of the ARP labeled, acrolein modified peptide EGIEC*EVINLR; monoisotopic m/z_{calc} 822.40; accuracy **Δ**(m/z) = 0.00 m/z

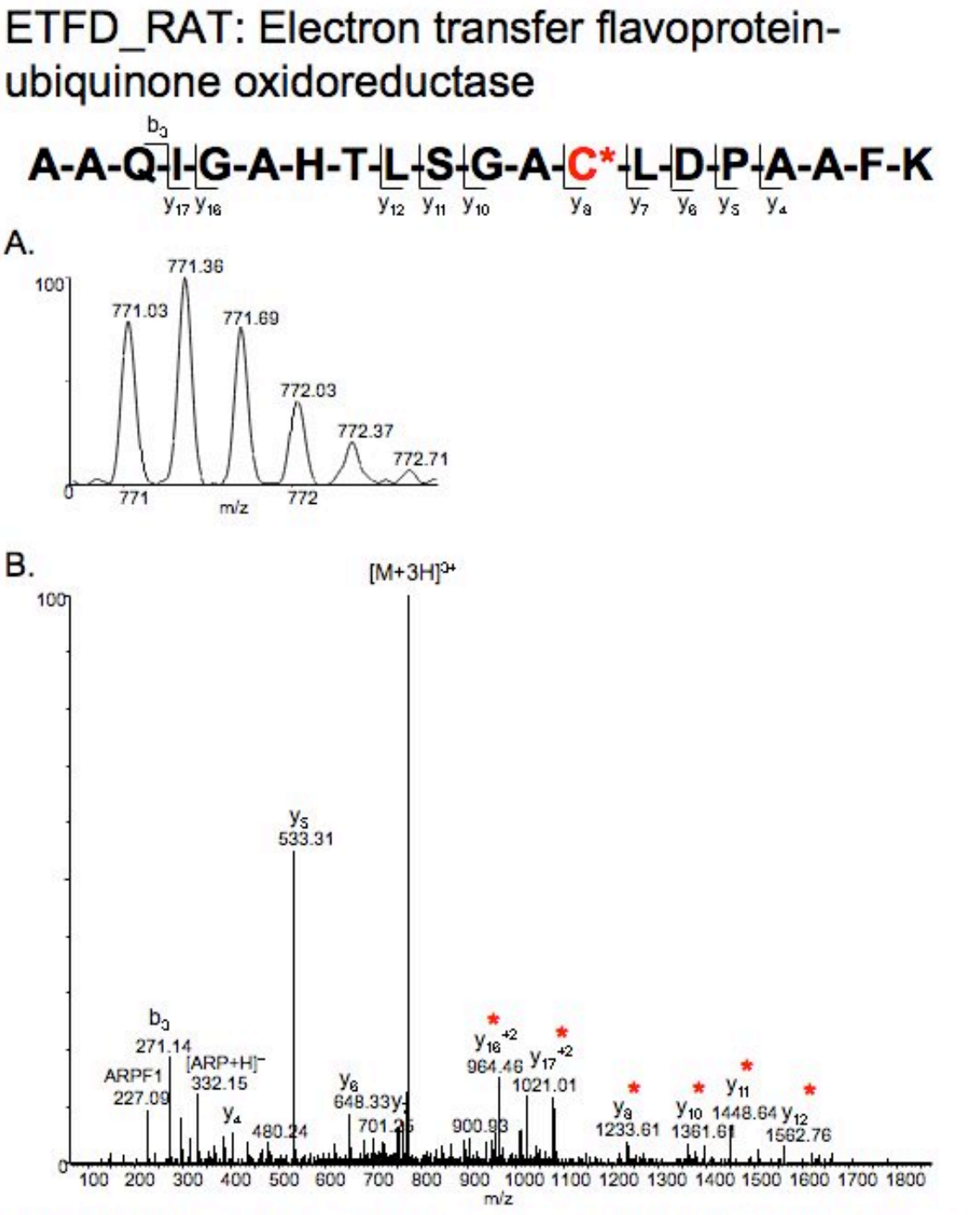

Figure SB63. (A) Full mass spectrum and (B) MS/MS spectrum acquired by ESI-Q-TOF of the $[M+3H]^{3+}$ ion of the ARP labeled, acrolein modified peptide AAQIGAHTLSGAC*LDPAAFK; monoisotopic m/z_{calc} 771.05; accuracy **Δ**(m/z) = -0.02 m/z

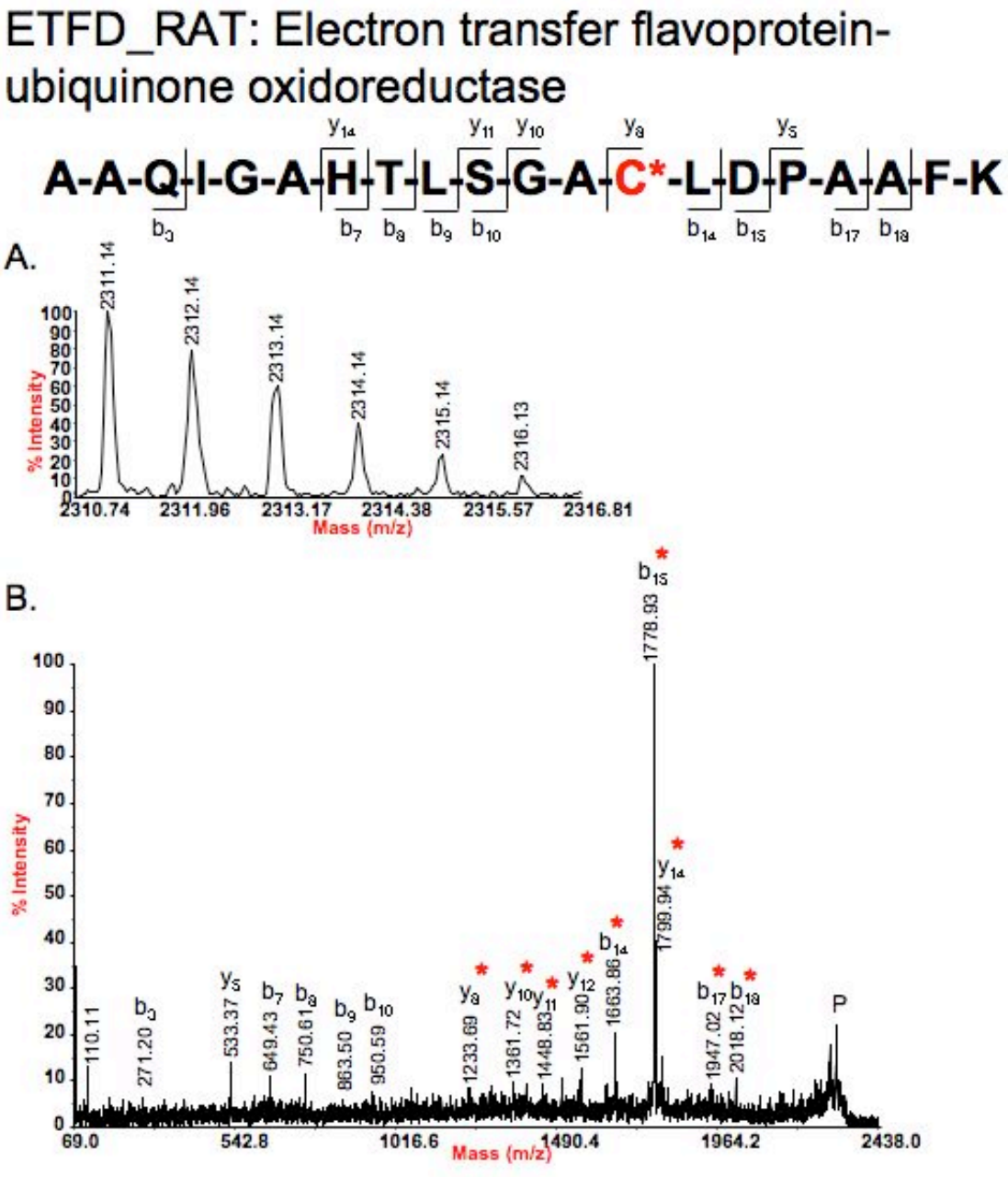

Figure SB64. (A) Full mass spectrum and (B) MS/MS spectrum acquired by MALDI-TOF/TOF of the $[M+H]^+$ ion of the ARP labeled, acrolein modified peptide AAQIGAHTLSGAC*LDPAAFK; monoisotopic m/z_{calc} 2311.13; accuracy **Δ**(m/z) = 0.01 m/z

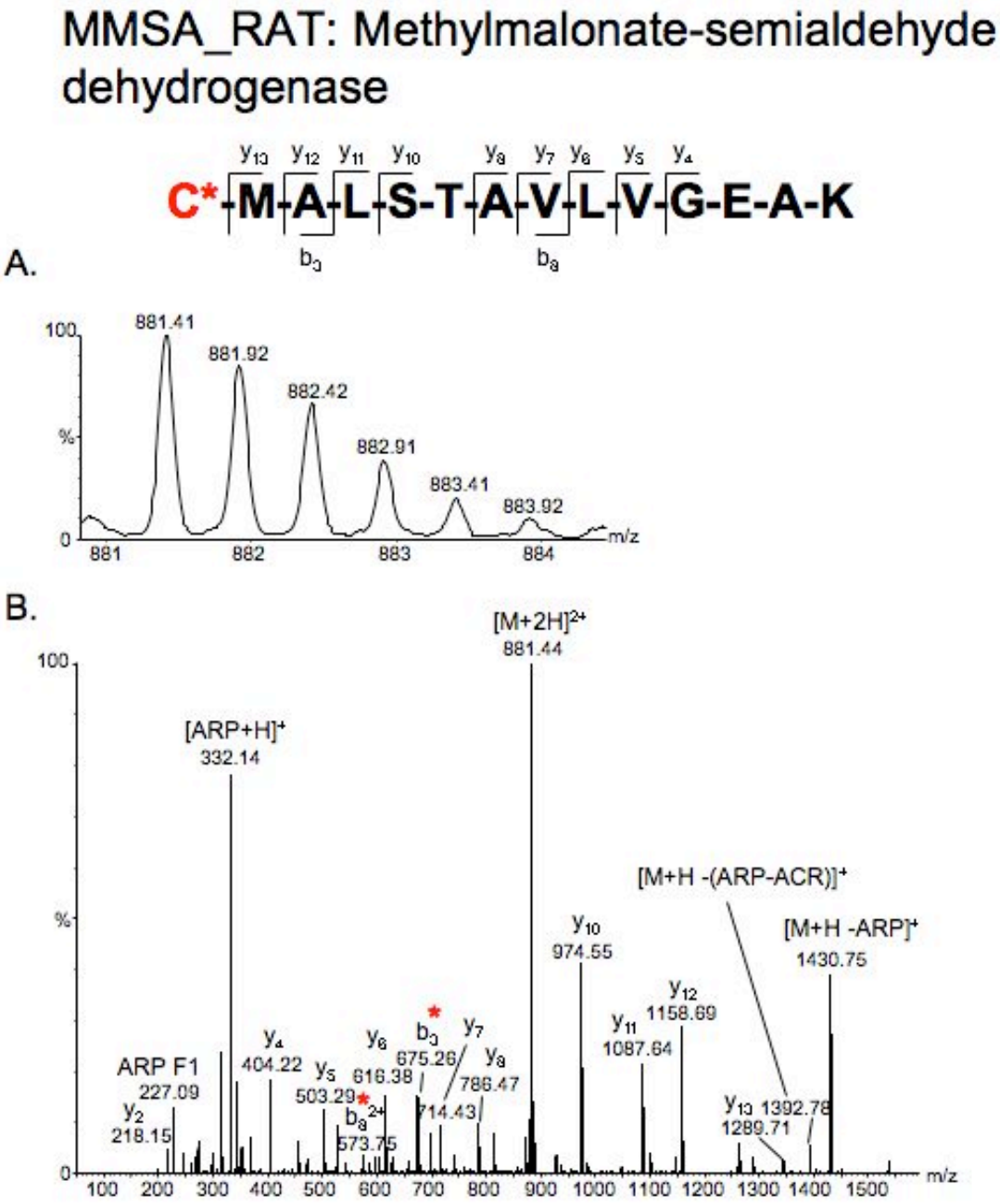

Figure SB65. (A) Full mass spectrum and (B) MS/MS spectrum acquired by ESI-Q-TOF of the $[M+2H]^{2+}$ ion of the ARP labeled, acrolein modified peptide C*MALSTAVLVGEAK; monoisotopic m/z_{calc} 881.44; accuracy $\Delta(m/z)$ = -0.03 m/z

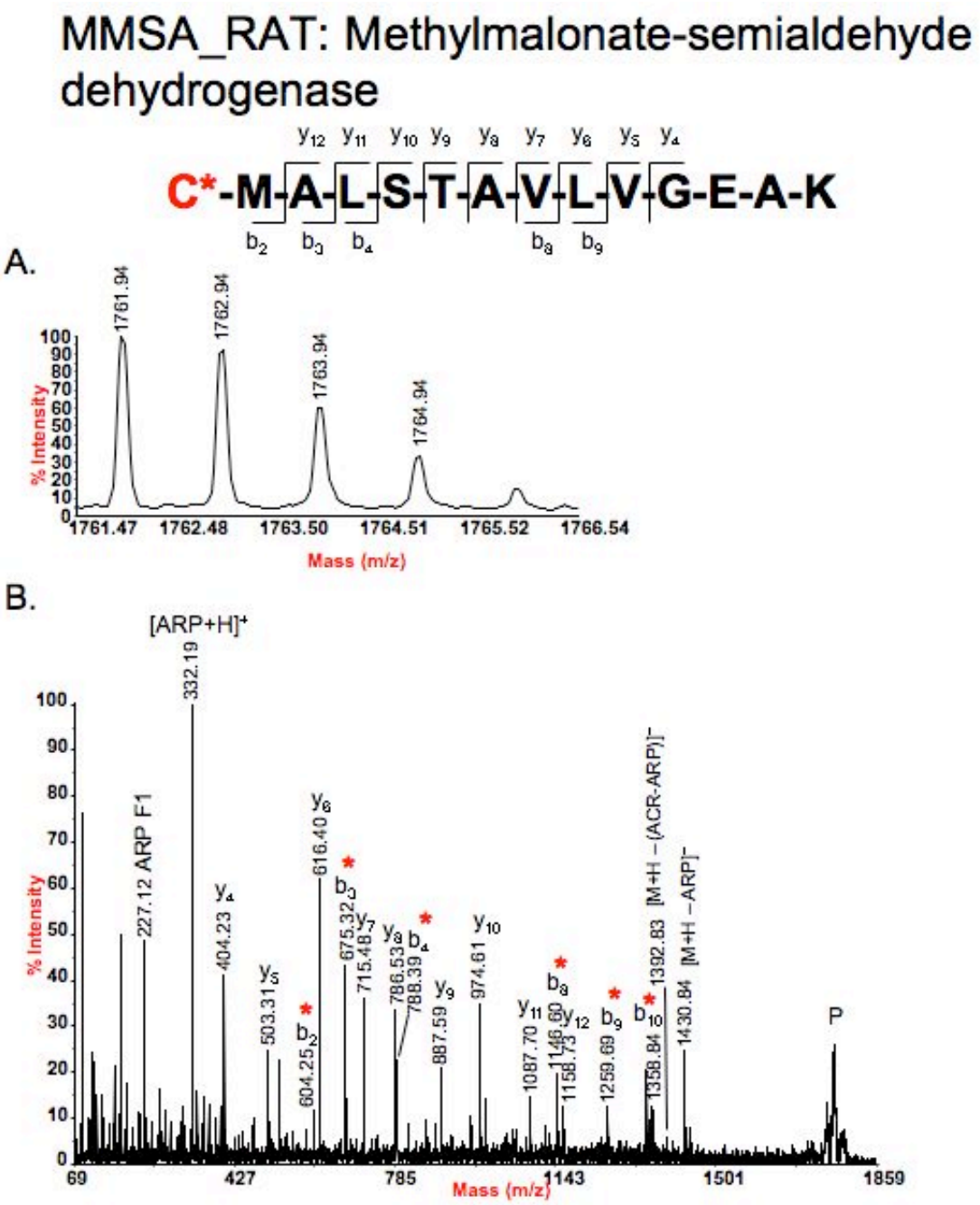

Figure SB66. (A) Full mass spectrum and (B) MS/MS spectrum acquired by MALDI-TOF/TOF of the $[M+H]^+$ ion of the ARP labeled, acrolein modified peptide C*MALSTAVLVGEAK; monoisotopic m/z_{calc} 1761.87; accuracy **Δ**(m/z) = 0.07 m/z

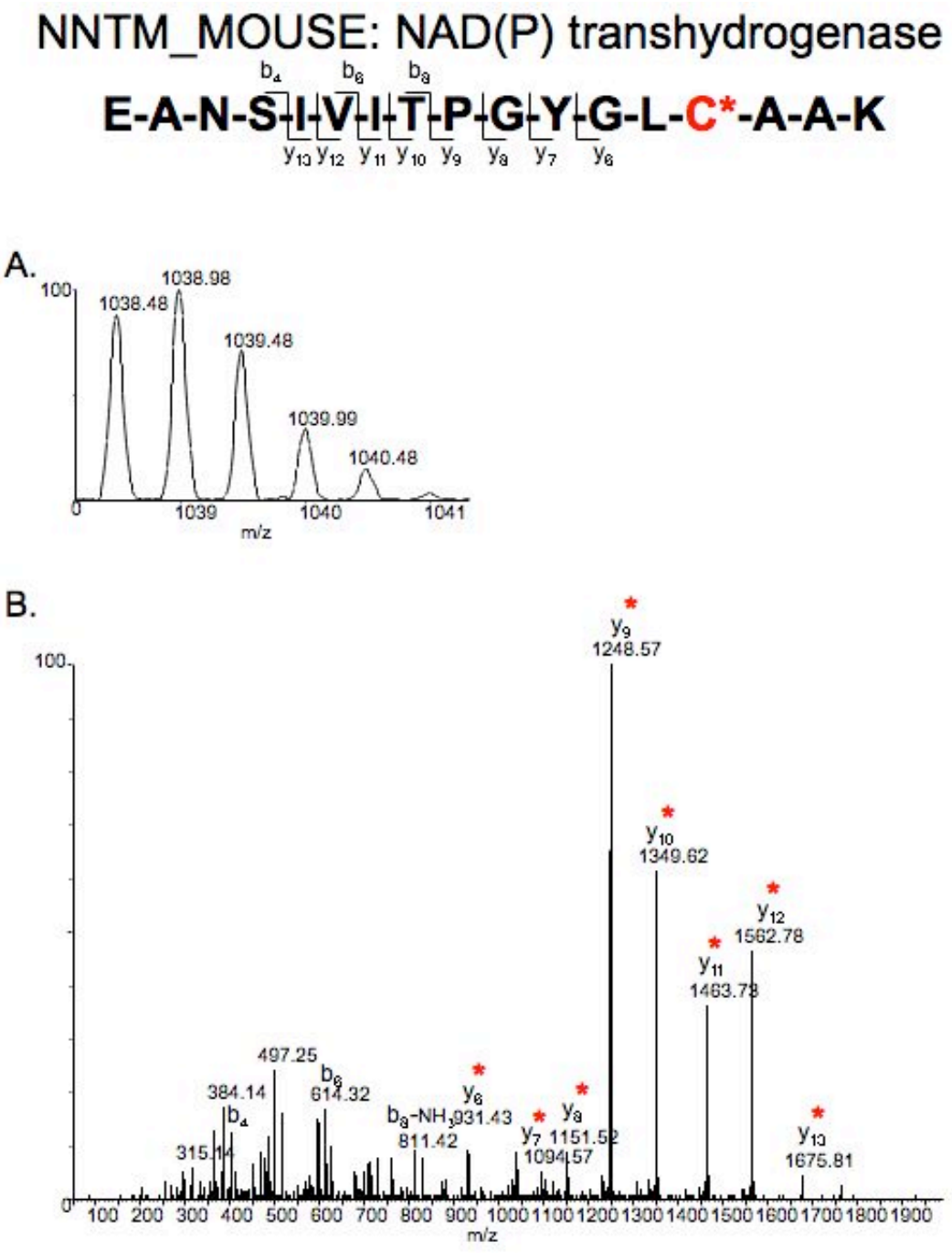

Figure SB67. (A) Full mass spectrum and (B) MS/MS spectrum acquired by ESI-Q-TOF of the $[M+2H]^{2+}$ ion of the ARP labeled, acrolein modified peptide EANSIVITPGYGLC*AAK; monoisotopic m/z_{calc} 1038.52; accuracy **Δ**(m/z) = -0.04 m/z

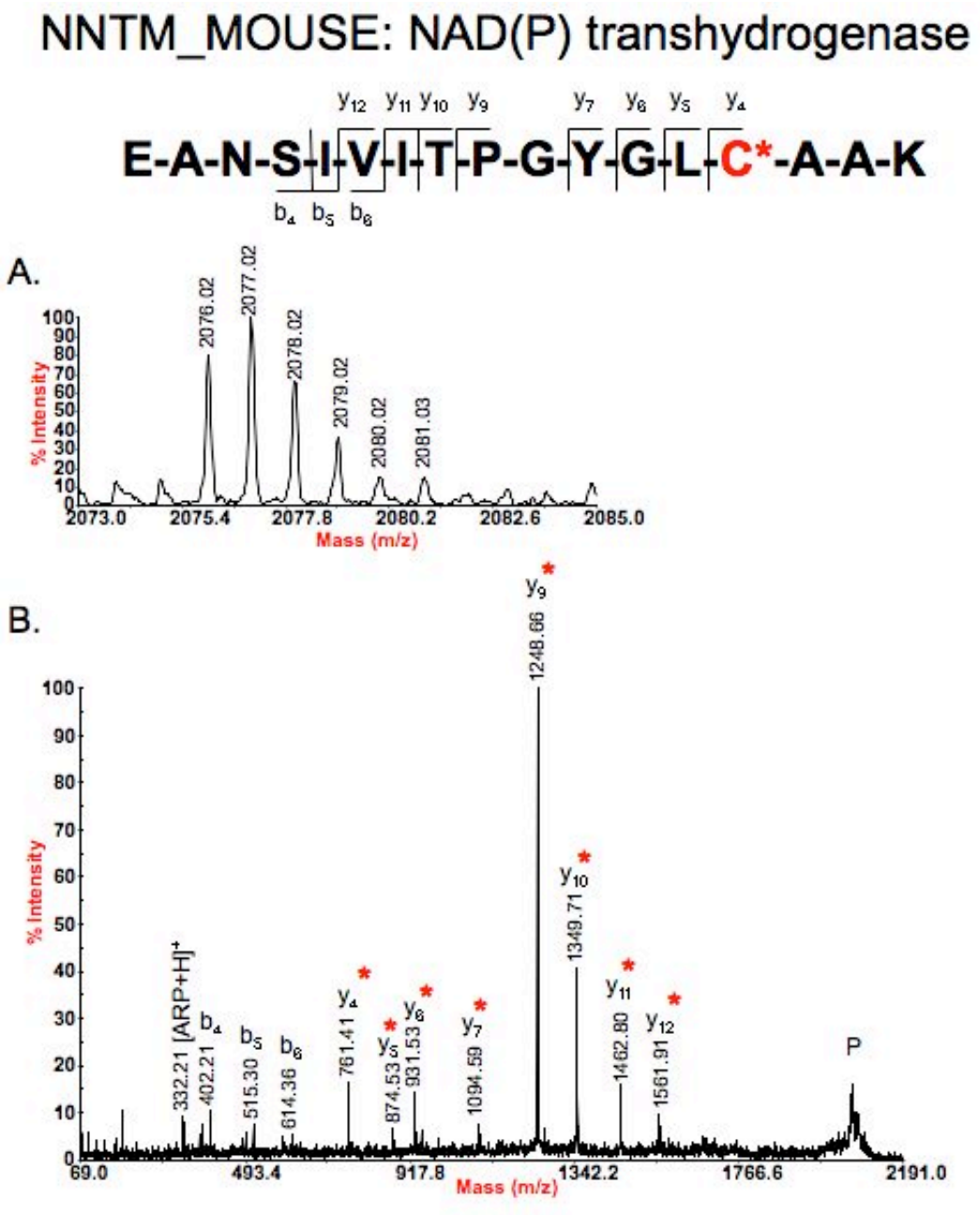

Figure SB68. (A) Full mass spectrum and (B) MS/MS spectrum acquired by MALDI-TOF/TOF of the $[M+H]^+$ ion of the ARP labeled, acrolein modified peptide EANSIVITPGYGLC*AAK; monoisotopic m/z_{calc} 2076.03; accuracy $\Delta(m/z)$ = -0.01 m/z

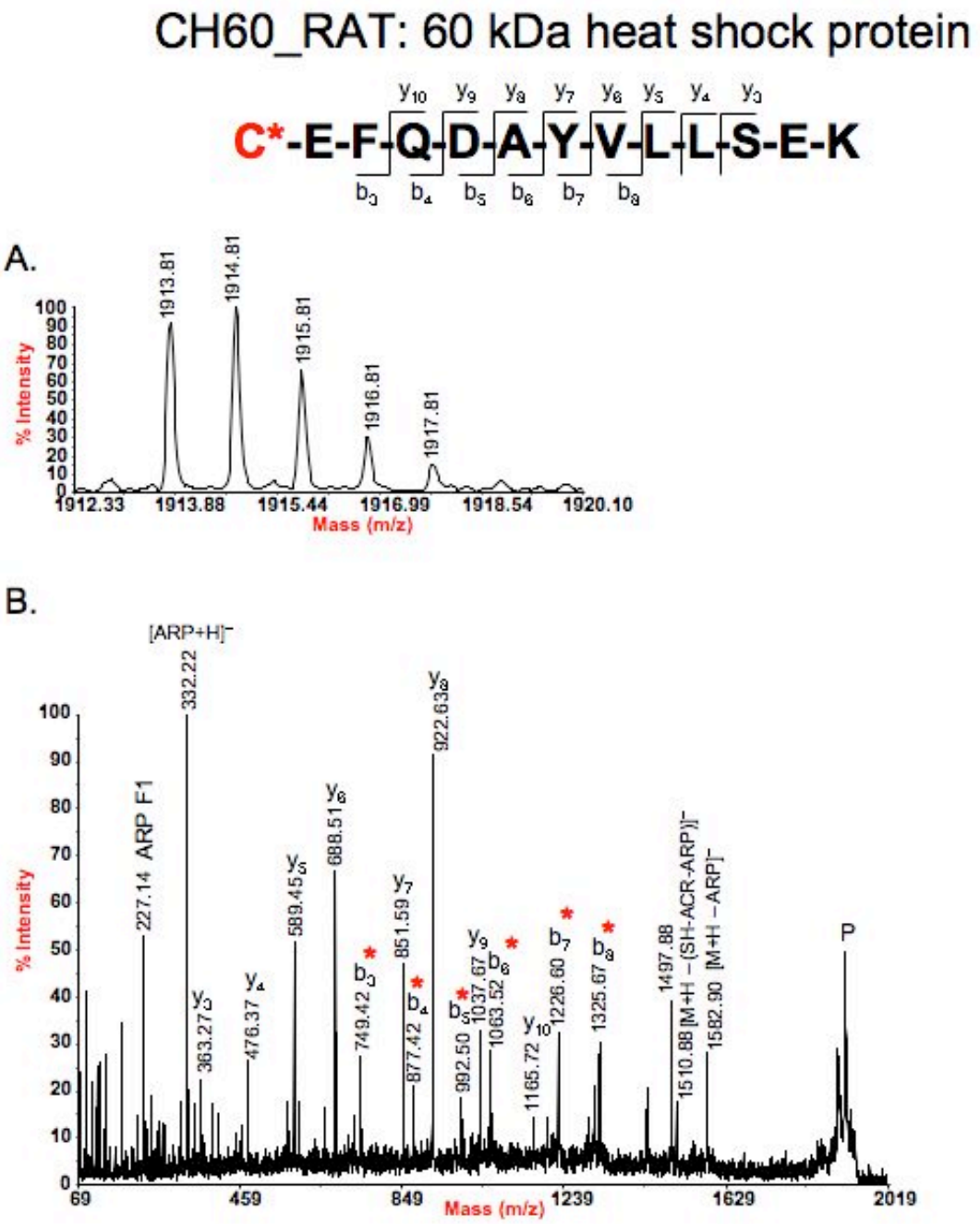

Figure SB69. (A) Full mass spectrum and (B) MS/MS spectrum acquired by MALDI-TOF/TOF of the $[M+H]^+$ ion of the ARP labeled, acrolein modified peptide C*EFQDAYVLLSEK; monoisotopic m/z_{calc} 1913.88; accuracy **Δ**(m/z) = -0.07 m/z

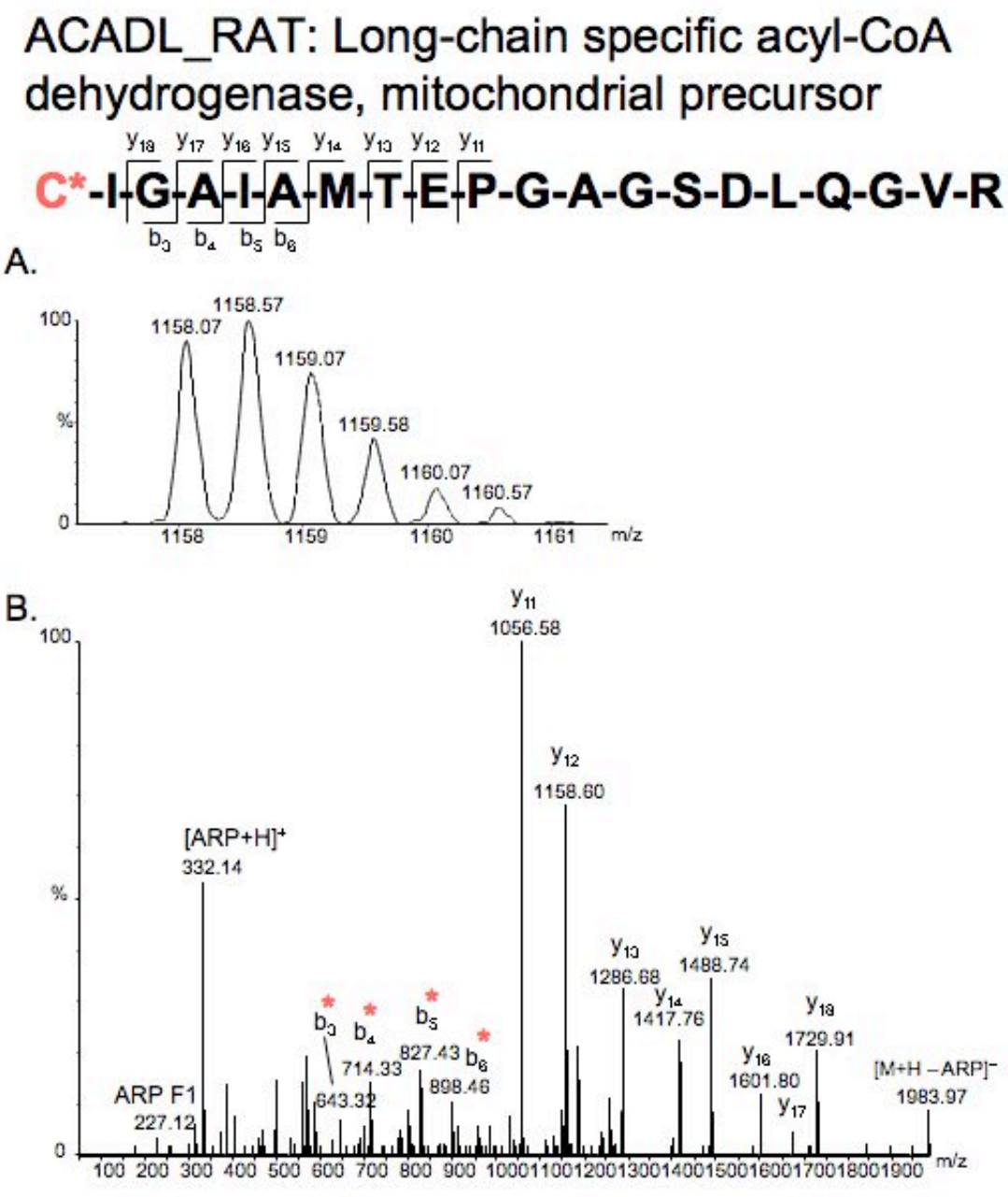

Figure SB70. (A) Full mass spectrum and (B) MS/MS spectrum acquired by ESI-Q-TOF of the $[M+2H]^{2+}$ ion of the ARP labeled, acrolein modified peptide C*IGAIAMTEPGAGSDLQGVR; monoisotopic m/z_{calc} 1158.05; accuracy **Δ**(m/z) = 0.02 m/z

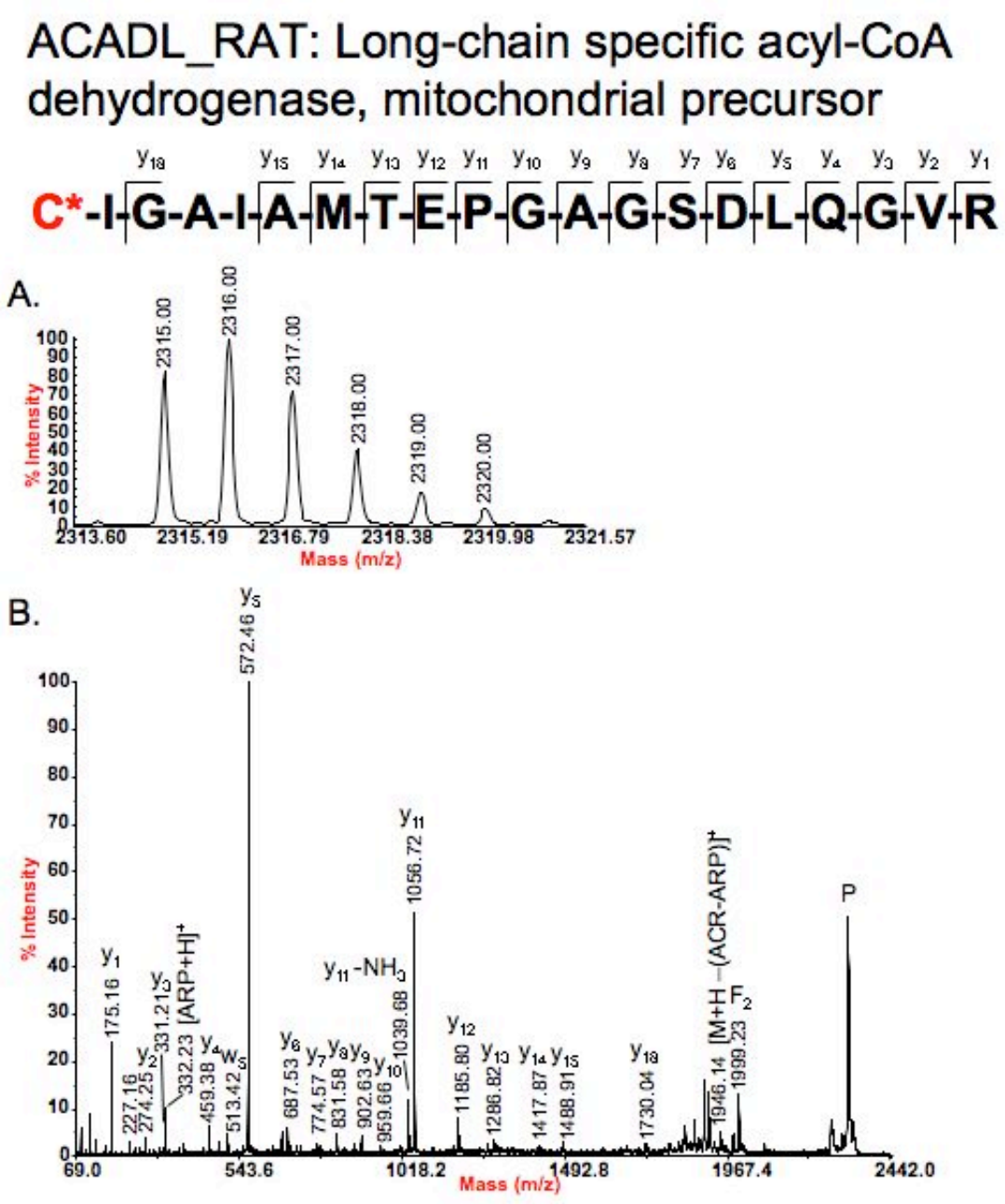

Figure SB71. (A) Full mass spectrum and (B) MS/MS spectrum acquired by MALDI-TOF/TOF of the $[M+H]^+$ ion of the ARP labeled, acrolein modified peptide C*IGAIAMTEPGAGSDLQGVR; monoisotopic m/z_{calc} 2315.09; accuracy **Δ**(m/z) = 0.01 m/z

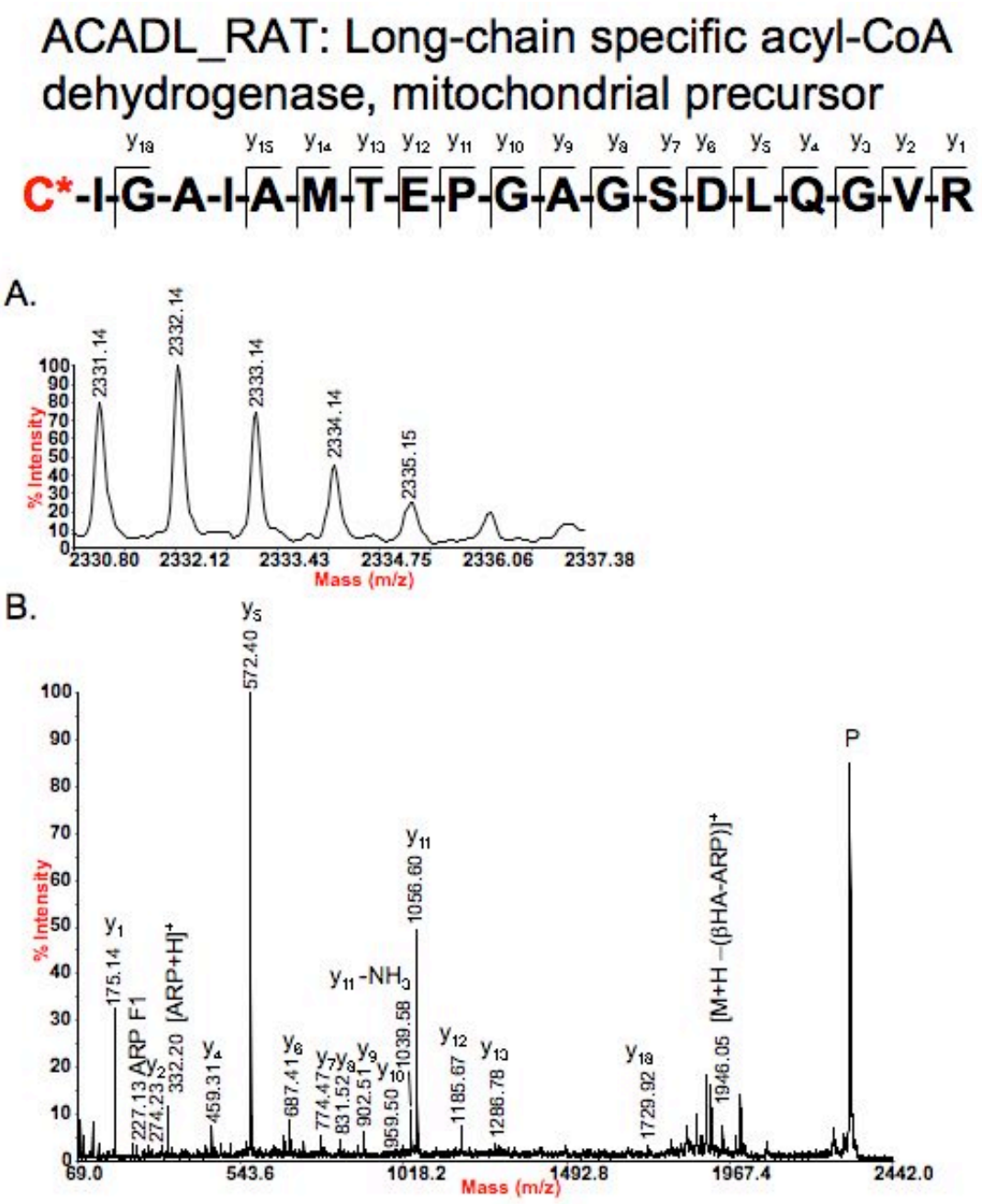

Figure SB72. (A) Full mass spectrum and (B) MS/MS spectrum acquired by MALDI-TOF/TOF of the $[M+H]^+$ ion of the ARP labeled, beta-hydroxyacrolein modified peptide C*IGAIAMTEPGAGSDLQGVR; monoisotopic m/z_{calc} 2331.09; accuracy **Δ**(m/z) = 0.05 m/z

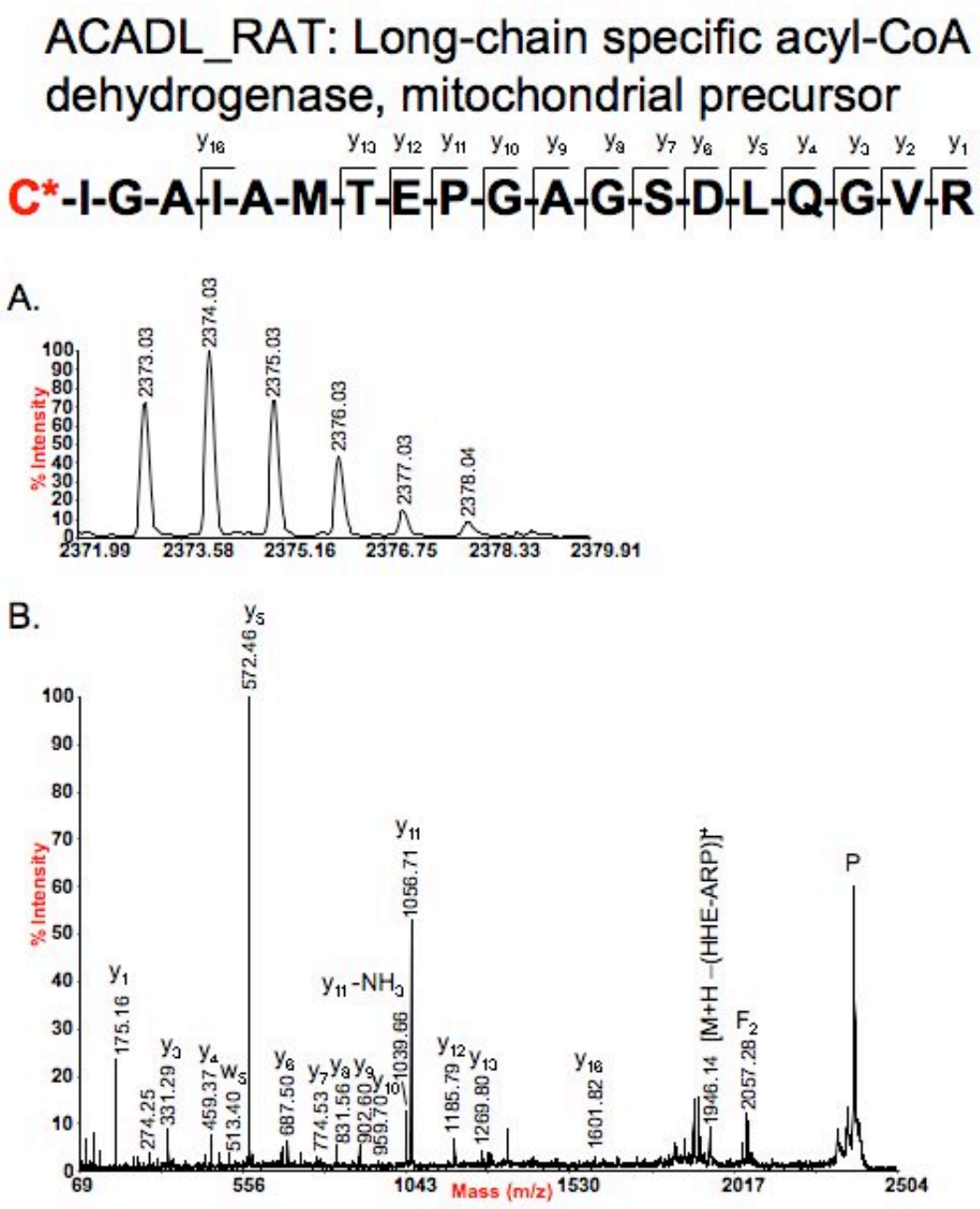

Figure SB73. (A) Full mass spectrum and (B) MS/MS spectrum acquired by MALDI-TOF/TOF of the $[M+H]^+$ ion of the ARP labeled, HHE modified peptide C*IGAIAMTEPGAGSDLQGVR; monoisotopic m/z_{calc} 2373.14; accuracy **Δ**(m/z) = -0.11 m/z

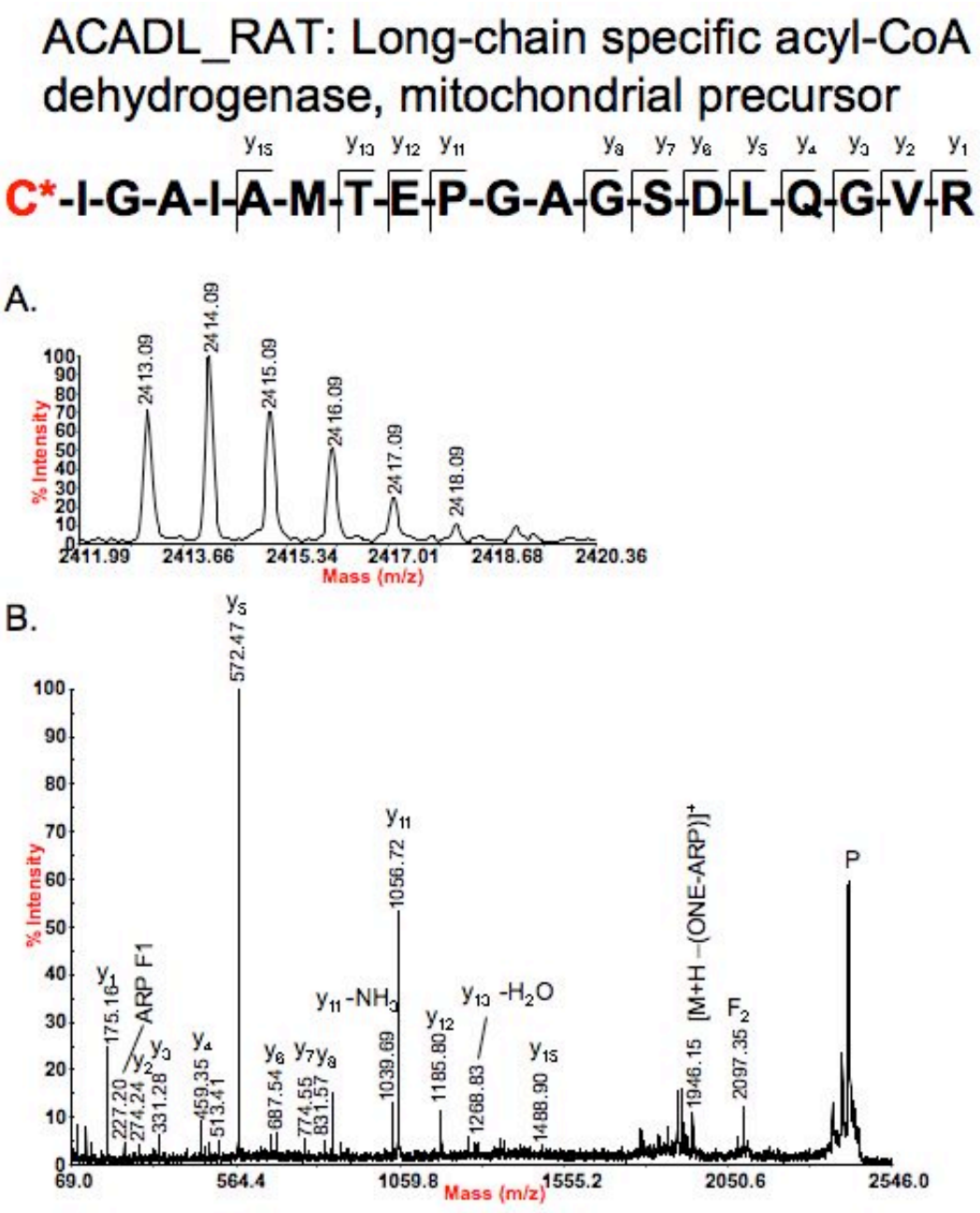

Figure SB74. (A) Full mass spectrum and (B) MS/MS spectrum acquired by MALDI-TOF/TOF of the $[M+H]^+$ ion of the ARP labeled, ONE modified peptide C*IGAIAMTEPGAGSDLQGVR; monoisotopic m/z_{calc} 2413.17; accuracy **Δ**(m/z) = -0.08 m/z

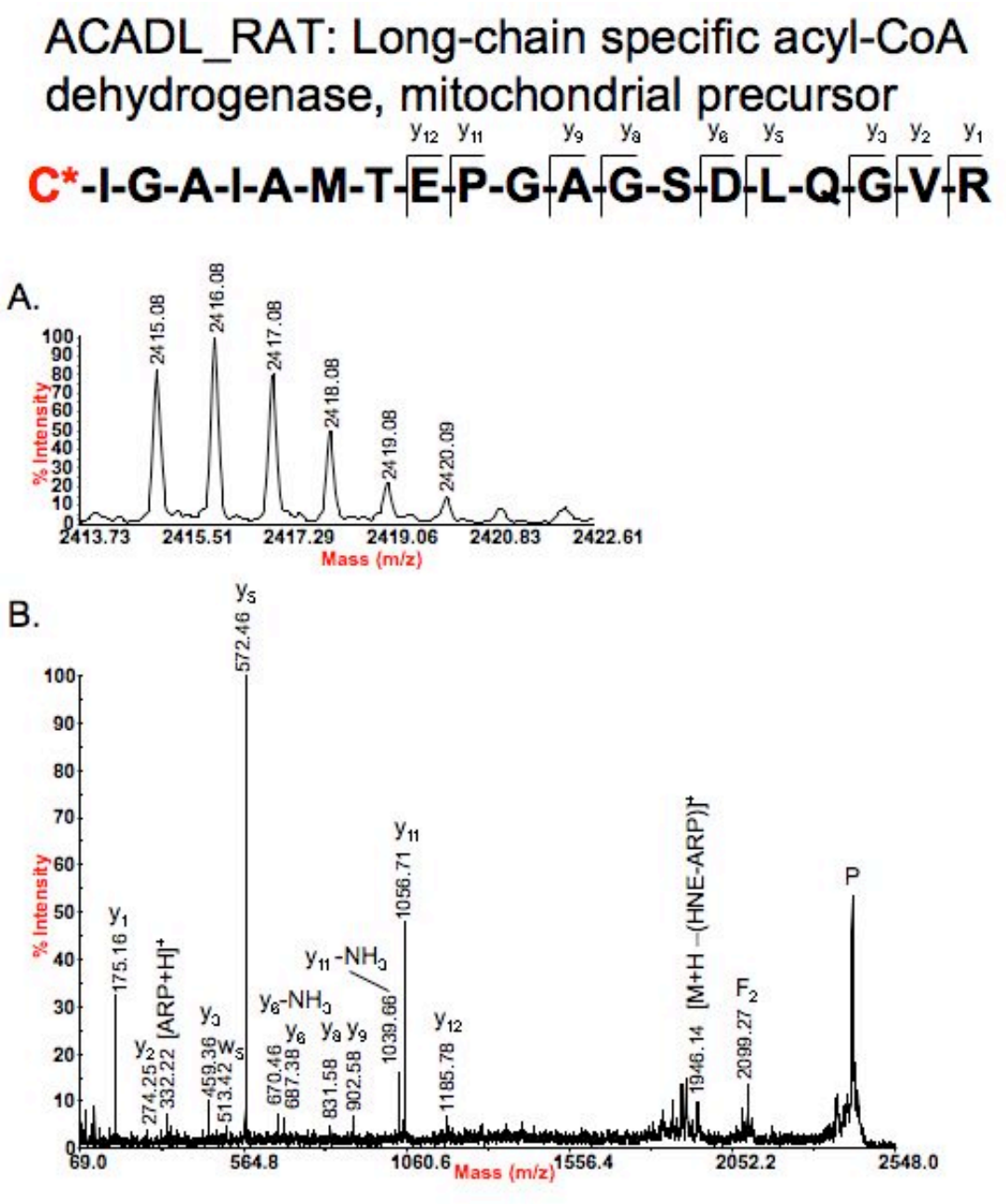

Figure SB75. (A) Full mass spectrum and (B) MS/MS spectrum acquired by MALDI-TOF/TOF of the $[M+H]^+$ ion of the ARP labeled, HNE modified peptide C*IGAIAMTEPGAGSDLQGVR; monoisotopic m/z_{calc} 2415.18; accuracy **Δ**(m/z) = -0.10 m/z

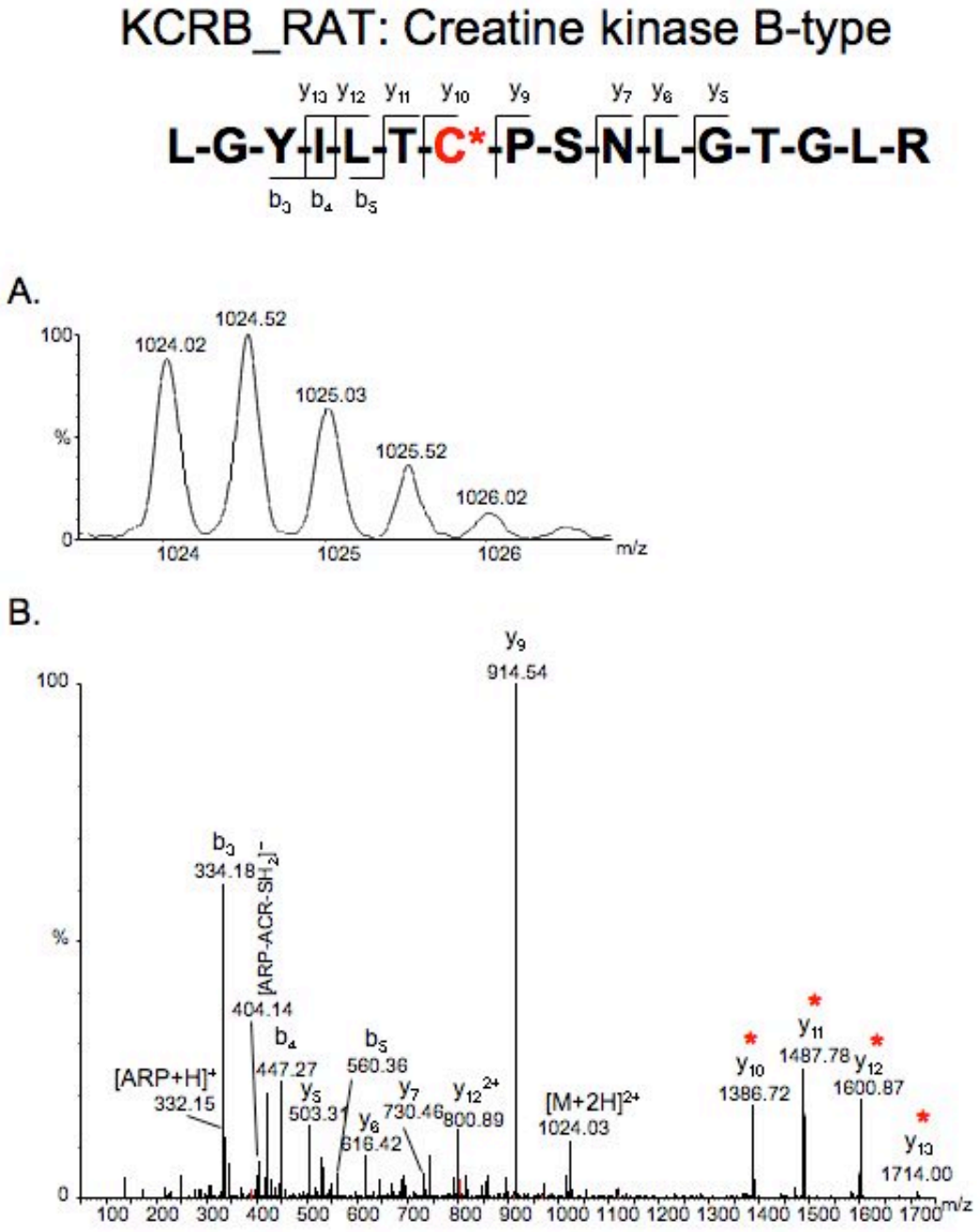

Figure SB76. (A) Full mass spectrum and (B) MS/MS spectrum acquired by ESI-Q-TOF of the $[M+2H]^{2+}$ ion of the ARP labeled, acrolein modified peptide LGYILTC*PSNLGTGLR; monoisotopic m/z_{calc} 1024.03; accuracy **Δ**(m/z) = -0.01 m/z

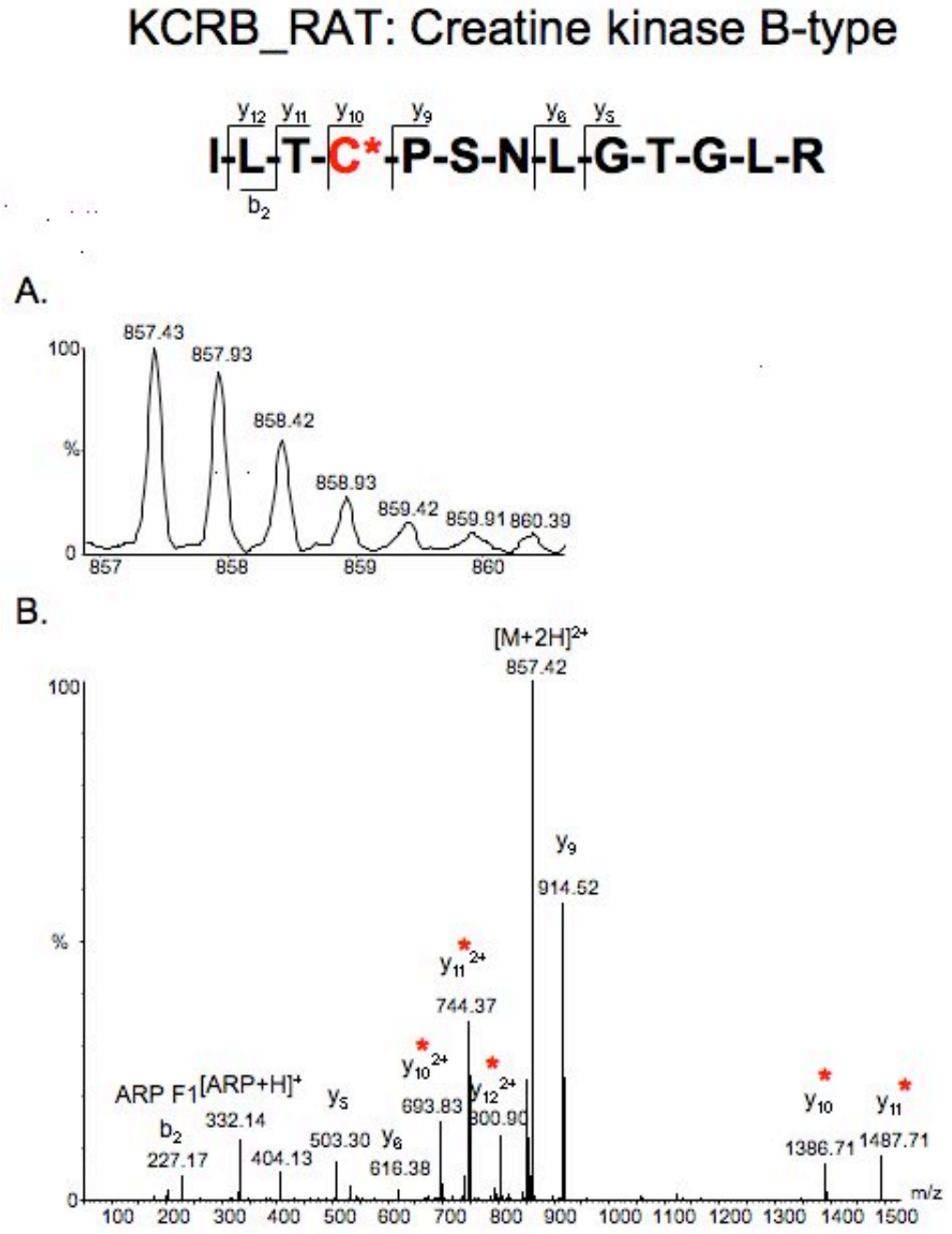

Figure SB77. (A) Full mass spectrum and (B) MS/MS spectrum acquired by ESI-Q-TOF of the $[M+2H]^{2+}$ ion of the ARP labeled, acrolein modified peptide ILTC*PSNLGTGLR; monoisotopic m/z_{calc} 857.44; accuracy $\Delta(m/z)$ = -0.01 m/z

Appendix C

Supplemental Material For Chapter 5

Table SC1. Mass spectrometry data of proteins identified in the gel regions (Figure 5.1A) that matched the immunoreactive bands in Figure 5.1B.

Region No.	Protein	Mass	pI	Sequence Coverage	Peptide No.	Mascot Score
3	**Heat shock protein HSP 90β (HS90B_HUMAN)**	**83,212**	**4.97**	**18%**	**12**	**537**
	Matching peptides			**Start-End**	**Mass**	**Score**
	IDIIPNPQER			73 - 82	1194.69	38
	ADHGEPIGR			169 - 177	951.47	29
	EDQTEYLEER			187 - 196	1311.58	60
	YIDQEELNK			276 - 284	1151.57	43
	TKPIWTR			285 - 291	901.55	42
	NPDDITQEEYGEFYK			292 - 306	1847.86	61
	ALLFIPR			331 - 337	829.56	38
	GVVDSEDLPLNISR			379 - 392	1513.85	55
	FYEAFSK			429 - 435	891.44	41
	LGIHEDSTNR			439 - 448	1141.58	38
	SIYYITGESK			482 - 491	1160.60	38
	EQVANSAFVER			492 - 502	1249.65	54
4	**Heat shock cognate 71kDa (HSP7C_HUMAN)**	**70,854**	**5.37**	**40%**	**19**	**1307**
	VEIIANDQGNR			26 - 36	1228.60	33
	TTPSYVAFTDTER			37 - 49	1487.77	54
	NQVAMNPTNTVFDAK Oxidation (M)			57 - 71	1665.78	77
	RFDDAVVQSDMK Oxidation (M)			77 - 88	1426.62	25
	SFYPEEVSSMVLTK Oxidation (M)			113 - 126	1632.82	87
	EIAEAYLGK			129 - 137	993.53	41
	TVTNAVVTVPAYFNDSQR			138 - 155	1982.03	112
	DAGTIAGLNVLR			160 - 171	1199.68	57
	IINEPTAAAIAYGLDK			172 - 187	1659.89	120

Table SC1 (Continued)

	STAGDTHLGGEDFDNR			221 - 236	1691.70	108
	MVNHFIAEFK Oxidation (M)			237 - 246	1251.66	56
	FEELNADLFR			302 - 311	1253.62	82
	SQIHDIVLVGGSTR			329 - 342	1481.87	90
	LLQDFFNGK			349 - 357	1081.55	64
	LLQDFFNGK Deamidation (N)			349 - 357	1082.54	49
	SINPDEAVAYGAAVQAAILSGDK			362 - 384	2260.20	81
	QTQTFTTYSDNQPGVLIQVYEGER			424 - 447	2774.38	33
	NSLESYAFNMK Oxidation (M)			540 - 550	1319.64	51
	NQTAEKEEFEHQQK			584 - 597	1745.78	87
6-1	**Protein disulfide isomerase A3 (PDIA3_HUMAN)**	**56,747**	**5.98**	**34%**	**14**	**691**
	LAPEYEAAATR			63 - 73	1191.62	73
	YGVSGYPTLK			95 - 104	1084.61	36
	QAGPASVPLR			131 - 140	995.57	27
	DASIVGFFDDSFSEAHSEFLK			153 - 173	2348.37	66
	LNFAVASR			297 - 304	877.53	34
	TFSHELSDFGLESTAGEIPVVAIR			306 - 329	2575.80	44
	FVMQEEFSR			336 - 344	1172.62	47
	FLQDYFDGNLK			352 - 362	1359.85	73
	VVVAENFDEIVNNENK			380 - 395	1833.08	37
	MDATANDVPSPYEVR			434 - 448	1664.86	63
	MDATANDVPSPYEVR.G Oxidation (M)			434 - 448	1680.81	32
	GFPTIYFSPANK			449 - 460	1341.86	60
	ELSDFISYLQR			472 - 482	1370.93	73
	EATNPPVIQEEKPK			483 - 496	1579.91	26
6-2	**Adenylyl cyclase-associated protein 1 (CAP1_HUMAN)**	**51,823**	**8.27**	**30%**	**18**	**1276**
	LEAVSHTSDMHR			18 - 29	1382.65	77
	LEAVSHTSDMHR Oxidation (M)			18 - 29	1398.61	29

Table SC1 (Continued)

	HAEMVHTGLK			72 - 81	1122.61	92
	HAEMVHTGLK Oxidation (M)			72 - 81	1138.52	76
	ALLVTASQCQQPAENK			85 - 100	1700.92	26
	ALLVTASQCQQPAENK Propionamide (C)			85 - 100	1771.97	76
	LSDLLAPISEQIK			101 - 113	1426.97	119
	EMNDAAMFYTNR			156 - 167	1462.72	94
	EMNDAAMFYTNR Oxidation (M)			156 - 167	1478.68	36
	EFHTTGLAWSK			199 - 209	1276.71	92
	EFHTTGLAWSK Oxidation (W)			199 - 209	1292.69	46
	KEPAVLELEGK			317 - 327	1212.73	91
	EPAVLELEGK			318 - 327	1084.63	78
	VENQENVSNLVIEDTELK			331 - 348	2073.26	107
	QVAYIYK			349 - 355	884.49	34
	VPTISINK			405 - 412	871.52	29
	SSEMNVLIPTEGGDFNEFPVPEQFK			434 - 458	2811.90	87
	SSEMNVLIPTEGGDFNEFPVPEQFK Oxidation (M)			434 - 458	2827.87	87
6-3	**Vimentin (VIME_HUMAN)**	**53,619**	**5.06**	**44%**	**17**	**1136**
	MFGGPGTASR			14 - 23	980.47	35
	SLYASSPGGVYATR			37 - 50	1495.87	95
	VELQELNDR			105 - 113	1115.59	63
	ILLAELEQLK			130 - 139	1169.90	90
	LGDLYEEEMR			146 - 155	1254.64	84
	LQEEMLQR			189 - 196	1046.53	51
	EEAENTLQSFR			197 - 207	1323.70	78
	KVESLQEEIAFLK			223 - 235	1534.02	44
	VESLQEEIAFLK			224 - 235	1405.95	48
	NLQEAEEWYK			283 - 292	1309.73	72
	FADLSEAANR			295 - 304	1093.55	41
	EMEENFAVEAANYQDTIGR			346 - 364	2187.24	129
	EMEENFAVEAANYQDTIGR Oxidation (M)			346 - 364	2203.19	29

Table SC1 (Continued)

	LQDEIQNMKEEMAR			365 - 378	1734.96	39
	ISLPLPNFSSLNLR			411 - 424	1571.17	84
	ETNLDSLPLVDTHSK			425 - 439	1669.06	42
	DGQVINETSQHHDDLE			451 - 466	1836.85	112
7	**Tubulin alpha-1B chain (TBA1B_HUMAN)**	**50,120**	**4.93**	**23%**	**7**	**439**
	TIGGGDDSFNTFFSETGAGK			41 - 60	2007.93	90
	AVFVDLEPTVIDEVR			65 - 79	1701.98	68
	QLFHPEQLITGK			85 - 96	1410.79	73
	EIIDLVLDR			113 - 121	1085.64	47
	NLDIERPTYTNLNR			216 - 229	1718.89	30
	IHFPLATYAPVISAEK			265 - 280	1757.02	69
	VGINYQPPTVVPGGDLAK			353 - 370	1825.04	62
8	**α-Enolase (ENOA_HUMAN)**	**47,139**	**7.01**	**24%**	**5**	**341**
	GNPTVEVDLFTSK			16 - 28	1406.75	74
	AAVPSGASTGIYEALELR			33 - 50	1805.02	46
	IGAEVYHNLK			184 - 193	1143.63	91
	VVIGMDVAASEFFR Oxidation (M)			240 - 253	1556.82	31
	YISPDQLADLYK			270 - 281	1425.74	99
9	**Actin, cytoplasmic 1 (ACTB_HUMAN)**	**41,710**	**5.29**	**53%**	**19**	**1607**
	AGFAGDDAPR			19 - 28	976.38	51
	AVFPSIVGR			29 - 37	945.58	57
	AVFPSIVGRPR			29 - 39	944.57	52
	HQGVMVGMGQK			40 - 50	1171.53	67
	IWHHTFYNELR			85 - 95	1515.81	81
	VAPEEHPVLLTEAPLNPK			96 - 113	1954.15	123
	TTGIVMDSGDGVTHTVPIYEGYALPHAILR			148 - 177	3183.91	141
	TTGIVMDSGDGVTHTVPIYEGYALPHAILR Oxidation (M)			148 - 177	3199.92	64

Table SC1 (Continued)

	DLTDYLMK			184 – 191	998.53	36
	DLTDYLMK Oxidation (M)			184 - 191	1014.45	40
	GYSFTTTAER			197 – 206	1132.52	75
	LCYVALDFEQEMATAASSSSLEK			216 - 238	2493.49	144
	LCYVALDFEQEMATAASSSSLEK Oxidation (M)			216 - 238	2509.39	76
	SYELPDGQVITIGNER			239 - 254	1790.97	108
	KDLYANTVLSGGTTMYPGIADR			291 - 312	2343.21	123
	DLYANTVLSGGTTMYPGIADR			292 - 312	2215.27	180
	DLYANTVLSGGTTMYPGIADR Oxidation (M)			292 - 312	2231.21	27
	EITALAPSTMK			316 - 326	1161.62	50
	QEYDESGPSIVHR			360 - 372	1516.68	112
12-1	**Carbonic anhydrase 2 (CAH2_HUMAN)**	**29,228**	**6.87**	**51%**	**10**	**770**
	HNGPEHWHK			10 - 18	1141.56	52
	QSPVDIDTHTAK			28 - 39	1311.71	74
	YDPSLKPLSVSYDQATSLR			40 - 58	2140.16	121
	ILNNGHAFNVEFDDSQDK Deamidation (NQ)			59 - 76	2063.97	104
	GGPLDGTYR			81 - 89	935.51	51
	YAAELHLVHWNTK			114 - 126	1581.86	111
	AVQQPDGLAVLGIFLK			133 - 148	1669.05	107
	VVDVLDSIK			159 - 167	987.61	58
	SADFTNFDPR			172 - 181	1169.56	62
	LNFNGEGEPEELMVDNWR Oxidation (M)			228 - 245	2165.09	30
12-2	**14-3-3 protein β/α (1433B_HUMAN)**	**28,065**	**4.76**	**21%**	**4**	**209**
	AVTEQGHELSNEER			30 - 43	1598.78	73
	EMQPTHPIR Oxidation (M)			161 - 169	1124.56	26
	TAFDEAIAELDTLNEESYK			196 - 214	2159.16	84
	DSTLIMQLLR Oxidation (M)			215 - 224	1205.66	26
13	**Peroxiredoxin-6 (PRDX6_HUMAN)**	**25,019**	**6.00**	**21%**	**4**	**163**

Table SC1 (Continued)

	PGGLLLGDVAPNFEANTTVGR			2 - 22	2098.18	27
	LPFPIIDDR			98 - 106	1085.62	73
	LSILYPATTGR			145 - 155	1191.71	34
	NFDEILR			156 - 162	906.50	29
17	**Histone H2B type 1-M (H2B1M_HUMAN)**	**13,981**	**10.31**	**46%**	**6**	**336**
	ESYSVYVYK			36 - 44	1137.49	72
	QVHPDTGISSK			48 - 58	1168.52	82
	AMGIMNSFVNDIFER 2 Oxidation (M)			59 - 73	1775.77	32
	LAHYNKR			81 - 87	901.43	25
	EIQTAVR			94 - 100	816.40	40
	LLLPGELAK			101 - 109	953.57	85

Table SC2. Mass spectrometry data of proteins identified in the gel regions (Figure 5.2A) that matched the immunoreactive bands in Figure 5.2B.

Region No.	Protein	Mass	pI	Sequence Coverage	Peptide No.	Mascot Score
1	Ribonuclease inhibitor (**RINI_HUMAN**)	**49,941**	**4.71**	**42 %**	**15**	**1090**
	Matching peptides			**Start-End**	**Mass**	**Score**
	WAELLPLLQQCQVVR Carbamidomethyl (C)			20 - 34	1853.14	33
	LDDCGLTEAR Carbamidomethyl (C)			35 - 44	1149.54	61
	VNPALAELNLR			54 - 64	1209.73	63
	SNELGDVGVHCVLQGLQTPSCK 2 Carbamidomethyl (C)			65 - 86	2398.23	104
	LSLQNCCLTGAGCGVLSSTLR Phospho (ST)			90 - 110	2176.19	25
	LSLQNCCLTGAGCGVLSSTLR 3 Carbamidomethyl (C)			90 - 110	2267.21	123
	ELTVSNNDINEAGVR			174 - 188	1630.81	106
	DSPCQLEALK Carbamidomethyl (C)			196 - 205	1160.57	64
	LESCGVTSDNCR 2 Carbamidomethyl (C)			206 - 217	1397.54	61
	LGDVGMAELCPGLLHPSSR Carbamidomethyl (C), Oxidation (M)			239 - 257	2025.01	89
	TLWIWECGITAK Carbamidomethyl (C)			260 - 271	1477.88	71
	ELSLAGNELGDEGAR			288 - 302	1530.77	127
	SCSFTAACCSHFSSVLAQNR 3 Carbamidomethyl (C)			322 - 341	2290.04	35
	ELCQGLGQPGSVLR Carbamidomethyl (C)			360 - 373	1513.84	74
	ELCQGLGQPGSVLR Carbamidomethyl (C), Deamidation (NQ)			360 - 373	1514.82	54
2	Protein disulfide-isomerase (**PDIA1_HUMAN**)	**57,081**	**4.76**	**57 %**	**30**	**2141**
	KSNFAEALAAHK			31 - 42	1158.56	86
	SNFAEALAAHK			32 - 42	1286.63	97
	ALAPEYAK			58 - 65	862.45	53
	VDATEESDLAQQYGVR			82 - 97	1780.86	125
	EADDIVNWLK			121 - 130	862.46	102

Table SC2 (Continued)

	QFLQAAEAIDDIPFGITSNSDVFSK			171 - 195	2713.54	110
	YQLDKDGVVLFK			196 - 207	1424.79	80
	DGVVLFK			201 - 207	777.44	31
	NNFEGEVTK			214 - 222	1037.48	32
	ENLLDFIK			223 - 230	991.58	76
	HNQLPLVIEFTEQTAPK			231 - 247	1965.13	164
	HNQLPLVIEFTEQTAPK Deamidation (NQ)			231 - 247	1966.13	41
	IFGGEIK			248 - 254	763.40	55
	THILLFLPK			255 - 263	1081.70	80
	ILFIFIDSDHTDNQR			286 - 300	1834.00	73
	ILEFFGLK			301 - 308	966.60	67
	LITLEEEMTK Oxidation (M)			317 - 326	1222.60	48
	YKPESEELTAER			327 - 338	1451.69	90
	ITEFCHR Carbamidomethyl (C)			339 - 345	962.44	49
	NFEDVAFDEK			376 - 385	1213.55	87
	NFEDVAFDEKK			376 - 386	1341.61	67
	QLAPIWDK			402 - 409	970.53	59
	QLAPIWDK Pyro-glu (N-term Q)			402 - 409	953.53	43
	LGETYKDHENIVIAK			410 - 424	1729.89	107
	DHENIVIAK			416 - 424	1038.52	72
	MDSTANEVEAVK Oxidation (M)			425 - 436	1309.58	39
	VHSFPTLK			437 - 444	928.48	45
	FFPASADR			445 - 452	910.41	44
	TVIDYNGER			453 - 461	1066.50	53
	FLESGGQDGAGDDDDLEDLEEAEEPDMEEDDDQK Oxidation (M)			469 - 502	3773.62	66
3	**Tubulin beta-2C (TBB2C_HUMAN)**	**49,799**	**4.79**	**21 %**	**8**	**453**
	INVYYNEATGGK			47 - 58	1328.58	105
	AVLVDLEPGTMDSVR Oxidation (M)			63 - 77	1617.84	36
	AVLVDLEPGTMDSVR Me-ester (DE); Oxidation (M)			63 - 77	1631.85	33
	IMNTFSVVPSPK Oxidation (M)			163 - 174	1335.69	78

Table SC2 (Continued)

	FPGQLNADLR			242 - 251	1130.63	66
	ALTVPELTQQMFDAK Oxidation (M)			283 - 297	1707.88	72
	YLTVAAVFR			310 - 318	1039.67	34
	EVDEQMLNVQNK Deamidation (NQ), 2 Me-ester (DE)			325 - 336	1475.74	29
4	β-Actin (**ACTB_HUMAN**)	**41,710**	**5.29**	**45 %**	**13**	**1026**
	DDDIAALVVDNGSGMCK Carbamidomethyl (C), 3 Me-ester (DE), Oxidation (M)			2 - 18	1837.85	93
	AGFAGDDAPR			19 - 28	976.47	80
	AVFPSIVGR			29 - 37	945.61	63
	DSYVGDEAQSKR			51 - 62	1354.64	55
	YPIEHGIVTNWDDMEK Me-ester (DE), Oxidation (M)			69 - 84	1977.00	81
	VAPEEHPVLLTEAPLNPK			96 - 113	1954.16	135
	DLTDYLMK Oxidation (M)			184 - 191	1014.51	64
	GYSFTTTAER			197 - 206	1132.57	53
	LCYVALDFEQEMATAASSSSLEK Carbamidomethyl (C), Oxidation (M)			216 - 238	2566.29	54
	SYELPDGQVITIGNER			239 - 254	1790.97	91
	EITALAPSTMK Oxidation (M)			316 - 326	1177.64	52
	QEYDESGPSIVHR Pyro-glu (N-term Q)			360 - 372	1499.75	99
	QEYDESGPSIVHR			360 - 372	1516.74	106
5	14-3-3 protein β/α (**1433B_HUMAN**)	**28,065**	**4.76**	**43%**	**9**	**754**
	AVTEQGHELSNEER			30 - 43	1598.73	106
	NLLSVAYK			44 - 51	907.56	55
	VISSIEQK			63 - 70	903.51	52
	YLIPNATQPESK			106 - 117	1360.78	67
	YLSEVASGDNK			130 - 140	1182.57	92
	QTTVSNSQQAYQEAFEISK Pyro-glu (N-term Q)			141 - 159	2142.10	93
	QTTVSNSQQAYQEAFEISK			141 - 159	2159.15	144
	TAFDEAIAELDTLNEESYK			196 - 214	2159.15	109
	DSTLIMQLLR Oxidation (M)			215 - 224	1205.69	36
6	Keratin, type II cytoskeletal 1 (**K2C1_HUMAN**)	**65,978**	**8.16**	**41 %**	**23**	**1714**

Table SC2 (Continued)

	SLNNQFASFIDK			186 - 197	1383.74	96
	SLNNQFASFIDKVR			186 - 199	1638.93	81
	FLEQQNQVLQTK			200 - 211	1475.82	89
	WELLQQVDTSTR			212 - 223	1475.81	71
	THNLEPYFESFINNLR			224 - 239	1994.10	71
	NMQDMVEDYR			258 - 267	1300.57	51
	NMQDMVEDYR 2 Deamidation (NQ); Me-ester (DE)			258 - 267	1316.57	37
	NMQDMVEDYR Oxidation (M)			258 - 267	1316.56	37
	NKYEDEINKR			268 - 277	1308.68	41
	YEDEINKR			270 - 277	1066.54	60
	TNAENEFVTIK			278 - 288	1265.68	95
	TNAENEFVTIKK			278 - 289	1393.76	88
	SLDLDSIIAEVK			344 - 355	1302.77	111
	SKAEAESLYQSKYEELQITAGR			365 - 386	2501.33	29
	YEELQITAGR			377 - 386	1179.64	75
	IEISELNR			396 - 403	973.56	39
	QISNLQQSISDAEQR Pyro-glu (N-term Q)			418 - 432	1699.90	47
	QISNLQQSISDAEQR			418 - 432	1716.90	96
	LNDLEDALQQAK			444 - 455	1357.73	103
	LALDLEIATYR			473 - 483	1277.77	51
	TLLEGEESR			484 - 492	1033.54	38
	GGGGGGYGSGGSSYGSGGGSYGSGGGGGGGR			519 - 549	2383.98	189
	GSYGSGGSSYGSGGGSYGSGGGGGGHGSYGSGSSSG			550 - 588	3312.35	119
	GYR					
7	Coronin-1A (**CORIA_HUMAN**)	**50,994**	**6.25**	**255**	**12**	**848**
	HVFGQPAK			13 - 20	883.43	62
	ADQCYEDVR Carbamidomethyl (C)			21 - 29	1155.41	49
	VSQTTWDSGFCAVNPK Carbamidomethyl (C)			30 - 45	1796.88	135
	EPVVTLEGHTK			122 - 132	1209.63	88
	DGGLICTSCR 2 Carbamidomethyl (C)			187 - 196	1138.48	35
	ILTTGFSR			234 - 241	894.52	45

Table SC2 (Continued)

	QVALWDTK			246 - 253	960.49	68
	RCEPIAMTVPR Carbamidomethyl (C); Oxidation (M)			344 - 354	1345.63	27
	DAGPLLISLK			384 - 393	1026.61	89
	AAPEASGTPSSDAVSR			417 - 432	1502.67	83
	KLQATVQELQK			439 - 449	1285.74	99
	LQATVQELQK			440 - 449	1157.64	68
8	Stress-induced-phosphoprotein 1 **(STIP1_HUMAN)**	**62,599**	**6.40**	**25 %**	**10**	**622**
	LDPHNHVLYSNR					
	KAAALEFLNR			33 - 44	1464.64	79
	AAALEFLNR			78 - 87	1132.63	47
	ELIEQLR			79 - 87	1004.58	38
	ELDPTNMTYITNQAAVYFEK Oxidation (M)			154 - 160	900.51	26
	DAIHFYNK			253 - 272	2364.19	108
	LAYINPDLALEEK			318 - 325	1007.45	45
	DCEECIQLEPTFIK 2 Carbamidomethyl (C)			352 - 364	1488.82	91
	LILEQMQK Oxidation (M)			416 - 429	1781.85	67
	DPQALSEHLK			506 - 513	1018.50	39
				514 - 523	1137.52	82
9	α-Enolase **(ENOA_HUMAN)**	**47,139**	**7.01**	**33%**	**9**	**617**
	EIFDSR			10 - 15	766.35	28
	GNPTVEVDLFTSK			16 - 28	1406.72	87
	AAVPSGASTGIYEALELR			33 - 50	1805.00	81
	IGAEVYHNLK			184 - 193	1143.58	91
	VVIGMDVAASEFFR Oxidation (M)			240 - 253	1556.80	57
	YDLDFK			257 - 262	800.38	28
	YISPDQLADLYK			270 - 281	1425.76	79
	VNQIGSVTESLQACK Carbamidomethyl (C)			344 - 358	1633.80	135
	YNQLLR			407 - 412	806.43	31
10	Purine nucleoside phosphorylase **(PNPH_HUMAN)**	**32,097**	**6.45**	**40 %**	**9**	**493**
	NTAEWLLSHTK			12 - 22	1299.71	57
	LTQAQIFDYGEIPNFPR			42 - 58	2009.05	39

Table SC2 (Continued)

	LVFGFLNGR			68 - 76	1022.64	35
	LVFGFLNGR Deamidation (NQ)			68 - 76	1023.62	35
	DHINLPGFSGQNPLR			134 - 148	1664.87	47
	FPAMSDAYDR Oxidation (M)			159 - 168	1188.52	36
	LGADAVGMSTVPEVIVAR Oxidation (M)			212 - 229	1801.02	67
	VFGFSLITNK			235 - 244	1125.69	69
	ANHEEVLAAGK			255 - 265	1138.61	108
11	**Carbonic anhydrase 2 (CAH2_HUMAN)**	**29,228**	**6.87**	**55 %**	**12**	**1153**
	HNGPEHWHK			10 - 18	1141.54	60
	QSPVDIDTHTAK Pyro-glu (N-term Q)			28 - 39	1294.62	91
	QSPVDIDTHTAK			28 - 39	1311.65	81
	YDPSLKPLSVSYDQATSLR			40 - 58	2140.18	149
	ILNNGHAFNVEFDDSQDK			59 - 76	2062.94	149
	GGPLDGTYR			81 - 89	935.45	62
	YAAELHLVHWNTK			114 - 126	1581.82	115
	AVQQPDGLAVLGIFLK			133 - 148	1669.02	120
	VVDVLDSIK			159 - 167	987.57	86
	SADFTNFDPR			172 - 181	1169.56	72
	EPISVSSEQVLK			213 - 224	1315.75	98
	LNFNGEGEPEELMVDNWR Oxidation (M)			228 - 245	2165.00	70

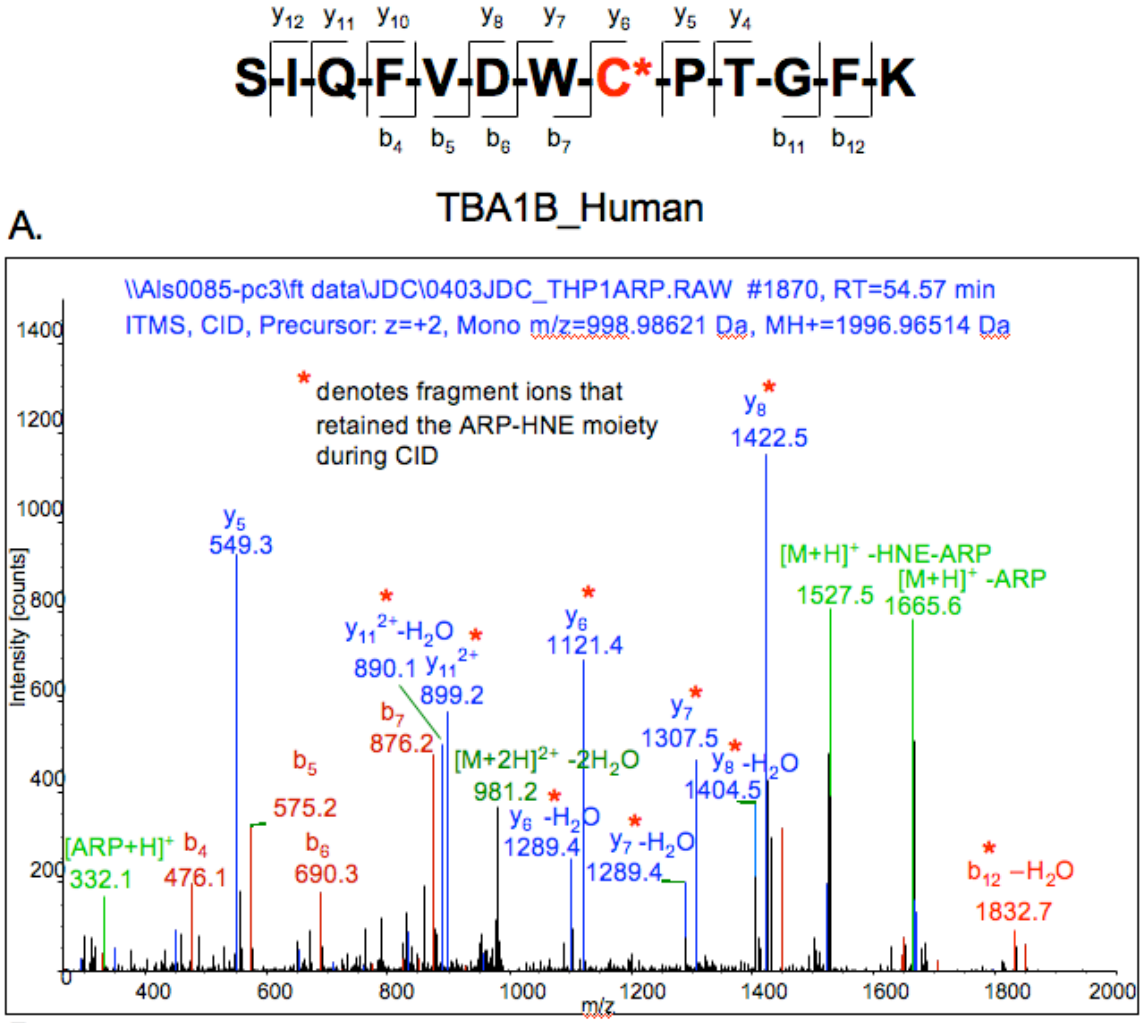

Mascot search result for the MS/MS spectrum depicted above:

#	b	b++	b*	b*++	b0	b0++	Seq.	y	y++	y*	y*++	y0	y0++	#
1	88.04	44.52			70.03	35.52	S							13
2	201.12	101.07			183.11	92.06	I	1909.93	955.47	1892.91	946.96	1891.92	946.47	12
3	329.18	165.09	312.16	156.58	311.17	156.09	Q	1796.85	898.93	1779.82	890.42	1778.84	889.92	11
4	476.25	238.63	459.22	230.12	458.24	229.62	F	1668.79	834.90	1651.76	826.39	1650.78	825.89	10
5	575.32	288.16	558.29	279.65	557.31	279.16	V	1521.72	761.37	1504.70	752.85	1503.71	752.36	9
6	690.35	345.68	673.32	337.16	672.34	336.67	D	1422.65	711.83	1405.63	703.32	1404.64	702.83	8
7	876.43	438.72	859.40	430.20	858.41	429.71	W	1307.63	654.32	1290.60	645.80	1289.62	645.31	7
8	1448.67	724.84	1431.64	716.33	1430.66	715.83	C	1121.55	561.28	1104.52	552.76	1103.54	552.27	6
9	1545.72	773.37	1528.70	764.85	1527.71	764.36	P	549.30	275.16	532.28	266.64	531.29	266.15	5
10	1646.77	823.89	1629.74	815.38	1628.76	814.88	T	452.25	226.63	435.22	218.12	434.24	217.62	4
11	1703.79	852.40	1686.77	843.89	1685.78	843.39	G	351.20	176.10	334.18	167.59			3
12	1850.86	925.93	1833.83	917.42	1832.85	916.93	F	294.18	147.59	277.15	139.08			2
13							K	147.11	74.06	130.09	65.55			1

Figure SC1. (A) MS/MS of the ARP-HNE modified peptide SIQFVDWC*PTGFK. (B) Full MS spectrum acquired by ESI-LTQ-FT, Δm = -0.44 ppm

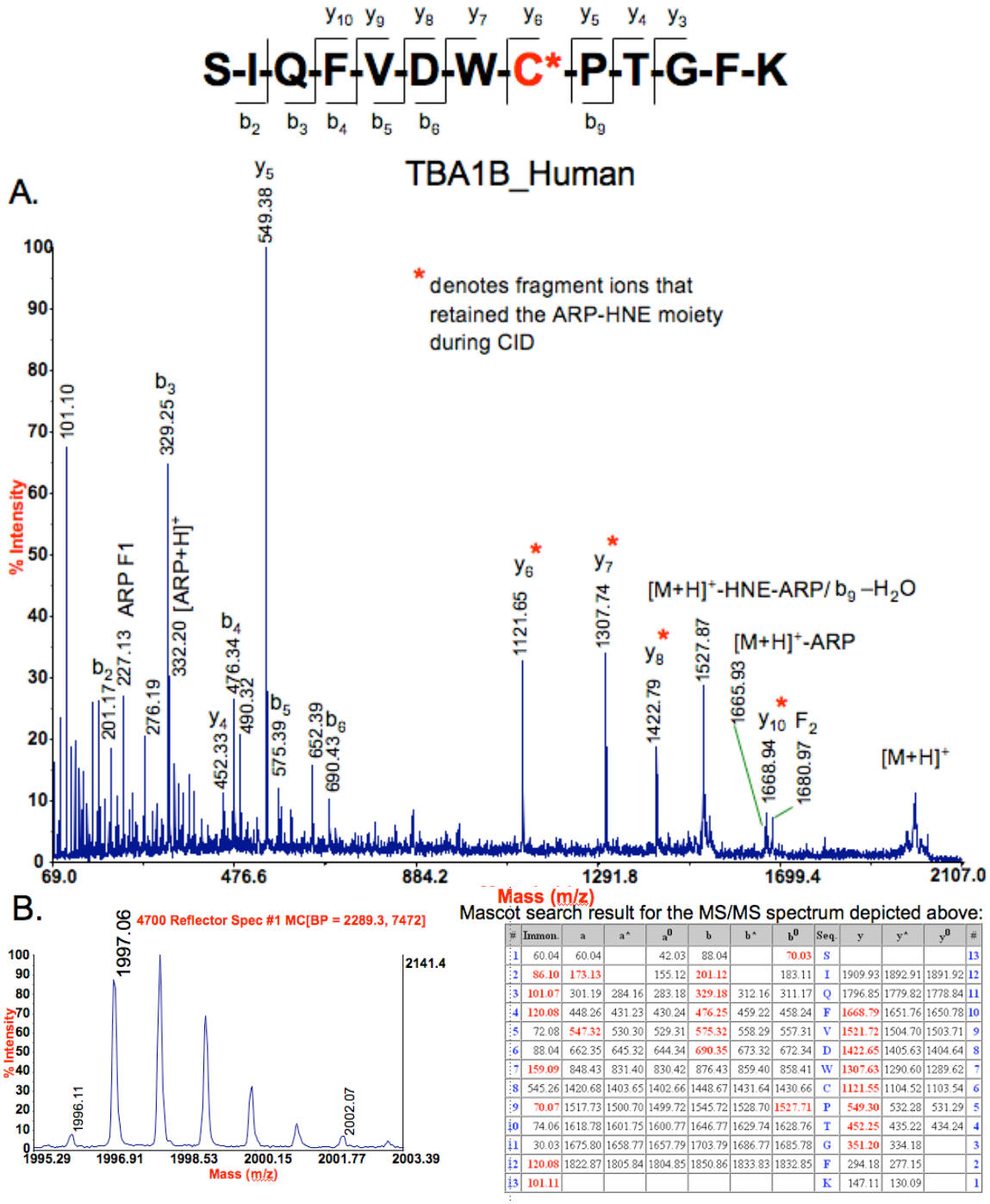

#	Immon.	a	a*	a0	b	b*	b0	Seq.	y	y*	y0	#
1	60.04	60.04		42.03	88.04		70.03	S				13
2	86.10	173.13		155.12	201.12		183.11	I	1909.93	1892.91	1891.92	12
3	101.07	301.19	284.16	283.18	329.18	312.16	311.17	Q	1796.85	1779.82	1778.84	11
4	120.08	448.26	431.23	430.24	476.25	459.22	458.24	F	1668.79	1651.76	1650.78	10
5	72.08	547.32	530.30	529.31	575.32	558.29	557.31	V	1521.72	1504.70	1503.71	9
6	88.04	662.35	645.32	644.34	690.35	673.32	672.34	D	1422.65	1405.63	1404.64	8
7	159.09	848.43	831.40	830.42	876.43	859.40	858.41	W	1307.63	1290.60	1289.62	7
8	545.26	1420.68	1403.65	1402.66	1448.67	1431.64	1430.66	C	1121.55	1104.52	1103.54	6
9	70.07	1517.73	1500.70	1499.72	1545.72	1528.70	1527.71	P	549.30	532.28	531.29	5
10	74.06	1618.78	1601.75	1600.77	1646.77	1629.74	1628.76	T	452.25	435.22	434.24	4
11	30.03	1675.80	1658.77	1657.79	1703.79	1686.77	1685.78	G	351.20	334.18		3
12	120.08	1822.87	1805.84	1804.85	1850.86	1833.83	1832.85	F	294.18	277.15		2
13	101.11							K	147.11	130.09		1

Figure SC2. (A) MS/MS of the ARP-HNE modified peptide SIQFVDWC*PTGFK. (B) Full MS spectrum acquired by MALDI-TOF/TOF, Δm = 0.10 Da

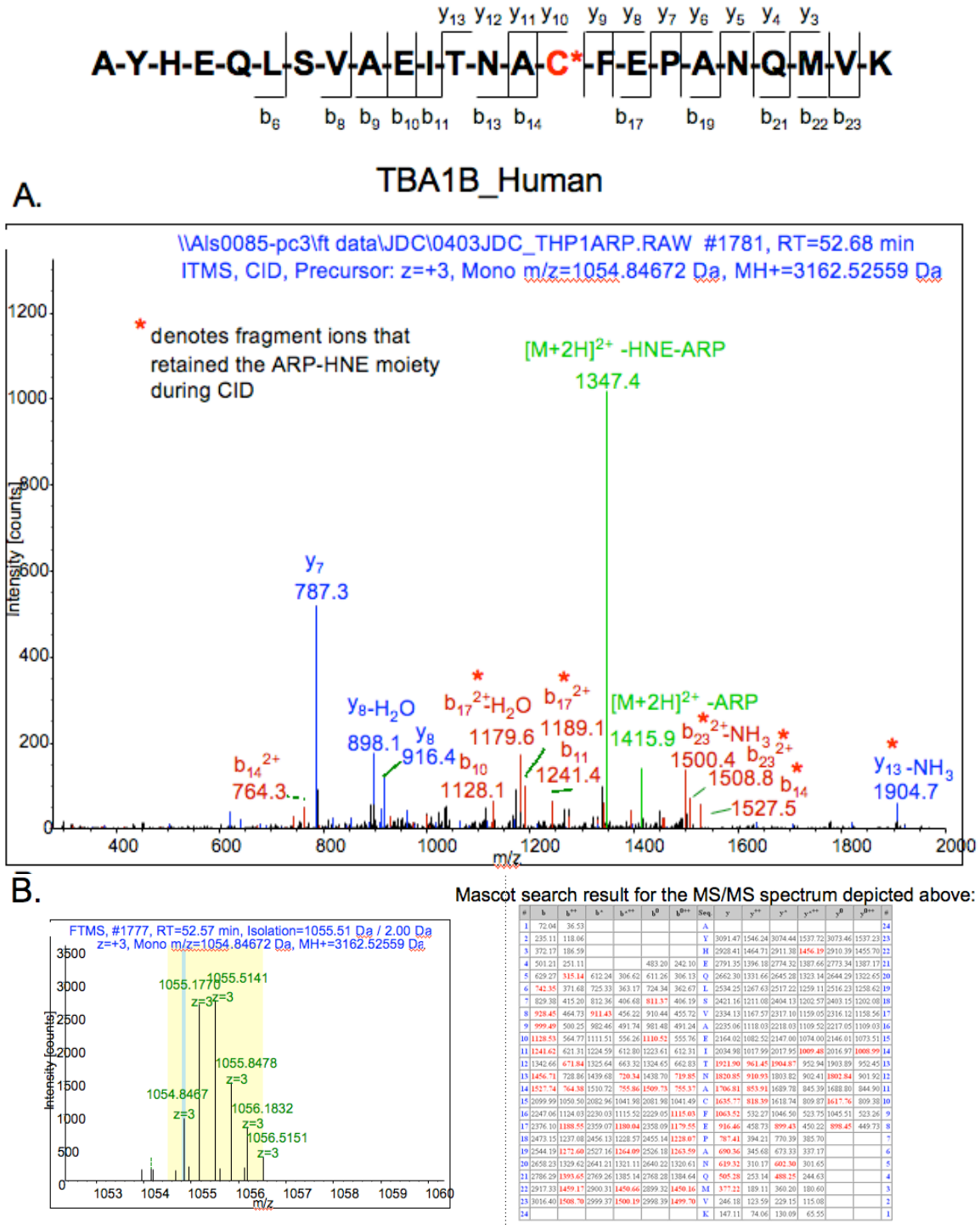

Figure SC3. (A) MS/MS of the ARP-HNE modified peptide AYHEQLSVAEITNAC*FEPANQMVK (B) Full MS spectrum acquired by ESI-LTQ-FT, Δm = 6.26 ppm

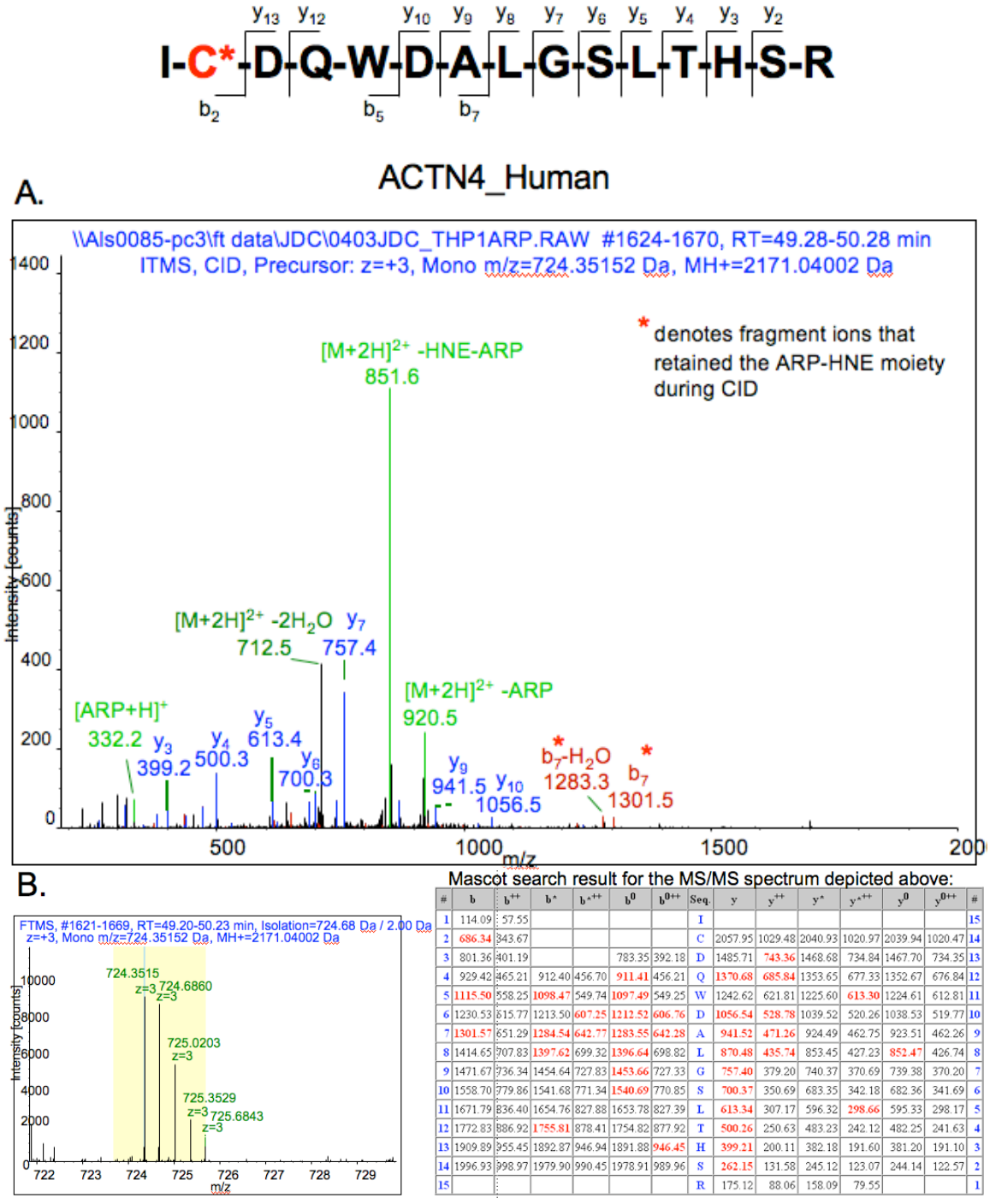

Mascot search result for the MS/MS spectrum depicted above:

#	b	b++	b*	b*++	b0	b0++	Seq.	y	y++	y*	y*++	y0	y0++	#
1	114.09	57.55					I							15
2	686.34	343.67					C	2057.95	1029.48	2040.93	1020.97	2039.94	1020.47	14
3	801.36	401.19			783.35	392.18	D	1485.71	743.36	1468.68	734.84	1467.70	734.35	13
4	929.42	465.21	912.40	456.70	911.41	456.21	Q	1370.68	685.84	1353.65	677.33	1352.67	676.84	12
5	1115.50	558.25	1098.47	549.74	1097.49	549.25	W	1242.62	621.81	1225.60	613.30	1224.61	612.81	11
6	1230.53	615.77	1213.50	607.25	1212.52	606.76	D	1056.54	528.78	1039.52	520.26	1038.53	519.77	10
7	1301.57	651.29	1284.54	642.77	1283.55	642.28	A	941.52	471.26	924.49	462.75	923.51	462.26	9
8	1414.65	707.83	1397.62	699.32	1396.64	698.82	L	870.48	435.74	853.45	427.23	852.47	426.74	8
9	1471.67	736.34	1454.64	727.83	1453.66	727.33	G	757.40	379.20	740.37	370.69	739.38	370.20	7
10	1558.70	779.86	1541.68	771.34	1540.69	770.85	S	700.37	350.69	683.35	342.18	682.36	341.69	6
11	1671.79	836.40	1654.76	827.88	1653.78	827.39	L	613.34	307.17	596.32	298.66	595.33	298.17	5
12	1772.83	886.92	1755.81	878.41	1754.82	877.92	T	500.26	250.63	483.23	242.12	482.25	241.63	4
13	1909.89	955.45	1892.87	946.94	1891.88	946.45	H	399.21	200.11	382.18	191.60	381.20	191.10	3
14	1996.93	998.97	1979.90	990.45	1978.91	989.96	S	262.15	131.58	245.12	123.07	244.14	122.57	2
15							R	175.12	88.06	158.09	79.55			1

Figure SC4. (A) MS/MS of the ARP-HNE modified peptide IC*DQWDALGSLTHSR (B) Full MS spectrum acquired by ESI-LTQ-FT, Δm = 1.26 ppm

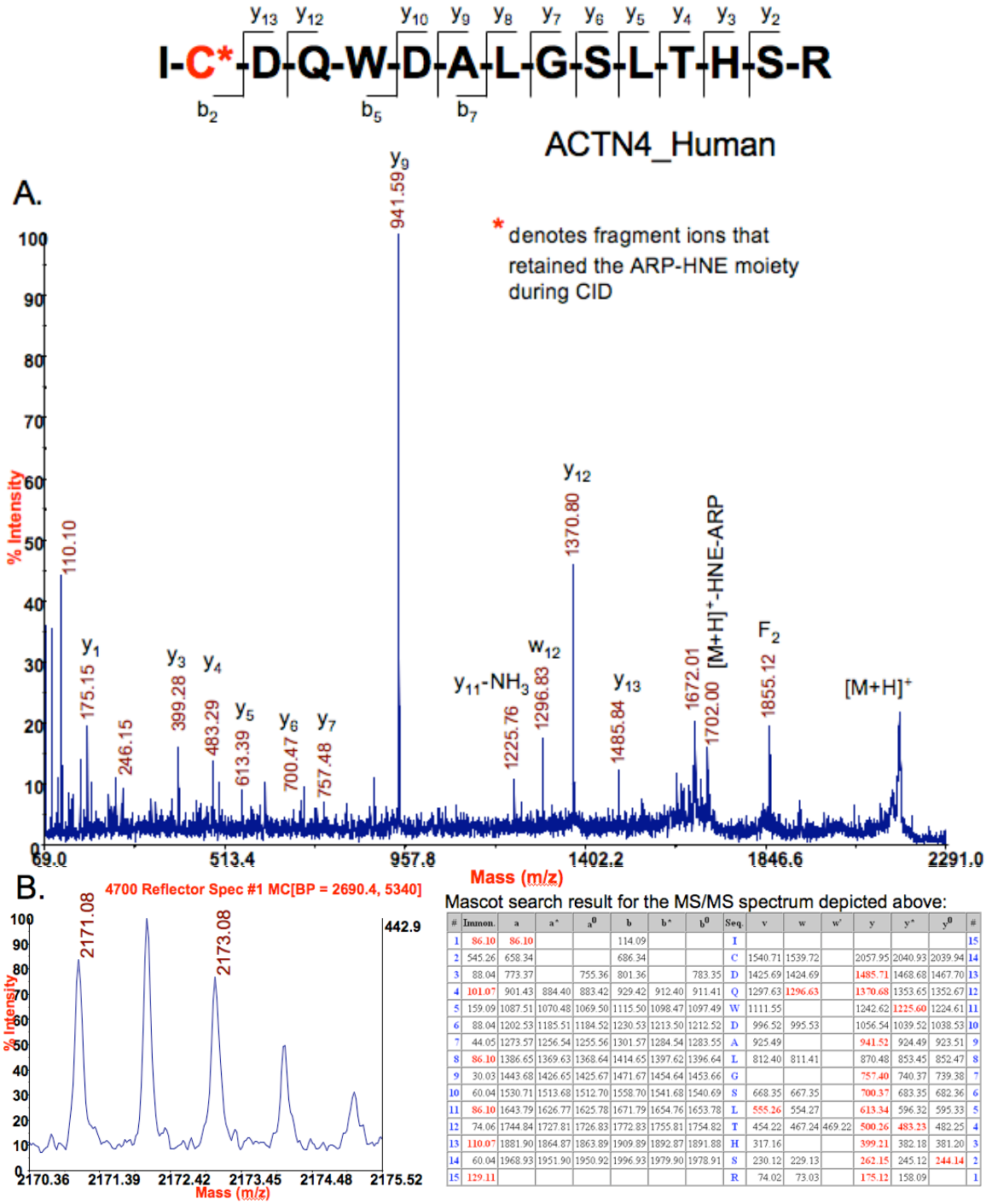

#	Immon.	a	a*	a⁰	b	b*	b⁰	Seq.	v	w	w'	y	y*	y⁰	#
1	86.10	86.10			114.09			I							15
2	545.26	658.34			686.34			C	1540.71	1539.72		2057.95	2040.93	2039.94	14
3	88.04	773.37		755.36	801.36		783.35	D	1425.69	1424.69		1485.71	1468.68	1467.70	13
4	101.07	901.43	884.40	883.42	929.42	912.40	911.41	Q	1297.63	1296.63		1370.68	1353.65	1352.67	12
5	159.09	1087.51	1070.48	1069.50	1115.50	1098.47	1097.49	W	1111.55			1242.62	1225.60	1224.61	11
6	88.04	1202.53	1185.51	1184.52	1230.53	1213.50	1212.52	D	996.52	995.53		1056.54	1039.52	1038.53	10
7	44.05	1273.57	1256.54	1255.56	1301.57	1284.54	1283.55	A	925.49			941.52	924.49	923.51	9
8	86.10	1386.65	1369.63	1368.64	1414.65	1397.62	1396.64	L	812.40	811.41		870.48	853.45	852.47	8
9	30.03	1443.68	1426.65	1425.67	1471.67	1454.64	1453.66	G				757.40	740.37	739.38	7
10	60.04	1530.71	1513.68	1512.70	1558.70	1541.68	1540.69	S	668.35	667.35		700.37	683.35	682.36	6
11	86.10	1643.79	1626.77	1625.78	1671.79	1654.76	1653.78	L	555.26	554.27		613.34	596.32	595.33	5
12	74.06	1744.84	1727.81	1726.83	1772.83	1755.81	1754.82	T	454.22	467.24	469.22	500.26	483.23	482.25	4
13	110.07	1881.90	1864.87	1863.89	1909.89	1892.87	1891.88	H	317.16			399.21	382.18	381.20	3
14	60.04	1968.93	1951.90	1950.92	1996.93	1979.90	1978.91	S	230.12	229.13		262.15	245.12	244.14	2
15	129.11							R	74.02	73.03		175.12	158.09		1

Figure SC5. (A) MS/MS of the ARP-HNE modified peptide IC*DQWDALGSLTHSR (B) Full MS spectrum acquired by MALDI-TOF/TOF, Δm = 0.08 Da

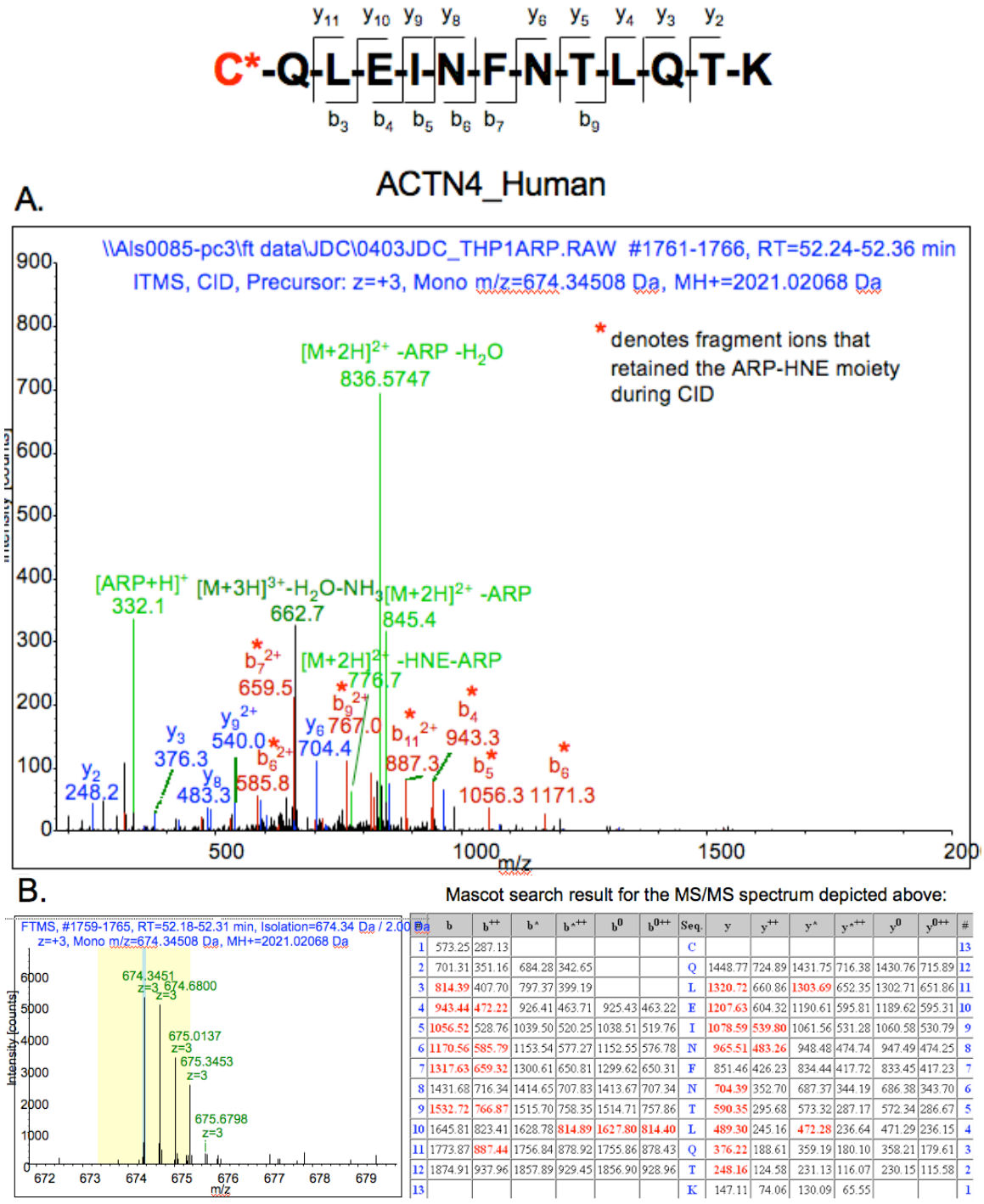

	b	b++	b*	b*++	b0	b0++	Seq.	y	y++	y*	y*++	y0	y0++	#
1	573.25	287.13					C							13
2	701.31	351.16	684.28	342.65			Q	1448.77	724.89	1431.75	716.38	1430.76	715.89	12
3	814.39	407.70	797.37	399.19			L	1320.72	660.86	1303.69	652.35	1302.71	651.86	11
4	943.44	472.22	926.41	463.71	925.43	463.22	E	1207.63	604.32	1190.61	595.81	1189.62	595.31	10
5	1056.52	528.76	1039.50	520.25	1038.51	519.76	I	1078.59	539.80	1061.56	531.28	1060.58	530.79	9
6	1170.56	585.79	1153.54	577.27	1152.55	576.78	N	965.51	483.26	948.48	474.74	947.49	474.25	8
7	1317.63	659.32	1300.61	650.81	1299.62	650.31	F	851.46	426.23	834.44	417.72	833.45	417.23	7
8	1431.68	716.34	1414.65	707.83	1413.67	707.34	N	704.39	352.70	687.37	344.19	686.38	343.70	6
9	1532.72	766.87	1515.70	758.35	1514.71	757.86	T	590.35	295.68	573.32	287.17	572.34	286.67	5
10	1645.81	823.41	1628.78	814.89	1627.80	814.40	L	489.30	245.16	472.28	236.64	471.29	236.15	4
11	1773.87	887.44	1756.84	878.92	1755.86	878.43	Q	376.22	188.61	359.19	180.10	358.21	179.61	3
12	1874.91	937.96	1857.89	929.45	1856.90	928.96	T	248.16	124.58	231.13	116.07	230.15	115.58	2
13							K	147.11	74.06	130.09	65.55			1

Figure SC6. (A) MS/MS of the ARP-HNE modified peptide C*QLEINFNTLQTK (B) Full MS spectrum acquired by ESI-LTQ-FT, Δm = 0.59 ppm

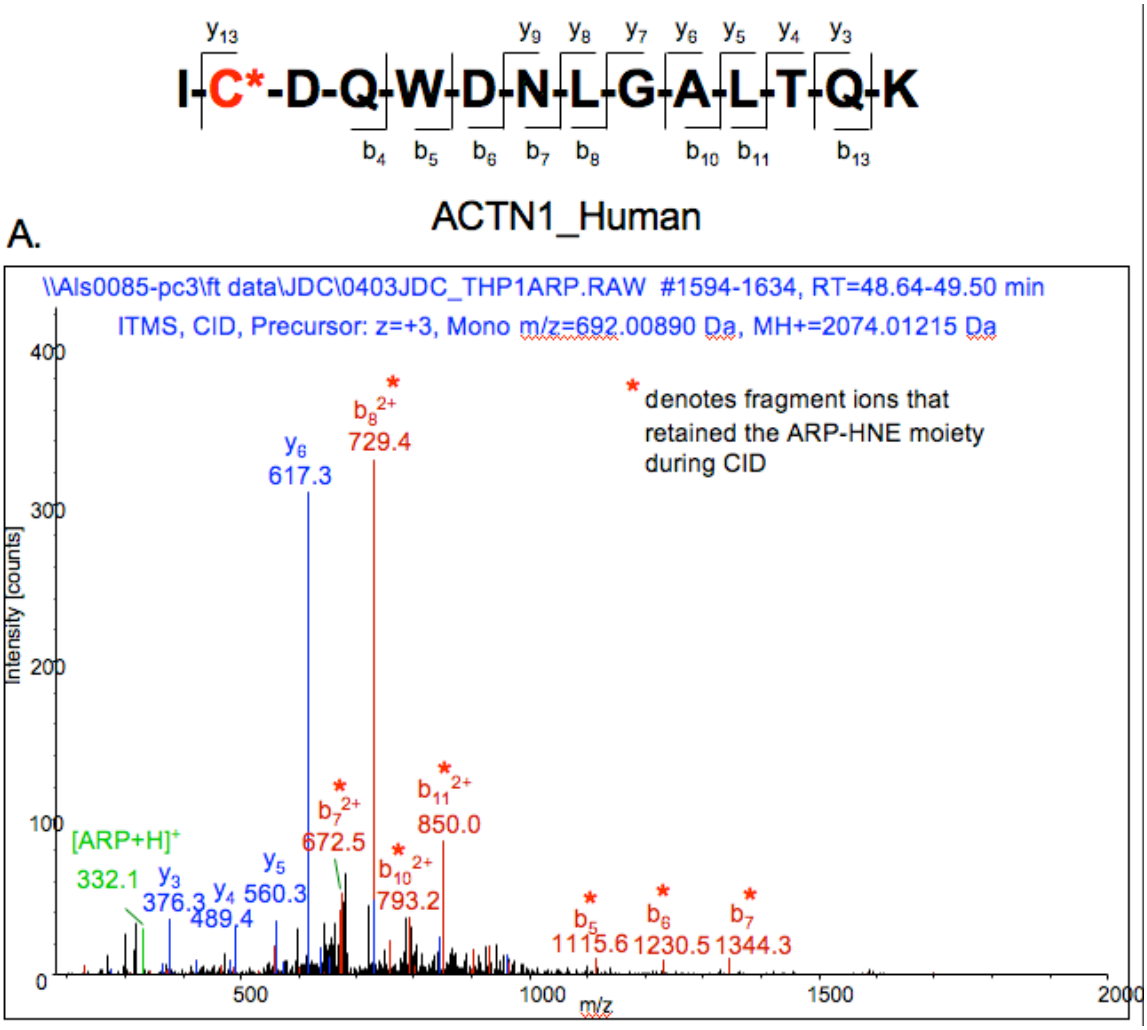

B.

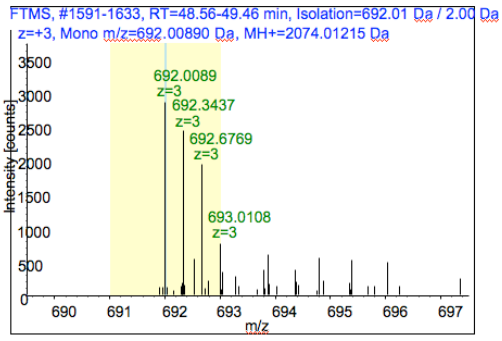

Mascot search result for the MS/MS spectrum depicted above:

#	b	b^{++}	b^*	b^{*++}	b^0	b^{0++}	Seq.	y	y^{++}	y^*	y^{*++}	y^0	y^{0++}	#
1	114.09	57.55					I							14
2	686.34	343.67					C	1960.93	980.97	1943.90	972.45	1942.91	971.96	13
3	801.36	401.19			783.35	392.18	D	1388.68	694.84	1371.65	686.33	1370.67	685.84	12
4	929.42	465.21	912.40	456.70	911.41	456.21	Q	1273.65	637.33	1256.63	628.82	1255.64	628.33	11
5	1115.50	558.25	1098.47	549.74	1097.49	549.25	W	1145.59	573.30	1128.57	564.79	1127.58	564.30	10
6	1230.53	615.77	1213.50	607.25	1212.52	606.76	D	959.52	480.26	942.49	471.75	941.51	471.26	9
7	1344.57	672.79	1327.54	664.28	1326.56	663.78	N	844.49	422.75	827.46	414.23	826.48	413.74	8
8	1457.66	729.33	1440.63	720.82	1439.64	720.33	L	730.45	365.73	713.42	357.21	712.44	356.72	7
9	1514.68	757.84	1497.65	749.33	1496.67	748.84	G	617.36	309.18	600.34	300.67	599.35	300.18	6
10	1585.71	793.36	1568.69	784.85	1567.70	784.36	A	560.34	280.67	543.31	272.16	542.33	271.67	5
11	1698.80	849.90	1681.77	841.39	1680.79	840.90	L	489.30	245.16	472.28	236.64	471.29	236.15	4
12	1799.85	900.43	1782.82	891.91	1781.83	891.42	T	376.22	188.61	359.19	180.10	358.21	179.61	3
13	1927.90	964.46	1910.88	955.94	1909.89	955.45	Q	275.17	138.09	258.14	129.58			2
14							K	147.11	74.06	130.09	65.55			1

Figure SC7. (A) MS/MS of the ARP-HNE modified peptide IC*DQWDNLGALTQK (B) Full MS spectrum acquired by ESI-LTQ-FT, Δm = 1.19 ppm

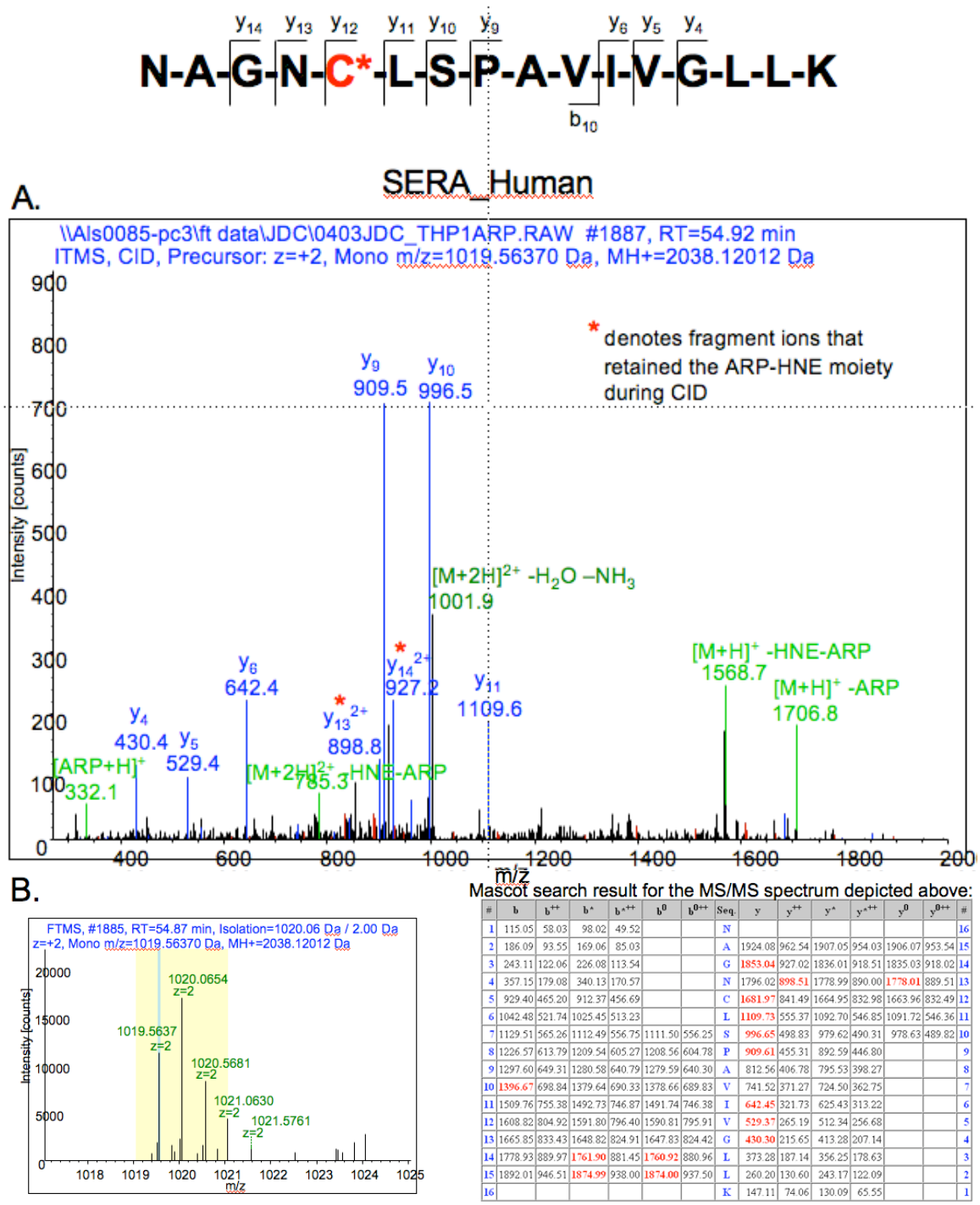

#	b	b++	b*	b*++	b0	b0++	Seq.	y	y++	y*	y*++	y0	y0++	#
1	115.05	58.03	98.02	49.52			N							16
2	186.09	93.55	169.06	85.03			A	1924.08	962.54	1907.05	954.03	1906.07	953.54	15
3	243.11	122.06	226.08	113.54			G	1853.04	927.02	1836.01	918.51	1835.03	918.02	14
4	357.15	179.08	340.13	170.57			N	1796.02	898.51	1778.99	890.00	1778.01	889.51	13
5	929.40	465.20	912.37	456.69			C	1681.97	841.49	1664.95	832.98	1663.96	832.49	12
6	1042.48	521.74	1025.45	513.23			L	1109.73	555.37	1092.70	546.85	1091.72	546.36	11
7	1129.51	565.26	1112.49	556.75	1111.50	556.25	S	996.65	498.83	979.62	490.31	978.63	489.82	10
8	1226.57	613.79	1209.54	605.27	1208.56	604.78	P	909.61	455.31	892.59	446.80			9
9	1297.60	649.31	1280.58	640.79	1279.59	640.30	A	812.56	406.78	795.53	398.27			8
10	1396.67	698.84	1379.64	690.33	1378.66	689.83	V	741.52	371.27	724.50	362.75			7
11	1509.76	755.38	1492.73	746.87	1491.74	746.38	I	642.45	321.73	625.43	313.22			6
12	1608.82	804.92	1591.80	796.40	1590.81	795.91	V	529.37	265.19	512.34	256.68			5
13	1665.85	833.43	1648.82	824.91	1647.83	824.42	G	430.30	215.65	413.28	207.14			4
14	1778.93	889.97	1761.90	881.45	1760.92	880.96	L	373.28	187.14	356.25	178.63			3
15	1892.01	946.51	1874.99	938.00	1874.00	937.50	L	260.20	130.60	243.17	122.09			2
16							K	147.11	74.06	130.09	65.55			1

Figure SC8. (A) MS/MS of the ARP-HNE modified peptide NAGNC*LSPAVIVGLLK (B) Full MS spectrum acquired by ESI-LTQ-FT, Δm = 0.63 ppm

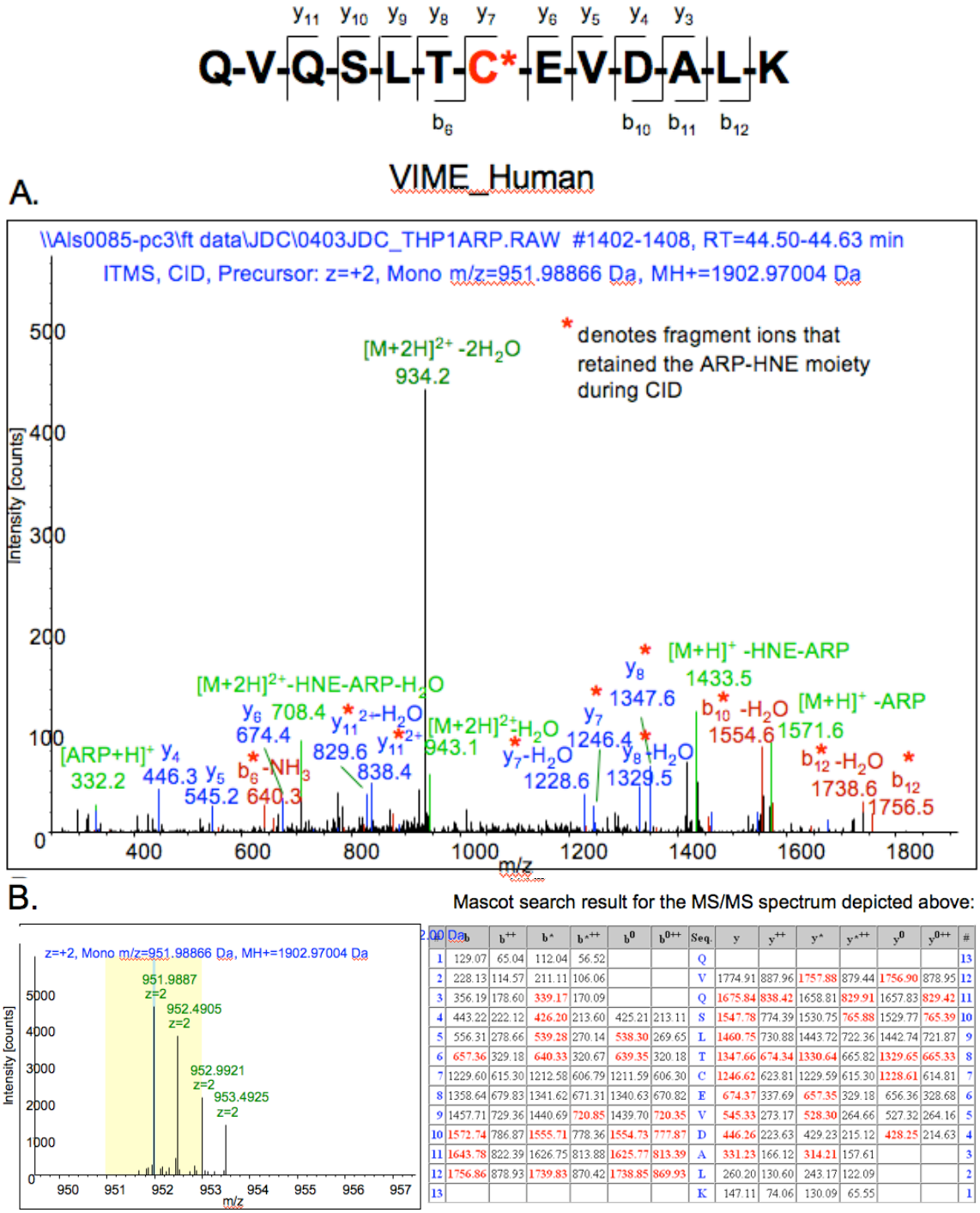

	b	b++	b*	b*++	b0	b0++	Seq.	y	y++	y*	y*++	y0	y0++	#
1	129.07	65.04	112.04	56.52			Q							13
2	228.13	114.57	211.11	106.06			V	1774.91	887.96	1757.88	879.44	1756.90	878.95	12
3	356.19	178.60	339.17	170.09			Q	1675.84	838.42	1658.81	829.91	1657.83	829.42	11
4	443.22	222.12	426.20	213.60	425.21	213.11	S	1547.78	774.39	1530.75	765.88	1529.77	765.39	10
5	556.31	278.66	539.28	270.14	538.30	269.65	L	1460.75	730.88	1443.72	722.36	1442.74	721.87	9
6	657.36	329.18	640.33	320.67	639.35	320.18	T	1347.66	674.34	1330.64	665.82	1329.65	665.33	8
7	1229.60	615.30	1212.58	606.79	1211.59	606.30	C	1246.62	623.81	1229.59	615.30	1228.61	614.81	7
8	1358.64	679.83	1341.62	671.31	1340.63	670.82	E	674.37	337.69	657.35	329.18	656.36	328.68	6
9	1457.71	729.36	1440.69	720.85	1439.70	720.35	V	545.33	273.17	528.30	264.66	527.32	264.16	5
10	1572.74	786.87	1555.71	778.36	1554.73	777.87	D	446.26	223.63	429.23	215.12	428.25	214.63	4
11	1643.78	822.39	1626.75	813.88	1625.77	813.39	A	331.23	166.12	314.21	157.61			3
12	1756.86	878.93	1739.83	870.42	1738.85	869.93	L	260.20	130.60	243.17	122.09			2
13							K	147.11	74.06	130.09	65.55			1

Figure SC9. (A) MS/MS of the ARP-HNE modified peptide QVQSLTC*EVDALK (B) Full MS spectrum acquired by ESI-LTQ-FT, Δm = 1.91 ppm

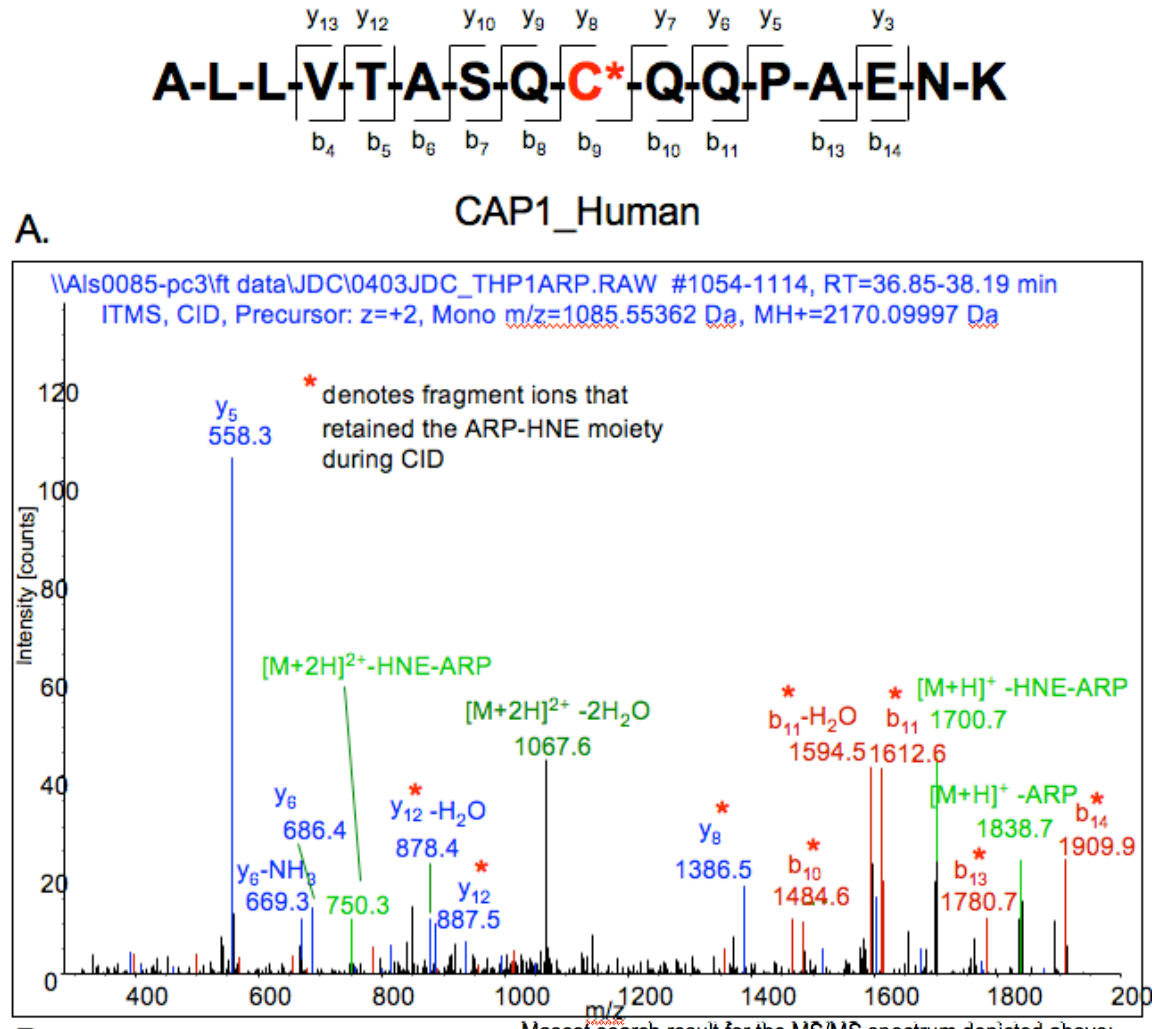

Mascot search result for the MS/MS spectrum depicted above:

#	b	b^{++}	b^*	b^{*++}	b^0	b^{0++}	Seq.	y	y^{++}	y^*	y^{*++}	y^0	y^{0++}	#
1	72.04	36.53					A							16
2	185.13	93.07					L	2099.06	1050.03	2082.04	1041.52	2081.05	1041.03	15
3	298.21	149.61					L	1985.98	993.49	1968.95	984.98	1967.97	984.49	14
4	397.28	199.14					V	1872.89	936.95	1855.87	928.44	1854.88	927.95	13
5	498.33	249.67			480.32	240.66	T	1773.83	887.42	1756.80	878.90	1755.82	878.41	12
6	569.37	285.19			551.36	276.18	A	1672.78	836.89	1655.75	828.38	1654.77	827.89	11
7	656.40	328.70			638.39	319.70	S	1601.74	801.37	1584.71	792.86	1583.73	792.37	10
8	784.46	392.73	767.43	384.22	766.45	383.73	Q	1514.71	757.86	1497.68	749.34	1496.70	748.85	9
9	1356.70	678.85	1339.67	670.34	1338.69	669.85	C	1386.65	693.83	1369.62	685.32	1368.64	684.82	8
10	1484.76	742.88	1467.73	734.37	1466.75	733.88	Q	814.41	407.71	797.38	399.19	796.39	398.70	7
11	1612.82	806.91	1595.79	798.40	1594.81	797.91	Q	686.35	343.68	669.32	335.16	668.34	334.67	6
12	1709.87	855.44	1692.84	846.93	1691.86	846.43	P	558.29	279.65	541.26	271.13	540.28	270.64	5
13	1780.91	890.96	1763.88	882.44	1762.90	881.95	A	461.24	231.12	444.21	222.61	443.22	222.12	4
14	1909.95	955.48	1892.92	946.97	1891.94	946.47	E	390.20	195.60	373.17	187.09	372.19	186.60	3
15	2023.99	1012.50	2006.97	1003.99	2005.98	1003.50	N	261.16	131.08	244.13	122.57			2
16							K	147.11	74.06	130.09	65.55			1

Figure SC10. (A) MS/MS of the ARP-HNE modified peptide ALLVTASQC*QQPAENK (B) Full MS spectrum acquired by ESI-LTQ-FT, Δm = 0.19 ppm

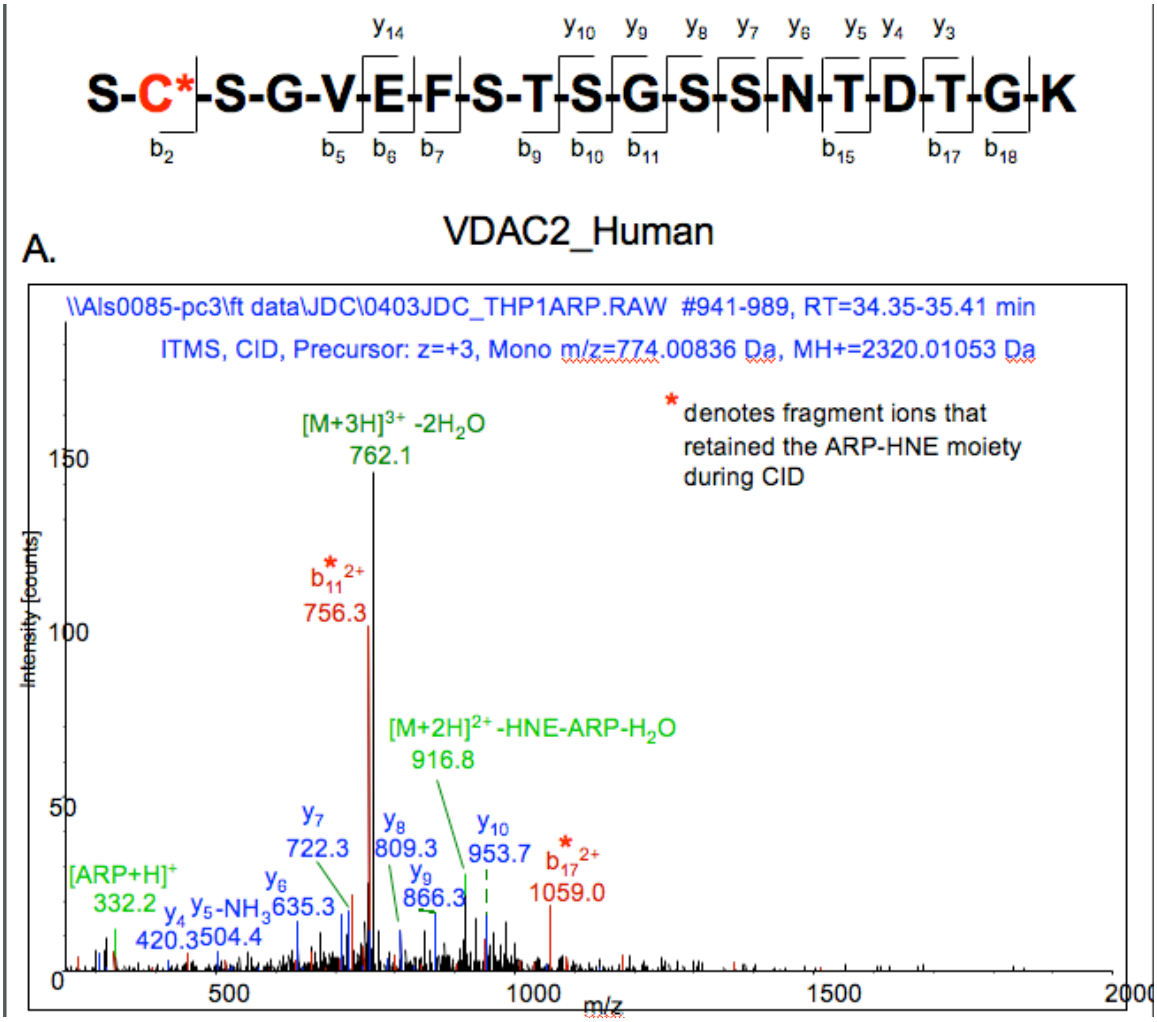

Mascot search result for the MS/MS spectrum depicted above:

#	b	b++	b*	b*++	b0	b0++	Seq.	y	y++	y*	y*++	y0	y0++	#
1	88.04	44.52			70.03	35.52	S							19
2	660.28	330.65			642.27	321.64	C	2232.97	1116.99	2215.95	1108.48	2214.96	1107.99	18
3	747.32	374.16			729.31	365.16	S	1660.73	830.87	1643.70	822.36	1642.72	821.86	17
4	804.34	402.67			786.33	393.67	G	1573.70	787.35	1556.67	778.84	1555.69	778.35	16
5	903.41	452.21			885.40	443.20	V	1516.68	758.84	1499.65	750.33	1498.67	749.84	15
6	1032.45	516.73			1014.44	507.72	E	1417.61	709.31	1400.58	700.79	1399.60	700.30	14
7	1179.52	590.26			1161.51	581.26	F	1288.57	644.79	1271.54	636.27	1270.55	635.78	13
8	1266.55	633.78			1248.54	624.77	S	1141.50	571.25	1124.47	562.74	1123.49	562.25	12
9	1367.60	684.30			1349.59	675.30	T	1054.46	527.74	1037.44	519.22	1036.45	518.73	11
10	1454.63	727.82			1436.62	718.81	S	953.42	477.21	936.39	468.70	935.41	468.21	10
11	1511.65	756.33			1493.64	747.32	G	866.39	433.70	849.36	425.18	848.37	424.69	9
12	1598.68	799.84			1580.67	790.84	S	809.36	405.19	792.34	396.67	791.35	396.18	8
13	1685.71	843.36			1667.70	834.36	S	722.33	361.67	705.30	353.16	704.32	352.66	7
14	1799.76	900.38	1782.73	891.87	1781.75	891.38	N	635.30	318.15	618.27	309.64	617.29	309.15	6
15	1900.81	950.91	1883.78	942.39	1882.79	941.90	T	521.26	261.13	504.23	252.62	503.25	252.13	5
16	2015.83	1008.42	1998.81	999.91	1997.82	999.41	D	420.21	210.61	403.18	202.09	402.20	201.60	4
17	2116.88	1058.94	2099.85	1050.43	2098.87	1049.94	T	305.18	153.09	288.16	144.58	287.17	144.09	3
18	2173.90	1087.45	2156.87	1078.94	2155.89	1078.45	G	204.13	102.57	187.11	94.06			2
19							K	147.11	74.06	130.09	65.55			1

Figure SC11. (A) MS/MS of the ARP-HNE modified peptide SC*SGVEFSTSGSSNTDTGK (B) Full MS spectrum acquired by ESI-LTQ-FT, Δm = 1.59 ppm

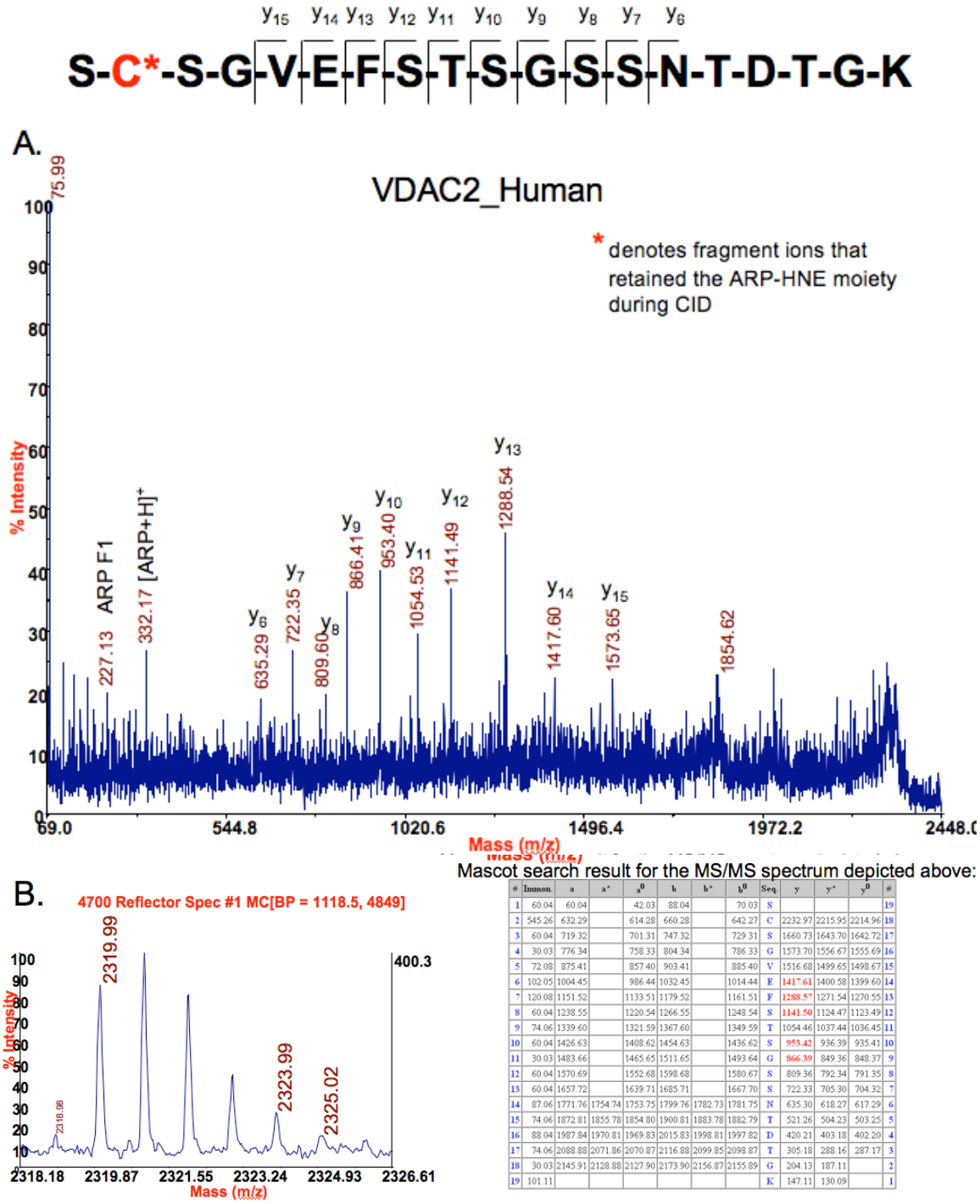

#	Immon.	a	a*	a0	b	b*	b0	Seq.	y	y*	y0	#
1	60.04	60.04		42.03	88.04		70.03	S				19
2	545.26	632.29		614.28	660.28		642.27	C	2232.97	2215.95	2214.96	18
3	60.04	719.32		701.31	747.32		729.31	S	1660.73	1643.70	1642.72	17
4	30.03	776.34		758.33	804.34		786.33	G	1573.70	1556.67	1555.69	16
5	72.08	875.41		857.40	903.41		885.40	V	1516.68	1499.65	1498.67	15
6	102.05	1004.45		986.44	1032.45		1014.44	E	1417.61	1400.58	1399.60	14
7	120.08	1151.52		1133.51	1179.52		1161.51	F	1288.57	1271.54	1270.55	13
8	60.04	1238.55		1220.54	1266.55		1248.54	S	1141.50	1124.47	1123.49	12
9	74.06	1339.60		1321.59	1367.60		1349.59	T	1054.46	1037.44	1036.45	11
10	60.04	1426.63		1408.62	1454.63		1436.62	S	953.42	936.39	935.41	10
11	30.03	1483.66		1465.65	1511.65		1493.64	G	866.39	849.36	848.37	9
12	60.04	1570.69		1552.68	1598.68		1580.67	S	809.36	792.34	791.35	8
13	60.04	1657.72		1639.71	1685.71		1667.70	S	722.33	705.30	704.32	7
14	87.06	1771.76	1754.74	1753.75	1799.76	1782.73	1781.75	N	635.30	618.27	617.29	6
15	74.06	1872.81	1855.78	1854.80	1900.81	1883.78	1882.79	T	521.26	504.23	503.25	5
16	88.04	1987.84	1970.81	1969.83	2015.83	1998.81	1997.82	D	420.21	403.18	402.20	4
17	74.06	2088.88	2071.86	2070.87	2116.88	2099.85	2098.87	T	305.18	288.16	287.17	3
18	30.03	2145.91	2128.88	2127.90	2173.90	2156.87	2155.89	G	204.13	187.11		2
19	101.11							K	147.11	130.09		1

Figure SC12. (A) MS/MS of the ARP-HNE modified peptide SC*SGVEFSTSGSSNTDTGK (B) Full MS spectrum acquired by MALDI-TOF/TOF, Δm = -0.02 Da

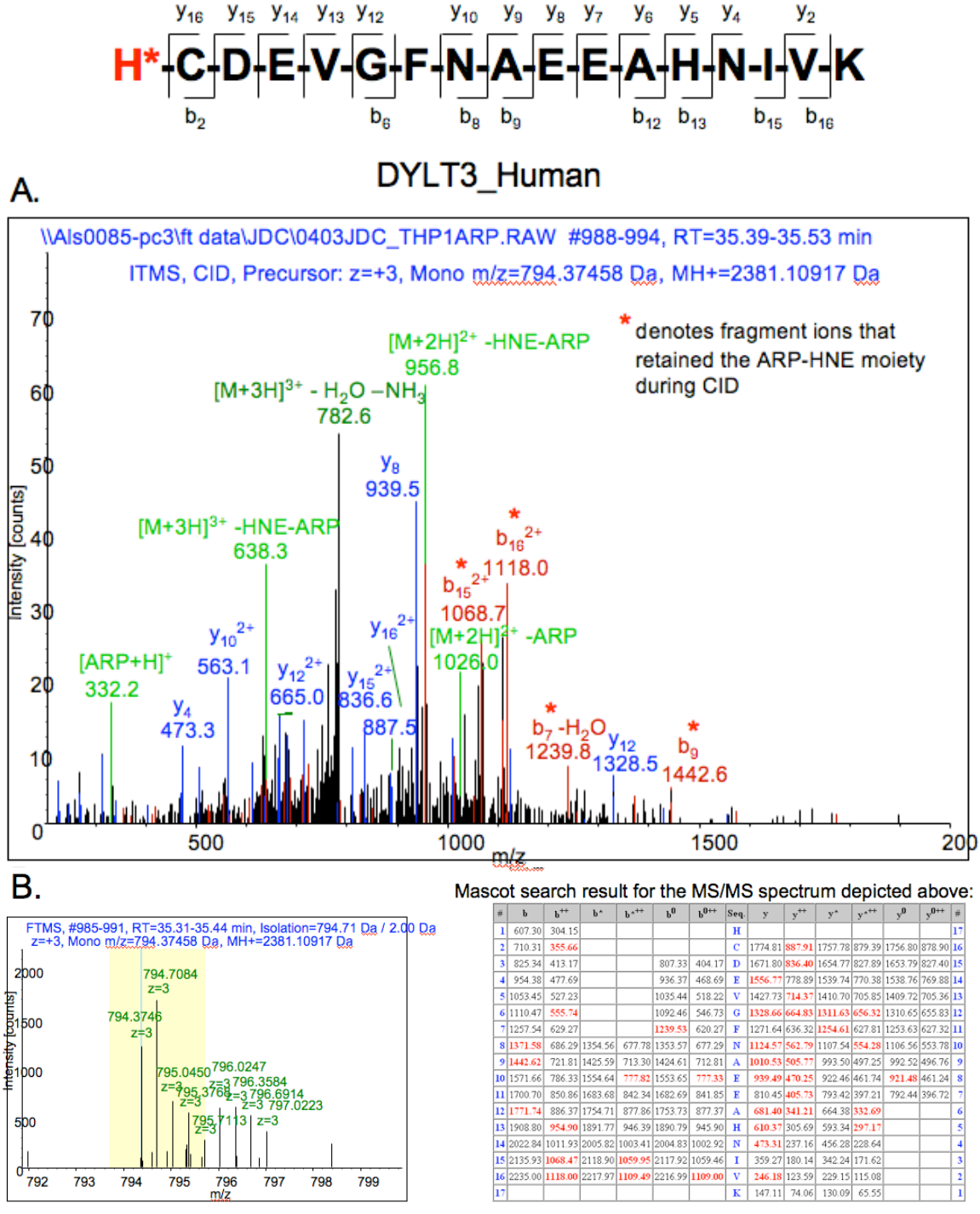

#	b	b++	b*	b*++	b0	b0++	Seq.	y	y++	y*	y*++	y0	y0++	#
1	607.30	304.15					H							17
2	710.31	355.66					C	1774.81	887.91	1757.78	879.39	1756.80	878.90	16
3	825.34	413.17			807.33	404.17	D	1671.80	836.40	1654.77	827.89	1653.79	827.40	15
4	954.38	477.69			936.37	468.69	E	1556.77	778.89	1539.74	770.38	1538.76	769.88	14
5	1053.45	527.23			1035.44	518.22	V	1427.73	714.37	1410.70	705.85	1409.72	705.36	13
6	1110.47	555.74			1092.46	546.73	G	1328.66	664.83	1311.63	656.32	1310.65	655.83	12
7	1257.54	629.27			1239.53	620.27	F	1271.64	636.32	1254.61	627.81	1253.63	627.32	11
8	1371.58	686.29	1354.56	677.78	1353.57	677.29	N	1124.57	562.79	1107.54	554.28	1106.56	553.78	10
9	1442.62	721.81	1425.59	713.30	1424.61	712.81	A	1010.53	505.77	993.50	497.25	992.52	496.76	9
10	1571.66	786.33	1554.64	777.82	1553.65	777.33	E	939.49	470.25	922.46	461.74	921.48	461.24	8
11	1700.70	850.86	1683.68	842.34	1682.69	841.85	E	810.45	405.73	793.42	397.21	792.44	396.72	7
12	1771.74	886.37	1754.71	877.86	1753.73	877.37	A	681.40	341.21	664.38	332.69			6
13	1908.80	954.90	1891.77	946.39	1890.79	945.90	H	610.37	305.69	593.34	297.17			5
14	2022.84	1011.93	2005.82	1003.41	2004.83	1002.92	N	473.31	237.16	456.28	228.64			4
15	2135.93	1068.47	2118.90	1059.95	2117.92	1059.46	I	359.27	180.14	342.24	171.62			3
16	2235.00	1118.00	2217.97	1109.49	2216.99	1109.00	V	246.18	123.59	229.15	115.08			2
17							K	147.11	74.06	130.09	65.55			1

Figure SC13. (A) MS/MS of the ARP-HNE modified peptide H*CDEVGFNAEEAHNIVK (B) Full MS spectrum acquired by ESI-LTQ-FT, Δm =3.28 ppm

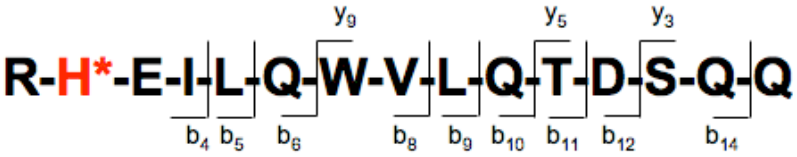

A.

LRC59_Human

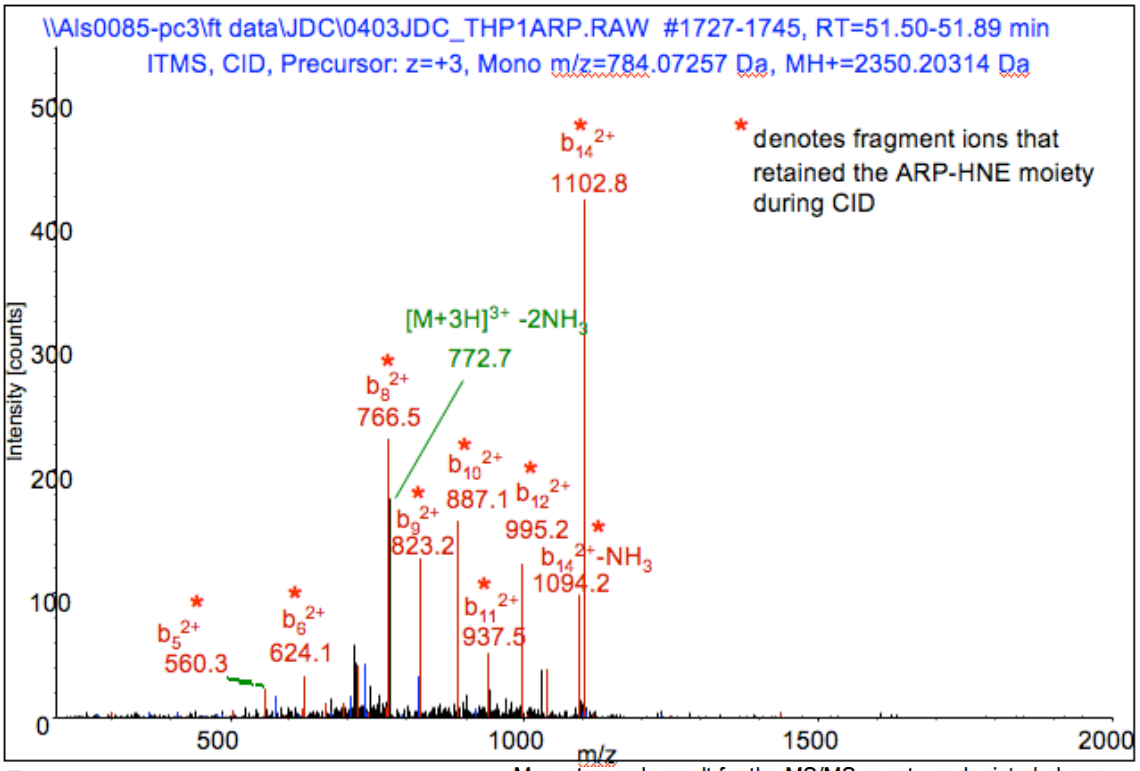

B.

Mascot search result for the MS/MS spectrum depicted above:

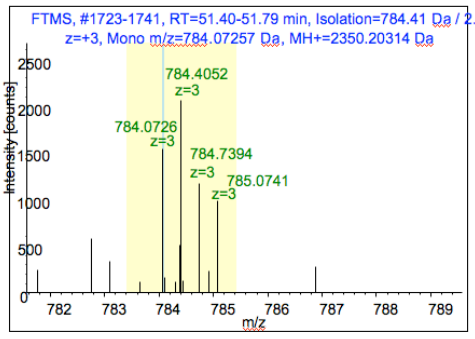

#	b	b++	b*	b*++	b0	b0++	Seq.	y	y++	y*	y*++	y0	y0++	#
1	157.11	79.06	140.08	70.54			R							15
2	763.40	382.21	746.38	373.69			H	2194.10	1097.55	2177.07	1089.04	2176.09	1088.55	14
3	892.45	446.73	875.42	438.21	874.44	437.72	E	1587.80	794.40	1570.77	785.89	1569.79	785.40	13
4	1005.53	503.27	988.50	494.76	987.52	494.26	I	1458.76	729.88	1441.73	721.37	1440.75	720.88	12
5	1118.61	559.81	1101.59	551.30	1100.60	550.81	L	1345.67	673.34	1328.65	664.83	1327.66	664.34	11
6	1246.67	623.84	1229.65	615.33	1228.66	614.83	Q	1232.59	616.80	1215.56	608.29	1214.58	607.79	10
7	1432.75	716.88	1415.73	708.37	1414.74	707.87	W	1104.53	552.77	1087.51	544.26	1086.52	543.76	9
8	1531.82	766.41	1514.79	757.90	1513.81	757.41	V	918.45	459.73	901.43	451.22	900.44	450.72	8
9	1644.90	822.96	1627.88	814.44	1626.89	813.95	L	819.38	410.20	802.36	401.68	801.37	401.19	7
10	1772.96	886.99	1755.94	878.47	1754.95	877.98	Q	706.30	353.65	689.27	345.14	688.29	344.65	6
11	1874.01	937.51	1856.98	929.00	1856.00	928.50	T	578.24	289.62	561.22	281.11	560.23	280.62	5
12	1989.04	995.02	1972.01	986.51	1971.03	986.02	D	477.19	239.10	460.17	230.59	459.18	230.10	4
13	2076.07	1038.54	2059.04	1030.03	2058.06	1029.53	S	362.17	181.59	345.14	173.07	344.16	172.58	3
14	2204.13	1102.57	2187.10	1094.05	2186.12	1093.56	Q	275.13	138.07	258.11	129.56			2
15							Q	147.08	74.04	130.05	65.53			1

Figure SC14. (A) MS/MS of the ARP-HNE modified peptide RH*EILQWVLQTDSQQ (B) Full MS spectrum acquired by ESI-LTQ-FT, Δm = 2.49 ppm

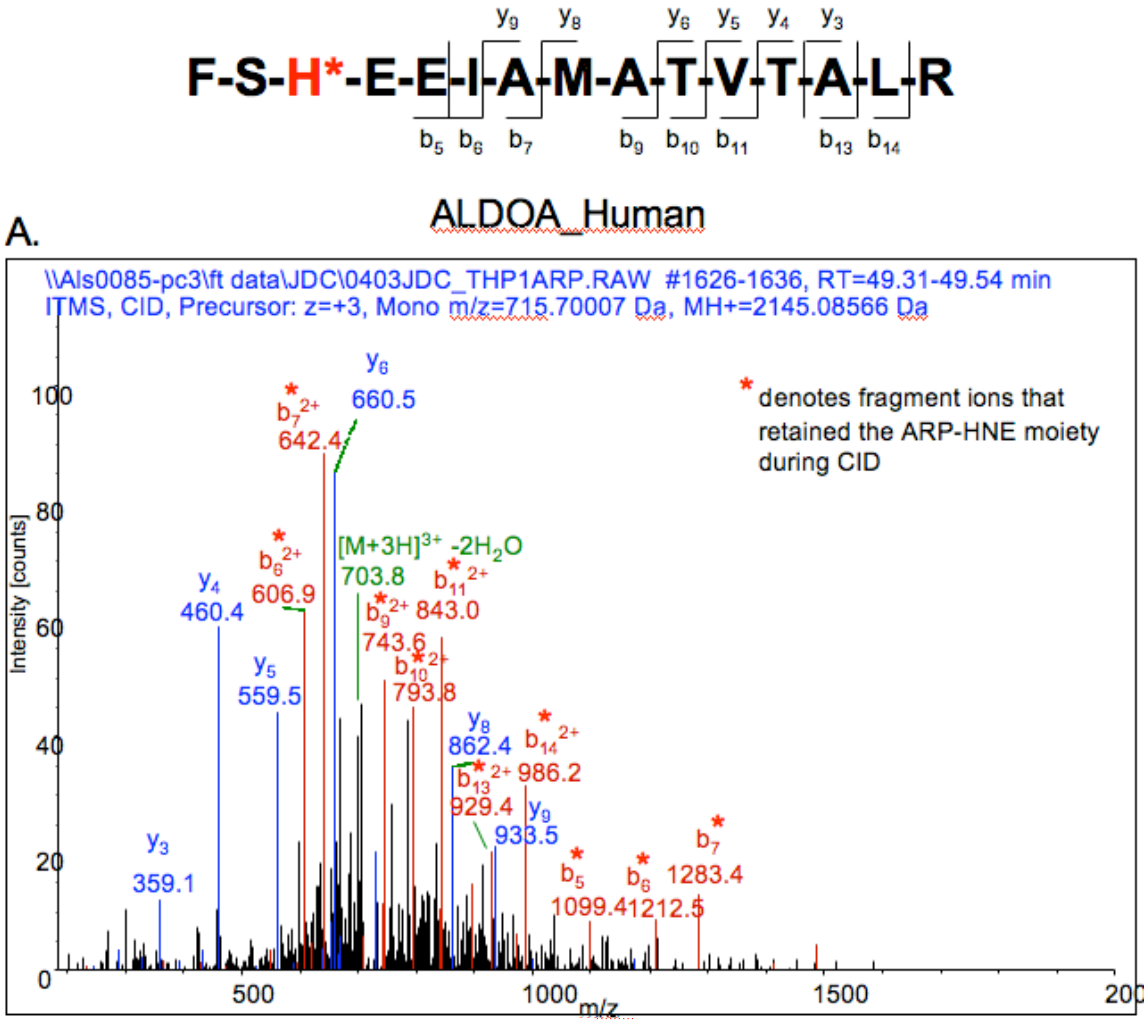

#	b	b++	b0	b0++	Seq.	y	y++	y*	y*++	y0	y0++	#
1	148.08	74.54			F							15
2	235.11	118.06	217.10	109.05	S	1998.01	999.51	1980.99	991.00	1980.00	990.51	14
3	841.40	421.20	823.39	412.20	H	1910.98	955.99	1893.96	947.48	1892.97	946.99	13
4	970.45	485.73	952.43	476.72	E	1304.69	652.85	1287.66	644.33	1286.68	643.84	12
5	1099.49	550.25	1081.48	541.24	E	1175.65	588.33	1158.62	579.81	1157.63	579.32	11
6	1212.57	606.79	1194.56	597.78	I	1046.60	523.80	1029.58	515.29	1028.59	514.80	10
7	1283.61	642.31	1265.60	633.30	A	933.52	467.26	916.49	458.75	915.51	458.26	9
8	1414.65	707.83	1396.64	698.82	M	862.48	431.74	845.45	423.23	844.47	422.74	8
9	1485.69	743.35	1467.68	734.34	A	731.44	366.22	714.41	357.71	713.43	357.22	7
10	1586.73	793.87	1568.72	784.87	T	660.40	330.71	643.38	322.19	642.39	321.70	6
11	1685.80	843.40	1667.79	834.40	V	559.36	280.18	542.33	271.67	541.35	271.18	5
12	1786.85	893.93	1768.84	884.92	T	460.29	230.65	443.26	222.13	442.28	221.64	4
13	1857.89	929.45	1839.88	920.44	A	359.24	180.12	342.21	171.61			3
14	1970.97	985.99	1952.96	976.98	L	288.20	144.61	271.18	136.09			2
15					R	175.12	88.06	158.09	79.55			1

Figure SC15. (A) MS/MS of the ARP-HNE modified peptide FSH*EEIAMATVTALR (B) Full MS spectrum acquired by ESI-LTQ-FT, Δm =1.15 ppm

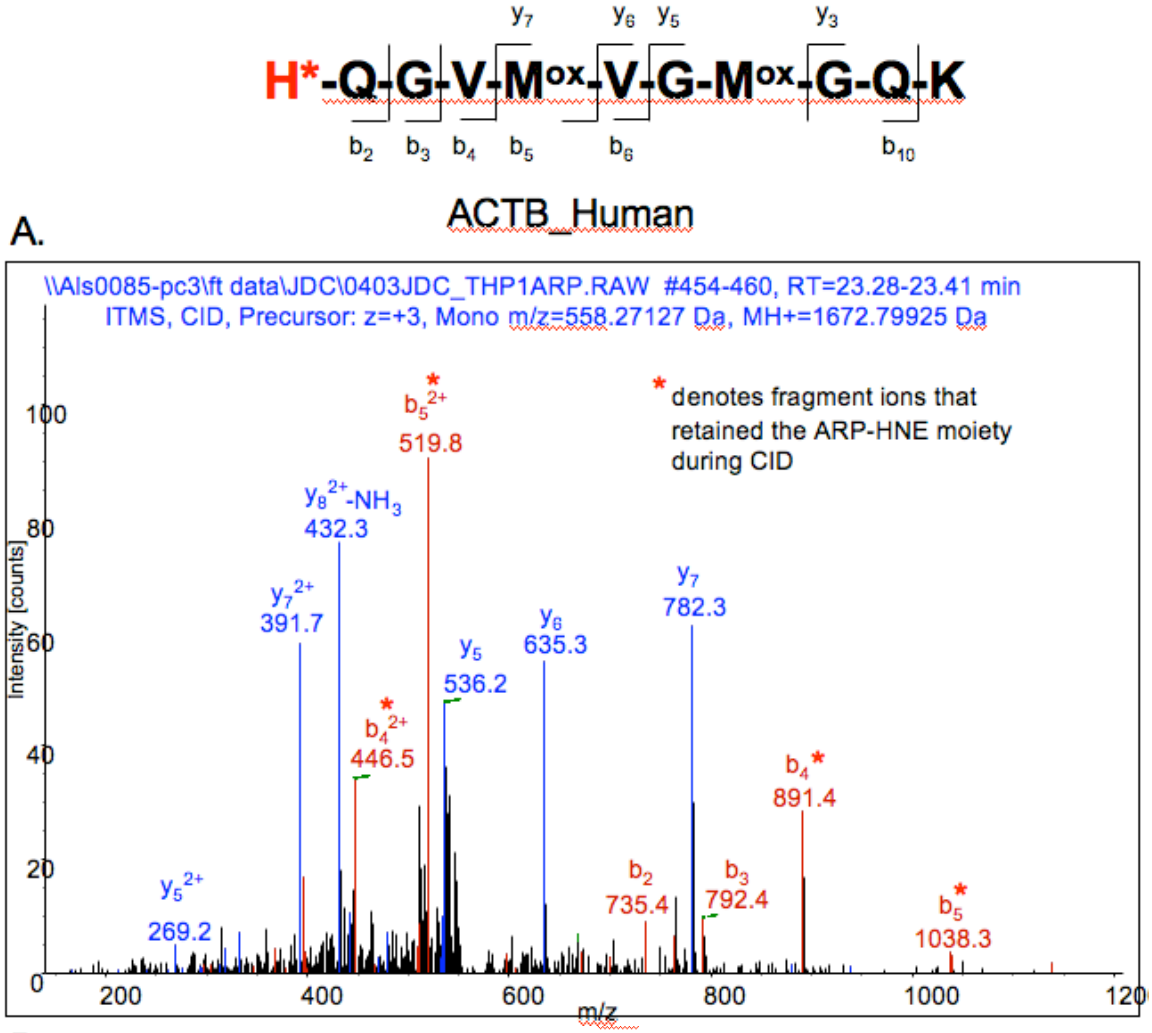

Mascot search result for the MS/MS spectrum depicted above:

#	b	b^{++}	b*	b*$^{++}$	Seq.	y	y^{++}	y*	y*$^{++}$	#
1	607.30	304.15			H					11
2	735.36	368.18	718.33	359.67	Q	1066.50	533.75	1049.48	525.24	10
3	792.38	396.69	775.36	388.18	G	938.44	469.73	921.42	461.21	9
4	891.45	446.23	874.42	437.72	V	881.42	441.21	864.40	432.70	8
5	1038.49	519.75	1021.46	511.23	M	782.35	391.68	765.33	383.17	7
6	1137.55	569.28	1120.53	560.77	V	635.32	318.16	618.29	309.65	6
7	1194.58	597.79	1177.55	589.28	G	536.25	268.63	519.22	260.12	5
8	1341.61	671.31	1324.58	662.80	M	479.23	240.12	462.20	231.60	4
9	1398.63	699.82	1381.61	691.31	G	332.19	166.60	315.17	158.09	3
10	1526.69	763.85	1509.66	755.34	Q	275.17	138.09	258.14	129.58	2
11					K	147.11	74.06	130.09	65.55	1

Figure SC16. (A) MS/MS of the ARP-HNE modified peptide H*QGVMVGMGQK (B) Full MS spectrum acquired by ESI-LTQ-FT, Δm = 1.43 ppm

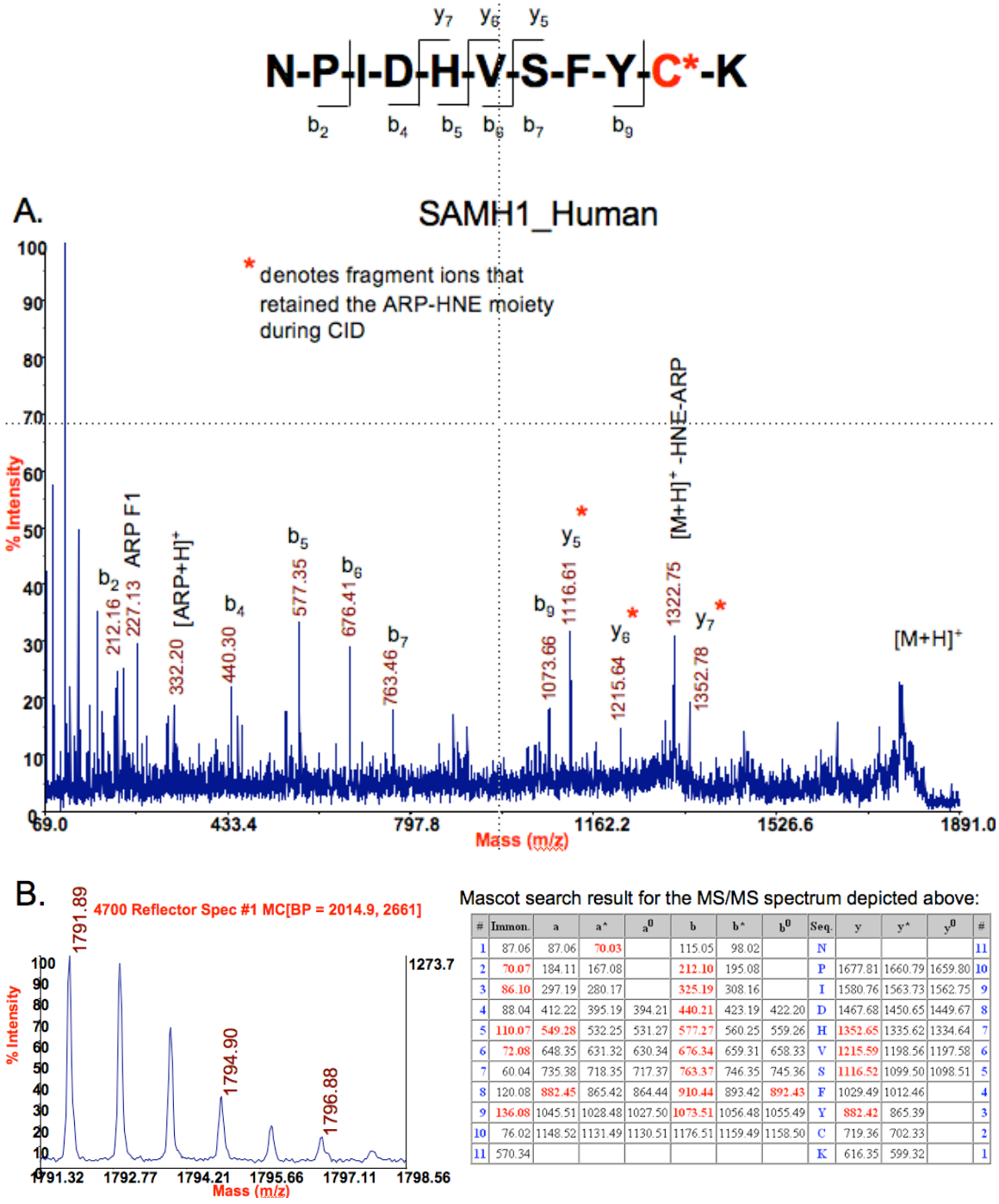

Mascot search result for the MS/MS spectrum depicted above:

#	Immon.	a	a*	a0	b	b*	b0	Seq.	y	y*	y0	#
1	87.06	87.06	70.03		115.05	98.02		N				11
2	70.07	184.11	167.08		212.10	195.08		P	1677.81	1660.79	1659.80	10
3	86.10	297.19	280.17		325.19	308.16		I	1580.76	1563.73	1562.75	9
4	88.04	412.22	395.19	394.21	440.21	423.19	422.20	D	1467.68	1450.65	1449.67	8
5	110.07	549.28	532.25	531.27	577.27	560.25	559.26	H	1352.65	1335.62	1334.64	7
6	72.08	648.35	631.32	630.34	676.34	659.31	658.33	V	1215.59	1198.56	1197.58	6
7	60.04	735.38	718.35	717.37	763.37	746.35	745.36	S	1116.52	1099.50	1098.51	5
8	120.08	882.45	865.42	864.44	910.44	893.42	892.43	F	1029.49	1012.46		4
9	136.08	1045.51	1028.48	1027.50	1073.51	1056.48	1055.49	Y	882.42	865.39		3
10	76.02	1148.52	1131.49	1130.51	1176.51	1159.49	1158.50	C	719.36	702.33		2
11	570.34							K	616.35	599.32		1

Figure SC17. (A) MS/MS of the ARP-HNE modified peptide NPIDHVSFYC*K (B) Full MS spectrum acquired by MALDI-TOF/TOF, Δm = 0.04 Da

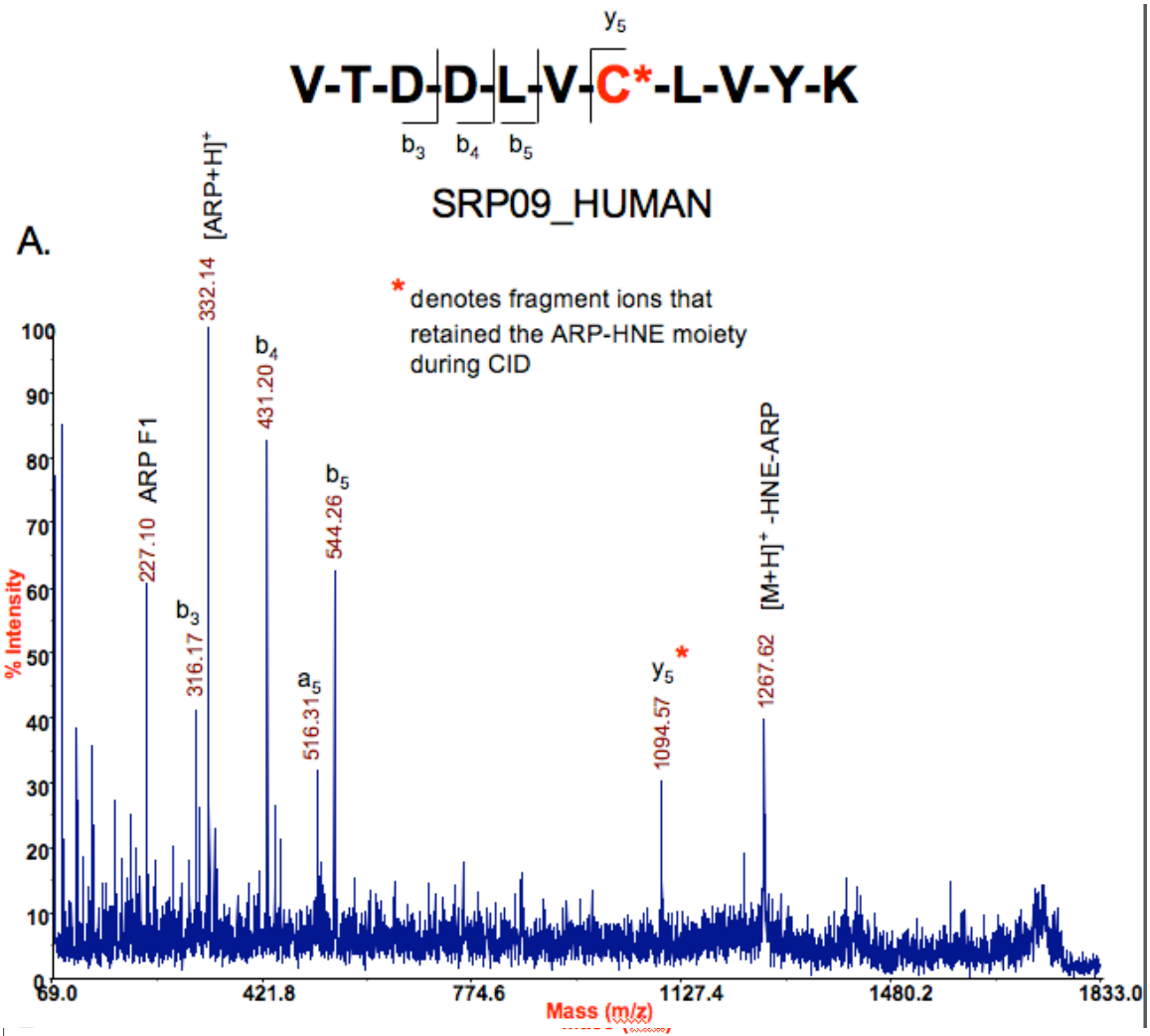

Mascot search result for the MS/MS spectrum depicted above:

#	Immon.	a	a^0	b	b^0	Seq.	y	y^*	y^0	#
1	72.08	72.08		100.08		V				11
2	74.06	173.13	155.12	201.12	183.11	T	1637.83	1620.80	1619.82	10
3	88.04	288.16	270.14	316.15	298.14	D	1536.78	1519.75	1518.77	9
4	88.04	403.18	385.17	431.18	413.17	D	1421.75	1404.73	1403.74	8
5	86.10	516.27	498.26	544.26	526.25	L	1306.73	1289.70		7
6	72.08	615.33	597.32	643.33	625.32	V	1193.64	1176.62		6
7	76.02	718.34	700.33	746.34	728.33	C	1094.57	1077.55		5
8	86.10	831.43	813.42	859.42	841.41	L	991.56	974.54		4
9	72.08	930.50	912.49	958.49	940.48	V	878.48	861.45		3
10	136.08	1093.56	1075.55	1121.55	1103.54	Y	779.41	762.39		2
11	570.34					K	616.35	599.32		1

Figure SC18. (A) MS/MS of the ARP-HNE modified peptide VTDDLVC*LVYK (B) Full MS spectrum acquired by MALDI-TOF/TOF, Δm = 0.17 Da

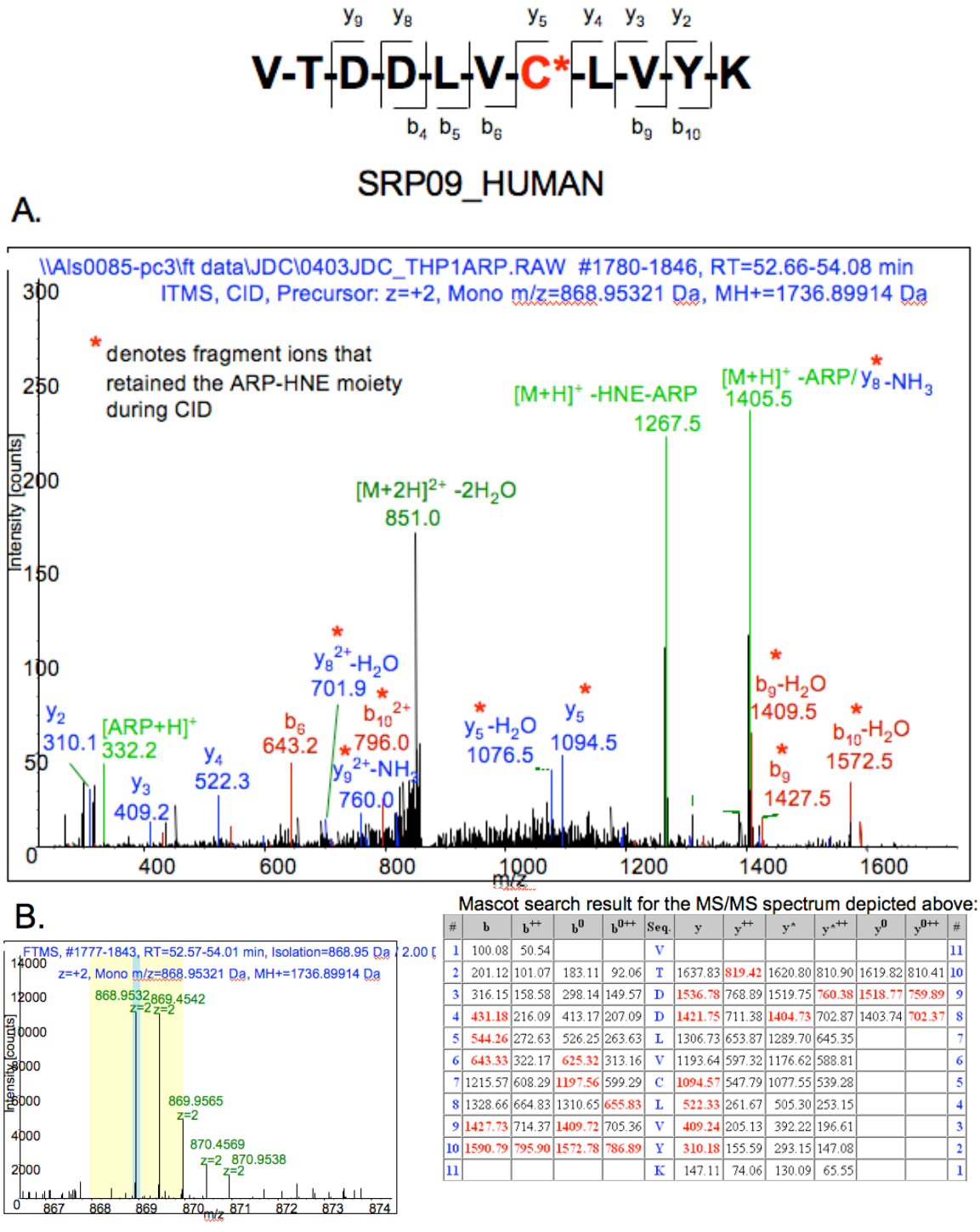

Mascot search result for the MS/MS spectrum depicted above:

#	b	b++	b0	b0++	Seq.	y	y++	y*	y*++	y0	y0++	#
1	100.08	50.54			V							11
2	201.12	101.07	183.11	92.06	T	1637.83	819.42	1620.80	810.90	1619.82	810.41	10
3	316.15	158.58	298.14	149.57	D	1536.78	768.89	1519.75	760.38	1518.77	759.89	9
4	431.18	216.09	413.17	207.09	D	1421.75	711.38	1404.73	702.87	1403.74	702.37	8
5	544.26	272.63	526.25	263.63	L	1306.73	653.87	1289.70	645.35			7
6	643.33	322.17	625.32	313.16	V	1193.64	597.32	1176.62	588.81			6
7	1215.57	608.29	1197.56	599.29	C	1094.57	547.79	1077.55	539.28			5
8	1328.66	664.83	1310.65	655.83	L	522.33	261.67	505.30	253.15			4
9	1427.73	714.37	1409.72	705.36	V	409.24	205.13	392.22	196.61			3
10	1590.79	795.90	1572.78	786.89	Y	310.18	155.59	293.15	147.08			2
11					K	147.11	74.06	130.09	65.55			1

Figure SC19. (A) MS/MS of the ARP-HNE modified peptide VTDDLVC*LVYK (B) Full MS spectrum acquired by ESI-LTQ-FT, Δm = 1.73 ppm

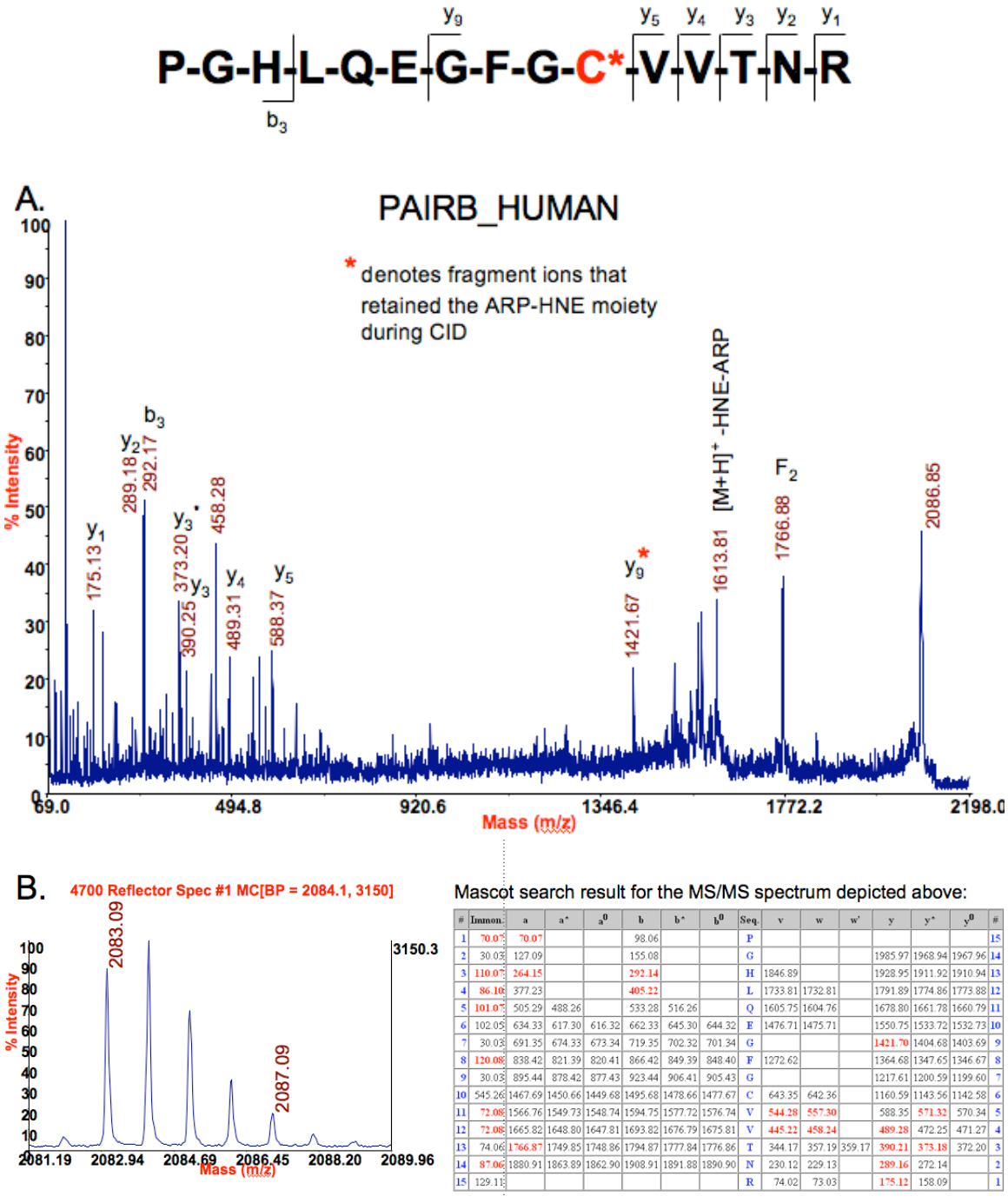

#	Immon.	a	a*	a0	b	b*	b0	Seq.	v	w	w'	y	y*	y0	#
1	70.07	70.07			98.06			P							15
2	30.03	127.09			155.08			G				1985.97	1968.94	1967.96	14
3	110.07	264.15			292.14			H	1846.89			1928.95	1911.92	1910.94	13
4	86.10	377.23			405.22			L	1733.81	1732.81		1791.89	1774.86	1773.88	12
5	101.07	505.29	488.26		533.28	516.26		Q	1605.75	1604.76		1678.80	1661.78	1660.79	11
6	102.05	634.33	617.30	616.32	662.33	645.30	644.32	E	1476.71	1475.71		1550.75	1533.72	1532.73	10
7	30.03	691.35	674.33	673.34	719.35	702.32	701.34	G				1421.70	1404.68	1403.69	9
8	120.08	838.42	821.39	820.41	866.42	849.39	848.40	F	1272.62			1364.68	1347.65	1346.67	8
9	30.03	895.44	878.42	877.43	923.44	906.41	905.43	G				1217.61	1200.59	1199.60	7
10	545.26	1467.69	1450.66	1449.68	1495.68	1478.66	1477.67	C	643.35	642.36		1160.59	1143.56	1142.58	6
11	72.08	1566.76	1549.73	1548.74	1594.75	1577.72	1576.74	V	544.28	557.30		588.35	571.32	570.34	5
12	72.08	1665.82	1648.80	1647.81	1693.82	1676.79	1675.81	V	445.22	458.24		489.28	472.25	471.27	4
13	74.06	1766.87	1749.85	1748.86	1794.87	1777.84	1776.86	T	344.17	357.19	359.17	390.21	373.18	372.20	3
14	87.06	1880.91	1863.89	1862.90	1908.91	1891.88	1890.90	N	230.12	229.13		289.16	272.14		2
15	129.11							R	74.02	73.03		175.12	158.09		1

Figure SC20. (A) MS/MS of the ARP-HNE modified peptide PGHLQEGFGC*VVTNR (B) Full MS spectrum acquired by MALDI-TOF/TOF, Δm = 0.07 Da

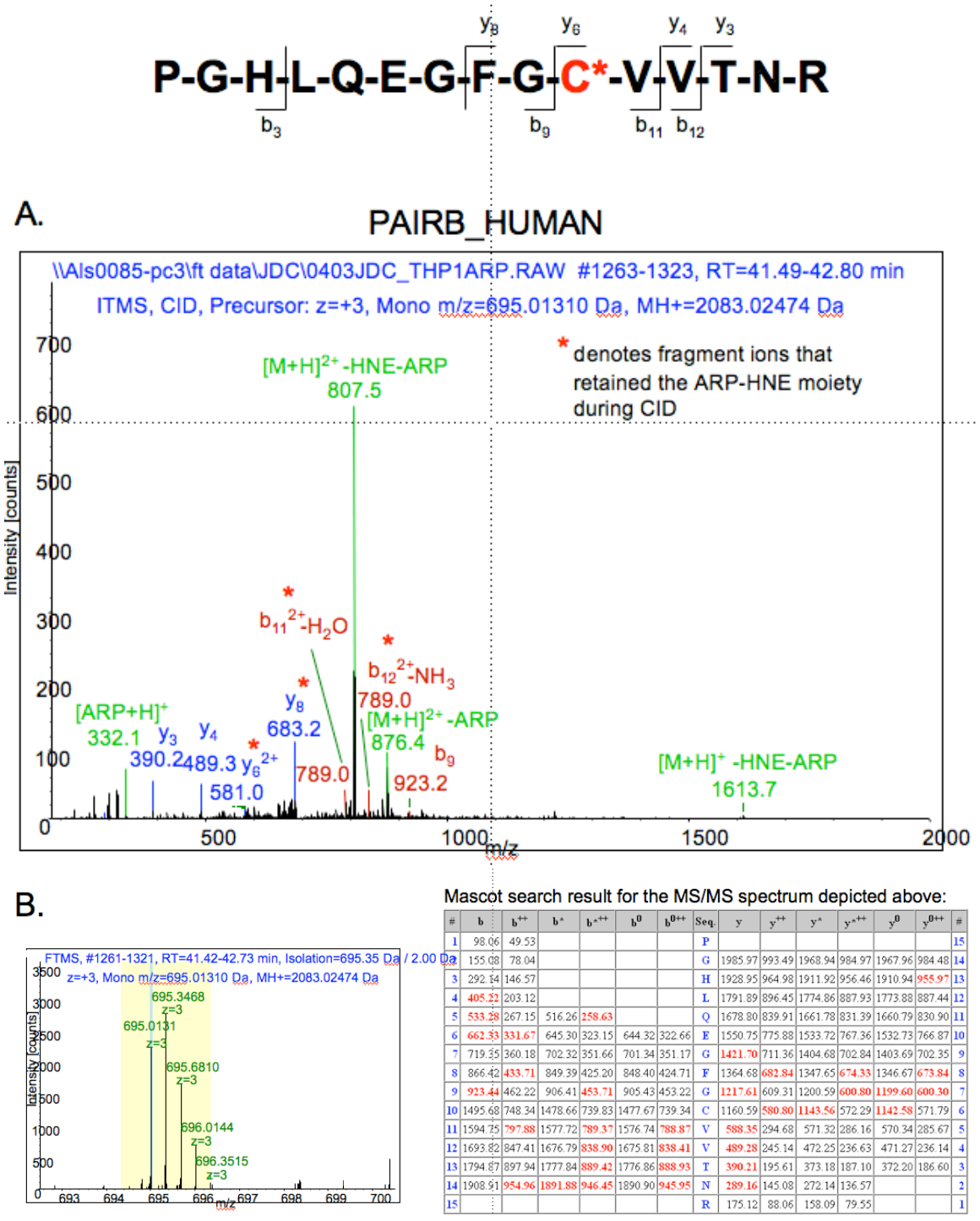

#	b	b++	b*	b*++	b0	b0++	Seq.	y	y++	y*	y*++	y0	y0++	#
1	98.06	49.53					P							15
2	155.08	78.04					G	1985.97	993.49	1968.94	984.97	1967.96	984.48	14
3	292.14	146.57					H	1928.95	964.98	1911.92	956.46	1910.94	955.97	13
4	405.22	203.12					L	1791.89	896.45	1774.86	887.93	1773.88	887.44	12
5	533.28	267.15	516.26	258.63			Q	1678.80	839.91	1661.78	831.39	1660.79	830.90	11
6	662.33	331.67	645.30	323.15	644.32	322.66	E	1550.75	775.88	1533.72	767.36	1532.73	766.87	10
7	719.35	360.18	702.32	351.66	701.34	351.17	G	1421.70	711.36	1404.68	702.84	1403.69	702.35	9
8	866.42	433.71	849.39	425.20	848.40	424.71	F	1364.68	682.84	1347.65	674.33	1346.67	673.84	8
9	923.44	462.22	906.41	453.71	905.43	453.22	G	1217.61	609.31	1200.59	600.80	1199.60	600.30	7
10	1495.68	748.34	1478.66	739.83	1477.67	739.34	C	1160.59	580.80	1143.56	572.29	1142.58	571.79	6
11	1594.75	797.88	1577.72	789.37	1576.74	788.87	V	588.35	294.68	571.32	286.16	570.34	285.67	5
12	1693.82	847.41	1676.79	838.90	1675.81	838.41	V	489.28	245.14	472.25	236.63	471.27	236.14	4
13	1794.87	897.94	1777.84	889.42	1776.86	888.93	T	390.21	195.61	373.18	187.10	372.20	186.60	3
14	1908.91	954.96	1891.88	946.45	1890.90	945.95	N	289.16	145.08	272.14	136.57			2
15							R	175.12	88.06	158.09	79.55			1

Figure SC21. (A) MS/MS of the ARP-HNE modified peptide PGHLQEGFGC*VVTNR (B) Full MS spectrum acquired by ESI-LTQ-FT, Δm = 1.71 ppm

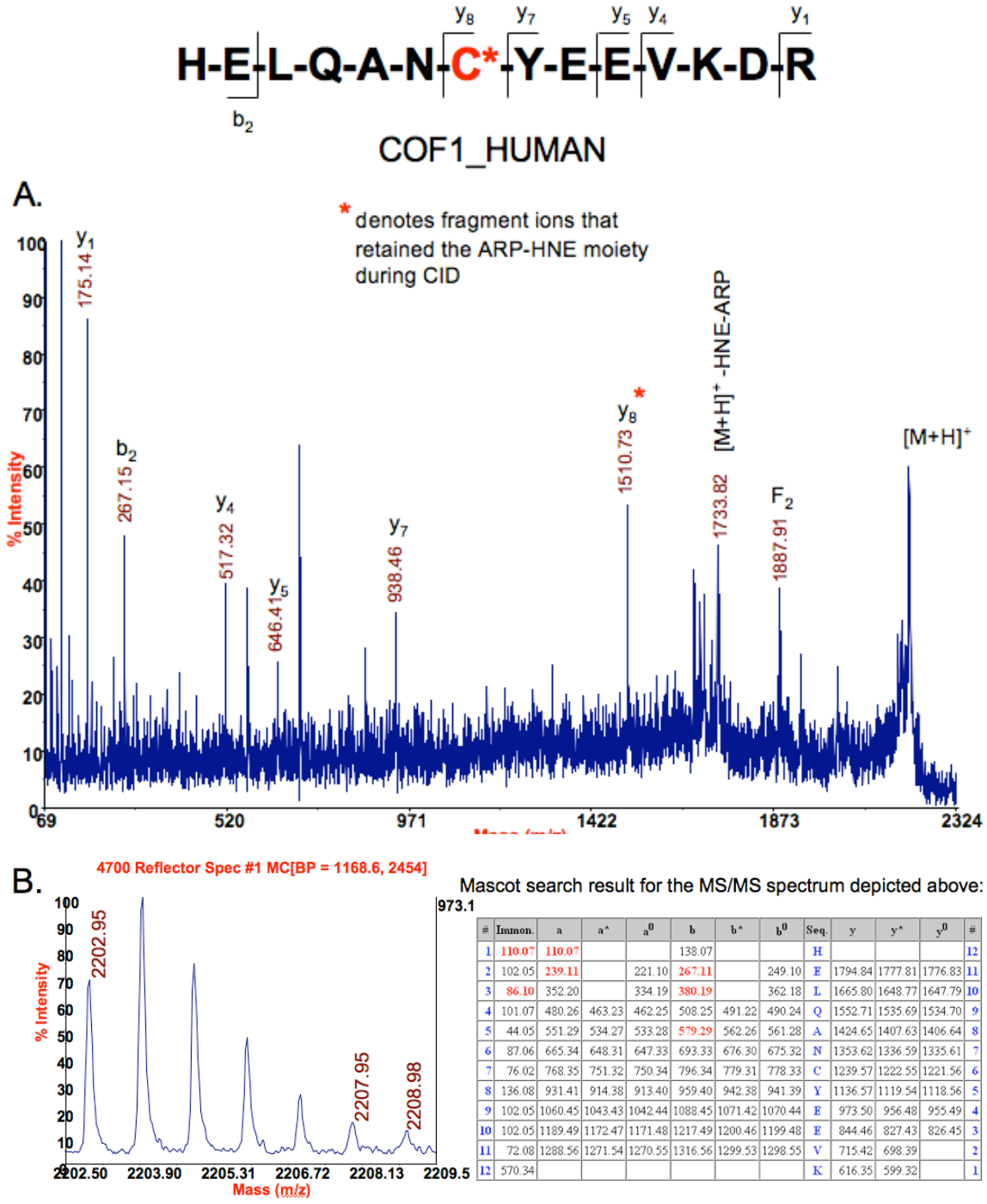

#	Immon.	a	a*	a0	b	b*	b0	Seq.	y	y*	y0	#
1	110.07	110.07			138.07			H				12
2	102.05	239.11		221.10	267.11		249.10	E	1794.84	1777.81	1776.83	11
3	86.10	352.20		334.19	380.19		362.18	L	1665.80	1648.77	1647.79	10
4	101.07	480.26	463.23	462.25	508.25	491.22	490.24	Q	1552.71	1535.69	1534.70	9
5	44.05	551.29	534.27	533.28	579.29	562.26	561.28	A	1424.65	1407.63	1406.64	8
6	87.06	665.34	648.31	647.33	693.33	676.30	675.32	N	1353.62	1336.59	1335.61	7
7	76.02	768.35	751.32	750.34	796.34	779.31	778.33	C	1239.57	1222.55	1221.56	6
8	136.08	931.41	914.38	913.40	959.40	942.38	941.39	Y	1136.57	1119.54	1118.56	5
9	102.05	1060.45	1043.43	1042.44	1088.45	1071.42	1070.44	E	973.50	956.48	955.49	4
10	102.05	1189.49	1172.47	1171.48	1217.49	1200.46	1199.48	E	844.46	827.43	826.45	3
11	72.08	1288.56	1271.54	1270.55	1316.56	1299.53	1298.55	V	715.42	698.39		2
12	570.34							K	616.35	599.32		1

Figure SC22. (A) MS/MS of the ARP-HNE modified peptide HELQANC*YEEVKDR (B) Full MS spectrum acquired by MALDI-TOF/TOF, Δm = 0.01 Da

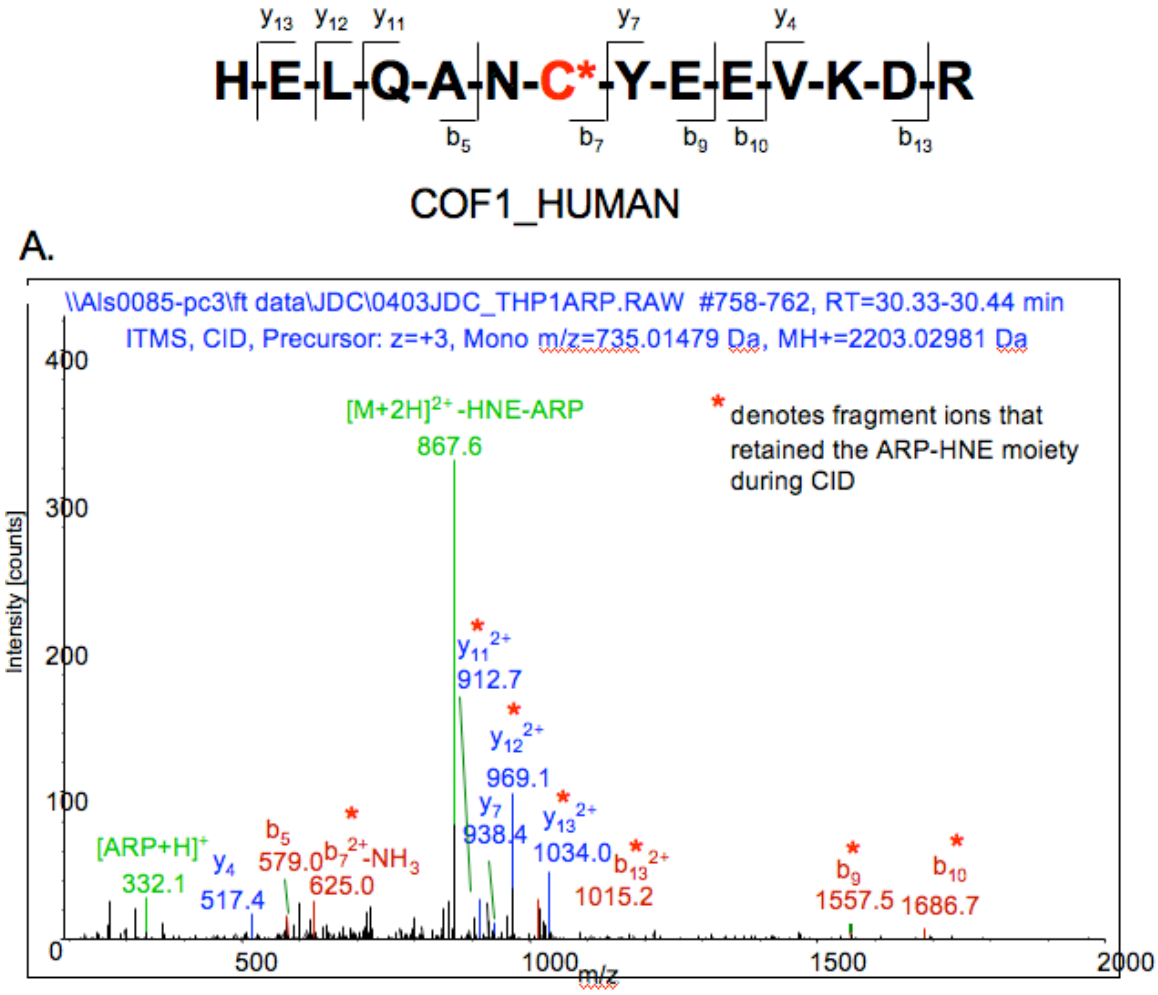

Mascot search result for the MS/MS spectrum depicted above:

#	b	b++	b*	b*++	b0	b0++	Seq.	y	y++	y*	y*++	y0	y0++	#
1	138.07	69.54					H							14
2	267.11	134.06			249.10	125.05	E	2065.97	1033.49	2048.94	1024.97	2047.96	1024.48	13
3	380.19	190.60			362.18	181.59	L	1936.93	968.97	1919.90	960.45	1918.91	959.96	12
4	508.25	254.63	491.22	246.12	490.24	245.62	Q	1823.84	912.42	1806.81	903.91	1805.83	903.42	11
5	579.29	290.15	562.26	281.63	561.28	281.14	A	1695.78	848.40	1678.76	839.88	1677.77	839.39	10
6	693.33	347.17	676.30	338.66	675.32	338.16	N	1624.75	812.88	1607.72	804.36	1606.74	803.87	9
7	1265.58	633.29	1248.55	624.78	1247.57	624.29	C	1510.70	755.86	1493.68	747.34	1492.69	746.85	8
8	1428.64	714.82	1411.61	706.31	1410.63	705.82	Y	938.46	469.73	921.43	461.22	920.45	460.73	7
9	1557.68	779.34	1540.66	770.83	1539.67	770.34	E	775.39	388.20	758.37	379.69	757.38	379.20	6
10	1686.73	843.87	1669.70	835.35	1668.71	834.86	E	646.35	323.68	629.33	315.17	628.34	314.67	5
11	1785.79	893.40	1768.77	884.89	1767.78	884.40	V	517.31	259.16	500.28	250.64	499.30	250.15	4
12	1913.89	957.45	1896.86	948.93	1895.88	948.44	K	418.24	209.62	401.21	201.11	400.23	200.62	3
13	2028.92	1014.96	2011.89	1006.45	2010.90	1005.96	D	290.15	145.58	273.12	137.06	272.14	136.57	2
14							R	175.12	88.06	158.09	79.55			1

Figure SC23. (A) MS/MS of the ARP-HNE modified peptide HELQANC*YEEVKDR (B) Full MS spectrum acquired by ESI-LTQ-FT, Δm = 1.28 ppm

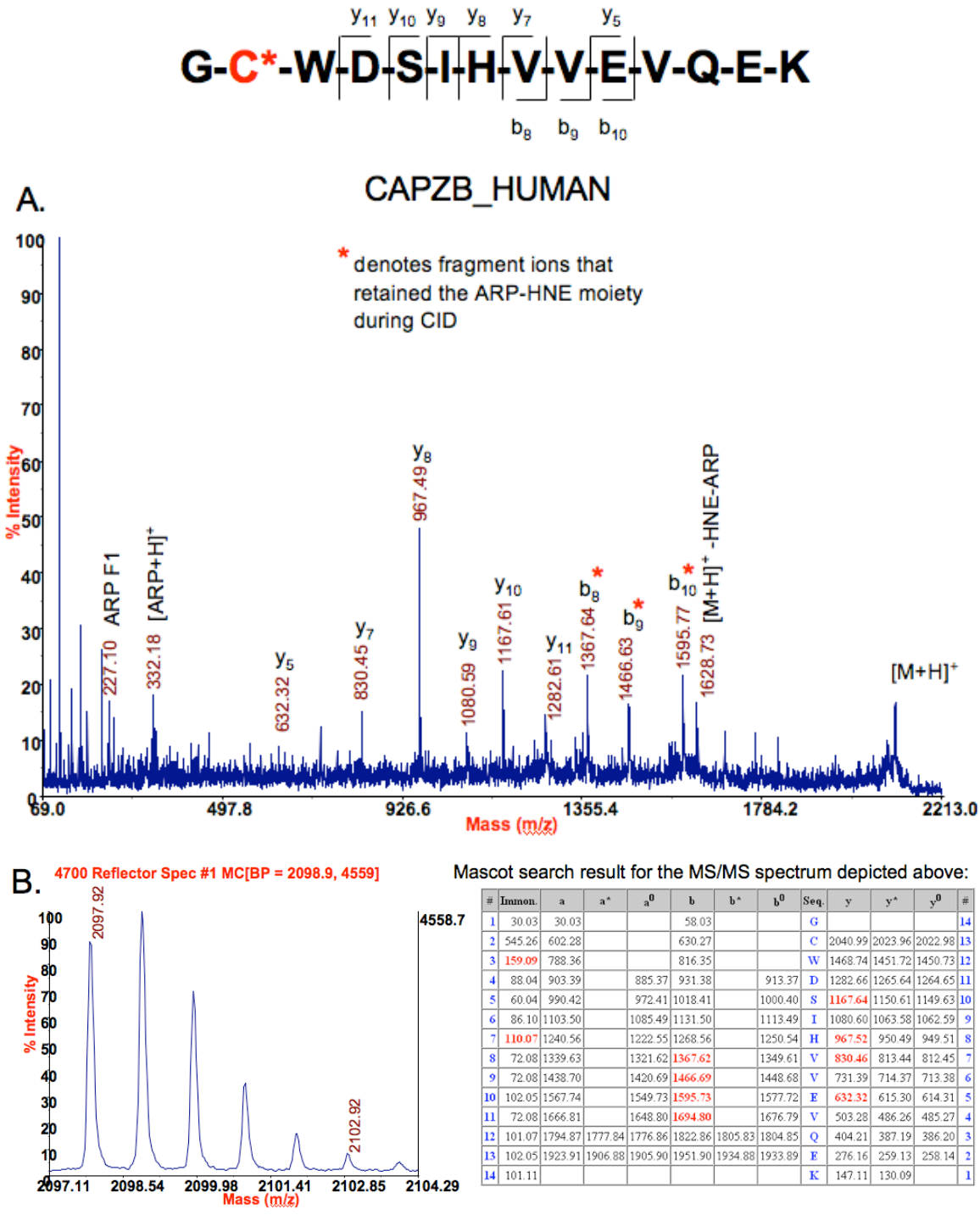

#	Immon.	a	a*	a0	b	b*	b0	Seq.	y	y*	y0	#
1	30.03	30.03			58.03			G				14
2	545.26	602.28			630.27			C	2040.99	2023.96	2022.98	13
3	159.09	788.36			816.35			W	1468.74	1451.72	1450.73	12
4	88.04	903.39		885.37	931.38		913.37	D	1282.66	1265.64	1264.65	11
5	60.04	990.42		972.41	1018.41		1000.40	S	1167.64	1150.61	1149.63	10
6	86.10	1103.50		1085.49	1131.50		1113.49	I	1080.60	1063.58	1062.59	9
7	110.07	1240.56		1222.55	1268.56		1250.54	H	967.52	950.49	949.51	8
8	72.08	1339.63		1321.62	1367.62		1349.61	V	830.46	813.44	812.45	7
9	72.08	1438.70		1420.69	1466.69		1448.68	V	731.39	714.37	713.38	6
10	102.05	1567.74		1549.73	1595.73		1577.72	E	632.32	615.30	614.31	5
11	72.08	1666.81		1648.80	1694.80		1676.79	V	503.28	486.26	485.27	4
12	101.07	1794.87	1777.84	1776.86	1822.86	1805.83	1804.85	Q	404.21	387.19	386.20	3
13	102.05	1923.91	1906.88	1905.90	1951.90	1934.88	1933.89	E	276.16	259.13	258.14	2
14	101.11							K	147.11	130.09		1

Figure SC24. (A) MS/MS of the ARP-HNE modified peptide GC*WDSIHVVEVQEK (B) Full MS spectrum acquired by MALDI-TOF/TOF, Δm = -0.09 Da

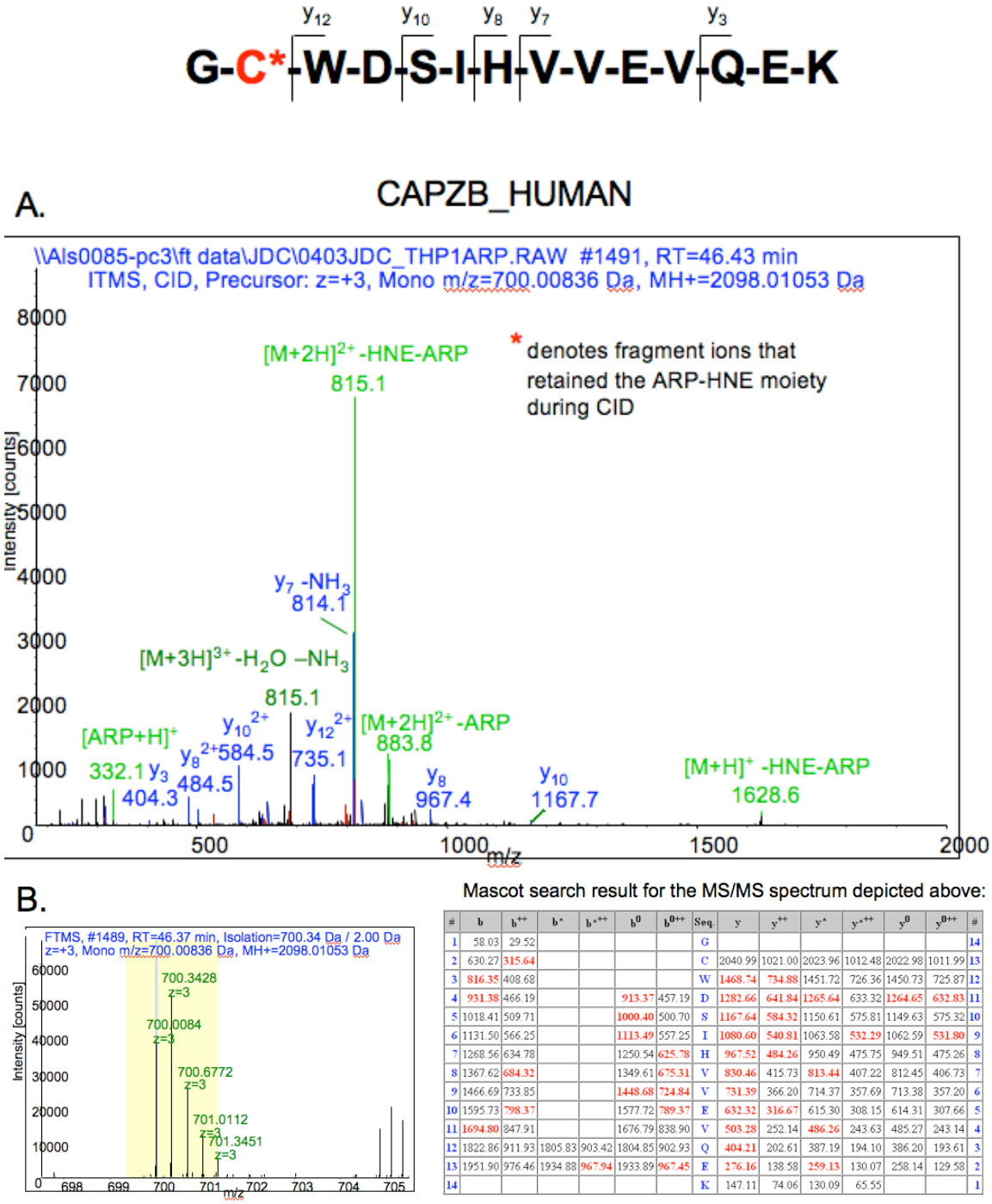

#	b	b++	b*	b*++	b0	b0++	Seq.	y	y++	y*	y*++	y0	y0++	#
1	58.03	29.52					G							14
2	630.27	315.64					C	2040.99	1021.00	2023.96	1012.48	2022.98	1011.99	13
3	816.35	408.68					W	1468.74	734.88	1451.72	726.36	1450.73	725.87	12
4	931.38	466.19			913.37	457.19	D	1282.66	641.84	1265.64	633.32	1264.65	632.83	11
5	1018.41	509.71			1000.40	500.70	S	1167.64	584.32	1150.61	575.81	1149.63	575.32	10
6	1131.50	566.25			1113.49	557.25	I	1080.60	540.81	1063.58	532.29	1062.59	531.80	9
7	1268.56	634.78			1250.54	625.78	H	967.52	484.26	950.49	475.75	949.51	475.26	8
8	1367.62	684.32			1349.61	675.31	V	830.46	415.73	813.44	407.22	812.45	406.73	7
9	1466.69	733.85			1448.68	724.84	V	731.39	366.20	714.37	357.69	713.38	357.20	6
10	1595.73	798.37			1577.72	789.37	E	632.32	316.67	615.30	308.15	614.31	307.66	5
11	1694.80	847.91			1676.79	838.90	V	503.28	252.14	486.26	243.63	485.27	243.14	4
12	1822.86	911.93	1805.83	903.42	1804.85	902.93	Q	404.21	202.61	387.19	194.10	386.20	193.61	3
13	1951.90	976.46	1934.88	967.94	1933.89	967.45	E	276.16	138.58	259.13	130.07	258.14	129.58	2
14							K	147.11	74.06	130.09	65.55			1

Figure SC25. (A) MS/MS of the ARP-HNE modified peptide GC*WDSIHVVEVQEK (B) Full MS spectrum acquired by ESI-LTQ-FT, Δm = 1.48 ppm

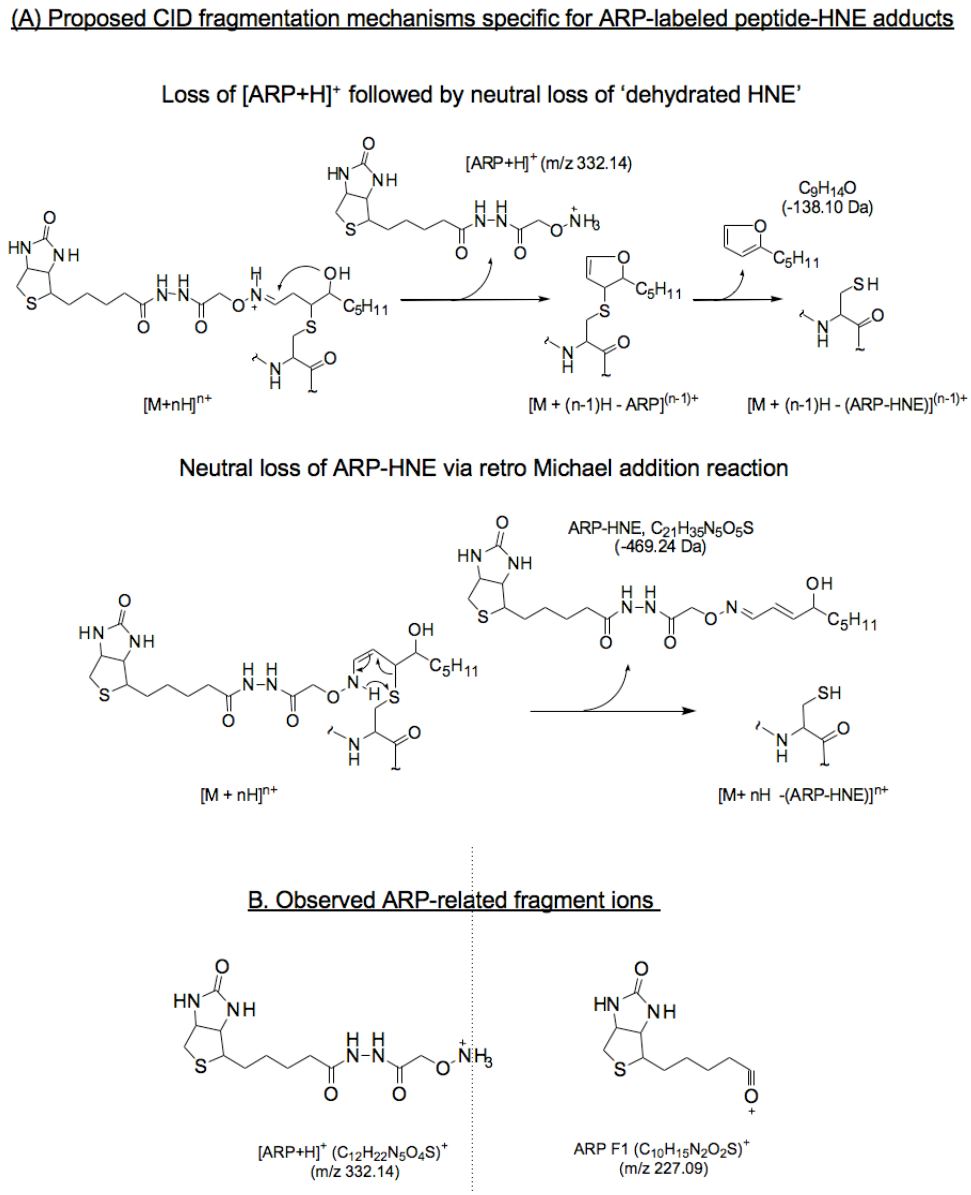

Figure SC26. (A) Proposed CID fragmentation mechanisms specific for ARP-labeled HNE-modified peptides. (B) Fragment ions generated by the ARP tag in CID MS/MS experiments

Appendix D

Supplemental Materials For Chapter 6

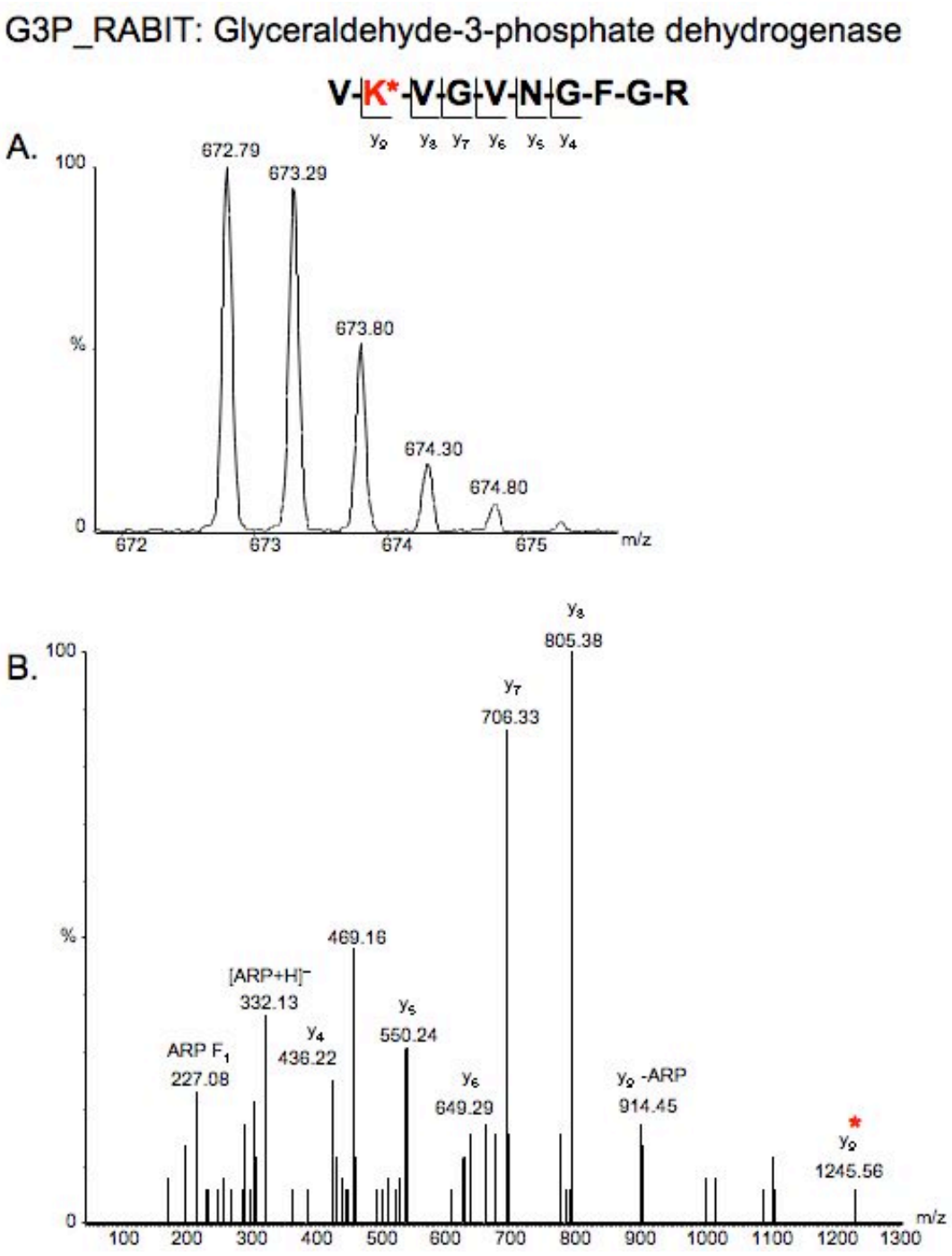

Figure SD1 – (A) Full mass spectrum and (B) MS/MS spectrum acquired by ESI-Q-TOF of the $[M+2H]^{2+}$ ion of the ARP labeled AAS modified peptide VK*VGVNGFGR; monoisotopic m/z_{calc} 672.85 ; accuracy $\Delta(m/z)$ = -0.06 m/z

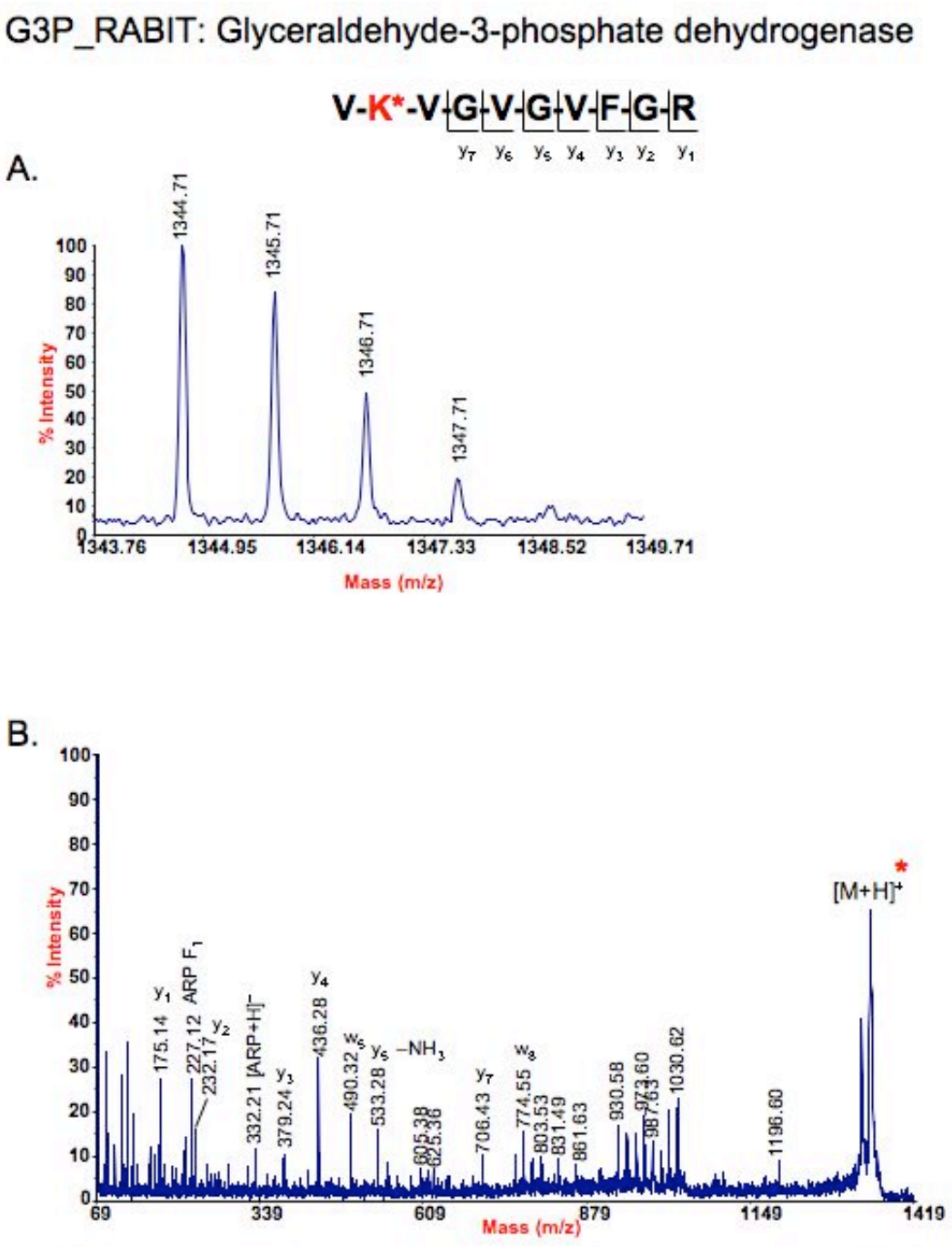

Figure SD2 – (A) Full mass spectrum and (B) MS/MS spectrum acquired by MALDI-TOF/TOF of the $[M+H]^+$ ion of the ARP labeled AAS modified peptide VK*VGVGVFGR; monoisotopic m/z_{calc} 1344.68; accuracy $\Delta(m/z)$ = 0.03 m/z

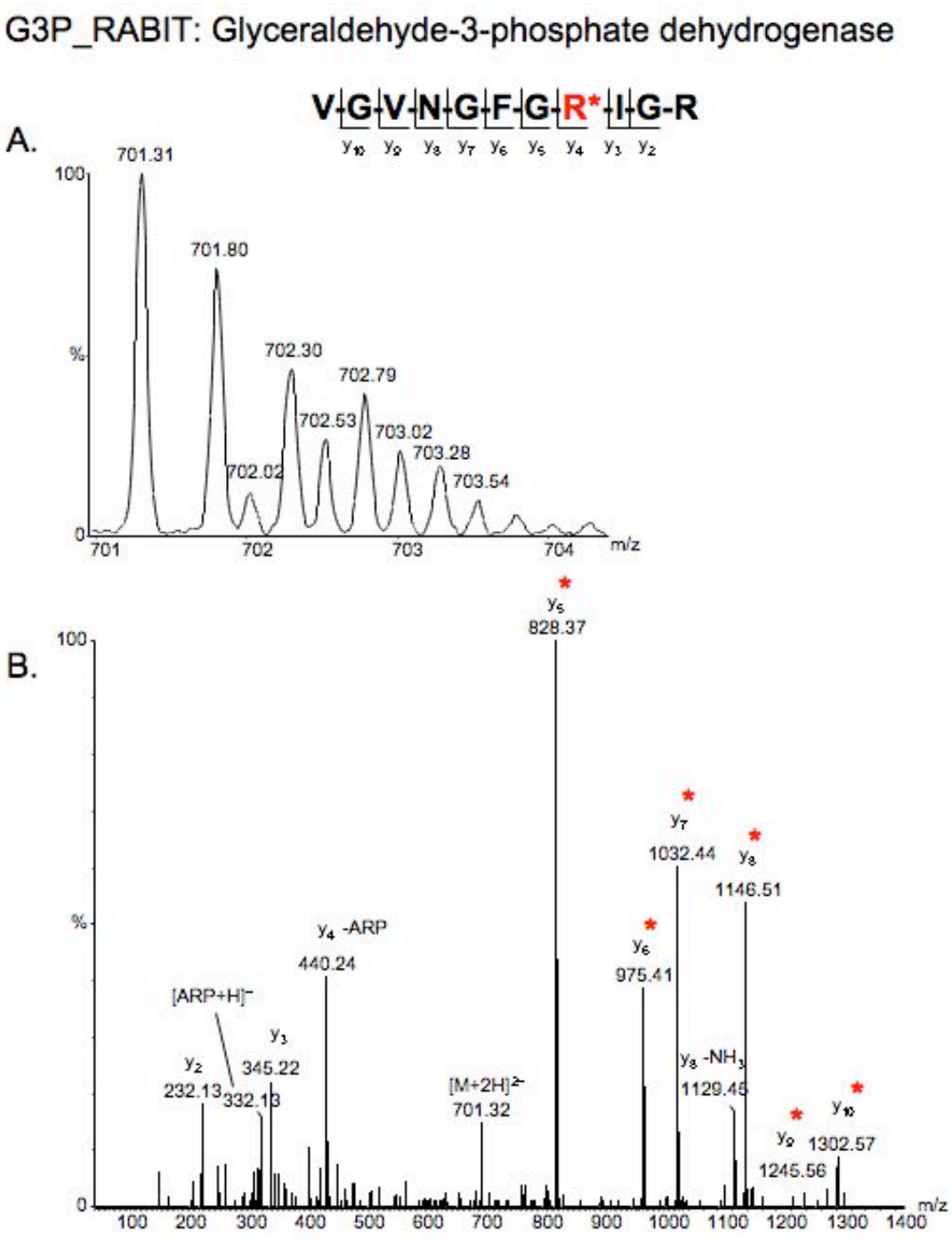

Figure SD3 – (A) Full mass spectrum and (B) MS/MS spectrum acquired by ESI-Q-TOF of the $[M+2H]^{2+}$ ion of the ARP labeled GGS modified peptide VGVNGFGR*IGR; monoisotopic m/z_{calc} 701.36; accuracy $\Delta(m/z)$ = -0.05 m/z

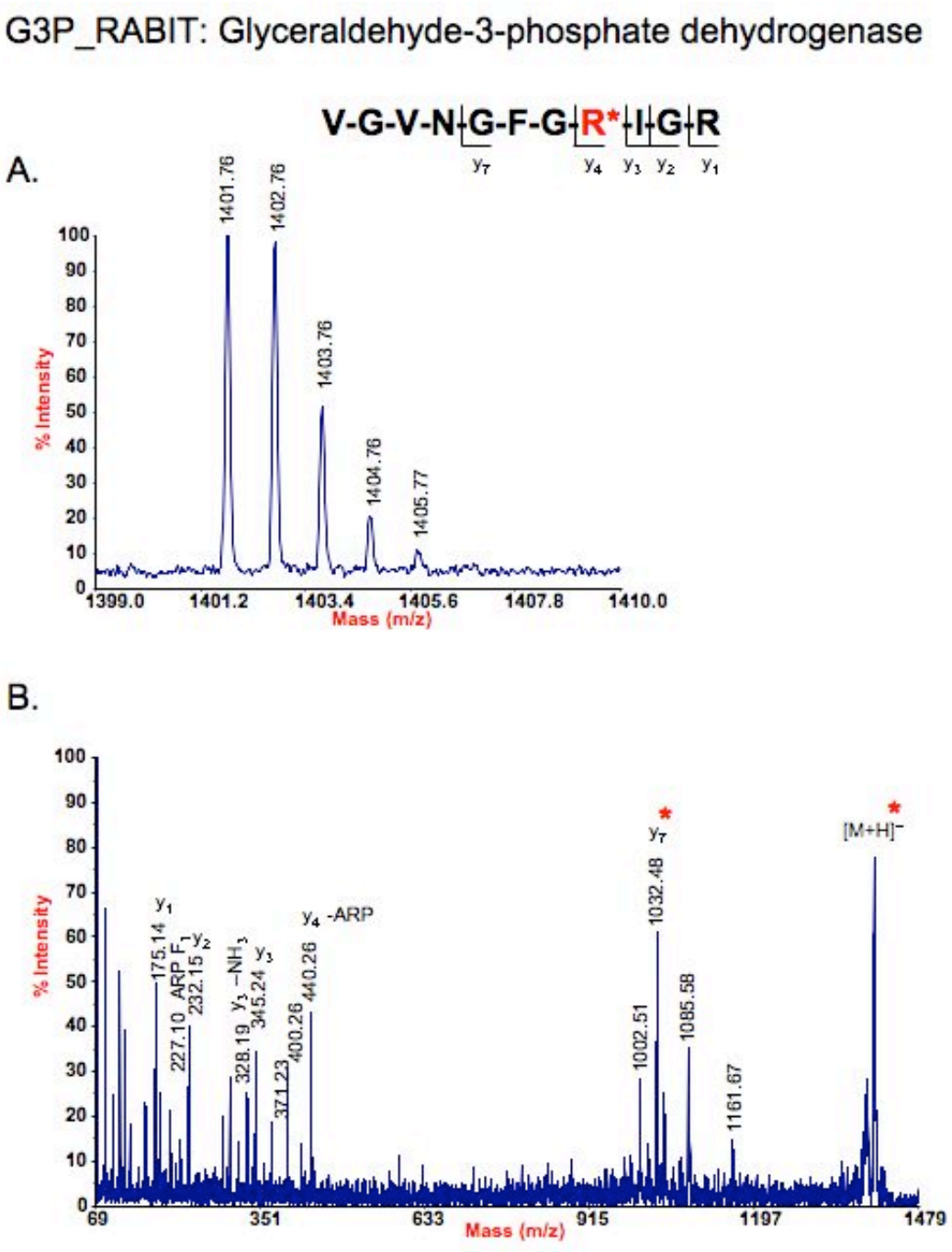

Figure SD4 – (A) Full mass spectrum and (B) MS/MS spectrum acquired by MALDI-TOF/TOF of the $[M+H]^+$ ion of the ARP labeled GGS modified peptide VGVNGFGR*IGR; monoisotopic m/z_{calc} 1401.71; accuracy $\Delta(m/z)$ = 0.05 m/z

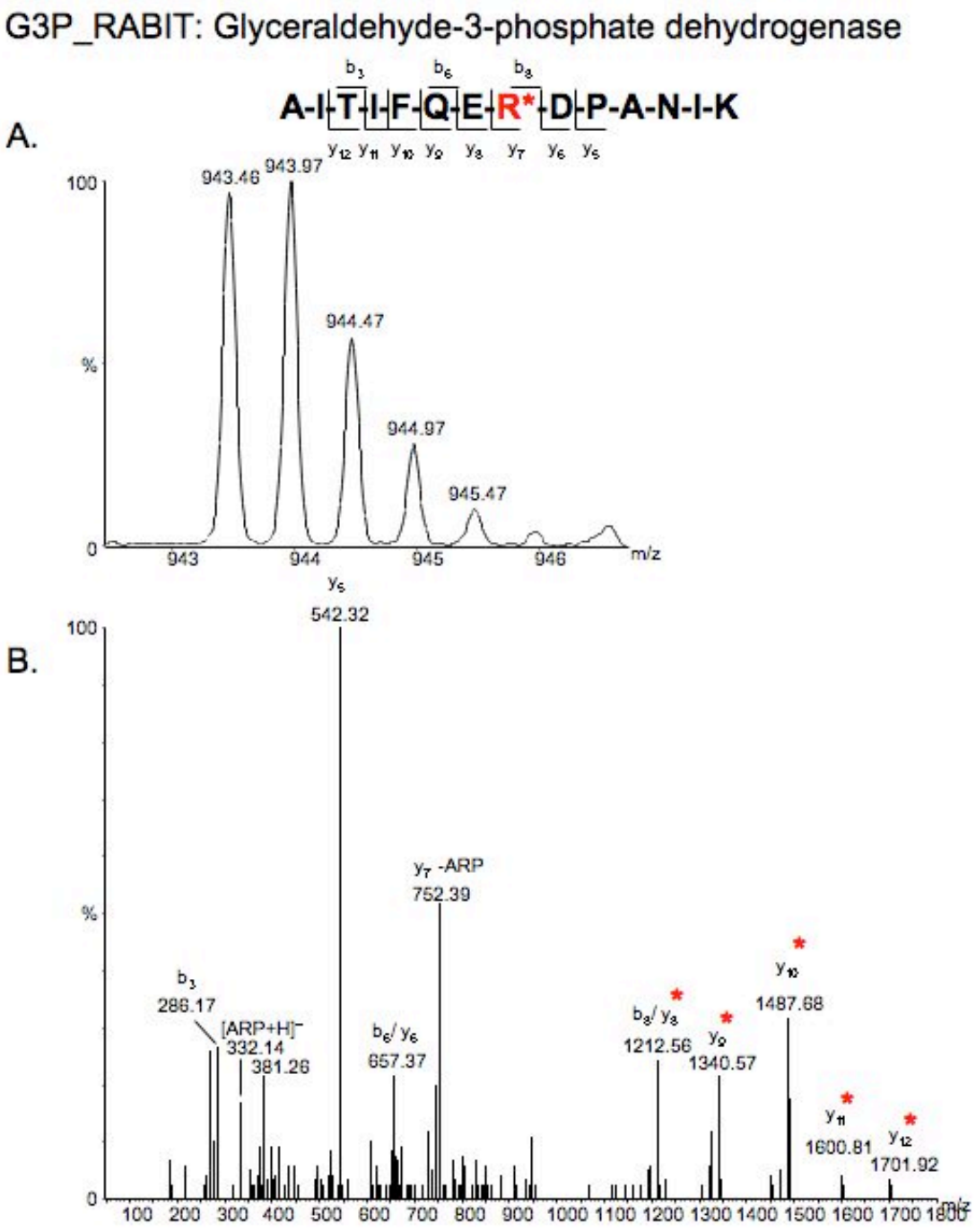

Figure SD5 – (A) Full mass spectrum and (B) MS/MS spectrum acquired by ESI-Q-TOF of the $[M+2H]^{2+}$ ion of the ARP labeled GGS modified peptide AITIFQER*DPANIK; monoisotopic m/z_{calc} 943.48; accuracy $\Delta(m/z)$ = -0.02 m/z

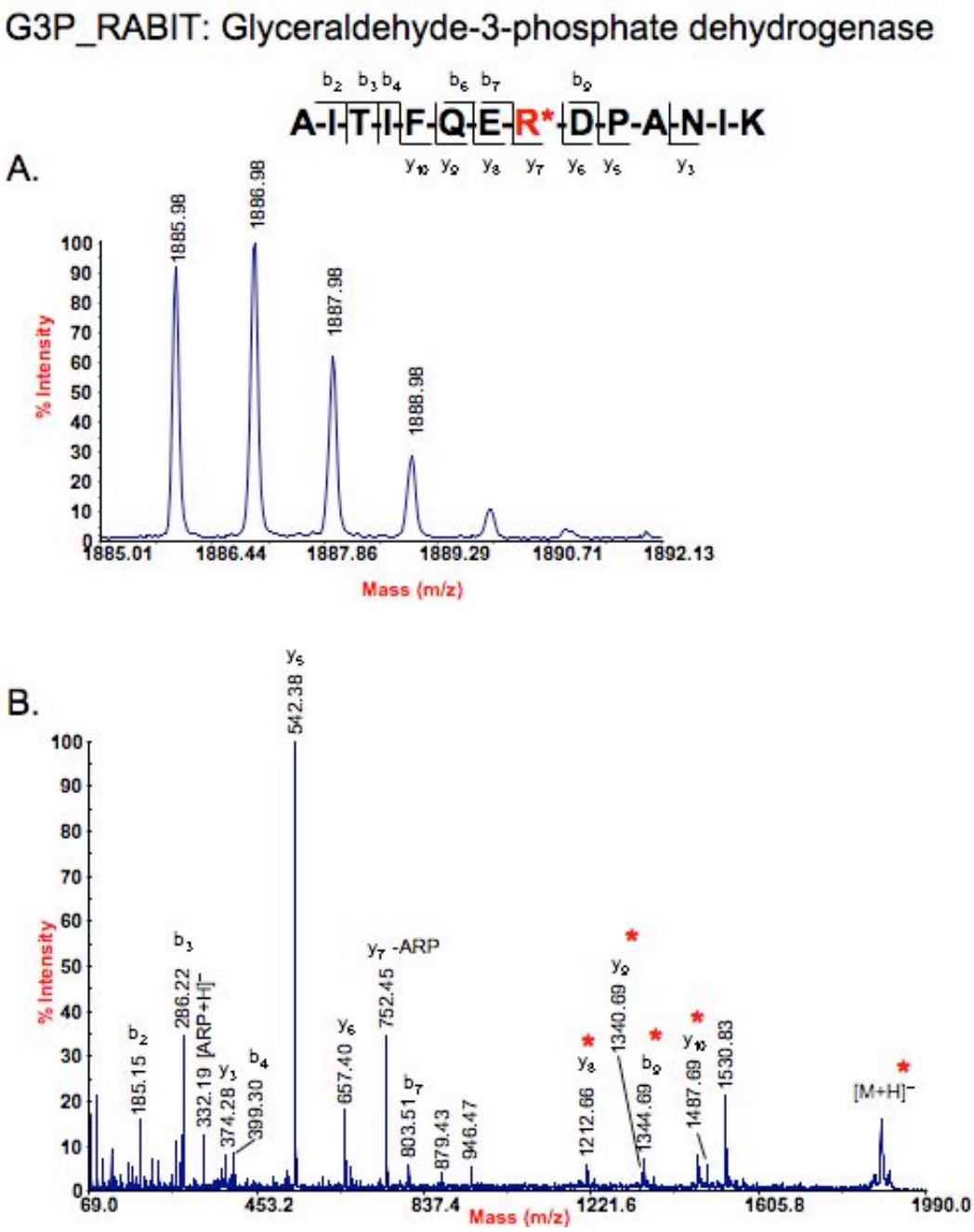

Figure SD6 – (A) Full mass spectrum and (B) MS/MS spectrum acquired by MALDI-TOF/TOF of the $[M+H]^+$ ion of the ARP labeled GGS modified peptide AITIFQER*DPANIK; monoisotopic m/z_{calc} 1885.95; accuracy $\Delta(m/z)$ = 0.01 m/z

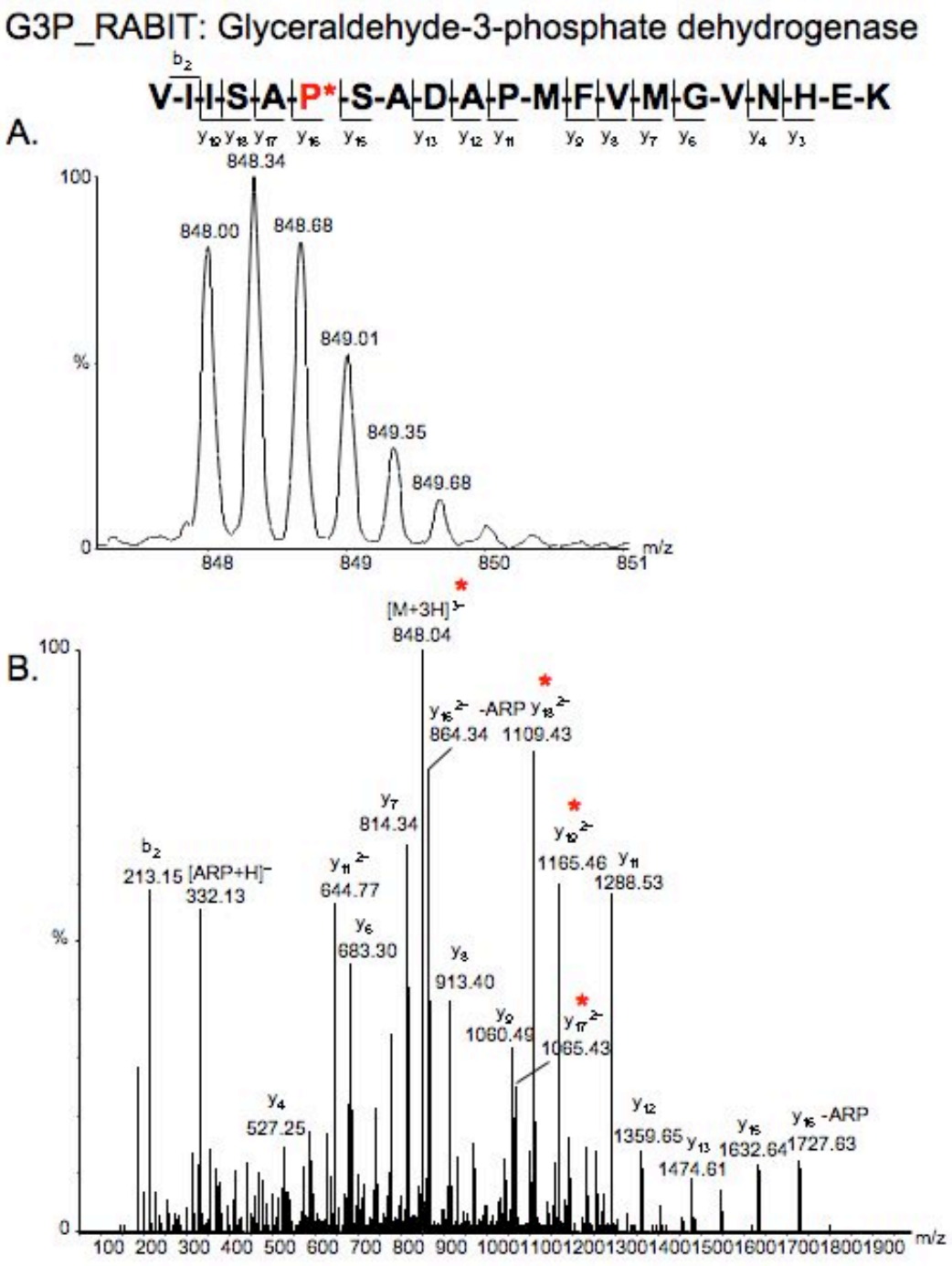

Figure SD7 – (A) Full mass spectrum and (B) MS/MS spectrum acquired by ESI-Q-TOF of the $[M+3H]^{3+}$ ion of the ARP labeled GGS modified peptide VIISAP*SADAPMFVMGVNHEK; monoisotopic m/z_{calc} 848.08; accuracy $\Delta(m/z)$ = -0.08 m/z

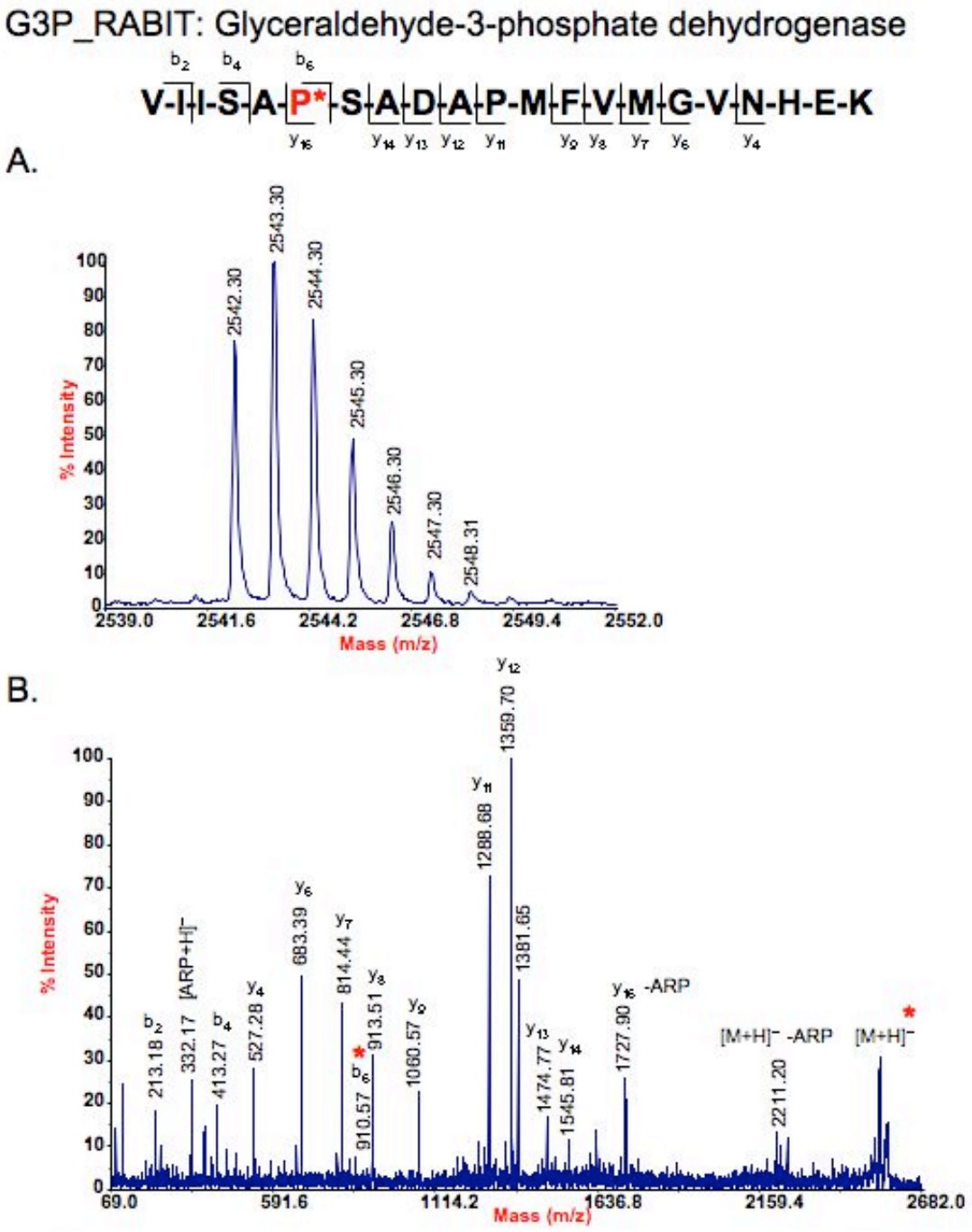

Figure SD8 – (A) Full mass spectrum and (B) MS/MS spectrum acquired by MALDI-TOF/TOF of the $[M+H]^+$ ion of the ARP labeled GGS modified peptide VIISAP*SADAPMFVMGVNHEK; monoisotopic m/z_{calc} 2542.23; accuracy $\Delta(m/z)$ = 0.07 m/z

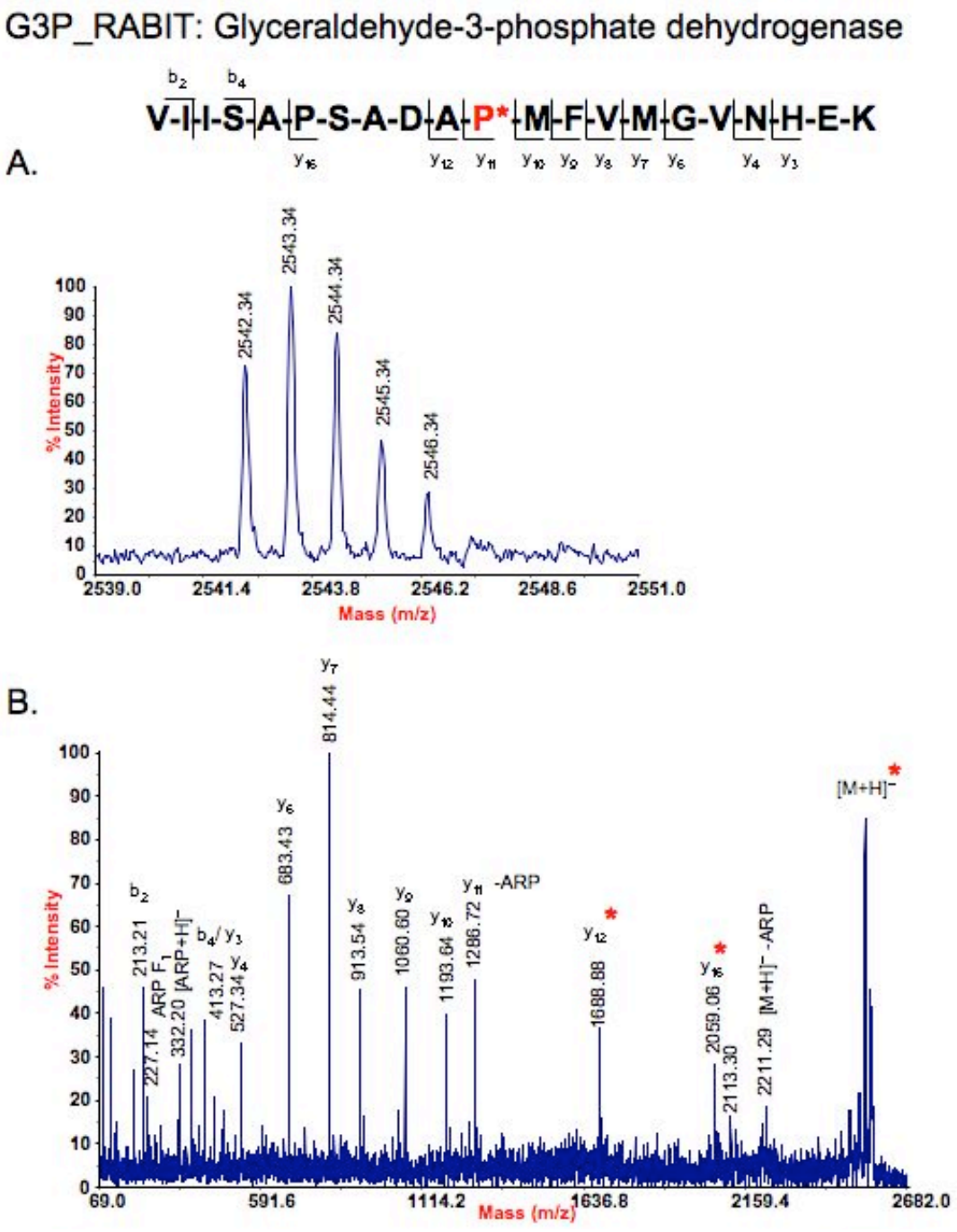

Figure SD9 – (A) Full mass spectrum and (B) MS/MS spectrum acquired by MALDI-TOF/TOF of the $[M+H]^+$ ion of the ARP labeled GGS modified peptide VIISAPSADAP*MFVMGVNHEK; monoisotopic m/z_{calc} 2542.23; accuracy Δ(m/z) = 0.11 m/z

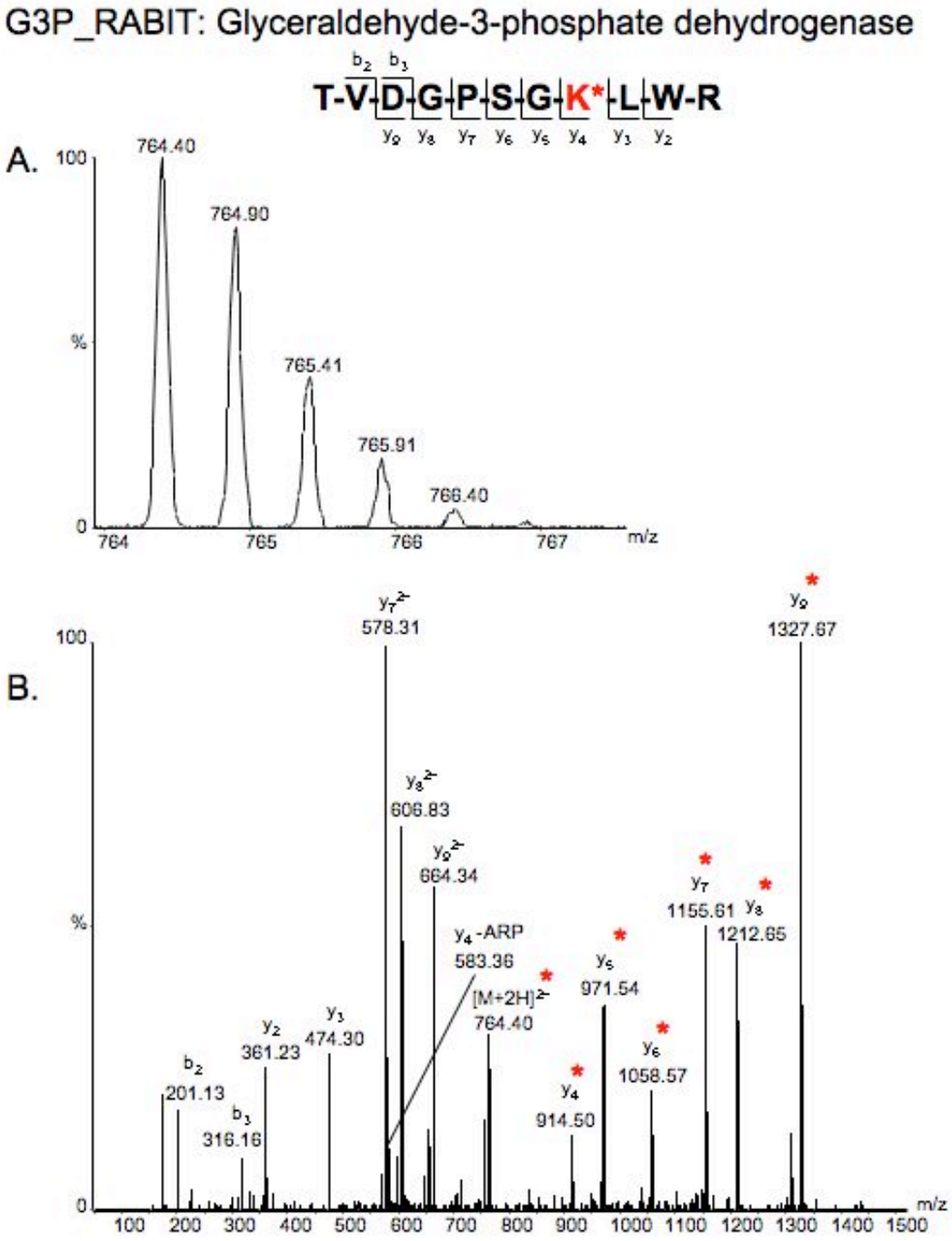

Figure SD10 – (A) Full mass spectrum and (B) MS/MS spectrum acquired by ESI-Q-TOF of the $[M+2H]^{2+}$ ion of the ARP labeled AAS modified peptide TVDGPSGK*LWR; monoisotopic m/z_{calc} 764.37; accuracy $\Delta(m/z)$ = 0.03 m/z

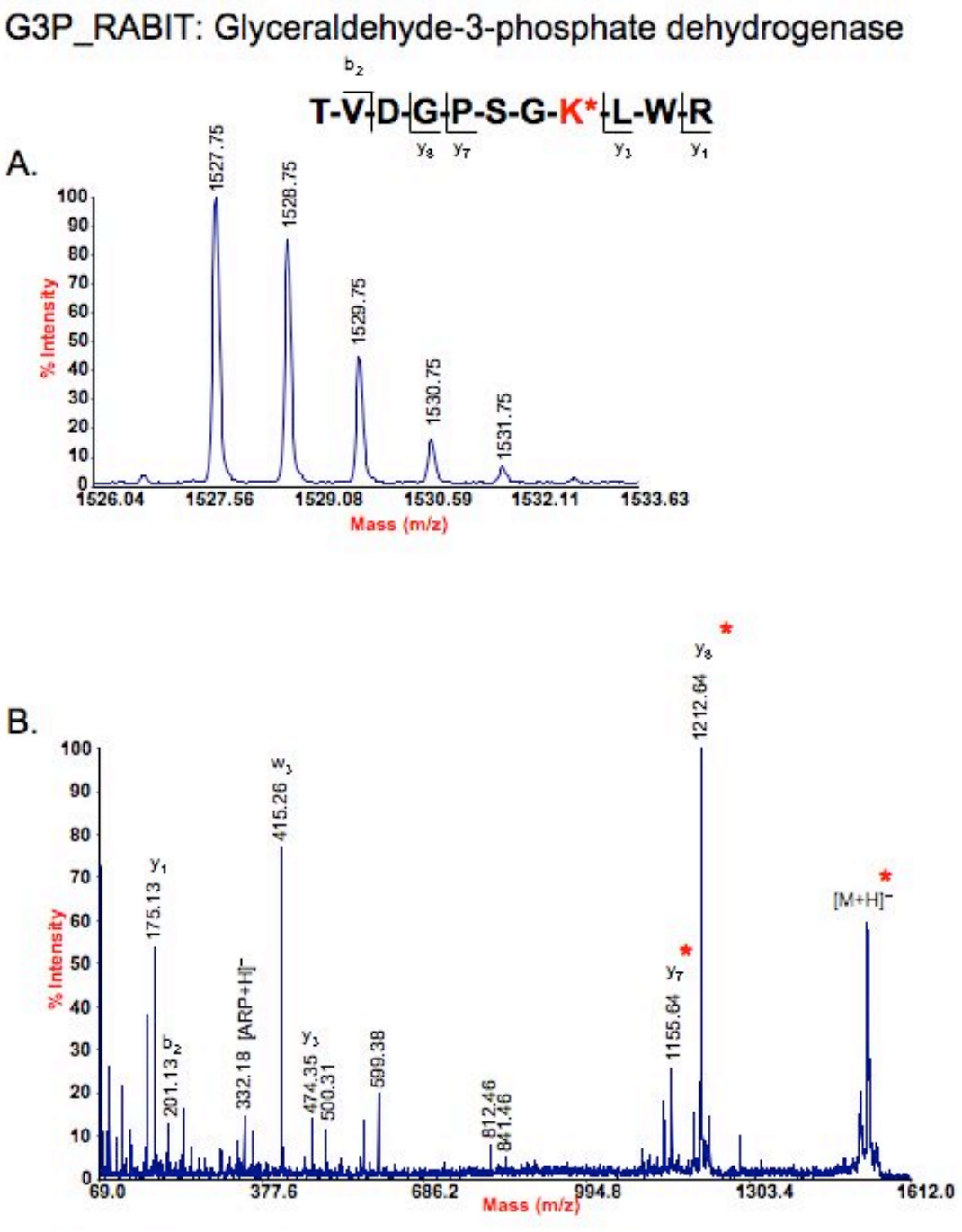

Figure SD11 – (A) Full mass spectrum and (B) MS/MS spectrum acquired by MALDI-TOF/TOF of the $[M+H]^+$ ion of the ARP labeled GGS modified peptide TVDGPSGK*LWR; monoisotopic m/z_{calc} 1527.74; accuracy $\Delta(m/z)$ = 0.01 m/z

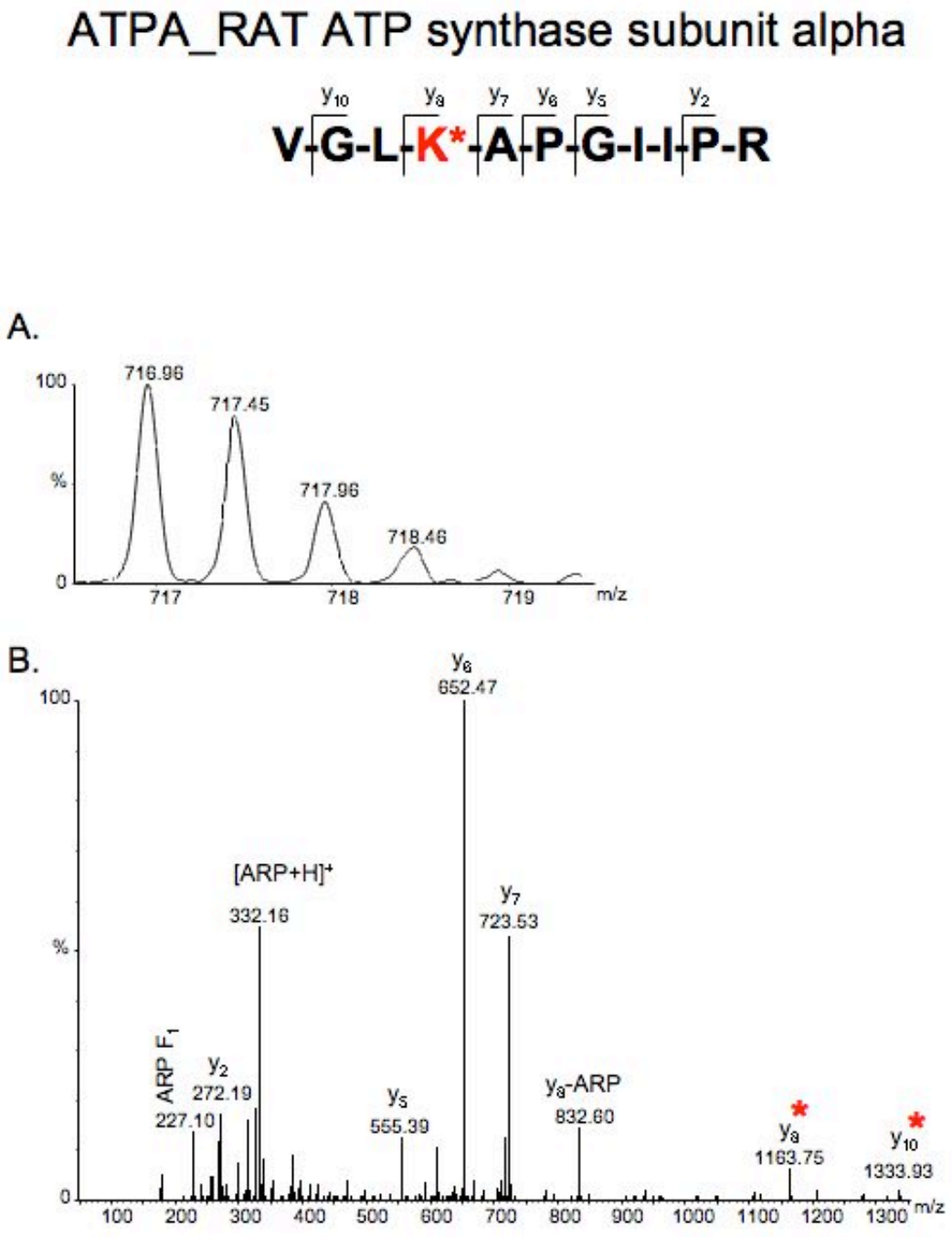

Figure SD12 – (A) Full mass spectrum and (B) MS/MS spectrum acquired by ESI-Q-TOF of the $[M+2H]^{2+}$ ion of the ARP labeled AAS modified peptide VGLK*APGIIPR; monoisotopic m/z_{calc} 716.91; accuracy $\Delta(m/z)$ = 0.05 m/z

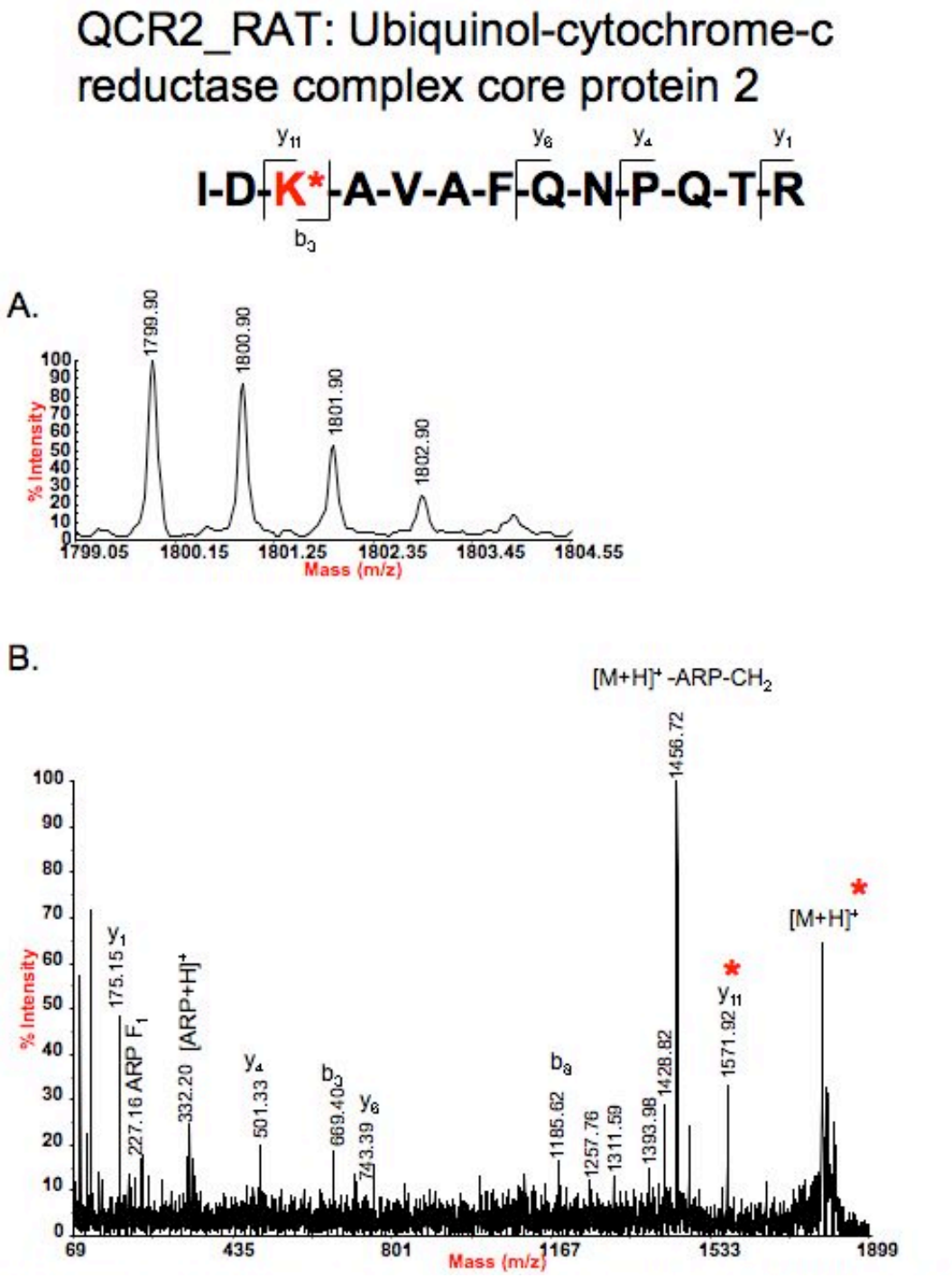

Figure SD13 – (A) Full mass spectrum and (B) MS/MS spectrum acquired by MALDI-TOF/TOF of the $[M+H]^+$ ion of the ARP labeled AAS modified peptide IDK*AVAFQNPQTR; monoisotopic m/z_{calc} 1799.89; accuracy $\Delta(m/z)$ = 0.01 m/z

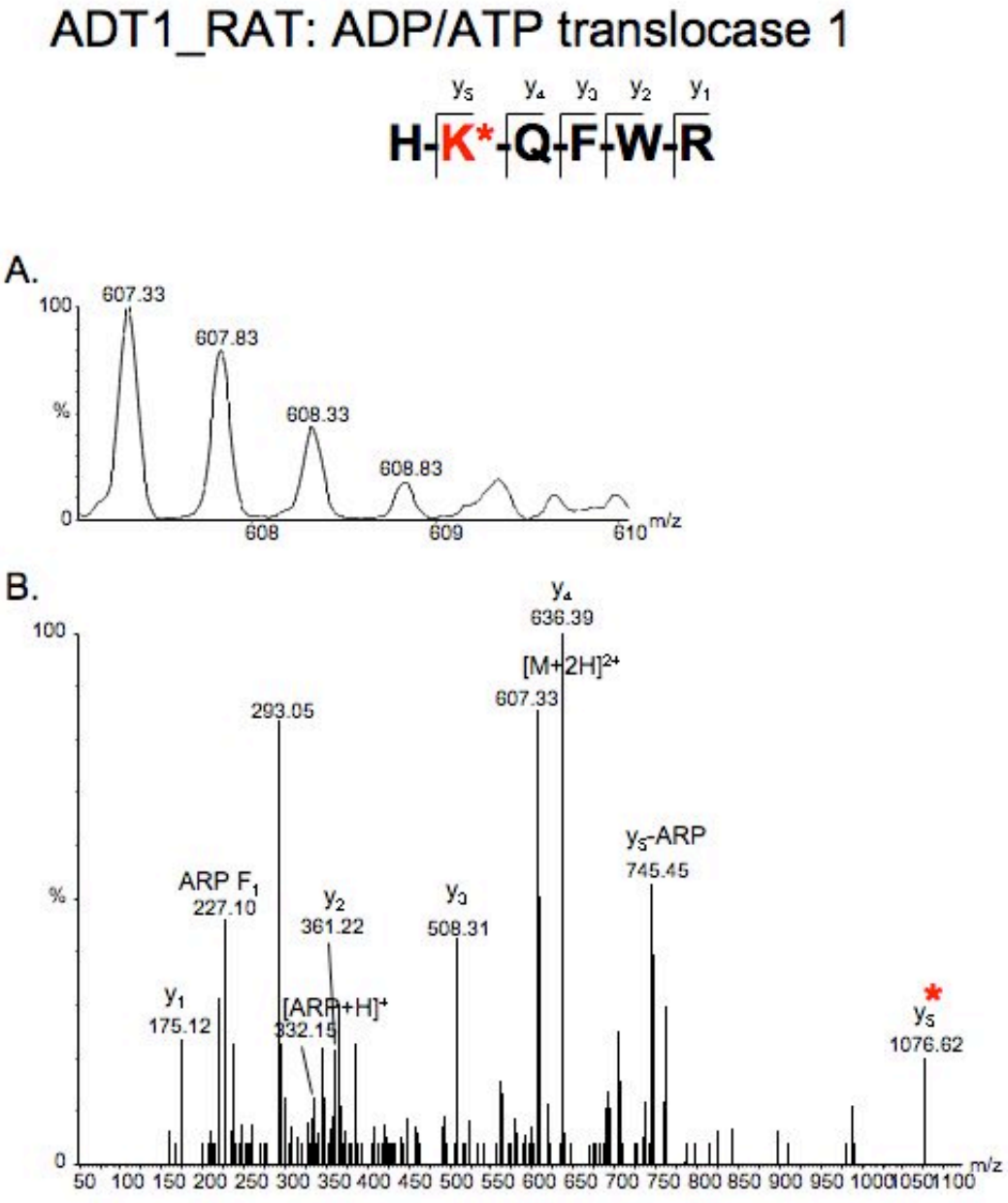

Figure SD14 – (A) Full mass spectrum and (B) MS/MS spectrum acquired by ESI-Q-TOF of the $[M+2H]^{2+}$ ion of the ARP labeled AAS modified peptide HK*QFWR; monoisotopic m/z_{calc} 607.29; accuracy $\Delta(m/z)$ = 0.04 m/z

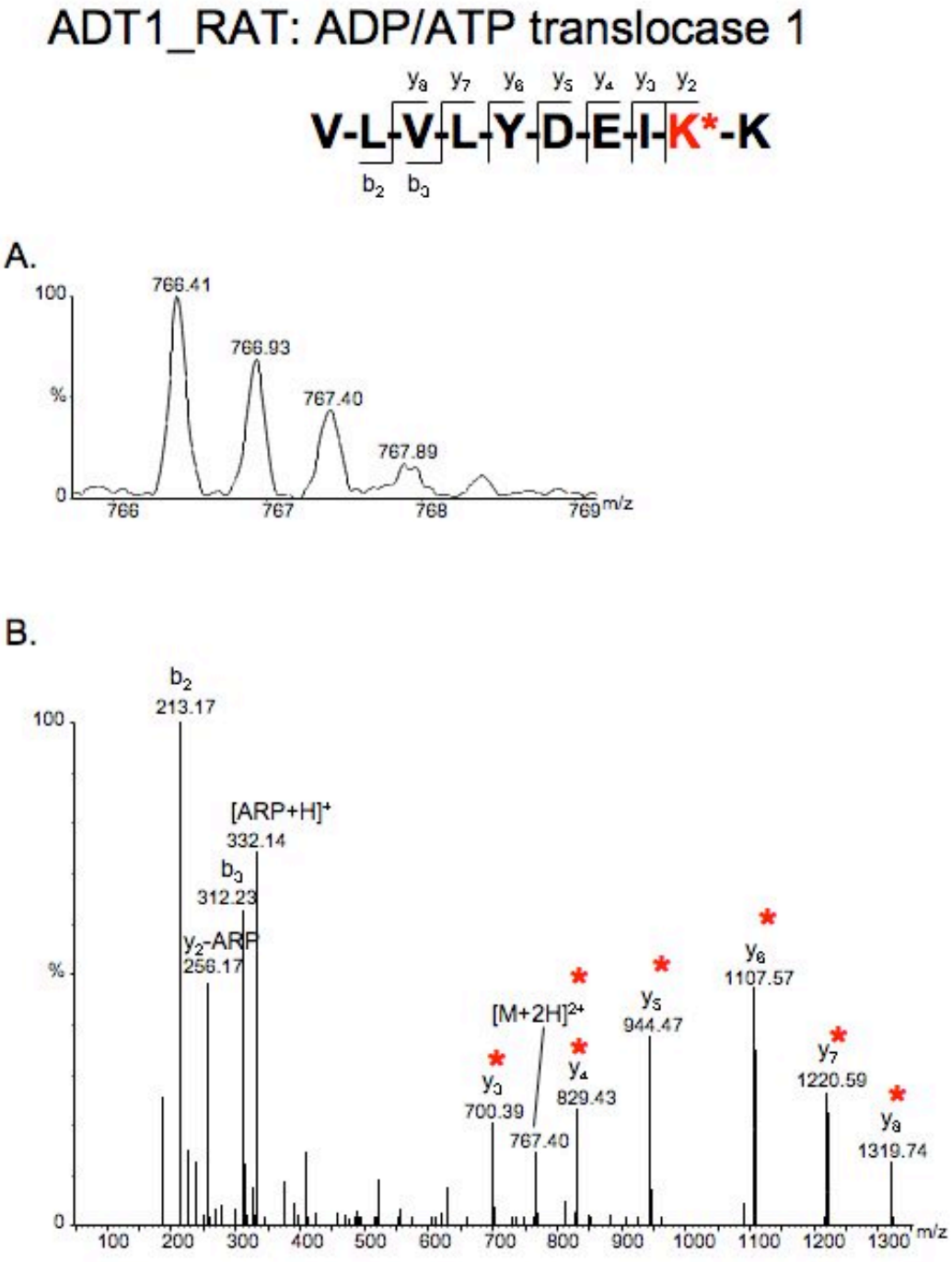

Figure SD15 – (A) Full mass spectrum and (B) MS/MS spectrum acquired by ESI-Q-TOF of the $[M+2H]^{2+}$ ion of the ARP labeled AAS modified peptide VLVLYDEIK*K; monoisotopic m/z_{calc} 766.41; accuracy $\Delta(m/z)$ = 0.00 m/z

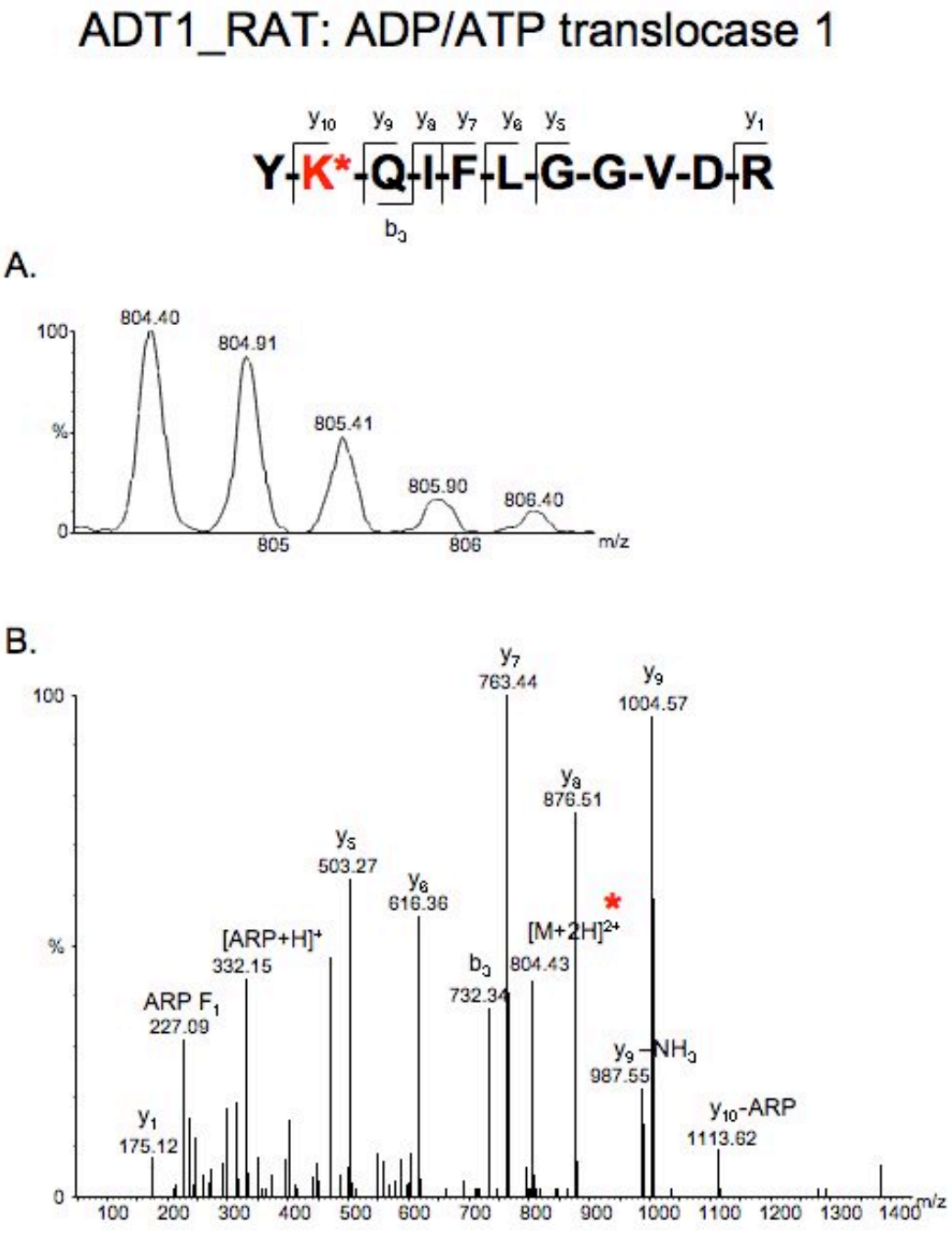

Figure SD16 – (A) Full mass spectrum and (B) MS/MS spectrum acquired by ESI-Q-TOF of the $[M+2H]^{2+}$ ion of the ARP labeled AAS modified peptide YK*QIFLGGVDR; monoisotopic m/z_{calc} 804.40; accuracy $\Delta(m/z)$ = 0.00 m/z

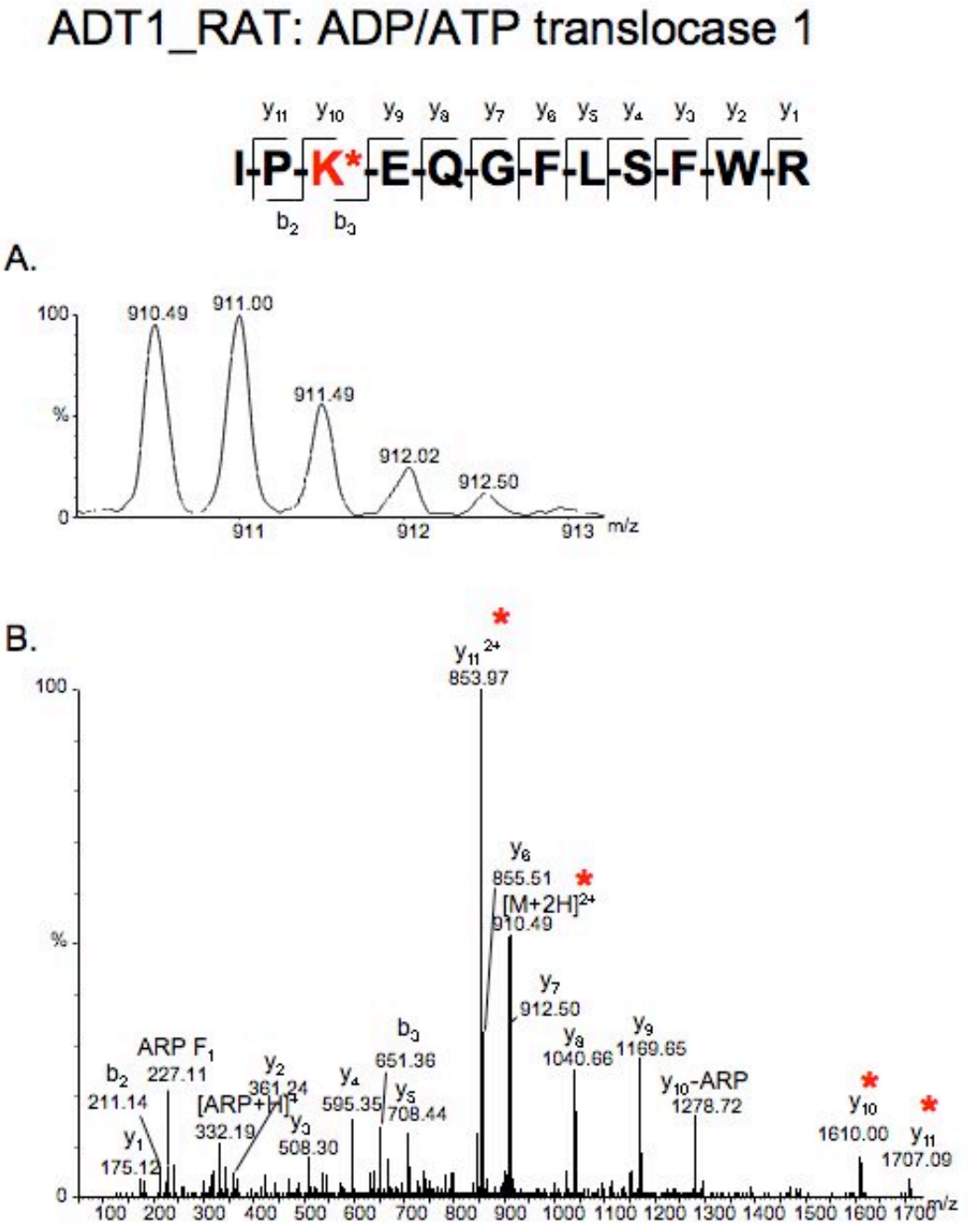

Figure SD17 – (A) Full mass spectrum and (B) MS/MS spectrum acquired by ESI-Q-TOF of the $[M+2H]^{2+}$ ion of the ARP labeled AAS modified peptide IPK*EQGFLSFWR; monoisotopic m/z_{calc} 910.45; accuracy $\Delta(m/z)$ = 0.04 m/z

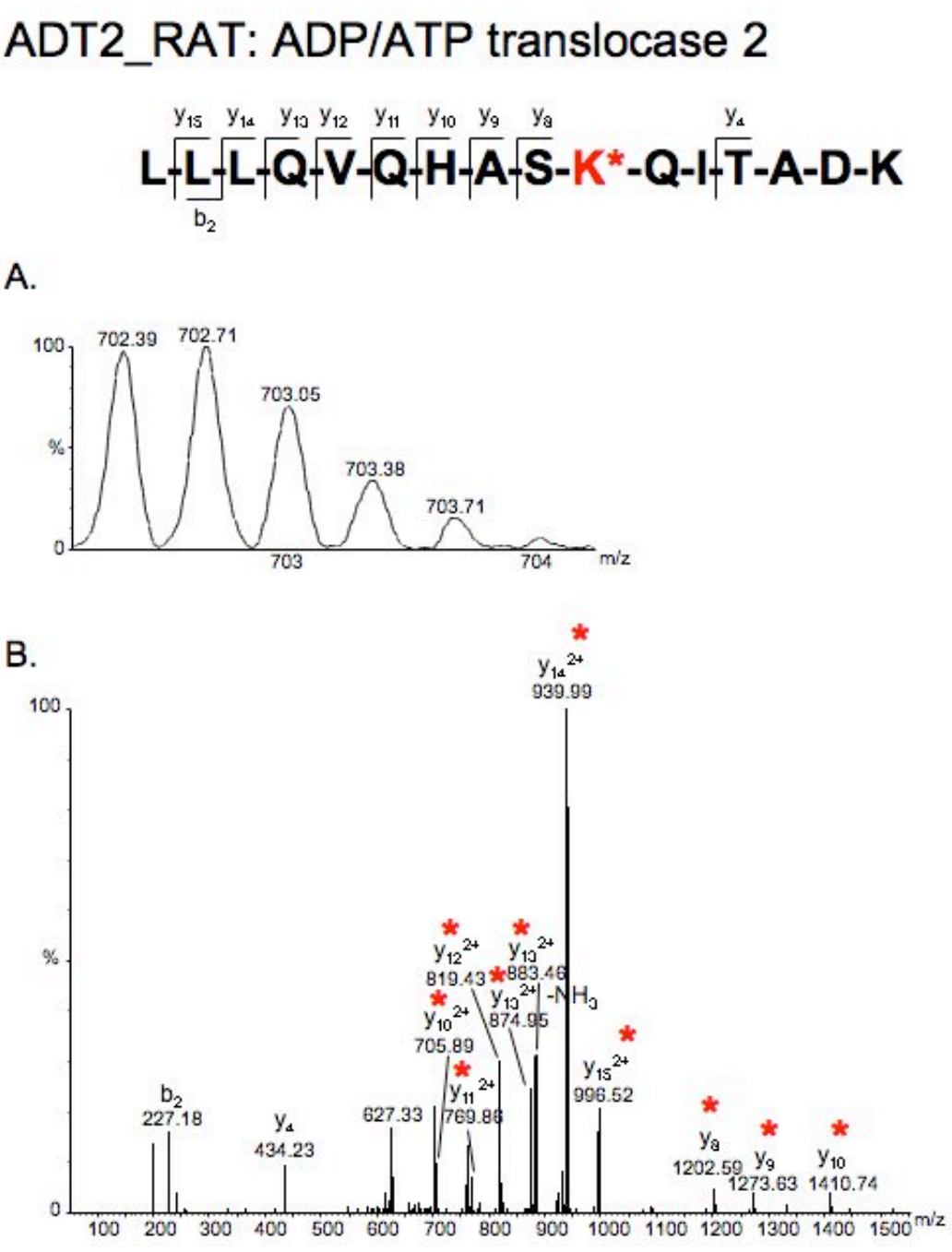

Figure SD18 – (A) Full mass spectrum and (B) MS/MS spectrum acquired by ESI-Q-TOF of the $[M+3H]^{3+}$ ion of the ARP labeled AAS modified peptide LLLQVQHASK*QITADK; monoisotopic m/z_{calc} 702.38; accuracy $\Delta(m/z)$ = 0.01 m/z

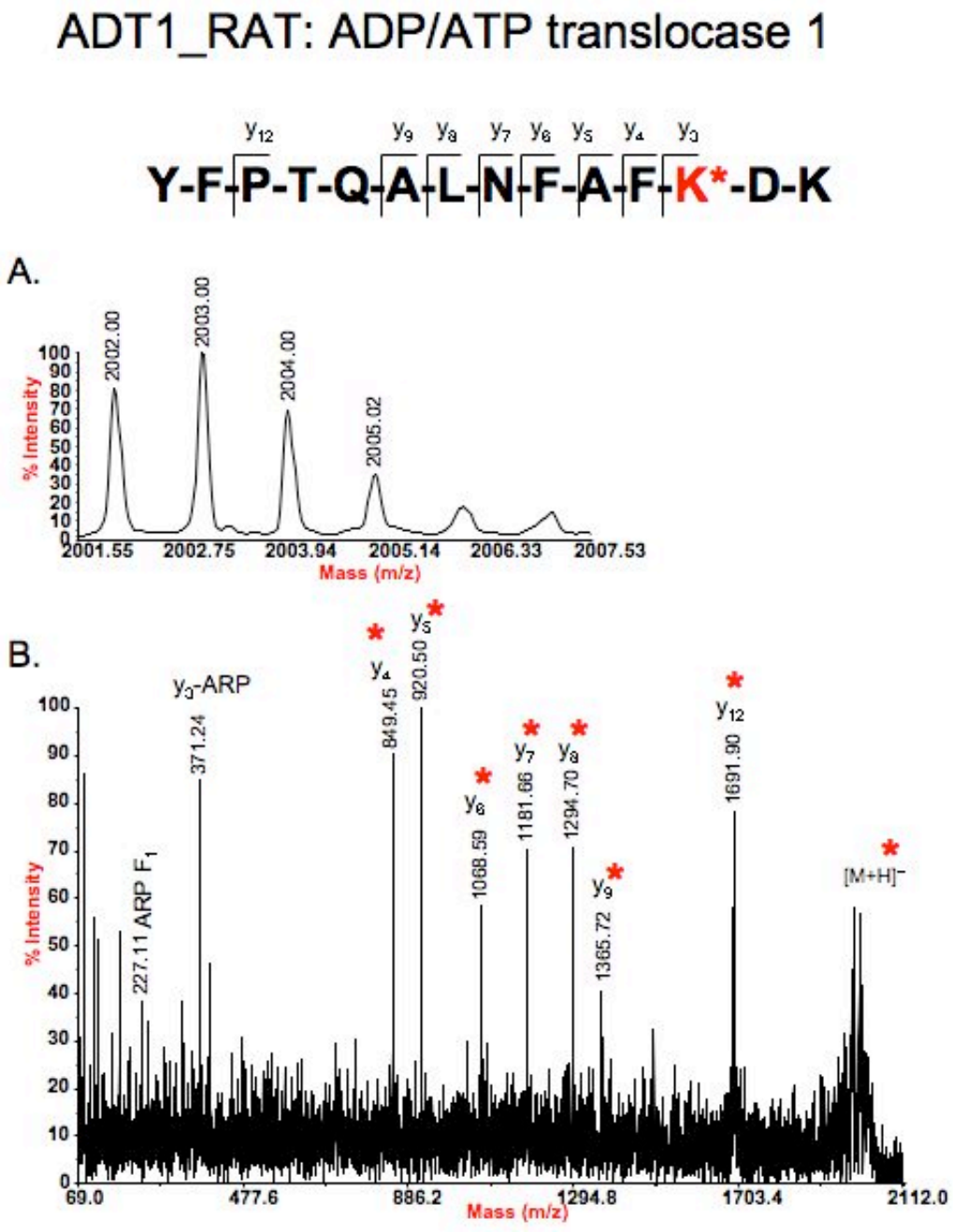

Figure SD19 – (A) Full mass spectrum and (B) MS/MS spectrum acquired by MALDI-TOF/TOF of the $[M+H]^+$ ion of the ARP labeled AAS modified peptide YFPTQALNFAFK*DK; monoisotopic m/z_{calc} 2001.95; accuracy $\Delta(m/z)$ = 0.05 m/z

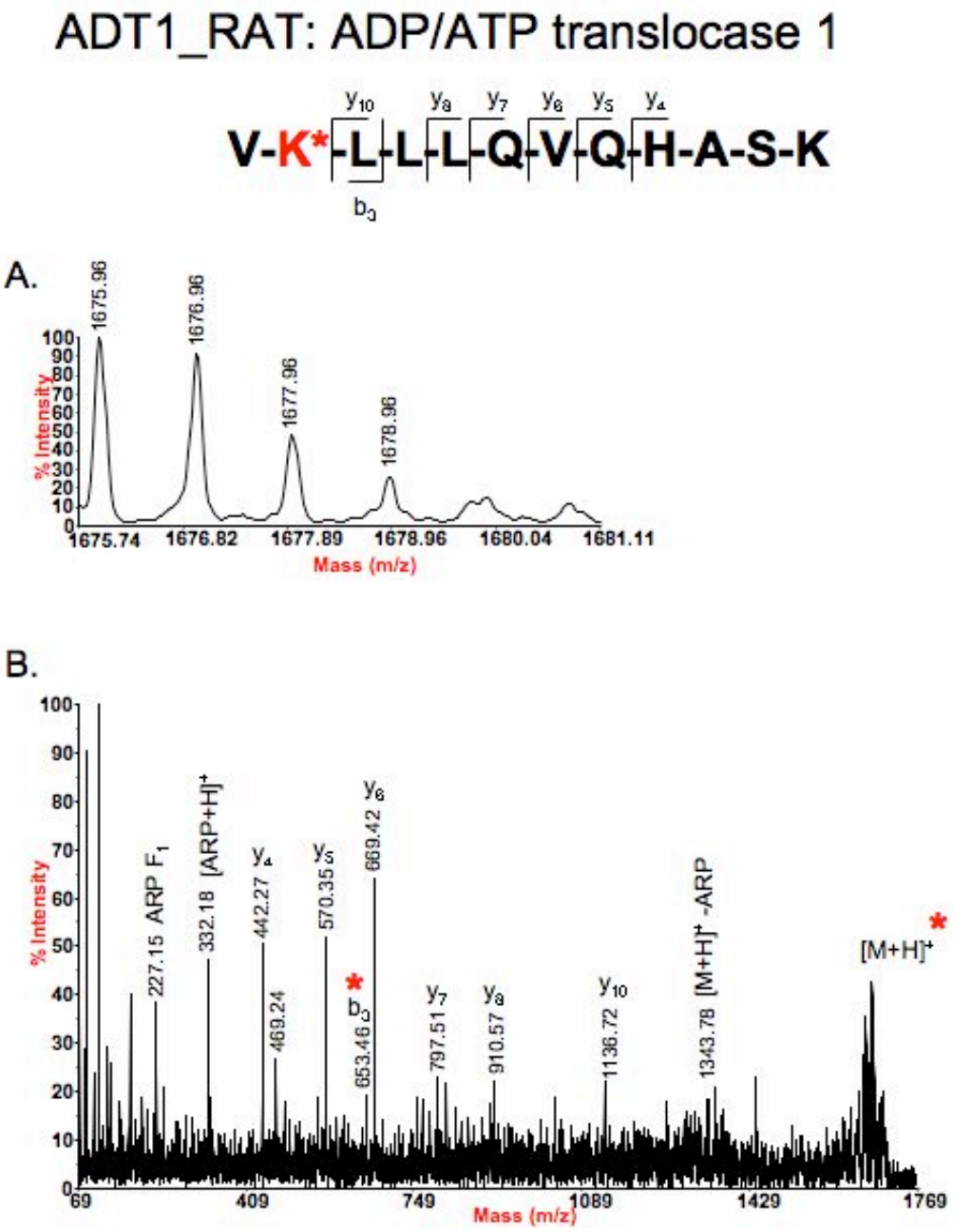

Figure SD20 – (A) Full mass spectrum and (B) MS/MS spectrum acquired by MALDI-TOF/TOF of the $[M+H]^+$ ion of the ARP labeled AAS modified peptide VK*LLLQVQHASK; monoisotopic m/z_{calc} 1675.93; accuracy $\Delta(m/z)$ = 0.03 m/z

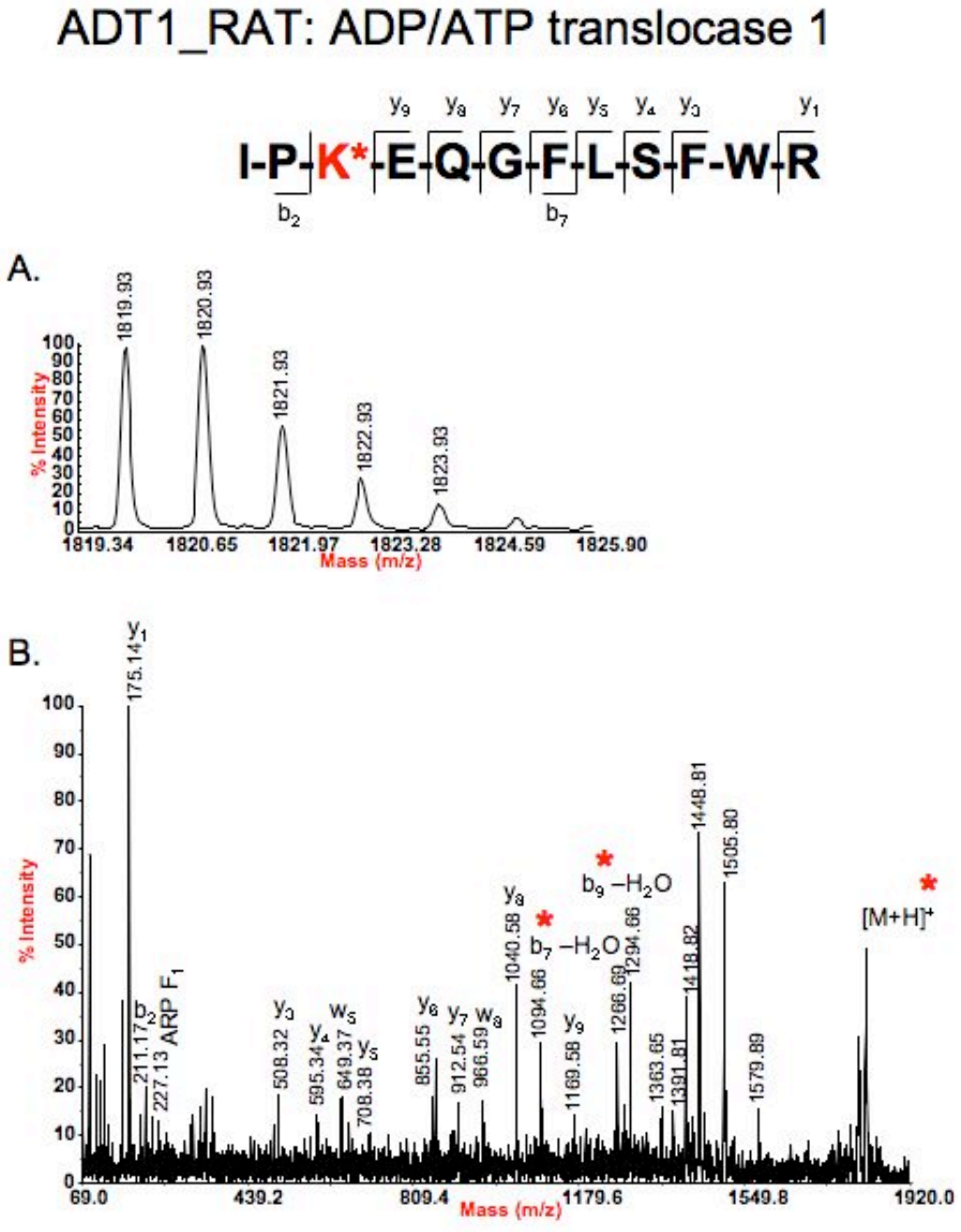

Figure SD21 – (A) Full mass spectrum and (B) MS/MS spectrum acquired by MALDI-TOF/TOF of the $[M+H]^+$ ion of the ARP labeled AAS modified peptide IPK*EQGFLSFWR; monoisotopic m/z_{calc} 1819.89; accuracy $\Delta(m/z)$ = 0.04 m/z

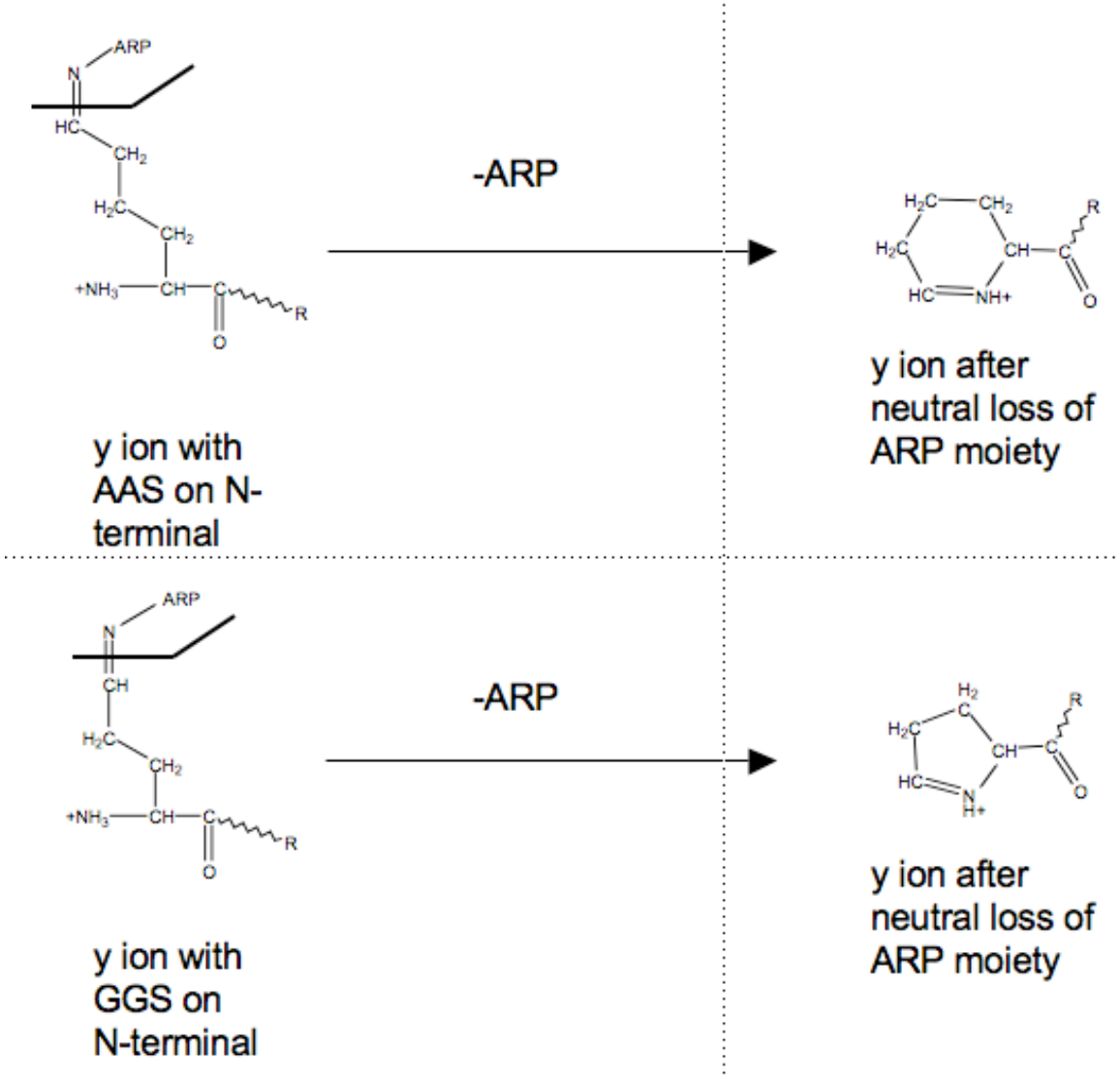

Figure SD22 – Diagram illustrating the neutral loss of the ARP moiety from y ions with an ARP labeled AAS or ARP labeled GGS residue located at the N-terminal location.